THE

American Journal of

ANATOMY

VOLUME 115

JULY SEPTEMBER NOVEMBER 1964

PUBLISHED BY

THE WISTAR INSTITUTE OF ANATOMY AND BIOLOGY

PHILADELPHIA PA

CONTENTS

No. 1 JULY 1964

No 2 SEPTEMBER 1964

No. 3 NOVEMBER 1964

The Influence of the Thyroid Gland on Polyploid Cell Formation in the External Orbital Gland of the Rat

RITA CARRIERE
Department of Anatomy State University of New York, Downstate Medical Center Brooklyn, New York

ABSTRACT The influence of the thyroid gland on the progressive accumulation of polyploid acinar nuclei in the rat external orbital gland was investigated. The numbers of polyploid nuclei were determined from nuclear size distribution curves, having first ascertained the correspondence between increased nuclear size and the polyploid state by microspectrophotometric determinations of the DNA in Feulgen-stained nuclei.

In the first experiment, the animals were kept 147 days, and controls showed increases in external orbital gland weight and polyploid cell formation with age. The presence of the thyroid was essential to these morphological changes, for they were prevented by thyroidectomy t 70 gm body weight. Treatment with thyroxine begun 103 days after thyroidectomy restored body and orbital gland weight gains and the formation of new polyploid cells. Treatment of thyroidectomized rats with growth hormone induced body growth, but failed to alter orbital gland weight and polyploidy The action of thyroid hormone on orbital gland cells was therefore not mediated through its effect on the release of anterior pituitary growth hormone and this contrasts with previously reported results of polyploidy studies in the livers of these same animals.

A second experiment was designed to study the interrelationship of the bserved thyroid effect with the stimulatory action of testis hormone reported in the literature The animals weighed 49 gm at the beginning of the experiment, their orbital glands weighed 54 mg and contained 41.0% polyploid nuclei. Eighty days after castration at 49 gm body weight, orbital glands weighed 153 mg and contained 88.9% polyploid nuclei of which 34.9% were above tetraploid size, whereas the glands of sham-oper ted controls weighed 214 mg and contained 91.5% polyploid nuclei of which 53.6% were above tetraploid size. Thus, the presence of the testis is not required for polyploid cell formation and orbital gland growth, although it can exert some stimulatory action in the course of normal development. On the other hand, thyroidectomy alone or thyroidectomy together with castration, prevented increases in gland weight or numbers f polyploid nuclei, again demonstrating the essential role of the thyroid. Treatment of thyroidectomized-castrates with thyroxine for 42 days, beginning 38 days after operation, led to the resumption of orbital gland weight gains (107 mg) and polyploid cell formation (91.4%) but treatment with testosterone did not. Thus, the thyroid control is independent of any concomitant testicular influence on these cells, whereas the stimulatory effect of testicular hormone requires permissive action of thyroid hormone.

In discussing these results, comparisons were made with the hormone control of liver growth and polyploidy and it was concluded that the formation of new polyploid cells is stimulated by those specific hormones which can promote cell division in liver parenchyma and external orbital gland acini. It was further noted that in both these tissues, there is an increase of basic nuclear size with age regardless of ploidy and that this nuclear growth also can be influenced by thyroid hormone

The external orbital gland of the rat is a flattened oval structure tightly adhering to the dermis in positions varying from near the base of the ear to midway between the eye and ear. Histologically it consists of acini of the serous type. This gland has been called the exorbital lachrymal gland, the gland of Loewenthal (who first described it in 1895) and by Latin authors, the juxta, or supra or preparotid gland (reviews by Walker '58 and Baquiche '59). It has also been mistaken for the parotid gland which is located just below it (see Baquiche, '59) In very young animals, the nuclei of its acinar cells are of uniform appearance, but before weaning, they begin to enlarge in progressively increasing numbers some attaining enormous sizes. This phenomenon has been shown to exhibit sexual dimorphism, enlarged nuclei being more numerous in glands from adult male albino rats than in those from adult fe-

males (Walker '58 Baquiche '59) Baquiche showed that the difference was due to male sex hormone since there were fewer large nuclei in castrated males and a greater number appeared after administration of testosterone to castrated males and to females. However it must be concluded that factors other than male hormone influence this phenomenon, since large nuclei begin to accumulate well before puberty and since they occur in females. Hormonal factors concerned with body and organ growth could conceivably exert an effect. Therefore the hypothesis that the thyroid gland might be implicated was examined, since it was shown to play a role in the accumulation of polyploid liver nuclei (Carriere '55 '62 Swartz, '60 *Geschwind et al.*, '60)

It has been found that external orbital gland cells may show very wide mitotic metaphase figures corresponding in size to the large nuclei, and that such figures contain higher numbers of chromosomes than smaller metaphase figures corresponding in width to smaller nuclei. It was therefore concluded that the large nuclei were polyploid (Teir 44) In the present investigation the relative DNA content of individual interphase nuclei was determined microspectrophotometrically to establish on a firmer basis the correlation between nuclear size and ploidy Once this was done the simpler technique of measuring nuclear sizes could be used to observe the changes in the relative numbers of polyploid nuclei in various experimental groups. *The influence of the thyroid gland* and its interaction with the testicular effect were studied in rats subjected to gland extirpations with and without hormone therapy

MATERIALS AND METHODS

The first experiment was designed to find out whether the thyroid could influence the formation of polyploid nuclei in orbital gland cells Ten 70 gm male Sherman rats were sham-operated and 50 were thyroidectomized the latter were subdivided into three groups 103 days later and injected twice daily for 44 days with saline solution, or thyroxine or growth hormone The sham-operated rats received injections of saline solution. This group is referred to as sham-operated age controls Since growth ceases about two weeks after thyroidectomy sham-operated rats corresponding to the final body weight of the saline-injected thyroidectomized rats (106 gm) were also added and all animals were killed 147 days after the beginning of the experiment. They were housed under conditions of controlled light and temperature (81 ± 3 F) To insure complete thyroid deficiency they were fed the iodine deficient diet described by Leblond and Eartly ('52) and drank 1% calcium lactate in distilled water during the first three weeks following operation (to prevent tetany due to possible total parathyroidectomy) and distilled water thereafter Injections were given at 12 hour intervals 3 μg/day of Na *dl-thyroxine until the rats reached 100 gm* body weight, and 6 μg/day afterwards and, initially 100 μg/day growth hormone (from the Connaught Laboratories Toronto Canada) with subsequent increases of the doses to maintain body weight gains. The growth hormone contained negligible TSH and ACTH contamination but it did contain some gonadotropic activity (Leblond and Carriere '55)

Completeness of thyroidectomy was verified (cessation of body weight gains absence of acidophiles in pituitary sections review by Eartly and Leblond, '54) Each group consisted of 6–8 animals at autopsy Tissues were fixed in Orth's fluid washed in 1% formalin weighed, sectioned at 6 μ and stained with hematoxylin and eosin. Body external orbital gland and seminal vesicle weights were subjected to analysis of variance and "t tests

A second experiment was designed to study the interrelationship of the thyroid and testicular hormones in their action on orbital gland cells Male Sherman rats *weighing 49 gm at the beginning of the* experiment were used. Eight were killed immediately to serve as initial controls (rather than use animals corresponding to the final weight of the thyroidectomized rats as in the previous experiment) 12

This experiment was carried out in the Department of Anatomy McGill University Montreal, Canada, and the biometric work was completed in the Department of Biology University of Montreal, with the aid of grants from the National Research Council of Canada, to Prof C P Leblond and to R. Carriere The author gratefully acknowledges her indebtedness to Prof C P Leblond.

were thyroidectomized, 12 were castrated, 52 were thyroidectomized and castrated and ten were sham-operated. After 38 days the doubly operated rats were subdivided into 4 groups to be injected twice daily with either saline solution, or thyroxine, or testosterone, or both hormones together The dosages were as follows 1 5 µg/day of thyroxine for ten days, then 3 µg/day for the rest of the experiment, and 250 µg/day of testosterone (in 1% Dupanol) for ten days and 500 µg/day afterwards. The animals were kept a further 42 days in quarters adjusted to 76 ± 3 F They were fed a commercial iodine deficient diet supplemented with 10% brewer s yeast and 1% pig liver (all from Nutritional Biochemicals Corp. Cleveland, O) They drank 1% calcium lactate in distilled water during the first four weeks, and distilled water thereafter Three weeks before the end of the experiment, respiratory infections spread among the animals those which were severely ill were eliminated and all others were given daily injections of 6 000 units of Combiotic (penicillin G and dihydrostreptomycin, Pfizer and Co.) for four days. At the end of the experiment, although most groups consisted of 8–10 animals there were only four in three of the groups, the sham operated age controls, the doubly operated rats receiving thyroxine and those receiving both hormones together The orbital glands, seminal vesicles, and several other organs were fixed in Bouin s fluid for 24 hours, washed in 70% alcohol, weighed, sectioned at 6 µ and stained with hematoxylin and eosin.

Histometric procedures

Nuclear sizes were measured at 1,000 × magnification in 200 acinar cells per animal taking the average of two diameters per nucleus, selecting all clearly outlined nuclei in eight randomly chosen areas per section. A Leitz screw micrometer having 29 divisions per µ was used. Many cells contained two nuclei; these were found to be of the same size range as nuclei in mononucleated cells and so they were included in the measurements. Nuclear size frequency distribution curves were prepared for each animal and it was found that the range of sizes for the various glands within an experimental group corresponded well and could be combined to plot the average distribution for each experimental group as a whole.

On examination of the histograms for experiment 1 it was found that the nuclear size classes were not clearly delineated (fig 2) and these curves were not analyzed further than to observe simply whether treatment altered the nuclear size distributions, i.e. whether it increased or decreased the numbers of nuclei in the larger size range Before carrying out the second experiment, several fixatives (Zenker Carnoy Bouin formalin) were tested, and Bouin s fluid was selected because it preserved the nuclei in a more regularly spherical shape. As a result, the size ranges for diploid and tetraploid nuclei were clearer (first curve of figure 3 as compared with the first curve of fig 2) and the histograms for experiment 2 could be analyzed mathematically to express the results on a more quantitative basis. The probability graph technique for analysis of polymodal curves (Harding 49 Kasten, '55 Carriere and Patterson, '62) was used to find the point marking the limit between diploid and tetraploid sizes in the average histogram for each experimental group (table 1) The percentage of nuclei beyond this nuclear size point, i.e., the percentage of polyploid nuclei, was determined for each individual animal, and the average percentage of polyploid nuclei for each experimental group could then be calculated and subjected to analysis of variance and "t tests. Changes in the number of nuclei beyond the tetraploid range were of interest in two of the groups. Therefore their probability graphs were used to find the limit between tetraploid nuclei and those of larger diameter the numbers of nuclei beyond this point were determined for individual animals, and the average for each group was then calculated. The graphical analyses also allowed the determination of the average diploid and tetraploid diameters. As with liver nuclear sizes (table 1 in Carriere and Patterson '62) all these values corresponded well with results obtained by simple inspection of the size distribution histograms, visualizing each peak as a bell-

males (Walker '58; Baquiche '59) Baquiche showed that the difference was due to male sex hormone, since there were fewer large nuclei in castrated males and a greater number appeared after administration of testosterone to castrated males and to females. However it must be concluded that factors other than male hormone influence this phenomenon, since large nuclei begin to accumulate well before puberty and since they occur in females. Hormonal factors concerned with body and organ growth could conceivably exert an effect. Therefore the hypothesis that the thyroid gland might be implicated was examined, since it was shown to play a role in the accumulation of polyploid liver nuclei (Carriere '55 '62; Swartz, '60; Geschwind et al 60)

It has been found that external orbital gland cells may show very wide mitotic metaphase figures, corresponding in size to the large nuclei and that such figures contain higher numbers of chromosomes than smaller metaphase figures corresponding in width to smaller nuclei. It was therefore concluded that the large nuclei were polyploid (Teir 44) In the present investigation, the relative DNA content of individual interphase nuclei was determined microspectrophotometrically to establish on a firmer basis the correlation between nuclear size and ploidy Once this was done the simpler technique of measuring nuclear sizes could be used to observe the changes in the relative numbers of polyploid nuclei in various experimental groups. The influence of the thyroid gland and its interaction with the testicular effect were studied in rats subjected to gland extirpations with and without hormone therapy

MATERIALS AND METHODS

The first experiment was designed to find out whether the thyroid could influence the formation of polyploid nuclei in orbital gland cells Ten 70 gm male Sherman rats were sham-operated and 50 were thyroidectomized the latter were subdivided into three groups 103 days later and injected twice daily for 44 days with saline solution or thyroxine or growth hormone. The sham-operated rats received injections of saline solution. This group is referred to as sham-operated age controls. Since growth ceases about two weeks after thyroidectomy sham-operated rats corresponding to the final body weight of the saline-injected thyroidectomized rats (106 gm) were also added and all animals were killed 147 days after the beginning of the experiment. They were housed under conditions of controlled light and temperature (81 ± 3°F) To insure complete thyroid deficiency they were fed the iodine deficient diet described by Leblond and Eartly ('52) and drank 1% calcium lactate in distilled water during the first three weeks following operation (to prevent tetany due to possible total parathyroidectomy) and distilled water thereafter Injections were given at 12 hour intervals: 3 μg/day of Na dl-thyroxine until the rats reached 100 gm body weight, and 6 μg/day afterwards, and, initially 100 μg/day growth hormone (from the Connaught Laboratories, Toronto Canada) with subsequent increases of the doses to maintain body weight gains The growth hormone contained negligible TSH and ACTH contamination, but it did contain some gonadotropic activity (Leblond and Carriere '55)

Completeness of thyroidectomy was verified (cessation of body weight gains, absence of acidophiles in pituitary sections, review by Eartly and Leblond '54) Each group consisted of 6–8 animals at autopsy Tissues were fixed in Orth's fluid, washed in 1% formalin, weighed, sectioned at 6 μ and stained with hematoxylin and eosin. Body external orbital gland and seminal vesicle weights were subjected to analysis of variance and t tests.

A second experiment was designed to study the interrelationship of the thyroid and testicular hormones in their action on orbital gland cells. Male Sherman rats weighing 49 gm at the beginning of the experiment were used. Eight were killed immediately to serve as initial controls (rather than use animals corresponding to the final weight of the thyroidectomized rats as in the previous experiment) 12

This experiment was carried out in the Department of Anatomy McGill University Montreal, Canada, and the histometric work was completed in the Department of Biology University of Montreal, with the aid of grants from the National Research Council of Canada, to Prof. C. P Leblond and to R. Carriere. The author gratefully acknowledges her indebtedness to Prof. C. P Leblond.

rately preserving their relative numbers. Our aim being only to ascertain that the large nuclei contained polyploid amounts of DNA, the above determinations were considered a satisfactory indication that nuclear size distributions could be used to count polyploid nuclei in tissue sections.

From the nuclear size distribution for young normal rats (fig. 3, first curve) and from the values obtained from the probability graph analysis (table 1) it is seen that: diploid and tetraploid nuclei overlapped at 6.5 μ; diploid nuclei averaged 5.7 μ in diameter; tetraploid nuclei ranged up to 8.2 μ and had an average diameter of 7.2 μ. As a matter of interest, the volume of a sphere of 5.7 μ diameter was calculated and found to be 96.7 μ^3. The diameter of a sphere twice this volume (193.5 μ^3) and hence, the expected tetraploid diameter was calculated and found to be 7.2 μ. In the older animals (second curve fig. 3) all values have shifted to the right, nuclei of a given ploidy were slightly larger, e.g. tetraploid nuclei now averaged 7.8 μ in diameter (fig. 3 and table 1). The volume of a sphere with this diameter is 247.3 μ. Volumes half and twice this size 123.6 μ^3 and 494.6 μ^3 respectively give calculated diameters of 6.2 and 9.8 μ for diploid and octoploid nuclei. These values are in keeping with the shape of the size distribution curve.

Since the nuclei were measured in 6 μ sections, and nuclear sizes ranged up to 15 μ or more, possible distortion of the true size frequency distributions by the presence of sectioned fragments of the largest nuclei must be considered. The larger fragment of a sectioned nucleus will of course include the equator and give the true diameter. The smaller fragment, on the other hand, may be cut very near the nuclear pole and would then show very light staining, little depth, and an indistinct nuclear membrane; such fragments can be excluded from the measurements. With smaller nuclei such as those in the diploid and tetraploid size range unrecognizable fragments are not sufficiently smaller than the equator to cause significant error in the size frequency distribution curve (for discussion, see Carriere and Patterson, '62). However it is conceivable that fragments of the largest nuclei may be cut far enough from the pole to remain unrecognized and yet still be far enough from the equator to have a significantly smaller diameter and appear among the diploid or tetraploid nuclei in the size distribution curves. To estimate the magnitude of such error a gland from an adult rat was sectioned at 6 μ and at 20 μ, and nuclei were measured in both sections. The size distributions may be compared in figure 1; the thicker section appeared to

INFLUENCE OF SECTION THICKNESS ON NUCLEAR SIZE DISTRIBUTION

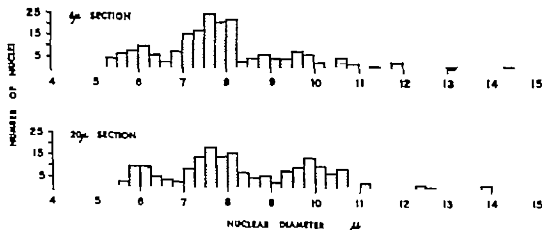


Fig. 1 The nuclear size distributions in 6 and 20 μ sections of an external orbital gland from an animal in the group of sham-operated age controls in experiment 2 (body weight, 280 gm).

contain fewer tetraploid nuclei and relatively more of higher ploidy It is obvious from the lack of significant change within the diploid range i.e. up to 6 5 μ that fragments of diameter below 6 5 μ can be recognized and excluded. Hence the percentage of diploid nuclei, or inversely the percentage of polyploid nuclei, the value of interest in this investigation will not be affected.

RESULTS AND CONCLUSIONS

Experiment 1

The size distribution for the orbital gland nuclei of sham-operated 106 gm rats (fig. 2) showed a range from roughly 4 μ up to 10 μ with most nuclei falling between 4.5 μ and 6.5 μ, and with the possibility of two widely overlapping peaks in this interval. As the rats grew to 374 gm body weight, the orbital glands increased in weight (table 2) nuclei were found to extend their size range up to 13 μ and a large proportion shifted away from 4 5–5 μ, towards 8 μ in diameter The numbers of polyploid nuclei had increased. Thyroidectomy prevented body growth (table 2) nd the age changes seen in the orbital ands of normal rats did not take place as may be seen from figure 2, where the nuclear size distribution is essentially the same as that of the younger sham-operated rats of similar body weight. Injections of thyroid hormone begun 103 days after thyroidectomy and continued for 44 days, increased body weight, orbital gland weight (table 2) and the numbers of nuclei in the larger size range (fig 2, fourth curve) To test whether this effect was associated with the action of thyroxine on the release of pituitary growth hormone thyroidectomized rats were given growth hormone injections. Body weight increased significantly but the external orbital glands showed no weight gains (table 2) and the numbers of polyploid nuclei were not augmented (fig. 2)

Thus thyroid hormone appeared to be essential to orbital gland growth and to the formation of polyploid acinar nuclei. This effect was independent of thyroid action on the release of growth hormone from the anterior pituitary It is not clear from this experiment whether or not the thyroid hormone can act independently of the influence exerted by the testis reported in the literature (Baquiche '59)

Experiment 2

The problem of the interaction of the effect of thyroid and testicular hormones on orbital gland cells was investigated in experiment 2, and the results are summarized in table 3 and figures 3 and 4 The fact that the relative numbers of polyploid nuclei increase with age may again be observed and in this case the histograms gave a clearer picture of ploidy distributions In the 49 gm rats diploid and tetraploid nuclei formed two clear peaks overlapping at 6 5 μ (fig 3 first curve) At 269 gm body weight (fig. 3 second curve) the overlapping point was 6 7 μ and most nuclei were beyond this i.e. polyploid nuclei had increased and the relative numbers of diploid nuclei were greatly reduced Tetraploid and octoploid nuclei predominated but were then also many much larger nuclei. There were only 41 0% polyploid nuclei in the glands of the 49 gm rats whereas there were 91.5% in those of the 269 gm rats (table 3)

TABLE 2

Experiment 1 The influence of the thyroid on body external orbital gland and seminal vesicle weights

Experimental groups Initial body weight 70 gm Killed 147 days after operation Injections last 44 days	Body weight	External orbital gland weight	Seminal vesicles weight
	gm ± S.E.	*mg ± S E.*	*mg ± S E.*
Sham-operated rats (weight control)	106.0 ± 2 7	129.5 ± 7.2	38 0 ± 2.0
Sham-operated age controls	373.6 ± 11.0	268 6 ± 21 7	386.4 ± 36 2
Thyroidectomized rats	105.7 ± 5.7	66.5 ± 7.3	39 4 ± 7.4
Thyroidectomized + thyroxine	215.6 ± 6.4	201.2 ± 21.9	287.8 ± 14 7
Thyroidectomized + growth hormone	151 1 ± 6.1	68.6 ± 10 5	90.5 ± 16.2

Seminal vesicle weights are included to allow assessment of testicular hormone activity

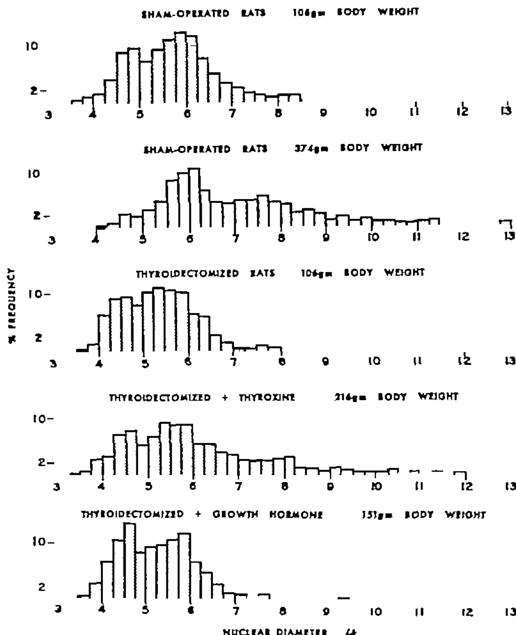


Fig. 2 Nuclear size distributions for the external orbital glands in experiment 1 The first curve represents the distributions for young sham-operated animals of body weight corresponding to the final body weight of untreated thyroidectomized rats; the second curve, that of sham-operated rats kept throughout the experiment, serving as ge controls; the other three curves illustrate the effect of thyroid extirpation in young animals, and of hormone treatments begun 103 days after operation and continued for 44 days.

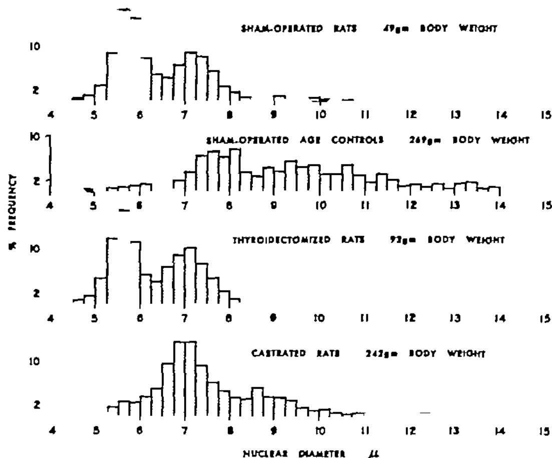


Fig. 3 Experiment 2, nuclear size distributions illustrating the influence of thyroidectomy or castration on nuclear size distributions in the external orbital gland. The 49 gm sham-operated rats illustrate conditions at the beginning of the experiment, or the time of operation and the sham-operated age controls were kept throughout the experiment, 80 days.

In the glands of thyroidectomized rats there were 45.3% polyploid nuclei, which was not significantly different from the 41.0% found in the initial controls the sham-operated 49 gm rats. Thyroid lack again prevented the accumulation of new polyploid nuclei. It should be noted that the tetraploid nuclei present at the time of gland extirpation remained intact, in contrast to the loss of tetraploid-sized nuclei seen in the liver (Carriere, '62) under such conditions.

Castration at 49 gm body weight did not prevent the growth of the gland (table 3) nor the formation of new polyploid nuclei, for they increased to 88.9% (table 3) However the degree of polyploidy was reduced in comparison with sham-operated rats of the same age. Total polyploid nuclei were similar in numbers (91.5% in the sham-operated age controls and 88.5% in castrates table 3) but there were only 24.9% of nuclei above tetraploid size in the castrated rats whereas there were significantly more 53.6% in the sham-operated age controls. Testis lack therefore did interfere with polyploid cell formation to some extent.

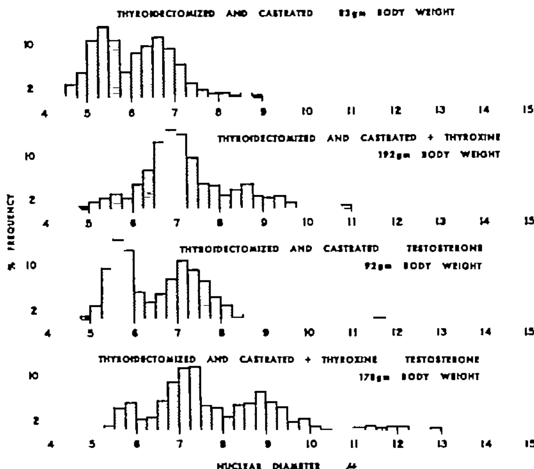


Fig. 4 Experiment 2, nuclear size distributions in the external orbital gland following thyroxine or testosterone treatment of thyroidectomized castrates. Injections were begun 28 days after gland extirpation and continued for 42 days. The curves serving as sham-operated controls for these are those shown in figure 3.

The combination of castration with thyroidectomy yielded results (table 3 and fig. 4 first curve) similar to thyroidectomy alone in that there was no significant difference in gland weight or in the numbers of polyploid nuclei. However in comparison with the sham-operated 49 gm rats there was a slight increase in polyploidy and this was found to be statistically significant (P = 0.02–0.01). These few new polyploid nuclei may well have been formed in the immediate post-operative period before complete thyroid deficiency was established (Leblond and Eartly '52). Treatment of the doubly operated rats with thyroxine increased the numbers of polyploid nuclei to 91.4% (table 3) and it can be concluded that the presence of testicular hormone is not necessary for the action of thyroid hormone on the orbital gland cells. However treatment of the doubly operated rats with testosterone failed to increase gland weight, or the numbers of polyploid nuclei, over the values found in saline-injected doubly operated rats (table 3 and fig. 4 third curve). Both hormones to-

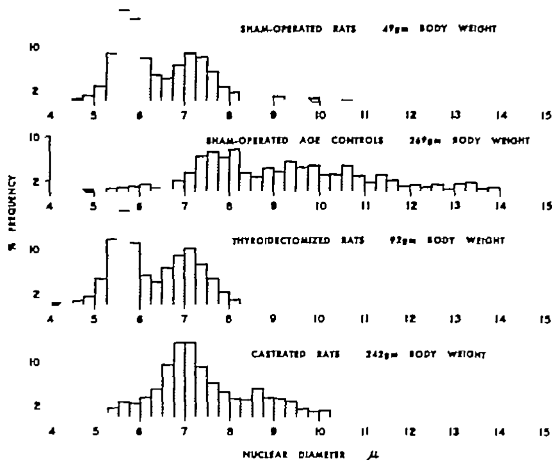


Fig. 3 Experiment 2, nuclear size distributions illustrating the influence of thyroidectomy or castration on nuclear size distributions in the external orbital gland. The 49 gm sham-operated rats illustrate conditions at the beginning of the experiment, or the time of operation and the sham-operated age controls were kept throughout the experiment, 80 days.

In the glands of thyroidectomized rats there were 45.3% polyploid nuclei, which was not significantly different from the 41.0% found in the initial controls the sham-operated 49 gm rats. Thyroid lack again prevented the accumulation of new polyploid nuclei. It should be noted that the tetraploid nuclei present at the time of gland extirpation remained intact, in contrast to the loss of tetraploid-sized nuclei seen in the liver (Carriere '62) under such conditions.

Castration at 49 gm body weight did not prevent the growth of the gland (table 3) nor the formation of new polyploid nuclei for they increased to 88.9% (table 3) However the degree of polyploidy was reduced in comparison with sham-operated rats of the same age. Total polyploid nuclei were similar in numbers (91.5% in the sham-operated age controls and 88.5% in castrates, table 3) but there were only 24.9% of nuclei above tetraploid size in the castrated rats whereas there were significantly more 53.6% in the sham operated age controls. Testis lack therefore did interfere with polyploid cell formation to some extent.

were fewer following castration, and their numbers were increased by the administration of testosterone (Walker '58 Baquiche '59) The experiments reported here showed on a quantitative basis that castration retarded but did not prevent, polyploid cell formation. New polyploid cells did arise in the absence of the testis and *so its hormone is not essential* to the process, and its stimulatory effect is not of the same magnitude as that of thyroid hormone. Furthermore a permissive action of thyroid hormone was found necessary for the response of orbital gland cells to testosterone, since polyploid nuclei did not increase in number when testosterone was injected to thyroidectomized-castrates in doses adequate to cause full growth of the seminal vesicles (table 3) On the other hand, orbital gland cells did not require an influence of testicular hormone to respond to thyroxine, for thyroxine injections promoted polyploid cell formation and orbital gland weight gains in thyroidectomized-castrates.

Our results clearly show then, that thyroid hormone is a major factor in the control of polyploid cell formation in the rat external orbital gland

B *The relationship between growth and polyploid cell formation*

The formation of larger polyploid cells appears, in general, to be associated with growth of the gland (tables 2 and 3) Experimental interventions retarding polyploid cell formation also interfered with weight gains, whereas gland weight increased following procedures (such as castration, thyroxine injection) allowing or stimulating polyploid cell formation. The relationship is further emphasized by the fact that treatment of thyroidectomized rats with growth hormone, which failed to elicit weight gains and polyploid cell formation in the external orbital glands increased both weight and polyploidy in the livers of the same animals (Carriere, '62) Parenthetically this is an interesting example of target organ specificity — external orbital gland cells did not respond to growth hormone at least not in terms of the processes considered here

The parallelism between gland weight and the relative numbers of polyploid cells is not a strict one however When values for individual rats within an experimental group were examined, the heaviest glands did not necessarily contain the highest numbers of polyploid nuclei. The relationship is apparent only upon comparing the average values for the various experimental groups. Moreover both Walker ('58) and Baquiche ('59) reported that as adult male albino rats grow older typical exorbital gland acini — with polyploid nuclei, tall pyramidal cells and canalicular lumen — are replaced to some extent by acini similar to those found in the Harderian gland with cuboidal epithelium, large vesicular lumen, and nuclei of uniformly small size (presumably diploid) Walker showed that as the rats grew from 278 to 376 gm body weight (roughly through 900 days from the age of three months) the numbers of Harderian acini increased. This change in the nature of the tissue places a limit on the generalization that polyploid nuclei increase in number with age or gland weight. In this connection, it should be noted that following treatment of thyroidectomized-castrates with testosterone in the present study there appeared to be a change in the structure of some acini toward the Harderian type. This involved increases of lumen size together with decreased cell height, giving forms intermediate between the two types. There were few if any typical Harderian acini. No attempt was made to count the numbers of acini undergoing such transformation and a subjective estimate suggests they constituted about one tenth of the tissue.

In liver (Carriere '62) there is also a parallelism between organ weight and the relative numbers of polyploid nuclei but again, this relationship is not a strict one for example, following thyroidectomy in juvenile (but not adult) rats the numbers of polyploid nuclei were gradually reduced and diploid nuclei were correspondingly increased, while liver weight remained unchanged. No such reduction was seen in the external orbital glands of these animals. Also, treatment of hypophysectomized rats with growth hormone increased liver weight and polyploidy but the numbers of polyploid nuclei increased more

PLATE 1

EXPLANATION OF FIGURES

Rat external orbital glands from experiment 2, Bouin fixation, hematoxylin and eosin staining, × 500.

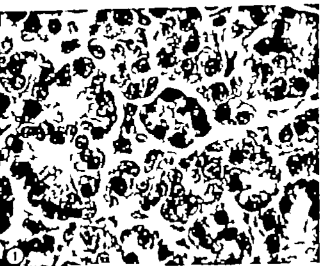
1 Gland from a 49 gm sham-operated rat. The nuclei re fairly uniform in size, for only two classes, diploid and tetraploid, are present in significant numbers.

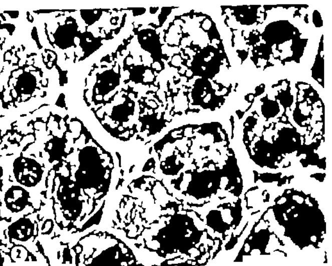
2 Gland from a 269 gm sham-operated rat. Few diploid acinar nuclei remain, and nuclei of very high degrees f ploidy have been formed.

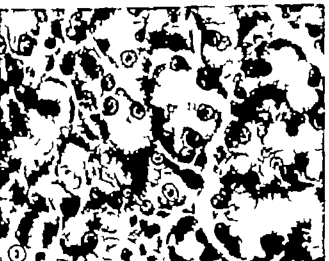
3 Gland from a rat thyroidectomized and castrated at 49 gm body weight, and kept 80 days afterwards.

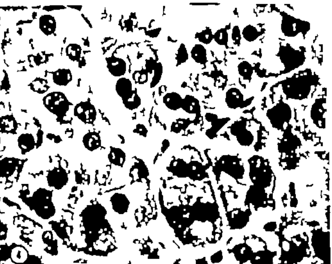
4 Gland from a rat thyroidectomized and castrated at 49 gm body weight, and treated with thyroxine for 42 days, beginning 38 days fter operation.

THYROID IN ORBITAL GLAND POLYPLOIDY
Rita Carriere











A Relationship Between Fine Structure and Function of Blood Vessels in the Central Nervous System of Rabbit Fetuses [1]

SHEILA DONAHUE

Department of Pathology Division of Neuropathology College of Physicians and Surgeons Columbia University and Neurological Institute of the Presbyterian Hospital, New York, New York

ABSTRACT The central nervous system of rabbit fetuses from the ninth to the twentieth day of gestation has been examined by phase contrast and electron microscopy Blood vessels are first seen in the neuroectodermal tissue at 11 days of gestation. They increase in number between 11 days and 20 days of gestation but there is no hange in their fine structure. The endothelial cells usually have voluminous cyto plasm which forms projections into the lumen of the vessels. These projections or flaps are a prominent feature of the fine structure of the endothelial cells during this period of growth of the central nervous system. Their function appears to be the impounding of material from the blood stream by curving over and coalescing with the plasma membrane, thus forming large vesicle Thorium dioxide injected into the blood stream, is taken up along with the constituents of the plasma and is seen in the large vesicles formed by the flaps, as well as in smaller vesicles formed directly from the luminal plasma membrane by the usual mechanism of pinocytosis. Flaps are usually located at the terminal bars. Thorium dioxide is not seen between the thickened cell membranes that form the terminal bar but is present in vesicles adjacent to the terminal bar.

Studies with the electron microscope have disclosed new details of capillary structure Bennett Luft and Hampton ('59) have suggested a morphological classification of blood capillaries in the various organs of vertebrata based on the structure of the endothelial cell on the presence or absence of a continuous basement membrane and on the presence or absence of a complete investment of peri capillary cells They suggest that these varying structural features of the capillary may be relevant to problems relating to exchange of materials between blood plasma and parenchymal cells

In the adult central nervous system the capillaries have a continuous basement membrane. The endothelial cells form a continuous lining without fenestrations or pores and the basement membrane is sur rounded by glial cells and glial cell proc esses (Dempsey and Wislocki, 55 Luse '56) In the cerebral cortex of the imma ture rat the capillary basement membrane is discontinuously present and is of variable width and density the endothelial cells have no pores or fenestrations and their cytoplasm is voluminous The basement membrane is completely surrounded but here nerve cells as well as glial cells take part in the investment (Donahue and Pappas, '61)

The present report describes blood vessels in the midbrain and spinal cord of rabbit fetuses from their first appearance at 11 days after mating, until the twentieth day after mating. This is a period of rapid growth in the central nervous system of the fetus.

MATERIALS AND METHODS

Dutch rabbits in which the period of gestation was usually 30 days were employed. The age of the fetus was calculated from the time of mating The dams were anesthetized with sodium pentobarbital, a midline abdominal incision was made and the uterus was located. Small incisions were made in the uterine wall

[1] This study was supported in part by a grant from the Association for the Aid of Crippled Children, by research grant B-1680(C4) and neuropathology training grant 2B-5062(C7) from the National Institute of Neurological Diseases and Blindness, U S Public Health Service, and by grant no. U-1075 from the Health Research Council of the city of New York.

Present address Department of Pathology Indiana University Medical Center 1 00 West Michigan Street, Indianapolis, Indiana 42807

away from the placental sites. The beating hearts could be seen with a dissecting microscope, and a small amount of Thorotrast (Testagar and Co. Inc. 24 to 26% stabilized colloidal thorium dioxide by volume 25% aqueous dextrin and 0 15% methyl parasept as a preservative) approximately 0 05 cm³ was injected directly into the heart of some of the fetuses. These were then wrapped in warm saline-soaked gauze and replaced in the abdominal cavity with the fetal circulation intact. They were removed for fixation 5 to 15 minutes later when the fetal hearts appeared to be failing. Other fetuses were removed and fixed immediately

After cutting the umbilical cord the fetuses were placed in a pool of 2% buffered osmium tetroxide (Palade, '52) They were then dissected and blocks of spinal cord and midbrain approximately 1 0 mm thick, were further fixed in cold *buffered osmium tetroxide for 30 minutes* to one hour They were then rapidly dehydrated (Ito '61) and embedded in Epon 812 (Luft, '61)

Tissues thus obtained from fetuses removed at 9 9¾ 10¾ 11 11¾ 12¾ 14 14¾ 17 17½ 18¾ 19¾ and 20 days after mating were sectioned with glass knives, on a Porter Blum microtome. Thick sections were examined with a phase contrast microscope Thin sections were stained with lead after the methods of Karnovsky ('61) and Millonig ('61) and examined in an RCA 3C or Siemens Elmiskop 1 electron microscope

OBSERVATIONS

Blood vessels are not present in the neuroectodermal tissue of fetuses younger than 11 days although they are occasionally seen before then in the surrounding connective tissue There is a rapid increase in the number of vessels per unit area, as shown in figure 1 (phase contrast microscope picture of the spinal cord of an 11¾ day fetus) and figure 2 (phase contrast picture at the same magnification of a 14 day fetus) The fine structure of the blood vessels of the nervous system does not change during the developmental period studied i.e. from day 11 to day 20 after mating. The close approximation of the plasma membranes of the neuro*ectodermal cells can be seen in figure 3* (arrows) The dense area between endothelial cells and neuroectodermal cells defined as the basement membrane is present discontinuously and varies in thickness and density (fig 3) In areas devoid of basement membrane the distance between the plasma membrane of the endothelial cell and that of the neuroectodermal cell is the same as the distance between the plasma membranes of neuroectodermal cells Pericytes cells which in the adult are fully enclosed by the basement membrane but do not participate in the formation of the luminal surface are difficult to define at this stage of development, since the basement membrane is incomplete In figure 3 (a blood vessel of a 14 day fetus) Thorotrast injected intracardially nine minutes before fixation, is seen as granules of thorium dioxide in a large vesicle (LV) in a cell process adjacent to the endothelial cell. This is probably the process of a pericyte since it is partially enclosed by basement membrane.

The cytoplasm of the capillary endothelial cell in the central nervous system of these fetuses is usually voluminous and contains numerous organelles. The perinuclear Golgi apparatus is prominent. The terminal bars are long and often tortuous. A conspicuous feature of these cells is the projection into the lumen of flaps or flanges usually located adjacent to the terminal bars. These flaps are larger and are seen more frequently than in capillaries in the adult central nervous system (Donahue and Pappas, '62) Their function appears to be the impounding of *material from the blood stream by curving* over and coalescing with the plasma membrane of the luminal surface of the endothelial cells thus forming large vesicles.

When thorium dioxide is introduced into the circulation it adheres to the cell surfaces (figs 3 4 5 6) of the endothelial cells and of the circulating blood cells. Particles are taken up by pinocytosis (Palade 53) i.e by invaginations from the endothelial cell surface forming small vesicles (fig. 4 arrow) In addition large vesicles containing thorium dioxide are formed by the flaps coalescing with the luminal cell surface as seen in figure 6.





FIG. 1 Phase contrast micrograph of the spinal cord of a rabbit fetus eleven and three-quarter days after mating. Cells of the ependymal layer (E) line the neural canal present on the left of the micrograph. One blood vessel (BV) is shown in the center and blood cell (BC) is seen in blood vessel in the mesenchyme at the upper right. × 810.

FIG. 2 Phase contrast micrograph of the spinal cord of 14 day rabbit fetus t the same magnification figure 1. Four blood vessels (BV) are shown. Cells of the ependymal layer (E) line the neural canal at the upper left of the micrograph. × 810.

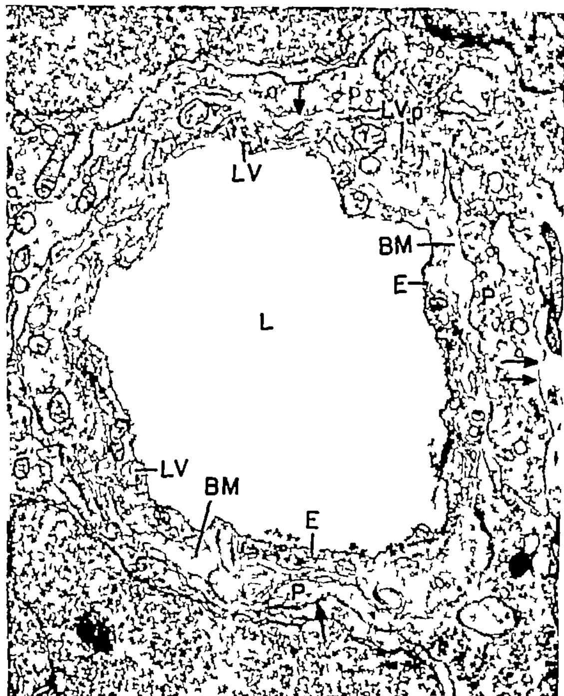


Fig. 3 A capillary in the spinal cord of rabbit fetus 14 days after mating. The close approximation of the plasma membranes of the neuroectodermal cells can be seen (arrows). Dense material forming the basement membrane (BM) is seen between the endothelial cells (E) and the processes (P) of the neuroectodermal cells. The basement membrane is discontinuously present and is of variable thickness and density. Where it is not present the distance between the cell membrane of the endothelial cell and the cell membrane of neuroectodermal cells is approximately the same as the distance between neuroectodermal cells (arrows). Thorium dioxide particles injected nine minutes before fixation, are present in the lumen (L) in many places adherent to the luminal surface of the endothelial cells. Large vesicles (LV) containing thorium dioxide particles are seen in the endothelial cell cytoplasm. One large vesicle (LV) is present in cell that is probably pericyte as it is partially enclosed by basement membrane. × 23,000.

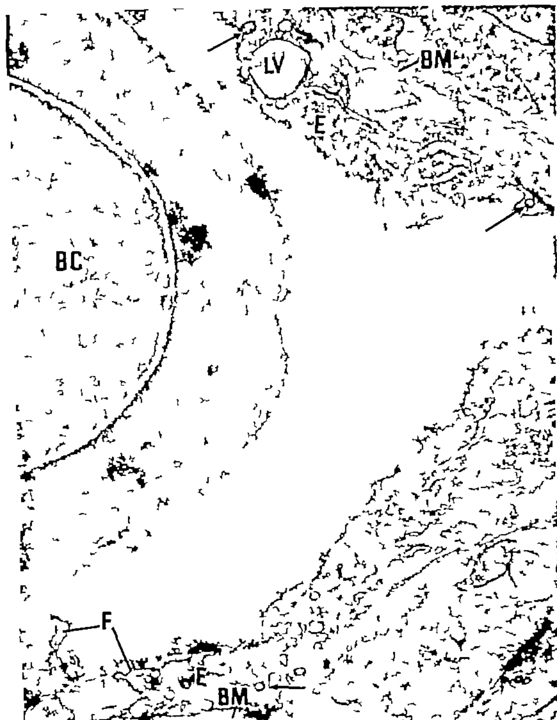


Fig. 4 Electron micrograph of part of blood vessel in the spinal cord of rabbit fetus 14 days after mating. Particles of thorium dioxide, injected intracardially nine minutes before fixation, are adhering to the blood cell (BC) and to the luminal surface of the endothelial cell (E). Small vesicles (arrows) in the endothelial cell cytoplasm contain particles of thorium dioxide. A large vesicle (LV) th t does not contain thorium dioxide is also present. I the lower left part of the micrograph, flaps (F) appear to be in the process f forming large vesicle. Basement membrane (BM) is discontinuously present. × 22,000.

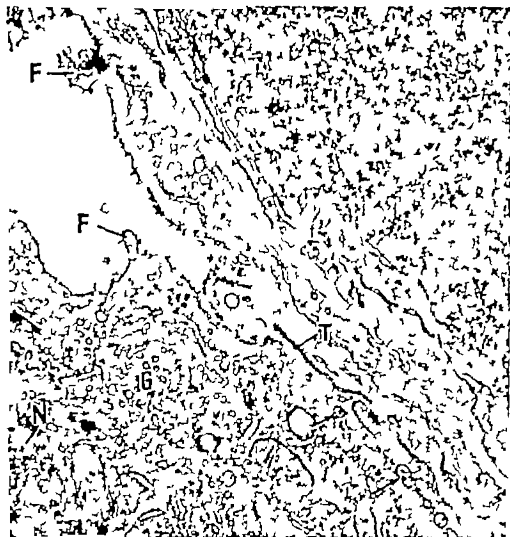


Fig. 5 An oblique section of capillary showing thorium dioxide adherent to the l minal surface of the endothelial cells. Flaps (F) or intraluminal projections to which thorium dioxide particles also adhere are present. A terminal bar is present t T The flaps associated with this terminal bar ppear t be turned in such w y that they are i close pproximation to the adjacent cell membrane and adherent particles of thorium dioxide are being impounded. Numerous vesicles containing thorium dioxide particles (rrows) extend for some distance toward the base of the cell beside the terminal ba (T) A large Golgi pparatus (G) is present near the nucleus (N) of this endothelial cell. Thorotrast wa injected int the circulation of thi 14 day fetus nine minutes before fix tion / 26,000

Flaps about to impound thorium dioxide particles are seen in figures 5 and 6 In figure 6 vesicles (V) containing such particles are shown It is probable that the flaps are always located close to the terminal bars but this relationship may be obscured by the plane of section In figure 5 particles of thorium dioxide are present in a large vesicle that is being formed by the flaps adjacent to the terminal bar (T) Many smaller vesicles containing thorium dioxide particles also are present and are seen extending towards the base of the cell in close relationship to the terminal bar

The presence of functioning flaps projecting into the lumen of blood vessels of fetuses of this period of gestation is not a

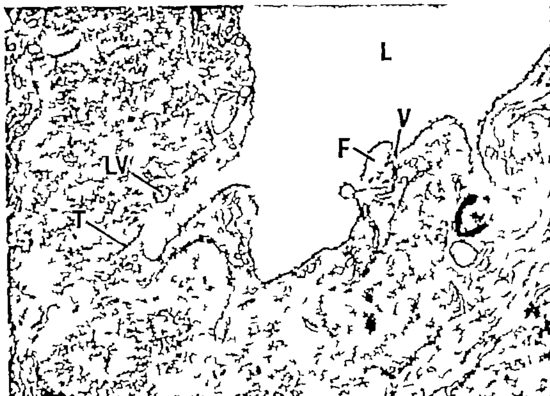


Fig. 6 Electron micrograph of part of blood vessel of rabbit fetus 14 days after mating. Thorium dioxide injected nine minutes before fixation, is present in the lumen (L) adhering to the endothelial cell membrane. Thorium dioxide particles are also seen in large vesicl (LV) adjacent to the terminal bar (T) Small vesicles containing thorium dioxide are present near this terminal bar A flap (F) projecting into the lumen appears to be about to form large vesicle by coalescing with the endothelial cell membrane. There is formed vesicle (V) containing thorium dioxide particles in the adjacent cytoplasm. × 22,000.

special condition related to the presence of thorium dioxide in the circulation Figures 7 and 8 show flaps in the blood vessels of a 14¾ day fetus that did not receive Thorotrast. The flaps are coalescing with one another and with the endothelial cell membrane forming large vesicles. Additional vesicles are present in the near by endothelial cell cytpolasm

DISCUSSION

The presence of another mechanism in addition to the usual process of pinocytosis, for the uptake of materials from the blood stream appears to be related to the state of activity of the tissue Between the eleventh and twentieth day is a period of rapid growth of the central nervous system of the rabbit fetus. We suggest that the formation of large vesicles by the flaps reflects activity of the blood vessels commensurate with this rapid growth. Flaps are also found projecting into the lumen of the capillaries of the normal adult central nervous system but they do not appear to form large vesicles by coalescing with the plasma membrane. Flaps or flanges and their function were described by Faw cett and Wittenberg ('62) in the counter current system of capillaries of the choroid rete of the fish eye where there is great activity Kisch ('60) demonstrated in longitudinal sections of capillaries in the left ventricle of the guinea pig heart that these are flaps not villous projections as they appear in transverse sections. In the capillaries of the traumatized sciatic nerve of the rat flaps impounding material and forming large vesicles are seen and the endothelial cell cytoplasm is more volumi-

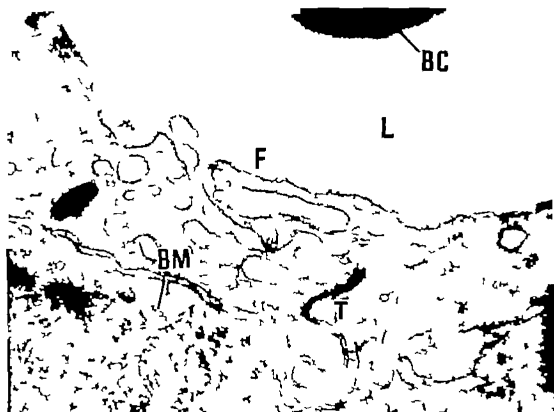


Fig. 7 Part of capillary from the spinal cord of rabbit fetus at fourteen and three-quarter ys after mating. Thorium dioxide was not injected into this fetus. However the formation of arge vesicles by the flaps (F) is shown. The relationship of the terminal bar (T) to the flaps is evident. A basement membrane (BM) is present between the endothelial cell and the neuroecto-dermal cell. A blood cell (BC) is seen in the lumen (L) of the capillary × 44,000.

ious than in the normal untraumatized nerve capillary (S Donahue and G L Kaye unpublished data) Thus in inflamed tissue where there is known to be increased capillary activity functioning flaps are observed.

The pathway of the membrane-enclosed thorium dioxide particles adjacent to the terminal bar in the endothelium of the rabbit cornea has been described by Kaye and Pappas (62) *in vivo* and by Kaye et al. *in vitro* (Kaye Pappas Donn and Mallett '62) They also described irregularities of the corneal endothelial cell plasma membrane to which numerous thorium dioxide particles adhered and there was pinching off of vesicles containing thorium dioxide from the base of the irregularities The circumstances of their experiments would allow the suggestion that the marker might have provided an additional stimulus to the activity of the flaps of the corneal endothelial cells. These experiments demonstrate the impounding of material by flaps forming large vesicles and the transport of material in smaller vesicles adjacent to the terminal bar in corneal endothelial cells.

Kaye et al ('62) also describes thorium dioxide in the space between corneal endothelial cells and point out that it is not present in the region of the intercellular space where the plasma membrane is thickened to form the terminal bar We have not observed thorium dioxide in the intercellular space between endothelial cells of blood vessels of the rabbit fetus nor have we seen thorium dioxide particles in the basement membrane. However the time interval in our experiment between injection of Thorotrast and fixation may have been too short (5 to 15 minutes) for these events to have occurred

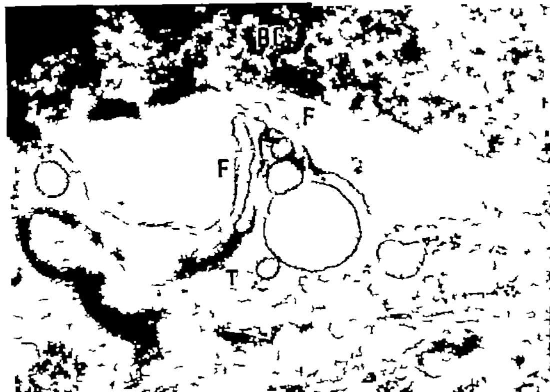


Fig. 8 A blood cell (BC) in the lumen of capillary of rabbit fetus at fourteen and three-quarter days after mating. A long tortuous terminal bar (T) is seen in the usual relationship to the intraluminal projections or flaps (F) which are curving over and coalescing to form large vesicles. N lectron opaque material or irritating substance was injected into the circulation of this fetus. × 51,000.

It should, perhaps be emphasized that we do not suggest that the method of uptake described i.e the impounding of material from the blood stream by flaps *or intraluminal projections of endothelial* cell cytoplasm replaced the usual pinocytotic mechanism. We believe that the latter is also very active in the blood vessels of the rapidly growing central nervous system of the rabbit fetus

LITERATURE CITED

Bennett, H. S., J H. Luft and J C. Hampton 1959 Morphological classifications of vertebrate blood capillaries. Am. J Physio., 196 381

Dempsey E. W and G. B Wislocki 1955 An electron microscopic study of the blood brain barrier in the rat employing silver nitrate as vital stain. J Biophysic. and Biochem. Cytol., 1 245.

Donahue, S., and G. D. P ppas 1961 The fine structure of capillaries in the cerebral cortex of the rat t various stages of development. Am. J Anat., 108 331

——— 1962 The fine structure of capillaries in the cerebral cortex of fetal and adult rats. In Proc. IVth Internat. Cong. Neuropath., Vol. II. ed. H. Jacob. G Thieme Verlag, Stutt gart, pp 77–80.

Donahue S., and G. I. Kaye 1962 Unpublished observations.

Fawcett, D W and J W ttenberg 1962 Structural specializations of endothelial cell junctions. Anat. Rec 142: 231

Ito, S 1961 The endoplasmic reticulum of gastric parietal cells. J Biophysic. and Biochem. Cytol., 11 333.

Karnovsky M. J 1961 Simple methods of staining with lead at high pH in electron microscopy J Biophysic. and Biochem. Cytol., 11 729

Kaye, G. I., and G. D Pappas 1962 Studies on the cornea. I. The fine structure of the rabbit cornea and the uptake and transport of colloidal particles by the cornea in ro. J Cell Biol., 12. 457

Kaye, G. I., G. D. Pappas, A. Donn and N Mallett 1962 Studies on the cornea II. The

uptake and transport of colloidal particles by the living rabbit cornea *in vitro*. J Cell Biol., 12: 481.
Kisch, Bruno 1960 Electron microscopy of the cardio vascular system an electron microscopic study with applications to physiology Charles C Thomas, Springfield, Illinois.
Luft, J H. 1961 Improvements in epoxy resin embedding methods. J Biophysic. and Biochem. Cytol., 9 409
Luse, S. A. 1956 Electron microscopic observations on the central nervous system. J Biophysic. and Biochem. Cytol., 2: 531
Millonig, G 1961 A modified procedure for lead staining of thin sections. J Biophysic. and Biochem. Cytol., 11 736.
Palade, G E. 1952 A study of fixation for electron microscopy J Exp. Med., 95 285.
——— 1953 Fine structure of blood capillaries. J Appl. Physics, 24 1424

Complete Dysraphism in 14 Somite Human Embryo

A CONTRIBUTION TO NORMAL AND ABNORMAL MORPHOGENESIS

A. S. DEKABAN AND G. W BARTELMEZ
Section on Child Neurology SN NINDB National Institutes of Health, Bethesda, Maryland and Department of Embryology
Carnegie Institution of Washington

ABSTRACT The youngest completely dysraphic human embryo of 2.75 mm G.L. has been reconstructed from the microscopic sections and studied in detail. Although the neural folds failed to close throughout the dorsal extent of this 14 somite embryo, the beginning of independent closure took place rostrally at the torus opticus. The last feature has been shown to be the usual event in normal embryos of this stage. Careful examination of other structures than the nervous system reveals only minor abnormalities. Thus, the dispersion of cells of somites I and II as well as loosening of other sclerotomes in this region has begun prematurely On the other hand, some retardation in the development of the pharynx, heart and nephros has been noted. Specifically the chorda, the mesenchyme, blood vessels and gut have been found to be normal.

The literature pertaining to the closure of the neural folds has been discussed. Also, the reports on experimental inhibition of the formation of the neural tube are discussed with special emphasis on the work of Davis (42) The available evidence refutes the contention that the closure of neural folds is induced by adjacent structures of whatever derivation. It ppears plausible as Davis demonstrated in his experiments that certain biochemical reactions within the neural epithelium may be involved in the process of normal closure of the neural folds.

Morphological findings in the present embryo do not support most of the previously advanced theories relating to the pathogenesis of dysraphic states.

Studies of congenital malformation in young human embryos are essential for the understanding of definitive teratological anomalies present in a proportion of newborn infants and in later life Such studies may also provide important clues for elucidation of normal morphogenesis during embryonic stages. Thus there exists a clear need for accumulation of well documented material concerning aberrations of development. So far only a few early human embryos with total dysraphism have been reported in the literature The specimen which constitutes the subject of this study is no. 779 of the Collection of the Carnegie Department of Embryology It is the youngest known totally dysraphic embryo (14 somites) It was utilized in part by Dekaban ('63 in press) in the study of anencephaly however there still remained a number of problems in this unique embryo which require further elucidation. Firstly it is desirable to study the state of development of ectodermal, entodermal and mesodermal structures and their relative position and relationship to the abnormality in closure of the neural folds this called for more detailed reconstruction of the total embryo Secondly there is a need for comprehensive evaluation of the available evidence on the closure of the neural folds. Thirdly the literature on experimental prevention of closing of the neural folds requires critical review With these and other objectives in mind we decided to reinvestigate in greater detail the morphology of this malformed human embryo

No 779 completely dysraphic embryo of 14 somites

This was the second pregnancy of a 37 year old white married woman whose first gestation resulted in a normal child. The initial course of the pregnancy was uncomplicated. The last menstrual period

Davis, J. O 1942 Photochemical spectral analysis of neural tube formation University of Missouri, Doctor's thesis.

ended on September 3rd and a spontaneous abortion occurred on October 12th.

Gross description. The entire specimen, consisting of decidua, clot and ovum, was available for examination. The ovum measured 16 × 14 × 12 mm and was entirely covered by villi from 5 to 9 mm long, most of them branching twice and many showing bulbous enlargements (early hydropic degeneration). The chorion was lined by a smooth membrane and filled with a clear fluid. The amnion was intact. The specimen was received, examined and most carefully processed at the Carnegie Laboratory of Embryology by H. M. Evans.

The embryo measured 2.75 mm G. L. Its caudal end was bent sharply to the left. Fourteen mesodermic somites were counted on the dorsolateral surface. The nervous system was grossly abnormal for this stage of development. The neural folds were open from forebrain to primitive streak. They were however conspicuously enlarged in the cephalic region as is the case in normal embryos of this stage. The cephalic flexure occurred, as in normal ...yos, at the midbrain level where the ... are narrower than at forebrain levels. ... prominence of the heart region was well marked. Caudal to the anterior intestinal portal the embryo was spread out on the yolk sac. The region of the forebrain overhung the yolk sac and the inferior end was bent slightly toward the yolk sac.

The embryo was embedded in paraffin. It was cut serially at 15 μ transverse to the rostral end and stained with hematoxylin and orange G. A complete set of photomicrographs was prepared by O. Heard at a magnification of 133 diameters. They were projected on bromide paper and on the basis of a preliminary wax model the photographs were oriented by the use of perpendicular guidelines according to the method developed by Lewis (15). Using these bromide prints Mr. Heard constructed a model of the embryo (fig. 1). Both the bromide prints and the model proved helpful in interpreting the microscopic sections and the prints were also used for the preparation of our reconstruction (fig. 2).

Description of the model. It is evident from the photograph of the model (fig. 1A) that the neural folds failed to fuse throughout most of the neuraxis. The cephalic flexure is about 90° and the cerebral end appears slightly smaller than that of the comparable 14 somite specimen of Heuser ('30). To what extent this is due to the more extensive post mortem changes is impossible to say. A significant finding is an incipient closure of the cephalic folds that extends dorsally from the torus opticus. This aspect will be discussed later in more detail. The optic and otic vesicles had formed in the usual locations. Similarly cranial neural crests are present. The caudal 35% of the neuraxis had been rotated to the left, possibly post mortem, and as a result of this the plane of section was oblique to the long axis of the embryo caudally (figs. 1A and 10).

Description of the reconstruction. A careful midsagittal projection reconstruction of the cephalic 65% of the specimen was prepared whereas the caudal 35% were reconstructed in the horizontal plane. The transition of these two planes is indicated by a line marked by an asterisk in the projection reconstruction (fig. 2). Complete reconstruction of chorda, gut, heart, as well as part of the ectoderm, permitted study of the relationship between these structures and the neural folds. Because of the considerable amount of morphological detail the description of various systems will be dealt with separately.

Nervous system. The outstanding feature of this embryo is the neural groove which is wide open in the region where the neural tube is normally closed at this stage of development. In the region of the midbrain and the adjoining hindbrain the neural folds resemble those of 3 to 4 somite embryos; caudally they gradually flatten out into a plate depressed in the midline as in presomite stages (figs. 6 to 9). It is significant for the understanding of anencephalic monsters with normal eyes that in this embryo closure of the folds had begun from the medial cephalic end of the neuraxis; an incipient neural tube had formed over the rostral one-third of the optic vesicles (fig. 1, B and C; figs. 2 and 3). The optic vesicles are relatively

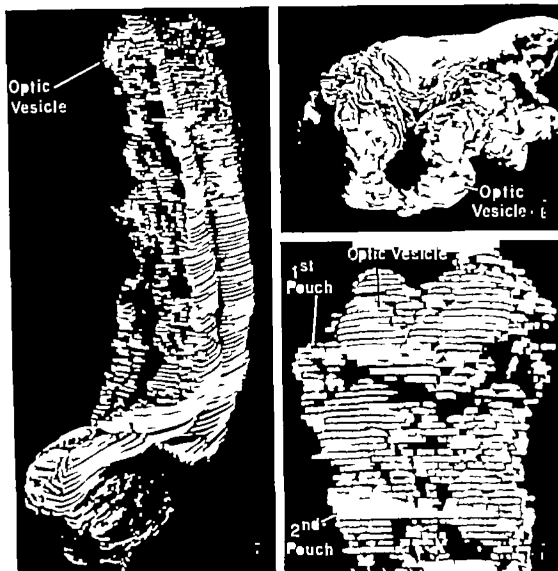


Fig. 1A, B and C Photographs of the original plaster model dissected to show the nervous system and the gut. Figure 1A presents the entire model viewed from the left. Note the nervous system with its trough like neural groove. The caudal end of the embryo is bent to the left. Figure 1B is head-on view of the rostral end of the model. Below are the optic vesicles where the neural tube has closed (see p. 28) The caudal forebrain and midbrain are wide open. Figure 1C shows the optic vesicles with the median seam of closure. Below is the ventral surface of the pharynx showing the first and second visceral pouches. They stand out clearly on the observer left.

smaller than in the 14-somite Heuser embryo and since they comprise the bulk of the forebrain as is normally the case it would seem that the forebrain was smaller than would be expected at this stage Two expansions of the neural folds in the region of the cranial flexure mark the midbrain as in the 13- and 16-somite embryos of figures 16 and 17 in Bartelmez and Evans ('26) In 779 the adjoining segment is indicated by a depressed basal plate and by the attachment of the trigeminal neural crest (fig. 2) As later stages show this segment gives rise to

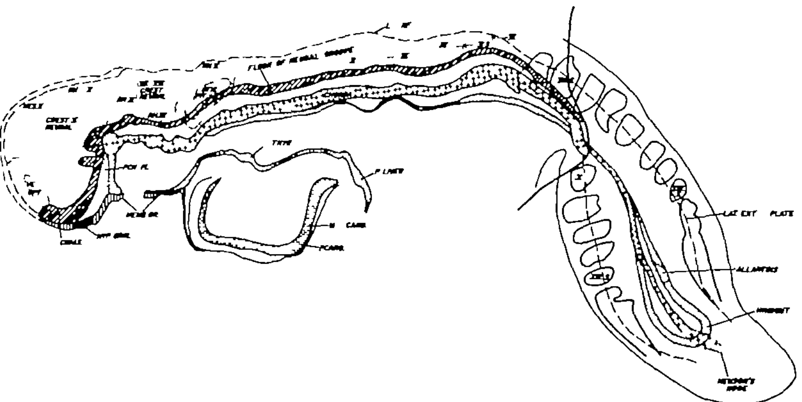


Fig. 2 Midsagittal projection reconstruction of the superior 65% of the dysraphic embryo. The inferior 35% is reconstructed in the horizontal plane that is parallel to the dorsal surf ce. line marks junction of the reconstructions.

Abbreviations

P CHIAS., Primordium chiasmatis
VES. OPT Vesicula optica
MES. II. Mesencephalon II.
HYP ORAL., Hypophysis oralis
MEMBR. OR., Membran oralis
RH., Rhombomeres
PCH. PL., Prechordal plate
IS., IIS., Somites I, II
LAT EXT N PLATE, Lateral extent of the neural plate indicating depth of groove
P THYR., Primordium of the thyroid
P LIVER, Primordium of the liver
M E. CARD Myo-epicardium
P CARD Pericardi m

rhombomeres I and II (Bartelmez and Dekaban, '62) A slight elevation of the neural folds indicates rhombomere III which is normally differentiating at this period. As in all embryos of the somite period, rhombomere IV is distinctive in form the VII–VIII neural crest to which it had given rise lies on its lateral surface. At this level the neural groove has narrowed, and the characteristic thickenings of the neural folds and depression of the floor are present (figs. 2 and 4 pl. 2) A normal otic pit is lateral to rhombomeres IV and V Rhombomere V is indicated by an elevation of the neural folds and by the proliferation of neural crest from their lateral edges which are typically loose in structure This crest extends toward the feebly developed second branchial pouch and represents that which later contributes to the glossopharyngeal ganglia.

Caudal to this level there are groups of neural crest cells attached here and there to the neural plate. This occipital and upper cervical crest agrees in extent with that figured by Heuser ('30 fig. 4) In 779 the neural crest cells are somewhat more abundant at the level of somites II and V

As the neural plate is followed caudally it becomes flatter (figs. 2 and 9) although the median groove extends caudally almost to Hensen's node. In figure 2 the lateral edge of the neural plate is indicated by a broken line In this embryo the space between the chorda and the floor of the nervous system is empty and is materially greater than in Heuser's specimen. In earlier well preserved embryos it is absent. In later stages fixed *in vivo* it is occupied by a loose mesenchyme with few cells. It would seem then that the space in the intermediate stages is due to the *post mortem* shrinkage of the adjacent mesenchyme which presumably has a higher water content than the rest. Since in 779 the thickness of the neural epithelium is fairly uniform where there is underlying mesenchyme and where as at the rostral end the nervous system is in contact with ectoderm, it would appear that the space is due primarily to a differential shrinkage of mesenchyme and not of the neural epithelium.

The space between the primordium of the oral hypophysis and the forebrain is also an artifact. In the Heuser embryo there is a loose fold of the surface ectoderm in this region. The hypophyseal primordium is a thickening of the surface epithelium marked off by lateral sulci and distinguished by cells larger than those of the adjoining ectoderm and by cytoplasm that has remained unstained.

Synopsis Complete dysraphism involving the entire neuraxis except at the rostral extremity where normal closure had occurred. Slight hypoplasia of the cephalic neural folds is present.

Chorda. The chorda is normal in form and structure. Where the axis of the embryo is twisted to the left the chorda is somewhat distorted (fig. 2) At the level of somite X in figure 2 the reconstruction on the midsagittal plane joins that on the horizontal plane. In the former the dorsoventral diameter of the chorda is plotted. Its transverse diameter is plotted in the horizontal projection. The failure of the cytoplasm of the chordal cells to stain serves to differentiate them they tend to be radially arranged. In the rostral one-third of the pharynx the chorda is still incorporated in the pharyngeal wall so that in the midline it forms the roof of the pharynx (figs. 2 and 4) The typical stages in its separation from the pharyngeal wall are present in the rostral levels of the first pouch (fig. 5) As far as the anterior intestinal portal, chorda and entoderm remain in contact; caudal to this they are more or less separated. In the region of the hindgut they are again in intimate contact, beyond this the chorda merges into the diffuse mass of cells which constitutes Hensen's node. It would appear that the development of the chorda was in most respects normal for this stage of development.

Somites. Caudal to the level of the second pharyngeal pouch there are irregular groups of mesodermal cells which we interpret as the dissociating first somite. They are separated from a somewhat more compact group by a dorsal aortic ramus. At the caudal end of this group there is a mass of radially arranged cells resembling a myotome. This entire group is the dissociating second somite. There is an aortic

ramus between it and the well differentiated somite III. Here dermatome myotome and sclerotome with a myocoel are present. The sclerotome had spread out caudally and is abnormally loose in structure as in somite II (fig. 8) Somite IV is similar in structure but lacks a myocoel. At this level the shift in the embryonic axis begins (fig. 9) Somite V is distorted on the embryo's left and has the peculiar large loose sclerotome; somites VI to XIV are normal in structure. As in the 14-somite embryo of Heuser somites XV and XVI are differentiating but are not yet separated from the segmental plate

Synopsis In general the cell population of the individual somites may be decreased The dispersion of the cells of somites I and II had begun prematurely as had the loosening of the sclerotomes of somites III to V The abnormal conditions in the prospective occipital and upper cervical levels are significant in view of certain anomalies especially the typical lordosis of these regions in intencephalus and anencephalus

Intermediate cell mass and nephric primordia. Between somites I to IV and the coelomic mesothelium the mesenchyma is very loose From the level of somite III to somite IX there are groups of 4 to 6 small cells closely applied to the surface ectoderm in this region. Occasionally they are radially arranged. The groups cannot be recognized in every section so they indicate a Wolffian duct regressing in the upper levels. In the VII–VIII intersomitic space there is a small vesicle in contact with the mesothelium At the level of the next two somites a larger nephric vesicle opens into the coelom (fig 9) The surface elevation corresponding to it resembles the nephric ridge first recognized in man by Wen ('28) The nephric primordia are retarded compared to this system in Heuser's specimen.

Synopsis Some retardation in the development of the nephros The entire *mesenchyme* appears normal except for post mortem shrinkage This is significant as it confirms the conclusion of Boerema ('29) and Davis ('42) that mesenchyme is not involved in the failure of the neural folds to close.

Vascular system. The pericardial cavity is almost filled by the myoepicardial mantle (figs. 2, 6 and 7)

The heart is simple in form similar to that of embryos of horizon X as described by deVries and Saunders ('62) The median axis of the myoepicardium is straight caudally where the broad mesocardium narrows it divides into right and left atria. The endocardium divides to form the first pair of aortic arches which loop around the first pharyngeal pouch. On the right, the arch and dorsal aorta are greatly dilated. On this side the second arch is forming

A series of intersegmental rami arise from each dorsal aorta between the levels of somites I–II as far as somites XI–XII. There are lateral aortic rami in the region of somites VII to IX here the nephric primordia were developing. In the region of somites VII to X intestinal rami reach the wall of the gut that has not yet separated from the yolk sac.

The primary cephalic vein extends forward to the region of the optic vesicle, giving off rami to the regions of the trigeminal and the acustico-facial neural crest Like the dorsal aortae the cephalic vein has alternately dilated and constricted regions. A series of interrupted vascular primordia corresponding in position to the cephalic vein can be recognized as far caudally as somite X.

Synopsis No gross abnormality of the vascular system is present. Compared with with the 14 somite embryo of Heuser the heart is somewhat retarded in development.

Gut At the rostral end of the pharynx *the cells are loosely arranged* this can be identified as the prechordal plate (fig. 2) There is an opening in the oral membrane such as does not appear normally until horizon XII The normal appearance of the cells at the rounded margins of the opening suggest that this condition is premature rather than the result of *post mortem* maceration. On the other hand the differentiation of the pharyngeal pouches is retarded. On the embryo's right there is a small area of contact of the first pouch with the surface ectoderm the minute branchial membrane is depressed. On the left the components of this mem-

brane seem to have been separated by shrinkage. The lateral invaginations into this pouch (fig. 5) agree with those which appear in all early human embryos. Grosser ('10) who first described them suggested that they might represent vestiges of internal gills. There is no evidence to support this. The position of the thyroid primordium caudal to the first pouch is normal for this stage (fig. 2) The second pouch is only indicated whereas in the 13-somite embryo of Wallin ('13) and the 14-somite Heuser embryo it had established contact with the ectoderm; in the latter a third pouch had appeared. In 779 as in the Heuser embryo the primordium of the liver is present. The gut is open from the level of somites II to VII. The relations of the hindgut to chorda and allantois are typical and there is an anal plate The allantoic duct is small and extends for 0 12 mm into the belly stalk. The intraembryonic coelom extends from the heart to the beginning of the segmental plate and is lined by typical tall mesothelium. Between the levels of somites II and X it communicates with the extraembryonic coelom.

Synopsis The pharynx is retarded but there is no malformation of the gut.

DISCUSSION

The investigation of morphology and structural relationship of definitive human monsters must, of necessity be based on (A) a detailed knowledge of normal development (B) evidence derived from experimental studies and (C) detailed studies of early stages of malformed human embryos. This last aspect is particularly important for the evaluation of dysraphic states which are by far the most frequent malformations of the nervous system.

A. Since the underlying abnormality in dysraphism is nonclosure of neural folds it is necessary to consider the formation of late stages of the neural plate and the morphological changes associated with rising of neural folds and their closure into neural tube One of the earliest differentiations in vertebrate embryos is thickening of the ectoderm which will give rise to the neural elements of the entire central and peripheral nervous systems. At this stage the neural ectoderm consists of a simple epithelium of columnar cells. These cells differ in shape because the relatively large nuclei lie at different levels. It is obvious from the inspection of a series of models and reconstructions (see Bartelmez and Dekaban, '62) that the general region of the brain is the first to appear This has also been demonstrated experimentally in various species of animals In the well known embryo "Gle of Spee the neural folds have begun to arise. It is significant that they occupy the entire dorsal surface of the rostral extremity of the embryo. The presence of taller epithelium in the rostral region of the neur axis is shown in the drawings of embryo "Gle (H. M. Evans in Keibel and Mall Vol. 2 '10 figs. 404 and 405) By the time two mesodermic somites have appeared in human embryos it is possible to identify forebrain midbrain and three hindbrain segments in the wide open neural folds (Ingall's embryo Bartelmez, '23 fig. 1) Only three human embryos are known which are sufficiently well preserved to give reliable evidences as to the level at which the neural folds begin to close. These embryos are (1) the 6-somite Huber embryo the folds of which are closed at the level of the second and third somites (Arey '38) (2) the 7 somite Schochet embryo (Heuser and Corner '57) which shows closure of the neural tube at the level of somites 3 to 5 and (3) the 7-somite embryo described by Payne ('25) which shows closure from somites 3 to 7 Arey ('38) and subsequently Sensenig ('57) demonstrated that no somites are differentiated rostral to the one which appeared first. In addition, Sensenig confirmed the finding that the first four somites contribute to the formation of the occipital region. From these data it would appear that closure of folds begins in the transitional region between future medulla oblongata and spinal cord. Closure progresses rapidly in both directions so that in the eight-somite embryo described by Bartelmez and Evans ('26 fig 12) it extends from the level of the caudal end of somite 7 to the otic plate. In the ten-somite embryo of Corner ('29) the closure had progressed slightly beyond the last somite but rostrally it had reached only to the level of the otic plate. This specimen

ramus between it and the well differentiated somite III. Here dermatome myotome and sclerotome with a myocoel are present. The sclerotome had spread out caudally and is abnormally loose in structure as in somite II (fig. 8). Somite IV is similar in structure but lacks a myocoel. At this level the shift in the embryonic axis begins (fig. 9). Somite V is distorted on the embryo's left and has the peculiar large loose sclerotome; somites VI to XIV are normal in structure. As in the 14-somite embryo of Heuser, somites XV and XVI are differentiating but are not yet separated from the segmental plate.

Synopsis. In general the cell population of the individual somites may be decreased. The dispersion of the cells of somites I and II had begun prematurely as had the loosening of the sclerotomes of somites III to V. The abnormal conditions in the prospective occipital and upper cervical levels are significant in view of certain anomalies, especially the typical lordosis of these regions in iniencephalus and anencephalus.

Intermediate cell mass and nephric primordia. Between somites I to IV and the coelomic mesothelium the mesenchyma is very loose. From the level of somite III to somite IX there are groups of 4 to 6 small cells closely applied to the surface ectoderm in this region. Occasionally they are radially arranged. The groups cannot be recognized in every section so they indicate a Wolffian duct regressing in the upper levels. In the VII–VIII intersomitic space there is a small vesicle in contact with the mesothelium. At the level of the next two somites a larger nephric vesicle opens into the coelom (fig. 9). The surface elevation corresponding to it resembles the "nephric ridge" first recognized in man by Wen ('28). The nephric primordia are retarded compared to this system in Heuser's specimen.

Synopsis. Some retardation in the development of the nephros. The entire mesenchyme appears normal except for post mortem shrinkage. This is significant as it confirms the conclusion of Boerema ('29) and Davis ('42) that mesenchyme is not involved in the failure of the neural folds to close.

Vascular system. The pericardial cavity is almost filled by the myoepicardial mantle (figs. 2, 6 and 7).

The heart is simple in form, similar to that of embryos of horizon X as described by deVries and Saunders ('62). The median axis of the myoepicardium is straight; caudally where the broad mesocardium narrows it divides into right and left atria. The endocardium divides to form the first pair of aortic arches which loop around the first pharyngeal pouch. On the right, the arch and dorsal aorta are greatly dilated. On this side the second arch is forming.

A series of intersegmental rami arise from each dorsal aorta between the levels of somites I–II as far as somites XI–XII. There are lateral aortic rami in the region of somites VII to IX, here the nephric primordia were developing. In the region of somites VII to X intestinal rami reach the wall of the gut that has not yet separated from the yolk sac.

The primary cephalic vein extends forward to the region of the optic vesicle, giving off rami to the regions of the trigeminal and the acustico-facial neural crest. Like the dorsal aortae the cephalic vein has alternately dilated and constricted regions. A series of interrupted vascular primordia corresponding in position to the cephalic vein can be recognized as far caudally as somite X.

Synopsis. No gross abnormality of the vascular system is present. Compared with with the 14 somite embryo of Heuser the heart is somewhat retarded in development.

Gut. At the rostral end of the pharynx the cells are loosely arranged; this can be identified as the prechordal plate (fig. 2). There is an opening in the oral membrane such as does not appear normally until horizon XII. The normal appearance of the cells at the rounded margins of the opening suggest that this condition is premature rather than the result of post mortem maceration. On the other hand the differentiation of the pharyngeal pouches is retarded. On the embryo's right there is a small area of contact of the first pouch with the surface ectoderm; the minute branchial membrane is depressed. On the left the components of this mem-

The following data are condensed from his table 2. After irradiating 17 embryos ranging from late presomite to six-somite stages for 12.5 seconds, he incubated them for 30 hours. In three of these the entire central nervous system was an open plate, in nine it was open for from one-fourth to three-fourths of its length and in five it was closed as far as in the control embryos.

Irradiation for 15 seconds and incubation for 30 hours resulted in 15 of the 17 embryos with open neural folds for one-fifth to three-fourths of the length of the nervous system the folds had closed normally in only two

When a group like the first was incubated for 54 hours the nervous system was open for one-fourth to one-third of its length in only five, whereas in 12 it had closed. This demonstrated that the irradiation for 12.5 seconds had not seriously injured the majority of the embryos and the inhibition was reversible.

Incubation for 54 hours after 15 seconds irradiation resulted in one monster with completely open neural plate, 12 with the neural folds open for one-sixth to one-half their length; in the remaining twelve the tube had closed. Such experiments provide evidence of individual variability in susceptibility

The chorda in normal early chicks is closely applied to the neural epithelium; these two structures are separated in embryos in which folding has been inhibited by irradiation (fig. 1 Davis, 42) The chorda is apt to be abnormally small although the cells appear normal. In addition, the mesenchyme underlying the nervous system is usually oedematous with pyknotic cells. By explanting normal neural plates freed of chorda and mesenchyme Davis showed that folding and tube closure proceeded normally This had also been demonstrated for Amblystoma by Boerema ('29) On the other hand, irradiated neural plates removed and explanted, failed to close over much of their extent.

These experiments showed that a substance or substances involved in folding were inactivated by irradiation. In 44 Davis presented striking evidence that a compound, probably related to vitamin D *within* the plate is responsible for the folding that forms the neural tube. His experiments have no bearing on the problem of the nature of the substance responsible for the original induction of the neural plate. In this connection he points out that experiments in which foreign substances are introduced into living embryos to induce a neural plate in indifferent ectoderm, are necessarily inconclusive since it is not possible to determine the part played by changes induced in the surrounding tissues by the experimental procedures.

Most of the experimental work on the influence of deleterious factors on early embryonic development has been done on the eggs of lower vertebrates since their environment can be readily modified and the changes produced can be readily followed *in vivo* In many adequate control experiments have not been made.

There appears to be no more extensive and careful study than that of Bellamy ('19) as to the periods in development at which growth and differentiation are inhibited by noxious factors of the environment. With an abundant supply of frogs eggs normally fertilized in an aquarium kept between 5 and 9 C he could run a series of experiments on the spawn of each pair of clasping frogs. The eggs were left within their protective envelopes of jelly Low temperature in the dark and nine chemical agents were used in a series of experiments run side by side with controls. The effects of the various agents were fundamentally similar

It is significant that all interferences with development which were begun shortly after fertilization ended in death prior to hatching, but in many such experiments a series of strikingly abnormal blastulae and gastrulae were produced; all of them showed that growth and/or differentiation had been inhibited. In one experiment two-celled eggs were exposed for 24 hours to KCN M/1000 and then transferred to KCN M/5000 During the ensuing day they developed into obviously retarded blastulae (see Bellamy's figs 7 10 and 11) At this time areas of plasmolysis of pigment appeared in the regions

is unique however in that the surface ectoderm overlies the lateral extremity of the neural folds as far forward as the midbrain. A similar condition appeared in the 17-somite embryo of Wen ('28) in which the surface ectoderm had already closed over the minute anterior neuropore In several other 17–19-somite embryos that have been described the neuropore is still open and although it varies in extent, it is at the level of the optic vesicle in every instance (Streeter 42) The closure is complete in the 20-somite C L. Davis embryo ('23) here the site of the final closure is marked by a small area where no boundary between superficial and neural ectoderm can be recognized This site is still clearly seen in the 22–23 somite and 25 somite embryos of Bartelmez and Blount ('54) as well as in the 25 and 28 somite embryos of Sternberg ('29) It is obvious then, that there is considerable variability in the closure of the anterior neuropore. This is due partly to a process which has been generally overlooked, namely the union of the neural folds which proceeds from the original rostral end of neural plate toward the closure that is advancing at the same time rostrally from the midbrain. This independent rostral closure was first noted by Johnston ('09) in lower vertebrates. The evidence for this in man is as follows all embryos of Streeter's horizon X have a terminal notch. This owes its origin to the bending of the nervous system around the end of the pharynx so that laterally the neural folds extend beyond the rostral end of the neuraxis in the midline (Bartelmez and Evans, '26 figs. 9–14 18 and 19; Heuser and Corner '57 fig. 1) In the 13-somite embryo of Wallin ('13 fig 2) and 12-somite embryo "Legge, the notch is disappearing in the 14-somite embryo of Heuser ('30 fig. 10) it is gone The two lateral primordia of the optic vesicles meet at the rostral end of the nervous system this can be seen in the eight-somite embryo of Bartelmez and Evans ('26 figs. 12 and 19) and the ten-somite Corner embryo ('29 figs. 1 and 11) Mall ('17) recognized that this marks the site of the optic chiasma and adopted the term "torus opticus which was first used by Froriep in '06 As the forebrain elongates it grows around the end of the pharynx so that in sections it appears to be ventral to the midbrain. The torus opticus however remains terminal in position. In the 14-somite Heuser embryo ('30 figs. 4 and 10) the torus appears elongated. As the subsequent stages show this apparent elongation is due to the fusion of the lateral moieties of the terminal notch (see Bartelmez and Dekaban, '62, figs. 64 67 68) The fused region is accordingly dorsal to the *primordium chiasmatis Obviously the closure of the folds is now proceeding from* the torus toward the closure that is extending forward from the midbrain. As might be expected, the location of the point of the meeting of the two seams of closure varies. Consequently neither the anterior neuropore nor its site of closure can be used as a landmark to indicate the original rostral end of the nervous system The primordium of the chiasma remains the original terminal end. The seam of closure of the lateral folds gives rise to the lamina terminalis and in part to the tela chorioidea ventriculi III. The closure of the posterior neuropore occurs in the more advanced embryos of Streeter's horizon XII which have 27 to 29 somites and are about 4 mm long. They belong to the end of the fourth week of gestation.

B Many experimental procedures have been used to interfere with the development of various vertebrate embryos. A variety of abnormalities including dysraphism ranging from spina bifida to anencephalus amyelus associated with other defects have been produced, (Stockard, '10 Stockard and Craig, '12) Thus far however *we have been able to find only one study* in which the formation of the neural tube was *specifically* inhibited. This was reported by J O Davis ('42 and 44) He also produced significant evidence as to the substance or substances which may be involved in the process of normal closure of the neural folds. Since most of his material is contained in his unpublished thesis we will discuss his findings at greater length. Using monochromatic ultraviolet light ranging from 2,483 A to 2 894 A, Davis irradiated chick embryos in early neural fold stages through an opening in the shell; subsequently he sealed the eggs and returned them to the incubator

Bartelmez, G. W with collaboration of M. P Blount 1954 The formation of neural crest from the primary optic vesicle in man. Carnegie Inst. of Wash. Publ. 603, Contribs. Embryol., 35 55–71

Bartelmez, G. W and H. M. Evans 1926 Development of the human embryo during the period of somite formation, including embryos with 2 to 16 pairs of somites. Carnegie Inst. of Wash. Publ. 362, Contribs. Embryol., 17 1–67

Bartelmez, G W and A. S. Dekaban 1962 The early development of the human brain. Carnegie Inst. of Wash. Publ. 621, Contribs. Embryol., 37 13–32.

Bautzmann, H. 1928 Experimentelle Untersuchungen über die Induktions-fähigkeit von Chorda und Mesoderm bei Triton. Arch. f. Entw-mechn., 114 177–225.

Bellamy A. W 1919 Differential susceptibility as basis for modification and control of early development in the frog. Biol., Bull., Woods Hole Mass 37 312–361

Boerema, I. 1929 Die Dynamik des Medullarrohrschlusses. Arch. f. Entw-mechn., 115 601–615.

Bonnevie, K. 1935 Vererbbare Missbildungen und Bewegungsstörungen uf embryonale Gehirnanomalien zurückführbar Erbarzt, Sonderarbeit. Z. Deutsch. Aerzterbl., 42: 145–150.

Bremer J L. 1906 Description of 4 mm human embryo. Am. J Anat., 5 459–480

Corner G. W 1929 A well-preserved human embryo of ten somites. Carnegie Inst. of Wash. Publ. 394, Contribs. Embryol., 20 81–101

Davis, C. L. 1923 Description of human embryo having 20 paired somites. Carnegie Inst. of Wash. Publ. 332, Contribs. Embryol., 15 1–51

Davis, J O. 1942 Photochemical spectral analysis of neural tube formation. University of Missouri, Doctor Thesis.

——— 1944 Photochemical spectral analysis of neural tube formation. Biological Bulletin, 87 73–95

Dekaban, A. S. 1963 Anencephaly in early human embryos. J Neuropath. and Exp. Neurol., 22: 533–548.

Dodds, G S., and E. DeAngelis 1937 Anencephalic human embryo 16 5 mm long. Anat. Rec., 67 499–505.

Evans, H. M. 1910 III. The development of the vascular system. Keibel and Mall Manual of Human Embryology Vol. 2, Chapter 18, pgs. 570–709

Frazer J E. 1921 Report of an anencephalic embryo. J Anat., 56 12–19

Froriep, A. 1906 Die Entwicklung des Auges der Wirbeltiere. Handbuch der Vergleichenden und Experimentellen Entwicklungslehre der Wirbeltiere. Vol. II, Teil II. pp 139–266 Ed. O. Hertwig Publ. Fischer Jena.

Grosser O 1910 The development of the pharynx and of the organs of respiration. Keibel and Mall Manual of Human Embryology Vol. 2, Chapter 17 pgs. 446–497

Groth, K. E. 1928 Ein Fall von Anencephalie mit Rachischisis bei einem 14 mm langen menschlichen Embryo, rekonstruktiv untersucht. Z. mikrosk-anat. Forsch., 14. 483–510.

Heuser, C. H. 1930 A human embryo with 14 pairs of somites. Carnegie Inst. of Wash. Publ. 131 Contribs. Embryol., 22: 135–153.

Heuser C. H., and G. W Corner 1957 Developmental horizons in human embryos; description of age group x, 4 to 12 somites. Carnegie Inst. of Wash. Publ. 611 Contribs. Embryol., 36 29–39.

Johnston, J B 1909 The morphology of the forebrain vesicle in vertebrates. J Comp. Neur 19 457–539.

Lewis, W H. 1915 The use of guide planes and plaster of Paris for reconstructions from serial sections; some points on reconstruction. Anat. Rec., 9 719–729.

Mall, F P 1917 Cyclopia in the human embryo. Carnegie Inst. of Wash. Publ. 226. Contribs. Embryol., 6 5–33.

Mann, I. C. 1937 Developmental abnormalities of the eye. Cambridge Univ Press London.

Mangold, O 1929 Das Determinations Problem. Das Nervensystem und die Sinnesorgane der Seitenlinie unter spezieller Berücksichtigung der Amphibien. Ergebn. d. Biol., 3 152–227

Padget, D. H. 1948 The development of the cranial arteries in the human embryo. Carnegie Inst. of Wash. Publ. 575 Contribs. Embryol., 32: 205–261.

Patten, B M. 1952 Overgrowth of the neural tube in young human embryos. Anat. Rec., 113 381–393.

——— 1953 Embryological stages in establishing of myeloschisis with spina bifida. Am. J An t., 93 365–395.

Payne F 1925 General description of a 7 somite human embryo. Carnegie Inst. of Wash. Publ. 361, Contribs. Embryol., 16 115–124

Politzer G. 1952 Über frühembryonale Encephalomyeloschisis beim Menschen. Wien. Ztschr Nervenh., 5 1 22.

——— 1954 Über Spaltbildungen des Gehirns und Rückenmarks menschlicher Embryonen und ihre Unterscheidung von Verletzungen. Wien. Ztschr Nervenh., 10 18–34

Sensenig, E. C. 1957 The development of the occipital and cervical segments and their associated structures in human embryos. Carnegie Inst. of Wash. Publ. 611, Contribs., Embryol., 36 141 151

Spemann, H., and H. Mangold 1924 Über Induktion von Embryonalanlagen durch Implantation artfremder Organisatoren. Arch. Entwmechan., 100: 599–638.

Sternberg, H. 1929 Über Spaltbildungen des Medullarrohres bei jungen menschlichen Embryonen, ein Beitrag zur Entstehung der Anencephalie und der Rachischisis. Virchows Arch., 272: 325–374

Stockard, C. R. 1910 The influence of alcohol and other anesthetics on embryonic development. Am. J Anat., 10 369–392.

Stockard, C. R., and D. M. Craig 1912 An experimental study of the influence of alcohol

on the germ cells and the developing embryos of mammals. Arch. Entwickl. Organ., 35 569–634

Streeter G. L. 1942 Description of age group XI, 13 to 19 somites, and age group XII, 21 to 29 somites. Carnegie Inst. of Wash. Publ. 197 Contribs. Embryol., 30: 211–245.

Vogel, F S. 1958 The association of vascular anomalies with anencephaly; a postmortem study of nine cases in one of which unilateral anencephaly was present in conjoined double monster. Am. J Path., 34 169–183.

——— 1961 The anatomic character of the vascular anomalies associated with anencephaly with consideration of the role of abnormal angiogenesis in the pathogenesis of the cerebral malformation. Am. J Path., 39 163–174

Vogel, F S., and J L. McClenahan 1952 Anomalies of major cerebral arteries associated with congenital malformations of brain with special reference to pathogenesis of anencephaly Am. J Path., 28 701–723.

Vries, E. de 1927 *Description of young human anencephalic and amyelic embryo.* Anat. Rec., 36 293–317

Vries, P A., de and J B de C. M. Saunders 1962 Development of the ventricles and spiral outflow tract in the human heart. Carnegie Inst. Washington Publ. 621 Contribs. Embryol., 37 87–114.

Wallin, I. E. 1913 A human embryo of 13 somites. Am. J Anat., 15 319–331.

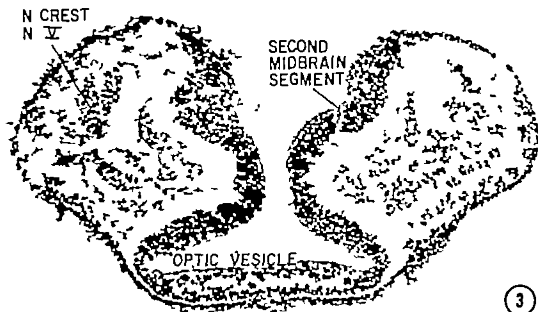
Wen, I. C. 1928 Anatomy of human embryos with 17 to 23 pairs of somites. J Comp. Neur., 45 301–376.

PLATE 1

EXPLANATION OF FIGURES

3 Section 1-8-2 passing through the optic vesicle, magnified × 178.

7 Section 1–5–13 passing through the first aortic arch magnified × 178



N PLATE
AMNION
CHORDA
FIRST
AORTIC
ARCH
FIRST
AORTIC
ARCH
AORTA
PHARYNX
ENDOCARDIUM
MYO EPICARDIUM
7

PLATE 2

EXPLANATION OF FIGURES

4 Section 1–3–7 passing through the neural crest of cranial nerves VII–VIII, magnified × 75.

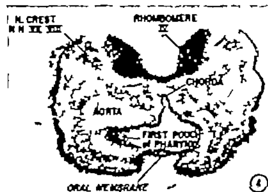
5 Section 1–3–12 passing through rhombomere IV magnified × 75

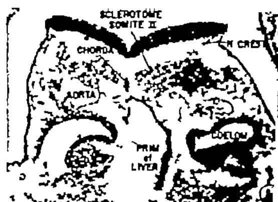
6 Section 1–4–6 passing through the otic pit, magnified × 75.

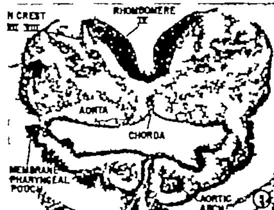
8 Section 2–1–11 passing through the second somite, magnified × 75.

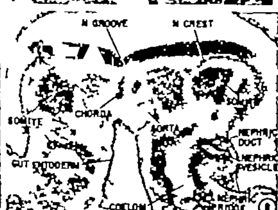
9 Section 2–2–16 passing through the fifth somite magnified × 75.

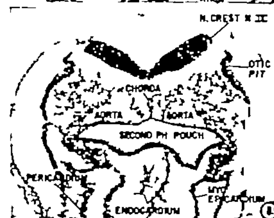
10 Section 2–3–12 cut obliquely through the somites 10–14 magnified × 61

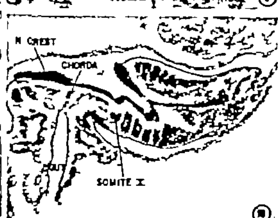

N. CREST
N N VII VIII
RHOMBOMERE
IV
CHORDA
AORTA
FIRST POUCH
of PHARYNX
ORAL MEMBRANE
6


SCLEROTOME
SOMITE II
CHORDA
N CREST
AORTA
COELOM
PRIM
of
LIVER


N CREST
VII VIII
RHOMBOMERE
IV
AORTA
CHORDA
MEMBRANE
PHARYNGEAL
POUCH
AORTIC
ARCH


N GROOVE
N CREST
SOMITE
CHORDA
AORTA
NEPHRIC
DUCT
NEPHRIC
VESICLE
GUT ENTODERM
COELOM


N. CREST N IX
OTIC
PIT
CHORDA
AORTA
AORTA
SECOND PH POUCH
PERICARDIUM
ENDOCARDIUM
EPICARDIUM


N CREST
CHORDA
SOMITE X

A Histologic Description of Certain Epithelial and Vascular Structures in the Kidney of the Normal Rat [1]

DON YOUNG AND STEVEN L. WISSIG

Department of Anatomy, University of California, San Francisco, California

ABSTRACT The cytology of the whole length of the collecting tubule of the rat kidney was studied by light microscopy. The tubule may be subdivided into four successive segments on the basis of the types of epithelial cells that form its lining. The morphology of other epithelial and vascular structures in the renal medulla and papilla was also studied. In fixed histologic specimens, morphologic characteristics of capillaries near the apex of the papilla and in retia mirabilia of the outer portion of the medulla suggest that their plasma is relatively concentrated in the living rat. First, plasma in capillaries of both regions stains deeply with certain histologic dyes. Second, in many specimens erythrocytes in capillaries near the apex of the papilla appear crenated. The significance of the morphologic findings is discussed with regard to current hypotheses concerning the physiologic function of the collecting tubule and other epithelial and vascular structures in the medulla and papilla.

It is interesting to note that morphologists have not in the past scrutinized the renal medulla and papilla as intensively as they have the cortex. Recently physiologists have gathered data revealing the significant role the papilla plays in forming concentrated urine (see review by Ullrich et al. '62). Such studies provide impetus for more thorough morphologic examination of this critical area, and this study reports observations obtained by light microscopy of certain of its epithelial and vascular components.

From its origin in the cortex at the termination of the distal convoluted tubule the collecting tubule passes successively through the cortex, the outer and inner zones of the medulla, and the papilla. Upon reaching the apex of the papilla it empties into the pelvis of the ureter and at this point, its lining epithelium becomes continuous with that coating the outer surface of the papilla. Descriptions of the structure of the collecting tubule along its length by both light and electron microscopy are found in a relatively small number of reviews and original articles. Sjöstrand (44) traced the historical evolution of our knowledge of the histology of the collecting tubule, and his monograph on the kidney should be referred to for detailed information concerning the earlier literature on this subject. More recently Rhodin (58a; '58b) appended newer findings from electron microscopy. However his description covers only the cortical portion of the tubule which he subdivides into two segments: an initial connecting part followed by the arched portion of the collecting tubule.

Sjöstrand (44) noted in the mouse kidney that the transition from distal tubule to connecting part of the collecting tubule takes place relatively abruptly. At the junction, the arrangement of mitochondria in a basal palisade characteristic of cells of the convoluted segment of the distal tubule terminates and the mitochondria of subsequent segments of the uriniferous tubule are more randomly scattered in the cytoplasm of the lining cells. Many authors have reported that two types of cells may be identified in the epithelium of the collecting tubule (see Sjöstrand, 44; von Möllendorf '30). The ordinary lining cells, which are numerically preponderant and are often referred to as "light" cells, are broad cells of cuboidal height. In the light microscope their cytoplasm appears relatively homogeneous and contains few

[1] This research was supported by research grant (H-4812) from the National Heart Institute of the National Institutes of Health.

[2] Summer Research Fellow of the United States Public Health Service.

granules vacuoles and mitochondria. The latter are located mostly in the base of the cell The second type of cell referred to as "dark or "intercalated" cells is slightly broader and taller than ordinary lining cells. It occurs singly and contains abundant cytoplasmic granules. The granules have been unequivocally identified as mitochondria on the basis of their fine structure (Rhodin '58a, '58b) The less numerous intercalated cells occur with greatest frequency in some of the cortical segments of the collecting tubule and are absent from its terminal segments (See Observations.)

The capillaries of the renal medulla and papilla receive arterial blood predominantly from efferent glomerular arteries arising from juxtamedullary glomeruli (von Möllendorf '30 Trueta et al 47 Ljungqvist and Lagergren, '62) The capillaries form long branching loops the vasa recta, which follow the same straight course towards and away from the apex of the papilla as do Henle s loops. Mammalian kidneys maintain an increasing osmotic gradient from the cortical border of the medulla to the apices of the renal papillae (Wirz et al '51 Bray '60) The cortex is isosmotic with the plasma of the general circulation, whereas the osmolarity at the apex of the papilla can be several times as great. The vasa recta maintain an active circulation to the medulla and papilla without disturbing the gradient. To do this effectively the vasa recta must act as a countercurrent diffusion exchange apparatus. Their walls must be permeable to small molecules in order to allow water to be shunted from the descending to the ascending limbs of their capillary loops Thus far several morphologic and physiologic studies have substantiated by indirect evidence that the vasa recta are indeed readily permeable to water For example several workers have shown that fluid in collecting tubules Henle s loops, and vasa recta at the apex of the papilla have roughly the same osmolarity (Wirz, '53 Gottschalk and Mylle '59 Ullrich et al. '61a) Longley and Burstone ('58) reported that blood plasma within capillaries of the renal papilla appears denser than elsewhere. Similarly protein-bound dyes circulating through the vasa recta display an increasing concentration gradient towards the apex of the papilla (Longley et al., '58) Furthermore, after being injected intravenously larger solutes reach the apex of the papilla much more rapidly than do smaller solutes injected simultaneously (Longley et al., '58 White et al. '60 Maganzini and Lilienfeld, '61 Lassen and Longley '61)

Apparently in order to ensure the efficient shunting of substances from descending to ascending limbs the vasa recta form a series of *retia mirabilia* as they pass through the outer portion of the renal medulla (Longley et al '60) These consist solely of bundles of intermingled ascending and descending limbs of the capillary loops. The two may be readily distinguished from each other in sections examined by electron microscopy because the descending limbs are lined by a continuous endothelium similar to that of muscle capillaries whereas the endothelium of the ascending limb is fenestrated and resembles peritubular capillaries of the renal cortex (Longley et al., '60) Classification of individual branches by light microscopy is more difficult to carry out.

The current report describes the histologic structure of the collecting tubule in the rat kidney from its origin in the cortex at the termination of the distal tubule to the point where it empties into the pelvis of the ureter at the apex of the renal papilla. In addition this report draws attention to morphologic characteristics of the vasa recta of the renal medulla and papilla which seem to be related to their role as a countercurrent *diffusion exchange apparatus in the urine-concentrating mechanism*

MATERIALS AND METHODS

Kidney specimens were obtained from 25 normal male and female rats of the Long Evans strain which had been receiving food and water *ad libitum*. They were kept in metabolic cages for several days prior to autopsy in order to record their output of urine. Only those rats excreting a normal daily volume (1.8–6.5 ml/100 g body weight/day average 3.7 ml/100 g body weight/day) were used in this study At autopsy the rats were anesthetized with

nembutal, and their kidneys were exposed through a midventral abdominal incision. *Usually only the left kidney but occasionally the right one as well, was fixed* either *in situ* by pouring fixative over the kidney with its circulation intact, or by first removing it from the rat after clamping the renal artery vein and ureter and then cutting it into small blocks under fixative A variety of techniques was used for preparing specimens for histologic examination. They were fixed either in glutaraldehyde (Sabatini et al., '63) acrolein (Luft, '59) or formaldehyde embedded in paraffin, celloidin, or polyester wax (Sidman et al., '61); *and stained with a modification* of Mallory s Azan procedure (Lillie '54) The most adequate preservation was achieved when the kidney was immersed initially *in situ* in acrolein fixative for 5–10 minutes. The kidney was then removed from the rat, and a segment containing the papilla and the portion of cortex to which it was attached was cut out for further fixation and subsequent embedding. Polyester wax was used most frequently for embedding as it facilitated cutting sections less than 5 μ thick. During sectioning the *specimens were oriented so that sections* contained parenchyma stretching from peripheral cortex to apex of the papilla. A Zeiss photomicroscope equipped with a plate camera attachment was used for photomicrography

OBSERVATIONS

Topography of the rat kidney

For ease of description, the rat s unilobar kidney may be subdivided into five zones (fig 1) *Zone I* comprises the cortex, and its principal parenchymal constituents are renal corpuscles and proximal distal, and collecting tubules. The medulla is usually divided into outer and inner zones, the former being further subdivided into an outer and inner band. *Zone II* the outer band of the outer zone of the medulla, contains the straight portions of proximal tubules, ascending portions of distal tubules, and collecting tubules. *Zone III* the inner band, contains thin (descending) limbs of Henle s loops, collecting tubules, and ascending portions of the distal tubules. The ascending limbs of the distal tubules that traverse Zones II and III are often termed thick limbs of Henle s loops. However under examination by light microscopy in this study this segment of the nephron of the rat appears morphologically identical with segments of the distal tubule located in the cortex (Zone I) At this stage it seems more reasonable, therefore, to refer to it as a part of the distal tubule rather than as part of Henle s loop. More than 30 years ago von Möllendorf ('30) also noted the close resemblance in some species between the thick, ascending limb of Henle s loop and the distal tubule. He proposed a classification for kidney tubules in which the thick, ascending limb of Henle s loop and the distal tubule were considered subdivisions of a single unit within the nephron, the Mittelstück. The thick, ascending limb of Henle s loop constituted the straight portion of the Mittelstück, and the distal tubule including the macula densa constituted its convoluted portion.

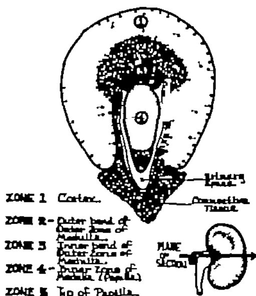


Fig. 1 Schematic view of rat kidney sectioned transversely at the level of the hilus. The approximate location and extent of the five zones into which the kidney is subdivided for the purposes of this study is illustrated.

The remaining portion of the kidney comprised principally of the papilla, is

Nembutal is the registered trade mark of sodium pentobarbital produced by Abbott Laboratories, North Chicago, Illinois.

usually classified as a single zone, the inner zone of the medulla. It contains collecting tubules as well as ascending and descending limbs of Henle's loops. Since as we shall point out later the apical portion of the papilla has several unique histologic properties which can best be dealt with separately we have subdivided the papilla into two parts the basal two-thirds (*Zone IV*) and the apical third (*Zone V*) In Zones IV and V the two limbs of Henle's loop are indistinguishable from one another and may be classified as thin limbs. In Zone V collecting tubules approach the apex of the papilla where they empty into the pelvis of the ureter and the descending limbs of the lengthiest Henle's loops upon reaching the nadir of their descent, make a U-turn and ascend back to the cortex. The large collecting tubules in this zone are often called papillary ducts.

Collecting tubule

After the techniques of fixation and staining described in Materials and Methods are applied to kidney specimens it is possible to demonstrate that the cytologic characteristics of the epithelial cells lining the collecting tubule change markedly along its length. For example the mitochondria of the lining cells in different zones vary in number and orientation and can serve as useful criteria for distinguishing individual cell types. On the basis of the types of cells forming the population of lining cells along its length the collecting tubule may be divided into four segments. The first segment corresponds to the connecting piece noted in earlier studies. Since it is usually found only after prolonged searching, we assume it to be of short length. It appears to arise by gradual transformation of the epithelium of the terminal portion of the distal tubule. Its cells are of roughly the same height and width as those of the latter On the basis of cytological properties two classes of cells may be identified in the epithelial lining transitional cells and ordinary lining cells. Transitional cells are usually scattered singly or in small groups in the lining epithelium (figs. 3 and 4) They are similar to ordinary lining cells except for one feature mitochondria tend to be arranged perpendicular to the basal surface of the cell in a manner reminiscent of the basal palisade they form in cells of the distal tubule (fig. 2) Since the number of mitochondria with this orientation is usually fewer than in cells of the distal tubule this type is considered to represent a transitional stage between lining cells of the latter and ordinary lining cells of the collecting tubule. Ordinary lining cells contain a moderate number of thin filamentous mitochondria scattered throughout their cytoplasm without sign of preferred orientation (figs 3 and 4) (A third, distinctive type of cell the intercalated cell, may occasionally appear in the initial segment but it does not usually occur in significant numbers in the lining epithelium before the second segment.) All of the cells of the segment are taller centrally where their nuclei are situated than in the region of their lateral border The matrix of the round nuclei of both transitional and ordinary lining cells is of homogeneous texture The abrupt transition from distal tubule to initial segment of the collecting tubule (i.e., the connecting piece) observed by Sjöstrand (44) in the mouse apparently does not occur in the rat.

The lengthy second segment of the collecting tubule begins in the cortex (Zone I) and traverses Zones II and III to terminate in the outer portion of Zone IV Two types of epithelial cells can be identified in its epithelial lining (figs. 5–8) ordinary lining cells like those of the first segment as well as scattered intercalated cells Intercalated cells are interspersed singly among the other epithelial cells and are generally taller and broader Their cytoplasm is distinctive for its rich content of relatively deeply staining mitochondria shaped like short rods or spheres. Their round nuclei are generally larger than those of ordinary lining cells and contain clumps of chromatin in their matrix. As the second segment nears Zone IV its epithelium becomes progressively lower in height. At its termination just within this zone, intercalated cells disappear from the epithelial lining.

The third segment of the collecting tubule another lengthy segment, extends throughout the remainder of Zone IV It is lined by a single type of cuboidal epithe-

lial cell, broad in width and of low height, which appears devoid of cytoplasmic organelles other than a few scattered mitochondria (fig. 9).

The fourth segment, the papillary duct, evolves gradually from its predecessor by progressive heightening of the epithelial lining until it reaches low or medium columnar. Only a single type of epithelial cell is present (fig. 10). Its apical surface is smooth and its cytoplasm appears relatively devoid of organelles except for a small number of thin, filamentous mitochondria. The borders between adjacent cells are especially prominent in this segment. When examined under high resolution with the light microscope the borders may present a perplexing appearance. Within the border often lie one or a string of several structures resembling small vesicles or vacuoles. The bases of the epithelial cells may appear vacuolated in a similar fashion. The exact nature and significance of this structural appearance is not yet known.

The epithelial lining of the terminal portion of the collecting tubule is continuous with that coating the surface of the papilla. Near the tip of the papilla, the latter, a cuboidal or columnar epithelium, consists of two types of cells. The numerically predominant of these resembles the cells lining the fourth segment of the collecting tubule. The second type occurs singly, is highly chromophilic, and appears to be either a degenerating cell or one that secretes mucus.

Vasa recta

Vasa recta passing through Zone III and the bordering portion of Zone II en route to and from the papilla are grouped in bundles to form numerous retia mirabilia (figs. 13 and 14). Not all capillaries traversing this region are included in retia; a substantial number pursue a solitary course between them. Above and below the retia, capillaries mingle randomly with tubules. An interesting morphologic attribute of capillaries in the retia is that their plasma stains avidly with some components used in the Mallory Azan procedure (fig. 14). The enhanced stainability of the plasma suggests that the concentration of its protein constituents is elevated above normal levels. In contrast, the plasma of capillaries passing individually through these zones stains with normal intensity. Wherever plasma in the lumens of capillaries in the retia does not stain so intensely that visualization of erythrocytes is obscured, the latter can be seen to retain a relatively normal outline (fig. 13).

Observations made in the present study seem to confirm earlier reports (Longley and Burstone, '58; Longley et al., '58) that a gradient of plasma concentration exists in the papilla of the kidney of the normally hydrated rat. Plasma generally stains most heavily and thus appears to be most concentrated in capillaries at the tip of the papilla (figs. 11 and 12). The plasma becomes progressively less concentrated with increasing distance from the tip. In normally hydrated rats, the gradient of increased staining of plasma is confined to the apical third of the papilla. Longley et al. ('58) reported that capillaries of the papilla contain few erythrocytes. This does not seem generally true for all capillaries near the apex; many contain a normal or high concentration of erythrocytes. Erythrocyte-rich and erythrocyte-poor capillaries at the apex often lie close together, and it is possible that the unequal distribution of erythrocytes in apical capillaries could be an artefact. In approximately two-thirds of the rats examined for this study, erythrocytes in capillaries near the apex appear crenated (figs. 15 and 16). In full-face view they display a scalloped outline, and when viewed edge-on they appear abnormally flattened. The zone in which erythrocytes are crenated coincides more or less with the zone in which the capillary plasma appears concentrated, i.e., the apical third of the papilla. The degree of crenation, like the apparent increase in concentration of plasma, increases progressively with proximity to the apex.

DISCUSSION

The morphologic characteristics of the epithelial lining of the collecting tubule change along its length in a sufficiently clearcut manner to permit us to subdivide it into four segments. In the past the existence of individual segments has been largely overlooked, and the collecting tubule has been dealt with as a single unit by

most morphologists and physiologists. On the basis of physiologic evidence the collecting tubule is assumed to carry out several steps in the overall process of urine formation, and several examples of these can be cited (Koch, '60) It secretes ammonia released by deamination of amino acids in its epithelium. It recovers sodium ions in exchange for hydrogen ions from fluid passing through its lumen. By adjusting its permeability to water in response to the level of antidiuretic hormone in the circulation, it purportedly regulates the rate at which water is withdrawn from the tubular lumen into the surrounding hypertonic papillary interstitium and thus plays an important role in the mechanism for secreting concentrated urine. It is not yet feasible to assign individual functions to each of the four segments of the tubule much less to individual types of cells in each segment, but some functions can be roughly localized within portions of the tubule The secretion of ammonia and exchange of cations are thought to take place near the origin of the tubule and participation in formation of concentrated urine is limited to the portion of the tubule located within the papilla.

Epithelial cells presumed to carry out active transport of ions commonly contain abundant mitochondria. Cells of this category occur in gastric glands (Sedar '55; Challice et al. '57) proximal and distal tubules (Sjöstrand and Rhodin '53 Pease '55) striated ducts of the parotid gland (Parks '61) and salt-glands of marine birds (Doyle, '60) It is possible that the mitochondria-rich intercalated cells scattered singly in the epithelium of the second segment of the collecting tubule function similarly It is interesting to recall in passing that the epithelial lining of the toad bladder which can also actively transport ions consists of four different types of cells and that one of these scattered singly among the other cells contains abundant mitochondria (Peachey and Rasmussen, '61; Choi, '63)

According to the currently prevalent theory of the means by which concentrated urine is secreted by the mammalian kidney Henle's loop in the renal papilla acts as a countercurrent multiplier and the vasa recta of the same region act as a countercurrent diffusion exchanger The theory asserts that the ascending and descending limbs of Henle's loop have radically different physiologic capabilities. The descending limb is permeable to sodium ions and water; the ascending limb is impermeable to both of these and, moreover, actively pumps sodium ions from its lumen into the papillary interstitium. The vasa recta are presumed to be permeable to salt and water throughout their descending and ascending limbs Coordinated operation of the countercurrent multiplier and diffusion exchanger produces a gradient of salt concentration in the interstitium of the papilla with maxmium concentration reached at the apex. Thus far the theory is supported by physiologic and, albeit to a lesser extent, morphologic evidence.

Throughout the renal papilla (Zones IV and V) both limbs of Henle's loop are classified as thin limbs. They are lined by squamous epithelium which appears only a shade thicker than the endothelium of the vasa recta. At all levels in the papilla, the limbs of Henle's loop appear identical with one another and therefore it is not possible to distinguish ascending from descending limbs. Structural distinctions between the two have not been reported even after more intensive examination by electron microscopy (Pease, '55; Rhodin, '58a) From a morphologist's point of view we can accept only with qualms the conclusion that the profound functional differences between ascending and descending limbs are not expressed structurally That the epithelium of Henle's loop appears not to have any of the distinctive morphologic properties of many of the other salt pumping epithelia furnishes additional grounds for uneasiness.

Several interesting features of the vasa recta of the renal medulla and papilla have come to light through morphologic investigations. To begin with, the intimate association between arterial and venous capillaries in the retia of the kidney ideally suits them to act as a countercurrent diffusion exchanger and these specialized structures situated at the gateway to the papilla may be the chief means responsible for making sure that the hypertonicity of its interstitium is not dissipated by its vascular supply Since the retia consist solely

of closely bunched capillaries, their structural design enables the capillaries in the retia, except those situated at the periphery to reach diffusion equilibrium with one another They cannot equilibrate readily with parenchymal elements for the latter are for the most part excluded from the retia. The remaining lengths of the capillary loops in the medulla and papilla below the retia presumably continue to act as countercurrent diffusion exchangers with the difference that, since they are dispersed individually at random in the parenchyma, they equilibrate primarily with adjacent limbs of Henle's loop and collecting tubules.

Examination by electron microscopy reveals that the fine structure of ascending and descending branches of the vasa recta in the retia mirabilia is quite different. Where these differences arise above the retia and how far they persist below have not yet been studied. The question why descending or "arterial" limbs of the retia are lined by continuous endothelium whereas ascending or venous limbs are lined by fenestrated endothelium may also be raised, although there is as yet no satisfactory answer On the basis of physiologic data gathered in studies of other organs, we have good reason to suspect, on the basis of this difference in morphology that the wall of the descending capillaries should be less permeable than that of the ascending (Mayerson et al. '60) Interestingly enough arterial and venous capillaries in the rete mirabile in the swim bladder of the toadfish show similar structural differences despite the fact that the role of the rete in this case appears to be to prevent gas rather than ions from escaping into the general circulation (Fawcett and Wittenberg, '59)

Assuming that the increased avidity for stains of plasma in the capillaries of certain regions is a sign of increased concentration of its proteins, we should draw attention to the observation that the concentration of plasma protein is elevated in two separate locales the retia mirabilia and the apex of the papilla The concentration may be higher at the apex for the plasma stains more avidly there and often the erythrocytes appear crenated. Plasma in vasa recta linking the two regions of elevated concentration appears to be of normal concentration. Since the walls of capillaries behave like semipermeable membranes (Pappenheimer '53) changes in concentration of the contents of capillaries should in turn reflect changes in osmolarity of the surrounding interstitium. A zone of increased osmolarity at the apex of the papilla is more or less consistent with the countercurrent theory but the tenets of the theory do not provide an explanation for the existence of a second zone of hyperosmolarity at the level of the retia mirabilia Intimations of the existence of hypertonic interstitium in the vicinity of the retia appeared in a recent preliminary report of an autoradiographic study (Mercer et al '63) However Bray ('60) using microcryoscopic techniques, measured the osmolarity of the cortex and the several subdivisions of the medulla of the rat kidney In disagreement with our findings he did not observe another region of pronounced hyperosmolarity associated with the retia mirabilia.

Ullrich and his colleagues recently published reports of two studies in which they examined the composition of blood samples obtained by micropuncture from vasa recta near the tip of the papilla of anesthetized hamsters. In one study (Ullrich et al. '61b) they compared the concentration of hemoglobin number of erythrocytes, and hematocrit of individual samples and concluded that erythrocytes in these capillaries are shrunken as a consequence of the hypertonicity of the plasma. Our observations confirm this finding. The other study (Ullrich et al. '61a) reports findings that do not seem compatible with our own. They found that the osmotic pressure of plasma from the vasa recta of the papillae of different animals ranged from 1.2–3.8 times as great as that of systemic plasma. In contrast, the concentration of plasma proteins in all plasma samples was more or less constant, averaging only 1.2 times as great as that of systemic plasma. On the basis of determinations of sodium and chloride concentration, they concluded that when the osmolarity of the plasma in the vasa recta exceeds that of systemic plasma, the additional solute consists chiefly of these two ions. These findings imply that ions can enter the *lumens* of vasa recta

faster than water molecules leave and therefore that the semipermeable capillary wall is actually less permeable to water molecules than to hydrated sodium ions with a diameter approximately three times as large. Furthermore if we assume that the glomerular membrane of mammals is relatively impermeable to protein and that approximately 10% of the fluid entering a glomerulus passes through the filter the *concentration of protein in the plasma of* efferent glomerular arterioles the principal source of blood for the papilla, should be approximately 1 1 times as high as that of systemic plasma According to their findings, the concentration of protein would be nearly the same in plasma entering the vasa recta as in vasa recta at the apex of the papilla, and no gradient of plasma protein concentration should exist in the medulla or papilla

A number of reports that contradict their findings can be cited. In this study as well as in an earlier one (Longley and Burstone 58) densely stained material believed to be concentrated plasma protein was observed in vasa recta near the apex of the papilla. Furthermore dyes bound to plasma protein in vasa recta increase progressively in concentration with increasing proximity to the apex of the papilla (Longley et al '60) Finally Thurau et al. ('60) found a gradient of increasing concentration of plasma albumin from the base to the apex of the papilla in vasa recta of the hamster kidney Maximum *concentrations ranging from* 2.1–2.9 as great as that of systemic plasma were reached at the apex.

Blood circulating through the renal medulla and papilla is drawn principally from efferent glomerular arterioles of juxtamedullary glomeruli These receive blood from intralobular branches of interlobular arteries a short distance after the latter arise from arcuate arteries Owing to the physical characteristics of blood flow through interlobular arteries (Pappenheimer and Kintner '56) erythrocytes under normal conditions are purported to be concentrated in an axial stream in the lumen of interlobular arteries whereas the periphery of the stream consists largely of plasma. Intralobular arteries branch at right angles from their parent artery As a consequence of the unequal distribution of the erythrocytes in the lumen of interlobular arteries intralobular arteries arising near the border of the medulla should, on the one hand, be perfused with blood containing few erythrocytes and blood perfusing peripherally situated intralobular arteries should on the other hand, be perfused with blood relatively enriched with erythrocytes. A further consequence of the "plasma-skimming" phenomenon is that the circulation to the medulla should contain few erythrocytes. Physiologic data obtained from micropuncture experiments substantiate the occurrence of "plasma-skimming (Ullrich et al. '61b) but, to our knowledge morphologic studies primarily designed to evaluate the validity of the hypothesis have not yet been carried out. Cursory inspection of our specimens, admittedly not ideal test objects for this purpose does not uncover an obvious scarcity of erythrocytes in the renal medulla or papilla, but this point requires additional scrutiny before more definite statements can be made

LITERATURE CITED

Bray G A. 1960 Freezing point depression of rat kidney slices during water diuresis and antidiuresis. Am J Physiol., *199* 915–918.

Challice, C. E., S. Bullivant and D. B. Scott 1957 The fine structure of some cytoplasmic inclusions of oxyntic cells. Exp Cell Res., 13 488–492.

Choi, J K. 1963 The fine structure of the urinary bladder of the toad, *Bufo marinus*. J. Cell Biol., *16* 53–72.

Doyle, W L. 1960 The principal cells of the salt-gland of marine birds. Exp. Cell Res *21*: 386–393.

Fawcett D W and J Wittenberg 1959 The fine structure of capillaries in the rete mirabile of the swim bladder of *Opsanus tau*. Anat. Rec., 133 274.

Gottschalk, C W and M. Mylle 1959 Micropuncture study of the mammalian urinary concentrating mechanism evidence for the countercurrent hypothesis. Am. J Physiol 196 927–936.

Koch, A. 1960 The kidney In Medical Physiology and Biophysics (edited by T C. Ruch and J F Fulton) W B Saunders Company 844–872.

Lassen N A and J B Longley 1961 Countercurrent exchange in vessels of renal medulla Proc. Soc. Exp. Biol. Med., 106 743–748.

Lillie R. D 1954 Histopathologic technic and practical histochemistry The Blakiston Company New York, 1–501

Ljungqvist, A., and C. Lagergren 1962 Normal intrarenal arterial pattern in adult and ageing

human kidney A micro-angiographical and histological study J Anat., 96 285–300.

Longley J B., and M. S. Burstone 1958 Observations on the renal medullary circulation. J Histochem. Cytochem., 6 89

Longley J B W G. Banfield and D C. Brindley 1960 Structure of the rete mirabile in the kidney of the rat as seen with the electron microscope. J Biophys. Biochem. Cytol., 7 103–106.

Longley J B., N. A. Lassen and L. S. Lilienfield 1958 Tracer studies on renal medullary circulation. Fed. Proc., 17 99

Luft, J H. 1959 The use of acrolein as fixative for light and electron microscopy Anat. Rec., 133 305.

Magantini, H. C., and L. S Lilienfield 1961 Demonstration of counter-current diffusion exchange in the vasa recta of the renal medulla. Proc. Soc. Exp. Biol. Med., 107 872–875.

Mayerson, H. S., C. G Wolfram, H. H. Shirley Jr., and K. Wasserman 1960 Regional differences in capillary permeability Am. J Physiol., 198 155–160.

Mercer P F N H Mercer and R. H. Wasserman 1963 Autoradiographic distribution patterns reflecting the concentrating mechanism in rat kidney The Physiologist, 6 233.

Pappenheimer J R. 1953 Passage of molecules through capillary walls. Physiol. Rev 33 387–423.

Pappenheimer J R., and W B. Kinter 1956 Hematocrit ratio of blood within mammalian kidney and its significance for renal hemodynamics. Am. J Physiol., 185 377–390.

Parks, H. 1961 On the fine structure of the parotid gland of mouse and rat. Am. J Anat., 108 303–329.

Peachey L. D., and H. Rasmussen 1961 Structure of the toad' urinary bladder as related to its physiology J Biophys. Biochem. Cytol 10 529–553.

Pease, D C. 1955 Fine structure of the kidney seen by electron microscopy J Histochem. Cytochem., 3 295–308.

Rhodin, J 1958a Electron microscopy of the kidney Am. J Med., 24 661–675.

——— 1958b Anatomy of kidney tubules. Int. Rev Cytol., 7 485–534.

Sabatini, D. D K. G. Bensch and R. J Barrnett 1963 Cytochemistry and electron microscopy The preservation of cellular ultrastructure and enzymatic activity by aldehyde fixation. J Cell Biol 17 19–58.

Sedar A. W 1955 Fine structure of parietal cells. Anat. Rec., 121 365–366.

Sidman, R. L., P A. Mottla and N Feder 1961 Improved polyester wax embedding for histology Stain Technol., 36 279–284

Sjöstrand, F 1944 Über die Eigenfluorescenz tierischer Gewebe mit besonderer Berücksichtigung der Säugetierniere. Acta Anat., 1 Suppl. no. 1 1–163.

Sjöstrand, F S and J Rhodin 1953 The ultrastructure of the proximal convoluted tubules of the mouse kidney as revealed by high resolution electron microscopy Exp. Cell Res., 4: 426–456.

Thurau K., T Sugiura and L. S. Lilienfield 1960 Micropuncture of renal vasa recta in hydropenic hamsters. Circulation Res., 8 383.

Trueta, J., A. E. Barclay P M. Daniel, K. J Franklin and M. M. L. Prichard 1947 Studies of the renal circulation. Charles C Thomas, Springfield, 1–187

Ullrich, K. J K. Kramer and J W Boylan 1962 Present knowledge of the countercurrent system in the mammalian kidney In Heart, Kidney and Electrolytes (edited by C. K. Friedberg) Grune and Stratton, New York, 1–37

Ullrich, K. J G. Pehling and M. Espinar-Lafuente 1961a Wasser und Elecktrolytflüss in vasculären Gegenstromsystem des Nierenmarks, Pflügers Arch. ges. Physiol., 273 562–572.

Ullrich, K. J G. Pehling and H. Stöckle 1961b Hämoglobinkonzentration, Erythrocytenzahl und Hämatokrit im vasa recta Blut. Pflügers Arch. ges Physiol., 273 573–578.

von Möllendorff, W 1930 Der Exkretionsapparat. In Handbuch der Mikroskopischen Anatomie des menschen, Band VII, Teil I, Verlag von Julius Springer Berlin, 1–328.

White, H. L., D C. Tosteson and D Rolf 1960 Roles of blood and urine flows in distributing THO and N = within kidney Fed. Proc., 19 363.

Wirz, H. 1953 Der osmotische Druck des Blutes in der Nierenpapille. Helvet. physiol. pharmacol. Acta, 11 20. (Cited by Ullrich et al., '62.)

Wirz, H., B Hargitay and W Kuhn 1951 Lokalisation des Konzentrierungsprozesses in der *Niere durch direkte Kryoscopie. Helvet.* physiol. pharmacol. Acta, 9 196. (Cited by Ullrich et al., '62.)

PLATE I

EXPLANATION OF FIGURES

2 A segment of the convoluted portion of distal tubule in Zone I crosses the field. Part of another lies along the upper margin of the figure. Blunt pseudopod protrude from the pices of a number of the cuboidal lining cell into th lumen of the tubules. Rodlets in the cytoplasm of the lining cells are identified as mitochondria. They seem to be beent from the pseudopods. In the basal cytoplasm, long filamentou mitochondria form prominent palisade normal to the basal surface of each cell. × 2,040.

3 A longitudinal section through a convol tion of the initial segment of collecting tubule in Zone I. It epithelial lining is formed by two different types of cells. The majority are ordinary lining cells, and mitochondria are distributed in their cytoplasm without any obvious pattern. Transitional cells can be recognized along the upper left margin of the tubule as well as elsewhere in its border by the fine filamentous mitochondria forming palisade in their basal cytoplasm. The cytoplasm near the pical borders of some lining cells appears free of mitochondria × 1 770





3

PLATE 2

EXPLANATION OF FIGURES

4 A cross section of an initial segment of collecting tubule in Zone I. Ordinary lining cells contain predominantly filamentous mitochondria in their cytoplasm. Mitochondria in transitional cell in the upper left margin of the tubule *form a palisade* in the base of the cell. × 2,240.

5 A cross section of the second segment of collecting tubule in Zone I. The lining cells are broader and not as tall as cells of the initial segment. The ordinary lining cells appear t contain filamentous mitochondria. The two more darkly stained cells in the epithelial lining are identified as intercalated cells. They stain more deeply because of the dense concentration of mitochondria in their cytoplasm. × 1,070.

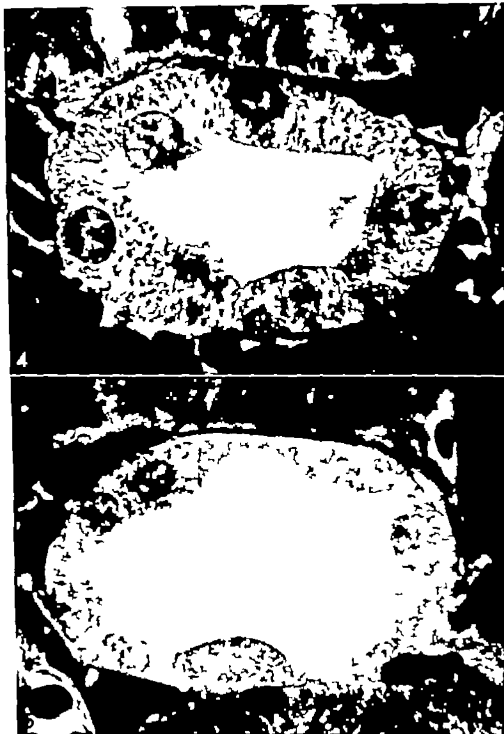

4
2

PLATE 3

EXPLAN TION OF FIGURES

6 A portion of the epithelial lining of the second segment of collecting tubule in Zone I. Two intercalated cells can be recognized by their dense population of mitochondria. They are broader than ordinary lining cells, and because they also are generally taller they protrude farther int the lumen. × 2,040

7 A tortuous collecting tubule in Zone II extends from left to right in the figure. In the center of the figure the plane of section grazes the epithelial wall of the tubule, and an intercalated cell is prominent in the tangentially sectioned epithelium. Its numerous mitochondria, largely of spherical form distinguish it from surrounding ordinary lining cells. A second intercalated cell (arrow) may also be present. Distal tubules ascending towards the cortex appear in the upper portion of the figure. In the lower portion lie straight portions of proximal tubules descending towards the papilla. × 1,840.

6

7

Abbreviations

CT collecting tubule
DT distal tubule
HL thin limb of Henle loop

PLATE 4

EXPLANATION OF FIGURES

8 A portion of the second segment of collecting tubule in the outer portion of Zone IV extends cross the figure from left to right. Just bove t lies limb of Henle s loop. Other parenchymal elements in the field are difficult to identify The epithelium lining the tubule is of low cuboidal height. Arrows indicate the location of three inter calated cells. Each of the ordinary lining cells lying between the two intercalated cells in the lower border of the tubule has single curious and unexplained protuberance in its pical border just over the nucleus. × 1 700

9 A portion f the third segment of collecting tubule in the inner portion of Zone IV Ordinary lining cells are the sole constituents of its epithelial lining, and they are of cuboidal height. Limbs of Henle loops (HL) also appear in the field. × 1,840.

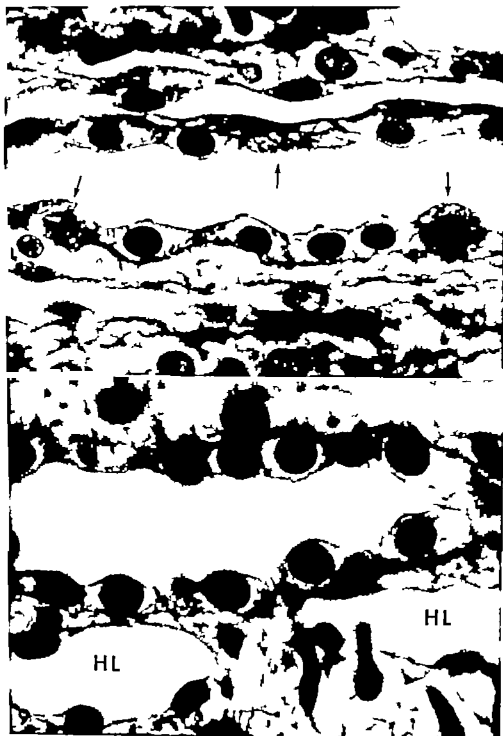

HL
HL

PLATE 5

EXPLANATION OF FIGURES

10 A portion of the fourth segment of collecting tubule situated near the pex of the renal papilla. Its epithelial lining is comprised of a single type of low columnar cell. The borders between adjacent epithelial cells are singularly distinct in this region. Structures resembling vesicles are poorly visualized in the intercellular borders as well as along the bases of number of epithelial cells. × 1 700

11 This figure illustrates the diverse appearance of some capillaries at the tip of the papilla. One capillary (A) cut in cross section contains erythrocytes that appear crenated, and no plasma is visible around them. A second capillary (B) contains crenated erythrocytes surrounded by homogeneous plasma of ppreciable density A third capillary (C) contains erythrocytes that are almost completely obscured by its densely staining plasma. Collecting tubules (CT) and limbs of Henle loops (HL) also appear in the field. Their lumens appear empty × 1,630.



10

CT
HL
A
HL
C
CT
B
HL
11

PLATE 6

EXPLANATION OF FIGURE

12 A longitudinal section through the tip of the renal papilla. Capillaries of this region form branching network and are easily singled out because deeply stained plasma opacifies their lumens. Collecting tubules in the field have broad, tortuou empty lumens bordered by tall cuboidal or low columnar epithelial cells. Limbs of Henle loops are almost bsent from the field. The capillaries and parenchymal tubules are separated from one another by substantial amounts of interstitial tissue. × 200.


12

PLATE 7

EXPLAN TION OF FIGURE

13 A longitudinal section through a rete mirabile passing through Zone III. Some capillaries of the rete contain plasma as well as erythrocytes, whereas others contain only plasma Erythrocytes in the capillaries h ve a relatively normal outline. The intensity with which plasm stains suggests th t it is more concentrated than in most other regions of the renal vascular bed. Parenchymal elements bordering the rete include limbs of Henle' loops (HL) collecting tubules (CT) and ascending portions of distal tubules (DT) × 970

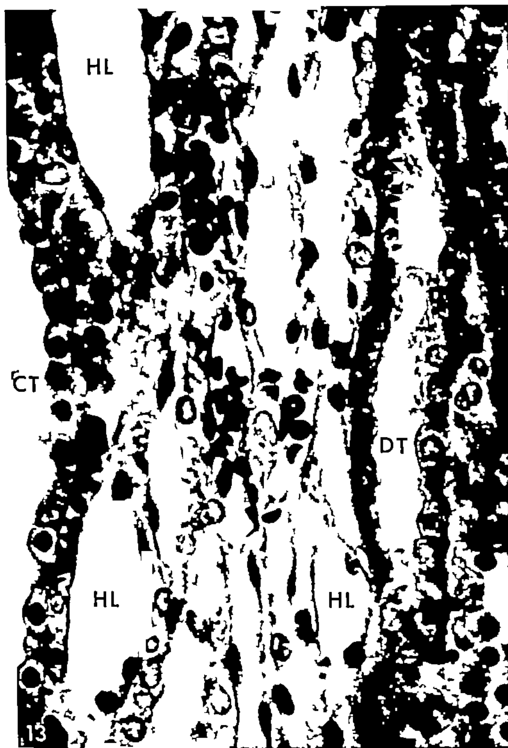

HL
CT
DT
HL
HL
13

PLATE 8

EXPLAN TION OF FIGURE

14 A longitudinal section of rete mirabile passing through Zone III. The plasma within capillaries of the ret stains so intensely that it obscures visualization f erythrocytes in the capillary lumens. The capillaries are bordered by limbs of Henle loops (HL) and ascending portions f distal tubules (DT) × 920.

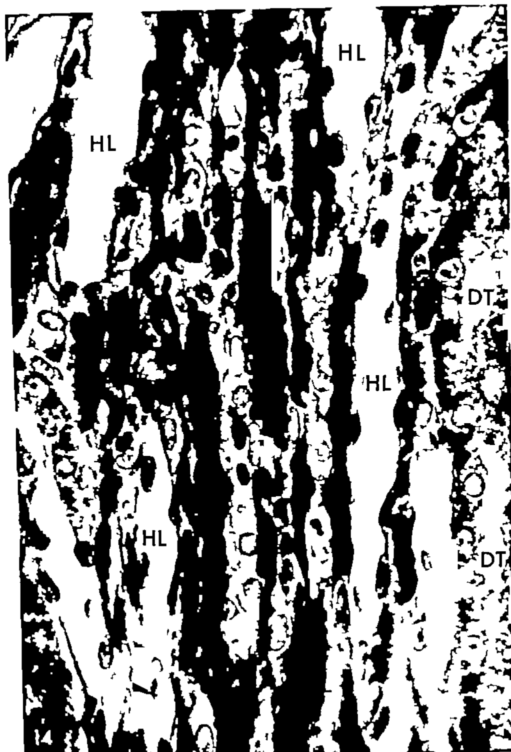

HL
HL
DT
HL
HL
DT
14

PLATE 9

EXPLAN TION OF FIGURES

15–16 Capillaries near the tip of the papilla. The erythrocytes in the capillary lumens are crenated. Viewed edge-on, they ppear as thin flattened discs and are no longer biconcave. In full-face view number display the classic scalloped outline characteristic of crenation. Their blood plasma is homogeneously stained. Portions of limbs of Henle loops and of fourth segments of collecting tubules also appear in the fields. Liberal amounts of interstitium separate ascular and parenchymal elements. The interstitium ppears to contain a single unique species of cell from which many fine cytoplasmic processes radiate to terminate on neighboring capillaries, Henle s loops or parenchymal tubules. The matrix f the interstitium ppears homogeneous and relatively devoid of connective tissue fibers. × 1 770 (fig. 15); × 1,840 (fig. 16)


15
16

An Electron Microscopic Study of the Ependyma and Subependymal Glia of the Lateral Ventricle of the Cat [1]

GEORGE H. KLINKERFUSS
Departments of Anatomy and Neurology Washington University School of Medicine Saint Louis, Missouri

ABSTRACT Portions of the wall of the lateral ventricles of the cat were obtained directly and after initial chrome-osmium perfusion. After further fixation they were embedded in Epon-812, sectioned on Porter-Blum microtome and examined in the electron microscope. Observations on the ultrastructure of ependyma and subependymal glia of the feline lateral ventricle are described. The ependyma contains pale cytoplasm with many vesicles, network of fibrils endoplasmic reticulum, Golgi apparatus and numerous dense mitochondria. Cilia are present along the luminal surface which have well defined basal body from which cross-striated rootlets diverge to make close contact with other ciliary rootlets and enter into complex relationships with specialized cell juncture composed of mitochondria in linear arrangement along an intercellular membrane studded with *zonula adherens* These rootlets thus form accommodating links between cilia and morphologic relation to the plasma membrane between ependymal cells. Theories of metachronal motion in ciliated mammalian epithelia may incorporate such structures in the future. Three varieties of subependymal glia are described. Oligodendrocytes are the least common but are observed in close relation to myelinated axons. Fibrous astrocytes send short processes beneath the ependyma, but ependymal astrocytes send thick processes deep into the underlying white matter. No ependymal cells are observed to send processes into the white matter and it is suggested that in the adult cat this is the property of the ependymal astrocyte

Ependyma of the lateral ventricles of mammals has received little specific attention by electron microscopists Tennyson and Pappas ('62) have examined the fine structure of the ependymal lining of the aqueduct in fetal, early postnatal and adult rabbits. Brightman and Palay ('63) recently have reported on ependyma of the third ventricle in the rat. Others who have contributed to the accumulated knowledge of the ultrastructure of ependyma include Luse ('56) Palay ('58) and Brightman ('61) on the ependyma of the rat Oksche ('58) of the frog; Duncan ('57) and Bellairs ('59) of the embryonic chicken; and Schultz, Berkowitz and Pease ('56) of the central canal in lamprey spinal cord.

Fleischhauer ('60 '61) emphasized the histologic variability of ependyma from various sites within the ventricular system of the cat. Draskoci, Feldberg, Fleischhauer and Haranath ('60) demonstrated a differential uptake of histamine between various areas of the cerebral ventricles in the cat. Feldberg and Fleischhauer ('60) showed a similar difference in uptake of bromphenol blue. They then considered a possible correlation between structure of ependyma and its underlying glia with this differential absorption.

Therefore a study of the ultrastructure of the ependyma lining the lateral ventricle of the cat is of interest both in the comparative study of ependymal cells among various species as well as between various areas in the ventricular system.

MATERIALS AND METHODS

Six adult cats were anesthetized with pentobarbital sodium and craniotomies performed leaving the dura intact. In three animals an 18 gauge hypodermic needle was placed in the left lateral ventricle by stereotactic technic. The animals were exsanguinated and simultaneously the ventricular systems perfused with Dalton's chrome-osmium fixative for 15 min-

[1] This work was supported in part by grants 5T1-GM 240-04 and NB-00485-11 from the United States Public Health Service, and by the Beaumont-May Institute of Neurology
Part of this work was performed during the tenure of Special Fellowship, NINDB, United States Public Health Service.

utes Blocks of the lining of the lateral wall of the body of the lateral ventricle were removed and placed in fresh fixative for an additional 30 minutes. In three animals tissue was quickly removed from the same part of the wall of the ventricle following exsanguination and placed directly into Dalton s solution.

Dehydration was by 10% increments of ethanol from 10 to 100% Tissue was then placed in toluene prior to infiltration in Epon-812. Polymerization was at 60 C for approximately 18 hours. Thin sections cut on glass knives in a Porter Blum microtome were mounted on uncoated grids and stained with lead or uranyl acetate. Sections were examined in a RCA EMU 2D or 3G electron microscope Orginal micrographs were at 2,000 to 11,000 diameters and subsequently enlarged photographically as desired.

OBSERVATIONS

The ependyma of the lateral ventricles of the adult cat fundamentally is similar to ependyma described in other mammalian species (Tennyson and Pappas '62 Brightman and Palay '63) It is a ciliated, cuboidal to columnar epithelium that rarely is ore than one cell thick (fig. 1) The ven- cular or luminal plasma membrane is complexly organized into numerous microvilli and also extends out along the cilia. Rarely a microvillus has a bulbous terminal expansion (fig. 2) There also are other membrane outlined structures containing vesicles and having only a narrow connection with the cell (fig 3) In addition to vesicles with or without dense centers some may even contain mitochondria having irregularly branched cristae (fig 4) The ependymal cytoplasm is pale with scant vesicular endoplasmic reticulum a prominent Golgi apparatus and numerous dense branched mitochondria (figs. 1 5) A tracery of delicate branching fibrils occurs throughout the cytoplasm (figs. 6 7) Along the luminal plasma membrane and at cell junctures these fibrils are arranged in a parallel array and occasionally form small bundles (figs 6 8) Prominent collections of perinuclear fibrils are absent in contrast to those reported in the rat (Brightman and Palay '63) Clear vesicles 20–100 mμ in diameter are distributed throuhgout the cytoplasm and multivesicular bodies are located in the portion in close association with basal bodies of cilia in some instances (figs. 6 9) These multivesicular bodies have a single membrane and contain packets of vesicles approximately 100-200 Å in diameter within a particular matrix (fig. 9) Large ovoid nuclei with well defined nucleoli are located near the base of the cell (figs. 1 5) No basement membrane separates ependymal cells from the subependymal glia and white matter (figs. 1 10)

In the cat, ependymal cilia contain the usual two central filaments surrounded by nine paired peripheral filaments radially arranged. In favorable sections condensations are observed midway between the central and peripheral filaments corresponding to subfibers (Gibbons and Grimstone '60) The proximal portion of each cilium is contained within a depression or pit in the cell surface the membrane of which is more dense than elsewhere (figs 11 12, 13) The plasma membrane at the neck of the cilium is narrowed with close packing of its peripheral filaments and termination of its two central filaments (figs. 12, 13)

The wall of the basal body is formed by a continuation of the nine peripheral paired filaments. They have a parallel course and are tubular in appearance. Although the center of the basal body remains pale it is surrounded by a dense filamentous sytoplasm (figs. 11 12, 13) that often is continuous with that about other basal bodies sometimes even joining the dense specialized cytoplasm at the intercellular junctures (figs. 7 13)

Each of the tubular filaments within the basal body gives rise to multiple cross-striated rootlets along the entire extent of the basal body including its termination. The tubular structure of the filaments disappears shortly after origin of the rootlet (fig 13)

The dense cytoplasm with its enclosed ciliary rootlets measures approximately 800–1 000 Å at its origin tapering to 80-100 Å through most of its length. Rootlets diverge widely from their basal bodies to intertwine with rootlets from neighboring basal bodies and sometimes extend deeply

into the cell (fig. 11) Their cross-striations form a characteristic by which they may be recognized when isolated from the basal body Rootlets from adjacent basal bodies repeatedly touch, fuse or cross although each basal body otherwise remains unconnected to its neighbor (fig. 14)

The cytoplasm immediately around the basal body as well as the rootlets deep in the cell are cross-striated by dense bands about 700–800 A apart (figs 11 12 13 14) that may be resolved into two electron dense lines separated by a pale central zone (fig 12) One or two narrower intraperiod lines occur within the primary banding (figs. 9 12 13) Cross-banding is apparent in unstained sections as well as after staining with either uranyl or lead acetate Mitochondria often occur in close apposition to the rootlets however no consistent relation of cristae to the periodicity of banding can be discerned. Some rootlets extend into a mitochondrial *zonula adherens* complex (fig. 15)

Cross-striated structures several mu in diameter are located adjacent to the nucleus (fig. 11) These structures are rarely seen and serial sections would be necessary to determine their exact origin, however it is possible that they may represent either a fusion of several rootlets or a tangential section of a centriole in which the tubular component is inapparent. They are the only perinuclear specialization of the cytoplasm that was seen in this study

The membranes of contiguous cells near their luminal surfaces are studded with *zonulae adherens* which in tangential sections form an almost continuous line (fig. 6) Two modifications of these membranes are noted. The first corresponds to the *zonula occludens* with fusion of the two cell membranes at the ventricular surface and occasionally even at deeper levels with the appearance of an adjacent *zonula adherens* immediately below (figs. 6 8) The second modification has a complex ultrastructure (figs. 2, 7 15 16) At the luminal surface cells usually are bound together by a *zonula adherens* with each cell membrane remaining distinct, but occasionally a *zonula occludens* tightly closes the intercellular space. *Zonulae adherens* extend for a short distance from the luminal surface of cells. Mitochondria palisade along each side of cell junctures. The space between mitochondria and plasmalemma is packed with fibrils and vesicles (fig 15) The fibrils are arranged parallel to the cell membrane and apparently have no attachment to the dense inner component of the *zonula adherens* The vesicles have a pale center and are indistinguishable from other cytoplasmic vesicles. Discrete cross-striated fibers, presumably ciliary rootlets pass between mitochondria into the fibrillar and vesicular region to terminate near the linearly arranged mitochondria (figs. 15 16) At deeper levels cell membranes possess no specialization and soon are separated by processes of underlying glia or by processes of other ependymal cells (figs. 5 and 10)

Three distinct types of glia underly the ependyma and occasionally occur side by side and hence are not the product of differential rates of fixation. The first and least common contains a large dense oval nucleus and a scant dense cytoplasm. The perinuclear region is dense because of its rich content of ribonucleoprotein (RNP) particles endoplasmic reticulum, and other organelles but with a notable absence of fibrils. Their infrequent elongated processes are small, contain densely packed fibrils and usually are oriented parallel to the surface of the ventricle (fig 10) Myelinated axons touch these cell bodies and their processes. The other and more common cell types have relatively clear cytoplasm of similar density to that of ependymal cells. Their nuclei are ovoid to elongated and contain pale areas in contrast to the homogeneous density of nuclei of the first cell type. Golgi apparatus RNP particles and endoplasmic reticulum are scattered sparsely throughout the pale cytoplasm Cell processes of moderate and small diameter course parallel to the base of the ependyma, intertwine irregularly with similar processes and remain relatively superficial in the white matter (fig 10) Other cells with identical cytoplasm send off large processes which plunge deep into the underlying white matter (fig. 17) Small branches arise perpendicularly from the large penetrating processes and interdigitate with myelinated axons and other cellular processes. Large

bundles of filaments fill the perinuclear cytoplasm as well as the processes. They intertwine among mitochondria and other cytoplasmic components and insert into the plasma membrane (figs. 17 18) Penetrating processes always arise from the underlying glial cells with pale fibrillar cytoplasm where the cell of origin can be identified.

Capillaries and small arterioles occur immediately beneath the subependymal glia as well as within the underlying white matter They have an endothelial lining identical with that of other cerebral vessels however each capillary is surrounded by a small extracellular space delimited by a double basement membrane that may be focally fused (figs. 19 20) This small extracellular space contains collagen. Occasionally the outer basement membrane extends between surrounding processes, enlarging the extent of the small extra cellular space (fig. 20)

DISCUSSION

The variation in ependyma as demonstrated by supravital technics (Feldberg and Fleischhauer '60) as well as by histochemical methods (Fleischhauer '61) places special limitations on the interpretation and comparison of various electron microscopic studies in different regions of the ventricular system of one species much less between different species. Such comparisons however are necessary to advance the growing inquiry into the ultrastructure of ependyma, its organelles and the subependymal glia.

The general appearance of ependymal cytoplasm in the lateral ventricle of the cat with minor exceptions does not differ significantly from previous descriptions of mammalian ependyma. There was no evidence of a perinuclear concentration of filaments as demonstrated by Brightman and Palay ('63) in the third ventricle of the rat, but rather a delicate network of branching filaments similar to that demonstrated by Tennyson and Pappas ('62) in rabbit ependyma. The cytoplasmic vesicular components were similar to those described by these authors. In addition there is in the cat a multivesicular body occurring with regularity near the ventricular surface of ependymal cells. This single membraned structure containing clear and dense vesicles is of unknown significance.

Since Fawcett and Porter's ('54) detailed description of the fine structure of the basal corpuscle its similarities, variations and functions have been the subject of extensive ultrastructural investigation (Sedar and Porter '55 Rhodin and Dahlman, '56 Gibbons and Grimstone '60, Fredricsson and Björkman, '62 Olsson, '63; Aitkin and Johnston '63 Dahl, '63, etc.) Fawcett and Porter ('54) noted in the mollusc that ciliary basal bodies have an electron dense wall enclosing a pale center a well formed basal plate and multiple rootlets with a constant 550–700 Å cross-banding. In amphibians they observed only one such rootlet for each basal corpuscle whereas there were no definite rootlets in the poorly developed ciliary basal bodies of mammals, although cross-banded structures did occur in adjacent cytoplasm.

The fine structure of basal bodies of mammalian ciliated epithelia is now being examined in detail in epoxy-embedded tissue stained by a variety of technics. Fredricsson and Björkman ('62) demonstrated distinct cross-striations similar to those noted in feline ependyma in basal bodies of cilia in epithelia of the human oviduct. Nagano ('62) described cross-striated fibrils with a 600 Å periodicity in the human spermatocyte that he considered to be associated with its centriole Tennyson and Pappas ('62) in their extensive study of the development of ependymal cells in the rabbit, mentioned banded rootlet fibers with a 500–700 Å periodicity in embryos but not in adults. Gibbons and Grimstone ('60) also referred to cross-striated, collagen-like fibers underlying some basal bodies of flagella in *Trichonympha*. Recently Grillo and Palay ('63) reported cross-striation of rootlets of cilia in Schwann cells of the rat autonomic ganglia, Dahl ('63) in neurons in the cerebral cortex of rats as has Olsson ('63) in both *Corella* and *Amphioxus* Most recently *Brightman and Palay* ('63) have demonstrated cross-striated bodies in the ependyma of the third ventricle of the rat but could not relate such structures to the basal body or ciliary rootlets. In comparative studies of the rat and mouse as well

as in the present study on the cat, cross-striations have been a common feature of ciliary rootlets in ependymal cells of adult mammals. They are less apparent in thin sections and hence can be overlooked unless specifically sought, and undoubtedly vary in frequency in different species although constantly present in the cat.

The tubular character of the wall of the basal body has been demonstrated by Rhodin and Dahlman ('56) in rat tracheal epithelium, where they noted that the triple tubular component fused into a net like structure deep within the basal body. They also described unstriated rootlets arising only from the tip of the basal body and then curving in a single direction. On the side of the basal body opposite to the direction of the rootlets there was an area of high cytoplasmic density perpendicular to the long axis of the basal body. In our material the basal body appeared similarly organized although rootlets diverged in many directions and arose along its entire extent. In addition the zone of cytoplasmic density entirely surrounded the basal body and was distinctly cross-striated. A very similar configuration of the basal body and rootlet origin was noted by Brightman and Palay ('63). In the present study even the center of the rootlet occasionally was tubular at its origin, a finding similar to that in ciliary rootlets in the avian oviduct (Aitkin and Johnston, '63).

Cross-striations of the cytoplasm surrounding the basal body and its rootlets are not as unusual as has been inferred. They have been observed in many species from protozoa (Sedar and Porter '55) to the human being (Fredricsson and Björkman, '62) and in all probability reflect a protein structure. The exact chemical nature of these cross-striations remains unknown although Olsson's ('63) recent observations of mitochondrial cristae closely apposed to the dense bands in lower chordates has been interpreted as suggestive evidence for a high local metabolic demand. In recent years stabilizing properties have been attributed to rootlets principally because of their superficial resemblance to collagen (Fawcett, '61) although light microscopists and physiologists had previously assumed that rootlets had a relationship to ciliary motion (e.g. Klein, '28; von Gelei, '32; Corliss '61).

Definite fusion and intersection of ciliary rootlets has been demonstrated in the ependyma of the cat. These interrelations are observed both adjacent to the basal body and as deep as the nucleus. These fusions might occur between rootlets of centrioles and basal bodies as well as between two or more basal bodies. In addition, ciliary rootlets extended between mitochondria linearly arranged at the specialized areas of cell junctures. A similar linear array of mitochondria along the plasmalemma has been described by Tennyson and Pappas ('62) in adult rabbit ependyma.

Previous investigations have not emphasized the recurrent close relationships that rootlets form with one another nor have they described the relationship of rootlets to cell junctures. The dangers of physiologic speculation from these anatomic observations are legion, but it is difficult to avoid considering a correlation between metachronal ciliary beat and the necessity of transmission of this rhythm between cilia, and indeed between cilia of different cells. The current theories of transmission have been reviewed thoroughly by Fawcett ('61) and by Sleigh ('62) and are beyond the scope of this paper. However if future investigations of other ciliated epithelia reveal similar ultrastructure an adequate explanation of metachronal ciliary activity should weigh the proximity of rootlets to the specialized plasmalemma and their close association to one another.

A detailed discussion of the specialization of the membrane between ependymal cells has recently been published by Brightman and Palay ('63) and this study confirms their observations. They have used the terminology proposed by Farquhar and Palade ('63) which also has been followed in this study.

Two, and possibly three, types of glial cells have been recognized in subependymal white matter in the cat. Previously Palay ('58) described fibrous astrocytes beneath rat ependyma. He compared them with those seen after stab wounds and described a cell containing numerous fi-

PLATE 1

EXPLANATION OF FIGURES

1 A low magnification of ependyma of the lateral ventricle of the cat illustrates single ependymal cell layer with underlying processes and myelinated axons. Portions of three ependymal cells are separated by plicated membranes which interdigitate complexly. Cilia and microvilli are seen in cross section at the luminal surface. Mitochondria are prominent above the nuclei. The clear cytoplasm contains many fibrils, RNA particles, ergastoplasm, vesicles and Golgi apparatus. Processes with similar cytoplasm to ependymal cells are noted at their base as is a single dark process containing closely packed fibril. N basement membrane separates ependymal cells from the underlying processes and myelinated axons. × 13,000.



PLATE 1

EXPLANATION OF FIGURE

1 A low magnification of ependyma of the lateral ventricle of the cat illustrates single ependymal cell layer with underlying processes and myelinated axons. Portions of three ependymal cells are separated by plicated membranes which interdigitate complexly. Cilia and microvilli are seen in cross section at the luminal surface. Mitochondria are prominent above the nuclei. The clear cytoplasm contains many fibrils, RNA particles, ergastoplasm, vesicles and Golgi apparatus. Processes with similar cytoplasm to ependymal cells are noted t their base as is single dark process containing closely packed fibril. No basement membrane separates ependymal cells from the underlying processes and myelinated axons. × 13,000.



PLATE 1

EXPLANATION OF FIGURES

2 The ventricular surface of ependymal cells exhibits microvilli and other cell processes with narrow bases extending into the ventricular lumen. At the center is an example of the close relationship of mitochondria to a tangentially sectioned plasma membrane with a *zonula adherens* at the cell surface. × 20,000.

3 A cell process similar to those in figure 2 contains numerous light and dark vesicles. × 20,000.

4 Similar processes to those in figures 2 and 3 contain mitochondria. In addition numerous vesicles are present. × 20,000.

PLATE 3

EXPLANATION OF FIGURES

5 A tangential section of ependymal cells demonstrates cilia and their basal bodies at upper right. In the lower half of the illustration processes of ependymal cells and of subependymal glia extend between cells. × 8,000

6 A tangential section through the most superficial portion of ependymal cells demonstrates microvilli and cilia at the luminal surface and numerous *zonulae adherens* form almost continuous lines between the three cells illustrated. A *zonula occludens* is illustrated at right center × 12,000



PLATE 4

EXPLAN TION O FIGURES

7 An example of mitochondria in close association with the specialized cell juncture containing severeal *zonulae dherens* is shown t left. In addition, it can be noted that the dense cytoplasm from a neighbor ing basal body becomes continuous with the dense fibrillar cytoplasm *along the cell membrane.* × 48,000.

8 An example of *zonula occl den* with a *zonula dheren* immedi tely deep to its inner extent. A small collection of parallel arranged fibrils course beside the cell juncture. × 70,000

9 A high magnification of two multivesicular bodies shows the single limiting membrane and the smaller size of their vesicles than those shown generally in the surrounding cytoplasm. × 50,000


8



PLATE 5

EXPLAN TION OF FIGURE

10 An ependymal cell is seen in the upper half of the illustration with typical plicated intercellular membranes. A fibrous astrocyte with an elongated nucleus and process extending parallel to the ventricular surface lies immediately beneath the ependymal cell. In close p-proximation with myelinated axon glial cell with dense cytoplasm is noted Fibrils are present in the process at right but are not apparent in the perinuclear cytoplasm. / 8,000



PLATE 6

EXPLAN TION OF FIGURE

11 A relatively thick section of portion of the pex of two ependymal cells illustrates cilia projecting from depression in the plasma lemma. The peripheral filaments of the cilia pack together nd the plasma membrane and cytoplasm become more dense at the neck of the cilium. Within the basal bodies the peripheral filaments f the cilium continue as the tubular component f the wall. The walls of the basal body are parallel in longitudinal sections but ellipsoid when sectioned obliquely Numerous rootlets penetrate deeply into the cytoplasm and come into close proximity to one another At upper left the rootlets from basal body pass into specialized cell junc ture A multivesicular body is present t lower right and cross-striated structure pproxim tely half micron cross is present t lower right. × 28,000

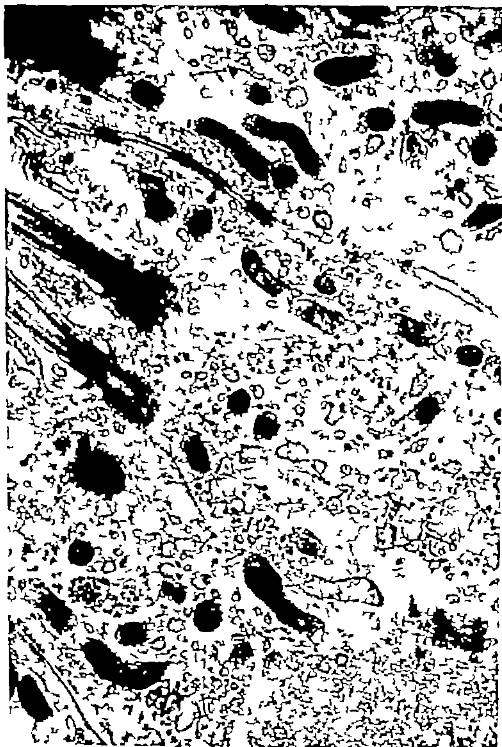


PLATE 7

EXPLAN TION OF FIGURES

12 A longitudinal section through three basal bodies and their cilia demonstrates the tubular character of the filaments of the wall and the cross-striations of the surrounding dense cytoplasm. In the central basal body the lucent center of the major cross-striation is evident. × 46,000.

13 A longitudinal section of two basal bodies and an oblique section of another constrasts th appearance produced by the plane of section The tubules of the wall are distinctly parallel in the lower basal body while they appear to converge in the pper example. Rootlets arise from the sides and termination of the tubules and course in close proximity to a mitochondrion The dense fibrillar cytoplasm sur rounding the basal body extends laterally and appears continuous with that of its neighbor × 46,000

14 Several rootlets illustrate how frequently anastomoses occur between these cross-striated tructures. At lower center rootlets from basal body or centriole join rootlets of second basal body almost t their origin. At lower right third cross-striated tructure almost touches the same rootlet. At upper right two rootlets ppear to cross. × 18,000.

12

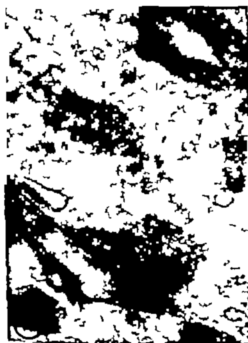




PLATE 6

EXPLANATION OF FIGURES

15 A high magnification of cell juncture which demonstrates the dark external component and less dense inner component of the *zonula adherens*. Mitochondria palisade on each side of the cell juncture and the space between is crowded with fibrils and vesicles. A cross-striated rootlet courses into close relation to the mitochondria and appears to be directed between them. The lucent center of the major cross-striation is apparent in the rootlet as are three or four intraperiod dense lines. × 50,000.

16 An example of a tangentially sectioned specialized cell juncture demonstrates cross-striated structure presumably ciliary rootlet, lying between mitochondrion and the nearby *zonula adherens* × 30,000.



PLATE 9

EXPLAN TION O FIGURES

17 An ependymal strocyte sends a large process deep within the peri ventricular white matter A small portion of the perinuclear cytoplasm is noted in the pper portion f the illustration while the giant process sending sm ll processes laterally descened between myelinated axons. Cl mps of filaments fill the center of the process with other organelles being present toward the periphery × 10 000

18 Several processes f subependymal astrocytes demonstrate cytoplasmic fil ments inserting into the cell membrane. × 20,000.

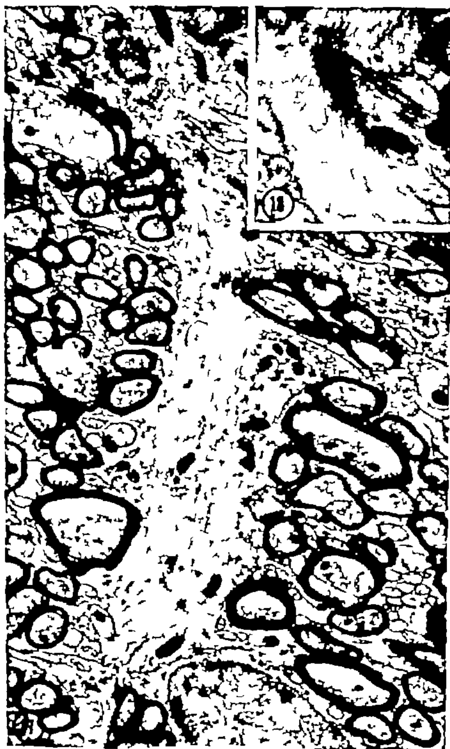

18

PLATE 11

EXPLAN TION O FIGURE

20 Another capillary demonstrates the extension of the basement membrane between astrocytic processes t upper right. Fusion f the two components of the basement membrane extend over several short segments in the center of the Ill stration. × 20,000.



The Anatomy of the Arterial Supply to the Cranial Regions of the Sheep and Ox

R. A. BALDWIN
Department of Physiology Royal Veterinary College London, N.W.1

ABSTRACT By means of neoprene latex injected preparations the anatomy of the arterial supply to the brain has been determined in the sheep and ox. In these two ruminant species, blood destined for the Circle of Willis and thence the brain must first pass through well-developed intra-cranial carotid rete. The main source of blood supply to the carotid rete in the sheep is from the external carotid artery via branches of the internal maxillary artery

In both the sheep and the ox, the internal carotid artery is poorly developed in the young animal and the portion proximal to the carotid rete is absent in the adult. The internal carotid artery in animals of all ages, can be traced through the rete to emerge as the efferent vessel, which divides to form the Circle of Willis.

In the ox, the main source of blood supply to the intra-cranial carotid rete is the external carotid artery via branches of the internal maxillary but, in addition the rete communicates directly with the vertebral arteries by way of the basi-occipital arterial plexus.

Unlike most other species, the basilar artery in both sheep and ox has only tenuous connections with the vertebrals. In both species, the basilar artery tapers caudally and is continued as the ventral spinal artery The basilar can therefore be regarded as caudally directed branch of the Circle of Willis in both these animals. A well-developed occipito-vertebral anastomosis is marked feature of the cephalic circulation in both sheep and ox.

Before proceeding to experimental studies on the cephalic circulation in the sheep and ox (Baldwin and Bell '63a '63b) it has been necessary to ascertain the routes by which arterial blood could reach the brain in these animals. Search of the literature revealed a paucity of reliable information on this topic the recognized text books of veterinary anatomy give the subject scanty consideration. Sisson ('53) refers only to major differences between the cerebral blood supply of the ox in comparison with the horse and hardly mentions the cranial vessels in the sheep. Chauveau (1891) also takes the comparative viewpoint using the horse as the type subject but gives some account of the distribution of the relevant vessels in both ox and sheep. Texts by Montane and Bourdelle ('17) and McLeod ('58) were not considered sufficiently complete or reliable to provide a basis for experimental work.

Tandler (1899) in his classical work on the arteries of the brain in a wide variety of mammals mentions the ox briefly and assumes the anatomy of these vessels in the sheep to be similar Schmidt ('10) gives an accurate account of the cranial blood vessels of the ox which has obviously provided a basis for the text of Ellenberger and Baum ('43) Ask-Upmark ('35) also considers that the cranial arteries of the sheep are identical with those of the ox. Daniel, Dawes and Pritchard ('53) describe the carotid rete and its formative arteries in a number of species including the sheep and ox, but they have necessarily concentrated upon these structures and only refer in passing to the vertebral arteries. Furthermore these latter authors were only able to examine one specimen of the ox, that of a four month-old calf

The carotid rete which is a striking feature of the cephalic circulatory system in both the sheep and ox is believed to have been discovered by Herophilus, although the first detailed account of it is given by Galen (Cole '44)

More recent investigations of the rete include those of Ask Upmark ('35 '44 and '53) Its histological structure has been

Present address Department of Physiology University of California Medical Center, Los Angeles 24, California.

studied by Boissezon ('41) and Legait ('45) Davis and Storey (43) have described the cranial blood vessels of the cat including an account of the rete The paper by Andersson and Jewell ('56) on the distri bution of carotid and vertebral blood in the brain and spinal cord of the goat contained some observations on the hemodynamic significance of the carotid rete

The present paper sets out the results of an anatomical investigation of the distribution of the arterial blood vessels of the cranial region in these two ruminant species.

MATERIAL AND METHODS

Material was examined from 20 oxen The specimens varied in age from one week to five years but the majority of the animals were calves a few weeks old Material was examined from 20 sheep ranging in age from birth to over four years Two pigs approximately four months of age, were examined. Direct measurements of the external diameter of the carotid and vertebral arteries were made on anesthetized animals under going surgical preparation for experi mental studies

Injection of Neoprene Latex

Fresh specimens of the sheep and calf both abattoir material and from animals employed in the experimental work, were used to prepare neoprene latex casts of the vessels of the head and neck.

The neck was usually severed between the fifth and sixth cervical vertebrae La tex was injected into the carotid arteries in the midcervical region following perfusion with saline in order to remove any remaining blood

On completion of the injection the specimens were placed in a dilute solution of hydrochloric acid for 24 hours in order to solidify the neoprene latex The skin which retards subsequent maceration was then removed and the specimens treated in various ways depending upon the type of preparation required

a *Preparation of a simple Neoprene latex cast* The skinned specimen was placed in concentrated hydrochloric acid for about seven days until the tissues were macerated sufficiently to allow careful removal of the latex casts. The casts were cleaned by placing them into water and removing any adherent tissue debris by brushing, or if fat remained attached to the cast, by placing it in 20% potassium hydroxide for a few days.

b *Preparation of Neoprene latex casts in relationship to the skull and cervical vertebrae* This technique was developed in order to preserve the relationship between the injected vascular system and the skeletal structures. After making a normal neoprene injection and hardening the latex in dilute hydrochloric acid the specimen was skinned and macerated in a water tank at 60 C when after a period of 7 12 days according to the size of the specimen an intact cast together with the skeletal structures remained

c. *Preparation of radiopaque Neoprene injections* A stabilized suspension of barium sulphate was added slowly with constant stirring to the neoprene latex until a mixture of two parts latex to one part barium sulphate was obtained. Barium sulphate in excess of this caused an increase of viscosity of the mixture and precluded successful injection. The radiopaque latex was injected in the usual way and the cast hardened by immersion of the specimen in acid formalin Stereoradiographs of such preparations have proved very useful in determining the relationship of the cranial blood vessels to the structures of the head and neck. These specimens have the further advantage that dissection can be carried out and more radiographs taken at subsequent stages

d. *Preparation of Neoprene latex casts of the venous system* These casts were made by retrograde injection of latex into the external jugular veins after perfusion of the specimen with normal 0.9% saline in the usual manner Specimens were also prepared in which both the arterial and venous systems were injected with neoprene latex simultaneously

Histological examination of the carotid rete

For microscopical examination formalin-fixed carotid retia from sheep and calves were sectioned at 5 µ and stained with hematoxylin -eosin or Masson's trichrome stain

Measurement of the common carotid and vertebral arteries in the living animal

These measurements were made with calipers on vessels exposed surgically for experimental studies. The common carotid arteries were measured in the mid-cervical region and the vertebral arteries on their extra-thoracic course near to the foramen transversarium of the sixth cervical vertebra.

OBSERVATIONS

Results in the Ox

The carotid rete The carotid rete in the ox is intra-cranial, lying sub-durally in the cavernous sinus It consists of two halves which are in communication anteriorly and posteriorly through numerous anastomotic vessels (pl. 1 fig. 4) The rete extends from the foramen orbito rotundum anteriorly to just beyond the foramen ovale posteriorly It is composed of a complex mass of intertwining anastomotic arteries which are largest on the dorsal surface. The two halves of the rete lie on each side of the pituitary body and, because of the anterior and posterior communicating branches, the rete effectively surrounds the pituitary body Arterial blood destined for the Circle of Willis can only reach this structure after passing through the rete. In the ox, the rete possesses an anterior V-shaped extension which enters the optic foramina, one arm of the V accompanying each optic nerve through the foramen (pl. 1 fig. 4) The distal ends of these extensions emerge into the orbital cavity to be joined by small branches from the arteria anastomotica

The rete receives an afferent blood supply from two branches of the internal maxillary artery the arteria anastomotica and the ramus anastomoticus the internal maxillary artery being the continuation of the external carotid artery (pl. 1 fig. 2) The internal carotid artery in the ox is thread-like and contributes to the rete only in the young animal. On the other hand, the large basi-occipital plexus, derived from the vertebral and occipital arteries constantly makes a large contribution to the rete posteriorly (pl. 2, fig. 8) Another but minor source of blood supply to the rete is from the accessory meningeal artery a branch of the superficial temporal artery These branches are given off in the temporal canal and enter the cranial

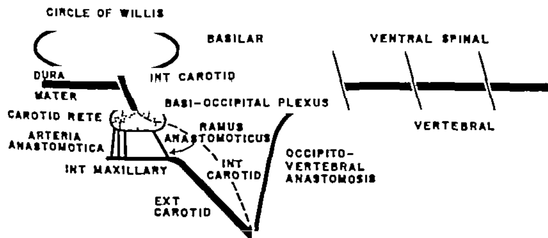


Fig. 1 Diagram illustrating the arrangement of the cephalic arteries in the calf. The dotted line indicates that the internal carotid artery does not persist in the adult.

cavity between the petrous temporal and the parietal bones and supply the lateral part of the rete

The rete has a single efferent vessel the homologue of the distal portion of the internal carotid. This vessel emerges from the dorso-medial surface (pl. 1 fig. 4) to pierce the dura mater before dividing into anterior and posterior branches which unite to form the Circle of Willis

Histological examination shows that the arterial network of the rete is surrounded by a delicate connective tissue adventitia with a layer of endothelial cells on the outside. These cells form the intima of the venous lake surrounding the arterial rete in the cavernous sinus

The Arteria Anastomotica. These vessels arise from the internal maxillary artery and enter the cranial cavity through the large foramen orbito-rotundum (pl. 2, fig. 5) In this foramen they are accompanied by the third fourth and sixth cranial nerves together with the maxillary and ophthalmic divisions of the fifth cranial nerve.

These arteries constitute the major route by which carotid blood from the internal maxillary artery enters the rete Usually three or four main arterial stems are deved from the internal maxillary artery d these subdivide as they enter the cranal cavity to supply the antero-lateral border of the rete. Immediately on entering the rete they ramify within it so that their subsequent distribution within this structure cannot be traced by dissection. In addition to the main branches of the arteria anastomotica supplying the rete other small branches arising just anterior to the main ones connect within the orbital cavity with the distal extra-cranial end of the V shaped anterior extension of the rete.

The ramus anastomoticus In the ox this is a small vessel arising from the internal maxillary artery which enters the cranial cavity via the foramen ovale along with the mandibular division of the fifth cranial nerve (pl. 2, fig. 5) The ramus anastomoticus enters the posterior-lateral border of the carotid rete to ramify immediately within it so that its subsequent course within the rete cannot be identified. The ramus anastomoticus is considerably smaller in diameter than the combined branches of the arteria anastomotica.

The internal carotid artery This vessel arises either from the common carotid artery at its division into occipital, external maxillary and external carotid arteries or from the base of the occipital artery It does not give off any branches during its course to the cranial cavity through the foramen lacerum but in the foramen exhibits a characteristic curl.

The vessel enters the rete caroticus ventrally near its posterior end, but unlike the other afferent vessels does not immediately *ramify within the complex* and lose its identity for its course through the rete can be clearly established by dissection (pl 3 fig 11) As shown by Daniel et al ('53) as the internal carotid passes through the rete it is joined by numerous branches so that it rapidly increases in calibre before emerging on the dorso-medial aspect of the rete as the single trunk which pierces the dura mater and divides into anterior and posterior branches to form the Circle of Willis

In specimens from animals a few weeks old the calibre of the internal carotid artery as revealed by latex injection, is almost equal to that of the ramus anastomoticus but with increasing age the internal carotid artery shows marked regression. It has been possible to demonstrate the internal carotid artery in animals 18 months old and in one case, it was still present unilaterally as a fine threadlike vessel in an animal four years old However it is not a significant source of blood to the rete in animals more than a few weeks old and usually is absent in animals over the age of 18 months When the rete from an adult animal is dissected although the internal carotid artery proximal to the rete has atrophied, the "intrarete portion persists and retains its individuality

The basi-occipital plexus. This large arterial plexus lie subdurally upon the basi-occipital bone (pl 2, fig 8) There is considerable individual variation in the size and complexity of the plexus.

The plexus is supplied posteriorly by the vertebral arteries and laterally by the condyloid branch of the occipital artery The plexus passes forward to unite with the posterior margin of the carotid rete con-

tributing some vessels to the posterior junction between the halves of the rete. Usually it takes the form of three large vessels which enter the rete with a supporting or a "bridging" vessel running between them as they join the rete

The occipital artery The occipital artery is one of the terminal branches of the common carotid artery At its origin there is a bulge which is considered to be the cardio-respiratory reflexogenic area of the carotid in ruminants.

The condyloid artery a large branch of the occipital enters the cranial cavity through the hypoglossal foramen and divides into two branches, the anterior limb uniting with the basi-occipital plexus and the posterior limb with the vertebral artery A large and important occipito-vertebral anastomosis occurs in the ox providing a link between the common carotid and vertebral arteries (pl. 1 fig. 2)

The vertebral arteries. These vessels arise from the subclavian artery on the left side and usually from the brachiocephalic trunk on the right side but occasionally the right vertebral may arise from the right subclavian artery adjacent to the brachiocephalic trunk.

The vertebral arteries leave the thoracic cavity anterior to the first rib and enter the foramen transversarium of the sixth cervical vertebra. Shortly after emerging from beneath the first rib the arteries give off a large branch which supplies the dorsal cervical musculature and which Sisson ('53) terms the dorsal cervical branch. A smaller dorsal muscular branch is given off immediately before the vertebral trunk enters the foramen transversarium of the sixth cervical vertebra.

The vertebral arteries have a typical course in the neck passing anteriorly in the foramina transversaria of the cervical vertebrae. At each intervertebral junction anastomotic branches are given off these cross the floor of the vertebral canal to unite with similar branches from the opposite vertebral. These branches also communicate with each other anteriorly and posteriorly forming irregular polygonal figures on the floor of the vertebral canal. The vertebral arteries and their anastomotic branches communicate with the ventral spinal artery by means of small anastomotic branches which penetrate the dura. Large branches to the cervical musculature are given off at each intervertebral junction.

The vertebral arteries leave the foramina transversaria at the junction of the second and third cervical vertebrae to enter the spinal canal and continue forward to the cranial cavity through the foramen magnum. In their course branches are given off at the atlanto-axial joint which emerge from the dorsal foramen in the wing of the atlas to supply the muscles in this region.

Just inside the cranial cavity the vertebral arteries unite with the anastomotic branches from the occipital arteries which have entered via the hypoglossal foramina, to constitute the basi-occipital arterial plexus which passes forward to unite with the rete caroticus (pl. 2, fig. 8) It is noticeable that in the ox the vertebrals make only insignificant connections with the basilar artery by way of the ventral spinal artery The relative diameters of the carotid and vertebral arteries in calves are given in table 1

The Circle of Willis After piercing the dura, the internal carotid arteries divide into anterior and posterior branches which form the well-developed Circle of Willis and this gives off three main branches, the anterior cerebral, the middle cerebral and the posterior cerebral arteries (pl. 3 fig 10) Numerous small thalamic arteries are also given off by the posterior communicating arteries. The Circle of Willis is completed rostrally by the small anterior communicating artery (pl. 2, fig 7) and posteriorly by the much larger posterior communicating arteries. In one specimen (a calf a few weeks old) it was possible to demonstrate that the anterior extension of the carotid rete communicated with the Circle of Willis by means of two small branches which pierced the dura and joined the Circle of Willis near the origin of the anterior cerebral arteries.

In the ox the basilar artery can be regarded as a branch of the Circle of Willis. This is in contrast to many other species where it is formed by the confluence of the vertebral arteries and passes forward to join the posterior communicating arteries In the ox the basilar artery tapers caudally and the disposition of the acute angles

a much more complex structure than in the sheep

In the sheep as in the ox, the internal carotid artery is not important in supplying blood to the rete, for usually it is impossible to demonstrate the artery in animals older than nine months although the distal portion between the rete and the Circle of Willis remains well developed and patent at all ages.

Daniel et al. ('53) claim that the sheep does not possess an internal carotid artery except for the distal portion between the carotid rete and the Circle of Willis. They describe a vessel which they term the ascending pharyngeal artery arising from the occipital artery They were only able to demonstrate this vessel in the near term *fetus. From their account and illustrations*, however it is likely that this is a misnomer for the internal carotid as described in this study The fact that the course of the vessel described by Daniel et al. ('53) *can be traced through the carotid* rete as one can trace the internal carotid artery in the calf supports the interpretation that this vessel in the sheep is in fact the internal carotid. In the carotid rete of the pig it has been possible to demonstrate that the ascending pharyngeal artery which is well-developed in the species, does not continue through the rete to join the Circle of Willis.

The sheep possesses a well-developed occipito-vertebral anastomosis in the form of a loop. The observation made by Canova ('09) that an arterial branch from the occipital enters the foramen in the lower border of the wing of the atlas vertebra and unites with the vertebral, has been confirmed.

The latex preparations have confirmed the observation by Daniel et al. ('53) that the basilar artery tapers caudally in the sheep. This is also so in the ox, so that in both species the basilar is reduced to the status of a posteriorly directed branch of the Circle of Willis with only tenuous connections with the vertebral arteries through the ventral spinal artery

In the sheep the vertebral arteries, close to their origin, are much smaller than those of the ox, in comparison with the common carotid arteries. In the sheep the vertebrals take no part in the supply of blood to the carotid rete. By way of the minor connecting branches with the small ventral spinal artery vertebral blood may pass to the spinal cord, which is the case in the goat (Andersson and Jewell, '56) Well developed side to side anastomoses between the vessels supplying both sides of the head and brain exist in the sheep, principally in the posterior communicating arteries of the Circle but also in the rete by means of a few connecting strands. Another side to side anastomosis is provided by the anastomosing vessels between the vertebral *arteries*.

As in the ox, the main connection between the intra-dural vessels of the Circle of Willis and extra-dura blood vessels of the rete caroticus is provided by the persistent distal portion of the internal carotid artery

The great difference between the cerebral circulation in the ox and sheep is the presence in the ox of a well-developed basi-occipital plexus which permits a direct communication of the vertebrals with the carotid rete and thence to the Circle of Willis. In the sheep vertebral blood has no direct access to the rete and is restricted to the cervical spinal cord and possibly to the posterior medulla oblongata.

ACKNOWLEDGMENT

I wish to thank Professor E. C. Amoroso for providing facilities for this investigation and Dr F R. Bell for his advice and help. I am also grateful to Miss J Harb for her technical assistance. The work was generously supported by the Animal Health Trust.

LITERATURE CITED

Andersson, B., and P Jewell 1956 The distribution of carotid and vertebral blood in the brain and spinal cord of the goat. Quart. J Exp. Physiol., 41 462–474.

Ask-Upmark, E. 1935 The carotid sinus and the cerebral circulation. An anatomical, experimental and clinical investigation. Including some observations on rete mirabile caroticum. Acta Psychiat., Kbh., Suppl., 6: 1–374.

——— 1944 Uber die makro-anatomisch zu beobachtendem Schutzvorrichtungen des Gehirns gegen vaskulare Insulte. Acta Path. Microbiol. Scand. Suppl., 54 530–538.

——— 1953 On the entrance of the carotid *artery into the cranial cavity in Stenops gracilis* and Otolicnus crassicaudatus. Acta Anat., 19 101–103.

Baldwin, B. A., and F R. Ball 1963a The anatomy of the cerebral circulation in the sheep and ox. The dynamic distribution of the blood supplied by the carotid and vertebral arteries to cranial regions. J Anat. (Lond.) 97 203–215.

——— 1963b The effect of temporary reduction in cephalic blood flow on the EEG of sheep and calf. Electroenceph. clin. Neurophysiol., 15 465–473.

de Bousseron, P 1941 Le reseau admirabile arteriel intracranien de l'agneau Bull. de la Soc. d'Hist. Nat. Toulouse., 76 299–304

Canova, P 1909 Die arteriellen Gefässe des Bulbus und seiner Nebenorgane bei Schaf und Ziege. Arch. Anat. Physiol. Lpz., An t. Abt. 1–48.

Chauveau, A. 1891 The comparative anatomy of the domesticated animals. 2nd English edition revised with the co-operation of Arloing S Trans. and Ed. Fleming, G London Churchill.

Cole, F J 1944 A history of Comparative Anatomy From Aristotle to the Eighteenth Century 1st ed. London Macmillan.

Daniel, P M., J D. K. Dawes and Marjorie M. L. Pritchard 1953 Studies of the carotid rete and its associated arteries. Philos. Trans. B 237 173–208.

Davis, D. Dwight, and Elizabeth H. Story 1943 The carotid circulation in the domestic cat. Zoological series Field Museum of Natural History Vol. 28 No. 1 Publication 527

Ellenberger W and H. Baum 1943 Handbuch der vergleichenden Anatomie der Haustiere Revised by O Zietzschmann, E. Ackerknecht and H Grau, 18th ed. Berlin Springer Verlag.

La Rocca, E. 1911 Le fasi di sviluppo di regresso dell' arteria carotide interna in "Bos T urus. Ric. Lab. Anat. Norm. Univ Roma, 16 107–113

Legait, E. 1945 Corpuscles nerv ux dans la parois des arteres du reseau admirable carotidien. C. R. Soc. Biol. Paris, 139 340–341

McLeod, W 1958 Bovine Anatomy 2nd. Ed. Revised by M. M. Trotter and J W Lumb, Minneapolis U.S.A. Burgess Publ. Co.

Montane L., and E. Bourdelle 1917 Anatomie regionale des animaux domestiques. Paris Librairie J -B Baillière et Fils.

Rogers, L. C. 1947 The function of the Circulus Arteriosus of Willis. Brain, 70 171–178.

Schmidt, K. 1910 Die arteriellen Kopfgefässe des Rindes. Int. Mschr Anat. Physiol., 27 187 264

Sisson, S. 1953 The anatomy of the domestic animals. Revised by J D Grossman, 4th Ed. Philadelphia and London W B Saunders Company

Tandler J 1899 Zur vergleichenden Anatomie der Kopfarterien bei den Mammalia. Denkschr Akad. Wiss. Wien 67 677–784

Abbreviations

A Arteria nastomotica
A.C., Anterior cerebral artery
A Com., Anterior communicating artery
B, Basilar artery
B O., Basi-occipital arterial plexus
C.C., Common Carotid Artery
C.R. Carotid Rete
C.O W Circle of Willis
E.C., External Carotid Artery
I.C., Internal Carotid Artery
I.M., Internal Maxillary Artery
I.D Inferior dental artery
M C., Middle cerebral artery
O Occipital Artery
O.F Optic foramina
P C., Posterior cerebral artery
P C.L., Processus Clinoideus
P.Com., Posterior communicating artery
R.A., Ramus Anastomoticus
V Vertebral Artery
V.S Ventral Spinal Artery
V.Ext., Anterior V-shaped Extension of the Carotid Rete

PLATE 1

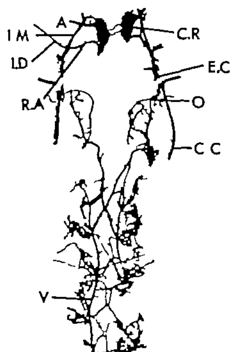
EXPLANATION O FIGURES

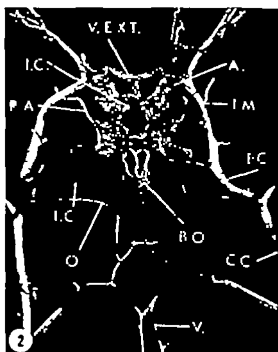
1 Sheep. Dorsal view of latex cast showing the disposition of the arteries concerned in the cerebral blood supply The Circle of Willis has been removed. (Approx. × ¼)

2 Ox. Dorsal view of latex cast showing the disposition of the arteries concerned in the cerebral blood supply The Circle of Willis has been removed (Approx. × ⅓)

3 Sheep. Dorsal view f latex cast of the carotid rete i itu The basi-occipital bone has been removed (Approx. × 2¼)

4 Ox. Dorsal view f latex of the carotid ret i itu The basi-occipital bone has been removed. (Approx. × 2½)


A
I M
I.D
C.R
E.C
R.A
O
C C
V
1


V. E X T.
I.C
A.
R A
I M
E C
I.C
B O
O
C C
V.
2


I C
P C L
C R.
3


O.F
V E X T
I.C
C R.
B O
4

PLATE 2

EXPLANATION OF FIGURES

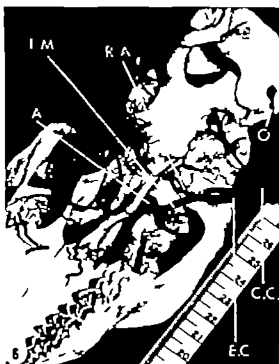
5 Ox. Ventro-lateral view of cast showing the arteries which enter the cranial cavity The arteria anastomotica enter *via* the foramen orbito-rotundum. The ramus anastomoticus enters *via* the foramen ovale and the occipital artery enters *via* the hypoglossal foramen (metric scale)

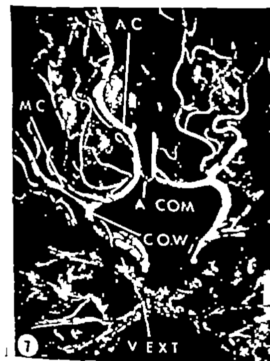
6 Sheep Ventral view of cast showing the arteries which enter the cranial cavity The arteria anastomotica enter *via* the foramen orbito rotundum. The ramus anastomoticus enters *via* the foramen ovale. The occipital artery enters *via* the hypoglossal foramen and large branch passes to the alar foramen in the wing of the atlas (metric scale)

7 Ox. Latex cast of the Circle of Willis displaying the anterior communicating artery The anterior V shaped extension of the carotid rete is also shown. (Approx. × 2)

8 Ox. Latex cast showing the basi-occipital plexus *in situ* The occipital artery is shown entering the cranial cavity *via* the hypoglossal foramen. (Approx. × 3)


A.
R.A.
I M.
E C
C C
O
5


I M
R A
A
O
C.C.
E.C
6


A C
M C
A COM
C.O.W.
V E X T
7


C R
O
B O
V.
8

Articular Remodeling in the Adult Human Temporomandibular Joint [1]

BENJAMIN C. MOFFETT JR.,[2] LENT C. JOHNSON,[3] JAMES B. McCABE[4] AND HAROLD C. ASKEW[4]

Department of Anatomy, University of Alabama Medical Center, Birmingham, Alabama

ABSTRACT Articular cartilage can proliferate sufficiently to alter the contours of joints, allowing them to adapt morphologically to various mechanical stresses. This remodeling has been classified into three types based on histologic criteria which were then applied to the temporomandibular joint. This joint has a fibrous type of articular tissue which is converted postnatally into fibrocartilage in the loaded areas. The thickness and cell population of this tissue and the amount of internal reconstruction in the subchondral bone vary from one part of the joint to another. These changes appear related to the distribution of mechanical stresses in the joint. Conclusions drawn are: The temporomandibular joint shows the following remodeling trends: progressive remodeling on the anterior part of the condyle, medial part of the tubercle, and roof of the mandibular fossa; regressive remodeling on the posterior part of the condyle and on the lateral part of the tubercle. A perforation in the disc causes progressive remodeling on the condyle and regressive remodeling on the tubercle at the perforation site. Articular remodeling merges gradually into osteoarthritis as the articular tissue breaks down. The net effect of remodeling that has become uncompensated or pathologic is: condyle flattened and enlarged, tubercle resorbed, disc perforated, and articular surfaces uneven. If the dentition is not restored or replaced, a high rate of temporomandibular remodeling occurs which will probably continue into osteoarthritis.

Joints have long been regarded as unchanging structures which maintain the same articular structure and cell population throughout adult life. A growing body of data indicates, however, that articular cartilages continue to proliferate after growth ceases and that they modify their shape throughout the entire lifetime of the individual. Johnson ('59) reviewed the evidence for this opinion and pointed out that the boundary between normal age changes and degenerative joint disease is difficult to define.

If such modifications of structure and contour occur in the temporomandibular joint, they would have a bearing on the clinical management of many problems involving this joint and the dentition. This paper will describe the evidence for articular remodeling of the temporomandibular joint.

The earliest presentation of the concept of articular remodeling is that of Ogston (1875, 1878). He described and illustrated in articular cartilage the presence of:

1. A zone of central growth located just superficial to the midpoint in thickness of the articular cartilage and consisting of cellular proliferation as shown by clones of new cartilage cells.

2. The lining up of these cartilage cells into cell columns just above the subchondral plate where they duplicate the pattern and behavior of an epiphyseal growth plate by adding to the subchondral bone.

3. The removal of disintegrating cells and cartilage from the superficial surface by means of articular movement with replacement of this tissue occurring by growth upward from the zone of central growth.

Ogston believed that cartilage continually renews itself from the zone of central growth and that it grows in two directions — towards the subchondral plate and towards the articular surface. His studies

---

[1] This investigation was supported by PHS research grants A-664 and A-[illegible]. It was completed during the tenure of Special Research Fellowship AF [illegible] from the National Institute of Arthritis and Metabolic Diseases, United States Public Health Service.

[2] Present address: Department of Anatomy, College of Medicine, Wayne State University, Detroit, Michigan.

[3] Armed Forces Institute of Pathology, Washington 25, D. C.

[4] University of Alabama Medical Center, Birmingham, Alabama.

of pathologic joints confirmed and reinforced his findings in normal joints The investigation by Mankin ('62) in which tritiated thymidine was injected into rabbit knee joints supports Ogston's interpretations on the presence of a proliferating zone in articular cartilage.

Detailed studies have been made on similar changes occurring in the pubic symphysis. Putschar ('31) observed that the articular tissue of the pubic symphysis proliferates excessively with each pregnancy and that the excess material is shed into the joint space at the end of pregnancy Todd ('20 '21) has described in detail the changes which occur in the subchondral bone of the pubic symphysis in both males and females. These changes are so regular they can be used by anthropologists as an indication of the individual's age between 18 and 50 years.

Articular remodeling in human joints has been classified by Johnson ('62) into three categories progressive regressive and circumferential. Progressive remodeling results from excessive proliferation and deposition of new cartilage with subsequent conversion to subchondral bone at a rate sufficient to add length to the end of the bone. The process is recognized by the presence of remnants of the older articular cartilage and subchondral plate in the space beneath the new joint. Dur the remodeling process thickening of the cartilage excessive numbers and hypertrophy of cartilage cells, and foci of ossification in the basal zone of calcified cartilage are seen.

Regressive remodeling results in a shortening of the length of the bone and is recognized by the presence of remnants of calcified cartilage in the upper layers of the intact articular cartilage During the remodeling, the subchondral plate is resorbed by osteoclasts the resulting cavities become filled in with connective tissue and this connective tissue then becomes chondrified. The increased thickness of the articular cartilage due to such retrograde extension is brought into balance by excessive loss of cartilage through wear at its free surface

Circumferential or peripheral remodeling results in an increased diameter of the chondro-osseous junction. It takes place at the margin of the articular cartilage through a combination of progressive remodeling, periosteal elevation, and metaplastic chondrification followed by ossification of the capsular ligamentous, and tendinous attachments.

Knowledge of the principles of articular remodeling provides a basis for deducing from histologic sections obtained at death the remodeling changes which have occurred and still are occurring in human temporomandibular joints. The calcified articular cartilage serves as a natural marker for determining the direction in which the remodeling is occurring and for measuring the amount of remodeling which has already taken place.

MATERIALS AND METHODS

One temporomandibular joint was obtained from each of 34 anatomy cadavers at the University of Alabama Medical Center All of these were unclaimed bodies 26 of them coming from the state mental hospitals. Two bodies were Caucasian the remainder were Negroes. The age range extended from 45 to 81 years and the series included approximately equal numbers of males and females (table 1) All observations will be in reference to the specimens in this age group unless specifically stated otherwise. The authors gratefully acknowledge the cooperation of the dental students at the University of Alabama who made these specimens available for study

The specimens were fixed *in situ* by a routine embalming procedure used to prepare cadavers for dissection. Radiograms were made of both joints in each cadaver and any joint that appeared unusual radiographically was included in those selected for study The majority of the joints were radiographically normal. After the joint had been removed as a block, it was x rayed again in order to determine the plane for histologic sectioning, which was either frontal or sagittal. The specimens were then cut on a band saw into slabs approximately 5 mm thick and these slabs were x-rayed. Several slabs from each joint were embedded in paraffin (some in celloidin) sectioned and stained with hematoxylin and eosin. The sections were then

Age	Specimen no.	Sex	Plane of section	Dentition	Grossly arthritic	Perforated disc	Articular zone	Remodeling activity: Articular tubercle, Crest and lower post. slope: Lateral	Medial	Upper post. slope	Tymp. plate	Fossa roof	Condyle: Ant. and sup.	Condyle: Post.
45	92	♂	S	O	no	no	F C	+R		al P			+P	al P
43	H 2	♂	F				C	al R	al P			no	+P	
55	70	♂	S	OA	no	no	C, F			+P				++R
														+P?
58	96	♂	S	E		no		++R	+P	+++P		+++P	+P	+P
56	E	♀	S				F C	no	al R	+P		al P	al P	+R
57	66	♂	S	O	no	no	F C	+R	al P	+P	+P	al P	al P	al P
61	D-2	♂	F				C, F	no	+++P			++P	+P	
61	L	♀	S		no	yes	C, F	no	al P	+++P	++P	+P	+P	+P
63	94	♂	F	N	no	no	F C	+R	+P					
63	72	♂	F	E	no	no	F C	+R	+P				+P	
64	83	♂	F	O2	yes	yes	C	+R	+P	+P		al P	++++P	
64	K	♀	S				F C	+R	al R	+P	+++P	al P	+P	no
66	74	♀	F				F C	+R	+R	+P			++P	
67	67	♂	S	E	no	no	F C	no	no	+P	no		+P	+R
67	90	♀	S	E	yes	yes	C	++R	++P	++R		al P	++P	++R
								+P		+P				
67	M	♀	S			thin	C	+R[10]	no	+P		++P	+P[10]	al R
68	F	♀	S				C, F	no	+R	+P		+P	+R	+P
										al R			+P	+R
69	B	♀	F				C, F	al R	al P	no			no	no
70	N	♂	S				C, F	+P	+P	+P	+P	no	no	+R
72	65	♀	F	O	no	no	F C	no	+P	+P			+P	
72	73	♀	S	A	no	no	C, F	no	+R	no			no	+P
73	I	♀	F				C, F	al R	no	+P		al P	+P	
74	88	♂	S	O	yes	yes	C		+++P	+++P		al P	al P	+P
75	J	♂	F				C, F			+P		al P	++P	
76	98	♀	F	OA	no	no	C	al R	al P	no		no	+P	
79	P	♂	S			yes	C	+R	++++P	al P		no	+P	+P
									+R					+R
81	71	♂	S	N		no	C	+R	al P	al P	no		al P	++R
81	68	♂	S		yes	yes	C	++R	+P	+P	++P	P	+++P	++R
?	60	♂	S	N	yes	yes	C	+++P	+P	no	++R	+++P	++P	++R
								+R			+++P			
?	91	♂	F	E		yes?	C, F	+P	+P	+P		al P	+P	
								+R					+R	

Key Blank spaces mean data not available.
Caucasian, remainder Negro.
S, sagittal; F, frontal.
O, occludable teeth; OA, occludable teeth anteriorly; O2, 2 occludable teeth; N, no occludable teeth; E, edentulous.
F fibrous, C, cartilaginous

R, regressive; P, progressive; range none, slight, to 4
Condyle contacts tympanic plate.
Cartilage pathologic on medial part of articular tubercle.
Condylar cartilage thickened at disc perforation.
Disc thinned posteriorly.
[10] Remodeling located adjacent to thinned part of disc.

studied and analyzed for the type degree and location of articular remodeling. Acknowledgment is made to the Armed Forces Institute of Pathology for the generous technical assistance they provided in histologic processing and photography

The terminology of the *Nomina Anatomica* is used for the gross features of the joint (fig 1) Thus the temporal surface of the joint is subdivided antero-posteriorly into the articular tubercle (articular eminence) and the articular surface of the mandibular fossa (that part of the fossa enclosed by the joint capsule) The contour of the articular tubercle is subdivided into a crest (the most inferiorly projecting point in its curvature) an anterior slope leading from the crest towards the most anterior attachment of the joint capsule on the temporal bone, and a slope which merges gradually into the mandibular fossa. The extraarticular surface of the mandibular fossa is that part which lies posterior to the petrotympanic fissure It consists of the tympanic portion of the temporal bone and is referred to here as the tympanic plate.

The term articular tissue is used in reference to what would ordinarily be the articular cartilage in other synovial joints. Certain parts of this tissue can be identified histologically as nonweight-bearing or nonloaded areas just as there are occlusal and nonocclusal surfaces on teeth. These will be referred to as the nonarticulating areas of the joint.

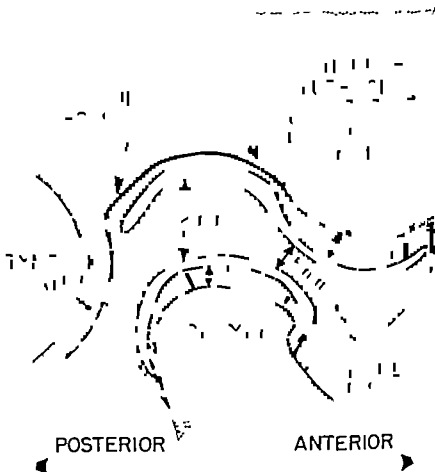


Fig. 1 Diagrammatic sagittal section of temporomandibular joint. The thicknesses of the articular tissue represent measurements obtained from histologic sections and are less than those found in unfixed fresh specimens.

OBSERVATIONS

Articular tissue

There is no hyaline articular cartilage present in this joint. The articular surfaces of the mandibular condyle and temporal bone consist only of fibrous connective tissue at birth which undergoes a varying degree of metaplastic conversion to fibrocartilage during postnatal life. In all specimens the deepest part of the articular tissue is calcified at the junction with the underlying bone

The ratio of chondrocytes to fibrocytes and the total number of cells present in the articular tissue vary in different specimens and in different areas of the same specimen. This cellular pattern shows no relationship with age and appears to depend largely on the mechanical factors associated with function.

Bundles of collagen fibers travel parallel to the joint surface and interlace with each other in this plane The deepest fibers extend into the subchondral bone This basic pattern is maintained even when the fibrous tissue undergoes a conversion to fibrocartilage.

The histologic characteristics of this articular tissue will be described separately for the condyle temporal bone, and articular disc. An important point to be made here however is that the thickness of the articular tissue is not constant throughout the joint. Thus the radiographic image, which corresponds to the contours of the subchondral bone does not represent the exact contour of the articular surface

Condyle

Articular tissue on the condyle is from 0.3 to 0.5 mm thick after the shrinkage due to chemical fixation and histologic processing. The hyaline growth cartilage is no longer present in this age range and there is no trace of its earlier existence between the articular tissue and the bone of the condyle.

The majority of specimens show a transition from fibrous tissue at the articular surface to fibrocartilage in the deeper layers (fig. 3) In some areas fibrocartilage may extend through the full thickness of the articular tissue (fig 4) Such zones usually show signs of proliferative activity increased thickness of the articular tissue a greater number of cartilage cells per unit area, often arranged in clones rather than singly and an increased amount of ground substance around the cells.

Cartilage cells generally are limited to the articular tissue on the antero-superior aspect of the condyle the area which is in contact with the articular tubercle during hinge and sliding movements of the joint. It is here that the tissue reaches its greatest thickness. The remaining tissue on the condylar surface merges imperceptibly with the periosteum of the mandible. At the periphery of the joint cavity and on the posterior aspect of the condyle is a covering of synovial tissue and its associated supply of blood vessels, lymphatics and nerves.

Temporal bone

The thickest layer of articular tissue on the temporal surface of the joint is seen at the articular tubercle (fig. 5) On the crest and the immediately adjacent posterior slope of the tubercle it is approximately 0 75 mm thick. Here as on the opposing surface of the condyle, the cartilage cells are most numerous and in some specimens they are distributed through the full thickness of the tissue Anterior to the crest the number of cartilage cells decreases. At the junction between the posterior slope of the tubercle and the roof of the mandibular fossa, a marked histologic change occurs The articular tissue becomes abruptly thinner and appears as a meager layer of fibrous connective tissue containing no cartilage cells Furthermore the tissue lining the mandibular fossa is often covered with a layer of vascularized and innervated synovial tissue (fig 6) This region is a nonarticulating part of the joint.

Articular disc

A sagittal section through the middle of the joint generally shows the disc to be thinnest and most compact at a point between the anterior surface of the condyle and the posterior slope of the tubercle Here the disc is very dense and contains more cartilage cells than in its peripheral portions. The bundles of collagen fibers are all parallel to the surfaces of the disc

latero-medial contour Laterally it is predominantly regressive. On the medial side progressive remodeling is most common

The roof of the mandibular fossa shows in the majority of specimens a slow orderly progressive remodeling. The articular tissue is thin the subchondral plate presents an even concave contour and the bone contains few osteones and no resorption cavities This part of the joint seems to have a relatively stable contour There is nothing to indicate that the thin bone separating the middle cranial fossa and its contents from the mandibular fossa is under mechanical stress or that any regressive remodeling occurs there which might ultimately result in communication between the cranial and articular cavities

Considering the specimens as a group (table 1) one can make a composite map or diagram showing the major distribution of the types of remodeling activity seen in different parts of the joint (fig 2) The distribution and frequency of remodeling described in table 1 are only rough approximations because serial sections were not made through the entire joint but were concentrated on any areas which showed radiographic and gross signs of alteration in form The data indicate however that the distribution of remodeling activity is not haphazard. Its more precise localization requires further study

The degree of remodeling activity present in a joint shows no correlation with age The rates and quantity of remodeling are evenly distributed throughout the entire age range studied and appear dependent on factors that must be regarded as functional or mechanical in origin. The striking feature is that all the joints studied showed remodeling activity in some part of the joint.

Remodeling and osteoarthritis

Remodeling activity is greatest in those specimens which also show the gross characteristics of osteoarthritis loss of the tangential fibers in the articular cartilage fibrillation, fissuring and shedding of the cartilage, and eburnation of the underlying bone (figs. 29–32) *Destruction and perforation of the articular disc is commonly seen in osteoarthritic joints but occasionally the perforation is also present* without any change in surface contour of the adjacent parts of the condyle and articular tubercle. In such cases however, one can see remodeling activity occurring beneath the articular surface at the level of the subchondral plate. When present this appears as a progression of subchondral bone on the condyle opposite the perforation (fig 18) or as a focus of early regression on the tubercle (fig. 22) The breakdown of the disc appears to be a stimulus for subsequent remodeling activity on the condyle and temporal bone at the site of perforation.

The pathologic specimens show the following trends in remodeling activity the articular surfaces become uneven (figs 31 and 32) the condyle becomes flattened and enlarged through a combination of progressive and circumferential remodeling, and the tubercle tends to be resorbed by regressive remodeling at the crest. The result of such changes is that the area of articular contact between the condyle and temporal bone is increased and the articular plane becomes more nearly parallel to the Frankfurt plane.

DISCUSSION

Histology

The temporomandibular joint is one of the few synovial joints which does not have articular surfaces composed of hyaline cartilage As Miles and Dawson ('62) point out, this has been attributed to the fact that the temporal and mandibular components of the joint are derived from membrane bone instead of from a cartilaginous model Actually however the condyle develops a cartilage growth center during fetal life and grows from that moment on by endochondral ossification in a manner comparable to that occurring at the epiphyseal growth plates of long bones with the exception that an ossification center which becomes an epiphysis does not appear

The presence of the fibrous articular tissue in this joint seems related to the fact that the articulating elements develop from a *discontinuous blastema* in contrast to the continuous blastema which is the embryonic precursor of joints possessing hyaline articular cartilage (Moffett '57) The

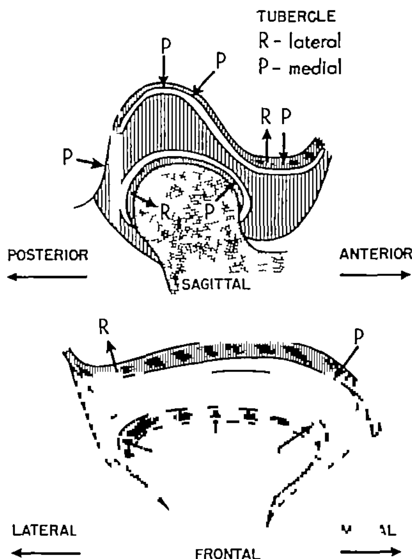


Fig. 2 Composite diagrams to summarize the major trends in distribution of remodeling activity in 30 adult temporomandibular joints. Upper diagram is a sagittal composite. Regressive remodeling (R) occurs predominately on the lateral part of the articular tubercle and progressive remodeling (P) on the medial part. Lower diagram represents frontal composite through the articular tubercle and the anterior half of the condyle

significance of this difference is that the embryonic interzone for the temporomandibular joint is mesenchymal and not blastemal. Condensations of this mesenchyme over the articular surfaces during embryonic and fetal life appear to be the precursor of the fibrous articular tissue seen in the fully developed joint. This hypothesis must be tested by studies on the embryology of other synovial joints which do not have hyaline articular cartilage such as the sternoclavicular joint.

The slow transformation of fibrous articular tissue into fibrocartilage during post natal life occurs in those parts of the joint which are bearing or loaded surfaces. Much evidence is available to indicate that cartilage can be induced to form in connective tissue at points where there is movement combined with pressure or me-

chanical loading. This is shown in the formation of pseudoarthroses following nonunited fractures as described by Murray ('36) Studies cited by Putschar ('60) illustrate that the collagen/chondroitin sulfate ratio in articular cartilage is correlated with function For instance Mathews ('52) has shown that the chondroitin sulfate content is higher in weight-bearing joints than in non weight-bearing joints. Similar differences can be demonstrated for the various areas within a joint, the higher values being located in the areas subjected to pressure This relationship between function and the morphological differentiation of cartilage was demonstrated in another manner by Akeson *Eichelberger and Roma* ('57) *who reported* that after an extremity had been inactivated by denervation, the chondroitin sulfate content of the articular cartilage decreased considerably

Schallock (42) has correlated the arrangement of collagen bundles in articular cartilage with the type of stress applied to that area In areas of sliding contact the fiber bundles cross each other at acute angles causing marked cleavage lines when the cartilage is experimentally punctured In pressure areas the collagen bundles cross in a rectangular pattern and little cleavage results upon puncturing

This type of physical differentiation of articular cartilage occurs apparently throughout the individual's lifetime Makowsky (49) observed that the differentiation begins at about the third year and continues to a peak at approximately 30 years of age

Articular remodeling

Against the background of the studies just cited the histologic picture seen in the temporomandibular joint takes on considerable functional significance The mechanical factors associated with function account for the gradual transformation of the fibrous articular tissue into fibrocartilage during postnatal life. This transformation occurs only in those parts of the joint which are articulating or pressure-bearing areas namely the anterior aspect of the condyle the central part of the articular disc, and the posterior slope and crest of the articular tubercle The roof of the mandibular fossa does not show this metaplastic transformation nor does the fibrous tissue display any proliferative response in that area The same functional stimuli which cause this differentiation to occur seem to be responsible for the proliferative response of the articular tissue and underlying bone which expresses itself in a *remodeling or reshaping of the* articular contours.

Since articular cartilage is avascular, its metabolic needs must be met by diffusion of fluid into the tissue from its surfaces. Although Ekholm ('55) has demonstrated that radioactive tracers do diffuse into articular cartilage from its deep surface in the knee joints of young rabbits, a variety of other evidence leads one to conclude that this path does not play a significant role in adults. It appears likely that adult articular tissue is supplied mainly from the synovial fluid on its articular surface Bywaters ('37) presents some evidence for this view and then attempts to calculate by means of a diffusion constant for glucose the maximum thickness of articular cartilage which could be supplied by diffusion from its surface His theoretical figure indicates that 3 mm is the critical thickness. This seems to be a reasonable approximation since most articular cartilage is thinner than this. The frequent occurrence of progressive remodeling in areas where the articular cartilage is visibly thickened makes it seem likely that insufficient nutrition induces the changes which follow cartilage proliferation namely expansion of the calcified zone vascular invasion from the underlying bone resorption of the calcified articular tissue, and finally advancement of the subchondral plate toward the articular surface.

It is more difficult to explain completely how the process of regressive remodeling is accomplished. When the subchondral bone is resorbed in regressive remodeling, mesenchyme fills in the resorption cavities and differentiates into articular tissue, thus increasing the thickness of the articular layer by adding to its deep surface The loss of cartilage on the articular surface which must occur in order to allow a regression of the contour and a reduction of the articular tissue to its usual thick

ness, cannot be explained by inadequate nutrition. It must be brought about by mechanical factors such as an increased attrition or wear rather than by metabolic factors.

Various types of evidence are available which indicate that joint contours do undergo regressive changes. Lawther ('56) compared the x ray contours of temporomandibular joints in two groups of male adults. The individuals who were edentulous for three years or more showed a decrease in slope of the articular tubercle and a decrease in height of the mandibular fossa when compared to similar aged individuals having good dentitions. Unpublished measurements by McCabe and Moffett on archaic Indian skulls show that in temporomandibular joints with clear-cut arthritic changes the posterior slope of the tubercle forms a smaller angle with the Frankfurt plane than that seen on the opposite normal joint in the same specimen or in comparable skulls with both joints normal. The same kind of regressive remodeling can be demonstrated roentgenologically on the articular tubercle if one follows the continuing arthritic changes in a patient.

Some of the relationships between function and articular remodeling in the temporomandibular joint have been demonstrated experimentally by Breitner ('40 '41) He extracted the maxillary molars and premolars in an adult rhesus monkey leaving the anterior teeth in occlusion After four weeks the posterior wall of the mandibular fossa and the posterior surface of the condyle showed histologic signs of bone resorption The changes were so extensive they could be recognized grossly

In another animal he raised the bite in the molar region by means of caps applied to the occlusal surfaces of the teeth This caused bone formation in the roof of the mandibular fossa and on the posterior surface of the condyle as well as bone resorption on the anterior surface of the condyle. Raising the bite in the incisal region produced the same effect on the joint.

By using intermaxillary rubber bands to pull the mandible anteriorly he induced the following changes in a young monkey bone formation on the posterior wall of the mandibular fossa and on the posterior surface of the condyle, as well as bone resorption on the posterior slope of the articular tubercle and on the anterior surface of the condyle

In another young animal the intermaxillary rubber bands were arranged to pull the mandible posteriorly This reversed the changes from that seen in the previous animal. The posterior wall of the mandibular fossa and the posterior surface of the condyle showed bone resorption. The anterior surface of the condyle and the posterior slope of the tubercle showed bone formation.

With these experiments Breitner demonstrated that changes in vertical dimension and in occlusal relationships cause bony changes in and about the temporomandibular joint and in other parts of the mandible These changes occurred rapidly as early as four weeks, and were essentially the same as those seen in alveolar processes during orthodontic treatment. In these short term experiments he did not mention or illustrate any changes occurring in the articular tissue One might expect, however that after the bony changes were stabilized much slower adaptive remodeling would develop in the articular tissue.

For setting the borderline between articular remodeling and degenerative arthritis one criterion seems useful – the integrity of the articular tissue. Remodeling might be defined as the changes associated with a proliferative response in the articular tissue Osteoarthritis, on the other hand represents the changes associated with a breakdown of the articular tissue fibrillation, fissuring eburnation and cystic alterations.

Not enough data are available to allow conclusions concerning the dental causes of temporomandibular joint remodeling. The amount of remodeling activity does seem to be correlated, however with the number of missing teeth Specimens with osteoarthritic changes are often edentulous. These relationships support the concept that the jaw joint is an articular triad with two points of contact provided by the temporomandibular joints and the third one by the dentition. Alteration in any one of these contact points will produce secondary changes in the other two just as hap-

pens in the articular triad between vertebrae.

LITERATURE CITED

Breitner C. 1940 Bone changes resulting from experimental orthodontic treatment. Am. J Orthodontics and Oral Surg., 26 521–546.

——— 1941 Further investigations of bone changes resulting from experimental orthodontic treatment. Am. J Orthodontics and Oral Surg 27 605–632.

Bywaters, E. G. L. 1937 Metabolism of joint tissue. J Path. and Bact., 44 247–268.

Ekholm, R. 1955 Nutrition of articular cartilage. Acta Anat., 24 329–338

Harrison, M. H. M., F Schajowicz and J Trueta 1953 Osteoarthritis of the hip a study of the nature and evolution f the disease. J Bone and Jt. Surg., 35B 598–626.

Johnson, L. C. 1959 Kinetics of osteoarthritis. Lab. Invest., 8 1223–1238

——— 1962 Joint remodeling as the basis for osteoarthritis. J Am. Vet. Med. Assoc., *141* 1237–1241

Lawther L. L. 1958 A roentgenographic study of the temporomandibular joint using special head positioner Angle Orthodontist, 26 22–33

Mankin, H J 1962 Localization of tritiated thymidine in articular cartilage of rabbits. I. Growth in immature cartilage. J of Bone and Jt. Surg., *44A* 682–698

M tthews, B F 1952 Collagen/chondroitin sulphat ratio of human articular cartilage related to function. Brit. Med. J 2 1295

Miles, A. E. W and J A. Dawson 1962 Elastic fibers in the articular fibrous tissue of some joints. Arch. Oral Biol., 7 249–252.

Moffett, B C. 1957 The prenatal development of the human temporomandibular joint. Carnegie Inst. Wash. Pub. 611 Contrib. to Embryol. 36 19–28.

Murray P D F 1936 Bones. A study of the development and structure of the vertebrate skeleton. Cambridge Univ Press.

Ogston, A. 1875 Articular cartilage. J Anat. and Phys., *10* 4–74.

——— 1878 On the growth and maintenance of the articular ends of the bones. J Anat. and Phys., *12* 503–517

Putschar W 1931 Entwicklung, Wachstum und P thologie der Beckenverbindungen des Menschen. Gusta Fischer Jena.

——— 1960 General pathology of the musculo-skeletal system. Handbuch der Allgemeinen P thologie 3 360–488.

Schallock, G 1942 Untersuchungen zur Pathogenese von Aufbrauchveränderungen an den knorpeligen Anteilen des Kniegelenkes Veröff Konstit. u. Wehrpath, *11* 1–66.

Todd T W 1920 Age changes in the pubic bone. I. The male white pubis. Am. J. Phys. Anthropol., *3* 285–334

——— 1921 Age changes in the pubic bone II. The pubis of the male negro-white hybrid. III. The pubis of the white female. IV The pubis of the female negro-white hybrid. Am. J Phys. Anthrop 4 1–70.

PLATES

Abbreviations

AT, articular tissue
B bone
C, fibrocartilage
CC, calcified cartilage
CO condyle
CZ, calcified zone
D disc

F fibrous tissue
M, mesenchyme
P progressive remodeling
R, regressive remodeling
SP subchondral plate
SV synovial villus
T tubercl

PLATE 1

EXPLANATION OF FIGURES

3–4 Articular tissue on mandibular condyle, 74 yr male (spec. no. 88) sagittal section 62 × The cell population and thickness of the articular tissue vary in different parts of the joint. Figure 3 Anterior part of condylar surface. A thin zone of calcified cartilage occurs at the junction with subchondral bone. Figure 4 Superior part of condyle sam specimen and magnification as in figure 3. The articular tissue is thickened, cartilage cells have formed clones and are distributed throughout the full thickness of the tissue.

5 Articular tissu on posterior slope of articular tubercle, 45 yr male (spec. no. H 2) frontal section, 44 × From bove downward are shown subchondral bone dark band f calcified cartilage, deep zone of fibrocartilage fibrous tissue on articular surface.

6 Articular tissue on roof of mandibular fossa, 74 yr male (spec. no. 88) sagittal section, 164 × N cartilage cells are present, the fibrous tissue is very thin and covered by two synovial villi (SV) containing blood vessels. This is histologically nonarticulating part of the joint.

7 Vascularized portion f articular disc in the mandibular fossa, 67 yr mal (spec. no 67) sagittal section 36 × The area bown is located just posterior to the condyle. The space along the right border is the inferior joint cavity Histologically this is nonarticulating area in which are found blood vessels nerves, adipose tissue and areolar tissue.

8 Temporomandibular joint, 74 yr male (spec. no 88) sagittal section, 3 × The large spaces seen in the bone of the mandibular fossa and rticular tubercle are mastoid air cells which sometimes extend into the squamous part of the temporal bone

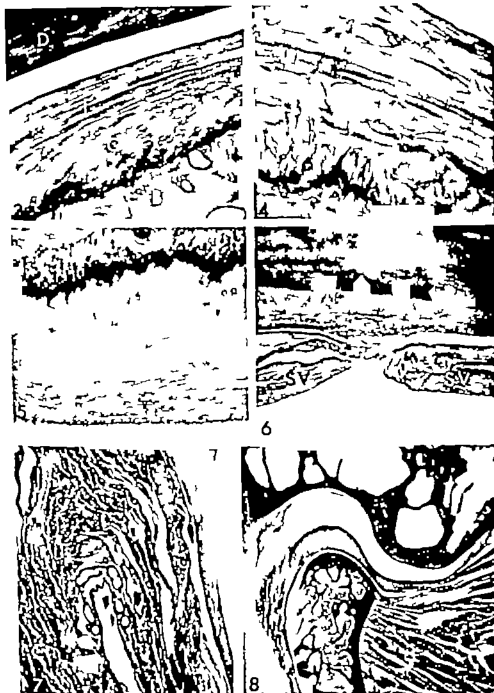

D
D
2
4
5
SV
SV
6
7
7
8

PLATE 2

EXPLANATION OF FIGURES

9 Roof of mandibular fossa, 61 yr female (spec. no. L) sagittal section, polarized light, 95 × The lamellar arrangement of the bone in this part of the joint indicates that very little internal reconstruction has occurred by means of replacement with osteones. This agrees with other evidence that the roof of the fossa is nonarticulating part of the joint. Compare with figure 10.

10 Articular tubercle just posterior to its crest, 64 yr female (spec. no. K), sagittal section, polarized light, 95 × The lamellar bone has been replaced by many generations of osteones indicating that this part of the joint is a loaded or articulating area subjected to mechanical stress.

11–12 Proliferation of articular tissue on the condyle opposite ttenu ted part of articular disc, 67 yr female (spec. no. M) sagittal section. Figure 11–10 × Area enclosed in the rectangle is enlarged in figure 12. Figure 12—58 × Articular tissue on condyle is thickened contains more than the usual number of cells per unit area and the calcified zone (C Z) has expanded.

13 Expansion of calcified zone into the overlying articular tissue on lateral half of condyle, 61 yr male (spec. no. D-2) frontal section, 25 × In this area the calcified zone (C Z) is thicker than the other layers of the articular tissue. Normally it is only thin band.

14 Progressive remodeling on the medial part of the articular tubercle 67 yr female (spec. no 90) sagittal section, 25 × The alcified zone has advanced toward the articular surface in the region marked by rrows and subchondral bone is invading the area deep to it.


9


10




CZ


D


14

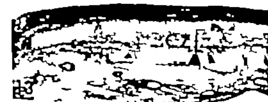

CZ

PLATE 3

EXPLANATION OF FIGURES

15 Progressive remodeling on the lateral part of the condyle, 61 yr male (spec. no. D-3) frontal section, 25 × The calcified zone has advanced toward the articular surface in the region marked by arrows and the tissue deep to it is being replaced with bone.

16 Progressive remodeling, lateral part of condyle 64 yr male (spec no. 93) frontal section 7.5 × Arrows indicate a cumulative series f stages in the dvancement of the calcified zone. An associated proliferation of articular tissue in this area has prevented the calcified tissue from reaching the joint cavity and in this manner the articular contour of the condyle has been altered.

17 Progressive remodeling, medial part of tubercle 65 yr male (spec. no. 96) sagittal section, 27 × The articular cavity appears in the lower left hand corner Running diagonally across the center of the photograph from upper left to lower right is an unresorbed band f calcified cartilage (C C) which marks the original location of the subchondral pl te prior to remodeling All of the bone seen on the lower side (articular side) of this calcified cartilage represents bone formed as result f progressive remodeling. The new subchondral plate (S P) and calcified zone (C Z) have advanced toward the articular surface for distance of more than 1 mm.

18 Condyle and articular disc 63 yr male (spec. unnumbered) sagittal section, 3 5 × Opposite perforation in the articular disc (D) is a localized area f early progressive remodeling (bounded by arrows) on the condyle The subchondral bone has advanced in this area even though change in contour has not yet occurred on the artic- la surface.

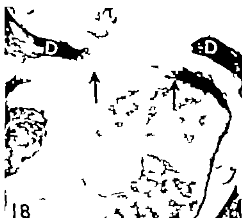
19 Junction between subchondral bone (S B) and articular tissue (A T), lateral part of rticul tubercle, 45 yr male (spec no. 92) sagittal section 36 × This is the first stage in regressive remodeling. A small localized area of bone resorption is seen immediately beneath the articular tissue The dark spots on the margins of resorption cavities are osteoclasts.

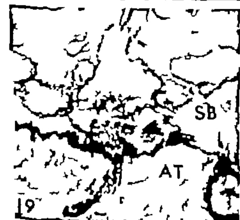
20 Regressive remodeling, lateral part of articular tubercle embalmed ad ver age unknown sagittal section, 7.5 × The resorption defect (outlined by rrows) in the subchondral bon represents an early tage in regressive remodeling. It is loc ted just posterior to the crest f the t bercle in loaded re where the disc (D) has become thinned almost to perforation.


15


D
16


SP
CZ
17


D
D
18


SB
AT
19


D
CO
20

PLATE 4

EXPLANATION OF FIGURES

21 Closer view of the resorption area shown in figure 20, 33 × As the resorption cavity enlarges it becomes filled with undifferentiated mesenchyme (M) This eventually differenti tes into articular tissue.

22 Regressive remodeling, lateral part of articular tubercle 79 yr male (spec no P) sagittal section, 25 × A deep and sharply bounded area of resorption (outlined by arrows) has occurred in the subchondral bone near the crest of the tubercle at point directly opposite the edge of perforation in the disc (D) It has been filled in with a fibrous tissue that is continuous with the articular layer

23 Extensive regressive remodeling t crest of articular tubercle, 55 yr male (spec. no. 96) sagittal section 3 × The contour f the subchondral bone on the tubercle (T) has been flattened by bone resorption t the crest. The dark wavy line enclosed in the rectangle (enlarged in fig. 24) is remnant of the old calcified zone and represents the former location of the subchondral plate.

24 Close up view of area enclosed by rectangle in figure 23 26 × The dark band marked by arrows is remnant of the old calcified zone It is located t the former level f the subchondral plate prior to resorption of the nderlying bone in regressive remodeling All of the fibrocartilage lying bove this band represents newly differentiated articular tissue which fills in the area where bone has been resorbed on the tubercle.

25 Temporomandibular joint, 55 yr male (spec. no. 96) sagittal section, 2.2 × Examination of the microscopic section under high power reveals progressive remodeling (P) on the posterior slope f the tubercle and on the roof of the mandibular fossa. Regressive remodeling (R) is occurring on the crest of the tubercle. Compare with figure 26.

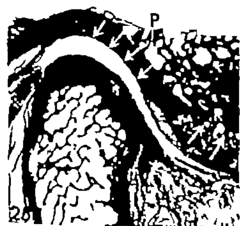
26 Tracing f the section shown in figure 25. The dotted line on the temporal part of the joint represents the contou of the subchondral plate prior t remodeling as determined from nresorbed remnants of the calcified zone The new contou shown in continuou line at the junction between bone (stippled) and articular tissue (horizontal stripe) is hanging toward flatter less steep articular tubercle


M
21


D
22


T
23


24


P
25

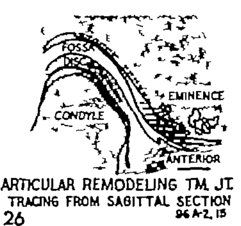

FOSSA
DISC
EMINENCE
CONDYLE
ANTERIOR
ARTICULAR REMODELING TM JT
TRACING FROM SAGITTAL SECTION
96 A-2, 15
26

PLATE 5

EXPLANATION OF FIGURES

27 Temporomandibular joint with perforated disc, 81 yr male (spec. no. 68) sagittal section, 2.2 × This joint is well within the category of osteoarthritis but its remodeling changes differ only in degree from those seen in figure 25. Observe that the severest changes occur opposite the perforation in the disc progressive and circumferential remodeling on the anterior part of the condyle, regressive remodeling on the crest of the tubercle. Compare with figure 28.

28 Tracing of the section shown in figure 27 The dotted lines on the condyle and temporal bone represent the contours of their subchondral plates prior to remodeling. The new contours at the junction between bone (stippled) and articular tissue (horizontal stripe) result in a flattened, enlarged condyle and a partially resorbed articular tubercle.

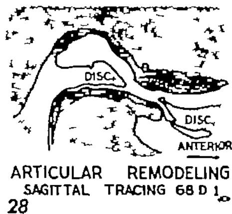
29 Posterior slope of tubercle, adjacent to crest, 67 yr female (spec. no. 90) sagittal section, 25 × Changes in articular tissue associated with osteoarthritis fissuring, fibrillation, and loss of the superficial, tangential fibers. The contour of the subchondral plate in this region has also become irregular and ragged through disorganized type of remodeling activity that appears to be progressive in one place and regressive in the next.

30 Upper posterior slope of articular tubercle, 67 yr female (spec. no. 90) sagittal section, 9 × Advanced changes in articular tissue associated with osteoarthritis. The articular tissue on this part of the tubercle (T) shows extreme fibrillation and shedding right down to the calcified zone in one area. This spot would shortly become eburnated bone. The convex curvature of the subchondral plate in this region is the result of progressive remodeling. The disc has become perforated allowing the condyle (CO) to come into direct contact with the tubercle.

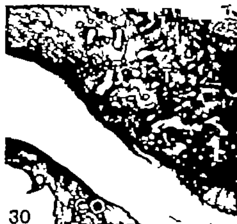
31 Temporomandibular joint, age unknown, male (spec. no. 69) sagittal section 3 × Disorganized type of remodeling associated with osteoarthritis. The condyle presents irregularities on its articular surface resulting from circumferential progressive, and regressive remodeling all occurring in adjacent areas. The disc (D) has disintegrated over most of the condyle.

32 Temporomandibular joint, age unknown, male (spec. no. 91) frontal section, 3 × Extreme irregularity of contour at anterior margin of condyle (CO) The shredded ppearance of the articular tissue on the lateral (left) part of the condyle and an irregular osteophyte (circumferential remodeling) on the medial aspect label this joint as osteoarthritic.


27


DISC.
DISC.
ANTERIOR
ARTICULAR REMODELING
SAGITTAL TRACING 68 D 1
28




30


31


32

Ultrastructure of Bovine Spermatozoa

I. THE HEAD OF NORMAL, EJACULATED SPERM [1,2,3]

R. G. SAACKE AND J. O. ALMQUIST

Dairy Breeding Research Center Department of Dairy Science
The Pennsylvania State University University Park

ABSTRACT The ultrastructure of the normal bovine sperm head has been studied and particular attention has been given to the morphology and coverings of the nucleus and the formation of the equatorial segment.

The bovine sperm head consists of homogeneous, flattened nucleus which is covered anteriorly by three-layered head cap and posteriorly by a loose thin, dense, post-nuclear cap. The nucleus measures approximately 0.2 to 0.3 μ in thickness. It tapers anteriorly to sharp point along the frontal portion of the head and thickens posteriorly to accommodate an implantation socket for the tail. The nuclear membrane is double and porous. Vacuoles or openings of variable size and shape are present in the nucleoplasm, predominantly in the posterior portion of the nucleus. The head cap measures approximately 350 to 600 Å in thickness. It consists of dense inner and outer membranes which envelop moderately electron dense middle layer. The head cap thickens across the frontal part of the head forming ridge on one side of the nucleus.

A sequence of structural alterations in the head cap provide evidence for the ppearance of the equatorial segment. The anterior portion of the head cap swells and deteriorates leaving the posterior portion intact as band about the center of the nucleus. This band represents the equatorial segment.

The literature on the ultrastructure of mammalian spermatozoa is voluminous and recent comprehensive reviews have been published by Anberg ('57) and Fawcett ('58). Of prime concern to the cellular physiologist is the integration of information on cellular metabolism, behavior and structure. Since the metabolism of bovine spermatozoa has been studied intensively and accurate information on fertility of individual bovine males is available through artificial breeding records it seemed advisable to define more clearly bovine sperm ultrastructure. Lack of information on normal head ultrastructure is particularly evident.

Most current knowledge of the bovine sperm head ultrastructure stems from the efforts of early workers studying whole cells (Baylor et al. 43 Bretschneider 48 49 Reed and Reed, 48) or partially disrupted cells (Wu and McKenzie, '55 Yasuzumi et al. '56) with the electron microscope. More recent studies involving thin-sectioning techniques with electron microscopy have revealed additional detail, particularly with respect to nuclear morphology and the relationship of the nuclear coverings (Bradfield '54; Blom and Birch-Andersen, '61; Rahlman, '61) Nevertheless, considerable disagreement still exists.

Confusion resides primarily in the characteristics and relationships of the nuclear coverings. Interpretations have been confounded by attempts to explain capacitation as well as the occurrence of the equatorial segment, a band readily observed across the center of the flat side of the fixed and/or stained head when examined under the light microscope.

Therefore the present investigation was undertaken to define further the ultrastructure of the normal bovine sperm head.

MATERIALS AND METHODS

Semen was collected by means of the artificial vagina from Holstein bulls. Ejaculates used had at least a volume of 3 ml, an initial motility of 60% and a sperm concentration of 700 × 10^6/ml.

---

[1] Authorized for publication July 1, 1962 as Paper no. 2798 in the Journal Series of the Pennsylvania Agricultural Experiment Station.

[2] Supported in part by the Pennsylvania State Association of Artificial Breeding Cooperatives

[3] The data contained in this paper are from thesis submitted by the senior author to the Graduate School of The Pennsylvania State University in partial fulfillment of the requirements for the degree of Doctor of Philosophy

The influence of any one bull was reduced by pooling single ejaculates collected from five different bulls. Semen was diluted either with previously heated skim-milk or a 2.9% solution of sodium citrate dihydrate.

Spermatozoa were centrifuged from the diluent at 4 C for 30 minutes at 750 g Centrifugation was carried out at 4 C instead of room temperature to reduce the resistance offered by motile sperm and to obtain a more equal distribution of motile and non-motile sperm in the pellet. The supernatant was decanted and the loose pellet of spermatozoa was transferred in pieces (approximately 3 mm) to a petri dish containing semisolid 2.5% agar at 29 C. The agar was permitted to solidify at room temperature following transfer

The use of agar as suggested by Blom and Birch Andersen (60) served to maintain the integrity of the loose pellets during fixation and the early stages of dehydration. The tissue then became sufficiently hard and the agar was no longer needed.

Pellets from each pooled sample were divided into two portions One portion was fixed in 1% osmium tetroxide buffered with veronal-acetate (Palade, 52) containing sucrose (Caulfield '57) and the other in potassium permanganate fixa- (Luft, '58) Both fixatives were buf -d at pH 7.2 to 7 4 Tissues were dehydrated in a graded series of ethanol baths and embedded in Araldite. Sections were cut with glass knives using a Porter Blum ultramicrotome and electron micrographs were made with an RCA EMU 2D electron microscope.

OBSERVATIONS AND DISCUSSION

Most measurements and descriptions of the bovine sperm head have been limited to the broad, flat side of the head. From this aspect, the approximate head measurement averages are: length 9 0 μ greatest width 4.5 μ and base width 1 7 μ. These values are based on measurements obtained by several investigators (Savage et al. '27; Bretschneider 48 Bonadonna et al., '59 Mukhergee and Dott, '60 Blom and Birch-Andersen, '61) Only when the cell is free floating, motile or fixed and sectioned is the thinner aspect apparent. A near-median sagittal section through the thin dimension of the head (fig. 2A) shows the relationship of its various components. In general these relationships are in close agreement with those observed by Blom and Birch-Andersen ('61) For comparison to the sagittal section, cross sections of the head positioned in the region in which each is believed to have originated, are presented in figs 2B C D and E.

The anterior 55 to 60% of the nucleus is tightly covered by a thick capsule, the head cap the posterior 40 to 45% is covered loosely by a thin sheath, the post-nuclear cap The cell membrane, which surrounds the entire cell, loosely envelops the head with the exception of an attachment along the base of the head (fig. 4).

A three-dimensional graphic illustration of the bovine sperm head is presented in figure 1 This illustration is based on information obtained from the present study as well as from pervious studies (Bradfield, 54; Blom and Birch-Andersen, '60 Rahlman, '61)

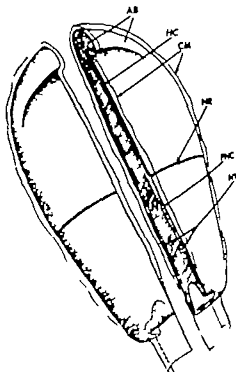


Fig. 1 Graphic illustration summarizing the ultrastructural f tures of the bovine sperm head. Apical body (AB); head cap (HC); cell membrane (CM); nuclear ring, (NR); nucleus, (N); post-nuclear cap (PNC); nuclear vacuoles, (NV).

The nucleus

The nucleus exhibits rather uniform thickness of from 0.2 to 0.3 μ. However there is a gentle taper of the anterior portion to a point along the frontal part of the head (fig. 2A and B) and a thickening near the base (fig. 2A and E). The thickening is especially apparent near the median line of the nucleus (fig. 2E) thereby providing a recess for the insertion of the tail. Blom and Birch-Andersen ('60) have described the attachment of the tail to the head as resembling a capitulum in a socket. The socket, however is not a complete one. It may be observed in sagittal sections through the neck cut on a plane parallel with the flat side of the head (arrow fig. 3) but not in sagittal sections cut at 90° to the flat plane of the head (fig. 4). The latter section reveals only the insertion of the tail into a concave recess at the base of the head. This relationship is shown in figure 1.

A basal plate distinctly separate from the nucleus but lining the implantation recess formed by the nucleus was reported by Nicander and Bane ('62) studying porcine spermatozoa. The same type of structure was observed in bovine sperm (fig. 6). The basal plate was not observed in all sections through the head base suggesting that it may not line the entire recess. Therefore this structure was omitted from figure 1 to avoid confusion.

The osmium- or permanganate-fixed and sectioned nucleus appears nearly homogeneous except for the presence of vacuoles (figs. 5 6 7 8). The term vacuoles is used here to include non-electron or low electron dense areas thus recognizing that they may be artifacts. Vacuoles were found throughout the nucleus, however they were most numerous posteriorly. In some instances they were observed as openings on the nuclear surface (fig. 6). Schnall ('52) reported a similar observation with human sperm. He postulated that such vacuoles may provide a means for eliminating gaseous metabolic waste from the nucleus. They also may represent a means by which the nucleoplasm protects itself against external osmotic gradients — forming and releasing vacuoles as the osmotic environment changes. Evidence for either hypothesis is still lacking. On the other hand, these structures may be deformities on the nuclear surface rather than vacuoles.

The two round vacuoles shown in figure 5 correspond to a series of four vacuoles along the same axis as reported by Blom and Birch-Andersen ('60). Their function is not known but their location suggests that they may be associated with the articulation mechanism.

The irregularity of number, shape and orientation of vacuoles shown in figures 7 and 8 indicates that they may be artifacts. Fawcett ('58) has suggested that nuclear vacuoles may arise from accidents in chromatin condensation during spermiogenesis. Such an explanation could apply to these vacuoles since they were most frequently observed in the posterior region of the nucleus where the greatest chromatin concentration occurs in the bovine sperm head (Salisbury et al., '61).

The nucleus is covered by a porous double nuclear membrane (fig. 10). The inner and outer layers appear to be continuous with one another at the pores. In many sections a thick, intermittent nuclear cover was observed outside of the nuclear membrane and under the loose post nuclear cap (fig. 14). Further characterization of this cover could not be resolved. Nicander and Bane ('62) observed a similar semi-electron dense layer under the region which they designated as the equatorial segment in boar spermatozoa.

The head cap

The head cap can be divided into three major layers: an inner membrane, an outer membrane and a homogeneous moderately electron-dense middle layer (fig. 11). The inner and outer membranes are continuous with one another at the posterior margin of the head cap so that the homogeneous material between them is completely enveloped by a single membrane (fig. 14). This general description agrees with previous interpretations of the head cap of cat spermatids by Burgos and Fawcett ('53) of human spermatozoa by Fawcett and Burgos ('56) and by Anberg ('57) and of epididymal porcine sperm by Nicander and Bane ('62). The inner and outer membranes of the head cap represent the wall of the acrosomic vesicle found during

Bishop M. W H., and A. Walton 1960 Spermatogenesis and the structure of mammalian spermatozoa. In Marshall's Physiology of Reproduction. Vol. 1 pt. 2, 3rd ed., Longmans Green and Co. Ltd. London. 1–129

Blom, E. 1963 The galea capitis and apical body in bull sperm and the fertilization process. Internat. J Fert., 8 447–452.

Blom, E., and A. Birch-Andersen 1960 The ultrastructure of the bull sperm. I. The middle piece Nordisk Vet. Med., 12: 261–279

——— 1961 An Apical Body" in the galea capitis of the normal bull sperm. N ture, 190: 1127–1128.

Bonadonna, J 1958 Enquiries on the sperms of domestic animals using the electronic microscope. First report On the microstructure of "bos taurus sperms. Proc. Eighth Pacific Sci. Cong., 4 455–490.

Bradfield, J R. G. 1954 The structure of mammalian spermatozoa. Proc. Intern. Conf Elec tron Microscopy London, p 599–607

Bretschneider L. H. 1948 An electron microscopial study of sperm. II. Measurements of the head. (Trans. Title) Jydschr Diergeneeskunde, 73 233–253.

——— 1949 An electron-microscopial study of bull sperm. III. Proc. Kon. Ned. Akad. Wetensch., 52 301–309

Burgos, M. H., and D. W Fawcett 1955 Studies on the fine structure of the mammalian testes. I. Differentiation of the spermatids in the cat (felis domestica) J Biophys. and Biochem. Cytol., 1 287–300.

Caulfield, J B 1957 Effects of varying the vehicle for osmium in tissue fixation. J Biophys. and Biochem. Cytol., 3 827–830

Chang M. C. 1957 A detrimental effect of seminal plasma on the fertilizing capacity of sperm. Nature 179 258–259

Clermont, Y., R. E. Glegg and C. P Leblond 1955 Presence of carbohydrates in the acrosome of the guinea pig spermatozoon. Exp. Cell. Res., 8 453–458.

F wcett, D W 1958 Structure of the mammalian spermatozoon. Intern. Review of Cytology 7 195–234

F wcett, D W., and M. H. Burgos 1956 Ob servations on the cytomorphosis of germi and interstitial cells of the human testis. Ci Foundation Symposium, Ageing in Transie Tissues, 2: 86–99

Luft, J H. 1956 Permanganate — A new fix tive for electron microscopy J. Biophys ar Biochem. Cytol., 2: 799–802.

Mukherjee, D P and H. M. Dott 1960 Effe of egg yolk-citrate and egg-yolk-glycine dilu on the morphology of bovine spermatozoa J Agric. Sci., 55 225–228.

Nicander L., and A. Bane 1962 Fine structu of boar spermatozoa. Zeitschrift fur Zellforsch ung, 57 390–405.

Palade, G. E. 1952 A study of fixation for ele tron microscopy J Exp. Med., 95: 285–298.

Rahlman, D. F 1961 Electron microscop study of mature bovine spermatozoa. J. Dai Sci., 44 915–920.

Reed, C. L., and R. P Reed 1948 Comparati study of human and bovine sperm by electro microscopy Anat. Rec., 100: 1 7

Salisbury G. W., W J Birge L. De La Torre and J R. Lodge 1961 Decrease in nuclear feulgen positive material (DNA) upon aging in in vitro storage of bovine spermatozoa. J Biophys. and Biochem. Cytol., 10 353–359.

Savage, A., W W Williams and N. M. Fowler 1927 A statistical study of the head length variability of bovine spermatozoa and its ap plication to the determination of fertility Trans. Roy Soc. Can. 34th Series Sec. 5, 21 425–450.

Schnall, M. 1952 Electron microscopic study of human spermatozoa. Fertility and Sterility 3 62–82.

Wu, S. H., and F McKenzie 1955 Microstructure of spermatozoa after denudation as revealed by the electron microscope. J. Anim. Sci. 14 1151–1166.

Yasuzumi G., W F Jimura, A Tanaka, H Ishida and J Maruda 1956 Submicroscopic structure of the sperm head as revealed by electron microscopy Okajimas Folia Anatomica Japonica. Part 1–2, 29 133–138.

PLATES

PLATE 1

EXPLANATION OF FIGURES

2 Osmium-stained sections of the head oriented on basis of probable origin. × 20,200

A Near median sagittal section showing location of the apical body (AB) head cap (HC) nuclear ring (NR) post-nuclear cap (PNC) nucleus (N) and cell membrane (CM)

B Cross section of frontal part of the head showing the lateral extremities of the pical body (AB) and thin nucleus (N) in this region.

C Cross section in region of the head cap (HC)

D Cross section in the vicinity of the post-nuclear cap (PNC) The increasing thickness across the nucleus suggests the section should be oriented obliquely Compare with posterior thickening of the nucleus in sagittal section 2A.

E Cross section through the base of the head showing the top of the implantation socket (IS) for the tail. The head thickens along the median line t the base to accommodate the socket.

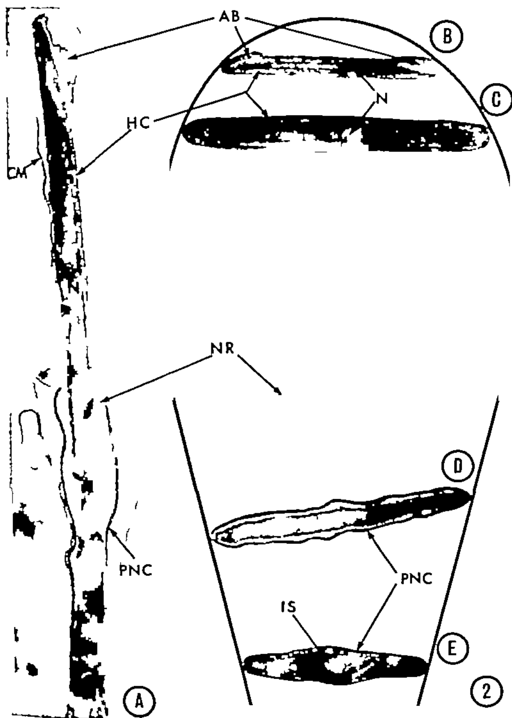

AB
B
C
N
HC
CM
NR
D
PNC
IS
E
2
A

PLATE 2

EXPLAN TION OF FIGURES

3 Osmium-stained sagittal section through the neck cut on plane parallel to the flat surf ce of the head. Left edge of nucleus may be ob-erved forming part of the socket (rrow) for ttachment of the tail. × 69 700.

4 Osmium-stained sagittal section through the neck cut t 90° to the fl t surface of the head. N evidence of socket is present in this typ of section. Attachment of the cell membrane along base of head i apparent (rrow) × 57,000


3


4

PLATE 3

EXPLANATION OF FIGURES

Figs. 5 to 8 Nuclear vacuoles (osmium stain)

5 Two round vacuoles at the base of the head.

6 A vacuole opening at the nuclear surface near frontal part of the head.

7–8 Irregular vacuoles found predominantly near the base of the nucleus. Figure 8 also shows the basal plate (BP) lining the recess at the base of the head.


5





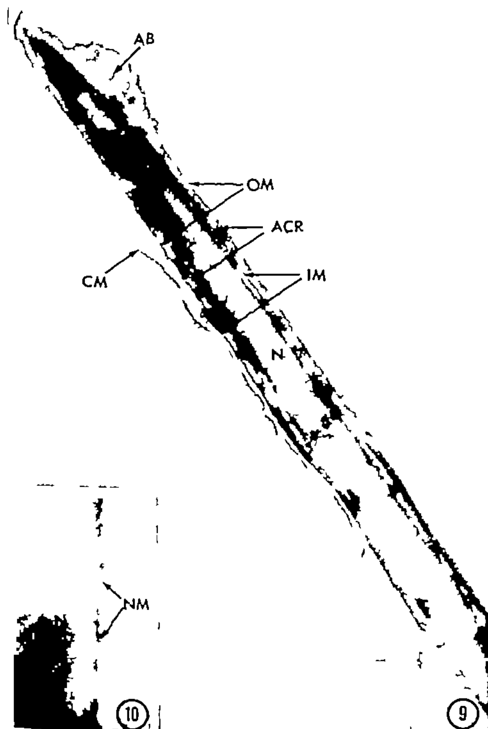

BP
8

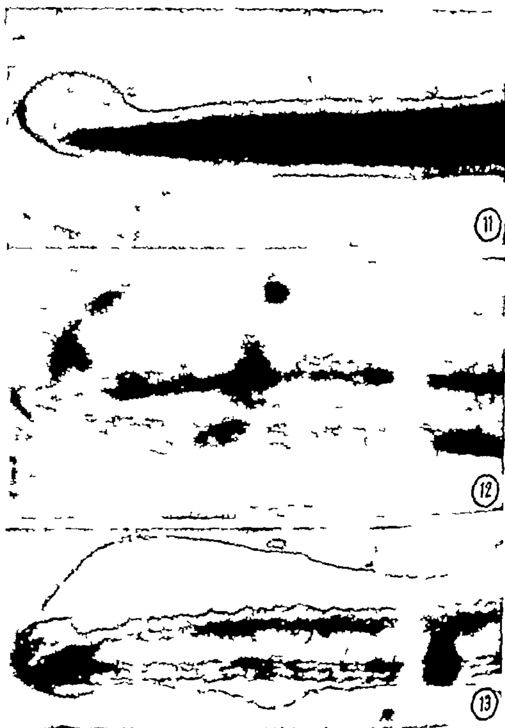
PLATE 4

EXPLANATION O FIGURES

9 Sagittal section (osmium stain) showing components of the head cap The head cap consists of three distinct layers thin, electron-dense outer membrane (OM); thick, moderately lectron-dense acrosomal layer (ACR); and thin highly electron-dense inner membrane (IM) The apical body (AB) appears as an enlargement of the acrosome on one sid of the nucleus. The cell membrane (CM) is the outermost covering. × 40,000.

10 High magnification of the nuclear surface (potassium permanganate stain) howing double porous nuclear membrane (NM) × 60,000.

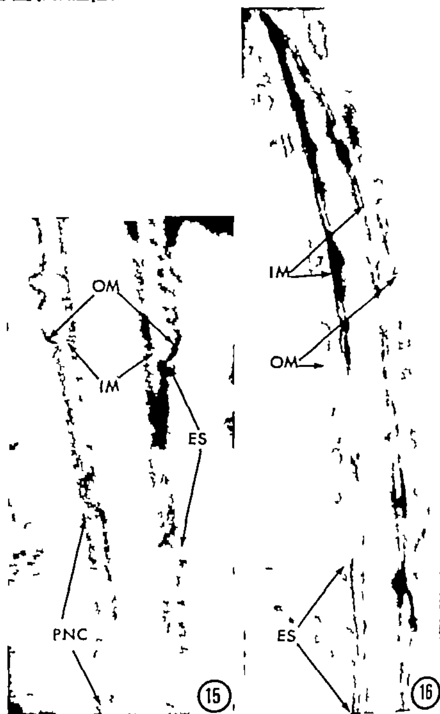

AB
OM
ACR
IM
CM
N
NM
10
9



11–13 Osmium-stained sagittal sections through the frontal part of the head showing variation in the appearance of the apical body. The more developed apical body in figure 12 is believed to have originated nearer the apex of the head. × 42,000

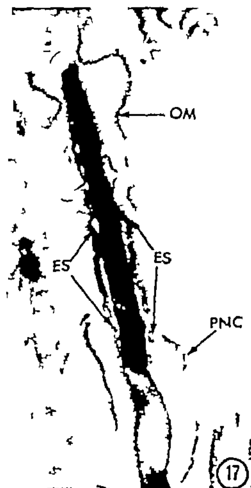


14 Near-median sagittal section (osmium-stain) through the posterior region of the head. In addition to the cell membrane (CM) in this region the nucleus is covered by the loose, electron-dense post-nuclear cap (PNC). A somewhat irregular moderately dense nuclear cover (NC) which could not be further resolved may be observed along the nuclear surface. The posterior margin of the head cap is pparent in the upper right hand corner. The arrow (HC) shows that the inner and outer membrane of the head cap are continuous with one another t this poin × 53,000.



15 Permanganate stained sagittal section in the region of the equatorial segment (ES) showing initial ph se of segment formation. The nterior portion f the head cap swells as noted by the sepa tion of the inner membrane (IM) and outer membrane (OM). × 57,000

16 Osmium-stained l section showing deterioration of the outer membrane (OM) with equatorial seg ES till intact The inner membrane (IM) also retains its identity × 40,000



17 Osmium stained sagittal section showing the equatorial segment (ES) as the intact inner and outer membranes of the posterior portion of the head cap. The anterior portion of the outer membrane (OM) is loose and will probably become detached from the head or deteriorate in place. Posterior to the equatorial segment is the post nuclear cap (PNC) × 22,000.

Ultrastructure of Bovine Spermatozoa

II. THE NECK AND TAIL OF NORMAL EJACULATED SPERM [1,2,3]

R. G. SAACKE AND J. O. ALMQUIST

Department of Dairy Science, The Pennsylvania State University, University Park, Pennsylvania

ABSTRACT The normal bovine sperm tail consists of the classical 9 + 9 + 2 fiber pattern bound anteriorly by the mitochondrial helix and posteriorly by the fibrous helix except for the last 2 to 3 μ.

The outer ring of nine coarse fibers originate as laminated columns, beginning from common base which is located in recess at the base of the head. The fibers taper posteriorly ending at different levels in the principal piece. Evidence is presented for the alternate contraction and expansion of the laminated segments of the coarse fibers in the neck — the probable mechanism for initiating the flagellar wave.

The mitochondrial helix is composed of several mitochondrial strands of different length. Each strand consists of several elongated mitochondria positioned end to end. Apparently the strands of mitochondria may begin or end at various locations along the middle piece. The number of turns in the mitochondrial helix was found to vary from approximately 65 to 75 turns among cells. The helix binds the axial fiber bundle with pitch of 20 to 25 over most of the middle piece. The mitochondria are double-walled and possess internal cristae that are vesicular or tubular in structure.

The fibrous helix consists of dense, circumferential strands of variable thickness and shape with two longitudinal elements on opposite sides of the helix. Both the circumferential strands and the longitudinal elements become thinner as they progress posteriorly

The tail of mammalian spermatozoa consists of three major regions as seen with the light microscope. Proceeding posteriorly they are the relatively thick middle piece, the thinner long principal piece, and the very thin, short terminal or end piece. The middle piece is joined with the head by a short, delicate segment referred to as the neck or implantation region.

As early as 1888 Ballowitz recognized that the sperm tail was more complex than the preceding description suggests Using the light microscope he observed occasionally that the tail frayed into a tuft of exceedingly fine fibrils. Later observations on whole and partially disrupted sperm under the electron microscope corroborated the early observations of Ballowitz that the flagellum was composed of several fibers (Baylor et al. 43 Bretschneider 49a, 49b Reed and Reed, 48; Randall and Friedlaender '50 Schnall, '52 Wu and McKenzie '55 Bonadonna et al. '58) Some of these studies revealed that the tail fibers were bound by a helix. The helical strands appeared thicker in the anterior portion of the flagellum than in the posterior portion (Bretschneider 49b Wu and McKenzie, '55) The middle piece was bound by the thicker helix and the principal piece by the thinner helix. The short terminal piece appeared to consist of the tail fibers without a helical cover (Baylor et al. 43) Thus, the three flagellar regions distinguishable with the light microscope were characterized ultrastructurally using the electron microscope.

Confusion concerning the number and arrangement of the flagellar subunits as well as characterization of the helix, prevailed until thin-sectioning techniques were employed with the electron microscope Subsequently much research has been undertaken to define the ultrastructure of the mammalian sperm tail. Several comprehensive monographs have been published (Anberg, '57 Fawcett, '58 '62)

Authorized for publication Oct. 14, 1963 as Paper no. [illegible] in the Journal Series of the Pennsylvania Agricultural Experiment Station.

[1] Supported in part by the Pennsylvania Association of Artificial Breeding Cooperatives.

The data contained in this paper are from thesis submitted by the senior author to the Graduate School of The Pennsylvania State University in partial fulfillment of the requirements for the degree of Doctor of Philosophy

Thin-sectioning techniques with electron microscopy have been successfully applied to the bovine sperm tail and neck (Bradfield '54 55 Blom and Birch-Andersen, '60 Rahlman, '61 Nicander and Bane 62) Nevertheless confusion still resides in the complete characterization of the mitochondrial and fibrous helix as well as the relationship of the flagellar fibers throughout the tail particularly their relation and origin in the neck region where they form the implantation structures Thus the present study was undertaken to delineate further the ultrastructure of the neck and tail of bovine spermatozoa.

MATERIALS AND METHODS

Semen was collected by means of the artificial vagina from Holstein bulls Ejaculates used had at least a volume of 3 ml an initial motility of 60% and a sperm concentration of 700 × 10^6/ml The influence of any one bull was reduced by pooling single ejaculates collected from five different bulls Semen was diluted either with previously heated skimmilk or a 2.9% solution of sodium citrate dihydrate.

Spermatozoa were centrifuged from the diluent at 4 C for 30 minutes at 750 g Centrifugation was carried out at 4 C instead of room temperature to reduce the resistance offered by motile sperm and to obtain a more equal distribution of motile and non motile sperm in the pellet The supernatant was decanted and the loose pellet of spermatozoa was transferred in pieces (approximately 3 mm) to a petri dish containing semisolid 2 5% agar at 20 C Following transfer the agar was permitted to solidify at room temperature

The use of agar as suggested by Blom and Birch-Andersen (60) served to maintain the integrity of the loose pellets during fixation and the early stages of dehydration The tissue then became sufficiently hard and the agar was no longer needed

Pellets from each pooled sample were divided into two portions One portion was fixed in 1% osmium tetroxide buffered with veronal acetate (P l de [illegible]) containing sucrose (Caulfield [illegible] nd the other portion in potassium per[illegible] nate fixative (Luft 56) Both fi[illegible] ere buffered at pH 7 2 to 7 4 Tissues were dehydrated in a graded series of ethanol baths and embedded in Araldite. Sections were cut with glass knives using a Porter-Blum ultramicrotome and electron micrographs were made with an RCA EMU-3 electron microscope.

OBSERVATIONS AND DISCUSSION

In contrast to the sperm head, the most widely accepted ultrastructural features of the mammalian sperm tail show considerably less species variation. The present study of the bovine sperm tail indicates that it also conforms quite closely to the general pattern described for other mammalian sperm. Modifications of the standard flagellar pattern were observed however it was difficult in most cases to ascertain whether any given variation was species-specific or merely unobserved in cells of other species.

Graphic illustrations of various segments of the bovine sperm tail are presented (figs. 1 to 4) These illustrations include information based upon interpretations of observations from the present study as well as those from previous studies of the bovine sperm cell (Baylor et al 43; Reed and Reed 48 Bretschneider 49a, b '50 Bradfield, 54 '55 Wu and McKenzie, '55 Blom and Birch-Andersen '60; Rahlman 61 Nicander and Bane '62a)

The length of the bovine sperm tail and its components are measured most advantageously in whole cell preparations However the thickness of the tail and its components barring preparational artifacts, can be measured from electron micrographs of cross sections or median sagittal sections Based on such sections, the middle piece was found to possess a relatively uniform diameter of from 0 85 μ to 0 72 μ A sharp decrease in flagellar diameter occurs at the junction of the middle piece and principal piece This is due to termination of the thick mitochondrial helix and the beginning of the thin fibrous helix (fig 1)

The anterior portion of the principal piece measured approximately 0 50 μ in diameter and tapered posteriorly to approximately 0.25 μ near the terminal piece

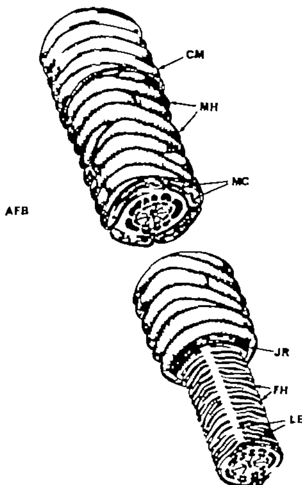


Fig. 1 Graphic illustration summarizing ultrastructural features of the middle piece and anterior portion of the principal piece. The cell membrane has been partially removed and the flagellum cut to show internal structure. Cell membrane (CM); mitochondrial helix, (MH); mitochondrial cristae, (MC); Jensen ring, (JR); fibrous helix, (FH); longitudinal element, (LE); axial fiber bundle, (AFB) consisting of the nine outer coarse fibers, the nine inner fibers or doublets and the central pair of fibers.

The axial fiber bundle

In the middle piece and anterior portion of the principal piece the axial fiber bundle (all fibers of tail) was found to consist of twenty fibers arranged concentrically in two rows of nine each around a central pair (figs. 1, 8 and 9). This arrangement, known as the 9 + 9 + 2 fiber pattern, has been described previously in spermatozoa of the bull (Bradfield, '55; Blom and Birch Andersen, '60; Rahlman, '61) as well as other mammals (Bradfield, '54, '55; Fawcett, '58; Anberg, '57; Telkka et al., '61). The inner ring of nine fibers or doublets (double fibers) plus the central pair collectively known as the axial filament complex or 9 + 2 fiber pattern, were found in the middle piece, principal piece and terminal piece. This complex is a truly classical arrangement in that it has been observed in many other flagella and cilia throughout the animal and plant kingdoms. Using a modified method of specimen preparation, Afzelius ('59) has clearly described this complex in the tail of the sea urchin sperm.

Based on the observations in the present study the axial filament complex may be

described as follows: The central pair appears as hollow tubes measuring 190 Å in diameter The nine doublets are spaced equally (approximately 100 Å apart) in a ring around the central pair One fiber member of each doublet appears hollow and the other moderately dense when examined in cross section (fig 8) The fiber members or subfibers of each doublet are positioned on the same circumference (approximately 0 1 μ from the tail center) and the dense subfiber is always located on the same side of the hollow subfiber of each doublet. The individual subfibers measure approximately 190 Å in diameter This measurement is in close agreement with that reported by Bradfield ('54)

The spatial relationships of the doublets to each other and the central pair as well as their individual diameters appeared uniform throughout the entire tail with the exception of the neck region where they originate and the terminal piece where they end. Fine radial spokes extending from the central pair to the dense subfiber of each doublet are apparent in some cross sections (figs 9 and 15) A very low electron dense matrix between the components of the axial filament complex is apparent also in some sections (fig. 8) The reason all sections were not uniform with respect to the presence of spokes and matrix could ot be ascertained.

Blom and Birch-Andersen ('60) compared the axial filament complex of bovine sperm with that of sea urchin sperm as critically defined by Afzelius ('59) The axial filament complex of sea urchin sperm features two hollow subfibers composing each doublet with one or two arms of varying length which extend laterally from some subfibers toward the adjacent doublet. Afzelius ('59) showed that the subfibers of each doublet were positioned nearly equidistant from the center of the central pair Radial spokes also were apparent extending from between the central pair toward each doublet.

The present data on bovine sperm indicated a modification in the axial filament complex which is in accord with that described by Telkka et al ('61) for guinea pig rat and bat sperm. These workers described an electron dense subfiber and a hollow subfiber as components of each doublet. The occurrence of a solid or semi-solid subfiber member and a hollow member in each doublet also was observed in the flagellum of protozoa (Gibbons and Grimstone, '60) and rooster sperm (Nagano '60)

In addition, Telkka et al. ('61) observed two small arms extending laterally from the dense subfiber of each doublet toward the adjacent doublet. There were indications that such arms were present in bovine sperm; however they could not be clearly resolved and were omitted from the interpretative illustration.

A modification in the radial spoke pattern was offered by Fawcett ('62) He described the pattern as consisting of linear densities in the matrix of the complex consisting of two curved lines connecting one member of the central pair to the other and nine radial lines connecting the central pair with the dense subfiber of each doublet. Thus the possibility exists that there are subtle connections between all elements of the axial filament complex.

The outer ring of nine dense longitudinal fibers (coarse fibers) were studied best from precise cross sections through the middle piece (figs. 8 and 9) in contrast to longitudinal sections (fig. 6) In cross sections these fibers appeared as large electron dense rods of varying cross sectional area and morphology They comprise the outer ring of the axial fiber bundle and each coarse fiber is located on the same radius as a doublet. In the middle piece there are three large coarse fibers (approximately 1 000 Å × 400 Å) five small fibers (approximately 400 Å), and one intermediate sized fiber (approximately 750 Å × 400 Å) Since these fibers taper as they pass down the middle piece into the principal piece, these measurements are only guides to the relative size of the coarse fibers.

Studying bull sperm Bradfield ('54) found three and occasionally four large fibers which exceeded the remaining coarse fibers in cross sectional area, while Blom and Birch-Andersen ('60) observed four large coarse fibers (main fibers) and five smaller fibers (secondary fibers) in the middle piece A possible explanation for the inconsistency of the findings of these studies to the present one may readily

in breed differences of the bulls used. A variation in the morphology and relative size of the coarse fibers among species is evident from the literature

As observed from cross sections of the middle piece two of the larger fibers are adjacent and a single large fiber is located on the opposite side of the ring An accepted numbering system for the coarse fibers begins with the single large fiber as 1 and proceeds in a clockwise direction As may be observed in figure 8 this results in the large fibers being numbered 1 5 and 6 the intermediate fiber 2 or 9 (depending upon which side of a cross section is examined) and the thin fibers 3 4 7 8 and either 2 or 9 (whichever is not intermediate in size) If flagellar cross sections are oriented such that the dense subfiber is to the right of the hollow subfiber within each doublet (when examined from the center of the section) then the number 9 fiber is always the intermediate sized fiber The coarse fibers are always oriented in strict relationship to the central pair This becomes apparent when an imaginary line is drawn through fiber 1 and between fibers 5 and 6 (fig 9) The line always bisects the axis of the central pair at right angles. Unlike the doublets and central pair the coarse fibers gradually become smaller as they pass posteriorly into the principal piece where they eventually disappear (fig. 15) As observed in sperm of other animals (Telkka et al. '61) the coarse fibers terminate at different levels within the principal piece Telkka et al. found that the largest fibers observed in the middle piece persist the longest while the smaller fibers terminate earliest i.e. fibers 3 and 8 disappear first followed by 4 and 7 and then 2 or 9 which ever is smallest. Fibers 1 5 and 6 terminate last. Wu ('63) has observed in bovine sperm that, although fibers 3 and 8 are much reduced in area, they persist farther down the principal piece than the other coarse fibers A closer examination in the present study corroborates this observation (fig 15) Thus, the order of fiber disappearance follows that outlined by Telkka et al. ('61) except that fibers 3 and 8 persist as small dense structures after the other seven coarse fibers terminate The distance over which the nine fibers terminate is probably quite short with respect to the length of the principal piece since sections showing missing fibers are not encountered frequently

If the coarse fibers are examined in cross sections obtained from the most anterior portion of the middle piece (just posterior to the neck) they appear nearly equal in cross sectional area (fig 7) They also have a core of moderate electron density with a border of greater density A longitudinal section of this region (fig 5) shows that the coarse fibers also become striated as they leave the middle piece and enter the neck region. The striations appear as highly electron dense areas approximately 300 Å thick, separated by moderately dense areas 130 Å thick. Although all the bands cannot be counted in figure 5 there are approximately 13 to 15 dense bands on each fiber

The origin of the doublets and central pair remains quite vague except that they most likely begin in the anterior region of the middle piece. In cross sections through this region (fig 7) no evidence of the doublets or central pair was found. However highly electron dense areas along the inside of each coarse fiber were observed. It is possible that the dense areas may represent the origin of the doublets which will eventually move away from the coarse fibers further down the middle piece. It also seems reasonable to believe that the course fibers give rise to the doublets or that both are of the same origin, since the additional ring of nine outer fibers is a modification in the spermatozoan flagella of higher forms of animal life.

The mitochondrial helix

The presence of the mitochondrial helix distinctively defines the middle piece of the sperm tail. In bovine sperm the helix makes approximately 65 to 75 turns from the neck to Jensen's ring (fig. 10) The number of turns in the helix varied within this range among three cells which were sectioned longitudinally through the entire middle piece.

The pitch of the spiral is about 20 to 25 over most of the middle piece but it is steeper than this in the neck region The helix is formed by an undetermined number of elongated mitochondria butting

end to end against one another (fig 12) There is also evidence that the helix is not single but rather composed of more than one string or strand of mitochondria (fig 13) In the neck region several mitochondria begin winding down the axial fiber bundle. Some of these terminate before they reach the base of the middle piece By the same token other strands of mitochondria probably begin part way down the middle piece (fig 13) The length of any one particular spiral or any one mitochondrion could not be determined accurately

In a median sagittal section of the middle piece (fig 6) the elongated tubular mitochondria of the helix are cut in cross sections and appear as a column of small spheres exterior to the axial fiber bundle. The diameter of the mitochondria is approximately 0 10 to 0 15 μ; however they appear to be considerably smaller in some cases The smaller diameters most likely represent the tapered terminus or beginning of a particular mitochondrion

The mitochondrial wall and internal mitochondrial membranes (cristae) are double (figs. 6 and 14) They also may be considered triple if the layer between the inner and outer membrane is included When the helix is viewed in longitudinal section (fig 12) the cristae appear to parallel the direction of the helix The cristae originate from the wall of the mitochondrion then turn and proceed parallel with the wall. They also exhibit occasional branching The cristae and their branches may be described as flattened or curved vesicles (fig. 6) and tubules (fig 14)

Occasionally cells without cristae were observed This has been shown to be a characteristic of spermatozoa fixed following death or injury of the cell (Saacke and Almquist '62, '63a) In these cases the cell membrane was usually severely damaged or missing.

Jensen's ring

Jensen's ring is an electron dense structure which surrounds the axial fiber bundle at the junction of the middle piece and the principal piece A sagittal section at this junction shows Jensen's ring in cross section on both sides of the axial fiber bundle (fig 11) From this view the ring may be described as an electron dense triangle with the base against the last turn of the mitochondrial helix and the apex pointing down the principal piece. This description agrees closely with the observations of Blom and Birch-Andersen ('60) The sides of the triangle are approximately 800 to 1 000 Å long and usually extend far enough to cover the first few winds of the fibrous helix.

Of particular interest is the attachment of the cell membrane to Jensen's ring (fig. 11) In some longitudinal sections of the tail the cell membrane appears to stop at the base of the triangle and begin again at the apex. Other sections clearly reveal that the cell membrane adheres closely to the ring without a break. The cell membrane is also anchored about the base of the head (Saacke and Almquist '64) Thus the head midpiece, and principal piece are distinct and separate with respect to the external environment of the cell. These attachments may be of significance during the traverse of the protoplasmic droplet down the middle piece as well as at the time of the shedding of the droplet They also may be important during capacitation when changes involving loss of the head cap are believed to occur Such changes could occur without disturbing the cell membrane surrounding the flagellum. On the other hand, a variation in selective permeability of the cell membrane among the segregated regions of the flagellum may favor cellular metabolism This idea is introduced only because of the elongated and separated aspects of the cellular components (cf nucleus and mitochondria)

Fawcett ('58) observed a physical contact of the cell membrane with part of a more elaborate Jensen's ring which he found in epididymal and testicular spermatozoa of the human Further attention should be given to this area in studies of the ultrastructure of bovine epididymal spermatozoa Fawcett ('58) suggested that a difference may exist in the structure of the annulus in ejaculated and epididymal sperm of man.

The fibrous helix and terminal piece

The fibrous helix binds the axial fiber ndle posteriorly beginning at the ter ination of the mitochondrial helix and tending to within 2 to 3 µ from the rmination of the axial filament complex ig. 2) The unbound end of the axial ament complex has been designated the rminal piece.

In a sagittal section of the principal iece, the helical strands are cut in cross ctions (fig. 11) The fibrillar windings are observed as closely-spaced thin, dense strands of variable shape and size. When the principal piece is cut in cross sections however the helical strands are viewed longitudinally (fig 15). The helical strands become thinner as they move posteriorly along the axial fiber bundle and, at the same time move closer to the axial filament complex as the coarse fibers disappear (fig 15) This accounts for the posterior taper of the principal piece (fig. 2)

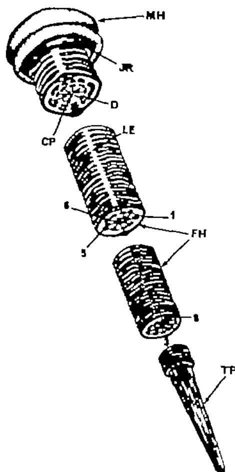


Fig 2 Graphic illustration of the principal piece and terminal piece. The cell membrane has been removed and the principal piece cut at various locations to show internal structure. Mitochondrial helix, (MH); Jensen ring, (JR); central pair of fibers (CP) doublet, (D) longitudinal element, (LE); fibrous helix, (FH); terminal piece (TP)

From cross sections of the principal piece two thickenings on opposite sides of the fibrous helix are apparent. The thickenings are always located on the same axis as the central pair of fibers The interpretations of these thickenings in other mammalian spermatozoa have varied from sectioning artifacts (Shultz Larson '58) to the presence of two longitudinal elements or rods which pass down on both sides of the principal piece (Bradfield, 53 '55 Fawcett, '58 '62 Telkka et al., '61) Longitudinal sections of the principal piece of bovine sperm obtained in the present study (figs. 16 to 18) support the latter interpretation The rods apparently begin at the anterior extremity of the fibrous helix and become thinner posteriorly They either disappear prior to the termination of the helix or become sufficiently small to escape detection in cross sections near the terminal piece (fig 15)

A reasonable proposal has been made by Fawcett ('58) that the existence of longitudinal rods precludes the presence of a helix. It is not clear however whether the circumferential strands lose their identity in the longitudinal elements or split and pass around them. Further study of this relationship should be conducted before the term helix is abandoned

The neck

The neck of the bovine sperm is characterized best by the lack of mitochondria and the presence of the laminated coarse fibers entering the recess or implantation socket at the base of the head (figs. 3 and 4) The beginning of the mitochondrial helix in relation to the base of the head varies sufficiently to conclude that the

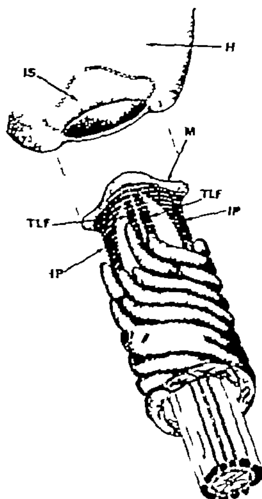


Fig. 3 Graphic illustration of the neck region. The cell membrane is removed and the tail separated from the head to show the articulation mechanism. Head, (H); implantation socket or head recess, (IS) matrix, (M); implantation plates (IP) thin laminated fibers, (TLF)

length of the neck probably ranges from 0.3 to 1 5 μ or more

A sagittal section through the neck on a plane with the flat surface of the head (fig. 20) shows two relatively large laminated fibers entering the head one on each lateral extremity of the head recess Blom and Birch-Andersen (60) have referred to these two structures as the implantation plates These workers believe that each plate is formed by the merger of two thick, coarse fibers which they found on each side of he axial fiber bundle. A sagittal section h ough one of the implantation plates at r ah ngles to that shown in figure 20 may be seen in figure 24 As the implantation plate is traced from its anterior base posteri in this figure it separates into more than one fiber The specific fibers which co tribute to the implantation plates ho ever could not be determined. One pr cluding factor is that the fibers we observed to be of nearly equal size in the middle piece just prior to entering the neck (fig. 7)

In addition to the two implanta plates, at least four other laminated fibe enter the base of the head. The tip of two of these fibers may be seen exten the head recess between the implan plates in figure 20 The present inte tation is that these two fibers make a 1 arc at the top of the head recess and p back down into the neck (fig. 23) The laminated fibers are positioned close t gether and are considerably thinner the the implantation plates. This relations is shown in the graphic illustration (fi 3 and 4) A cross section through th neck region of a boar spermatozoon p sented by Nicander and Bane (62b) show that a fifth small fiber is present in th neck along with the two implanta plates

A homogeneous matrix across the t of the laminated fibers forms a comm base for the insertion of the fibers in the head recess (fig. 20) The comm base is held in the head recess by a li (fig. 20) on each side of the recess th a modified ball and socket joint is p duced (fig. 3)

Blom and Birch-Andersen (60) de scribed the articulation mechanism a consisting of a capitulum, formed by th merger of the implantation plates, whi fits into the concave base of the head o socket. They suggested that the rema ing fibers may attach directly to the b of the head. In the present study n evidence of a physical connection of a fiber elements with the head was fou The thin fibers as well as the implanta tion plates, are considered to form th common cap which fits into the base of the head The cap appears to be held p place merely by the lips formed at ea end of the opening into the head

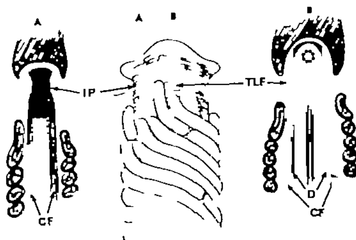


Fig. 4 Two-dimensional sagittal sections through the neck region (A and B) Section A shows the relationship f the implantation plate (IP) to the coarse outer fibers (CF) The implantation plate on each side splits forming some of the coarse fibers that extend down the tail.

Section B shows thin laminated fiber (TLF) which is continuous at the top of the head recess This section also shows the possible origin of the doublets (D) budding aw y from the coarse fibers.

A possible role of the laminated portion of the coarse fibers may be advanced on the basis of the sagittal section through the two implantation plates shown in figure 22. The implantation plate on the left of this figure appears to be in a state of contraction while the plate on the right is in the expanded state Thus the alternate contraction and expansion of the laminated fibers in this region may initiate the flagellar wave.

Although considerable debate still exists on the pattern of the flagellar wave the size and therefore strength, of the implantation plates would suggest a two-dimensional or planar wave. This is supported by the suggestion of Blom and Birch-Andersen ('60) that the implantation plates are formed by the thicker outer fibers on each side of the axial fiber bundle. These fibers are known to be dominant in size throughout much of the tail However similar contraction and expansion of the thinner laminated fibers in the neck region would contribute to the wave to a lesser degree but in the third dimension.

Thus the present interpretation favors a predominantly two-dimensional flagellar wave but with some movement in the third dimension Such a mechanism might be compared with the flat, figure-of eight, flagellar pattern proposed by Gray ('58) for bull sperm.

The presence of the proximal centriole in the recess at the base of the head was confirmed however its morphology remains speculative The characteristic ring of beads was observed only in sagittal sections of the neck when the head was cut at or about 90 to its flat plane (figs. 25 and 26) Fawcett ('58) has stated that the proximal centriole of the spermatozoon is no different than the typical centriole of a somatic cell. The typical centriole takes the form of a cylinder with a wall composed of nine rods arranged longitudinally Thus, the centriole shown in figure 25 might represent a cross section of the cylinder An oblique section through the cylinder is shown in figure 21 The cylinder is located at the base of the head oriented at about 70–80 to the tail on an axis across the greatest dimension of the head. An excellent electron micrograph presented by Nicander and Bane ('62b) shows the proximal centriole of a boar spermatozoon as consisting of nine tubular triplets i e each of the nine tubes constituting the centriole contain three separate tubules.

Further research should be conducted to clarify the morphology of the proximal centriole and the relationship of the flagellar fibers to each other and the centriole in the neck region. Ultrastructural individuality among sperm also should receive more attention. Based on ultrastructural variations particularly those observed in the mitochondrial helix cells may possess a variety of features which are capable of normal physiological function

ACKNOWLEDGMENTS

We wish to thank Dr P Grun for his technical advice on the microscopy techniques and the use of facilities of the Department of Botany and Plant Pathology

Messrs J Comer and S Irving for their technical advice on the microscopy and the use of facilities of the Electron Microscopy Section of the Mineral Constitution Laboratory

Mrs V Holter for the interpretative graphic illustrations

LITERATURE CITED

Afzelius, B. 1959 Electron microscopy of the sperm tail. J Biophys. Biochem. Cytol., 5 269–278

Anberg, A. 1957 The ultrastructure f th human spermatozoon. Acta Obstet. Gynecol. Scand., Suppl. 2, 36 1–133.

Ballowitz, E. 1888 Untersuchungen uber die Struktur der Spermatozoen Zugleich ein Beitrag zur Lehre vom Feineren Bau der contraktilen Elemente. Arch. Micr Anat., 32 401–473.

B ylor M. R. B A Nalbandov and G L. Clark 1943 Electron microscope study of sperm. Proc. Soc. Med 54 229–232.

Blom, E., and A. Birch-Andersen 1960 The ultrastructure of the bull sperm I. The middle piece. Nordisk Vet. Med., 12: 261–279.

Bonadonna, J 1958 Enquires on the sperms of domestic animals using the electron microscope First report on the microstructure of "bos taurus sperms. Proc. Eighth Pacific Sci. Cong., 4 455–490.

Bradfield, J R. G. 1954 The structure of mammalian spermatozoa. Proc. Intern. Conf. Electron Microscopy London. p. 599–607

——— 1955 F ber patterns in animal flagell and cilia. Symp. Soc. Exptl. Biol 9 306–334.

Bretschneider L. H 1949 An electron-microscopial study of bull sperm. III. Proc. Kon. Ned., Akad. Wetensch., 52: 301–309.

——— 1949b An electron-microscopial study of sperm. IV The sperm tail of bull, horse and dog. Proc. Kon Ned Akad Wetensch., 52: 526–534

——— 1950 Elektronen-Mikroskopische [illegible]turuntersuchung an Spermien. V Proc. Ned. Akad. Wetensch., 53 531 541.

Caulfield, J B 1957 Effects of varying [illegible] vehicle for osmium in tissue fixation. J Biophys. and Biochem. Cytol., 3. 827–830

F wcett, D W 1958 Structure of the mammalian spermatozoon. Intern. Review of Cytology 7 195–234.

——— 1962 Sperm tail structure in relation to the mechanism of movement. Proc Sym. on Spermatozoan Motility Amer. Assoc Adv Sci., New York, Publ. no. 72, p. 147–169

Gibbons, I. R., and A. V Grimstone 1960 On flagellar structure in certain flagellates. J Biophys. Biochem. Cytol 7 697–715

Gray J 1958 The movement of the spermatozoa of the bull. J Exptl. Biol., 35 96–108

Luft, J H. 1956 Permanganate — A new fixative for electron microscopy J. Biophys and Biochem. Cytol., 2 799–802.

Nagano, J 1960 The fine structure of the sperm tail of the domestic fowl (*Gallus domesticus* J Appl. Physics 31 1844 (abst.).

Nicander L., and A. Bane 1962a New observations on the fine structure of spermatozoa. Intern. J Fert., 7 339–344.

——— 1962b Fine structure of boar spermatozoa. Zeitschrift fur Zellforschung, 57 [illegible]–406.

Palade G E. 1952 A study of fixation for electron microscopy J Exp. Med., 95 285–297

Rahlman, D F 1961 Electron microscopic study of mature bovine spermatozoa. J Dairy Sci., 44 915–920.

Randall, J T and M. H. G. Friedlaender 1950 The microstructure of ram spermatozoa Exp Cell. Res., 1 1–32.

Reed, C. I. and B P Reed 1948 Comparative study of human and bovine sperm by electron microscopy Anat. Rec., 100: 1 7

Saacke, R. G and J O Almquist 1961 The structure of bovine spermatozoa freeze-dried with and without glycerol. J Dairy Sci 44 674

——— 1963 Ultrastructure of bovine spermatozoa subjected to various lethal agents. J Dairy Sci., 46 636.

——— 1964 Ultrastructure of bovine spermatozoa I. The head of normal, ejaculated sperm. Amer J Anat., 115: 143–162

Schnall, M. 1952 Electron microscopic study of human spermatozoa Fertility and Sterility, [illegible] 62–82.

Schultz-Larsen, J 1958 The morphology of the human sperm Opera Ex Domo Biologiae [illegible] reditarial Humanae Universitatis Hafniensis 41 1–121.

Telkka, A., D W F wcett and A. K. Christensen 1961 Further observations on the structure of the mammalian sperm tail. Anat. Rec 14[illegible] 231–246.

W S. H 1963 Personal Communication

Wu, S. H and F M Kendle 1955 Microstructure of spermatozoa after denudation as revealed by the electron microscope J An Sci., 14 1151 1166.

PLATES

PLATE 1

EXPLANATION OF FIGURES

Figs. 5 to 9 Osmium-stained sections of the middle piece.

5 Sagittal section through the neck and anterior extremity of the middle piece showing relations of the outer coarse fibers in this region. × 66,000.

6 Median sagittal section of the middle piece. From the outside margin to the center it shows the cell membrane, a row of mitochondrial cross sections, an outer coarse fiber, a doublet, and a center fiber. Distinct vesicular cristae are apparent within the mitochondria. Occasional, small mitochondrial cross sections probably represent the tapered beginning or terminus of a mitochondrial strand. × 57,600.

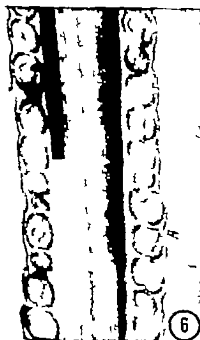
7 Cross section through the middle piece near the neck. The outer coarse fibers are nearly equal in size and the mitochondria are arranged at a sharp angle down the tail. Note the absence of a central pair and doublets. The highly electron dense, inside edge of each coarse fiber may represent the origin of the doublets. × 63,000.

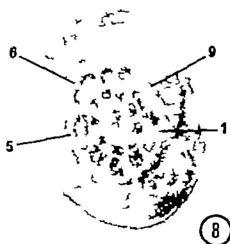
8 Cross section through the middle piece showing components of the axial fiber bundle. The large fibers (1, 5, and 6) and the intermediate sized fiber (9) are numbered for orientation. A hollow and a dense subfiber constituting each doublet is apparent. × 91,000.

9 Cross section through the middle piece showing the orientation of coarse fibers. A line passed through fiber 1 and between fibers 5 and 6 always bisects the axis of the central pair at right angles. Fine radial spokes between the central pair and solid subfiber of each doublet are apparent. × 78,000.


5


7


6


6
9
5
1
8


9

PLATE 2

EXPLANATION OF FIGURES

Figs. 10 and 11 Osmium-stained sagittal sections through the middle piece and anterior portion of the principal piece.

10 Low magnification electron micrograph showing entire length of the middle piece. In this cell the helix makes approximately 70 turns about the axial fiber bundle. × 15,400.

11 High magnification electron micrograph showing the junction of the middle piece and principal piece. The cell membrane (CM) anchors itself on Jensen ring (JR) Occasionally membranous vesicles (MV) are found immediately under the cell membrane. × 44,500.


CM
CM
JR
MV
10
11

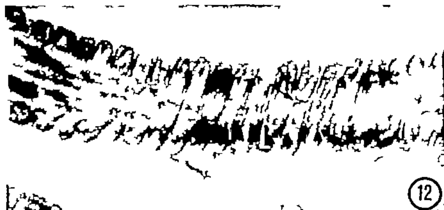
PLATE 2

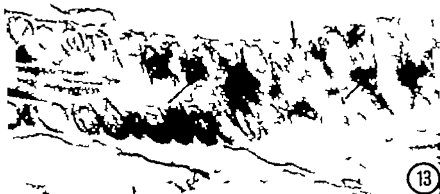
EXPLANATION OF FIGURES

Figs 10 and 11 Osmium-stained gittal section through the middle piece and anterior portion of the principal piece

10 Low magnification lectron micrograph showing entire length of the middle piece In this cell the helix makes pproximately 70 turns bout the axial fiber bundle 15 400.

11 High magnific tion lectron microgr ph showing the junction of the middle piece and principal piece The cell membrane (CM) anchors itself on Jensen ring (JR) Occ sionall membranous esicles (MV) are found immediately under the cell membrane. × 44 500


12


13

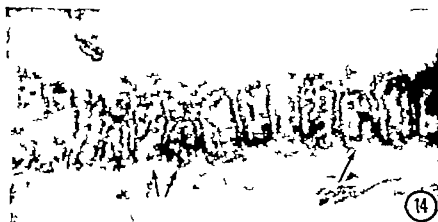

14

PLATE 4

EXPLAN TION OF FIGURES

Osmi m tained section of the principal piece

15 Cros section t different lev l long the principal piece anterior region A; middle region, B; and posterior region, C. The principal piece tapers in posterior direction with the longitudinal lements (LE) nd ircumferential tr nd (CS) of the fibrous helix becoming thinner The coarse fibers become thinner in posterior direction and eventually disappear Fibers 3 and 8 section C persi t farther down the principal than the other seven fibers (arrow) 47,300.

16 Sagittal section f principal piece howing continuity of one longitudinal lement (arrow) in contr t to the circumferential trand on the other side of the axial fiber bundle A periodicity of electron dense area along the inside nd outside edge of the longitudinal lement suggests that the circumferential trands may p s around the longitudinal element. × 60 000.

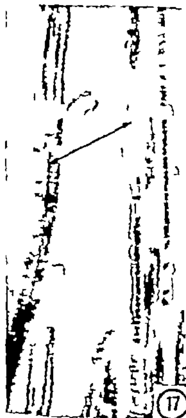
17 Low m gnific tion lectron micrograph comparing two gittal sec tions of the principal piece The ppearance of the longitudinal element (arrow) and circumferential trand may be compared. × 22,000

18 High m gnific tion of the longitudinal lement × 48,500.

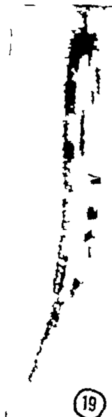
19 Oblique section showing the end of the fibrou helix and beginning of the terminal piece The axial filament complex i bserved to extend beyond the helix thereby forming the tapered terminal piece × 35,000


CS
LE
C
B
B
A
15


16


17


18


19

Persistent Stunting Following X Irradiation of the Fetus

ROBERTS RUGH, LYSE DUHAMEL, ALAN W OSBORNE AND A. VARMA

Radiological Research Laboratory Department of Radiology Columbia University New York

ABSTRACT CFI female mice were time mated and the embryos at each gestation day from 0.0 to 18 0 were x-rayed to 100 and the young carried to four months at which time a skeletal study was made. With this exposure the litters were reduced in size, following irradiation at certain gestation ages, and there was neo-natal mortality so that this skeletal study is based upon the survivors to four months and represents the maximum development under the conditions of irradiation. The sex ratio was not altered by this irradiation. Male mice of this strain are always heavier than the females of the same age, and this exposure reduced the over-all average of either sex by 2.5 grams. The skeletal measurements were taken from 1,006 radiographs of the living animals, and the averages calculated for each gestation day There were sex differences in stunting, even when x-irradiation occurred before day 9 0. *When the differences were pronounced the female was the more adversely* affected. The highest statistical significance in skeletal effects of seven measurements was between 11 and 13 days, when the embryo shows the earliest skeletal differentiation. Such mice were topographically well developed.

Stunting is a frequent sequela of embryonic and fetal x-irradiation, as has been well established. The amount of stunting with respect to dose of x-irradiation and the persistence of stunting for an extended post-natal period have not been so well established, although Russell ('54 '58 '60) reported skeletal effects of 200 to 400 exposures. It was the purpose of this project, using large numbers of mice to determine statistically the effect of a standard dose of x-rays (100 r) at each of the prenatal stages from 0 0 through 18.0 days gestation, as determined on the four month old adult mouse Using a standard dose of x-irradiation it is possible to establish those prenatal stages when the skeletal primordia are particularly *radiosensitive*.

MATERIALS AND METHOD

The mouse used was the CFI non-Swiss albino strain. Virgin females of more than two months of age were exposed during a two hour period to mature males of the same strain, and those with vaginal plugs at the end of this period were segregated and labeled as to the time of conception. Since the x-irradiation to be used was the LD50 for embryos of certain ages, the litter mate survivors would most likely have reduced vitality as would their mothers so that foster mothers were provided for all newborn mice of this project. Foster mothers comprised similar females simultaneously mated, but never x-irradiated, whose young were removed at birth and replaced by a litter which had been x-rayed in utero. When this exchange was made in a new box, with new shavings and new environment the foster mothers generally accepted the new litter without any difficulty and nursed them regularly as their own.

The x-ray conditions were as follows Dual tubes were used in cross fire spaced 72 cm each from the center of the gravid uterus. The voltage of the machine was *184 KVP* and the *milliamperage of each* tube held at 30 with filtration of 0.28 mm Cu and 0.50 mm Al, HVL of 0 6 mm Cu, and dose in air 50 r per minute The previous experience of x irradiating five mice at a time (which increases slightly the irradiation due to scatter) and within a

---

Supported by Project AT(30-1)-2740 for the Atomic Energy Commission, and aided by PH grant RH-81.
From the Department of Radiology Columbia University

Assistant Professor, Biostatistics, Department of Public Health, Columbia University

porous polyethylene container (which absorbs slightly the irradiations) gave the estimated rads absorbed by the embryos or fetuses very close to the dose in air at that position The exposure was thus two minutes in all cases

For the radiographs the mice were not anesthetized but were immobilized with strips of masking tape Five mice were fastened to the carrier of a sheet of 10 × 12 DuPont x-ray film which was then properly identified with lead letters and numbers and placed at a uniform distance of 20 inches from a diagnostic x ray tube The voltage used was 40 milliamperes 10 and the uniform exposure was two seconds The films gave excellent contrast (see illustrations) Each and every mouse skeleton was thus radiographed and this was later mounted on an x ray viewing box and each bone measurement taken under a hand lens of 10 × magnification All measurements were made by the same person

The mice were part of an experiment designed to determine the long term sequelae of embryonic and fetal x irradiation so that most of them are still alive 14 months of age However it is believed that the skeleton has reached a state of development by four months of age so that that age was selected for this particular study of skeletal effects

EXPERIMENTAL DATA

The statistical data from this project are presented in the several tables below While the experiment began with 25 males and 25 females for each set of variables and 50 each for the controls these numbers could not be held against the occasional losses due to accidents or to other and natural causes Chief among these was diarrhea The best cure for this condition is to treat the regular food with tetracycline hydrochloride (soluble Polyotic) for a 1–2 week period By four months, when the skeletal study was made the minimum number of males surviving for any gestation age group was 18 and for the females it was 16 while 45 and 43 of the males and females of the controls survived All of the averages are based upon the number of survivors at the time of the examination

A total of 307 pregnancies were provided for this study plus 12 control pregnancies At certain gestation ages the loss in embryos due to 100 r x irradiation was sufficient to require twice the usual number of pregnancies Since the skeletal study was made on the survivors at four months it is well to present here the litter average and 30 day post natal survival of mice x irradiated at different gestation ages

Among the controls there were 53.1% males and 46.9% females born. This compared with 53.0% males and 47.0% females among those x-irradiated so that this exposure did not shift the balance of the sexes by selectively eliminating one or the other While there were fewer controls than the total of x-irradiated embryos the deaths during the first 30 post-natal days affected a higher percentage of the controls where 15 % of the males and 17.7% of the females died due to undetermined factors During this same period and considering all gestation ages together there were 0.6% deaths among the x-irradiated male and 10% among the females However among those delivered none of the controls was born dead or had a gross anomaly while 39 out of 2,257 (1.7%) of those x irradiated were born dead or anomalous

The average litter size of all of the x-irradiated pregnancies was 7.60 which was lower but not significantly so, than the 8.00 average for the controls. Such reduction as existed for the various stages represented intra-uterine deaths and resorption and these occurred more frequently among the very early stages of pregnancies. (0.0 days or immediately after conception) There was also some litter size reduction on days 0.5 to 1.0, 7.0 and 8.0 The stunting data of this paper are derived from embryonic and fetally x irradiated mice that not only came to term, but which also survived the critical first 30 post-natal days plus three more months. Thus, the data really concern the healthiest of the survivors at maturity

Surviving males of this strain whether controls or x-irradiated experimentals, were always heavier than were the surviv-

TABLE 1

Effect on litters of 100 R x-rays at different gestation ages mice

Gestation day	Pregnancies	Number delivered			Litter av.	Dead in 30 days		Eaten	Abnormal or born dead
		Total	Male	Female		Male	Female		
Controls	12	96	51	45	8.00	8	8	1(1.0%)	0
0 0	24	110	56	54	4 58	1	2	0	1
0 5	20	135	59	78	6.75	2	0	0	0
1.0	16	108	63	45	6.75	4	5	0	0
2 0	11	78	38	38	6.90	1	4	1(1.3%)	0
3 0	18	128	69	59	7 11	11	11	19(15.0%)	0
4.0	13	98	55	43	7 53	10	5	18(18.0%)	1
5.0	14	104	49	55	7.50	8	4	0	0
6 0	12	87	46	41	7 25	2	4	0	0
7.0	18	109	62	47	6.05	4	1	1(1.0%)	0
8 0	17	107	62	45	6.29	3	3	0	23(21.5%)
9 0	14	137	73	64	9 78	7	10	0	2
10 0	19	134	78	56	7 05	10	9	24(17.0%)	6
11 0	16	136	69	67	8.50	5	8	7(5.1%)	0
12 0	19	174	93	81	9 15	21	15	12(7.0%)	0
13 0	14	98	50	48	7 00	2	2	10(10.0%)	4
14 0	13	118	62	56	9 07	10	4	10(9 0%)	0
15 0	12	108	56	52	9.00	2	2	0	0
16 0	14	125	70	55	8.93	7	10	0	0
17 0	12	105	50	55	8.75	6	7	0	0
18 0	11	90	52	38	8.18	1	2	0	0

ing females at four months of age. The over-all average of all mice x-irradiated to 100 r in utero from 0 0 to 18.0 days gave 30.5 grams for the males and 24 0 grams for the females, a mean loss from the con trol average of about 2.5 grams per mouse of either sex. This does not tell the entire story however as the data show that the greatest single depression in weight oc curred when the males were exposed on gestation day 13 (31% loss) and the females on gestation day 12 (28% loss) although day 13 was also low for the females (23% loss in weight) (see fig. 1) As will be shown below the greatest depression in bone or skeletal growth occurred when the x-irradiations were administered on day 11 or 12 (table 2 and fig. 2)

These average weight data were all subjected to statistical analysis. The standard deviation was estimated from the differ ence between the highest and the lowest weight of the individual males and females separately For the males it was 3.32 grams and for the females 2.38 grams based on a large number of degrees of freedom. The mean weight for each batch of x-irradiated mice was compared with the control, using the standardized normal deviate. Taking into account that for each sex 20 compari sons are made the absolute critical value was 3 02 for each sex. Statistically significant reductions in body weights occurred for the males following x-irradiation on days 5 and 9 through 18 with the most pronounced effects on days 12 through 14 For the females there was a statistically significant reduction in average weight when the x-irradiation occurred on days 8 through 18 with the most drastic reduc tions on days 11 through 14 Thus, the second half of gestation appeared to be the period of most significant stunting by x rays.

For the skeletal data a total of 917 x-ir radiated and 88 control mice were radiographed and seven of their skeletal measurements were taken, making a total of 7,035 measurements for the statistical analyses. The seven measurements taken included two of the skull (lateral and antero-posterior) and lengthwise measurements of the spine humerus ulna, femur and tibia. For the skull the AP measurement was from the most posterior aspect of the occiput to the anterior limit of the frontal bone. For the skull LAT the maximum width was determined. The spine was measured from the tip of the odontoid process to the end of the fourth sacral vertebra. For the other long bones the maximum length was determined. Other

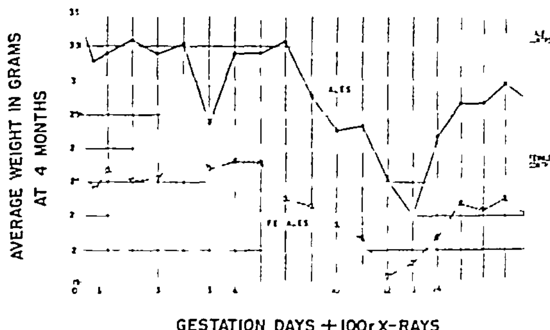


Figure 1

and smaller bones might well have shown some reduction but these particular bones were chosen as representative and rather accurately measurable

The table above presents the average of the seven skeletal measurements of male and female mice x-irradiated at each of the gestation days 0 0 through 18 0 If the skeletal data from males and females are plotted separately certain sex differences in response become apparent (fig 2) There is little deviation from the control measurements following 100 r x rays to the mouse embryo during the first half of gestation or from 0 5 to 9 0 days with the possible exception of the ulna of the female exposed on day 3. Since days 2 and 4 fit into this depression it cannot be an artefact but there is at present no explanation of this disparity of the female ulna as compared with the reaction of the male ulna. The humerus then the spine and the ulna (in that order) appear to be more affected in the female than in the male when x-irradiations occur prior to 9 0 days gestation. On the whole it appears that 100 r does not seriously affect skeletal growth of either male or female when the exposure occurs before 9 0 days gestation (fig. 2)

Followin gestation day 9 0 the situation is quite different so that a detailed statistical analysis has been made of three particular measurements takin into consideration the limits of variation within each averaged group. The measurements considered were of the spine tibia, and the For each bone the measurements within each sex were compared against the non-irradiated controls givin 38 comparisons for each bone The critical level was therefore taken as the standardized deviate correspondin to 1 76 × 0 03 for each comparison. An estimate of the variability was obtained from the ranges observed in each sample. The resulting degrees of freedom are some 500 and therefore taken as the "true value The absolute value of a standardized normal deviate to be exceeded is 3 81 For all of the bones and for both sexes the highest statistical significance is obtained at 11 through 13 days of gestation As the bones are highly correlated in their development there is not too much significance in the fact that the danger period for radiation coincides for all of the bones studied The effect appears to be over all and therefore the fetally x irradiated mice may be grossly stunted but topographically normal A

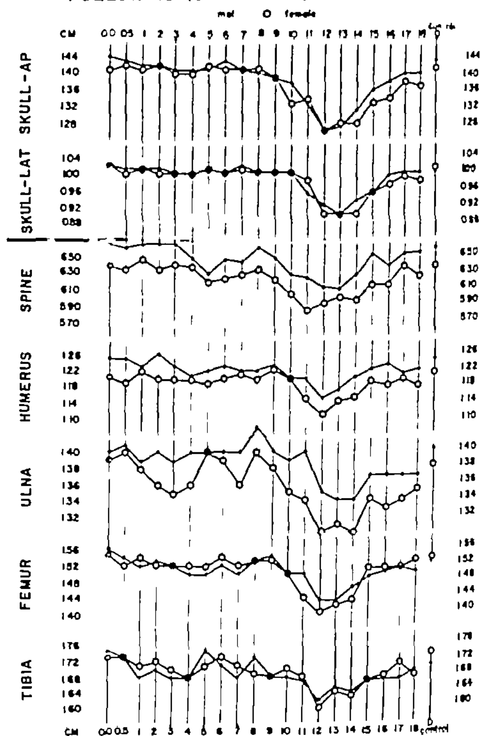
TABLE 2

Mice at four months of age following 100 R x-rays during embryonic stages

Gest. age x-rayed	Sex	No.	Av. wt.	Average measurements skeleton in millimeters: Skull Lat.	Skull Ap.	Spine	Humerus	Ulna	Femur	Tibia
			gm							
Controls	male	45	33.7	1.00	1.43	6.59	1.24	1.40	1.52	1.70
Controls	female	43	26.3	1.01	1.41	6.35	1.21	1.38	1.53	1.73
0.0 da.	male	24	34.1	1.02	1.44	6.62	1.25	1.40	1.56	1.75
0.0 da.	female	24	25.7	1.02	1.41	6.37	1.20	1.39	1.55	1.73
0.5 da.	male	23	32.2	1.01	1.43	6.60	1.25	1.41	1.54	1.73
0.5 da.	female	24	24.7	1.00	1.42	6.33	1.19	1.40	1.52	1.73
1.0 da.	male	25	32.5	1.01	1.42	6.64	1.23	1.39	1.52	1.68
1.0 da.	female	19	25.7	1.01	1.41	6.45	1.22	1.38	1.54	1.71
2.0 da.	male	23	33.3	1.01	1.42	6.64	1.26	1.40	1.53	1.70
2.0 da.	female	25	25.1	1.00	1.42	6.31	1.20	1.36	1.52	1.72
3.0 da.	male	24	32.6	1.00	1.41	6.64	1.23	1.39	1.52	1.68
3.0 da.	female	23	25.2	1.00	1.40	6.38	1.20	1.35	1.52	1.70
4.0 da.	male	21	33.1	1.00	1.41	6.48	1.21	1.40	1.50	1.68
4.0 da.	female	16	27.2	1.00	1.40	6.36	1.20	1.36	1.52	1.69
5.0 da.	male	21	25.6	1.01	1.41	6.29	1.22	1.40	1.50	1.75
5.0 da.	female	25	25.9	1.01	1.42	6.19	1.19	1.40	1.52	1.71
6.0 da.	male	25	33.7	1.00	1.43	6.45	1.23	1.40	1.53	1.71
6.0 da.	female	25	26.3	1.00	1.41	6.21	1.20	1.39	1.54	1.73
7.0 da.	male	25	32.7	1.02	1.41	6.41	1.22	1.40	1.50	1.68
7.0 da.	female	25	26.2	1.01	1.41	6.26	1.21	1.36	1.52	1.71
8.0 da.	male	23	33.4	1.00	1.40	6.60	1.22	1.43	1.53	1.73
8.0 da.	female	22	24.1	1.00	1.41	6.31	1.20	1.40	1.53	1.77
9.0 da.	male	23	30.2	1.00	1.39	6.46	1.23	1.40	1.54	1.68
9.0 da.	female	22	23.6	1.00	1.39	6.30	1.22	1.38	1.53	1.68
10.0 da.	male	25	28.2	1.00	1.38	6.26	1.20	1.39	1.50	1.68
10.0 da.	female	22	22.6	1.00	1.33	6.02	1.20	1.35	1.50	1.70
11.0 da.	male	25	28.5	0.95	1.33	6.23	1.20	1.40	1.50	1.67
11.0 da.	female	23	21.6	0.96	1.34	5.83	1.16	1.34	1.44	1.68
12.0 da.	male	25	25.1	0.92	1.26	6.10	1.15	1.35	1.43	1.62
12.0 da.	female	23	19.5	0.90	1.26	5.90	1.11	1.30	1.40	1.60
13.0 da.	male	23	23.1	0.90	1.27	6.09	1.17	1.34	1.43	1.65
13.0 da.	female	20	20.3	0.90	1.28	5.99	1.14	1.31	1.42	1.64
14.0 da.	male	23	27.7	0.93	1.31	6.25	1.20	1.34	1.46	1.64
14.0 da.	female	25	21.7	0.90	1.28	5.95	1.15	1.30	1.43	1.63
15.0 da.	male	24	29.7	0.95	1.36	6.50	1.22	1.37	1.49	1.67
15.0 da.	female	24	23.8	0.95	1.33	6.13	1.19	1.34	1.51	1.67
16.0 da.	male	23	29.7	0.99	1.38	6.33	1.23	1.37	1.50	1.67
16.0 da.	female	24	23.4	0.97	1.34	6.13	1.18	1.33	1.51	1.68
17.0 da.	male	18	30.9	1.00	1.40	6.52	1.21	1.37	1.51	1.67
17.0 da.	female	18	24.1	0.99	1.38	6.37	1.20	1.34	1.51	1.71
18.0 da.	male	23	30.1	1.00	1.40	6.64	1.22	1.37	1.50	1.69
18.0 da.	female	21	25.1	0.96	1.37	6.24	1.18	1.33	1.53	1.68

Note. Each figure represents an average taken from the number of males or females shown in column under No.

In some cases animals died between the weight-taking and the skeletal radiogram, but in each case the average derived was based upon the actual number of survivors either weighed or radiogrammed.



MOUSE SKELETON AT 4 MONTHS OF AGE
FOLLOWING 100r X-RAYS TO EMBRYO
male
O female
CM
SKULL-AP
SKULL-LAT
SPINE
HUMERUS
ULNA
FEMUR
TIBIA
control

Figure 2

this time no bones are formed and osteoblasts are just beginning to appear from sclerotome. Ossification begins on day 15.

With regard to the measurements of the spine, there were seven gestation periods when 100 r x-rays resulted in statistically significant reductions namely days 5 10 through 14 and 16 for the males and the same number of days but with a slightly different distribution for the females, namely 10 through 16 The most radiosensitive days with respect to the spine were 12 and 13 for the males and 11 and 12 for the females. This could suggest slightly earlier spine development in the female.

With regard to the tibia, the male mice showed statistically significant stunting following 100 r x rays on days 12 through 14 while the females showed such reductions in the tibia on days 9 and 11 through 16. Here as in most of this study female sensitivity seemed to precede the male by one day whether in regard to average weight or specific bone measurements. Curiously the males showed a statistically significant and unexplained *increase* in tibia average length when the x-irradiations occurred on day 5 For the males the maximum stunting effect occurred when the x-irradiations were on day 12 and while it was on the same day for the females, the effect was considerably greater (10.24 over 3.81)

With regard to the ulna, it has already been pointed out that for some reason this bone shows a significant reduction in the female, as compared with the male on days 2 through 4 with the greatest stunting on day 3 of gestation. There is another drop on day 7 In addition when males were x rayed on days 12 through 14 there was a significant stunting of the ulna (maximum at days 13 and 14) while the females showed significant stunting following exposures on days 11 through 17 with the maximum reductions on days 12 and 14 Again the females reacted a day earlier than the males.

Consistently day 11 showed the beginning of x-irradiation stunting (with the exception of the female ulna on day 3) although the ulna and the skull-AP of the female and the spine of both sexes showed significant effects earlier on day 10 In most instances, the maximum effect on any long bone was on the bone of the female as opposed to the male (fig. 2)

For illustrative purposes a search was made for the control and the x-irradiated male and female on gestation day 12 which had skeletal measurements closest to those of the mean for those conditions and sex. The data of the following table 3 when compared with the mean of table 2, indicate that the mice chosen do in fact represent the means for the four sets of conditions.

Having identified those four mice which best exemplified the controls and the x irradiated mice at 12 days gestation, a set of radiographs were taken of these mice to demonstrate the skeletal effects (plate 1) It will be noted that at first examination there is no evidence of gross reduction in size between the controls (nos. 1 and 3) and the comparable male (no 2) and female (no. 4) x-irradiated experimental mice selected as most closely representative of the means. These are mice which survived x-irradiation to 100 r at 12 days gestation and also survived the critical

TABLE 3

Skeletal measurement	Males				Females			
	Controls (45)		12 G D. 100 (25)		Controls (43)		12 G.D. 100 (12)	
	A	D-2 no. 5	XIII (a-3) no. 5	A	A	D-15 no. 5	XIII (e-6) no. 3	A
Skull lat.	1.00	1 00	0.90	0.92	1.01	1.0	0 90	0 90
Skull ap	1 43	1 40	1.30	1 28	1 41	1 4	1.3	1 26
Spine	6.59	6.5	6.1	6 1	6.35	6.3	5.9	5 9
Humerus	1.24	1.2	1 1	1 15	1.21	1.2	1 1	1 11
Ulna	1 40	1 4	1 3	1.35	1.36	1 4	1.3	1.3
Femur	1.52	1.5	1 4	1 43	1.53	1.5	1 4	1 4
Tibia	1 70	1 7	1 6	1.62	1 73	1 7	1.6	1.6

first 30 days of postnatal adjustment and were radiographed at four months of age Upon closer examination it can be seen that there is an over all reduction in size involving probably every bone of the body with the x irradiated female showing relatively the greatest stunting (no 4) (A study is in progress to determine whether this amount of x irradiation has any sequelae aside from stunting such as reduction of life span or the incidence of tumors and leukemia) Such mice appear *to be quite normal but this study reveals* statistically significant stunting when the x irradiation occurs at certain gestation ages

DISCUSSION

Mammalian embryos develop in an aquatic and homeostatic environment relatively protected against the vicissitudes normally encountered by embryos of poikilothermic forms and yet some 5% of all human births bear congenital anomalies Whether these are of genetic origin or are due to traumatic imbalance in the physical environment or to both factors has not yet been determined There are a variety of extrinsic conditions which can cause congenital anomalies through the other (Rivers et al '59 Kalter and Warkany '59 Fraser '59 Lock '62) one of which is rapidly gaining respect namely ionizing radiations (Levy et al '59 Rugh et al 59–'63)

In analyzing congenital anomalies one must remember that there are two aspects of the problem There is the abnormal environment which may be physical or chemical or both and there is the reacting embryo Embryos of some strains are inherently resistant to damage and others are highly susceptible At some stages of development congenital anomalies are more readily produced than at others some anomalies may be caused over a relatively long developmental period while others may have a very limited time of susceptibility the embryo is a mosaic of sensitivities some organs tissues and cells being sensitive at one moment while others later to be sensitive are resistant and finally since the embryo is composed of undifferentiated cells it is able to redirect the undamaged cells to fill the gap caused by the destruction and removal of susceptible cells This power of redirection of undamaged and as yet undifferentiated cells is not new to the experienced embryologist (nor to the embryo) but it has been erroneously described as recovery or repair These terms have an entirely different meaning in the hospital clinic than they might for the embryo. Actually there is abundant evidence in the literature and data from this paper that support the contention that cell death in *the embryo does not result in a localized* deficiency but rather in an over all stunting or generalized deficiency which does not seriously affect the topography of the individual but does reduce his overall mass

With regard to the extrinsic factors these may alter th chemical or enzymatic reactions which are highly critical for certain developmental processes may have abscopal effects rather than direct may start a chain of biochemical reactions and may have thresholds and intensity variables These concepts are the more plausible when we remember that the embryo is not a conglomeration of unrelated parts but that there seems to be an over all controlling organization which continually integrates the parts of the developing embryo toward an organism functional as a whole

Highly penetrating x or gamma rays delivered in a short period, have the advantage of a clean traumatizing agent without the unknown and indeterminable residual and lingering effects of chemicals or isotopes. The interval of exposure can be limited to seconds or minutes without further contamination so that the time and developmental stage factors can be sharply delimited. In these experiments the age of the embryo was controlled to within two hours and the x irradiation to two minutes

The most significant studies of x-ray effects on the rodent skeleton have been reported by Russell and Russell ('50 '57). They found the critical period for anterior shift in the thoraco-lumbar border from 7.5 to 8 5 days with the peak of reaction at 8 5 days in the mouse Exposures to as little as 25 r on day 8 5 altered the rib development in B alb C mice but the strain 129 and (C57 × NB) F hybrids

were rather resistant to such skeletal changes. L. B Russell ('56) reported that on increasing the dose the period of response can usually be lengthened and the incidence and degree of abnormality usually can be increased. The vertebral column and thorax of newborn mice had been examined after irradiations on days 0.5 to 13.5 following fertilization. They also stated that "Irradiation during the first five days (prior to the implantation of the embryo in the uterus) leads to all-or-none effects there is a high incidence of death shortly after irradiation but those embryos that survive are normal. Since the doses used were 100 to 400 r this is a very significant statement, if the survivors are truly normal.

Similar studies have been made on the digits of mouse embryos (Neyfakh '60) in which it was found that 300 r x-rays during the gestation period of 10 to 12 days caused reduction of 1 to 4 digits or increases of 1 or 2 digits. Forelimb digits were reduced by exposures on day 11 but the same irradiation caused reduction of hindlimb digits on days 11 or 12. Rabbits exposed to 300 r on day 13 showed the most pronounced effect on bone development with lengthwise retardation and delay in the appearance of ossification nuclei in the long bones of the extremities Ehling and Randolph ('62) described skeletal anomalies in the F following x-irradiation of the post-spermatogonial stages of male mice, mating them with normal females. This effect was not congenital but genetic.

Following the atomic bomb in Japan there have been numerous studies on the skeletal development of children who were exposed in utero to ionizing radiations. Plummer ('52) described microcephaly with mental retardation in seven out of 11 children exposed in utero within 1,200 meters of hypocenter while among the other four there was one with small head measurements but without obvious mental retardation. Greulich et al. ('53) stated that our findings indicate that the physical growth and development of the children who survived the atomic bombing of Hiroshima and Nagasaki was adversely affected by the experiences and that some of the retardation in their height, weight, and skeletal development was still evident at the end of '50 five and one-half years after the bombing." Sutow ('54 '55) stated that females exposed during the first half of gestation had mean height, weight, and head circumference significantly less than the controls while the males showed only the mean head circumference to have a significant reduction. Irradiation during the second half of gestation had no skeletal effects but thier I.Q ratings were lowered. The effects on the skeleton were spina bifida, lumbarization sacrolization, shortened phalanges accessory epiphyses at the bases of the metacarpal bones, and neural arch defects. Yamazaki et al. ('54) stated that the mean height and head circumference of children born to mothers with major signs of radiation exposure were significantly smaller than the controls, and that fetal, neonatal, and infant mortality assumed significant proportions only when the exposure occurred during the second or third trimesters of pregnancy

Other studies have been directed toward determining the roentgen exposure of a gravid uterus during routine obstetrical and gynecological procedures. Mobius ('51) stated that with a combination of antero-posterior lateral, and sitting positions the aggregate exposure of the gravid uterus in diagnostic radiology could be kept to less than 1 r with a skin dose of 6 to 8 r By precision coning precision centering, marking the area of the fetal head protecting the fetus with a lead apron etc. there should be a minimum fetal exposure (Kendig, '60) Payne ('60) found that the greatest exposure of the fetus occurred in pelvimetry but was never more than 2.1 r while Berman and Sonneblick ('57) found it to be 2 to 4 r and for hystero-salpingography it could be 3.2 r They stated that "there should be no hesitation in utilizing indicated diagnostic procedures in obstetrics and gynecology if the technique is properly carried out However Pitter and Svejda ('52) reported a two year old girl who had been examined in utero at four five and six months for diagnostic purposes, and this child had syndactyly brachydactyly microphthalmus microcornea, strabismus hypertropia amelogenesis and odontogenesis imperfecta. Exposures were not given but

must have exceeded the normal diagnostic levels

Specific skeletal effects have been caused by drugs (e g 6-aminonicotin amide) administered on days 10 or 11 to mice resulting in malformations of both the axial and appendicular skeletons and often causing cleft palate (Pinsky and Fraser '59) Cleft palate can be readily produced by x rays on day 10 (Ershoff and Bavetta '59) or on day 11 (Callas '62)

Gestation age at the time of x ray insult appears to bear a significant relation to the nature and the degree of skeletal modification Johnson ('33) described the time and appearance of ossification centers in the albino mouse and this was generally about day 15 and took four days so that irradiation on day 11 or 12 preceded the onset of ossifications Exposures on days 11 or 12 must therefore include the early differentiating and highly sensitive osteoblasts Wodard ('57) stated that both the anabolic and catabolic processes in bone are damaged by external irradiation and that such damage as is inflicted appears slowly and lasts for a long time Clinically significant bone effects of x irradiation include stunting of growth in children generalized and patchy demineralization athologic fractures total disintegration bone and osteogenic sarcomas even after single exposures.

This current study reveals effects on various parts of the skeleton following x irradiation at the various stages of development from 0 0 to 18 days. The major effects follow exposure on days 11 through 15 While there is an over all effect, resulting in generalized but topographically normal stunting there are certain *bones which are more drastically affected* than others The exposure to 100 r x rays is not normally within the diagnostic range (e g. fluorescopy) but it can occur in special and accident cases It is far below the LD 50/30 level of 630 roentgens for the mouse or 500 roentgens for the human.

CONCLUSIONS

1 A total of 319 timed pregnancies in CFl mice provided the material for this study to determine the effect of 100 r x-rays delivered at each of the gestation periods from 0 0 to 18 0 days The major part of this study dealt with the skeleton and stunting

2. The skeletal study was made on only those mice which survived to four months of age thus representing the maximum or optimum development of the skeleton following developmental x irradiation.

3 The greatest reduction in litter size followed 100 r on day 0.0 or immediately after fertilization The exposure to 100 r on gestation days 3 4 10 and 13 caused such severe congenital anomalies that the mothers killed and ate more than 10% of the live-delivered fetuses.

4 The exposure to 100 r did not alter appreciably the sex ratio of mice delivered (53% males and 47% females) nor the ratio of those dying within the first 30 post natal days. In this latter group the highest mortality occurred among those x rayed on days 3 4 9 10 12 and 14

5 The highest incidence of congenital anomalies seen at birth occurred following 100 r delivered on day 8 0 This is the time of onset of neurogenesis, but not of osteogenesis which is not active until about day 15

6. Male mice of the CFl strain are always heavier than the females at four months of age Exposure of the developing mouse to 100 r reduced the over all average weight of the survivors at four months by about 2.5 gm for each sex. There were statistically significant reductions in average body weights of males following exposure on gestation days 5 and 9 through 18 with the greatest reductions following exposure on days 1 –14 For the females weight reductions occurred following exposures on days 8 through 18, with the greatest effects on days 11–14 Thus stunting *is a more* likely sequela of embryonic x irradiation when it occurs during the second half of gestation, after organogenesis has begun

7 For the skeletal data 1,005 mice were radiographed, and seven skeletal measurements taken and averaged. There were sex differences in skeletal stunting even when x-rayed before day 9. Where the differences were pronounced *the female* was the more adversely affected.

8 The statistical analysis of the skeletal development following 100 r at the various gestation stages showed that after

nine days the highest significance was obtained when the irradiation occurred on gestation days 11 through 13 Since the effects appear to be over-all, the mice ex posed on these days were grossly stunted but appeared to be topographically normal.

Extrapolation of gestation age in days: mouse — human

Mouse	Human	Mouse	Human
1	1	9	25
2	2	10	28
3	4	11	32
4	6	12	36
5	8	13	39
6	12	14	45
7	16	15	54
8	20	16	70

LITERATURE CITED

Aleksandrovich, E. I. 1959 Bone changes in the postnatal period in the offspring of rabbits subjected to the action of ionizing radiation t different periods of pregnancy Med. Radiol., 4: 30–34 (in Russian)

Berman, R., and B P Sonnenblick 1957 Intravaginal measurement of radiation dose incident to -ray pelvimetry and hysterosalpingography Am. Jour Obstet. Gynec., 74 1 12.

Callas, G. 1962 Embryology of -ray induced cleft palate in mice. Anat. Rec., 142. 336 (abs.) also Anat. Rec., 145 61–71 (1963)

Ehling, U H., and M. L. Randolph 1962 Skeletal abnormalities in the F generation of mice exposed to ionizing radiations. Genetics, 47 1543–1555.

Englhoff B. H and L. A. Bavetta 1959 Effects of -irradiation during the formative period of tooth development on the teeth and periodontium of rats and the effects of such treatment on subsequent caries susceptibility Prog. Rep. DA-49 007-MD-768.

Fraser F C. 1959 Antenatal factors in congenital defects. In Problems and Pitfalls. New York and Jour Med., 59 1579–1605.

——— 1959 Causes of congenital malformations in human beings. Jour Chron. Dis., 10: 97 110.

Greulich, W W C. S. Crismon and M. L. Turner 1953 The physical growth and development of children who survived the tomic bombing of Hiroshima or N gasaki. Jour Pediatrics, 43 121 145.

Johnson, M. L. 1933 The time and order of appearance of ossification centers in the albino mouse. Am. J Anat., 52: 241–271

Kalter, H., and J Warkany 1959 Experimental production of congenital malformations in mammals by metabolic procedures. Physiol. Rev 39 69–115.

Kradig, T A. 1960 Reduction of fetal irradiation in pelvimetry Radiology 75 608–611

Levy B R. Rugh, A. Lanin, M. Moss and N Chilton 1953 The effect of single and subacute x-ray exposure to the fetus on skeletal development A statistical study J Morph., 93 561–571

Lock, F R. 1962 Human congenital anomalies — Some current concepts. Abs. and Gynec., 20 867–873.

Mobius, W 1951 Roentgen doses during gynecological roentgen diagnostic procedures. Fort schr a.d.Geb.d.Röntgenstrahlen 75 734–739

Neyfakh, A. A. 1960 On reduction of the digits in mouse embryos following -ray irradiation. Arkh. Anat. Gistol. i. Embriol., 39 74–82.

P yne F L. 1960 Progress of medical science. Gynecology and obstetrics. Radiation safety in Obstetric-Gynecologic practice. Am. Jour Med., Sci., 240: 782–791.

Pinsky L., and F C. Fraser 1959 Production of skeletal malformations in the offspring of pregnant mice treated with 6-aminonicotinamide. Biologia Neonatorum, 1 106–112.

Pittar J and J Svejda 1952 Effects of x-radiation on the origin of malformations in human fetuses. Ophthalmologica, 123 386–393 (in German)

Plummer G. 1952 Anomalies occurring in children exposed in utero to the atomic bomb in Hiroshima. Pediatrics, 10 687–693

Rivers, T M., J Warkany F C. Fraser J G. Wilson, D D Matson and R. McIntosh 1959 Conference on congenital malformations. Jour Chron. Dis., 10 83–151.

Rugh, R. 1961 Effect of low level -irradiation on the fertilized egg of the mammal. Exp. Cell. Res., 25 302–310. (See also Am. Jour Roent. Rad. Ther Nucl. Med., 87 559–566.)

——— 1962 The impact of ionizing radiations on the embryo and fetus. Am. Jour Rad. Ther Nucl. Med., 89 182–190.

Rugh, R., and E. Grupp 1959 X-irradiation exencephaly Am. Jour Roent. Rad. Ther Nucl. Med., 81 1026–1052.

——— 1959 Exencephaly following -irradiation of the preimplantation mammalian embryo. Jour. Neuropath. Exp. Neur 18 468–481

Rugh, R., and M. Wohlfromm 1963 Can the mammalian embryo be killed by -rays? J Exp Zool., 151 227–244

Russell, L. B 1950 X-ray induced developmental abnormalities in the mouse and their use in the analysis of embryological patterns. J Exp Zool., 131 329–395

——— 1957 Effects of low doses of x-rays on embryonic development in the mouse. Proc. Soc. Exp. Biol. Med., 95 174–178.

——— 1960 Radiation hazards during embryonic development. IX Int. Cong. Radiology Munich 1959 (1006 Abbildungen)

Russell, L. B and W L. Russell 1950 Changes in the relative proportions of different axial keletal types within inbred strains of mice brought bout by -irradiation at critical stages in embryonic development. Genetics, 35 689.

——— 1954 Pathways of radiation effects in the mother and the embryo. Cold Spring Harbor Symposium on Quant Biol., 19 50–59

Knezevic ('60) reported the presence of secretory granules in the perivascular connective tissue space and, also within the cytoplasm of the endothelial cells in the rabbit

In the present paper observations concerning the locations and form of secretory products in the adenohypophysis of the rabbit will be presented and the significance of the findings in relation to the possible mechanisms of release and transport of hormone containing material from parenchymal cells into the circulating blood will be discussed.

MATERIALS AND METHODS

Virgin estrous rabbits of the New Zealand white strain with an average weight of 2.5 to 3.5 kg were used The animals were anesthetized with intravenous nembutal for removal of the calvaria A lethal dose of nembutal was then administered and the hypophysis removed carefully divided in pieces of 1 to 2 mm and fixed in 1% osmium tetroxide dissolved in Clark's modification of White's saline (Clark '63) The elapsed time between death of the animal and immersion of the gland in fixative was two to three minutes. After one hour in fixative tissues were hydrated in alcohol and embedded in Epon 812 (Luft '61) or English Araldite (Richardson et al. '60) The sections were cut on a Porter Blum ultramicrotome model MT 1 stained with either lead hydroxide (Millonig '61) or uranyl acetate (Watson '58) and examined in RCA microscopes models EMU-3C and EMU-3G

OBSERVATIONS

Extrusion of secretory granules The majority of cells in the adenohypophysis of the rabbit contain granules which for each type of cell attain a typical maximum diameter In the virgin estrous rabbit a few cells contain granules with a maximum diameter of 600 to 800 mμ. A great number of the cells contain granules of 300 to 400 mμ diameter A moderate number of large cells contain granules with a diameter of 100 to 200 mμ. From comparisons by light and electron microscopes of adjacent sections it has been possible to identify cells containing granules of the 300 to 400 mμ size as well as those with 600 to 800 mμ granules as acidophiles The large cells with the 100 to 200 mμ diameter granules were classified as basophiles on the basis of their positive periodic-acid-Schiff reaction. In most cases it is possible to distinguish a smooth perigranular membrane surrounding the dense granule In acidophiles the perigranular membrane is very closely applied to the mature granules while in the basophiles it is usually separated by a more noticeable interval from the granules (figs. 1 4) Most of the acodophile cells seen are packed with granules (fig. 4) whereas in the basophiles the granules, although quite numerous are usually more widely separated (fig 1) In sparsely granulated cells the granules are frequently found lined up very near the plasma membrane (fig 8) This condition is not limited to that part of the cell adjacent to the basement membrane but is seen around the entire periphery The smooth perigranular membrane is sometimes seen to be in contact with the plasma membrane (fig 1).

Granules are seen lying in shallow depressions between the plasma membrane and the parenchymal basement membrane (figs. 1 2) The latter is often deformed to follow the contour of the granule (fig 1) In this location the perigranular membrane is usually but not invariably absent, suggesting that it becomes continuous with the plasma membrane in the process of discharge The finding of extruded granules is not confined to the basal part of the cells but has also been observed in large and small spaces between adjacent cells (figs. 3 4) These intercellular spaces into which cilia and cytoplasmic projections often protrude are continuous with the space between the parenchymal cell membrane and the basement membrane adjacent to it (fig 4) The granules found in the intercellular spaces are frequently seen enclosed within a perigranular membrane In some instances a small but distinct rim of cytoplasm is observed surrounding the individual granules (fig. 4), suggesting that the granules are contained in either projections from cells outside the plane of section or that they are contained in projections that have been pinched off The latter possibility appears the more likely inasmuch as the granules

) observed have a symmetrical rim and o projections containing granules have een seen cut in longitudinal section.

Parenchymal cells in perivascular space .s reported in the rat by Rinehart and arquhar ('55) and Lever and Peterson '60) processes or portions of parenchymal ells are also sometimes seen in the peri ascular space in the rabbit (fig. 9) They re not surrounded by basement memrane but rather appear to have discontinuous strands of basement membrane naterial attached to them. The site of enetration of the process through the arenchymal basement membrane has not een observed although the portion of the ell on each side has an identical appear ance. Immediately outside the plasma nembrane of some of the processes granles are seen lying free in the perivascular pace. These granules are identical with hose inside the process and those in the nearby parenchymal cell (fig 9) Contrary o the findings of Lever and Peterson ('60) he granules found free in the perivascular space retain their perigranular membrane

Fate of extracellular granules Although the secretory granules have not een found in actual passage through the parenchymal basement membrane they must in some manner cross this barrier for it is not uncommon to see granules in perivascular space i.e., between the parenchymal and endothelial basement membranes (figs. 5 6 9) It is of interest to note that all the granules we have found lying free in this location were surrounded by a perigranular membrane.

Electron-dense granules have been observed within the thicker portions of the endothelial cells of capillaries in the adenohypophysis (fig. 7) These granules have a perigranular membrane and are of the same size and appearance as those seen in adjacent parenchymal cells. Granules indistinguishable from those of pituitary cells or those in the endothelial cells have also been observed in the lumen of the capillaries (figs. 8 10) In such cases most of the granules had a distinct peri granular membrane and lie in close proximity to small projections or microvilli of the endothelial cytoplasm (figs. 8 10)

The endothelium of the capillaries of the anterior hypophysis is very thin and fenestrated in most places. The openings do not appear to be complete but are bridged by a very thin membrane (figs. 2, 8 12, 13) In other regions the endothelium is thicker and contains numerous pinocytotic vesicles of various sizes; some are large and surrounded by a continuous rim of endothelial cytoplasm (fig 11) while others are surrounded by a fenestrated layer (figs. 12, 13) The material contained within these vesicles resembles more closely the material occupying the perivascular space than the plasma within the capillary lumen.

DISCUSSION

The process of secretion in an endocrine gland such as the adenohypophysis involves not only synthesis consolidation, storage and release of the hormones by the cells but also requires that the released secretory products find their way into the circulatory system. All of these steps in the secretory process of the anterior hypophysis save the last, have been studied by many investigators (Farquhar et al., '54a, b '57 '61a,b; Green and Van Breemen, '55 Rinehart and Farquhar '55; Ichikawa, '59 Lever and Peterson, '60 Yamada and Sano '60 Löblich and Knezevic '60 Sano 62 Schelin, '62; Garwood and Latta, '63) in various species. The formation and release of secretory products are well documented but the evidence bearing on the problem of passage of these products into the circulation has been lacking

One mechanism for release of secretory products from the pituitary cells has been reported in the rat by Farquhar ('61a) Ichikawa ('59) Lever and Peterson ('60) in the mouse by Sano ('62) and in the rabbit by Löblich and Knezevic ('60) This is a merocrine type of release in which the perigranular membrane comes into contact with the internal surface of the parenchymal plasma membrane and fuses. An aperture forms at the site of fusion so that the perigranular membrane then becomes the cell membrane and the naked granule is released into the extra cellular space. This has come to be considered by many as the only mechanism of hormone release in the anterior pituitary; however the observations presented

here lead us to postulate that an additional mechanism occurs in the secretory activity of this gland This mechanism is tentatively called a microapocrine type of secretory release in which small blebs of cytoplasm containing secretory granules are pinched off from parenchymal cells into the intercellular spaces Small projections containing granules protruding into intercellular spaces granules surrounded by a narrow rim of cytoplasm lying in the same spaces and granules surrounded only by a perigranular membrane found in this and other extracellular sites are evidence in support of this mechanism. The small blebs of cytoplasm released in this way may dissolve in the extracellular space and thus liberate the contained secretory granules enveloped by the perigranular membrane Further supporting evidence is given by the fact that in sections showing such free granules the integrity of the parenchymal cells was maintained and no signs of disruption or cell damage were apparent A study of serial sections should provide additional information relative to this particular question.

The observation of processes of parenchymal cells extended through the basement membrane into the perivascular space was first made in the rat by Rinehart and Farquhar ('55) and Lever and Peterson ('60) showed in the same species such processes in which many secretory granules were being discharged by the merocrine process Although these observations have not been confirmed in the mouse (Yamada and Sano '60) or in the human (Schelin '62) our findings indicate that it does occur in the rabbit (fig 9) The release of secretory products directly into the perivascular space could well be the mechanism by which the pituitary reacts to situations requiring sudden changes in hormone concentration in the blood It has not been possible to trace the processes far enough to determine whether they are detached portions of cells or simply a process which has extended through the basement membrane to discharge its granules

Once liberated from the parenchymal cells the secretory products must reach the blood stream in order to have an effect on the distant target organs. Although no concrete evidence exists accounting for the movement of dissolved materials, a concentration gradient presumably exists which would establish and facilitate the direction of diffusion of hormones through the basement membranes the ground substance in the perivascular space and even across the tenuous membrane bridging the fenestrae of the endothelium. Rinehart and Farquhar ('55) and Farquhar ('61) demonstrated pinocytotic vesicles in the thicker portions of the endothelium and suggested that in such places there is an active transport of dissolved substances across the endothelial wall. Our observations that large pinocytotic vesicles in the endothelium (figs. 11 13) contain a material which resembles the ground substance of the perivascular space rather than the plasma in the capillary lumen supports the theory that hormones may be transported by pinocytosis from the perivascular space into the circulation.

The fact that we have observed membrane-bound granules indistinguishable from those in the epithelial cells lying free in intercellular spaces in the perivascular space within the cytoplasm of endothelial cells as well as in the lumen of capillaries indicates that movement of intact secretory granules toward the circulating blood does occur We can theorize that the motive force which transports the granules in their extracellular course might be provided by the movements of the parenchymal cells which change the shape and extent of the intercellular spaces, perhaps aided by the action of cilia that are often found protruding into these spaces (fig 3) Although the basement membranes have been considered to be the principal barrier to diffusion we have observed a few times an appearance suggesting that intact granules can cross them. We have confirmed the report by Farquhar ('61b) that electron-dense granules having perigranular membranes are sometimes seen within the thicker portions of endothelial cells (fig 7) Were it not for finding such granules in the perivascular spaces as well as in the lumen of the capillaries, we would presume that the granules in the endothelial cells have a different origin

from those of the parenchymal cells How ever as we have indicated above the granules found in the capillary lumen present the same morphological characteristics, i.e., distinct perigranular membrane size and electron density as those seen in other intra- and extra-cellular locations. In addition, the fact that they are frequently found in the vicinity of cytoplasmic projections of endothelial cells (figs. 8 10) strongly suggests that they have just been discharged. Löblich and Knezevic ('60) while not presenting photographic evidence, suggested that intact granules could be actively transported across the endothelial cytoplasm in the rabbit adenohypophysis. In the present study it has been possible by systematic survey at high magnification of every capillary visible in each section, to accumulate sufficient data to warrant proposal of the theory of active transport of intact secretory granules as well as dissolved hormone-containing material into the circulation.

LITERATURE CITED

Clark, S. L., Jr. 1963 The thymus in mice of strain 129/J studied with the electron microscope. Am. J Anat., 112: 1–34

Farquhar M. G. 1961 Origin and fate of secretory granules in cells of the anterior pituitary gland. Trans. N Y Acad. Sci., 23: 346–351.

——— 1961b Fine structure and function in capillaries of the anterior pituitary gland. Angiology 12 270–292.

Farquhar, M. G., and J F Rinehart 1954a Electron microscopic studies of the anterior pituitary gland of castrate rats. Endocrinology 54: 516–541

——— 1954b Cytologic alterations in the anterior pituitary gland following thyroidectomy An electron microscope study Endocrinology 55 857–876.

Farquhar M. G and S. R. Wellings 1957 Electron microscopic evidence suggesting secretory granule formation within the Golgi apparatus. J. Biophys. Biochem. Cytol., 3 319–322.

Garwood, V F and J S. Latta 1963 Electron microscopic observations on the secretory process in prolactin cells of the mouse anterior pituitary (Abstract) Anat. Rec., 145 231–232.

Green, J. D., and V L. Van Breeman 1955 Electron microscopy of the pituitary and observations on neurosecretion. Am. J Anat., 97 177 203.

Hartley M. W W H. McShan and H. Ris 1960 Isolation of cytoplasmic pituitary granules with gonadotrophic activity J Biophys. Biochem. Cytol., 7 209–218.

Herlant, M. 1952 Séparation des activites du lobe antérieur de l'hypophyse par la méthode des centrifugations différentielles. Ann. Endocrinol., 13 611–623.

Hymer, W C., and W H. McShan 1963 Isolation of cytoplasmic pituitary granules by column chromatography J Cell Biol., 13 350–354.

——— 1963 Isolation of rat pituitary granules and the study of their biochemical properties and hormonal activities. J Cell Biol., 17 67–86.

Ichikawa, A. 1959 Electron microscope study on secretion of the rat adenohypophysis. Acta Anat. Nipp 34: 460–482.

Lever J D and R. R. Peterson 1960 Cellular identities in the pars distalis of the rat pituitary Trans. N Y Acad. Sci., 22: 504–508.

Löblich, H. J and M. Knezevic 1960 Elektronenoptische Untersuchungen nach akuter Schädigung des Hypophysen-Zwischenhirnsystems. Beitr zur Path. Anat., 122 1–30.

Luft, J. H. 1961 Improvements in epoxy resin embedding methods. J Biophys. Biochem. Cytol., 9: 409–414.

Maillard, M. 1963 Origine des grains de sécrétion dans les cellules de l'antéhypophyse embryonnaire du rat; rôle de l'appareil de Golgi. J Microscopie, 2 81–94

McShan, W H., and R. K. Meyer 1949 Gonadotropic activity of granules isolated from rat pituitary gland. Proc. Soc. Exp Biol. and Med., 71 407–410.

——— 1952 Gonadotropic activity of granule fractions obtained from anterior pituitary of castrated rats. Endocrinology 50 294–303.

McShan, W H., R. Rozich and R. K. Meyer 1953 Biochemical properties of fractions obtained from rat anterior pituitary glands by differential centrifugation. Endocrinology 52: 215–222.

Millonig, G. 1961 A modified procedure for lead staining of thin sections. J Biophys. Biochem. Cytol., 11 736–739.

Richardson, K. C., L. Jarrett and E. L. Fink 1960 Embedding in epoxy resins for ultrathin sectioning in electron microscopy Stain Tech., 35 313–323.

Rinehart, J F and M. G Farquhar 1953 Electron microscopic studies of the anterior pituitary gland. J Histochem. Cytochem., 1 93–113.

——— 1955 The fine vascular organization of the anterior pituitary gland. Anat. Rec., 121 207–239

Sano, M. 1962 Further studies on the theta cell of the mouse anterior pituitary as revealed by electron microscopy with special reference to the mode of secretion. J Cell Biol., 15 85–98

Schelin, U 1962 Chromophobe and acidophile adenomas of the human pituitary gland. Acta P th. Microbiol. Scand., Supp. 158.

W tson, M L. 1958 Staining of tissues for electron microscopy with heavy metals. J Biophys. Biochem. Cytol., 4 475–478.

Yamada, K., and M. Sano 1960 Electron microscopic observations of the anterior pituitary of the mouse. Okajimas folia. Anat. Japon., 34: 449–475.

Abbreviation

CL Capillary lumen
E Endothelium
EB *Endothelial b sement membrane*
IS Intercellular space
PB Parenchymal basement membrane
PS Perivascular space

PLATE 1

EXPLAN TION OF FIGURES

1 Portion of basophile in the process of discharging three secretory granules (arrows) The liberated granules, without perigranular membranes, lie between the plasma membrane and the parenchymal basement membrane A distinct perigr nular membrane surrounds the granules within the cytoplasm. × 37,800.

2 A basophile granule (arrow) lying in an irregular depression of plasma membrane ha not undergone any notice ble dissolution. The nature of the tructures intervening between the extruded granule and the capillary lumen can be observed. × 25,200.

PS
PB
1
CL
ED
PS
PB
2

PLATE 2

EXPLAN TION O FIGC 6

3 A free membrane bound cidophile gr ule (rrow) and several cytoplasmic processes occupy an intercellular spac along with cili m protruding from parenchymal IL 9,00

4 A acidophile on the left and basophile on the right bound an intercellular pace in which tw secretory gra ules be seen, ach urrounded by thin rim of cytopla m The intercellular pace is continuous t the arrow with the pac between the parenchymal cell nd the adjacent basement membr ne ,8,200

IS

3

PB

PS

IS

4

PLATE 4

EXPLAN TION OF FIGURE

8 Tw intact gran les (rrows) having imil r haracteristics to those in the basophile t the upper left, an be bserved ly ng free in the lumen f e pillary The typical fenestrated and thick portions of the endothelium are demonstrated A prominent nucleus and occasional pinocytotic vesicles n be seen in the thick portions. Note the cytopl mic projection or microvillus near the free granule on the left × 30,000


PR
PS

PLATE 5

EXPLANATION OF FIGURES

9 Processes of basophile (arrow) lying in the perivascular space. They have the same morphology the basophile seen t the lower right. The processes are not urrounded by basement membrane although some intermittent strands of basement membrane can be detected Some of the granules (ircles) appear to h been liberated. × 19,000

10 A secretory granule which is of the same size nd densit a those in the nearby acidophile lies free in the lumen of capillary A microvillus (arrow) projects from the endothelial cell near the granule × 37,800.

11 A large vesicle projecting int the capillary lumen appears to have small esicle (arrow) coalescing with it The large esicle has a conti uou rim of endothelial cytopla m urrounding it The contents more closely resembles the material in the perivascula pace than it does that in the capillary lumen. × 38,200.

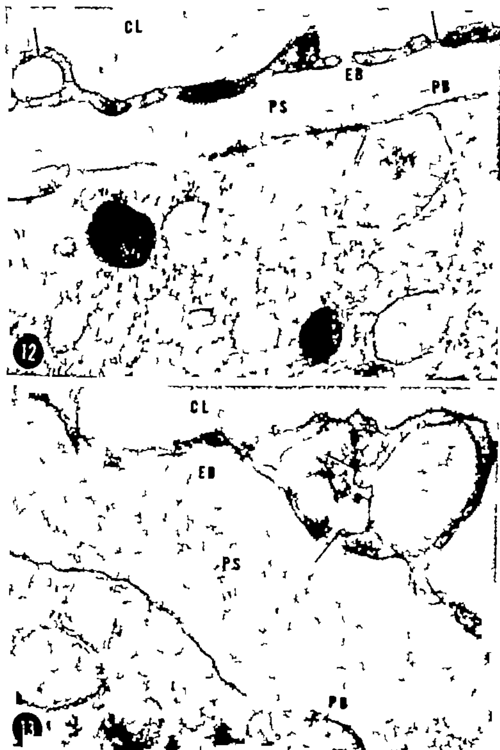

CL
EB
10
CL
E
PB
11

PLATE 6

EXPLAN TION OF FIGURES

12 A esicle surrounded by the fenestrated endothelium contains dense material. Note that the fenestrae are bridged by membrane (ar row) × 51,000

13 Small esicles in the endothelial wall ppear to be alescing with and or dhering to the large vesicle which is encl ed in part by fenestrated endothelium. The material within the Large vesicle has the same ppearanc that in the perivascula pa 39,000.


CL
EB
PB
PS
12
CL
EB
PS
PB
13

or simple immersion of whole opened atria or large pieces of ventricle in 0 005% methylene blue in saline adjusted to pH 3 6 In many cases heart tissue was treated first by perfusion and then dissected pieces of the perfused heart im mersed Additional immersion solution was occasionally injected with a syringe and small needle beneath the epi- or endocardium. Following perfusion and/or im mersion various portions of the heart such as the entire opened right or left atrium, the interatrial septum or selected areas of the ventricles were aired and then fixed in 8% ammonium molybdate Following fix ation the tissues were thoroughly washed dehydrated with alcohol and finally cleared and studied in benzyl benzoate

The advantage of tissues prepared for study in this manner is that one may focus through the entire thickness of the atrial walls or through a several millimeter thick portion of the ventricular wall and easily determine the relative disposition of vari ous types of nerve end formations.

OBSERVATIONS

Classification of nerve endings

Before describing the types of sensory endings found in various parts of the heart, it is necessary to describe briefly and compare the types of sensory endings found in somatic and vascular tissues. In such tissues as the skin, fasciae aponeu roses tendons ligaments joint capsules and periosteum three basic types of sen sory nerve endings are usually found (Miller and Kasahara, '59a, '59b '63 Ralston et al. '60; Miller et al. '58 '60) These may arbitrarily and simply be di vided into 1 Free fiber endings which are little branched or unbranched termina tions of small myelinated or unmyelinated fibers 2. Complex unencapsulated endings resulting from the repeated branching of terminal fibers and which are distinctly discrete but unencapsulated structures (e.g. Ruffini, Ruffini-like or Golgi-type endings) 3. Encapsulated endings, characteristically discrete and sur rounded by a capsule of modified Schwann cells or connective tissue elements (e g. Meissner's corpuscles Krause end bulbs Golgi Mazzoni ends or the various sized Vater-Pacinian corpuscles.

In blood vessels small myelinated fibers may terminate in sensory endings of the free fiber type, or the dendrites of one or several fibers may anastomose to form an end net. The end-net may well be the most abundant type of vascular sensory element but it is difficult to identify because of its remarkable morphological similarity to the autonomic motor plexus. Unless experimental nerve root sections are performed (Polley '55) or special histochemical technics are used differentiation of the sensory and motor elements in blood vessels is very difficult.

Apart from such specialized areas as the aortic arch carotid sinus, pulmonary artery and origin of the renal arteries, complex unencapsulated endings (baroreceptors) are rarely found in blood vessels.

Encapsulated endings of the Vater-Pacinian type are found in the walls of the larger veins.

The sensory nerve endings found in the heart are: 1 end-nets 2. complex unencapsulated endings and 3. encapsulated endings.

The end-net (fig 12) is formed by the anastomoses of the branched dendrites of several apparently different myelinated fibers. It is a prominent and constant feature of the entire endocardium. Since free fiber endings seem to be absent from cardiac tissue the end-net may either represent free fiber endings in the heart, or be a sensory element peculiar to vascular tissue

It should be pointed out that the end-net nerve terminals are not usually demonstrable with heavy metal technics, and therefore workers such as Chabarowa ('57) and Nonidez ('39) do not explicitly describe these nerve endings. Holmes ('57), however was able to demonstrate these endings with both methylene blue and silver technics. Workers with methylene blue on the other hand, have consistently described indicated or pictured these structures (Michailow '08 Meyling '53, Woollard, '26 Mitchell, '56)

Complex unencapsulated endings in the heart are referred to in the literature as diffuse or compact type nerve endings. Endings of moderate sized myelinated fibers which are much branched and occupy a considerable area may be termed diffuse

of complex unencapsulated endings. ...ly large or large myelinated ...bers arise more spatially circumscribed ... of varying size and form. These may be termed compact types of complex unencapsulated endings. Intermediate or ... forms are always found, which emphasizes the artificiality of this or any other classification.

Encapsulated endings are compact, circumscribed nerve end formations that are surrounded by a definite connective tissue capsule. Such endings are exceedingly common in many tissues, but with the exception of the horse (Michailow '08) are rare in the hearts of mammals thus far described.

Epicardium

Atria. In our experience, the atrial epicardium as compared to the endocardium is only sparsely supplied with sensory nerve endings. We have observed both diffuse and compact types of complex unencapsulated endings in the substance of the epicardial connective tissue (figs. 1, 2, 4 and 6). Occasionally an end-net like formation was seen lying just above the outer surface of the myocardium but it was not certain whether this was a sensory end-net or merely part of the general epicardial nerve plexus. The relative sparsity of sensory endings in the epicardium was surprising to us as Dogiel (1898) and more recent Russian workers (Chabarowa, '59) state that these endings are very abundant in the epicardium. In our entire series of over 75 animals however we found not even one specimen to be richly supplied with epicardial sensory endings.

Area of sinu-atrial node. Immediately surrounding the sinu-atrial node and elsewhere in the substance of the atrial epicardium are various sized groups of ganglion cells. With methylene blue some of the nerve cell bodies of these ganglia stain well, while the satellite cells surrounding ... prevent the cell body from staining. The synaptic contacts between pre- and post-ganglionic neurones is well visualized in these areas. In no case did we ever see a sensory fiber ending on the pericapsular apparatus of cardiac ganglion cells. Sensory fibers ending on cardiac ganglion cells have been described by some Russian workers (Khabarova, '62).

With our technics we were not able to demonstrate nerve fibers terminating within the nodal tissue. Recently Torii ('62) with the electron microscope has beautifully and unequivocally demonstrated nerve terminals ending in relation to elements within the nodal tissue.

Ventricles. As in the atrial epicardium a wide variety of both diffuse and compact types of complex unencapsulated endings were encountered (figs. 7–11). End-nets were generally absent from the epicardium proper but were characteristic of the coronary vasculature. Differentiation of motor and sensory end-nets in smooth muscle areas is difficult without experimental nerve root sections.

Myocardium

Bundles of mixed myelinated and unmyelinated nerves follow connective tissue septa between muscle bundles and ultimately extend to the endocardium. With our technics we were unable to demonstrate sensory terminals ending about myocardial muscle fibers. Occasionally however amyelinated fibers course directly over myocardial muscle fibers in both the atria and ventricles and these are presumably the motor terminations of post-ganglionic sympathetic nerves (figs. 34–36).

Endocardium

Atria. The atrial endocardium is richly innervated. End-nets and diffuse and compact varieties of complex unencapsulated sensory endings occur profusely in this region. Certain locations are more abundantly and consistently well innervated than others; these are the areas about the entrance of the inferior vena cava into the right atrium, the opening of the pulmonary veins into the left atrium, and the bases of the interatrial septum.

All three varieties of nerve endings (end-net, diffuse and compact) may occur in the same location, or each type may occur separately. The end-nets frequently arise from variously sized myelinated fibers (fig. 12). It appeared to us that the end-net structure arose from the anastomosed dendrites of several (two to six or even more) nerve fibers (fig. 12). As far as one

is able to determine with the light microscope the branching ends of several fibers anastomose with one another Michailow ('08) observed and described precisely this phenomenon in the horse atrial endocardium and pointed out that while the end-net might appear to originate from several different fibers in reality the apparent fibers of origin might be collaterals of a single parent fiber branching at a higher level. The end-nets were seen most frequently on the posterior and inferior aspects of the atrial endocardium as well as on the interatrial septum.

In some areas the end-nets may be the only elements present (fig. 12) but more frequently occur together with complex unencapsulated endings (fig. 14)

The most characteristic feature of the atrial endocardium is the wealth and variety of complex unencapsulated sensory nerve endings varying in form from diffuse rambling structures to discrete compact elements (figs. 13–26) Morphologically these endings are the homologues of stretch receptors in other types of tissue and in the heart are termed baroreceptors by the physiologists.

While these endings may be encountered almost anywhere in the atrial endocardium they are most abundant in the areas about the openings of the great vessels and on the interatrial septum. They are rare or absent in the auricular endocardium.

The nature and variety of these type endings can best be appreciated from the photographs (figs 13–26) Here it is apparent that in all four mammalian species represented the same basic types of structures are present, but in each species the endings have a slightly different appearance. While it is difficult to describe these species differences, the terminal structures of the dog and monkey appear a little more coarse and less delicate than those of the cat and lamb After one has studied a sufficient number of specimens from a particular species, it is possible to recognize the species by the appearance of the sensory terminals.

The diffuse type of endings arise from fibers approximately 4 to 6 μ in diameter and the branches and ramifications of one fiber may occupy an area of several square millimeters. There are no anastomoses between the terminal branches of different nerve fibers.

Fibers giving rise to the large compact endings are usually the largest found in the heart and range from 8 to 14 μ in diameter The terminal apparatus from these fibers vary in size from 50 to 350 μ. The approximate number of these large discrete endings ranges from 100 to 300 in the endocardium of the dog.

Ventricles The ventricular endocardium (apart from the valvular endocardium) is much different from the atrial in that only end nets and no other type of sensory endings have been observed. In the ventricular endocardium there is a rich nervous plexus (figs. 27–29). Many of the myelinated fibers in this plexus give rise to sensory end-nets. No particular association of sensory end-nets with the Purkinje bundles was noted although in the lamb where the bundles are more superficially located there are abundant overlying nerve fibers (fig. 28).

Valves

The endocardium of both surfaces of the leaflets of the mitral and tricuspid valves are well endowed with end-nets and occasional complex endings (figs. 30–33) The aortic and pulmonary valve leaflets show only infrequent patches of end-nets. From the tricuspid and mitral valve leaflets nerve fibers course over the chordae tendineae

Pulmonary artery and aortic arch

While this study was not primarily concerned with these structures, excellent photographs of the sensory nerve endings in these interesting areas were obtained and are included here.

In the adventitia of the base of the pulmonary artery and the inferior aspect of the aortic arch (figs. 37–41) there are numerous end-nets and large complex unencapsulated endings. These have been thoroughly described and illustrated in the extensive studies of Abraham ('55, '56, '61)

DISCUSSION

After a century of morphological study of the intrinsic innervation of the heart

a more complete picture is emerging. From 1860 to 1890 the emphasis was primarily on the nature of the motor endings on myocardial muscle fibers. With the advent of methylene blue in the 1880's attention was directed more to the sensory innervation. From the 1890's to the present, many authors have described a variety of sensory nerve endings in the heart.

An excellent historical summary of the motor innervation of cardiac muscle is given in the papers of Berkeley (1895) and Smirnow ('00) The consensus in the 1890's was that in many myocardial areas, but not all, the muscle is innervated by simple unbranched or few branched endings of amyelinated nerve fibers which are in intimate direct contact with the muscle fiber Little was added to our knowledge of myocardial muscle innervation until the recent ultrastructural studies of Fawcett and Selby ('58) and Virágh and Porte ('61) The electron micrographs corroborated the earlier viewpoint that myocardial muscle fibers are innervated by simple branched or unbranched terminal of unmyelinated nerve fibers much in the same way as the smooth muscle of blood vessels or visceral structures is innervated. Whether these endings in the heart muscle are the terminal branches of sympathetic or parasympathetic nerve fibers remains undetermined, although the supposition is that they represent the terminals of postganglionic sympathetic fibers. Neither sufficient nor appropriate histochemical studies, nor observations following successful total heart sympathectomies or parasympathectomies have been carried out to resolve this problem.

A host of Russian workers (Khabarova, '62) have described sensory nerve endings associated with the intrinsic cardiac ganglia, but this concept is far from generally accepted and its significance unclear Our preparations show numerous synapses within the cardiac ganglia, but nothing to suggest the endings of sensory fibers.

Goertler ('61) and others feel that the bundles of Purkinje fibers coursing down the interventricular septum are covered by sensory elements that are specifically related to the conduction fibers. While we have observed this apparent relationship in the lamb heart, we conclude that the sensory endings are not necessarily functionally related to the conduction fibers, but are rather a part of the general endocardial sensory apparatus.

There is little doubt that both the epicardium and endocardium are well supplied with sensory nerve endings. The majority of the sensory endings in the epicardium are complex unencapsulated in nature These are remarkably similar in structure to the same type of endings that occur in the dermis, fasciae, aponeuroses tendons, joint capsules, or periosteum. In the heart, as in other tissues these endings are probably associated with the function of denoting change in tissue position or a change in the degree of tension or stretch existing in the tissue. Such receptors are termed "stretch receptors in most of the body but referred to as baroreceptors in the heart.

Dogiel, in his early classical article of 1898 presents beautiful drawings of complex unencapsulated endings. A multitude of Russian workers have since elaborated on the nature and disposition of these receptors. While the Russian workers state that the epicardial nerve endings are remarkably abundant, neither Woollard nor we have been able to find these endings in great profusion. Regardless of their number they comprise the dominant epicardial sensory element.

The coronary vasculature is well endowed with both motor and sensory networks but without resort to special histochemical technics and experimental dorsal and ventral root sections the nature and extent of the sensory network is difficult to ascertain.

The atrial endocardium is the most profusely innervated area of the heart. Nearly all workers since Smirnow (1895) and Berkeley (1895) have described a wealth of sensory nerve endings in this location. Virtually all students of cardiac innervation have described and illustrated a large variety of complex unencapsulated terminals varying from diffuse to compact in general form (Smirnow 1895 Berkeley 1895 Woollard, '26; Nettleship '36 Nonidez, '39 Holmes '57 '58 and many others) While numerous drawings of these endings have been published, very few good photographs have appeared in

print. Since interpretation plays a con siderable role in neurohistology it is im perative that photographic evidence ac company descriptive accounts

The end net formation so prominent in both the atrial and ventricular endocar dium was first recognized and described by Michailow ('08) but largely overlooked until Holmes ('57 '58) clearly depicted it and emphasized its separateness from the diffuse and compact types of endings It is interesting that the more recent Russian workers (Khabarova '62) fail to recognize this remarkable structure Preoccupation with heavy metal technics explains in part the failure to visualize nerve terminals made up of very small sized fibers.

The fact that the end-net is derived from myelinated fibers and shows non-specific cholinesterase staining about the network fibers (Holmes '58) is indicative of its sensory nature In almost every variety of sensory apparatus in the heart the terminal branches have been described ending in relation to specialized types of cells (Dogiel 1898 Khabarova '62) The demonstration of such elements depends in part on the particular technic used as well as on the interpretation of the observer The ultimate solution of this prob[illegible] awaits ultrastructural study similar to [illegible] of the interstitial cell problem in rela tion to smooth muscle motor innervation

The central distribution of the various types of sensory nerve endings in the heart *is only partially solved.* Woollard ('26) Nettleship ('36) Nonidez ('39) Holmes ('57) and Chabarowa ('59) by means of differential vagal and sympathetic sec tions have described results indicating that the large complex unencapsulated endings found mostly in the atrial endo-cardium travel mainly with the vagus nerves and terminate in medullary centers. That some baroreceptors end in the upper thoracic spinal cord is maintained by Kha barova ('62) The central termination of the end-nets remains undetermined.

There is little doubt that the complex endings found in both the epi- and endo-cardium are stretch or baroreceptors. Thus these cardiac endings are both mor phologically and functionally homologous to similar endings throughout the body

Establishment of the true nature and function of the end-net endings awaits further investigation Likewise the nature and disposition of fibers mediating pain from the heart remains undetermined

LITERATURE CITED

Abrahám, A. 1955 Über die Stelle und Struktur der Receptoren im Aortabogen des Rindes Acta Biol. Szeged, *1:* 125–129.

——— 1956 Über die Struktur und die Endigungen der Aorticusfasern im Aortenbogen des Menschen mit Berücksichtigung der Cholinesterase Aktivität der Pressoreceptoren. Z. mikr -anat. Forsch., *62:* 194–229.

——— 1961 Struktur und Endigungsform der Fasern des Nerven aorticus im Aortenbogen des Schweines. Z. mikr -anat. Forsch., [illegible] 409–426.

Berkeley H. J 1895 The intrinsic nerve supply of the cardiac ventricles in certain vertebrates. The John Hopkins Hospital Reports. Report in Neurology II, 4 248–275.

Chabarowa, A. J 1959 (Same authoress listed below as Khabarova, A. I.) Die afferente Innervation des Herzens. Z. mikr -anat. Forsch., 66 236–250.

——— 1961 Ueber die Rezeptorischen Felder im Herzen. Z. mikr -anat. Forsch., 67 [illegible]

Dogiel, A. S. 1898 Die sensiblen Nervenendigungen im Herzen und in den Blutgefässen der Säugethiere. Arch. mikr Anat., 52: 44–[illegible]

Fawcett, D W and C. C. Selby 1958 Observations on the fine structure of the turtle atrium. J Biophys. Biochem. Cytol., 4 63–71.

Gerlach, L. 1868 Cited in Schäfer, E. A., [illegible] Textbook of Microscopic Anatomy Longmans, Green and Co., London, p. 325.

Goerttler K. 1961 Struktur und Bedeutung der Purkinjefasern im Herzen. Verhand. d. Deutschen Gessell. f Kreislauf., 27 [illegible]–301.

Holmes, R. L. 1957 Structures in the atrial endocardium of dog, which stain with methylene blue and the effects of unilateral vagotomy J Anat., 91 259–266.

——— 1958 Nervous structures in the mammalian atrial wall. J. Physiol., 142: [illegible]

Khabarova, A. I. 1963 (Same authoress as Chabarowa, A. J above.) The Afferent Innervation of the Heart. Consultant's Bureau, New York.

Meyling, H. A. 1953 Structure and significance of the peripheral extension of the autonomic nervous system. J Comp. Neur., 99: [illegible]

Michailow S. 1908 Die Nerven des Endocardiums. Anat. Anz., 32: 87 101.

Miller M. R., H. J Ralston III and M. Kasahara 1958 The pattern of cutaneous innervation of the human hand. Am. J. Anat., 102: [illegible]

——— 1960 Advances in Biology of Skin Ed. by W Montagna. Pergamon Press, New York. Vol. 1 Cutaneous Innervation. Chap. 1, 1–47.

Miller M. R. and M. Kasahara 1959 The pattern of cutaneous innervation of the human foot. Am. J Anat., *105* 233–256.

1959b The cutaneous innervation of the human female breast. Anat. Rec., 135: 153–168.
—— 1963 Observations on the innervation of human long bones. Anat. Rec., 145 13–17
Mitchell, G. A. G. 1956 Cardiovascular Innervation. E. & S. Livingstone, Ltd., Edinburgh.
Nettleship, W A. 1936 Experimental studies of the afferent innervation of the cat' heart. J Comp. Neur 64: 115–133.
Nonidez, J. F 1939 Studies on the innervation of the heart. Am. J Anat., 65 361–413.
Palley E. H. 1958 The innervation of blood vessels in striated muscle and skin. J Comp. Neur., 103 253–287
Ralston, H. J III, M. R. Miller and M. Kasahara 1960 Nerve endings in human fasciae, tendons, ligaments, periosteum, and joint synovial membranes. Anat. Rec., 136 137–148.
Smirnow A. 1895 Ueber die sensiblen Nervenendigungen im Herzen bei Amphibien und Säugetieren. Anat. Anz., 10: 737–749
—— 1900 Zur Frage von der Endigungen der motorischen Nerven in den Herzmuskeln der Wirbeltiere. Anat. Anz., 18 105–115.
Torii, H. 1962 Electron microscopic observations of the S-A and A V nodes and Purkinje Fibers of the rabbit. Jap Circ. J 26 39–50.
Virágh, S., and A. Porte 1961 Eléments nerveux intracardiaques et innervation du myocarde. Étude au microscope électronique dans le coeur de rat. Z. Zellforsch., 55 282–296.
Woollard, H. H. 1926 The innervation of the heart. J Anat., 60: 345–373.

PLATE 1

EXPLANATION OF FIGURES

The nerve endings demonstrated in all figures were stained by methylene blue perfusion and/or immersion.

The straight black line at the bottom of each photograph represents 100 μ of distance.

In the explanation of figures "C.U.E." is the abbreviation for complex unencapsulated ending.

1 Dog. Right atrial epicardium. This is a diffuse type of C.U.E., and is very similar to endings often seen in the connective tissues of the capsules and ligaments about joints.

2 Monkey. Right atrial epicardium. A compact C.U.E. This type of formation is often seen in fascial structures.

3 Cat. Left ventricular epicardium. A compact C.U.E. This type of structure is very similar to the Ruffini ending found in the dermis of human glabrous skin.

4 Dog. Left atrial epicardium. A compact C.U.E.

5 Lamb. Left atrial epicardium. Similar to figure 4.

6 Cat. Left atrial epicardium. A compact C.U.E. Two spherical bulb-like structures arise from the two branches of a single fiber.

7 Lamb. Left ventricular epicardium. A large diffuse type of C.U.E. Such structures are frequently seen in fasciae, aponeuroses, and periosteum.

8 Lamb. Left ventricular epicardium. A spread out, but basically compact type of C.U.E. This ending is characteristic of the Golgi-type endings found in retinacula and tendons.

9 Dog. Left ventricular epicardium (near the apical dimple). This is diffuse type of C.U.E.

10 Dog. Left ventricular epicardium near the atrio-ventricular junction. Compact C.U.E.

11 Cat. Left ventricular epicardium. Compact C.U.E.

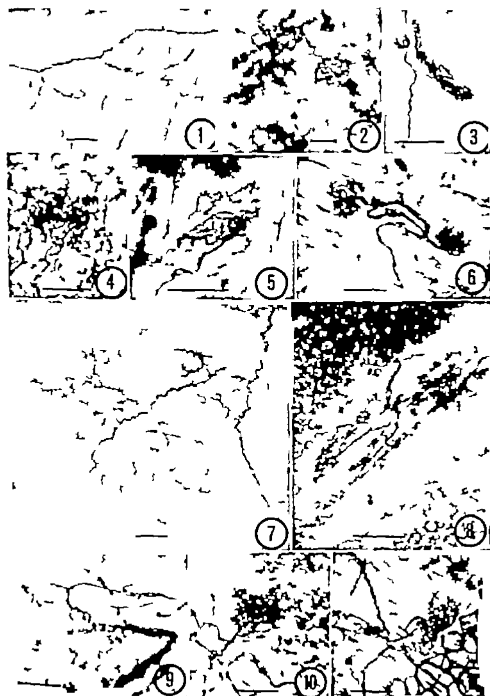

1
2
3
4
5
6
7
8
9
10

PLATE 2

EXPLANATION OF FIGURES

12 Dog Right trial endoc rdium A end net sensory terminal. Several small myelinated fibers re seen bifurc ting to form terminal end-net The terminal branches of several fibers seem to fuse thu forming an ana tomotic end-net.

13 Dog Right trial endocardium at the point of junction with the inferior ven ca a. Diffuse C.U.E. All the terminal in this view emanate from single parent fiber The terminal f separate fibers never ana tomose in this type f ending.

14 Dog. Right atrial endocardium. The network in the background is an end net. The larger more heavily stained fiber entering the upper left part of the field is seen supplying compact C U.E.

15 Monkey Right atrial endocardium. A very fine fibered diffuse C.U E.

16 Dog. Right trial endocardium in the vicinity of the inferior vena ca Diff se types of C U.E.

17 Lamb. Right atrial endocardi m. Diffuse C.U.E. the individual ter minal of which are longate d tending toward compaction.

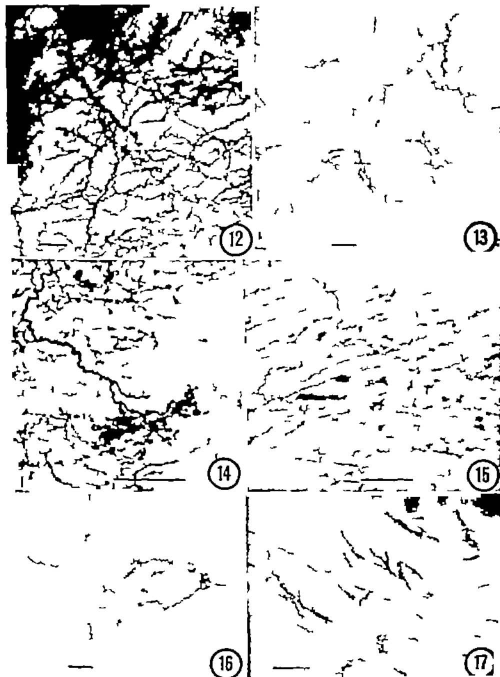

12
13
14
15
16
17

PLATE 3

EXPLAN TION FIGURES

18 Cat. Left trial endocardi m. Diffuse C U.E. with individual ter minals tending toward compaction

19 Cat. Right trial endoc rdi m. Diffuse C.U E.

20 Lamb Right trial endocardium. Diffuse C.U.E.

21 Monkey Left trial endocardium Diffuse C U.E.

22 Dog. Left trial endocardi m. Compact C.U.E.

23 Monkey Left trial endocardium. Compact C.U.E.

24 Lamb. Left trial endocardium. Compact C.U E.

25 Cat. Right trial endocardium near inferior ven cava. Compact C.U.E.

26 Cat. Left trial endocardium near entrance f pulmonary ein Compact C U E.

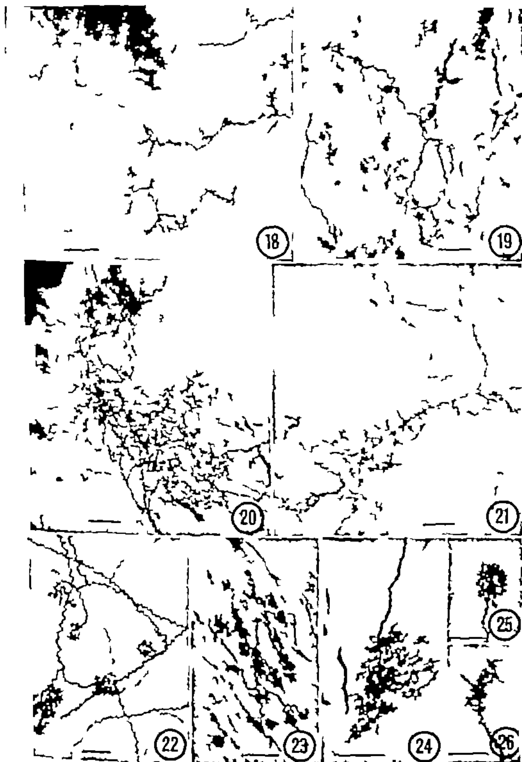

18
19
20
21
22
23
24
25
26

PLATE 4

EXPLANATION OF FIGURES

27 Cat. Endocardium of the right side of the interventricular septum Sensory end-net in the ventricular endocardium.

28 Lamb. Endocardi m of the left interventricular septum. In this view one sees mal ly the b-endocardial ple us but some of the fibers form sensory end-nets

29 Monkey Endocardium f right interventricular septum. Sensory end-net.

30 Monkey Mitral al e Sensory end net.

31 C t Mitral valv C.U.E.

32 Monkey Tricuspid valve Sensory end-net

33 Lamb Tricuspid al C.U E.

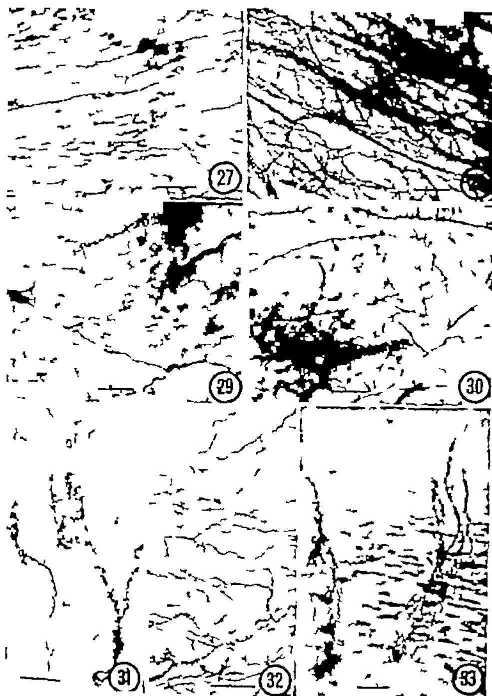

27
29
30
31
32
33

PLATE 5

EXPLAN TION OF FIGURES

31–33 Dog. Left trial myocardium. Several thin "beaded" unmyelinated fibers re seen runni g acros and p rallel to the myocardial muscle fibers. The are f intimate contact between the nerve nd muscle fibers represent ynaptic points nd are multiple (ynapses en pa sant") These rel tionships ha been verified by ultrastructural tudies (see discus ion)

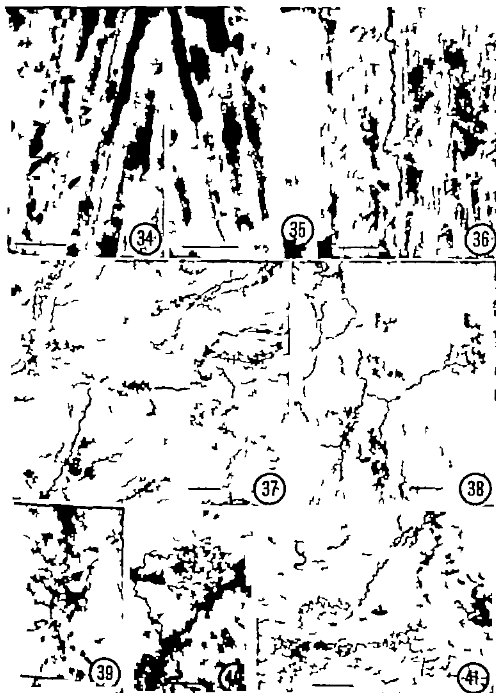
36 Monkey Left ventricular myocardium. Same 34 and 35.

37 Cat. Aortic rch. Several C.U.E. 1 the drentitla of the inferior spect of the aortic rch.

38 Lamb Aortic arch Same a 37

39 Monkey Aortic arch Same as 37

40–41 Dog. Aortic rch. S me as 37


34
35
36
37
38
39
40
41

Cyclic Changes of Interstitial Gland Tissue of the Human Ovary [1]

H. W. MOSSMAN, MARILYN J. KOERING AND DARWIN FERRY JR.
Department of Anatomy, University of Wisconsin, Madison, Wisconsin

ABSTRACT Three distinct types of gland cells occur in adult human ovaries and those of other mammals. These are (1) Interstitial gland cells formed from the theca interna cells of degenerating (atretic) follicles, hence present from infancy to old age; (2) Thecal gland cells formed from th theca interna cells of ripening follicles, hence present only in individuals that are sexually mature or nearly so, and in these only at or near the time of ovulation; (3) Luteal cells formed from the granulosa cells of ovulated follicles and from the undifferentiated stroma cells surrounding these, and in certain species also from the same sources in relation to atretic follicles. These latter are the so-called accessory corpora lutea. Primary and accessory corpora lutea are present normally only after ovulation occurs and appear to function for relatively short time unless pregnancy ensues. In certain species other types of gland cells occur in the ovary and mesovarium; these include the paraluteal cells of the human ovary. Paraluteal cells are not persistent thecal gland cells, but are differentiated from surrounding stroma after the thecal gland disappears. They are probably intermediate stages in the differentiation of luteal cells from stroma cells. Planimetric measurements and computations made from serial sections of human ovaries indicate that in non-pregnancy and early pregnancy the volume of interstitial gland tissue is less than 1% of the total ovarian volume. However in the last trimester of gestation, the relative amount of interstitial gland tissue increases rapidly to roughly from 4% to 6% of the total ovarian volume. The largest amount in our series was 5.6%. Luteal gland tissue at the height of its development in the first trimester of gestation reached 31% of the total ovarian volume. In human ovaries the cells of the interstitial gland tissue of late pregnancy seem to be consistently larger and to have more finely granular cytoplasm than those of early pregnancy or nonpregnancy. The literature shows that mammalian interstitial gland cells of comparable origin to the human cells discussed in this paper have the following characteristics which are known to be indicative of steroid secretors. Numerous birefringent, acetone soluble autofluorescent granules which react with sulphuric acid and are Schultz and Schiff positive; mitochondria with anastomosing tubular cristae; and smooth tubular endoplasmic reticulum. Physiological studies so far reported have indicated possible estrogen, androgen, and progesterone production by interstitial gland cells, but all of the evidence is too scanty, indirect, and at times contradictory to be convincing. Since interstitial gland cells are present from birth to old age, and show cycles of abundance and differentiation correlated with the reproductive age and cycles, they may prove to be the most important ovarian gland cells when their function is fully understood.

The interstitial gland may be the most important gland of the human ovary. It is the first gland tissue to form, being present, at least periodically, in the human ovary from before birth (Fraenkel and Papanicolaou, '38; Potter, '53) until well after the menopause. On the other hand, the thecal gland, an important source of estrogens, is apparently active only when a follicle is in the last few days of the ripening process, and the luteal gland is ordinarily formed from a ruptured follicle secreting progesterone in significant amounts during just a few days of the middle third of the menstrual cycle, or, in the case of pregnancy, for only the first two or three months of the gestation period.

There are several types of glandular tissue in human and other mammalian ovaries and in the adjacent mesovaria, which are usually classed as interstitial gland. (For a review of this matter see Brambell, '56.) However, the type with which we are concerned in this paper is that which differentiates from the relatively embryonic tissue of the theca interna of degenerating large secondary follicles and degenerating vesicular (Graafian) follicles of all sizes, except those follicles which are essentially ripe before atresia

[1] Supported by NIH Summer Fellowship grant [illegible], NIH Training Grants [illegible], [illegible], and [illegible], and NIH Research Grant HE [illegible].
[2] Present address: Regimental Headquarters, 14th Armored Cavalry, APO 26, New York.

sets in In these ripe or nearly ripe follicles the majority of the theca interna cells have already differentiated into functional thecal gland cells and have lost the pluripotentiality they possessed earlier hence little or no interstitial gland tissue is produced by such follicles.

Because crops of vesicular follicles are produced and undergo atresia in rhythmic fashion the amount and cytological differentiation of interstitial gland tissue is also rhythmic Probably this is true even in infants and children

Although known and described in the human ovary and in those of many other mammals for a century (Schrön 1863 Pflüger 1863) and called interstitial gland by Bouin s student Limon in 1901 the significance and importance of this gland has been generally overlooked by both anatomists and physiologists even by many of those who are especially concerned with the physiology of reproduction (Also see Bouin '02 and Limon '02–03) There are several reasons for this Probably most important is the constant confusion as to what is meant by interstitial tissue and the failure to recognize it as a gland or to differentiate it from the thecal gland or corpus luteum The term "inter stitial is itself unfortunate and inaccurate s a descriptive term when applied to the ary connoting as it does merely someing in the spaces between other presumably more vital elements Many students of the ovary have failed to observe the differences between the interstitial gland cells of the theca interna of atretic follicles and the thecal gland cells of ripe follicles or have denied their existence entirely in certain species For example McKay et al ('61) succeed in describing in detail the atresia of various sizes of human follicles without mentioning interstitial gland tissue although they show a clear example of it in their figures 27 and 28 Also Nelson and Greene ('53 and 58) speak of hyperplasia and hypertrophy or "luteinization of the theca interna of atretic follicles but object to calling these cells interstitial gland cells Obviously they do not distinguish clearly between what they call "luteinization of the theca interna of a ripening follicle (actually thecal gland formation) and that of an atre ic follicle (interstitial gland formation) Yet few who have made reasonably extensive comparative studies of ovaries fail to recognize the existence and distinctiveness of these types of ovarian glandular tissue It is unfortunate that in some of the species most commonly studied the interstitial gland cells are relatively inconspicuous (pig) or perhaps somewhat difficult to distinguish from other gland cells in ordinary histological sections (rat)

Yet there is considerable morphological evidence of the steroid secreting nature of the type of mammalian interstitial gland cells with which we are dealing here namely those that are derived from the theca interna of atretic follicles. Dempsey and Bassett ('43) showed that the interstitial gland tissue of the rat contains substances giving the characteristic histochemical reactions of steroid hormones (birefringent crystals autofluorescence acetone-soluble keto-compounds, and sterol substances reacting with sulphuric acid. Claesson and Hillarp ('48) demonstrated Schulz positive sterols in the interstitial gland of the rat guinea-pig, and rabbit. They could show no appreciable increase in sterol production by the interstitial gland at parturition in any of these species nor during the entire lactation period in rats and guinea pigs. Dawson and McCabe ('51) demonstrated in the infantile and juvenile rat ovary cellular inclusions in both the primary and secondary interstitial gland tissue which were osmiophilic sudanophilic Schiff-positive, Schultz-positive birefringent and acetone-soluble in formalin-fixed frozen sections. Rennels ('51) also showed that in the immature rat these cells reacted to hormonal manipulation of the pituitary-gonad axis as one would expect if the inclusions demonstrated by the histochemical methods were gonadal hormones or their direct precursors. Claesson Diczfalusy Hillarp and Hogberg ('48) had shown similar effects of gonadotropic stimulation on the lipids of the pregnant rabbit ovary Deane ('52) concluded from histochemical studies on the rat during the estrous cycle that, "Sites of steroid formation are the theca interna of normal follicles the granulosa of follicles becoming atretic at the time of ovulation, the corpora lutea, and the interstitial

tissue. Ben-Or ('63) concludes from similar studies on the mouse that the interstitial gland is the principal source of oestrogens.

Several electron microscopic studies have demonstrated that steroid secreting cells of the adrenal cortex, interstitial tissue of the testis and corpus luteum are characterized by an anastomosing, tubular smooth endoplasmic reticulum. Muta ('58) has, to our knowledge published the only such study of ovarian interstitial gland. Using the mouse ovary he also demonstrated in the interstitial cells the characteristic smooth endoplasmic reticulum of steroid secretors. Belt and Pease ('56) considered only the mitochondria of steroid secretors and mention that the interstitial cells of the rat ovary have mitochondria with characteristic tubular cristae, but that this feature is more pronounced in theca interna cells and even more marked in luteal cells.

Still it must be admitted that completely clear-cut physiological proof is lacking as to whether or not interstitial gland cells are actually hormone secretors, and certainly there is only a little direct evidence as to what their presumed endocrine product is. Falck ('59) presented evidence that in the rat it is an estrogen however Falck, Menander and Norastedt ('62) obtained only androgen effects. Production of progestins by interstitial tissue of the rabbit is strongly indicated by the work of Hilliard, Archibald and Sawyer ('63) who found that rabbit ovaries from which all corpora lutea and large follicles had been removed by cauterization released approximately as much total progestin/hr/mg tissue as control ovaries with intact follicles. Yet Kilpatrick, Armstrong, and Greep ('62) showed that rabbits with apparently normal interstitial gland tissue but without corpora lutea, did not maintain a progestational endometrium It must be pointed out, however that the latter data were derived incidentally from animals which had been or were being treated with gonadotrophins and which had also been hypophysectomized. Obviously it is still possible that the most significant product of ovarian interstitial gland may be neither estrogen, an androgen nor a progestin.

Anyone who takes the trouble to examine microscopically the ovaries of a variety of mammalian species must certainly be impressed by the universal persence of interstitial gland cells derived from the theca interna of degenerating vesicular follicles by the cyclic fluctuation in abundance of this tissue and by its typical endocrine gland characteristics in both cytology and vascularity It is because of our conviction as to its importance as an endocrine tissue and because we feel strongly that it should be the subject of intense physiological investigation, that we have undertaken, not only to call attention again to its prominence in the human ovary but to attempt to show by quantitative methods that it occurs in significant amounts and that it undergoes a marked rhythm in abundance correlated with the pregnancy cycle

We have chosen for study the pregnancy cycle rather than the menstrual cycle, because we have obtained reasonably normal ovaries from this period and because the size and development of the fetus is a fairly accurate method of determining the stage of gestation, whereas clinical records of menses are very unreliable criteria for the stages of the menstrual cycle. Endometrial characteristics can, of course be used for determining the stages of the cycle in nonpregnant women, if one knows that the cycles of the individual were normal at the time of death or removal of the genital tract, but usually this is uncertain, or else it is definitely known that the reproductive physiology was abnormal.

MATERIAL AND METHODS

The ovaries used in this study were removed surgically or during autopsies from two children and fourteen women four pairs were from patients with apparently normal ovarian cycles but for whom the exact phase of the cycle is unknown, and five pairs and two singles were from women in various stages of pregnancy two were from women who had de-

Specimen numbers [illegible], 81, and 110 were provided by our Department of Surgery and of Gynecology and Obstetrics, and were of great value because they could be fixed promptly. [illegible] autopsy specimens [illegible] Numbers 101 and [illegible] Gordon Worley Jr. and by Dr. Richard A. [illegible] respectively. [illegible] from our Department of Pathology [illegible] the cooperation especially of Dr. Gabriele [illegible] Mrs. Ruth Zevall [illegible] work. We wish to express our appreciation [illegible] of these.

TABLE 1

Pertinent data on ovaries studied

Ovary number	Patient's age	Phase of cycle	Time before fixation	Fixative	Cause of death, or reason for oophorectomy
	years				
143	2 ½	nonpregnant	17 hours	10% F	brain tumor
121	7	nonpregnant	—	Baker's F	—
135	25	nonpregnant	—	AFA	myocardial failure
106	29	nonpregnant	12 hours	AFA	myocarditis
112	18	nonpregnant	3 hours	10% F	uremia and ulcers
125	38	nonpregnant	5 minutes	AFA	adenocarcinoma of breast
93	27	2 months	—	10% F	poliomyelitis
51	39	3½ months	5 minutes	10% F	hysterosalpingo-oophorectomy for breast malignancy
49	42	4 months	2 hours	Levi's	hysterosalpingo-oophorectomy for breast malignancy
80	43	4½ months	—	10% F	—
119	46	5½ months	immediate	AFA	hysterosalpingo-oophorectomy for breast malignancy
104	—	8½ months	—	10% F	—
96	21	8½ month	6 hours	Z+2% F	auto accident
131	—	term	1½ days	Baker's F	postpartum hemorrhage
142	25	term	10 hours	AFA	cerebral aneurysm
116	22	1 month postpartum	1 day	AFA	—

Small portion of each ovary removed by pathologist not included in our measurements.

livered within an hour or two of death and one was approximately one month post partum (table 1). None of these had a definite record of recent hormone therapy or of pathology of a type known to have gonadotropic effects, but for five individuals there was no clinical record available (table 1).

The ovaries were fixed in various solutions: alcohol formol acetic acid, 10% formalin, Baker's formalin, or Levi's. They were stored in 70% alcohol and later dehydrated and cleared by the alcohol cyclohexanone method, embedded in paraffin and sectioned serially. Every fiftieth section was mounted and stained with Groat's tetrachrome stain.

The sections were studied under the microscope and the significant interstitial gland masses of each section were identified and roughly outlined on paper. Then, using an Edinger microprojector with these rough outlines as guides, the enlarged image of each section was projected onto paper at known magnification and the peripheral extent of the ovary as well as of each interstitial and luteal area was accurately outlined and then traced twice with a Keuffel and Esser Co. 4236M planimeter and the average of the two readings was used. The planimeter readings gave the area of each outline in cm². These areas were plotted on mm graph paper. The abscissa represented the number of sections and the ordinate the areas. A line was drawn connecting the tops of the ordinates and the area was then measured by the planimeter. The data for each portion

measured (whole ovary corpus luteum, and interstitial gland masses) were substituted in the following formula which gave the approximate volume of each From these volumes the percentage volume of the interstitial tissue and luteal tissue in relation to the whole ovary and in relation to the volume of both ovaries together was computed. (For details of this method see Dornfeld et al. 42.)

$$\text{Volume} = \frac{PYX}{M^2} \times 100\ (\text{mm}^3/\text{cm}^3) \times \frac{T}{1000}$$

P = planimeter reading of plotted areas
Y = cm²/vertical cm of graph
X = number of sections/horizontal cm of graph
T = thickness of sections in micra
M = magnification factor

It is obvious that such measurements are accurate only in a relative sense and that much depends upon the judgment of the person tracing the outlines of the tissue masses. In order not to exaggerate the amount of gland tissue present, the outlines were drawn as nearly as possible just within the average boundaries of the interstitial and luteal tissue masses all nonglandular core areas of atretic follicles and corpora lutea were measured and deducted from their total areas and numerous atretic follicles having only scattered groups of interstitial gland cells around their periphery were not measured and therefore are also excluded from the totals. Hence, it is felt that the percentages given represent very conservative estimates of the active tissues actually present in these ovaries.

OBSERVATIONS

Table 2 and figure 1 present the quantitative data. The exact computed volumes are given because the error in measurement and computation is unknown. We did find that the volume of a fixed ovary as determined by the displacement method is reduced by about one-third when determined by the planimeter method after dehydration and sectioning However except for some variation in methods of fixation, each ovary was subjected to the same treatment and therefore to the same errors It is believed that differences in the percentage volumes given are certainly significant when they are as great as they are between early and late gestation specimens (table 2 and figs. 2 and 3) Probably they are not significant between the individuals having under 1% of interstitial gland tissue as the relative error must have been much greater where the amounts are so small.

Comparison of the absolute volumes and the percentages of interstitial gland tissue in relation to luteal tissue (table 2 and fig. 1) shows that the volume of interstitial gland often amounts to from one-third to one-half that of the luteal gland at its most functional state. Certainly this indicates that the interstitial gland is voluminous enough to have real functional significance

Although our sample of ovaries is small, the low amount of interstitial gland in early pregnancy the sharp rise in late pregnancy and the sudden drop just after delivery seems to represent a definite and consistent trend (fig 2) However the erratic fluctuations in the amount of luteal gland in these same individuals (table 2 and fig. 1; also commented upon by Forleo '61) warns of the danger of giving too much weight to quantitative differences in small samples. Yet when one looks to the qualitative changes in the luteal tissue there is no doubt that there is a consistent rapid rise in cytological differentiation in the first few weeks of gestation and then a consistent gradual decline from the functional to a degenerating condition in late gestation. Obviously qualitative changes in luteal tissue are better correlated with its known physiology than are its quantitative fluctuations. For this reason we have paid considerable attention to the cytological nature of the interstitial gland cells in the different reproductive phases

Contrary to what we have been led to expect from comparative studies human ovaries have a much greater percentage and greater absolute amount of interstitial gland tissue in late pregnancy than in the early months (figs. 1 and 2) and the cells differ cytologically from those of early gestation or of the non-pregnant woman (figs. 6 7 14 and 15) Since this tissue differentiates from the theca interna of degenerating follicles it should be most abundant during and just after the periods of greatest follicular atresia. To our knowl-

TABLE 2

Computed vol mes i mm nd percentage vol mes of luteal and interstitial gland tissue

Identification number		Whole ovary	Luteal gland tissue		Interstitial gland tissue		
		mm	mm	%	mm	% each ovary	% [illegible]
106	Right	1877	4	0.2	1.4	0 07	
	Left	2368	3	0.1	2.5	0.11	
	Total	4245	7		3.9		[illegible]
112	Right	1860	0	0	5.5	0 24	
	Left	1524	11	0.7	6 6	0 43	
	Total	3384	11		12.1		[illegible]
125	—	2089	116	5.5	10.2	0 49	
	—	2819	15	0.5	7.4	0 26	
	Total	4908	131		17.6		[illegible]
93	Right	801	0	0	2.0	0 24	
	Left	1129	356	31.5	3 0	0 27	
	Total	1930	356		5.0		[illegible]
51	Left	3727	210	5.4	17.0	0 45	
49	Right	1458	0	0	20 4	1.40	
	Left	3970	910	23.0	27.3	0 69	
	Total	5328	010		47 7		[illegible]
80	Right	2750	0	0	7.0	0.25	
	Left	3738	600	16.0	14.0	0.37	
	Total	6488	600		21.0		[illegible]
119	Right	2223	16	0 7	2 2	0 09	
	Left	3452	199	5.8	4 4	0.12	
	Total	5675	215		6.6		0.11
104	Right	1317	0	0	52	3 94	
96	Right	2257	0	0	134	5 95	
	Left	2810	548	19.5	109	3.86	
	Total	5067	548		243		4 8
131	Right	3937	519	13.2	163	4.14	
	Left	3330	0	0	232	6 97	
	Total	7267	519		395		[illegible]
142	Right	2977	130	4 4	118	3 96	
	Left	2382	0	0	183	7 68	
	Total	5359	130		301		[illegible]
118	Right	2506	0	0	1.3	0 05	
	Left	1943	0	0	1.6	0 08	
	Total	4449	0		2 9		[illegible]

edge in most mammalian species the maximum number of atretic follicles is present during late proestrus estrus and early postestrus, or early pregnancy if fertilization has occurred In most mammals this is the period of the greatest abundance and greatest cytological differentiation of interstitial gland tissue. There is certainly much of this tissue in human ovaries during early pregnancy but it is strikingly more abundant late in gestation, which indicates that an even greater wave of growth and atresia of follicles occurs during gestation probably early in the third trimester

In early pregnancy and in nonpregnancy the thickness of the zone of internal gland tissue around atretic follicles, although highly variable, appears to be somewhat greater than that of the theca interna of normal follicles of similar diameter (figs. 6 7 and 11) The gland cells are

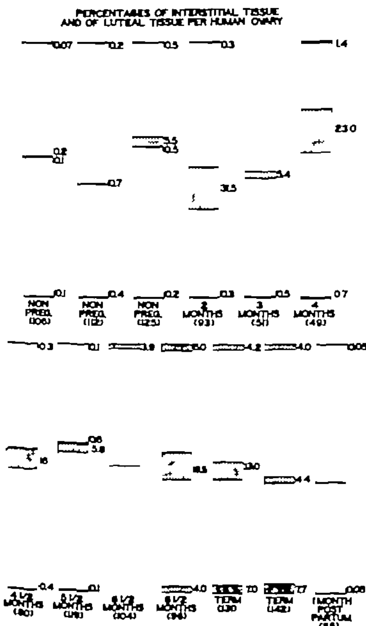


Fig. 1. With the exception of (51) and (104) each bar represents 100% of the total volume of pair of ovaries. The heavy black transverse line near the middle of each bar divides it into an upper portion representing the percentage volume of the right and lower portion representing the percentage volume of the left ovary. (Only the left ovary of 51 was available and only the right of 104.) The percentage of the volume of the right ovary occupied by interstitial gland tissue is represented by the diagonally hatched area at the upper end of each bar and for the left ovary by similar area at the lower end. Likewise the percentage of each ovary occupied by luteal tissue is represented by crosshatched area at the central end of the portion representing the ovary in which the corpus was located. In several cases the percentages were too small to be represented this way but in all cases the numerical percentages are given at the right of the corresponding areas.

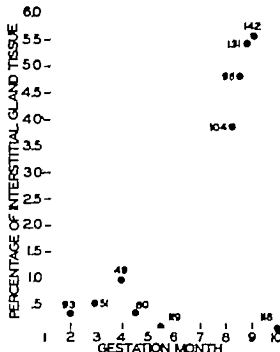


Fig. 2 The percentage of interstitial gland tissue in each pair of ovaries is plotted against the month of gestation, including the first post partum month. In the case of ovary 51 and 104 the percentage is based on only one ovary The trend is obviously toward a marked increase in interstitial gland volume late in gestation.

grouped in short cords arranged in radiate fashion around the remnants of the follicular cavity They are spheroidal and their cytoplasm appears relatively clear and unstained because of the presence of numerous coarse vacuoles the contents of which have disappeared during the technical procedures (figs. 6 8 and 14) The cords are separated by capillaries and by fine strands of collagen (not clearly shown in the figures) which are most conspicuous at or near the outer and inner margins of the zones of interstitial gland cells.

The gland cells of later pregnancy are most numerous and best developed just before or at parturition (figs. 2 13 and 15 to 19) They are also arranged in radiate cords around atretic follicles, but in general, form relatively thicker and more compact zones than in early pregnancy In comparison with the interstitial gland cells observed in early gestation and nonpregnancy these cells are more often elongated or polyhedral but perhaps most noticeable is their distinctly granular and relatively nonvacuolar cytoplasm (cf figs 14 and 15) A month after parturition the outlines of atretic follicles could still be determined but the components of these areas were no different than the surrounding stromal cells of the cortex. Apparently human interstitial gland cells revert to embryonic, inactive, fibroblast-like types as they seem to do in other mammals.

In the larger atretic follicles it was difficult to distinguish between the degenerating theca and the interstitial gland tissue. In general degenerating thecal cells have less vacuolar cytoplasm, are not arranged in radiate cords and are separated by negligible amounts of collagen. The granulosa may still be partially intact in these larger follicles. Interstitial gland tissue cells are smaller have more lightly stained cytoplasm are usually arranged in cords with collagen alternating with the cells. Many of the largest atretic follicles show little or no interstitial gland tissue (fig 18)

There is no doubt that interstitial gland tissue develops around atretic follicles in infancy and childhood. Besides those of two and one-half and seven years illustrated in figures 3 4 and 5, we have also seen it in small amounts in ovaries of an infant of 13 months and a child of three years. More ovaries of infants and prepubertal children should be studied to demonstrate more clearly whether it occurs in definite cycles and in what amounts. We have also seen it in menopausal ovaries although in such small amounts that attempts at quantitative measurements would seem unfruitful at present

Two other cell types that are related to or associated with interstitial gland cells were also observed; lutealized granulosa of atretic follicles and paraluteal cells.

Within several follicles surrounded by interstitial gland tissue parts of the granulosa had become lutealized (figs 9 and 19) The remainder of the granulosa had usually sloughed and in many cases the lumen of the follicles had been obliterated. These masses of lutealized granulosa cells, usually known as the accessory corpora lutea, were found only in two pairs of ovaries — one at three months, and one at five and one-half months of gestation

When accessory corpora lutea were distinct and sufficiently large they were measured, and the quantity was added to the total luteal volume computed for the respective ovary. The cells of accessory corpora lutea were always similar to those of the main corpus luteum of the same pair of ovaries, and were distinctly larger than and cytologically distinct from the interstitial gland cells enclosing them (figs. 9 and 19). These things are generally true of accessory corpora lutea of other mammals.

Paraluteal cells were observed in the infoldings and adjacent borders of the corpora lutea of most ovaries, even in one ovary at parturition. These cells resemble the interstitial gland cells in size and appearance (fig. 10). The outer cells of paraluteal masses often grade smoothly into the surrounding undifferentiated stroma cells. Likewise their innermost cells commonly include transitional types intergrading with true luteal cells.

DISCUSSION

We have demonstrated by a reliable quantitative method that there is a pronounced rhythmic variation in the amount of interstitial gland tissue in the human ovary during the pregnancy cycle and that this tissue exists in sufficient amounts to be of functional significance as an endocrine gland. We have also demonstrated that this tissue is organized histologically like an endocrine gland, that the cells of homologous structures in other species resemble steroid secreting endocrine gland cells and that in man as in other mammals they undergo a rhythm in cytological features which is correlated with the pregnancy cycle.

However unless we succeed in making it clear that this tissue is not the same as thecal gland or luteal gland tissue little will have been accomplished by this investigation. Confusion as to the identity of these three tissues has existed so long, especially among pathologists and endocrinologists and has been so widely disseminated, that it will be difficult to break down the general acceptance of these traditionally established misconceptions. Nevertheless, it seems advisable to again restate a simple and correct classification of ovarian glandular tissues as applied to mammals.

The theca interna is usually present around secondary follicles and growing vesicular follicles. It is composed of "embryonic rapidly multiplying, fibroblast like cells derived from the surrounding stroma, and it contains a rich capillary plexus. During the final preovulatory growth period of the follicle these cells enlarge greatly and differentiate into steroid secretors. Their ratio of nucleus to cytoplasm is low in contrast to their earlier condition and their cytoplasm is noticeably granular in ordinary histological preparations. The capillaries are now conspicuous and often congested. The theca interna is at this time a functional *thecal gland*, an important secretor of estrogens during the proestrous and estrous periods (Corner '38 and Harrison '62). When the follicle ovulates these thecal gland cells may persist temporarily around the developing corpus, but they undergo rapid degeneration and completely disappear within a few days in all species where this has been studied carefully. If a ripening follicle with an already differentiated thecal gland undergoes atresia instead of ovulation then the differentiated thecal gland cells degenerate completely.

If a follicle undergoes atresia after its theca interna has developed, but before the final ripening and formation of functional thecal gland (and probably more than 99% of mammalian follicles do this) then the still embryonic theca interna differentiates into an *interstitial gland*. The nature of these gland masses varies widely in different mammalian groups but in general the cells become rounded or polyhedral but not as large as the thecal gland cells of ripe follicles nor do they have as much cytoplasm in relation to the nucleus. They tend to be arranged in rows or groups of cells radiating outward from the margin of the disappearing cavity of the follicle. Between these rows lie capillaries which, however are seldom conspicuously dilated. The cytoplasm of these gland cells usually appears relatively clear in ordinary preparations, because it contains large rounded vacuoles rather than granules. If stained with osmium or other stains reacting with steroids these vacuoles are seen to be filled

with steroid material (Stafford, Collins and Mossman 42; Stafford and Mossman 45; Mossman and Judas 49 Dawson and McCabe '51; Harrison '62)

As pointed out previously since atresia of follicles in most mammals so far studied occurs from infancy to old age the type of interstitial gland derived from the theca interna of degenerating follicles is the first major adult type of ovarian gland to appear *It occurs periodically often constantly* throughout life even beyond the active reproductive period because some follicles grow and undergo atresia beyond the period when any are able to mature and achieve ovulation. We have found this to be true of the human female but we have not included menopausal ovaries in this investigation.

Lest there be any misunderstanding of the nature of the interstitial gland tissue with which this investigation is concerned, it should be pointed out that we are not dealing with the form found in the female embryo and early fetus nor are we including a number of known adult types not derived from the theca interna of degenerating follicles. Since these other adult types are either inconspicuous or absent from the human ovary it seems appropriate to disregard them here.

The *luteal gland* (pregnancy gland or corpus luteum) is the best known of the ovarian glands both as to morphology and function. Luteal cells usually begin to differentiate from the follicular epithelium of a ripe follicle just before ovulation and develop very rapidly for the first few days after ovulation. They undergo most of *their hyperplasia before ovulation but in* many species mitoses still occur among the young luteal cells for several days after ovulation especially if the individual is pregnant. In many species apparently most commonly among larger forms, an early accretion of luteal cells occurs around the periphery of the corpus by differentiation of surrounding pluripotential" stroma cells. In any case there is a rich invasion into the luteal mass by capillaries from the former thecal gland plexus. The luteal cells usually become much larger than those of either the thecal or interstitial glands and are often not very osmiophilic during their early functional stages although steroid substances can be demonstrated in them by more specific tests.

Several types of luteal gland cells have been described by various workers and various origins have been ascribed to them (Corner 19; Harrison, '62) However, it is not clear in most cases whether these are actually different stages in differentiation of a single cell type or whether they do actually represent distinct cell species. *The senior author has observed two clearly* distinct glandular cell types only in corpora lutea of Artiodactyla (cloven hoofed mammals) and Cetacea (whales). In all other forms including man, his observations suggest simply different degrees of differentiation This is especially obvious in those species where accretion of stroma cells is prominent. Man is one of these. We believe the paraluteal cells of the human ovary are simply transition stages in the differentiation of stroma cells into luteal cells. This is not to say that they might not have a function different in degree or quality from that of mature luteal cells

Finally one must admit that paraluteal cells do pose a problem of interpretation, especially in man. We believe they differentiate from stromal cells *after* the thecal gland has degenerated not directly from thecal gland cells as so many authors have implied. We base this chiefly on comparative studies by the senior author (Stafford, Collins and Mossman, 42, Stafford and Mossman 45 Mossman and Judas, '49), and on the *following reports*.

Corner (45) says of the rhesus ovary. "The theca interna cells retain their iden*tity after ovulation*. They are not distinguishable during the period of days 4 to 6, but afterwards can sometimes be distinguished. In the corpus luteum of pregnancy and the corpus aberrans, the theca interna cells or paralutein cells are readily distinguishable in the bases of the folds and at the periphery of the corpus. Corner Jr ('56) on the human ovary states that "the theca interna and granulosa became indistinguishable on day 1, but that on day 6 theca interna and granulosa are again distinguishable. In the light of the overwhelming comparative evidence and these statements and illustrations of the Corners there seems to be little

that in the rhesus monkey and man thecal gland cells are distinct entities degenerate immediately after ovulation, and that paraluteal cells then differ from the adjacent stroma. Whether these latter are merely developmental steps in the differentiation of luteal cells of identical nature to those of granulosa origin, or are themselves a second distinct species of luteal gland cell is not clear. Sallman and Stein (41) found the interstitial gland cell to be indistinguishable from the paraluteal cell. We agree that this is true in many cases, but to go into this matter adequately would take us too far afield. At present we think the evidence favors the interpretation that paraluteal cells are developmental stages in the differentiation of true luteal cells, that at one stage in this process they resemble interstitial gland cells, may indeed be identical with them and in some cases may fail to differentiate any further.

If there are three distinct glands characteristically present in all mammalian ovaries, as seems to have been amply demonstrated in the literature then the time has come to designate each by its specific name and to stop the loose use of the terms "thecal tissue" and "luteinization". The names which we believe best suited in view of past usage and nature of each are *thecal gland*, *interstitial gland* and *luteal gland*.

Admittedly "interstitial gland" is not an ideal term and may need considerable qualification to distinguish between interstitial tissue of thecal origin in contrast to that derived from ovarian or mesovarial stroma, medullary cord epithelium, or rete epithelium, as happens in various mammal groups. It has good historical precedent, however as Limon ('01) and Bouin ('02) used it correctly over 60 years ago.

Perhaps the most irresponsible misuse of terms and the one most often repeated, is that of "luteinization" to refer to any enlargement or hypertrophy of cells associated with the ovary regardless of whether or not there is the slightest evidence of the relation of the hypertrophied cells to the luteal gland. In fact the term has been used frequently where there is direct evidence that the tissue designated has no relation whatever to luteal tissue.

We would emphasize, as a postscript to this, that undifferentiated ovarian tissue both epithelial and stromal, is rather highly pluripotential, even in the adult. It differentiates into a variety of definitive tissues as a complicated response to both genetic factors and to environmental inducing and organizing influences mechanical and chemical. In such a complicated system a great variety of aberrations from the normal or usual are apt to occur. This is evident in the complexity of pathological tumors which often do not clearly simulate any normal tissue although they may produce a preponderance of a certain endocrine action. It is also evident in the intermediate types of cells one often sees in such structures as accessory corpora lutea. This form of atretic follicle usually contains normal interstitial gland cells, some more centrally located true luteal gland cells and many intermediate cell types that cannot be categorized as either (fig. 9).

With this orientation as a background, the specific problem of the changes in ovarian interstitial gland tissue in relation to the reproductive cycle in man and other mammals can be discussed. Although to our knowledge no real attempt to measure the volume of interstitial gland tissue has been made previously it has been recognized for years that interstitial gland tissue does increase during gestation in many mammals (bat — Athias '20; water shrew — Price '53 certain monkeys and man — Cohn, '03 Seitz, '06 Wallart, '08 Watrin, '24; Dubreuil, 48 Nelson and Green, '58 Forleo '61).

If the ovarian interstitial gland of man is a hormone producer then it is reasonable to believe that it must function either in storage or secretion whenever it is present in a differentiated condition, which we have seen is from infancy to the menopause. Since the tissue appears to fluctuate greatly in amount and in degree of cytological differentiation, one must assume that its function is also periodic or rhythmic, reaching its maximum in late gestation when the tissue is most voluminous. Again we must caution that there is as yet no completely convincing *physiological* evidence as to what this function is or in fact that female interstitial gland tissue has a specific function.

Reproductive Organs. New York Oxford University Press.

Pflüger E. F W 1863 Die Eierstöcke der Säugethiere und des Menschen. Leipzig.

Potter E. L. 1953 Pathology of the Foetus and Newborn. Year Book Publishers, Chicago.

Price M. 1953 The reproductive cycle of the water shrew Proc. Zool. Soc. Lond., 123 599–621

Rennels E. G. 1951 Influence of hormones on the histochemistry of ovarian interstitial tissue in the immature rat. Am. J Anat., 88 63–108

Schroeder R. 1930 Die weiblichen Genitalorgane Handbuch d. mikr Anat. d. Menschen., 7 329–569 Springer Berlin.

Schrœn, O. 1863 Beitrag zur Kenntnis der Anatomie und Physiologie des Eierstocks der Säugethiere. Zeitschr f wiss. Zool., 12: 409–426.

Seitz, L. 1906 Die Follikelatresie während der Schwangerschaft, insbesondere die Hypertrophie und Hyperplasie der Theca interna Zellen (Theca-luteinzellen) und ihre Beziehungen zur Corpus luteum-Bildung. Arch. Gynaek., 77 203

Stafford W T., and H. W Mossman 1945 Ovarian interstitial tissue and its relation to the pregnancy cycle in the guinea pig. Anat. Rec., 93 97–107

Stafford, W T., R. F Collins and H W Mossman 1942 The thecal gland in the guinea pig ovary Anat. Rec., 83 193–207

Wallart J 1908 Untersuchungen über das Corpus luteum und die interstitielle Eierstocksdrüse während der Schwangerschaft. Z. Geburtsh. Gynäk., 63 520–536.

Watrin M. 1924 Étude histochimique et biologique du corps jaune de la femme. Arch. Int. Méd. Exp., 1: 97

Watzka, M. 1957 Weibliche Genitalorgane Das Ovarium. Handbuch d. mikr. Anat. d. Menschen., 7 1–178, Springer Berlin.

PLATE 1

EXPLANATION OF FIGURES

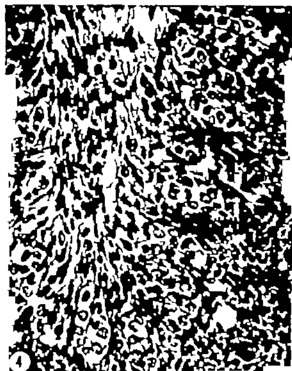
3 Ovary of two and one-half year old child showing large atretic follicle surrounded by interstitial gland tissue. 143 L. × 12.6.

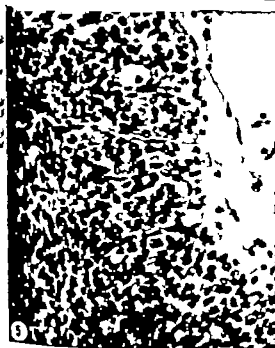
4 Wall of the atretic follicle shown in figure 3. Note the short rows of typical interstitial gland cells. 143, L. × 345.

5 Wall of an atretic follicle of a seven year old child showing short rows of relatively undifferentiated interstitial gland cells. 121 L. × 310.

6 Wall of an atretic follicle of a woman of 18 years showing the relatively undifferentiated interstitial gland cells typical of nonpregnancy 112, L. × 210.


3


4


5


6

PLATE 2

EXPLANATION OF FIGURES

All figures are from the left ovary of no. 51 a woman t three and one-half months of gestation

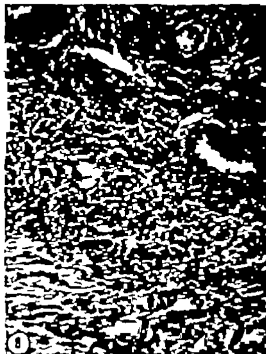
7 Wall of tretic follicle showing interstitial gl nd cells at various degrees of differentiation together with numerous endothelial and fibroblast nuclei. × 260

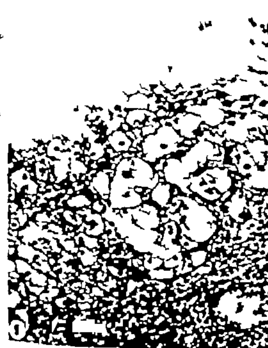
8 More mature interstitial gland tissue of a follicle in late atresia. × 220.

9 Luteal gland tissue (actually a small accessory corpus luteum) occurring in the central portion of an interstitial gland mass formed from an tretic follicle Note that most of these l teal cell are intermediate in morphology between interstitial gland cells and fully differentiated luteal cells shown in figure 10. × 220

10 Outer edge of the primary corpus luteum howing luteal cells at top paraluteal cell centrally and stromal connective tissue at the bottom. Note the close similarity of m ny paraluteal cells to interstitial gland cells. Note also th t toward the top they resemble luteal cells and that toward the bottom they are small and lie among the stromal fibers Examination f sections of this and similar paraluteal masses indicates that they in fact differentiate from tromal cells and that they must often continue their differenti tion ntil they become true luteal cells. × 330.


7


8


9

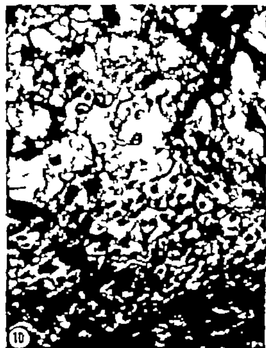

10

PLATE 3

EXPLANATION OF FIGURES

11 A medium sized (3 mm) vesicular follicle showing the relative thickness of the granulosa (g) and the thin vascular theca interna (n) the cells of which are in early stages of differentiation into thecal gland cells. Note the gradual transition from the thecal cells to those of the stroma of the theca externa an indication of their derivation from the stroma. 119 L. × 220

12 Interstitial gland cells differentiating in the theca interna of an atretic follicle at five and one-half months of gestation. The arrangement in radiate cords is clear as is the small size of the cells and their high ratio of nucleus to cytoplasm. 119 L. × 420.

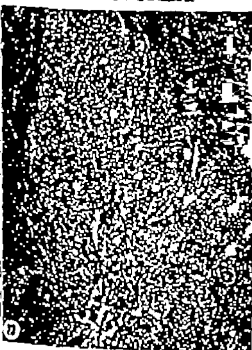
13 Characteristically well developed interstitial gland mass at eight and one-half months of gestation. Obviously such masses must include cells differentiated from stroma far beyond the limits of the theca interna at the time follicular atresia began since mitosis of interstitial gland cells is rarely if ever seen. 104 B. × 85.

14 Detail of mature interstitial gland tissue at eight and one-half months of gestation. Note the nuclei of capillary endothelium crowded between the rows of gland cells. These latter show the characteristic granular cytoplasm and nuclei of average chromaticity of the interstitial cells of late pregnancy and should be compared with figure 15 which is of mature interstitial cells at three and one-half months of gestation. 104 B. × 420.

15 Detail of typical mature interstitial gland tissue of early gestation (3½ mos.) showing the characteristic vesicular cytoplasm and highly chromatic nuclei. Note that the cells are also smaller than those of late pregnancy shown in figure 14. The more irregular arrangement of the cords of cells is not a constant difference (Cf. figs. 7 and 8 of the same ovary in which the cells are more regularly aligned). 51 L. × 420.


11


12


13


14


15

The Structure of the Functional Pronephros in Larvae of *Ambystoma opacum* as Studied by Light and Electron Microscopy [1]

A. KENT CHRISTENSEN [2]
Department of Anatomy Harvard Medical School, Boston, Massachusetts

ABSTRACT The functional pronephros in early larvae of *Ambystoma opacum*, studied in serial sections, consists of an anterior and posterior nephrostome, respective proximal tubules which fuse into a common proximal tubule a ciliated intermediate segment, and distal tubule, which leaves the pronephros posteriorly as the nephric duct. In the coelom medial to each pronephros is glomus, arising from the dorsal aorta.

In electron micrographs of osmium-fixed, methacrylate-embedded pronephros and glomus, the fine structure generally resembles that seen in adult kidneys. Proximal tubule cells show brush border of irregular microvilli, tubular invaginations, resorption granules, and very few basal infoldings. Cells of the distal tubule have numerous radially-oriented mitochondria, and the basal infoldings are generally well developed. The fine structure of the nephric duct seems to resemble that of the distal tubule. Cells of the nephrostomes and intermediate segment bear cilia of usual fine structure, and contain melanin granules, lipid droplets and slender mitochondria. The glomus resembles glomerulus in having an endothelium with sparse pores, basement membrane, and epithelial cells with numerous interdigitating foot processes.

The similarity at the fine structure level between the pronephros and the more posterior mesonephros and metanephros of adult vertebrates suggests the serial homology of vertebrate nephrons, and thus constitutes further evidence for the archinephros or holonephros theory of the origin of vertebrate kidneys.

The nature and significance of the pronephros has been debated for nearly a century Many of the earlier workers held that it constituted the remnant of a primitive kidney distinct from the adult kidneys of modern vertebrates. This view has suffered considerably in the light of subsequent embryological and comparative studies. The more modern view well summarized by Fraser ('50) denies the primitive nature of the pronephros, and emphasizes the essential unity of the nephrogenic material, maintaining that the pronephric tubules are basically the same both structurally and functionally as those which develop more posteriorly and give rise to the mesonephros [3] and metanephros.

With the advent of the electron microscope it is now possible to gain further evidence on this question by examining the pronephros and its associated glomus to see if they possess the elaborate specializations of fine structure seen in adult kidneys (Pease '55; Rhodin, '58 '63). The present investigation describes the fine structure of the pronephros and glomus in early larvae of the marbled salamander *Ambystoma opacum*. In such larvae the pronephros is particularly well developed and is known to be serving as a functional kidney (Howland '21)

MATERIALS AND METHODS

Eggs of *Ambystoma opacum* (Gravenhorst) were obtained from a professional collector Mr J C. Nicholls, who collected them in Cherokee County North Carolina. After hatching in mid-October (see Noble and Brady '33) the larvae were kept in a constant temperature room (about 18 C) and were fed *Enchaetreus* worms. Some of the larvae were killed a day or so after hatching when they were 19 mm long

[1] This material has been published in abstract ('61, Anat. Rec., 139: 215), and has been cited as personal communication (Fox, '63, p. 5). Part of the writing of this paper was done during the tenure of Public Health Service grant number AM-05428 from the National Institute of Arthritis and Metabolic Diseases.

[2] Present address: Department of Anatomy, Stanford School of Medicine, Stanford, California.

[3] Many authors prefer the term "opisthonephros" (Kerr, '19, p. 221) in referring to the kidney of adult anamniotes, since this organ arises from that portion of the nephrogenic plate which furnishes both the mesonephros and metanephros of amniotes. However the term "mesonephros" seems to be more widely used, especially among embryologists, and is utilized in this paper. This usage is defended by Fraser ('50, pp. 168–170).

and had just begun to feed. Others were killed a week later when they were 20–21 mm long.

For observations with the light microscope whole larvae were fixed overnight in 10% acrolein in distilled water at refrigerator temperature. The tissues were dehydrated in increasing concentrations of a 1:1 mixture of methyl alcohol methyl cellosolve in distilled water, followed by a 1:1 mixture of methyl cellosolve-chloroform and were infiltrated and embedded in polyester wax. This method (Sidman, Mottla and Feder, '61; Feder, personal communication) provides excellent preservation of cytological detail. Ten micron serial sections were cut through both pronephroi in each of three larvae, and were stained with the Mallory triple staining technique. Two pronephroi were reconstructed, one from a 19 mm and the other from a 20 mm larva. The latter served as a basis for figure 2. To reconstruct a pronephros serial sections were projected and traced on paper and the course of the various tubules was mapped out on the tracings by means of a system of colors and numbers. These data were then used as a guide in constructing a clay model. Because of the complexity of the organ, the usual wax reconstruction technique was not employed, since the inner convolutions of the tubules would have been difficult to follow in such a model.

For electron microscopy the cervical region of the larva was excised and fixed one and a half hours in cold 1.3% osmium tetroxide buffered with s-collidine (Bennett and Luft, '59) and containing 5% sucrose. The tissues were dehydrated over a period of about an hour in increasing concentrations of 1:1 methyl alcohol methyl cellosolve in distilled water, and were then left about three hours in three changes of alcohol-cellosolve. They were then infiltrated and embedded in prepolymerized 1:4 methyl and *n*-butyl methacrylates catalyzed with 1.5% Luperco CDB. Final polymerization was effected by ultraviolet light. Sections cut on a Porter Blum MT 1 microtome were picked up on celloidin-covered, carbon-coated grids, stained with lead hydroxide (Watson, '58) and sandwiched with a thin carbon coat. The sections were viewed in an RCA EMU 3 electron microscope.

OBSERVATIONS

The pronephros and glomus of *Ambystoma opacum* larvae are similar in overall structure to those described in larvae of other urodeles (Field, 1891; Rabl, '04; Howland, '21; McCurdy, '31). The pronephros shows a similar pattern of organization (fig. 1) to a single primary mesonephric nephron of the adult urodele kidney, and is believed to function in a similar way. In the case of the pronephros blood filtrate passes into the coelom through the walls of the glomus, and is subsequently drawn into the two nephrostomes by the action of cilia which line the nephrostomal epithelium. The filtrate then passes along the two proximal tubules into the common proximal tubule and hence through the ciliated intermediate segment into the distal tubule. Absorptive and excretory processes may take place in the proximal and distal tubules. The distal tubule becomes the nephric duct posteriorly. For a discussion of pronephric function and other aspects of the pronephros in amphibian larvae, see Fox ('63).

The actual location and configuration of the pronephros of a 20 mm larva of *A. opacum* is shown in figure 2. The pronephros (*pr*) lies in the dorsolateral body wall of the neck region (fig. 2A and fig. 1) and is bounded dorsally by the cervical musculature, laterally by the scapula, and medially by the peritoneum and the coelom. Lying within the coelom medial to the pronephros on each side is a glomus (*g*), a vascular tuft which arises from the dorsal aorta (*a*). In a more detailed view (fig. 2B) the pronephros, as reconstructed from serial sections, is seen to consist of a mass of convoluted tubules. The organ is approximately ¾ mm long, ¼ mm high and ⅓ mm wide. Anteriorly and posteriorly the two nephrostomes (*n*) open from the coelom as two short ciliated ducts, each about 30 μ in outside diameter. These connect with the proximal tubules (*p*) and the proximal tubule leads into the distal tubule (*d*) via a ciliated intermediate segment (*is*).

In figure 2C the tubules are spread apart to allow the configuration of the

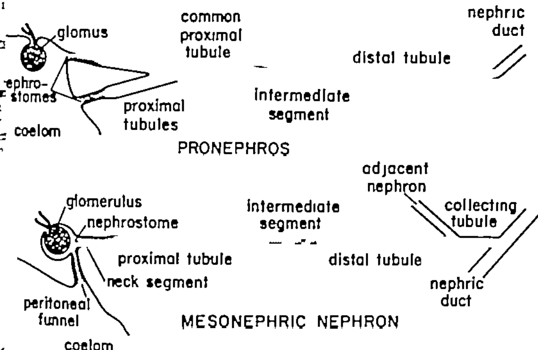


Fig. 1 In these two diagrams the basic organization of the whole pronephros and associated glomus on one side of salamander larva is compared with that of single primary mesonephric nephron in adult salamander (the latter diagram adapted from Chase, '23) The correspondence between the various structures in the two cases is suggested by observations with the light microscope and is further borne out by electron microscopy

roximal and distal tubules to be visualized more clearly The proximal tubule (p) is somewhat irregular or saccular in contour and the outside diameter is generally about 80 µ. The distal tubule (d) is more even in outline and is smaller in diameter usually between 50 and 60 µ. After it arises from the intermediate segment (is) the distal tubule passes to the posterior pole of the pronephros then back to the region of the intermediate segment, and finally posteriorly again eventually to become the nephric duct (nd) The space between the various tubules is occupied for the most part by sinusoids (fig. 4) which arise from the posterior cardinal vein and form an extensive vascular network throughout the pronephros.

The general pattern of organization of the pronephros in the 19 mm larva was the same as that of the 20 mm larva described above but there were some differences in the details of coiling of tubules, which may merely reflect individual variation In particular the course of the distal tubule was somewhat more complicated.

The nephrostome The ciliated epithelium of the nephrostome (fig. 4) varies in height from about 10 µ near the junction with the proximal tubule (np) to about 14 µ near the mouth of the nephrostome (n) where it is continuous with the squamous epithelium lining the coelom Near the mouth of the nephrostome the epithelial cells are closely packed together and their oval nuclei, which nearly fill the cells, are often oriented perpendicular to the epithelial surface. A tuft of cilia arises from the central region of the luminal surface of each cell. The cytoplasm contains numerous melanin granules and a considerable number of filamentous mitochondria, which are randomly oriented in the cytoplasm and tend to be obscured by the melanin granules.

Under the electron microscope the various organelles of the epithelial cells can be seen in greater detail (fig 5) The

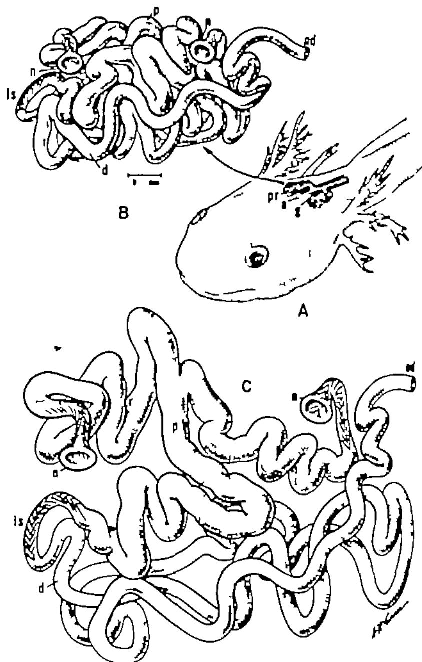


Fig. 2 The pronephros of 20 mm larva of *Ambystoma opacum*, as reconstructed from serial sections. *A* The pronephros (*pr*) on each side lies in the dorsolateral body wall of the neck region. Extending from the dorsal aorta ( ) into the coelom medial to each pronephros is a glomus (*g*) *B* A closer view of the right pronephros shows the two nephrostomes (*n*) and convolutions of the proximal (*p*) and distal (*d*) tubules, as well as the intermediate segment (*is*) and nephric duct (*nd*) C In this drawing the various portions of the pronephric tubule are spread part so their course can be followed more clearly The anterior and posterior nephrostomes (*n*) open into the corresponding proximal tubules, which unite as the common proximal tubule (*p*) The latter connects, by way of the intermediate segment (*is*) with the distal tubule (*d*) which is continuous posteriorly with the nephric duct (*nd*)

mitochondria (*m*) are of small diameter, averaging about 0.25 μ, and contain cristae in moderate abundance. The Golgi complex (*gc*) and agranular endoplasmic reticulum (*er*) are fairly well developed. The nucleus is not unusual, except that it occasionally contains granular inclusions (*inc*) of unknown nature. Lipid droplets (*lp*) occur but are less prominent than the melanin granules (*mg*) The cilia in the central tuft, like those in other amphibians (Fawcett and Porter '54 Bargmann, Knoop and Schiebler '55) have a basal plate (*bp*) Striated rootlets (*sr*) with a 750 Å periodicity extend down from the basal bodies (*bb*) In some micrographs, a feltwork of very fine fibrils is visible underlying the luminal surface of the cell at the level of the basal bodies (Fawcett and Porter '54)

The proximal tubule In cross sections of proximal tubules seen with the light microscope (fig. 4 *p*) the epithelial cells bulge somewhat into the lumen, their height ranging from about 5 μ at the junctions of cells up to 15 μ at the level of the nucleus. The epithelium is generally lower in the common proximal tubule When the cells are seen in surface view (*ps*) the nuclei are oval or round, but where tubules are cut in the usual cross section the nuclei appear more flattened. The individual cells show the same general features as are seen in the proximal tubules of adult kidneys, namely a brush border numerous resorption granules, and a moderate number of mitochondria located mostly in the basal portion of the cells. The brush border is variable in height, averaging about 3 μ. Granules occur most commonly in the apical cytoplasm, and often vary considerably in abundance from one cell to another The cells also contain occasional melanin granules, sometimes in small clusters. Mitochondria are more abundant in the cells of the anterior and posterior proximal tubules than in the common proximal tubule. In their mitochondrial content and general shape the cells of the common proximal tubule therefore resemble those of the straight portion of the proximal tubule in the mammalian metanephros (Rhodin, '58, '63)

As seen in the electron microscope (figs 6–8) the brush border (*br*) consists in general of irregular and interconnected evaginations of the cell surface. Uniform, cylindrical microvilli like those composing the brush border in adult kidneys are rarely seen. Components of the endoplasmic reticulum are common within the irregular microvilli (figs. 7 and 8 *er*) which may be an indication that the irregularities are normal, and not merely artifacts of preservation.

Tubular invaginations, about 600 Å in diameter originate from the plasma membrane at the base of the brush border and pursue an irregular course into the apical cytoplasm (*ti*, figs. 6 and 7) These tubular invaginations appear more electron dense than nearby elements of the agranular endoplasmic reticulum (*er*) This greater density may not be due entirely to contained material, for in cases where the invaginations are cut in cross section the limiting membrane shows considerable density and when the limiting membrane is seen in surface view (fig. 9) there appears to be an irregular pattern of oblong profiles along the membrane The significance of this fine structure is unknown.

The characteristic granules observed with the light microscope appear in electron micrographs as vacuoles which are filled to one degree or another with a flocculent precipitate (figs. 6 and 7 *gr* *v*) The granules vary in size but are commonly about 1 μ in diameter Miller has presented evidence in the proximal tubule of the mouse kidney that vacuoles give rise to granules by the accumulation of protein absorbed from the lumen of the proximal tubule by way of the tubular invaginations ('60) and that the granules may be considered to be lysosomes, since they contain acid phosphatase ('62) Gérard and Cordier ('34) showed in the pronephros of larval anurans that the proximal tubule cells are capable of actively taking up a wide variety of materials from the lumen of the tubule

Occasional proximal tubule cells contain small, dense, membrane-bound inclusions (fig 10) about 0.2 μ in diameter which are found throughout the cytoplasm but are more numerous in the basal half of

the cell The chemical nature of these structures is unknown but they bear a close morphological resemblance to inclusions interpreted as emulsified fat droplets by Palay and Karlin ('59) in their study of fat absorption in mouse intestinal epithelial cells.

The intermediate segment As seen with the light microscope the ciliated intermediate segment (fig 4 *is*) is essentially similar in structure to the deeper portions of the nephrostomes In electron microscope sections it was impossible to distinguish between these two segments since identification would have required extensive serial sections a procedure which in electron microscopy is so difficult that the probable rewards did not seem to justify the work involved

The distal tubule The epithelial cells of the distal tubule are generally flatter than those of the proximal tubule the cell height varying from about 6 μ to as little as 2 μ, and at the level of the nucleus up to 9 μ The cells lack the characteristic granules seen in the proximal tubule but like the proximal tubule cells may contain occasional single or clustered melanin granules. Under the light microscope the distal tubule cells show no brush border or at most a faint suggestion of one; the electron microscope reveals sparse stubby microvilli on the luminal surface of some the cells

In both light and electron micrographs, the most prominent feature of distal tubule cells is the general abundance of mitochondria usually oriented radially with regard to the tubule (fig. 12) Cases were observed where the mitochondria were more numerous than those shown in figure 12 while in other cases cells showed fewer mitochondria (fig 11) Also prominent in electron micrographs of these cells are numerous infoldings of the plasma membrane at the base of the cell (fig 12) These basal infoldings partially compartmentalize the cytoplasm and enclose the radially-oriented mitochondria. In the deeper portions of the infoldings, the two opposing membranes sometimes seem to give way to what might appear in section to be a series of vesicles arranged in linear order (*fen* fig 12) However it is more likely that these are merely places where the basal infoldings contain irregular fenestrations, and therefore in section appear discontinuous (Tormey '63)

The nephric duct. There is little change in the structure of the distal tubule, as seen by either light or electron microscope as it leaves the confines of the pronephros and continues posteriorly as the nephric duct. Observations were made with the electron microscope only on the most proximal portion of the nephric duct. However in light microscope serial sections the epithelial cells generally resemble distal tubule cells throughout the length of the duct, for example in their abundant radially-oriented mitochondria. There were some minor differences the epithelium was slightly higher (usually about 9 μ, and about 11 μ at the level of the nuclei), the nuclei were somewhat more closely-spaced, and the melanin granules seemed more numerous. In 19 mm larvae the anterior mesonephric tubules are already connected to the nephric duct and are showing signs of cellular differentiation.

The glomus. The glomus consists of a mass of interconnected capillary loops arising from the dorsal aorta and extending into the coelom on each side adjacent to the posterior half of each pronephros The capillary endothelium is covered throughout by an epithelial layer which is a reflection of the parietal peritoneum and is homologous with the visceral layer of Bowman's capsule in renal corpuscles of the adult kidney

In a low power electron micrograph (fig 13) the glomus is seen to have basically the same organization as that found in the glomeruli of the adult amphibian mesonephros (Pak Poy '57) At higher magnification (fig. 14) the structure of the endothelium (*end*) the epithelium (made up mostly of foot processes, *fp*) and the basement membrane (*bm*) can be seen to better advantage. The endothelium is irregular in thickness, and in its thinner areas is penetrated by scattered pores which seem to be less numerous than those described in amphibian mesonephric glomeruli (Pak Poy '57) The epithelial cells send out cytoplasmic processes (*cp*) which ramify over the surface of the basement membrane into foot processes (*fp*), and these interdigitate with the foot processes

cesses of adjacent epithelial cells. The foot processes are generally coarse and [1] but frequently become fine and closely apposed. The cell bodies of the epithelial cells sometimes lie directly the basement membrane but for the most part the epithelial layer on the capillary is made up of the foot processes.

basement membrane seems to be quite swollen in the present material probably a preservation artifact. In areas where it appears to be most nearly intact, the basement membrane is commonly about 3,500 A thick, although there is considerable variation. A thin outer layer of the basement membrane, about 600 A thick and lying next to the foot processes, seems to be less subject to preservation damage. Processes of cells are frequently observed in the basement membrane between the endothelium and epithelium (fig. 14 pc) In some cases these may derive from endothelial cells, although similar processes were reported by Pak Poy ('57) in glomeruli of adult frogs and toads, and were interpreted by this author as deriving from so-called "pericapillary cells.

DISCUSSION

The fundamental studies of Howland ('21) and of other workers (see Fox, '63) have shown that the pronephros of larval urodeles plays an important role in water balance and excretion until it is superseded later in larval development by the mesonephros The findings reported in the present investigation demonstrate that this functional pronephros and its associated glomus exhibit the same general pattern of cellular fine structure as has been described in the mesonephros and metanephros of adult vertebrates.

The fine structure of the *proximal and* distal tubules has been described in mammals (Rhodin, '58 '63 and others) reptiles (Anderson '60) amphibians (Bargmann, Knoop and Schiebler '55 Fawcett, '58 Karnovsky '63; Christensen '63) and bony fish (Gritzka, '63) In the pronephros described here the brush border of the proximal tubule is similar to that of other vertebrate kidneys in being composed of numerous microvilli, although the pronephric microvilli are generally more irregular in form than the cylindrical microvilli seen in most other kidneys, including those of adult frogs (Fawcett, '58 Karnovsky '63) However similar irregular microvilli have been described as characteristic of the proximal tubule in the fish *Fundulus heteroclitus* (Gritzka, '63) Although these irregular microvilli could be preservation artifacts (Maunsbach, Madden and Latta, '62) the presence of numerous and prominent elements of the endoplasmic reticulum in the microvilli (figs. 7 and 8) may suggest that the form is normal. The tubular invaginations and apical granules of the proximal tubule in the pronephros correspond in morphology to those described in other kidneys although attention has not previously been called to the patterns visible in surface views of the walls of the tubular invaginations.

The proximal tubule cells of the pronephros lack appreciable basal infoldings and the mitochondria do not exhibit the striking orientation seen in the distal tubule The same is generally true in the adult amphibian mesonephros (Karnovsky '63 Christensen '63; Peyrot and Massimello, '61) On the other hand, in proximal tubule cells of the mammalian metanephros, there is some tendency toward basal infoldings and mitochondrial orientation, although less so than in the distal tubule

The distal tubule cells of the pronephros resemble those of adult kidneys in having sparse microvilli on the luminal surface in some cases, numerous mitochondria generally oriented radially with regard to the tubule and basal infoldings of the plasma membrane which enclose the mitochondria in basal compartments. The mitochondria and basal infoldings are variable in abundance but where well developed are comparable to those described in adult kidneys.

The fine structure of the glomerulus has been described in mammals (Pease '55 Rhodin '63 and others) birds (Pak Poy and Robertson '57 Prestage and Beams, '57) reptiles (Pak Poy '59; Anderson, '60) amphibians (Pak Poy '57; Bargmann, Knoop and Schiebler '55) and in bony fish (Pak Poy '58) The glomus described in the present study is basically similar in fine structure to the glomerulus

of the adult amphibian mesonephros, which has essentially the same pattern of organization as that of the mammalian metanephros except that some of the cellular specializations are less highly evolved

The present findings provide new evidence for the current theory of vertebrate kidney evolution Near the turn of the century two conflicting views were in vogue to explain the phylogenetic origin of vertebrate kidneys. One view originally put forth especially by German workers maintained that during the course of evolution the vertebrates had successively developed three separate and distinct adult kidneys, the pronephros the mesonephros and the metanephros and that this evolutionary history was recapitulated during the embryonic development of higher vertebrates. The other view originally held mostly by British and American workers, claimed that the pronephros, mesonephros and metanephros were merely regional specializations of a single primitive kidney the archinephros (Lankester 1877 p. 429) or "holonephros (Price 1897) which was thought to have extended the full length of the body cavity in some hypothetical ancestral vertebrate According to this latter interpretation, as it eventually came to be understood the pronephros emerged in vertebrate evolution as a [illegible]l kidney an anterior differentiation of the archinephros designed to arise early in embryological development and thereby satisfy larval excretory needs until the more posterior mesonephros could be fully developed.

The basic question at issue between these two rival theories was the degree of serial homology in the vertebrate excretory system and it is therefore not surprising that a central issue was to what extent the pronephros, mesonephros and metanephros resembled each other As comparative and embryological evidence was accumulated increasing similarities between the three kidneys emerged and the archinephros theory became more and more widely accepted. However the peculiarities of the pronephros still remained a problem for those who held this theory Thus Goodrich wrote in '30 (pp 680 and 683):

> When the development of the mesonephros and metanephros was accurately worked out it had to be admitted that they are essentially of the same nature and that the peculiarities of the metanephros are related to its late [embryological] appearance and more specialized structure. The comparison of the mesonephros with the pronephros is, however, not so easily made, and there is still much doubt as to the exact relation they bear to each other.

After making this statement, Goodrich proceeded to review some of the evidence that the pronephros and mesonephros were indeed serially homologous, as claimed by the archinephros theory Since that time, additional findings, many of them arising from experimental embryology have served to further substantiate the archinephros theory and it now seems to have gained near universal acceptance. The evidence for this theory has been admirably marshaled by Fraser ('50).

The results of the present investigation further corroborate the archinephros theory by showing that the various cell types of a functional pronephros and glomus exhibit the same striking specializations of fine structure that have been described for corresponding cell types in the mesonephros and metanephros of a wide variety of vertebrates.

An additional implication of the present findings concerns the terminology used to designate the various segments of the pronephric nephron. In the past there has been considerable variation in usage, often because of differing embryological findings and interpretations. Thus the anterior and posterior proximal tubules have been variously called "secretory," "urinary" or "excretory" tubules while that portion which is here called the common proximal tubule has often been referred to as the "collecting tubule" or the common duct. The tubule extending from the intermediate segment back to the cloaca is generally considered as one unit, the archinephric

Many modern textbooks of comparative anatomy, while subscribing in general to the archinephros theory, still convey the impression that the basic [illegible] nephric renal corpuscle evolved from a [illegible] nephric type, through an enlargement of the [illegible] by folds of peritoneum to form Bowman's capsule and peritoneal funnel. However, the best embryological evidence has long suggested the [illegible] the primary mesonephros nephron is the basic [illegible] brate nephron, and that the pronephric type [illegible] from it by secondary changes involving [illegible] out of the peritoneal funnel and the fusion of several segmental glomeruli to constitute [illegible] glomus (see Fraser, '50).

segmental" duct or by some authors pronephric primary or nephric duct. Since portions of the pronephric are here shown to correspond in details of their fine structure to the proxi and distal tubules of adult kidneys, it seems reasonable and desirable to employ a nomenclature which reflects this similarity. Such a terminology has been utilized throughout the present study (fig. 1). Although the archinephric duct seems to exhibit a distal tubule structure over most of its length, and may possibly subserve a distal tubule function, only that portion which lies within the confines of the pronephros is called the distal tubule in the present paper the remainder being termed the nephric duct. The above interpretations based on fine structure criteria, are in essential agreement with the conclusions of Jaffee (see '63) based on vital staining and phenol red transport.

ACKNOWLEDGMENTS

The author would like to thank Dr Don W Fawcett and Dr Elizabeth D Hay for ng the manuscript and offering valuable suggestions. The larvae used in this study were obtained through Dr Hay's kindness. The first two figures were prepared by Mrs. Gertrude H Turner

LITERATURE CITED

nderson, E 1960 The ultramicroscopic structure of reptilian kidney J Morph 106: 205–241.

ergmann, W A. Knoop and T H. Schiebler 1958 Histologische, cytochemische und elektronenmikroskopische Untersuchungen am Nephron (mit Berücksichtigung der Mitochondrien) Zeitschr f Zellf 48: 386–422

ennett, H. S and J H. Luft 1959 s-Collidine as basis for buffering fixatives. J Biophysic. Biochem. Cytol., 6 113–114

hase B. W 1923 The mesonephros and urogenital ducts of Necturus maculosus Rafinesque. J. Morph., 37 457–531

hristensen, A. K. 1963 Fine structure of an exceptional kidney in the salamander Batrachoseps J Cell Biol 19 13A (Abstract)

awcett, D W 1958 Structural specializations of the cell surface. In Frontiers in Cytology Ed. by S L. Palay Yale Univ Press, New Haven. Chap 3 pp 19–41

Fawcett, D. W and K. R. Porter 1954 A study of the fine structure of ciliated epithelia J Morph 94 221 281

Field, H. H. 1891 The development of the pronephros and segmental duct in Amphibia Bull Mus Comp Zool Harvard, 21 201–340

Fox, H. 1963 The amphibian pronephros. Quart. Rev Biol., 38 1–25.

Fraser, E. A. 1950 The development of the vertebrate excretory system. Biol. Rev 25 159–187

Gérard, P and R. Cordier 1934 Recherches d'histophysiologie comparée sur le pro- et le mésonéphros larvaire des Anoures. Zeitschr f. Zellf 21 1–23.

Goodrich E. S. 1930 Studies on the Structure and Development of Vertebrates. Macmillan and Company London.

Gritzka, T L. 1963 The ultrastructure of the proximal convoluted tubule of euryhaline teleost F. ndulus heteroclitus Anat. Rec., 145 235–236 (Abstract)

Howland, R. B. 1921 Experiments on the effect of removal of the pronephros of *Amblystoma punctatum*. J Exp. Zool., 32 355–395.

Jaffee O. C. 1963 Cellular differentiation in the anuran pronephros. Anat. Rec., *145* 179–182.

Karnovsky M. J 1963 The fine structure of mitochondria in the frog nephron correlated with cytochrome oxidase activity Exp. and Mol. Path., 2 347–366.

Kerr J G. 1919 Text-book of Embryology Vol. 2. Macmillan and Co London.

Lankester E. R. 1877 Notes on the embryology and classification of the animal kingdom Comprising revision of speculations relative to the origin and significance of the germ layers Quart. J Micr Sci 17 399–454

Maunsbach A. B., S. C. Madden and H. Latta 1962 Variations in fine structure of renal tubular epithelium under different conditions of fixation. J Ultrastr. Res., 6 511–530.

McCurdy H. M. 1931 Development of the sex organs in *Triturus torosus*. Am. J Anat., 47 367–403.

Miller F 1960 Hemoglobin absorption by the cells of the proximal convoluted tubule in mouse kidney J Biophysic. Biochem. Cytol., 8 689–718.

——— 1962 Acid phosphatase localization in renal protein absorption droplets Proc. Fifth Intern. Congr of Electron Micr (Ed by S S Breeze, J) Academic Press, New York. Vol. 2, p. Q–2.

Möllendorff W von 1930 Der Exkretionsapparat. In Handbuch der mikroskopischen Anatomie des Menschen. Ed. by W von Möllendorff Julius Springer Berlin Vol 7 part 1 pp 1–328.

Noble G K and M K. Brady 1933 Observations on the lif history of the marbled salamander Ambystoma opacum Gravenhorst Zoologica. *11* 89–130.

Pak Poy R. K F 1957 Electron microscopy of the amphibian renal glomerulus. Austral J Exp Biol. and Med. Sci 35 583–594

——— 1958 Electron microscopy of the piscine (*Carassius auratus*) renal glomerulus

Because of the cytological similarities at the light microscope level, von Möllendorff (see '30, pp. 169–201) one of the outstanding authorities on kidney cytology used the terms for proximal (*Hauptstück*) and distal (*Mittelstück*) tubules to describe the respective segments of the amphibian pronephros

Austral J Exp. Biol. and Med. Sci., 36 191–210

——— 1959 Electron microscopy of the reptilian glomerulus. Austral. J Exp. Biol. and Med. Sci 37 153–162.

Pak Poy R. K. F., and J S. Robertson 1957 Electron microscopy of the avian renal glomerulus. J Biophysic Biochem. Cytol. 3 183–192.

Palay S L., and L J Karlin 1959 An lectron microscopic study of the intestinal villus II The pathw y f fat bsorption. J Biophysic Biochem. Cytol., 5 373–384

Pease D C. 1955 Fine structure of the kidney seen by electron microscopy J Histochem and Cytochem., 3 295–306

Poyrot, A., and C Masaimell 1961 Le rein du Triton crété (*Triturus cristatus carnifex* Laur) étude morphologique cytologique et cytochimique Zeitschr f Zellf 54 764–792.

Prestage J J and H. W Beams 1957 The structure f renal corpuscles in the sparrow *Passer dom sticus domesticus* as revealed by the electron microscope Proc Iow Acad. Sci. 64 670–679

Price G. C. 1897 Development of the excretory organs of a myxinoid, Bdellostoma stouti Lockington. Zool. Jahrb., Abt. f Anat 10 [illegible]

Rabl H 1904 Über die Vorniere und die Bildung des Müller schen Ganges bei Salamandra maculosa. Arch. f. mikr. Anat., 64 [illegible]

Rhodin J A. G. 1958 Anatomy of kidney tubules. Intern. Rev Cytol 7 485–534.

——— 1963 Structure of the kidney In Diseases of the Kidney Ed. by M. B. Strauss and L. G. Welt. Little Brown and Co Boston Chap. 1 pp. 1 29

Sidman, R. L., P A. Mottla and N Feder 1961 Improved polyester wax embedding for histology Stain Technol 36 279–284.

Tormey J M. 1963 Fine structure of the ciliary epithelium of the rabbit, with particular reference to infolded membranes, "vesicles, and the effect of Diamox. J Cell Biol 17 641–659

Watson M. L. 1958 Staining of tissue sections for electron microscopy with heavy metals. II Application of solutions containing lead and barium. J Biophysic Biochem. Cytol 4 727–730

PLATE 1

EXPLAN TION O FIGURES

3 Transverse section through the cervical region f 19 mm larva of *Ambystoma pecum* bowing the pronephros (*pr*) sectioned near its posterior pole and the glomus (*g*) on each side The pronephros lies deep to the scapula (*sc*) and adjoins the coelom ( ) in which are seen the esophagus ( ) and lungs (*l*) The connection between the glomu on the left and the dorsal aorta ( ) is shown in this section. Above the aorta are the notochord (*t*) and spinal cord (*sp*) At the xtreme left and right in the figure are sections of the gills. × 82

4 T ansverse section near the anterior pole of the left pronephros of a 19 mm larva. The ciliated epitheli m of the anterior nephrostome ( ) is continuou with the parietal peritoneum (*pp*) Although the nephrostome passes out of the plane f section, it re-enters the section t the junction (*p*) with the anterior proximal tubule of which three other sections (*p*) are visible one in surface view (*ps*) Except for the ciliated intermediate segment (*is*) all the other profiles are f th distal tubule (*d* and unmarked) Sinusoids containing red blood corpuscles (*rbc*) occupy the space between tubules. × 255

sp

nt

p

g

a

c

ln

st

3

e

np

p

p

d

ps

rbc

ls

4

pp

PLATE 2

EXPLAN TION OF FIGURE

5 Nephrostomal epithelial cell. The basal bodies (*bb*) of the cilia give rise to striated rootlets (*sr*) with 750 A periodicity and at the base of each cilium is basal plate (*bp*) The mitochondria (*m*) are of small di meter about 0.25 μ average and the background cytoplasm contains agranular endoplasmic reticulum (*er*) and an lement of the Golgi complex (*gc*) In one area of the cytoplasm are numerous melanin granules (*mg*) between which are found distorted lipid droplets (*lp*) The nucleus contains gra ular inclusion (*inc*) of unknown nature × 14,200


bp
bb
m
sr
er
gc
inc
lp
mg
5

PLATE 3

EXPLANATION OF FIGURE

6 Proximal tubule cell. At the base of the sparse and irregular microvilli of the brush border (*br*) are invaginations of th plasma membrane the tubular invagin tions (*ti*) which extend down into the apical cytoplasm. Vacuoles (*v*) are thought to become granules (*gr*) by accumulating material absorbed from the lumen by way of the tubular inv ginations (Miller '60) Agranular endoplasmic reticulum (*er*) nd Golgi omplex (*gc*) are also seen i the cytoplasm. There are few mitochondria (*m*) and no h- the basal infoldings occur at the base f the cell (lower left


br
v
er
gr
m
gc
6

PLATE 4

EXPLANATION OF FIGURES

7 The apex of a proximal tubule cell bowing in greater detail the brush border tubular invaginations (*ti*) and granule (*gr*) The microvilli f the brush border are irregular in form, and commonly contain elements f the endoplasmic reticulum (*er*) × 22,000.

8 Horizontal section through the brush border showing cross sections of the very irregular and anastomosing microvilli Small profiles of endoplasmic reticulum (*er*) are frequently seen. × 23,700.

9 The limiting membrane of tubular invagin tion seen in surface view Note the uneven pattern of oblong profiles (arrows) along the membrane. The significance of this fine structure is unknown × 53,000

10 Small, dense, membrane-bound inclusions about 0.2 μ in diameter re seen in occasional proximal tubule cells and are here shown among mitochondria The chemical ture of these inclusions is unknown, but they closely resemble structures described as emulsified fat droplets (Palay and Karlin '59) × 25,000

7

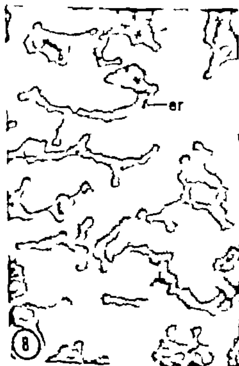






PLATE 5

EXPLANATION OF FIGURES

11 Distal tubule cell. The lumen of the tubule is t upper left and sin soid, lined by n endothelium (*end*) and containing red blood cells (*bc*) is t the lower right. The mitochondria and basal infoldings characteri tic of distal tubule cell are f moderate number in this cell. × 6,000

12 Base of a di tal tubule cell showing somewhat oblique sections of oriented mitochondria and of basal infoldings, some of which ppear to be fenestrated (*fen*) In this study distal tubul cells with more numerous mitochondria and still more striking basal infoldings than those shown here were not uncommon. × 21,000.

rbc
end
11
fen
fen
12

PLATE 6

EXPLANATION OF FIGURES

13 Glomus. In this low power lectron micrograph several capillaries (*cap*) of the glomus are shown surrounded by the coelomic space ( ). The nuclei of number of endothelial cells (*end*) and epithelial cells (*ep*) re present i the field Cytoplasmic processes (*cp*) extend out from the epithelial cell to ramify over the capillary basement membrane i t atten ted foot processes, which interdigitate with those of adjacent epithelial cells. The foot processes constitute most of the epithelial layer covering the capillaries, except occasionally when the ell body itself happens t lie against the basement membrane (ar row) A leucocyte (*wbc*) partially occludes the lumen of one of the capill ries. Some cells contain clusters of melanin granules (*mg*) × 3,800.

14 Capillary wall of th glomus, t higher magnificatio The endothelium (*end*) is irregular i thickness. The baseme t membrane is inadequately preserved except for a thin outer l yer (*bm*) which is covered by the foot processes (*fp*) from the epithel al cells. In the basement membrane region between the endotheli m and epithelium re cell processes (*pc*) which may derive from endothelial cells, or possibly from so-called pericapillary cells (Pak Poy 57) × 14,500

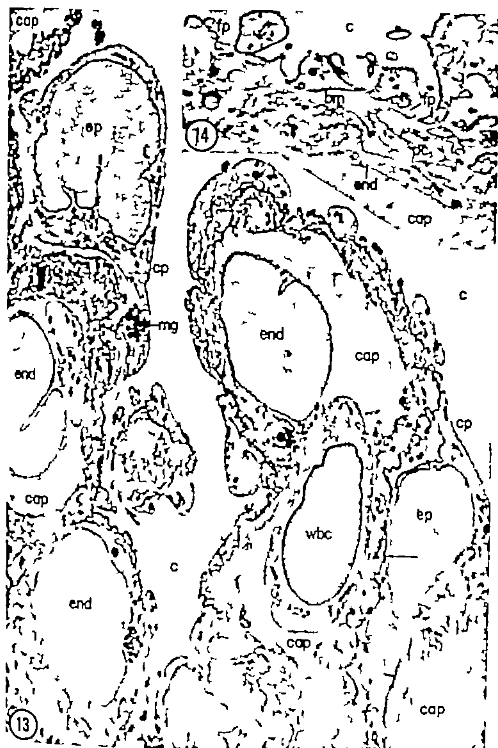

cap
fp
c
bm
fp
14
ep
pc
end
cap
cp
c
mg
end
cap
end
cp
ep
wbc
cap
c
end
cap
cap
13

PLATE 6

EXPLAN TION OF FIGURES

13 Glomus. I this low power lectron micrograph, several capillaries (*cap*) of the glomus are shown urrounded by the coelomic space ( ) The nuclei of a number of endothelial cell (*end*) and epithelial cells (*ep*) are present in the field. Cytoplasmic processes (*cp*) extend out from the epithelial cell t ramify over the capillary basement membrane into attenu ted foot processes, which interdigitate with those of adjacent epithelial cells. The foot processes constitute most of the epithelial layer covering the capillaries, except occasionally when the cell body itself happens to lie again t the basement membrane (ar row) A leucocyte (*wbc*) partially occludes the lumen of one of the capillaries. Some cells contain clusters of melanin granules (*mg*). × 3,800

14 Capillary wall of the glomus, at higher magnification The endothe li m (*end*) is irregular i thickness. The basement membrane is inadequat ly preserved, except for thin outer l yer (*bm*) which is covered by the foot processes (*fp*) from the epithelial cells. In the basement membrane region between the endothelium and epithelium are cell processes (*pc*) which may derive from endothelial cells, or possibly from so-called pericapillary cells (Pak Poy '57) × 14,500

Structural and Functional Aspects of Rodent Salivary Glands Including Two Desert Species [1]

JOHN M. SHACKLEFORD AND CHARLOTTE A. SCHNEYER
University of Alabama Medical Center Birmingham, Alabama

ABSTRACT The submaxillary glands of the adult desert rat, antelope squirrel, rat, mouse and hamster have in common low levels of amylolytic enzyme in comparison with the relatively high levels of parotid gland amylase in these rodents. Submaxillary gland acini are classed as seromucous secreting although there is some variation in the carbohydrate histochemistry of these secreting units. Granular tubules are absent in antelope squirrel submaxillary glands and they are present in the submaxillary glands of the desert rat, rat, mouse and hamster. Electron micrographs reveal the presence of numerous basal folds in the acini of antelope squirrel submaxillary and parotid glands. These structures were not observed in the salivary gland acini of the hamster Golgi membranes and "immature secretion granules are topographically intimate in parotid glands of the hamster and antelope squirrel. In the submaxillary glands of these two rodents, the secretory material appears to originate in relation to the endoplasmic reticulum and secondarily the granules become associated with diffusely arranged system of Golgi membranes. The sublingual glands of all the rodents of this study are predominantly ones that produce mucous secretion and contain well developed striated duct systems. Of the salivary glands investigated in this study the parotid glands of the rat, mouse and desert rat produce an isotonic saliva; the saliv f the other glands is definitely hypotonic.

The morphology of the salivary glands of desert rodents does not appear to have been previously described even though these structures may play a role in adaptation to desert conditions (Bartholomew and Hudson, '61 Schmidt-Nielsen and Schmidt-Nielsen '53) It was therefore of interest to investigate the morphology of the salivary glands of desert rodents in comparison with laboratory rodents. The two desert rodents used in this investigation were the desert rat and antelope squirrel, and the laboratory rodents the hamster rat and mouse Comparison of functional characteristics of the desert and laboratory animals was also undertaken since a correlation between structure and function has been suggested previously (Shackleford and Klapper '62a, '62b and '62c Schneyer and Schneyer '58 '60a and '60b)

METHODS AND MATERIALS

Three fixatives were used in the preparation of tissues for light microscopic studies. These were Bouin's buffered 10% formalin and Zenker formol (90 parts Zenker's fluid and 10 parts formaldehyde) Paraffin sections were examined after staining with the Masson, hem t x lin and eosin and a modification of Masson's technique Histochemical stains employed were the periodic acid Schiff Alcian blue buffered toluidine blue and the p-hydrazinobenzenesulfonic acid reaction (Shackleford, '63a) Alcian blue and periodic acid Schiff reactive substances were characterized using the malt diastase bull testis hyaluronidase (McManus and Mowry '60) and *Vibrio cholera* neuraminidase (Spincer and Warren, '60) digestion techniques.

Submaxillary and parotid glands from the hamster (*Cricetus auratus*) and the antelope squirrel (*Citellus tereticaudus*) were fixed for electron microscope studies. Small fragments of the glands were fixed in buffered osmium tetroxide (pH 7.4 with sodium acetate-sodium veronal buffer) and embedded in methacrylate or epon Thin sections of epon embedded material were stained by the lead hydroxide method of Millonig ('61) The sections were examined with Phillips 100-B and Phillips 75-B electron microscopes.

Physiological studies were performed on adult desert rats (*Dipodomys deserti* and *Dipodomys merriami*) antelope squirrel white mice Long Evans rats and hamsters

[1] This study supported by U S Public Health Service grants DE-01228 03 and D 1674.

fasted for 24 hours prior to experimentation The saliva evoked in response to stimulation by injection of pilocarpine nitrate (2 mg/300 gm animal) was collected directly from the duct orifice by micropipette and diluted immediately with double-distilled water for subsequent electrolyte determination by Coleman flame photometry Glands were homogenized in phosphate-buffered saline centrifuged, and the supernatant was used as the enzyme source. Amylase activity is expressed as the number of milligrams of reducing substance (as glucose) per mg of tissue and was determined using a modification (Schneyer and Schneyer '56) of the method of Myers Fiee and Rosinski ('44)

RESULTS

Light microscopy of desert rat and antelope squirrel submaxillary glands The submaxillary gland of the male desert rat is structurally similar to that of the male white mouse The acinar cells exhibit acidophilic staining properties and are finely granular A basophilic ergastoplasmic zone can be recognized at the base of the cell on either side of the rounded acinar nuclei (fig 1) The granular cytoplasm of the acini is periodic acid Schiff (PAS) positive but does not stain appreci with Alcian blue Sulfation (method of Mowry '58) produces a toluidine blue metachromasia in the acinar cytoplasm and the p-hydrazinobenzenesulfonic acid (PBSA) reaction indicates a concentration of vicinal hydroxyl groups consistent with a seromucous classification for the secretion Most of the submaxillary gland parenchyma of the male desert rat is occupied by large convoluted granular tubules. The granular tubules are composed of tall columnar cells with a basally located rounded nucleus Basal striations similar to that of striated ducts can be distinguished below the nucleus. The apical two-thirds of the granular tubule cells is filled with acidophilic granules which are PAS positive and Alcian blue negative These granules stain orthochromatically with toluidine blue after sulfation and stain light green with toluidine blue (0.01% at pH 2.8) after the PBSA reaction It is probable that PBSA reacts in direct proportion to the concentration of vicinal hydroxyl groups (1,2-glycols) yellow-green to green staining, with 0.01% toluidine blue at pH 2.8 is characteristic of serous secreting cells in which some PAS positive material is present. A sex dimorphism of the granular tubules is apparent in the submaxillary glands of the desert rat, similar to that reported by others in the mouse (Lacassagne '40 Junqueira et al '49).

The submaxillary gland of the antelope squirrel in most respects is very different from that of the desert rat. With the light microscope the ergastoplasmic zone is inconspicuous. Nuclei of acinar cells are basally located and rounded or oval shaped. The acinar cytoplasm stains with acid dyes, is moderately positive to Alcian blue, and reacts strongly with PAS. The Alcian blue staining is comparable to submaxillary gland acini of the female hamster or to acini of the dog parotid gland. Granular tubules, which are a prominent feature of submaxillary glands of hamster desert rat mouse and Long-Evans rat, are absent in the antelope squirrel. A well developed striated duct system is present, however (fig 2) Submaxillary glands of the antelope squirrel closely resemble the submaxillary gland of the common grey squirrel (unpublished data)

The PBSA-toluidine blue reaction stains submaxillary acini of the antelope squirrel a pale blue color Hyaluronidase digestion removes most of the Alcian blue positive material in stromal elements of submaxillary glands of desert rat and antelope squirrel. Hyaluronidase also slightly reduces the Alcian blue staining in antelope squirrel submaxillary acini and hyaluronidase plus neuraminidase digestion markedly reduces the Alcian blue reaction in the same area The possible significance of these results will be discussed subsequently Malt diastase digestion did not significantly reduce PAS staining in submaxillary glands of the antelope squirrel or the desert rat in comparison with sections known to contain glycogen (cf guinea pig submaxillary gland striated ducts or striated ducts of the [illegible] parotid gland (Shackleford, '63)).

Ultrastructural comparison of hamster and antelope squirrel submaxillary glands Electron micrographs of hamster submaxillary glands reveal structures similar

to those described by Scott and Pease ('59) and Leeson and Jacoby ('59) in the rat submaxillary gland. Among prominent features of acini of hamster submaxillary gland are a well developed *endoplasmic* reticulum (ER) with attached ribonucleoprotein (RNP) particles, a somewhat flattened electron dense nucleus, a few scattered mitochondria and intercellular canaliculi (figs. 7 8) The secretory granules, at the base of the acinar cell are mostly enclosed by ER membranes but lose this association in areas adjacent to the acinar lumen or the intercellular canaliculi (fig 7) Here, there is evidence to support the contention of Palade ('59) that, as the ER relationship to the secretory granules is lost, the smooth Golgi type membranes become closely associated with the secretion. Mitochondria of hamster submaxillary gland acini are sparsely distributed throughout most of the cytoplasm and are elongated or irregularly shaped without any particular orientation. Basal infolded plasma membranes are rarely observed in acinar cells of hamster submaxillary glands.

The short intercalated ducts and small number of striated ducts in the hamster submaxillary gland are structurally very similar to the same *ducts of* the hamster parotid gland. Since striated and intercalated ducts are much longer and more easily studied in the parotid gland, these structures are reserved *for* description along with other components of the hamster parotid gland. The granular tubules of *the* hamster submaxillary gland are composed of simple *columnar* epithelium with rounded, basally located nuclei. The granules of the apical two-thirds of the cells are of many sizes and shapes and vary considerably in electron density ER membranes are poorly developed and are not a striking feature of the granular tubule epithelium. Conversely infoldings of the plasma membrane are numerous and are topographically intimate with large numbers of mitochondria (figs. 9 10) As pointed out by Rhodin ('58) in regard to the kidney tubules, and by Parks ('61) in reference to the striated ducts of the mouse parotid gland, the infoldings may represent *complex* interlockings of adjacent epithelial cells. In the region *of* the nucleus the infoldings appear to branch, anastomose and form highly complex configurations. Close to the apex of the granular-tubule cell numerous vesicles are observed which *appear to the derived from* "pinched off" portions of the double infoldings of the plasma membrane. A well developed system of Golgi membranes is frequently present in a position apical to the nucleus of granular tubule cells (fig. 11) This observation is contrary to the findings of Scott and Pease ('59) who report the presence of Golgi membranes at *the base of the cell only and away from* the granule formations In hamster granular tubules a Golgi complex is occasionally observed in positions either apical or basal to the nucleus.

Acinar cells of the submaxillary gland of the antelope squirrel contain secretory granules which are slightly more electron dense than those of hamster submaxillary *acini*. *Characteristic nuclear chromatin* aggregations which are striking in light micrographs of salivary glands from the desert rodents (figs. 1 2) are also very *prominent in electron* micrographs (fig 12) The chromatin aggregates are Feulgen positive and are present in all tissue preparations regardless of fixation. In contrast to the hamster submaxillary acini of antelope squirrel exhibit *only scattered* ER membranes. The ER membranes and associated RNP particles are frequently located in close association with secretion granules *at the base of the acinar cells but* the same membranes are rarely even seen in a definite parallel array A few mitochondria, a diffused type Golgi membrane system, *and intercellular canaliculi* are also present. Occasionally small nerve "terminals can be observed between the basal portions of adjacent acinar cells. *Frequently the basal plasma membrane* appears to "infold" and form highly complex smooth membrane systems within the acinar cells (fig. 13) This arrangement *of smooth membranes is* rarely encountered in the salivary gland acini of the hamster

Intercalated ducts of submaxillary and *parotid glands of antelope* squirrel are characterized by low cuboidal epithelium with very little evidence of secretory activity ER membranes and Golgi membranes

are poorly developed and are not a striking feature of the intercalated duct cell (fig 14) Plasma membranes of adjacent cells form interdigitations at their basal aspect and desmosomes are located toward the cell apices. Mitochondria, having no particular orientation within the cells, are present in moderate numbers

Striated ducts of the submaxillary and parotid glands of the antelope squirrel contain large numbers of mitochondria which are closely related to infolded plasma membranes (fig. 15) Golgi membranes are poorly developed in comparison with those of the granular tubules. Desmosomes are frequently observed which attach the apices of neighboring cells. The apical cytoplasm usually contains numerous vesicles or vacuolated areas and the lumen of the striated duct is characterized by many microvillous-projections

Light microscopy of desert rat and antelope squirrel parotid glands Parotid glands of desert rats (fig 3) are not remarkably different from those of previously described rodents (Shackleford and Klapper '62c) The principal exception to this similarity would be the "pawn ball nuclei present in the salivary glands (as well as in certain other exocrine glands) of both the desert rat and the antelope squirrel. Acini of desert rat parotid glands typical with respect to the well defind zone and the PAS positive Alcian blue negative reactions in the secretory granules. Intercalated ducts composed of flattened cuboidal non-granular epithelium connect the acini with the striated ducts. The striated ducts are typical and exhibit some PAS staining which is not digestible with diastase.

Parotid glands of the antelope squirrel are characterized by a very strong PAS reaction in the acini (fig. 4) The PBSA reaction produces a dark green coloration of the acini when stained with 0 01% toluidine blue at pH 2.8 The Alcian blue reaction is negative in all the parenchymal elements of the parotid gland of the antelope squirrel. Intercalated and striated ducts are morphologically similar to those of the submaxillary glands. Occasionally nuclei of the striated ducts are strongly stained with PAS This nuclear carbohydrate is located between the chromatin aggregates described previously and is not digestible with diastase.

Ultrastructural comparison of hamster and antelope squirrel parotid glands Electron micrographs of hamster parotid acini reveal a well developed ER, a discrete Golgi system apical to the nucleus, intercellular canaliculi and secretion granules which are slightly more electron dense than those of the hamster submaxillary gland The nuclei are oval or rounded in shape and are located at the base of the acinar cells. The secretion granules are, for the most part, limited to cytoplasmic areas apical to the nucleus and they are closely related to the Golgi membranes (figs. 16 17) Mitochondria are typically sparse and basal infoldings of plasma membranes are characteristically absent in the acini of hamster parotid glands. Nerve endings" located between adjacent acinar cells are frequently observed in hamster parotid glands. These endings closely resemble those reported by Scott and Pease ('59) in the parotid gland of the rat.

Intercalated ducts of the hamster parotid gland possess a moderately well developed ER and few scattered mitochondria. The nuclei are flattened and the apical one-half of the cells contain extremely electron dense secretion granules (fig 18) The intercalated duct granules are not as irregular in size and shape as those of the granular tubules in the hamster submaxillary gland. The ER membranes and attached RNP particles are not arranged in a definite parallel array as they are in the acini of the parotid gland of the hamster Desmosomes are present at the plasma membranes toward the cell apices.

Striated ducts of the hamster parotid gland are composed of simple columnar epithelial cells containing a rounded, centrally located nucleus. Apices of the cells contain granules of much smaller dimensions than those of hamster granular tubules. Protoplasmic projections into the lumina are fewer in number and larger than those of the antelope squirrel striated ducts. Desmosomes are present at the plasma membranes of adjacent cell apices. Infoldings of the plasma membrane are a prominent feature of the basal one-half of the striated duct cell. These smooth mem-

ranes are topographically intimate with elongated mitochondria whose long axis is perpendicularly oriented toward the base of the striated duct cell (figs. 19 20). Structures similar to the lysosomes described by de Duve ('50) are occasionally seen scattered among the mitochondria.

Acinar cells of the parotid gland of the antelope squirrel possess a moderately well developed system of ER membranes a discrete Golgi system, numerous electron dense secretion granules and a moderate number of mitochondria (fig 22). In lead stained epon sections of the antelope squirrel parotid gland, peripheral nerve endings are observable as topographically to adjacent acinar cells (figs. 22, 24). Secretory granules appear to originate as definite membrane-limited structures in the region of the Golgi complex (figs. 22, —). This apparent relationship of immature secretory granules and Golgi membranes is not as apparent in the submaxillary glands of either the hamster or the antelope squirrel. Though not as extensive as in the antelope squirrel submaxillary gland acini, smooth membranes are frequently present in the basal aspect of the parotid gland acini of the antelope squirrel. These membranes have definite continuity with the surface plasma membrane of the acinar cells (fig. 25). A well defined desmosome and microvilli are illustrated at the junction of two acinar cells bordering an intercellular canaliculus (fig 26).

Intercalated and striated ducts of the parotid gland of the antelope squirrel are not remarkably different from those in the submaxillary gland of this animal. As previously mentioned, the striated ducts of the submaxillary gland are much more numerous per unit area than in the parotid gland of the antelope squirrel.

The ultrastructure of interstitial plasma cells. In addition to the usual type of interstitial cells e.g. fibroblasts and mast cells, there are cells present in the salivary glands of most mammals which have a structure very much like the plasma cell. These cells mostly fill in the spaces between adjacent salivary gland acini. The "interstitial plasma cell" is characterized by a rounded, usually eccentrically placed nucleus. The cytoplasm is filled with rough ER membranes which limit very large vesicles or cisternae (fig 21). Upon observation of a number of these cells the size of the cisternae varies considerably. Extremely dilated cisternae with the associated ER membranes are frequently seen to be detached from the remainder of the cell. This brief description of the inter acinar cell is included here because of its possible role in the secretory mechanism. In any biochemical analysis of saliva therefore this cell should be considered as a possible source and site of synthesis of certain salivary proteins and other organic compounds.

Comparison of sublingual glands in the desert rat and antelope squirrel. The sublingual glands of the antelope squirrel and desert rat have a similar gross relationship to the submaxillary glands as in certain other rodents e.g. the rat, mouse and hamster. That is, the submaxillary and sublingual glands are enclosed in a common connective tissue capsule and the two glands are separated by a band of irregular connective tissue only. Sublingual glands of both the desert rat and the antelope squirrel are composed largely of mucous acini which react strongly to PBSA, PAS and Alcian blue (figs. 5 6). Nuclei are typically flattened or oval in shape and lie at the extreme base of the acinar cells. Striated ducts are present and well developed in the sublingual glands of the antelope squirrel and desert rat but only very short intercalated ducts are present. The mucous acini of the desert rat frequently open directly into the striated ducts. Demilunes appear to be totally absent in the antelope squirrel sublingual gland. Conversely in the sublingual gland of the desert rat, there are many acinar cells which stain slightly with PAS and are negative to Alcian blue. On morphological grounds these cells are considered to be demilune formations.

Hyaluronidase and neuraminidase considerably reduce the Alcian blue staining of antelope squirrel sublingual glands. Alcian blue staining which is removed by neuraminidase probably reflects the presence of sialic acid in the mucous acini. Reduction in Alcian blue staining after bull testis hyaluronidase treatment was not totally unexpected since sulfated mucopolysaccharides (chondroitin sulfates A

or C) are sometimes in the sublingual gland acini of other mammals. One possibility that should be considered in the enzymatic digestions is the presence of proteolytic enzyme in sufficient quantity to give non-specific results.

Comparison of amylase and electrolyte secretions in the rodents From the data included in table 1 it is clear that most rodent submaxillary glands (unstimulated and obtained from animals fasted for 24 hours prior to experiment) are consistently low in amylase levels. This is true for submaxillary glands of the rat, mouse hamster desert rat and antelope squirrel where values lie in the range of 0 01 to 0.25 mg reducing substance per mg gland. Conversely amylase levels in the parotid glands are consistently high and range from 55 to 87 mg/mg gland in the desert rat to as high as 500 mg/mg gland in the antelope squirrel and 600 mg/mg gland in the Long Evans rat (Schneyer and Schneyer '56 '60b) The guinea pig is the only rodent thus far studied where a high amylase level is found in the submaxillary as well as in the parotid glands (Schneyer unpublished data)

The pattern of Na and K secretion by the submaxillary glands of rat (Schneyer and Schneyer '60a) hamster desert rat and antelope squirrel (table 1) is generally ... with saliva distinctly hypotonic to serum produced in each case. In general, following stimulation of the glands by the parasympathomimetic agent, pilocarpine, Na is low (usually below 25 meq/1) and K high (about 48 meq/1) Only in the case of submaxillary saliva of the mouse is this pattern somewhat altered, for, while Na levels are again similar to those of the rodents already mentioned, K is consistently high (initially) and the submaxillary saliva of mouse begins to approach isotonicity The saliva from parotid gland of the mouse desert rat (table 1) and Long Evans rat (Schneyer and Schneyer, '60a) exhibits high levels of Na (initial values for Na range from an average of 96 to 142 meq/1) and is isotonic, or nearly isotonic with serum. Na in parotid saliva of the hamster and antelope squirrel is, on the other hand, comparatively low, (initial levels in hamster range from 7 to 35 meq/1) while those of parotid saliva of the antelope squirrel range from 43 to 62 meq/1 K of parotid gland saliva is high in the hamster (average initial value of 96 meq/1) and relatively low in the mouse, desert rat, and antelope squirrel (K values range from an average initial level of 21 meq/1 in the desert rat, which is similar to levels reported for the Long Evans rat (Schneyer and Schneyer '60a), to 36 meq/1 in the mouse) In considering the sum of the two chief cations (Na plus K) of the salivas of parotid glands of the mouse, desert rat and Long-Evans rat

TABLE 1

Amylase levels of rodent salivary glands and electrolyte levels of the salivary secretions

Animal	Submaxillary glands N	Submaxillary glands K	Submaxillary glands Amylase	Parotid glands N	Parotid glands K	Parotid glands Amylase
	meq/l saliva	meq/l saliva	mg/mg gland	meq/l saliva	meq/l saliva	mg/mg gland
Mouse	23 ± 4 (3)	102 ± 5 (4)	0 10 ± 0.19	96 ± 17(3)	36 ± 7 (5)	163 ± 19 ([illegible])
	17 ± 6 (3)	73 ± 10(3)		117 ± 13(7)	19 ± 5 (5)	
Hamster	17 ± 11(5)	46 ± 3 (3)	0.04 ± 0.01(8)	14 ± 16(3)	96 ± 23(3)	114 ± 1[illegible](4)
				33 ± 12(4)	64 ± 16(4)	
Desert Rat	27 ± 14(3)	66 ± 19(3)	0.07 ± 0.05(7)	142	21	79 ± 17(4)
Antelope Squirrel	23 ± 7 (3)	38 ± 9 (3)	0.05 ± 0.05(4)	51 ± 10(4)	33 ± 4 (4)	278 ± 1[illegible]([illegible])

Values presented in each case are means ± standard deviations number in parenthesis refers to number of animals. The values for Na and K were determined on saliva samples obtained immediately after initiation of flow following intraperitoneal injection of pilocarpine when second value is also presented, such value refer to samples obtained 3 min to 8 min after initiation of flow Amylase is expressed as mg reducing substance (as glucose) per mg of tissue.

Data not included here on the rat may be found in the published papers of Schneyer and Schneyer ('58, '60).

Range of average values for several strains of mice (Schneyer, '58).

Only single values here obtained.

roduce isotonic secretions whereas the arotid salivas of the hamster and antelope squirrel are hypotonic.

DISCUSSION

In comparing the salivary glands of the desert rodents with those of common laboratory rodents it appears that the similarities are more striking than the dissimilar characteristics. The salivary glands of the desert rat, for example, are morphologically histochemically and physiologically closely related to the salivary glands of the white mouse, and laboratory rat. More specifically desert rat and white mouse salivary glands have submaxillary gland acini which histologically and histochemically may be classified as seromucous. In the male, large granular tubules occupy most of the submaxillary gland parenchyma. Very low amylase levels are present in the submaxillary glands of white mice laboratory rats (Schneyer and Schneyer '58 '60a, '60b) and desert rats, while relatively high levels of this enzyme are demonstrable in the parotid glands. Potassium (K) is high in the submaxillary gland saliva whereas sodium (Na) is high in the parotid glands of these animals. The sublingual glands are composed predominantly of mucous-secreting acini.

Parotid gland amylase levels are consistently high in all rodents thus far tested. The guinea pig is the only rodent which exhibits a high submaxillary gland amylase (Schneyer unpublished data) There is, to some extent, an inverse relationship between amylase levels and mucous secretions in mammalian salivary glands. This is particularly true in salivary glands in which the sialomucin content is very high. Salivary glands which produce a seromucous secretion and are classified as seromucous glands e.g., submaxillary glands of most rodents (excepting that of the guinea pig) and the parotid glands of the dog and cat, are also reported to be low or lacking in amylase content (Shackleford and Klapper '62c). Exceptions to this relationship are the parotid glands of the cow and sheep which exhibit low levels of amylolytic enzyme in the saliva but yet are classified as serous glands (Shackleford and Klapper '62c; Burgen and Emmelin, '61) Morphological and histochemical studies are an invaluable aid in classifying salivary glands therefore, but caution should be exercised in making conclusions without the additional information provided from biochemical analysis. Serous acini of most salivary glands, for example, are reactive to the periodic acid Schiff (PAS) method for tissue carbohydrate. The presence of PAS positive material should by no means justify the conclusion that mucins are present. In this regard, however there is admittedly some confusion as to the exact biochemical definition of mucin. If the mucins are considered as protein-carbohydrate complexes in which hexose hexosamine fucose and sialic acid taken together compose about 70% of the molecule (Hashimoto and Pigman, '62) then it should be clear that all PAS positive materials in salivary gland epithelial cells are not mucin. In this regard the *p*-hydrazinobenzenesulfonic acid (PBSA) reaction should be of value in estimating the concentration of vicinal hydroxyl groups in the glycoproteins of epithelial cells (Shackleford, '63a)

Electrolyte levels in rodent salivas cannot be predicted with any consistency on the basis of presently available morphological and histochemical methods. Na and K in antelope squirrel parotid saliva, for example, is closer to the electrolyte levels of rat submaxillary glands than it is to most parotid glands. As a result of the high K values and low Na levels in the hamster parotid and in mouse submaxillary gland, the electrolyte secretions of these two glands are similar The only salivary glands of this study which can be considered to have an isotonic saliva are the parotid glands of the rat, mouse and desert rat. Whereas the salivas of mouse submaxillary glands can be said to approach isotonicity it is evident that all salivas (other than that of the desert rat, mouse and rat parotids) are definitely hypotonic. It should be emphasized at this point that there are no morphological criteria by which electrolyte levels can be estimated. Speculation on transport of electrolytes on the basis of striated duct morphology for example, seems fruitless at this time. In this regard it is interesting to note that children with cystic fibrosis of the pancreas may produce sweat in which

PLATE 1

EXPLANATION OF FIGURES

1 Submaxillary gland of the male desert rat. Granular tubule at arrow Observe close resemblance to male white mouse. Hematoxylin, orange-G aniline blue stain. × 640.

2 Submaxillary gland of the antelope squirrel. Granular tubules are absent in this rodent. Typical "pawn ball" nucleus at arrow. Striated duct in lower portion of the picture. Hematoxylin, orange-G, aniline blue stain. × 640.

3 Parotid gland of the desert rat. Striated ducts (at arrows) are smaller than those of the antelope squirrel parotid (cf fig. 4). Hematoxylin, orange-G, aniline blue stain. × 160.

4 Parotid gland of the antelope squirrel. Acini are strongly PAS positive. Striated duct at arrow. Periodic acid Schiff hematoxylin stain. × 160.

5 Sublingual gland of the desert rat. Acini exhibit strong acidic carbohydrate staining. Alcian blue-Feulgen stain. × 160.

6 Sublingual gland of the antelope squirrel. All acinar cells are the mucous secreting type. Alcian blue-Feulgen stain. × 160.

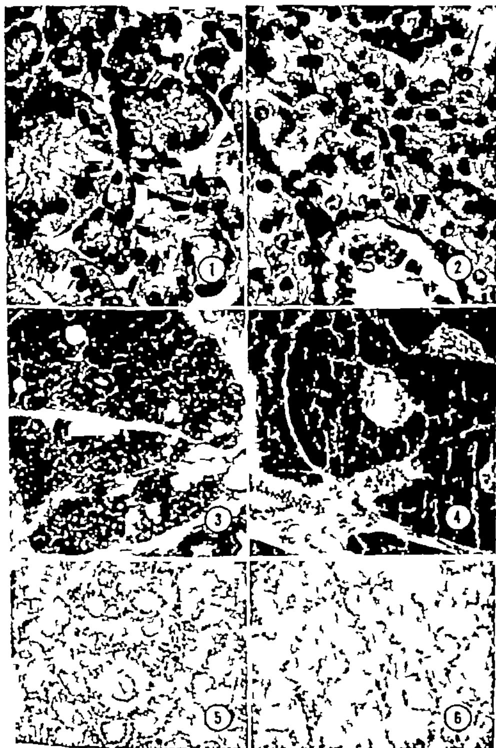

1
2
3
4
5
6

PLATE 2

EXPLANATION OF FIGURES

7 *Hamster submaxillary gland* Acinar cells containing numerous secretion granules (S) few scattered mitochondria (M) Golgi membranes (G) and granular (rough-surfaced) endoplasmic reticulum (R) Note that the more basally placed secretion granules are closely related t granular reticulum whereas those near the canaliculus (t arrow) are related to smooth membranes. Electron micrograph, lead stained epon section. × 13,500

8 Hamster submaxillary gland. Secretion granules (S) of acinar cell just apical to nucleu (N) Electron micrograph, lead-stained epon section. × 15,000.

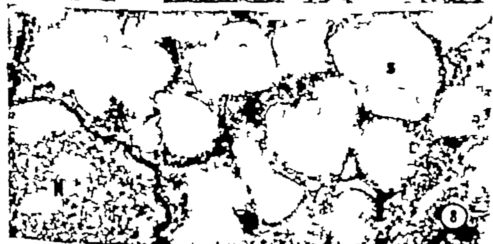

S
N
8

PLATE 3

EXPLANATION OF FIGURES

9 Hamster submaxillary gland. Granular tubule epithelium shows an abundance of mitochondria and smooth membranes in basal one-third of cells. Apical two-thirds of cells contain secretion granules of varying size and electron density. Cell with nucleus (N) contains numerou small vesicles in apical cytoplasm. Microvilli project from the apices of some cells into the tubule lumen at right of micrograph. Electron micrograph, lead stained epon section. × 4,000.

10 Hamster submaxillary gland. Picture illustrates intimate relationship of infolded plasma membranes and mitochondria in basal portion of granular tubule cell. Electron micrograph, methacrylate section. × 40,000.

11 Hamster submaxillary gland. Golgi membranes t apex of granular tubul cell nucleus. Electron micrograph, methacrylate section. × 32,000.


10


11

PLATE 4

EXPLANATION OF FIGURES

12 Antelope squirrel submaxillary gland. Acinar cell contains numerous secretion granules (S) and an extensive system of Golgi membranes (G) Granula reticul m (R) is sparse. Electron micrograph, lead stained epon section. × 9,000

13 Antelope squirrel submaxillary gland. Picture ill strates basal folds of plasma membrane (t arrows) in an acinar cell. Electron micrograph lead stained epon section. × 33,000

G

S

G

N

S

12

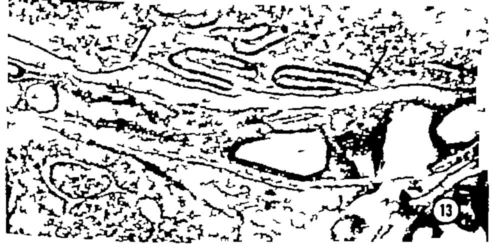


PLATE 6

EXPLANATION OF FIGURES

16 Hamster parotid gland. Notice abundant granular reticulum in portions of acinar cells. Canaliculus bove nucleu at left is studded with microvilli. Structure at arrow containing two small mitochondria is probably a nerve ending. Electron micrograph lead stained epon section × 10,500.

17 Hamster parotid gland. Portions of acinar cell to illustrate close relationship of gran lar reticulum to Golgi membranes. Membranes of the granular reticulum appear to converge toward the Golgi region right of center Electron micrograph, lead stained epon section. × 33,000

S

m

N

16



PLATE 7

EXPLANATION OF FIGURES

18 Hamster parotid gland. I tercalated duct cells show secretion granules (S) of much greater lectron density than those of acinar cells. Lumen of duct is left of center in upper portion of micrograph. Electron micrograph lead stained epon section. × 6,000

19 Hamster parotid gland Base f striated duct illustrates continuity of plasma membrane with smooth membranes within the cell. A small nerve fiber accompanies the blood vessel in lower half of micrograph Electron micrograph lead stained section. × 15,000


N
N
S
18

PLATE 8

EXPLANATION OF FIGURES

20 Hamster parotid gland. Tangential section through striated duct to show abundance of mitochondria and their intimate relationship to smooth membranes. Electron micrograph, lead stained epon section. × 7,500

21 Hamster parotid gland. Micrograph illustrates typical morphology of an interstitial "plasma cell. Nucleus (N); Cisterna (C); Golgi region (G) Electron micrograph, lead stained epon section. × 21,000

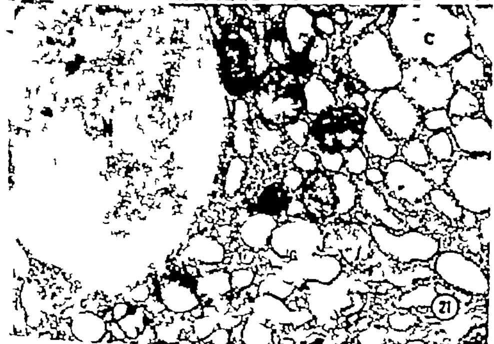

C
N
21

PLATE 9

EXPLANATION OF FIGURES

22 Parotid gland of the antelope squirrel. N is relationship of nerve ending" (at arrow) between two acinar cells. Acinar cells exhibit sparsely distributed granular reticulum and abundant secretion granules (S). Note relationship of "immature secretion granules to Golgi membranes (G). Electron micrograph, lead stained epon section. × 7,000

23 Higher magnification of Golgi region in lower right corner of figure 22. × 16,000.

24 Higher magnification of nerve ending" in figure 22. Note "synaptic vesicles and small mitochondrion. × 32,000.


S
N
N
N
22
23
24

PLATE 10

EXPLANATION OF FIGURES

25 Parotid gland of the antelope squirrel. Acinar cell show smooth membranes which are continuous (at arrows) with the basal plasma membranes. Electron micrograph, lead stained epon section. × 44,000.

26 Parotid gland of the antelope squirrel. Portions of two adjacent cells close to an intercellular canaliculus. Note microvilli projecting into the lumen and desmosome (t arrow) Electron micrograph of lead stained epon section × 40,000.


25
26

Morphological and Histochemical Observations on Trophoblast and Decidua of the Basal Plate of the Human Placenta at Term [1]

G. DALLENBACH-HELLWEG AND G. NETTE
Department of Pathology, Dartmouth Medical School, Hanover New Hampshire

ABSTRACT The trophoblastic cells of the basal plate at the end of pregnancy still have an important hormonal function, in contrast to the decidual cells which appear to exert their main function at the onset of pregnancy. Possibly the decidual cells are functionally replaced by the basal trophoblastic cells, which phagocytize and destroy them. Although both types of cells are structurally quite similar and appear to produce the same hormones but at different times, genetically they are very different. They degenerate morphologically in much the same way but the cause for the retrogressive change for each is distinct. The trophoblastic cells degenerate with reticulin-fibrinoid inclusions which they have mainly phagocytized. The decidual cells perish with collagen inclusions formed from collagen fibers they in turn produced.

The possibility that the placenta might be active endocrinologically was first suggested with Halban's discovery ('05) that a human pregnancy could persist following ovariectomy. Although in the decades following Halban's publication the histology of the placenta was exhaustively studied, morphological identification of placental hormones proved unsuccessful.

During the last few years the morphological study of the placenta has been stimulated by the biochemical demonstration of a group of hormones in the placenta itself or in maternal or cord blood. The greatest attention has been given the trophoblastic layer of the villi with the result that one now is able with fair assurance to localize in the syncytium the presence or formation of steroids (without differentiating between estrogen and progesterone) gonadotropin, and growth hormone. Estrogen and progesterone were most likely demonstrated histochemically (Wislocki and Bennett, 43 Dempsey and Wislocki, 44 Ashbel and Hertig '52). Although the histochemical reactions for ketosteroids are not entirely specific (Karnovsky and Deane, '55) the recent demonstration of steroid 3β-Ol-dehydrogenase in the syncytium by Deane offered further proof for the presence of these steroid hormones. Nevertheless the two hormones are still not specifically identifiable. Estrogen was also detected in the aqueous humor of rabbit eyes in which placental tissue had been transplanted but in which only the syncytium had survived (Stewart, '51); it was found as well in the media of in vitro cultures of syncytium from late pregnancies (De Clerck, '58). Recently gonadotropin was demonstrated immunohistologically in the syncytium (Midgley and Pierce '62) and also in the amnion and in small amounts in the chorionic plate (Thiede and Choate '63). A growth hormone, prolactin like substance was also detected immunohistologically in the syncytium (Sciarra et al., '63). Corticosteroids (Johnson and Haines '52; De Courcy et al. '52) and relaxin (Zarrow et al., '55) were detected biochemically in maternal blood. That ACTH is present in maternal blood was strongly suggested by Jailer and Knowlton ('50).

Which cells of the placenta, because of their fine structures might produce hormones? Fujimura ('21) pointed out that the syncytial and cytotrophoblastic cells, as well as the large and small decidual cells, display the morphological prerequisites for the formation of hormones. Wislocki ('51) was the first to draw attention to the high metabolic activity in respect to protein formation of the basal trophoblastic cells, especially at the end of preg-

[1] This work has been supported by the aid of the United States Public Health Service Grant GM-09473-02.

nancy. Because the abundant RNA in these cells represented a prerequisite for protein synthesis he also suspected gonadotropin was formed in these cells. Ortmann ('55), Bargmann and Knoop ('59) and Weber ('61) again pointed out that the basal trophoblastic cells because of these special features were especially adapted for the synthesis of hormones. Wislocki ('53) and Latta and Beber ('57) demonstrated in the basal trophoblastic cells protein-bound SH-groups which they interpreted as evidence of the formation of ACTH or gonadotropin. Furthermore Thomsen and Willemsen ('59) believed that the PAS positive substances demonstrated in these cells at the end of pregnancy even after diastase digestion might represent a formation of gonadotropin. Since the basal trophoblast of the entire placenta has a volume of about 1.8 cm more than twice the size of the pituitary it may be regarded in respect to its mass as an important endocrine gland (Ortmann '55).

As is evident from table 1, enzymes, lipoids, polysaccharides, RNA and protein-bound SH groups have been localized histochemically in various placental cells. One does not know, however, whether these substances are important for the metabolism of the cells, for the production of hormones or for the fetus. Consequently we have compiled from the world literature on the one hand, the results of studies on the basal plate (see table 1) and on the other hand have attempted to fill in some of the gaps by our own studies (see table 2). In addition to the basal trophoblastic cells, our interests concern the decidual cells as well, for in the basal plate they are often in close relation to the trophoblast.

MATERIALS AND METHODS

We studied 92 human placentae. 22 were obtained from spontaneous deliveries at term, 31 were from Caesarean sections at or near term but mostly prior to the onset of labor, three were from forceps deliveries at term, one from the sixth month, six from the fifth month, 20 from abortions at the second–fourth month and nine from currettements in the first month. The placentae from Caesarean sections performed prior to the onset of labor seemed to us to guarantee the best possible preservation of the morphology of the mature placenta, for under these conditions one would not expect hormones or other active substances needed for the onset of labor or delivery to have been discharged already. A few placentae which were obtained by Caesarean section after the onset of labor served for comparison but are included in the 92 specimens.

The placental material, obtained shortly after delivery or operation and still warm, was cut into blocks 3 mm thick and either fixed in 10% formalin, Carnoy's, Bouin's, San Felice's and basic lead acetate or frozen in a petroleum-ether bath at minus 70 C. Paraffin embedded and frozen sections respectively were made at 4 µ, and histological and histochemical methods carried out (table 2).

The isoelectric points of various cell structures were determined with both methylene blue and orange G at graduated pH's (after Pischinger) and compared with the fluorescence microscopic method with acridine orange (after Schümmelfeder and Stock).

The *histologic staining techniques* performed were: hematoxylin-eosin, Lendrum's phloxine-tartrazin, azan after Heidenhain, kresazan after Romeis' chromalum hematoxylin phloxine after Gomori, Masson's trichrome stain; Pentachrome after Movat, reticulum stain of Gomori, PTAH, fibrin stain of Weigert.

Histochemical reactions: Gomori's aldehyde fuchsin stain; Sudan black B, Luxol fast blue after Pearse, PAS reaction with and without diastase, toluidine blue after fixation in formalin and in 0.4% basic lead acetate; Alcian blue at pH 2.8 and 1.0, Astra blue after Ploch (with 0.5% solution of Astra blue in 2–3% tartaric acid) mucicarmine; Feulgen; gallocyanin-chrome alum, acridine orange at pH 4.8 and 6.0 before and after RNAse digestion (after Schümmelfeder et al. modified by Dallenbach); methyl-green-pyronin according to Taft; and tetrazonium reaction before and after benzoylation and after dinitro-fluoro-benzene, demonstration of SH-groups after Chèvremont and Frédéric, after Rebhun, after Adams (specific for cystin, see Pearse) and after Barrnett and Seligman, the re-

TABLE 1

Compilation of results from the world literature of studies on the cells of the basal plate

	Trophoblastic cells		Large decidual cells		Small decidual cells	
Mitochondria	+	(Wislocki, '51)	−	(Fujimura, '21)	+	(Fujimura, '21; Baker et al., 44)
Nuclear inclusions	+	(Ortmann, '55)				
Alkaline phosphatase	−	(Wislocki, '51; Thomsen, '55; McKay Hertig et al., '58)	(+) −	(Wislocki, '51) (McKay Hertig et al '58)	+	(Thomsen, '55)
Acid phosphatase	− −+ (+)	(Wislocki, '51) (Thomsen, '55) (McKay Hertig et al '58)	+	(Wislocki, Dempsey 48; Thomsen, '55; Strauss, Hiersche '62)		
Esterase	+	(Wislocki, '53; McKay Hertig et al., '58)	−	(Zacks, Wislocki, '53; McKay Hertig et al., '58)	+	(Zacks, Wislocki, '53)
5-Nucleotidase	+	(Thomsen et al., '56; McKay Hertig et al., '58)	−	(Thomsen et al., '56 McKay Hertig et al., '58)		
Succinic dehydrogenase	+	(Wislocki, '53; Ortmann, '55)				
Lipoids	− (+)	(Wislocki, '51) (Thomsen et al., '56)	+ (+) Sudan black B − Baker test − Nile blue + Osmium +− polarized light −	(Fujimura, '21) (Wislocki et al., 49) Ortmann '55		
Glycogen	+	(Driessen, '07; Flesch, '11; Wislocki, '51; McKay Hertig et al., '58; Thomsen, '58)	+	(Baker et al, 44; Ortmann, '55; Wislocki et al., '55; McKay Hertig et al., '58; Brontigh, Traub, '62)	+	(Baker et al., 44)
Diastase resistant polysaccharides	+	(Ortmann, 49; Wislocki, '51; Thomsen et al., '59; Lewin, '60)	−	(Latta, Beber '57)	+	(Wislocki et al 48)
Ribonucleic acids	+	(Dempsey Wislocki, 45; Ortmann, 49; Wislocki, '51; McKay Hertig et al., '58; Weber '61 Bleyl, '62)	(+) −	(McKay Hertig et al., '58) (Dempsey Wislocki, 45)	+	(Wislocki, Dempsey '48)
Protein bound SH groups	+	(Wislocki, '53; Latta, Beber '57)				
Aniline blue granules					+	(Baker et al., 44)

TABLE 2

The results of ar n ogical and histochemical tudies of the basal plate

			Trophoblastic cells			Decidu l cells		
			Protein inclusions	Glycoprotein inclusion	Fibrinoid inclusion	Small decidual cells	X-cells	Collagen inclusions
Lipoids	Neutral f ts lipoproteins	Sudan black B	−	−	−	−	−	−
	Phosphatides	Luxol fast blue	−	−	−	−	−	−
Polysaccharides	Glycogen	PAS	−	+	−	+	−	−
	neutral m co-polysaccharides	PAS after diastase	−	+	−	+	−	−
		metachromasia	−	−	−	−	−	−
	acid muco-polysaccharides	alcia blue at pH 2.0	−	+	(+)	(+)	−	+
		alcian blue at pH 1.0	−	−	−	−	−	+
		mucicarmine	−	−	−	−	−	−
Nucleic acids	DNA	gallocyanin chromalum	−	−	−	−	−	−
		feulgen	−	−	−	−	−	−
		acridine-orange t pH 6.0	+	−	−	−	+	−
	RNA	acridine-orange at pH 4.8	−	−	−	−	−	−
		methylgreen-pyronin	−	−	−	−	−	−
		methylgreen-pyronin after RNase	−	−	−	−	−	−
Proteins	Histidine	tetrazoni m	+	+	(+)	+	+	(+)
		tetrazonium after benzoylation	−	−	(+)	−	(+)	(+)
	Tryptophan arginine, cystine cysteine	tetrazonium after dinitrofluorobenzene	+	+	−	+	+	−
	Fibrin	Weigert	+	−	−	−	+	−
		PTAH	+	−	−	−	+	−
		Ad ms	−	+	(+)	(+)	−	+
	SH groups	B rrnett nd Seligman	(+)	(+)	−	−	(+)	−
		Chèremont Fréderic	−	(+)	−	−	(+)	−
		aldehyde-fuchsin	−	+	−	+	−	−
	IEP	methylene blue	pH 4.6	pH 4.0	4.4–4.6	3.8	4.09	4.8
Histological stains	Azan	Heidenhain	red	blue	blue	blue	red	blue
	Kresazan	Romeis	red	blue-violet	blue	blue- iolet	red	blue
	Trichrome	Masson	red	blue	blue	blue	red	blue
	Pentachrome	Mov t	red	blue-green	light green	blue-green	red	green
	Phloxine-t rtrazin	Lendrum	red	tan	ligh yellow	brown-tan	red	ligh yellow
	Chromhematoxylin-phloxine	Gomori	red	blue-black	li ht grey	brown	red	li ht grey
	Reticulum	Gomori	− black well [illegible]	[illegible]	+	− [illegible]	− [illegible]	+

action for non-specific esterase with -naphthylacetate according to Pearse; and iron reaction with Prussian blue. From time to time we used several different modifications of one histochemical reaction and have tabulated therefore, only that method which seemed to us to be the most suitable for the placenta. At all times sections were stained with appropriate control methods (see Pearse) Besides the original method for toluidine blue sections were left in the 0.1% solution until definite overstaining was evident in order to obtain permanent preparations after rapid dehydration

RESULTS

(1) *Trophoblastic cells*

Even in H. & E. sections one may recognize the trophoblastic *cells in the basal* plate by their dense basophilic granular cytoplasm and by their large nuclei. In general, these cells are round; only where they penetrate the decidua are they chiefly spindle-shaped, with rather long processes, none of which appear to communicate with one another With the reticulum stain the trophoblastic cells may be especially well differentiated from the decidual cells occasionally crowded about them Whereas each individual decidual cell is enveloped by reticulum fibers the trophoblastic cells lie free in the ground substance. This difference was also observed by Wislocki and Bennett (43) In addition, with the azan stain the trophoblastic cells may be readily recognized by their granular dark brown cytoplasm in contrast, the cytoplasm of the decidual cells is bright gray

The *nucleus* of the trophobalstic cell is outlined by an irregularly wavy membrane. Besides coarser clumps of chromatin, the nucleus contains 1–2 prominent nucleoli, which react positively with methods for RNA (bright red with methyl green-pyronin, orange-red with acridine orange from pH 3 4 to 8 0 negative after RNAse digestion at pH 4.8 and 6.0) The majority of the nucleoli abut against the nuclear membrane. At times they may even protrude into the cytoplasm without a recognizable nuclear membrane intervening, as if they were being extruded from the nucleus. There are furthermore rounded structures within occasional nuclei which closely resemble large nucleoli, but which fail to stain for RNA. We refer to them as nuclear inclusions. They may become so large that they occupy most of the nucleus (fig 3A) In rare nuclei, vacuoles may be identified, some of which contain a small inclusion.

The *cytoplasm* of most of the trophoblastic cells is especially rich in RNA appearing from coarse to finely granular Occasionally this RNA is accumulated in the periphery of the cell, but at other times it is concentrated in the paranuclear region Consequently these cells are strongly *basophilic*. Their cytoplasm also contains diffusely scattered esterase-positive particles (fig 1) In addition, a large proportion of these cells contains numerous vacuoles, distributed like a string of beads at the periphery of the cytoplasm. Among this type of trophoblastic cells in the basal plate there are occasional groups of other rounded cells with less cytoplasm which appears optically empty by the usual histological stains (fig. 2A) This *clear cell* type of trophoblastic cell resembles most closely the young cytotrophoblastic cells of the cell columns at the beginning of pregnancy With special stains these clear cells contain abundant dense homogeneous substances in droplet form that are PAS-positive, digestible with diastase, alcian blue-negative and non-metachromatic thus representing glycogen (see fig 2B)

If further special stains are employed, one may recognize in the *basophilic trophoblastic cells* several different types of *cytoplasmic inclusions*

(a) The most prominent inclusions are homogeneous, intensely refractive round intracytoplasmic particles, mostly of the approximate size of a nucleolus (fig 3C) but sometimes as large as the nucleus (fig 3B) Their histochemical and staining reactions are compiled in table 2. It is evident therefrom, that the inclusions are strongly acidophilic and, in the absence of lipoids and polysaccharides consist of proteins apparently without a prosthetic group. With the reticulum stain these pure *protein inclusions* are enclosed by a thin black shell Some of them are located in vacuoles, as if they were becoming liquefied or being formed. Others are situated in the paranuclear region among the RNA gran-

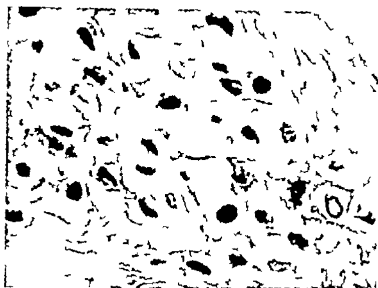


Fig. 1 Term placenta of spontaneous delivery. Esterase positive granules in the trophoblastic cells of the basal plate. Esterase reaction. Magnification × 615.

ules and still others are distributed randomly throughout the cytoplasm. Some of the nuclear inclusions described above (fig. 3A) give the same staining reactions (for more detail see Dallenbach-Hellweg and Nette ('63a).

These pure protein inclusions must be differentiated from indistinct, finely granular intracytoplasmic particles which are found in some basophilic trophoblastic ells and which may be detected only with e reactions for *fibrin*. These particles re most frequently observed near large akes of fibrin whereas in the fibrin-deficient regions they are absent. In contrast to the protein inclusions the fibrin particles are strongly positive for SH groups with the method of Chèvremont Frédéric.

(b) Following diastase digestion some of the basophilic trophoblastic cells are found to contain round or angular PAS positive basophilic inclusions which are also Alcian blue positive at pH 2.6 negative at pH 1.8 and non-metachromatic. In addition the react positively w tetrazonium a th the method SH groups (2) In the a of metachro e positive reac th aldehyde f ven without o n cannot be -groups in a polysaccha refore it y lain esence of S phil Scott and

Hence histochemically these inclusions seem to consist of glycoproteins containing a neutral mucopolysaccharide and a basophilic protein the latter being responsible for the low isoelectric point. These *glycoprotein inclusions* are generally smaller and more frequent within a cell than the pure protein inclusions (fig. 4). They lie often within vacuoles, parasclear or diffusely scattered in the cytoplasm and some may even be in the nucleus (for detail see Dallenbach-Hellweg and Nette ('63b).

The glycoprotein inclusions are to be differentiated from irregularly crenated particles which may be randomly dispersed throughout the cytoplasm of occasional basophilic trophoblastic cells. These latter particles even the smallest, are distinctly impregnated with the methods for *reticulum* and some also stain blue with the azan and Masson trichrome methods. Since however the silver stains have not been proven to be specific for reticulum, we are cautious in interpreting their true nature. In contrast to the glycoprotein inclusions they are never seen within vacuoles.

(c) In some basophilic trophoblastic cells on may distinguish deep invaginations of cell membrane into the cytoplasm e of these indentations may be so l at they almost replace the

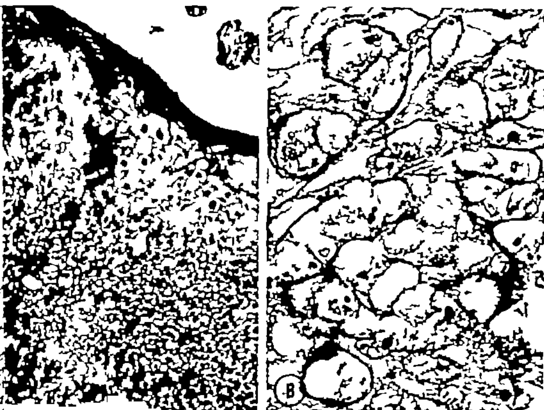


Figure 2

A Cross section through basal plate of term placenta of forceps delivery. At upper right intervillous space; at upper half basophilic trophoblastic cells; at lower half the "clear" trophoblastic cells. Phloxin-Tartrazin stain. Magnification × 132.

B "Clear" trophoblastic cells with intracytoplasmic PAS positive droplets. PAS stain. Magnification × 640.

trophoblastic cell, hence the cell, appearing as a ghost, can be identified as such only by its outline. These invaginations may contain variable amounts of fragmented reticulum fibers in a "fibrinoid" ground substance. Thus, in tangential sections they may be confused with the intracytoplasmic "reticulum inclusions" mentioned above. One is able, however, to differentiate the *fibrinoid" inclusions* by their membrane-like outline representing the indented membrane of the cell. These invaginations are generally broad-based, or they communicate by a narrow stalk of ground substance with that surrounding the cell (fig. 5A). Although the ground substance consists chiefly of fibrinoid, it contains as well fine fragments of destroyed reticulum fibers and in contrast to fibrinoid in other parts of the body it stains like collagen. These fibrinoid" inclusions, indeed, resemble closely the collagen inclusions of the decidual cells (Hamperl, '58; Dallenbach-Hellweg, '61). These two types of inclusions may be differentiated from each other, however, by noting the type of cells in which they are located — whether trophoblastic or decidual.

Occurrence of the inclusions. Of interest is the fact that the pure protein inclusions in the trophoblastic cells are found almost exclusively in those placentae which are obtained by elective Caesarian section prior to the onset of labor. In contrast, the placentae of the Caesarian sections carried out after several hours of labor, and those of the spontaneous de-

ions of the basal trophoblastic cells are synthesized in the cell, most likely in the paranuclear region of the endoplasmic reticulum where the smallest inclusions can always be found. Since some are located in vacuoles they may very well be secreted from the cell by means of liquefaction processes. From all the results discussed it seems sensible to regard the intracytoplasmic and intranuclear pure protein and glycoprotein inclusions as the morphological representation of hormones that is, the inclusion could be the hormone itself, or be a nonspecific carrier substance.

Since the pure *protein inclusions* occur or are formed in the mature placenta shortly before the inception of labor as shown by the studies of placentas obtained by elective Caesarian section but cannot be demonstrated in the placentas delivered following spontaneous labor these inclusions apparently are discharged during the few hours of labor Therefore logically one searches for an analogue for a similar rapidly disappearing hormone biochemically detectable in the placental blood. *Relaxin* is the only hormone which fulfills all of these conditions Its chemical structure corresponds significantly with the histochemical results already discussed. We (F Dallenbach and G. Dallenbach-Hellweg) have carried out immunohistological studies with fluoresceein-labeled rabbit-anti-relaxin serum using the Coons-Kaplan technique. We were able to show that the pure protein inclusions of the basophilic trophoblastic cells and the granules of the *endometrial granulocytes* of the early decidua react positively with the antisera, while all the controls were negative. Hence we believe that these inclusions do represent relaxin or its carrier substance (for detail see Dallenbach and Dallenbach-Hellweg '63) This observation appears to confirm the hypothesis that the same hormone can be found and probably synthesized in different cells and at different times.

One might, in addition, propose as so many authors before us have assumed, that the *glycoprotein granules* in the basophilic trophoblastic cells represent remnants of *gonadotropin* Their location is identical with the immunohistological localization of gonadotropin in the syncytium by Midgley and Pierce and in syncytium and amnion by Thiede and Choate One might assume furthermore that the granules of the *small decidual cells* which also contain glycoproteins, represent gonadotropin as well a non-specific glycoprotein here, however would have to be excluded. The possibility still remains, that these small decidual cells actually represent trophoblastic cells which have migrated into the decidua. The reticulum fibers enveloping them, however support the contention that they are of decidual origin These cells could very well be of the same kind as the small decidual cells mentioned by Wislocki and Dempsey ('48). In contrast, we believe that Fujimura ('21) and Baker et al. (44) have seen the endometrial granulocytes for they described small decidual cells with pyknotic nuclei, numerous mitochondria, and acid-fuchsin stainable granules in the nuclear indentations.

In all likelihood the large decidual cells have no important hormonal function at the end of pregnancy Our results agree with those mentioned (Fujimura '21 Baker et al., 44 Ortmann, '55 McKay et al., '58 Thomsen '59 Wislocki and Padykula '61) Whether the glycogen substances in the *clear trophoblastic cells* represent true products of cellular synthesis or are only those of storage is difficult to decide The clear cells are poorer in RNA than the remaining trophoblastic cells, but show prominent nucleoli and disclose no degenerative changes. One may assume that they have maintained not only the structure of the young cytotrophoblast of the cell columns, from which the trophoblastic cells of the basal plate are thought to be developed (Wislocki and Padykula) but have retained as well their original content of glycogen. On the other hand the *basophilic trophoblastic* cells, which are occasionally multinucleated might very well be derived from or have a close relation to the syncytial cells of the villi which invade the decidua to form the basal plate. The syncytial cells of the villi and the basophilic trophoblastic cells of the basal plate apparently represent differentiated cells of the trophoblast capable of producing hormones.

The *fibrinoid"* *inclusions* apparently represent the onset of degeneration of trophoblastic cells The complete destruction of these cells, like that of the decidual cells caused by the collagen inclusions can be similarly followed step by step If we look for an explanation for the formation of the fibrinoid inclusions two processes appear to be significant: (1) it seems logical to assume that the trophoblastic cells on invasion of the decidual tissues phagocytize the remnants of the fragmented reticulum fibers (see also Hertig and Rock, 41; Hertig et al '58) It would then be conceivable that in aging trophoblastic cells this debris of reticulum and fibrinoid" substance piles up gradually until excessive accumulation causes the cell to degenerate slowly (2) In addition there seems to be another process that plays a role. In this a collapse is passively induced in some of the aging trophoblastic cells by the encroachment of the fibrinoid ground substance against the cell to form invaginations which eventually compress the cell. The degeneration of the basal trophoblastic cells appears to be enhanced by either or both of these two processes although it should be pointed out that only very few trophoblastic cells at term have undergone marked degeneration. On the contrary most are as we ave shown above highly active at the ! of pregnancy

The *collagen inclusions* of the decidual cells appearing so similar to the fibrinoid inclusions of the trophoblastic cells develop without doubt by another means (see Wessel '59 Dallenbach-Hellweg '61) especially since the decidual cells are capable of producing collagen fibers and are imbedded in an intact collagen-reticulum ground substance

CONCLUSIONS

At the end of pregnancy the trophoblastic cells of the basal plate are still highly active in protein synthesis. Their nuclei contain prominent nucleoli and occasionally inclusions and vacuoles. Their basophilic cytoplasm is very rich in RNA in protein-bound SH groups in different enzymes and in peripherally located vacuoles With special stains one may recognize different types of cytoplasm inclusions (1) intensely refractive round pure protein inclusions (2) diastase resistant PAS positive particles (glycoproteins) and (3) fibrinoid inclusions. Groups of "clear cell" trophoblastic cells containing glycogen may be differentiated from the more numerous basophilic trophoblastic cells in the basal plate

The decidual cells at term appear inactive Only occasional glycogen granules are found within them, but many contain collagen inclusions Amongst these ! decidual cells there are a few granulocytes with protein granules, and small cells with PAS positive granules resistant to diastase (glycoproteins). T pure protein inclusions of the basophilic trophoblastic cells undoubtedly are formed within the cell. These inclusions as well as the granules of the endometrial granulocytes, have been shown by immunohistological studies to represent relaxin The glycoprotein inclusions in the basophilic trophoblastic cells may be related to the formation of gonadotropin. This might possibly hold true also for the glycoprotein granules of the small decidual cells. The clear trophoblastic cells may be remnants of the cytotrophoblastic cells of the cell columns, while the basophilic trophoblastic cells appear to be closely related to the syncytial cells of the chorionic villi. Hence the basal plate at term apparently contains endocrinologically active derivatives of the syncytiotrophoblast namely the basophilic trophoblastic cells as well as derivatives of the cytotrophoblast namely the clear trophoblastic cells. The fibrinoid inclusions in the trophoblastic cells and the analogous collagen inclusions in the decidual cells are regarded as indicating regressive processes.

ACKNOWLEDGMENT

We gratefully acknowledge the helpful criticisms suggestions and careful review of this manuscript given us by Professor Dr A T Hertig We wish to express our appreciation and thanks to Dr Hans Jürgen Brähler and Miss Dorothea Da for their invaluable help

LITERATURE CITED

Altmann, H W 1949 Über die Abgabe [illegible] Kernstoffen in das Protoplasma der menschlichen Leberzellen. Z. Naturforsch 4b [illegible]

——— 1955 Zur Morphologie der Wechselwirkung von Kern und Zytoplasma. Klin. Wschr 33: 306–314.

Ashbel, R., and A. T Hertig 1952 Histochemical demonstration of ketosteroids in normal, abnormal and neoplastic placenta. J N t. Canc. Inst., 13 221 222.

Baker, B. L., S. J Hook and A. E. Severinghaus 1944 The cytological structure of the human chorionic villus and decidua parietalis. Am. J Anat 74 291–325.

Bargmann, W 1955 Die funktionelle Morphologie der Hormonbildungsstätten. Klin. Wschr 33. 323–328.

Bargmann, W and A. Knoop 1959 Elektronenmikroskopische Untersuchungen an Plazentarzotten des Menschen. Zeitschr f Zellforsch., 50 472–493.

Barnett, R J 1958 Some aspects of protein histochemistry with special reference to protein hormones. In S L. Palay Frontiers of Cytology Yale University Press, New Haven, p 264.

Barnett, R. J and A. M. Seligman 1952 Histochemical demonstration of protein-bound sulfhydryl groups. Science, 116 323–327

Beyl, U. 1962 Fluoreszenzmikroskopische Untersuchungen an überlebenden menschlichen Plazenten mit Acridinorange. Zeitschr f. Zellforsch 56 404–424

Cottier H. 1961 Cytologische Aspekte der Plasmaprotein-synthese. Bull. Schweiz. Akad. Med. Wiss., 17 50–60.

Dallenbach, F D Personal communication.

Dallenbach, F D., and G. Dallenbach-Hellweg 1964 Immunohistologische U tersuchungen zur Lokalisierung des Relaxins in menschlicher Plazenta und Decidua. Virch. Arch. path. Anat 337 301–316.

Dallenbach Hellweg, G. 1961 Über die Ruckbildung von Deciduazellen unter Auftreten von Kollagenstoschlüssen. Virch. Arch. path. Anat., 334 196–205.

Dallenbach Hellweg, G and G. Nette 1963a Über Proteineinschlüsse in basalen Trophoblastzellen der reifen menschlichen Plazenta. Virch. Arch path. Anat., 336 536–543

——— 1963b Über Glykoproteideinschlüsse in Trophoblastzellen der menschlichen Plazenta und die Frage ihres Zusammenhangs mit der Bildung von Gonadotropin. Zeitschr f Zellforsch 61 145–158

Deane H 1963 Sites of steroid hormone production in the trophoblast of man and rat. Proc 2nd Rochester Trophoblast Conference Nov 4–5, 1963.

DeClerck, P 1958 Sécrétion d'oestrogènes par le syncytiotrophoblaste humain en culture In Snoeck, J Le placenta humain, Masson et Cie., Paris. 515–529

DeCourcy C., Ch Gray and J B Lunnon 1952 Adrenal cortical hormone in human placenta. Nature, 170 494

Dempsey E. W and G. B. Wislocki 1944 Observations on some histochemical reactions in the human placenta with special reference to the significance of the lipoids glycogen and iron. Endocrinol., 35 409–429

——— 1945 Histochemical reactions associ ted with basophilia and acidophilia in the placenta and pituitary gland. Am. J Anat., 76 277–301.

Driessen, L. F 1907 Über Glykogen in der Plazenta. Arch. f Gynäk., 82: 278–301

Flesch, K. 1911 Glykogen in der menschlichen Plazenta. Monatsschr f Geburtsh. u. Gynak., 34 21–34

Fuhrmann, K. 1963 Histochemische Untersuchungen über Hydroxysteroid Dehydrogenase Aktivität in Nebennieren und Eierstöcken von Ratten und Kaninchen. Arch. f Gynak., 197 583–600

F jimura, G. 1921 Cytological studies on the internal secretory functions in the human placenta and decidua. J Morph., 35 485–580

Glick, D 1949 Techniques of Histo- and Cytochemistry Interscience Publishers, New York, London.

Gropp, A., and K. Hupe 1958 Zytologische Beobachtungen am Zellkern und der Kern-membran in Gewebekulturen. Verh. deutsch. Ges. P th., 268–274

Halban, J 1905 Die innere Sekretion von Ovarium und Placenta und ihre Bedeutung für die Funktion der Milchdrüse. Arch. f. Gynak 75 353–441

Halmi N S. 1952 Differentiation of two types of basophils in the denohypophysis of the rat and the mouse. Stain technol., 27 61–64

Hamperl, H. 1954 Über endometriale Granulocyten (endometriale Körnchenzellen) Klin. Wschr 32: 665–668.

——— 1958 Über Kollageneinschlüsse in Deciduazellen. Klin. Wschr 36 939–940.

Hellweg, G. 1957 Über Auftreten und Verhalten der endometrialen Kornchenzellen im Verla f der Schwangerschaft, im krankhaft veränderten Endometrium und berhalb des Corpus teri Virch. Arch. path. Anat., 330 658–680.

——— 1954 Über endometriale Körnchenzellen Arch. f Gynäk., 185 150–186.

Hertig, A. T and J Rock 1941 Two human ova of the previllou stage having an ovulation age of about 11 and 12 days respectively Contrib. Embryol 29 127–156

Hertig, A. T E. C. Adams, D G M Kay J Rock W J Mulligan and M. F Menkin 1958 A thirteen-day human ovum studied histochemically Am. J Obst. Gynec., 76 1025–1043.

Jailer J W and A. L Knowlton 1950 Stimulated adreno-cortical activity during pregnancy in an addisonian woman. J Clin. Invest 29 1430–1436

Johnson, R H., and W G. Haines 1952 Evidence of small amount of adrenal cortex hormone activity in human placenta. Science, 116 456–457

Karnovsky M. L., and H. W Deane 1955 Aldehyde formation in the lipide droplet of the adrenal cortex during fixation as demonstrated chemically and histochemically J Histochem Cytochem., 3 85–102

Latta J S and Ch R Beber 1957 The differ ntiation f a special form of tropholla t in tl hum n placenta Am J Obst Gyn 74: 105–110

Lendrum A C 1947 The Phloxine-Tartrazin method as general h tologic l stain an l for the demonstration of inclusion bodies J Path Bact 59: 399–401

Lewin I 1960 Histochemische Untersuch ungen n Plaze tten von Extraut eingravidität n Gynaecologia 149 184 192.

McKay D G A T Hertig I C A l ms an l M V Ri l ardson 1958 Histochemical obser v tion on the h man plac nta Obstetr and Gynec 12 1 30

Midgley A R nd G B Pierce 1962 Immuno-hi tochemical localiz tion f h m n chorio le gon dotropi J Exp Med 115 289 294

Movat H Z 1955 Demonstration of all con nectiv tissue element in a single section Arch f Pathol 60 289 295

Ortmann R 1949 Über K rnsekretion Kolloid und V uolenbildu ng in Beziehung z m Nu cleinsäuregehalt in Trophobl stkernen H n der menschlichen Plazenta Zeitschr f Zellf rsch 34 562–581

——— 1955 Hi tochemisel Untersuchungen i me schlicher Pl zen t mit besonderer Berü ksicl tigu g l Kernkugeln (K rneinsch lüsse) und ler Pl sm lipoi leinschlüsse Zelt schr f A t Entwickl gesel 119 28–54

Pearse A G E 1955 C pper phthalocy nins a phospl olipid tains J Path and B ct 70 554–557

——— 1961 Histochemistry theoretic l and applied Little Brow & Co Boston

Petry G 1962 Die Morphologi ler äusser! H der Placent best hender fet m ternen K in t kte Arc! f Gy äk 198 74 81

Pioch W 1957 Über lie Darstellung sa rer M opolysa h ride mit der K pferphthalo y Inf rbstoff Ast ld Virch Arcl path An t 330 337 340

Pischinger A 1926 Di Lage les isoel ktrischen Punktes histologische Elemente l Grundlage il re verschiedenen Färbbark it Zeitschr f Zellforsch l 3 169 197

Romeis B 1948 Mik oskopisel Tech ik Leibnitz München

Schümmelfeder N 1950 Die Fluor hromierung des lebenden überl benden und toten Proto pl sm s mit dem basische F rbstoff A ridinor range und ihre Bezieh g Stoffwechsel k tivität der Zelle Virel Arcl path A t 318 119 154

Schümmelfede N K J Ebsch ner and E Krogh 1957 Die Grundl ge der diff renti Fluoro chromierung von Ribo nd Desoxy ibon kle i säure mit Acridinora ge N turwi 44 467–468

Schümmelfeder N nd F P Stock 1956 Die Bestimmung des Uml deberei hes (isoelek trischer Punkt) von Gewebeleme t mit dem Fluorochrom Acridinora ge Zeitschr f Zell forsch 44 327–338

Scott H R and B P Clayton 1953 A com parison of the st ining affinities of aldehyde-fuchsi n and the Schiff reagent J Histochem Cytochem 1: 336 340.

Sci ra J J S I Kaplan and M M Grumbach 1963 Loc lization f anti h um n growth hor mone serum within the h m n placenta: Evi dence for a human chorionic growth hormone-Prol ctin Nature 199 1005 1006.

Stew rt H L 1951 Hormone secr tion by human pl c nta grown i ye of rabbit Am J Obst Gynec 61: 990 1000

Str u s G nd H D Hirsch 1962 Untersu hungen zur Problematik ler histochemischen Fermentlok li tion i der Pla enta Arch f Gynäk 198 187 199

Szontágh F E and A Tra l 1962 Zur Histo chemie de Trophobl sten Z Geburt h Gynäk 159: 68 76.

Thiede H A and J W Choat 1963 Chorionic gonadotropin locali tion i the human pl cent by immu ofluorescent st ini g Obste trics and Gynecology 22: 433–443

Thomsen K 1955 Über die Aktivität der alkalischen Ph sph tase in d r menschlichen Pl zenta Ar h f Gynäk 187: 1 19

——— 1955 Histochemisch Untersuchungen über lie sau e Ph sphat se in der mensch lichen Plazent Arch f Gynäk 187: 264 281

——— 1958 Studien zur Histochemie der Pla zenta Gebu t h u Fr uenheilk 18 851 300

Thomsen K and Ch L ar zen 1956 Untersu hungen über die Lok lis tion succinoxydin Substr ts n ler mensc hlichen Pl zenta Arch f Gynäk 187: 462–477

Thomsen K a l R P ka 1956 Über die Aktivität der Nucleoti ase in der men chlichen Pl zent Arch f Gynäk 188 97 111

Thomsen K and R Willemsen 1957 Histo chemische Unter s gen über die P sph tomonest der Chorionepithelien Arch endocrinol 30 161 174

Weber J 1961 Th it of production gonadotropi in in the placent at term Act obst et gynec Sc nd 40 139 161

W sel W 1959 Die menschlichen Deciduazellen u l ihre Kollagenfeinstruktur im Elektronenmikroskop Vir l Arch path Anat 332 224 275

Wislocki G B 1951 The histology and cytochemistry of th basal pl t nd septa placentae in th norm l placent delivered at f ll term Anat Rec 109 359

——— 1953 Succinic dehydrogenase reaction nd protei bound sulfhydryl groups in human placenta Anat Rec 115 380–381

Wislocki G B and H B Bennett 1943 The histology and cytology of the human nd monkey plac nt with special reference to the trophobl st Am J Anat 73 335–449

Wislocki G B and E W Dempsey 1955 The chemic l histology of the human placenta or decidu with reference to mucopolysaccharides glycogen lipids and acid phosphatase Am J Anat 83 1–41

——— 1965 Electron microscopy of the human placenta. Anat. Rec., 123 133–149

Wislocki, G. B., and H. A. Padykula 1961 Histochemistry and electron microscopy of the placenta In: W. C. Young Sex and Internal Secretions, Williams & Wilkins Co., Baltimore, 883–957

Zacks, S. L., and G. B. Wislocki 1953 Placental esterases. Proc. Soc. Exp. Biol. Med. 84 438–441

Zarrow M., E. Holmstrom and H. Salhanick 1955 The concentration of relaxin in the blood serum and other tissues of women during pregnancy J. Clin. Endocr. and Metab., 15 22–27

PLATE 1

EXPLANATION OF FIGURES

3A Large nuclear inclusion in basophilic trophoblastic cell of placenta from elective Caesarian section at thirty-sixth week. Phloxine-Tartrazin stain. Magnification × 1,200. (From Dallenbach-Hellweg and Nette, '63a.)

3B Large protein inclusion in basophilic trophoblastic cell of basal plate of placenta from elective Caesarian section at thirty-ninth week. Phloxine-Tartrazin stain. Magnification × 1,500.

3C Prominent nucleoli and numerous cytoplasmic protein inclusions of the trophoblastic cells of the basal plate of term placenta from elective Caesarian section. Azan stain. M gnification × 830

3D Placenta from elective Caesarian section at 37 weeks gestation. In the middle between large cells of the basal plate an endometrial granulocyte. Phloxin-Tartrazin stain. Magnification × 675.

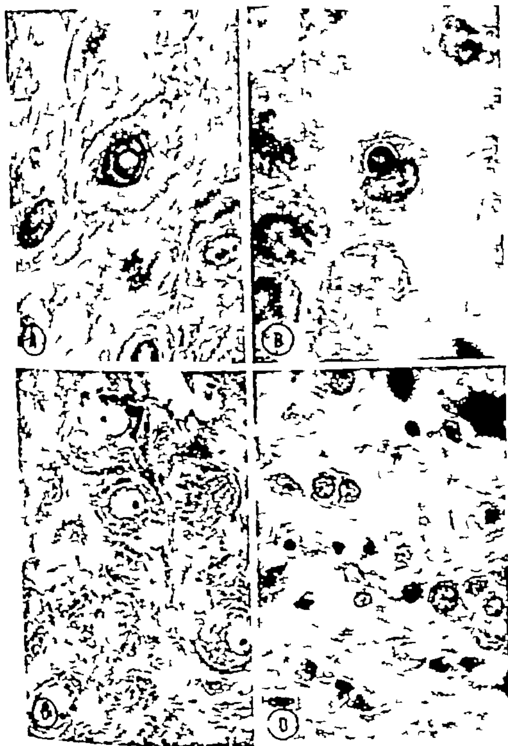

A
B
C
D

PLATE 2

EXPLANATION OF FIGURES

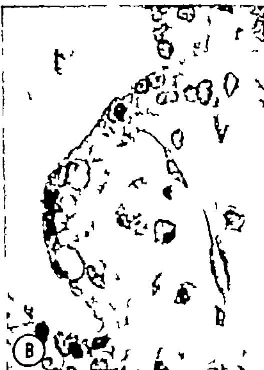
4A Numerous glycoprotein inclusions (black) in basophilic trophoblastic cells of the basal plate of term placenta following spontaneous delivery Aldehyde-fuchsin stain. Magnification × 600

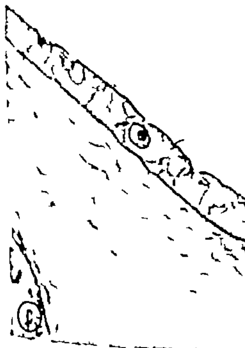
4B Nine weeks old placenta. Infranuclear vacuoles with glycoprotein particles in the syncytial layer of chorionic villus. Alcian blue stain (only faintly visible in black and white reproduction) Magnification × 715.

4C Amnion of a term placenta of spontaneous birth. Vacuole containing glycoprotein inclusions within the epithelial layer PAS stain after Diastase digestion. Magnification × 745. (From Dallenbach-Hellweg and Nette, '63b.)

4D Term placenta. Small decidual cells showing intracytoplasmic PAS positive granules amidst large decidual cells and remnants of degenerated cells. PAS stain after diastase digestion. Magnification × 640.


A


B


C


D





5A Trophoblastic cell of basal plate showing fibrinoid inclusion and stalk, both surrounded by cell membrane. Term placenta from elective Caesarian section. Azan stain. Magnification × 1,600

5B Collagen inclusion surrounded by cell membrane in a decidual cell of the basal plate of five months old placenta. Masson trichrome stain. Magnification × 1,600.

Placentation in the Spotted Hyena (*Crocuta crocuta* Erxleben) With Particular Reference to the Circulation [1]

RALPH M. WYNN AND E. C. AMOROSO

Department of Obstetrics and Gynecology State University of New York, Downstate Medical Center Brooklyn, New York, and the Royal Veterinary College University of London, England

ABSTRACT A study of the placenta of the spotted hyena (*Crocuta crocuta* Erxleben) based on five specimens from early in the second third of pregnancy to full term, is presented. Resembling the dog and cat in the retention to term of large allantois and medium-sized yolk sac, the hyena is unique among Carnivora in the possession of hemochorial villous placenta, allied structurally more to that of New World monkeys than to the other carnivores. The intimacy of the fetal and maternal circulations is further increased by so-called intraepithelial capillaries in the syncytial trophoblast. The hyena, unlike most carnivores, possesses no central hematoma or marginal deposit of pigment, and lacks specialized structures in the chorionic membrane. The cytotrophoblast, however, does undergo modifications associated with phagocytosis of histotrophe in the paraplacental regions and in the junctional zone of the placenta proper

The principal mode of entry of maternal blood is directly into the subchorial zone, into which uterine arteries, carried up in crescent of gestational endometrial tissue at the margin of the placenta, empty Smaller arteries reach the subchorial zone in maternal septa that traverse the entire trophoblastic zone. Major arteries do not discharge blood at the base of the placenta, but basal drainage constitutes the sole means of return of blood to the uterine veins. The phylogenetic significance of the morphogenesis and vasculature of the placenta of *Crocuta* is discussed.

Despite the common occurrence of the spotted hyena in the Old World tropics and the unrestricted hunting of the species permitted by the African authorities, a comprehensive account of the development and detailed structure of the placenta has hitherto been unavailable The classical description by Matthews ('39) of the reproductive tract of *Crocuta crocuta* gives no information regarding placentation, and the more recent report by Morton ('57) is an account of the placenta and membranes based on a single, full-term specimen. The remaining information on this subject is confined to a brief note by Matthews ('54) and to the observations of Amoroso ('55 '59a, '59b '60 '61) which stimulated the present investigation.

Interest in the placenta of the spotted hyena derives from two principal sources. Firstly the histological differences between the placentation of this genus and that of the carnivores in general present an interesting basis for reconsidering the phylogenetic significance of the features of placental structure to which Mossman ('37) drew attention. Secondly the intraplacental vascular relationships in *Crocuta* represent a striking example of perfection in countercurrent flow the significance of which was first pointed out by Mossman ('28) In the present investigation, a morphogenetic approach is presented with particular emphasis placed on the maternal circulation and its relationship to that in man and the other Primates.

MATERIALS AND METHODS

The present study is based on the placentas and accessory organs of five hyenas ranging in gestational age from early in the second third of pregnancy to full term. In order of increasing age the specimens are designated S/1 W/2, G81/3 G100/4 and L/5 respectively The most recent specimen hyena W/2, consists of the complete uterus and adnexa of an animal estimated as being in mid-pregnancy or about 55 days from term based on the average length of gestation of 110 days, as

[1] This work was supported in part by a USPHS research grant, RG-4434, from the National Institutes of Health.

quoted by Matthews ('39) both the sterile cornu and the one containing the fetus were opened as was the abdomen of the fetus to allow more adequate penetration of the fixative, but relationships of fetus to placenta and membranes and of placenta to uterus remained intact. The specimen was received in good condition in 10% neutral formalin The pregnant animal was shot in Kenya and the specimen flown to London through the courtesy of Dr A. M. Harthoorn of the Faculty of Veterinary Science of the Royal College at Nairobi The remaining four specimens were received in formalin from Tanganyika through the courtesy of Dr L. Harrison Matthews F R. S of the London Zoological Society The specimen designated Hyena S/1 is estimated as early in the second third of pregnancy or about 45 days gestational age it consisted of a uterus with intact placenta and membranes from which the fetus had been removed. Specimens G81/3 and G100/4 consisted of uteri containing intact placentas and membranes of animals estimated as 85 and 95 days pregnant, respectively the fetuses had been removed prior to arrival in the laboratory The largest specimen, Hyena L/5 consisted of e bisected uterus with term-sized fetus situ

Observations and drawings of the gross anatomy were made prior to cutting the specimens. Slices through the five placentas and of the uteri of Hyena S/1 and W/2 and the uterine adnexa of W/2 were transferred to 70% 90% and 100% ethanol. Membrane relationships were preserved by immersion in 1% celloidin hardening in 15% chloroform in ethanol, and clearing in cedarwood oil. The placental segments were embedded in paraffin and cut through in their entirety at either 5 µ or 7 µ. Most sections were stained with Harris hematoxylin and eosin the remainder were stained with the periodic acid-Schiff reagent Turnbull's or Prussian blue, or the Mallory Masson or Wilder reticulum method. Significant histological details, as revealed by ht microscopy were subjected to blac h e and color photomicrography From pe men W 2 somewhat better preserv h n th others thin sections were cut at 2 µ stained with Azure II and studied under oil. Thin sections of tissue from this animal were prepared for electron microscopy by embedding in araldite certain sections were prepared from material than had been fixed in formalin alone others were made from tissue that had been postfixed with osmic acid for two hours. All sections were treated with lead hydroxide.

OBSERVATIONS

Gross anatomy of the uterus and conceptus Specimen S/1 consisted of an opened uterus containing a placenta with membranes in one horn, and an apparently nonpregnant horn. The fetus had been removed but a fold of allantois was found overlying the cavity The yolk sac was readily identified between the amnion and the allantochorion. The placental band formed an incomplete annulus, measuring 16 cm in length 5.3 cm in its greatest width and 0.8–1.2 cm in thickness.

Specimen G81/3 comprised an opened uterus with placenta and membranes intact within the pregnant horn. The placenta formed a bilobed incomplete annulus measuring 20.0 cm in total length. The lobes were almost equal in size measuring 9.5 × 5 0 × 1 0–1.2 cm and 10.5 × 5.5 × 1 0–1.2 cm respectively The yolk sac was identified between allantois and amnion extending along the paraplacental chorion.

Specimen G100/4 consisted of a uterus with one pregnant and one nonpregnant cornu. The gravid horn contained a placental band comprising a trilobed incomplete annulus. The total length of the band was 21 5 cm and the average width 6 6 cm The largest lobe measured 8.5 × 7.0 × 1.5 cm and the smallest, 3.2 × 5 × 1.2 cm The intermediate lobe itself divided by a fairly deep central sulcus measured 4.2 × 8.0 × 1 4 cm. A gap of 4.2 cm. over which the endometrium was lined only by paraplacental chorion, separated the two ends of the placental annulus.

Specimen L/5 consisted of a bisected uterus containing a full-term fetus, attached by its umbilical cord to a trilobed central placental annulus. The largest lobe measured 11.0 × 10 0 the smallest was 4 0 cm long and 5.5 cm in average width

and the intermediate lobe measured 10 0 × 5 5 cm. Including a paraplacental gap of 11.0 cm, the total length of the annulus was 38.0 cm. The thickness of the pla cental band varied from 1 0–1 4 cm. In this placenta, as well as in the three previously described, each lobe received branches of both umbilical arteries and was drained by tributaries of both umbili cal veins. The fetus of Hyena L/5 measured 290 mm from crown to rump The umbilical cord was quite short, measuring only 5.0 cm in length.

Hyena W/2 (figs. 1 and 2) the most recent and complete specimen, consisted of a dorsoventrally flattened gravid uterus with its adnexa and a cuff of vagina. The two uterine cornua joined almost at right angles to form the short corpus uteri which was partially divided internally by a me- dian longitudinal septum, the cornual lu- mina remaining separate almost to the cer vical os. The ovaries were relatively smooth and white. A large corpus luteum on the left measured 2.0 cm in its greatest diam- eter doubling the size of the ovary whereby a smaller corpus luteum on the right measured 1.2 cm in largest diameter The ovaries lay in bursae (fig. 5) the walls of which were well padded with fat, and in which natural slit-like openings cm in length were found. The oviducts measured 12 cm in length, each consisting of a fimbriated extremity infundibulum, ampulla and isthmus.

Each uterine cornu had been opened, as had the abdomen of the fetus contained in the left side. The endometrium of the nonpregnant right horn was deeply folded. Since the gestation sac on the left had been previously entered to facilitate pres- ervation of the fetal tissues no observa- tions of the amniotic or allantoic fluids were possible. The fetus (fig. 4) measur ing 152 mm CR, was attached by the 6 cm umbilical cord to the placenta. The fetus was a male with prominent phallus and well scrotal pouches (fig. 7) The vestiges of a yolk sac were identifiable between the larger allantois and the amnion, which latter encased both the yolk sac and the umbilical cord. A large vitelline vein tra versed the fetal abdomen to end in the vicinity of the duodenal cap; the vitelline artery crossed the peritoneal cavity as a firm white cord joining the left leaf of the mesentery of the small gut (fig 3) The two umbilical arteries and the two veins ran relatively straight courses through the cord both arteries and both veins sup- plied and drained, respectively both lobes of the placenta. The mesoderm of the cord was fairly dense and vascularized by small vessels, more prominently in the central area. The placenta itself consisted of an incomplete bilobed annulus with a 5 0 cm gap bridged by the paraplacental chorion. The lobes were divided by a very deep cleft (fig. 1) each measuring 8.5 × 5.3 cm. Near the margin the depth of the placental mass was reduced to 0 6 cm whereas at its thickest portion it measured 1 6 cm (fig 8)

In Hyena W/2 as in the other pla centas the fetal surface appeared shiny and purplish-blue. No evidence of pig- ment deposits at the margin or of central or peripheral hematomata was found. The maternal surface was shaggy and yellow ish-gray and presented the orifices of ve- nous channels. Cross section of the pla- cental lobe revealed the following areas grossly distinguishable a thick but shiny allantochorion overlying a subchorial blood sinus a dark-staining labyrinth, in which perpendicular striations could be seen a clearly defined junctional and glandular zone in which some greenish pigment, fading rapidly after fixation, was found. Beneath the placental site the pale stain- ing myometrium was found (fig. 8)

For purposes of description the placenta may be divided into four zones. Starting at the inner or fetal side, the first zone is that of the chorionic plate (actually the fused allantois and chorion) and the sub- chorial sinus. The inner surface of the chorionic plate is covered by cuboidal to columnar allantoic endoderm and its outer surface by syncytial trophoblast. The inner surface has occasional folds projecting into the allantoic cavity (fig 34) and its outer surface, of course, bears the vascular chorio-allantoic projections or stem villi, which cross the area of the subchorial maternal blood sinus toward the "laby rinth.

The second zone is the labyrinth proper or trophoblastic zone made up of the elab- orately branched spongework of chorio-

allantoic villi, between which are the narrow intervillous maternal blood spaces continuous with the subchorial sinus and corresponding to the trophoblastic tubules of a labyrinthine placenta (figs. 18–22) Here fine strands of chorionic mesoderm covered by syncytial trophoblast are in direct contact with the maternal blood. The strands occasionally appear to fuse with others of similar size to form a laby rinthine arrangement, or frequently end freely as true villi particularly in the more advanced placentas, in which a greater number of capillaries appear indenting the trophoblastic covering in almost an intraepithelial fashion.

The third zone is the junctional region where attachment or penetration of the endometrium by the trophoblast occurs Here tips of chorionic processes contact the endometrium by either their syncytial epithelium or by fronds of columnar cytotrophoblast (fig 9) The maternal tissue in this zone consists of glandular debris *blood and giant cells. A few remnants of* dilated uterine glands are found in this basal area whence the placental blood drains into the subjacent uterine veins

The narrow fourth or deep glandular zone contains the bases of endometrial glands separated by scant areolar tissue and attaches to the myometrium. The foregoing description, though applicable to the major portion of the placental mass fails to consider several specialized regions that differ significantly histologically and may be of importance functionally Among these must be included the placental mar gin, the interlobular groove and the para placental chorion, all of which will be described subsequently

The yolk sac and allantois In common with other members of the Order Car nivora the hyena retains a large and permanent allantois, which even late in pregnancy can be recognized with its endodermal lining of cuboidal cells (fig 10) The yolk sac on the other hand though still recognizable even at term becomes relatively smaller and less conspicuous as the placenta ages. A small sac derived from the vascular splanchnopleure is found collapsed and generally T-shaped Each arm of the T has a somewhat bulbous tip by which it is attached to the inside of the chorion. The thin walled structure is lined by deeply staining, tall columnar cells with vesiculated cytoplasm (fig 13) As the conceptus ages, the prominence of the sac decreases and the lining epithelium becomes lower and less clearly vacuolated (fig 11)

The amnion and umbilical cord. The amnion is surrounded by the allantois with which it fuses and by which it is vascularized Although in other Carnivora amniogenesis occurs by folding, no information on this point is available for the hyena, of which the earliest stages have not been examined. The umbilical cord, even at term when it measures about 6 cm in length, contains two arteries and two veins as well as smaller vitelline vessels and the allantoic duct (fig. 12) The mesenchyme in the center of the cord is slightly denser than at the periphery but is not particularly well vascularized, a feature shared by most Carnivora except the wolverine, according to Wislocki and *Amoroso* ('56)

Endometrium. Before describing the structure of the placental mass proper it is helpful to consider the changes in the endometrium of the nonpregnant cornu and in that underlying the nonplacental and paraplacental areas of the gravid horn The sterile horn exhibits the changes usually associated with pseudopregnancy in other animals namely a glandular enlargement, with the individual glands separated by only thin strands of connective tissue (figs. 14 and 15) The glands narrow markedly at the base of the endometrium and follow a brief course therein As pregnancy advances, the endometrium begins to degenerate resulting in the shedding at term of the entire glandular zone of the mucosa, except for the flattened bases of the glands, together with blood and debris into the uterine lumen.

An incidental observation concerns the ovaries during pregnancy Although none of the five used in the present series contained more than one conceptus, the one specimen in which the adnexa were available for study revealed two well developed corpora lutea, the one on the side of the pregnancy somewhat larger than that on the contralateral side. The ovarian [illegible] high stroma outside the corpora lutea showed a high degree of cellular hypertrophy and the number of follicles visible either to the naked eye or microscopically was very small (fig. 9). With regard to the hyperthecosis and the rarity of follicles, the hyena ovary bears certain histological resemblance to that found in the so-called Stein-Leventhal syndrome in the human female.

Paraplacenta. In the paraplacental region, where a tongue-like extension of the allantochorion from the placental band remains in contact with the endometrium, in the manner of the smooth chorion in the human embryo the membrane is thrown into low folds that contact irregularities in the surface of the uterus. The epithelium of the chorion in this area is cuboidal and strips easily from the loose connective tissue that supports it. The chorionic epithelium, though lower than that of the cytotrophoblastic fronds of the placenta proper or of the marginal zone (fig. 38) shares the features associated with phagocytosis elsewhere including a vacuolated cytoplasm, in which granules and disintegrating erythrocytes can be found. The subjacent endometrium remote from the major placental mass shows changes similar to those in the subplacental endometrium (fig. 16) and in places the degenerative changes in the paraplacental endometrium are more striking than in the main placental area (fig 17). Specializations in the chorionic membranes, such as the rosettes of large clear cells described by Amoroso ('52) in the dog, are absent in the sections studied.

Trophoblastic zone The placenta proper is composed of strands of chorionic mesoderm, covered by syncytial trophoblast, that radiate obliquely outward from the chorionic plate toward the basal endometrium (fig. 30) In general, the fetal elements of the placenta comprise not so much a trabecular network forming a labyrinth of trophoblastic lamellae, as an essentially villous system (figs. 18–22) in which the greatly branched, slender villi are not entirely free, but exhibit occasional syncytial junctions. In certain areas in the earliest specimen, particularly in the subchorial and marginal regions areas of transition from the labyrinthine to the villous placenta can be observed (fig. 37) resulting in a condition rather like that described by Wislocki ('29) in the monkey Even later in development, the interruption of tenuous syncytial connections between terminal chorionic strands converts the labyrinth in those areas to a villous state. Some of the main villous stems can be traced throughout the placenta to the basal plate (figs. 19 and 20) to which they are attached by their syncytial coverings (fig 48); others reach the depths of the intervillous space, but remain unattached with cytotrophoblast capping the villous tips that often occlude the mouths of uterine glands (fig 49) The maternal blood throughout the placenta is in direct contact with the chorionic epithelium a true hemochorial relationship. In serial sections the course of the maternal blood within the labyrinth can be traced from the subchorial sinus (fig 47) an extensive space lined by syncytiotrophoblast, whence it escapes through numerous ostia communicating with the underlying intervillous space. After leaving the subchorial sinus the blood pursues a circuitous course through the fetal portion of the placenta, eventually reaching the decidua to empty into the uterine veins but remaining at all times in contact with the trophoblastic lamellae or villi.

The allantoic vessels (fig 30) supplying the placenta are large structures present at the axes of the radiating mesodermal cores. Repeated branching of the vessels within the axial mesenchyme of the chorionic processes results in a network of tortuous capillaries in the terminal villi. The drainage of the fetal capillary blood is back toward the chorionic plate in a direction opposite to that of the maternal capillary circulation, an excellent example of countercurrent flow

Although the hemochorial condition is present at all stages of placental development in the present series as the placenta ages, the intimacy of the maternal and fetal circulations increases. The decrease in thickness of the histological barrier is effected by a reduction in the amount of connective tissue within the villi and by a proliferation of fetal capillaries in closer approximation to the trophoblastic lining (figs. 23–28) Furthermore as term is reached, the fetal capillaries approach the syncytial epithelium so intimately as to indent it and assume what has been described by Bonnet ('02) in the dog and Goldstein ('26) in the pig, and more recently by Amoroso ('52) and Wislocki and Amoroso ('56) in other species as an intraepithelial position (fig 29) This reduces the anatomical barrier to the fetal capillary wall and a greatly attenuated

ing exception to his criteria for establishing interordinal relationships among the mammals.

The typical carnivore placenta, exemplified by the dog, develops by an essentially diffuse projection of short villi, vascularized by allantoic vessels, into the gland and crypt mouths of the endometrium. Most modern carnivore placentas resemble the postulated primitive ancestral type in the possession of an endotheliochorial labyrinth with retention of a permanent large allantois and a relatively large and persistent yolk sac. In its retention to term of a large allantoic vesicle and a medium-sized yolk sac, the hyena fulfills two of Mossman's major criteria for classification within the order Carnivora. With regard to the third ordinal criterion, the orientation of the disc to the uterus, which is antimesometrial or possibly irregular in other carnivores, there is no information about the hyena, since earliest stages of placentation are not available for study. Mossman's fourth and fifth ordinal criteria concern the anatomy of the placental barrier, which in other carnivora is endotheliochorial and labyrinthine, but in the hyena is hemochorial and villous.

In features of lesser phylogenetic significance but of equal interest, the structure of the placenta of *Crocuta* shows additional differences from other carnivores. Within the Order Carnivora, Amoroso ('52) has described a labyrinth that is regular and lobulated in the cat, and irregular and nonlobulated in the seal. In the hyena, septa of maternal connective tissue divide the intervillous space, but neither well defined lobules nor a true labyrinth is present. A sequence among the Carnivora can be established based on the progressive reduction in thickness of the maternal capillary walls. In the wolverine (Wislocki and Amoroso '56) and other mustelids, the maternal capillaries are large sinusoidal vessels lined by prominent cuboidal epithelium and surrounded by a thick amorphous matrix. In such cases the term "vasochorial," as suggested by Wislocki and Amoroso ('56), seems particularly applicable to the placental barrier. In the dog, cat and bear, the maternal capillaries are lined by lower endothelial cells with less supporting matrix, a more typical "endotheliochorial" *relationship*. In the hyena, however, the maternal endothelium has entirely disappeared, creating a hemochorial condition. In *Crocuta*, furthermore, the placenta, particularly at term, is characterized by a multitude of intrasyncytial capillaries. A series of carnivores has been described by Amoroso ('55) based on the prominence of capillaries in an apparently "intraepithelial" location. There is a gradation within the Order beginning with the timber wolf and ending with the grey Atlantic seal, in which there is maximal development of these capillaries. Amoroso ('55) *has* emphasized, furthermore, the widespread occurrence of such capillaries in ungulates and lower animals.

Hematomata. Among the carnivores there is considerable variation in the size, number and distribution of hematomata and related structures. The hyena placenta is unusual, however, in the complete absence of large central and smaller marginal hematomas, such as characterize the wolverine, or of pigmented borders, such as those found in the cat (brown) and dog (green). The subchorial sinus of the hyena, moreover, is not morphologically comparable to the hematomas of other carnivores, since in *Crocuta* the maternal blood space is lined on all sides by chorionic epithelium and originates, as in man and rodents, basal to the endometrium. In the typical carnivore hematoma, the stagnant maternal blood lies between the uterine epithelium and the chorion, arising by extensive hemorrhage from the maternal vessels through the uterine epithelium. In the opinion of Amoroso ('52, '55) the typical carnivore hematoma is related more to structures such as the chorionic vesicle of the pig than to the true hemochorial condition.

The amount and location of extravasated maternal blood also differ among the carnivores. In the hyena, the early invasion of the trophoblast must outstrip the proliferative reaction of the uterus and so effect erosion of the maternal blood vessels over a wide area. The resulting diffuse lake in which maternal blood circulates is thus established, differing from the stagnant hematomata of other carnivores.

In a very recent report, Biggers and Creed ('62) describe the hematoma of the raccoon as representing the hemochorial condition in a carnivore placenta. Again, the persistence of uterine glands and derivatives of maternal epithelial tissue indicates relationship to the condition in the dog and cat, rather than to that of the human placenta.

Endometrium. The hyena differs further from other carnivores in the greater destruction of maternal glandular elements beneath the placenta and the absence of a thick spongy glandular zone. Giant endometrial cells, lacking in most Carnivora except the cat in which they are present along the maternal vessels (Wislocki and Dempsey '46) are prominent at the base of the placenta in the hyena. Matthews ('54) mentions a resemblance between the "decidual" giant cells of the hyena's placeta and those of the mares. It is clear from the aforementioned observations that among the Carnivora there are significant differences in the mode and extent of reactivity of the maternal tissues to the invading trophoblast.

The labyrinth. The hemochorial condition, arising from extensive erosion of maternal vessels associated with suppression of maternal capillary growth, may develop along lines leading to either a labyrinthine or a villous state. The histologic resemblance in mid-pregnancy and at term of the placenta of *Crocuta* to that of certain platyrrhine monkeys, as described by Wislocki ('29) Hill ('32) Mossman ('37) and Amoroso ('52) suggests that the hyena too develops massive early trophoblastic proliferation. There thus results greater dependence on histotrophe in New World monkeys and the hyena than in catarrhine monkeys, apes and man, in which there is greater and earlier freedom of individual villi. By whatever means the hemochorial condition in the hyena develops, it is clear that for the most part the result is a villous placenta, rather than primarily a labyrinth as suggested by Morton ('57). As Wislocki ('29) demonstrated so clearly in the anthropoids and as has here been shown in *Crocuta*, transitions from the labyrinthine to the villous condition are common. Indeed, Stieve (41) believed that the placentas of all anthropoids, including man, were basically labyrinthine, consisting of intercommunicating networks formed by the fusion of chorionic lamellae, with fetal vessels running in uninterrupted fashion between the strands.

Cytotrophoblast. The specializations of the columnar trophoblast in the hyena placenta appear related to those areas of the chorion actively engaged in the absorption of histotrophe and extravasated blood. Amoroso ('55) suggests analogies to the chorionic vesicles of *Loris* the irregular areolae of the sow the endometrial cups of the mare and the central and marginal hematomas of other carnivores. In man and monkeys further comparison with the cell columns, which consist almost entirely of cytotrophoblast, can be made. In those carnivores possessing an endotheliochorial labyrinth, such as the dog and cat, the lamellae at the junctional zone are capped with cytotrophoblast (Duval, 1894 1895) resembling very closely the fetal epithelium of the junctional zone in the hemochorial hyena placenta. Cellular trophoblast of very similar appearance, though somewhat taller occurs in the conspicuous marginal fronds of the hyena, here the chorionic epithelium is slightly lower than that described by Duval in the hematomal area of the cat, but somewhat higher than that in the dog. The third location of phagocytic tall columnar trophoblast in the hyena is the lining of the interlobar sulci.

Columnar trophoblast of a similar but lower type, perhaps more accurately described as cuboidal, occurs in the paraplacental and non-placental areas in *Crocuta* and shares the features associated with phagocytosis. In these areas the underlying chorionic mesenchyme often appears more basophilic and more strongly positive for iron. In a general sense the placenta proper of the hyena, with its syncytial-lined intervillous space is adapted to hemotrophic functions, whereas the paraplacental areas, conspicuously lined by cytotrophoblast, are involved more closely in the absorption of histotrophe. The membranous chorion of the hyena though sharing with that of other carni-

vores the ability to engulf particulate matter is unusual in its lack of specialized structures.

Vasculature In its main features, namely the entry of maternal blood into the fetal placenta through maternal septa and the exit of venous blood from its base the circulation in the placenta of the hyena appears at first to bear a resemblance to that of both the New World monkeys and the typical labyrinthine placenta of carnivores as described by Amoroso ('52) from which the hemochorial placenta of *Crocuta* may have been derived. Although in the single specimen of hyena placenta that he examined, Morton ('57) described an absence of maternal septa penetrating to the chorionic plate, in the present series such septa were consistently found furthermore they contained maternal arteries as described by Duval (1895) in the cat and dog (1894) In the hyena, however the principal arterial supply is at the margin, where the maternal vessel communicates directly with the subchorial sinus the smaller vessels in the maternal septa discharge their blood at or very near the top of the septum, thereby also communicating directly with the subchorial sinus It is important to recognize that the arterial blood in *Crocuta* is not discharged at the basal plate into the intervillous space, as in the case of the macaque (Ramsey '56 '60)

The circulation in the placenta of the hyena is in several respects reminiscent of that postulated by Bumm (1893) for the human placenta, including high septal entry of arterial blood and diffuse basal venous drainage In Bumm's scheme the placental arteries open high enough upon the septa to ensure insofar as the blood falling back toward the decidual plate bathes the functional villi, countercurrent flow of fetal and maternal blood. Though Ramsey ('56 '60) has clearly shown that the human placental circulation differs greatly from that described by Bumm the vascular relationships in the hyena placenta of the present series are remarkably similar to those in Bumm's human model. In this regard it is significant that in *Crocuta* no major or medium-sized placental arteries were observed to enter the base of the intervillous space. What might be misinterpreted as arteries are large veins that drain the base of the labyrinth. A further semantic point of some significance arises with reference to the term subcorial lake, as proposed by Spanner ('35) in his theory of human placental circulation based on overflow filling Unlike the subchorial "lake of Spanner the subchorial sinus of the hyena receives arterial, rather than venous, blood.

As Ramsey ('60) points out, in both the labyrinthine and villous placentas of epitheliochorial syndesmochorial and endotheliochorial types the blood in the maternal and fetal vessels flows in opposite directions. Initial contact of the reduced fetal blood is thus made with maternal blood in the venous state and increasingly arterialized blood is gradually encountered. Since maximal passage across a permeable membrane occurs when flow is of the opposing variety the countercurrent distribution of maternal and fetal blood within the placenta allows for maximal efficiency In the hemochorial villous placenta of *Crocuta* and man, the intervillous space is substituted for the closed system of maternal capillaries. In these terms, the placental circulation of the spotted hyena approaches perfection in countercurrent flow as a result of the complete septa that carry arterial blood directly to the subchorial sinus.

Reproduction. Although the atypical anatomy of the hyena's placenta might form a sufficient basis for considering *Crocuta* an extraordinary carnivore, other aspects of its reproduction are equally curious. The virtual absence of external sexual dimorphism in the adult hyena has, according to Matthews ('39) led to the widespread belief that the hyena is a hermaphrodite. Authors as widely separated by the ages as Aristole (*Historia Animalium*) and Hemingway (*Green Hills of Africa*, '36) have described intersexual transformation in the hyena. Matthews explains this misconception on the basis of the large penis like clitoris and scrotal pouches of the female.

With regard to a phylogenetic scheme for the Mammalia based on comparative morphogenesis of the fetal membranes, the placenta of *Crocuta* has raised some

interesting problems. The structural specializations of the trophoblast, particularly the previously undescribed ultrastructure of the syncytium, have provided additional material for study. Definitive solution of both problems, however, must await acquisition of the earliest stages of placentation and tissue more suitably prepared for electron microscopy.

ACKNOWLEDGMENTS

Valuable assistance was rendered by Mr A. R. Goffin and Mr D. Woulds in the photography of the specimens, and by Dr A. M. Lawn in the electron microscopy.

LITERATURE CITED

Amoroso, E. C. 1952 Marshall's Physiology of Reproduction, Vol. 2, 3rd ed. Ed. by A. S. Parkes, Longmans, Green and Co., London, Chap. XV 127–311.

——— 1955 The anatomy of the placental barrier. In: Gestation. Transactions of the First Conference. Ed. by L. B. Flexner. Josiah Macy Jr. Foundation, New York, 119–224.

——— 1959a The biology of the placenta. In Gestation. Transactions of the Fifth Conference. Ed. by C. A. Villee. Josiah Macy Jr. Foundation, New York, 15–76.

——— 1959b Comparative anatomy of the placenta. Ann. N. Y. Acad. Sci., 75: 855–872.

——— 1960 The Placenta and Fetal Membranes. Ed. by C. A. Villee, Williams and Wilkins Co., Baltimore, Chap. I, 3–28.

——— 1961 Histology of the placenta. Brit. Med. Bull., 17: 81–90.

Biggers, J. D., and R. F. S. Creed 1962 Two morphological types of placentae in the raccoon. Nature 194: 103–105.

Bonnet, R. 1902 Beiträge zur Embryologie des Hundes. Anat. Hefte, 20: 323–499.

Bumm, E. 1893 Über die Entwicklung des mütterlichen Blutkreislaufes in der menschlichen Placenta. Arch. Gynäk., 43: 181–195.

Duval, M. 1894 Le placenta des carnassiers. J. Anat. Paris, 30: 189–240.

——— 1895 Le placenta des carnassiers. J. Anat. Paris, 31: 38–80.

Goldstein, S. R. 1926 A note on the vascular relations and areolae in the placenta of the pig. Anat. Rec., 34: 25–35.

Hill, J. P. 1932 The developmental history of the primates. Phil. Trans. Royal Soc. London, Series B, 221: 45–178.

Matthews, L. H. 1939 Reproduction in the spotted hyaena, Crocuta crocuta (Erxleben). Phil. Trans. Royal Soc. London, Series B, 230: 1–78.

——— 1954 Remarks on the placenta of the spotted hyaena, Crocuta crocuta. Proc. Zool. Soc. London, 124: 198.

Morton, W. R. M. 1957 Placentation in the spotted hyena, (*Crocuta crocuta Erxleben*). J. Anat. London, 91: 374–382.

Mossman, H. W. 1926 The rabbit placenta and the problem of placental transmission. Am. J. Anat., 37: 433–497.

——— 1937 Comparative morphogenesis of the fetal membranes and accessory uterine structures. Contr. Embryol. Carneg. Inst., Washington, 26: 129–246.

Ramsey, E. M. 1956 Distribution of arteries and veins in the mammalian placenta. In Gestation. Transactions of the Second Conference. Ed. by C. A. Villee, Josiah Macy Jr. Foundation, New York, 229–251.

——— 1960 The Placenta and Fetal Membranes. Ed. by C. A. Villee. Williams and Wilkins Co., Baltimore. Chap. III, 36–62.

Romer, A. S. 1945 Vertebrate Paleontology. The University of Chicago Press, Chicago, Chap. XIX, 370–371.

Spanner, R. 1935 Mütterlicher und kindlicher Kreislauf der menschlichen Placenta und seine Strombahnen. Z. Anat. Entwicklungsgeschichte, 105: 163–242.

Stieve, H. 1941 Bemerkungen über den Blutkreislauf in der Plazenta des Menschen. Z. Gynäkol., 65: 370–379.

Wislocki, G. B. 1929 On the placentation of the primates, with a consideration of the phylogeny of the placenta. Contrib. Embryol. Carneg. Inst., Washington, 20: 51–80.

Wislocki, G. B., and E. W. Dempsey 1946 Histochemical reactions in the placenta of the cat. Am. J. Anat., 78: 1–45.

Wislocki, G. B., and E. C. Amoroso 1956 The placenta of the wolverine (*Gulo gulo luscus* (Linnaeus)). Bull. Mus. Comp. Zool. Harvard, 114: 91–100.

PLATE 1

EXPLAN TION FIGURES

1 Hyena W/2. Placenta in situ, showing deep sulcus separating lobes of the incomplete annulus.

2 Hyena W/2. Uterus with placenta in situ and attached fetus. The amnion is fused to the allantois, forming a thick, but shiny allanto-amnion.

3 Hyena W/2. The fetal abdominal wall is reflected to show vitelline stalk (V) traversing abdomen.

4 Hyenas L/5 and W/2. The larger fetus is t term (approximately 110 days) The smaller fetus (W/2) is from pproximately the middle of gestation.







4

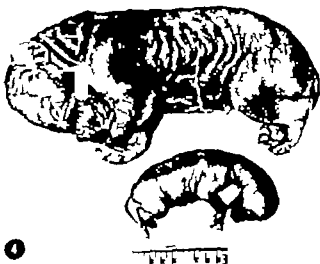


PLATE 2

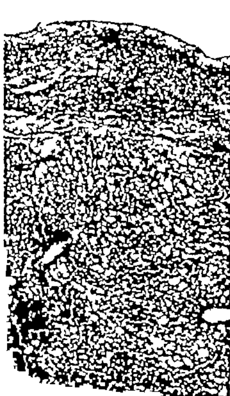
EXPLANATION OF FIGURES

5 Hyen W/2. The uterus with placenta in situ and fetus removed. The corn join t pproximately right angle t form the short corpus uteri. The cervix and both oviducts are shown. The ovary on the side of the nonpregnant horn is smooth and white, lying in bursa heavily padded with fat.

6 Photomicrograph of ovary seen in figure 5. Follicles are relatively scarce in the superficial cortex. There is great cellular hypertrophy of the stroma. × 58

7 External genitalia of male fetus of Hyena W/2. The prominent phallic protuberance and bifid scrotal pouches characterize both sexes t this stage of development.





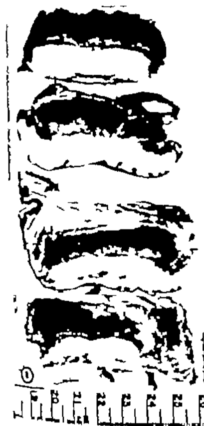

7

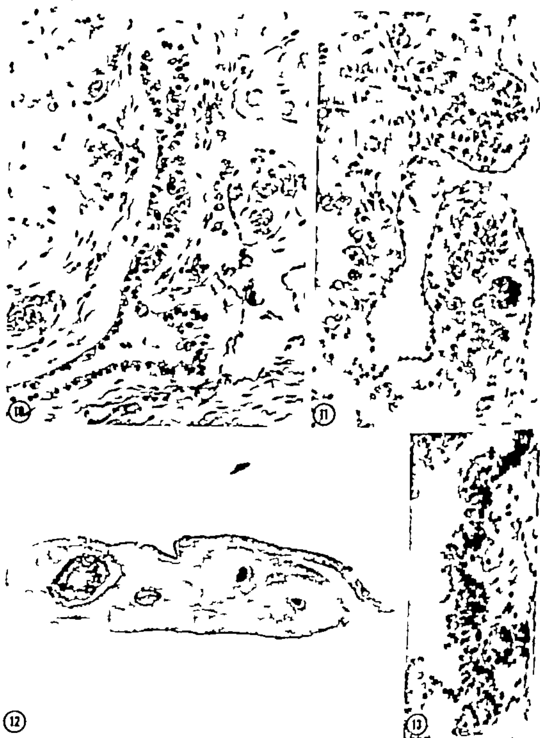
PLATE 3

EXPLANATION OF FIGURES

8 Cross sections of placenta (W/2) showing grossly distinguishable zones (1) fetal surface covered by allantochorion; (2) dark trophoblastic zone exhibiting perpendicula striations; (3 and 4) thin lighter junctional and glandular zones overlying the (5) pale myometrium.

9 Transect of placenta (S/1) showing bottom of trophoblastic zone and intervillous space (IVS) attachment of columnar trophoblast (C) junctional zone (J) and deep glandular zone (G) with underlying myometrium (M) Compare with figure 17 × 123


1



10 Allantois f specimen G100/4 showing persistent membrane lined by cuboidal to columnar epithelium. × 221

11 Yolk sac of G100/4 approximately 95 days gestational ge. The endodermal lining is still intact. Compare with figure 13 × 221

12 Umbilical cord of L/5 showing persistence to term of two umbilical arteries, two veins, and allantoic duct. × 9

13 Yolk sac of earliest pecimen (S/1) pproximately 45 days gestational ge The endodermal lining is taller and the mesenchyme thicker than in figure 11 × 221









14-15 Endometrium of nonpregnant horn of 8/1. There is considerable glandular dilatation. An exudate appears in the uterine lumen × 44

16 Endometrium underlying nonplacental region of pregnant horn of 8/1 The glands are even more widely dilated than in figures 14 and 15. × 44

17 Transformation of the endometrium underlying paraplacental area of pregnant horn in 8/1 The reaction of the maternal tissue in the deep glandular zone is comparable to that underlying the placenta seen in figure 9

PLATE 6

EXPLANATION OF FIGURES

18 Low power photomicrograph of placenta of S/1 showing chorionic plate ( ) trophoblastic zone (t) functional zone (j) and thin deep glandular zone (g) overlying the myometrium (m) The general structure is less clearly villous than that of figures 19–22. Masson. × 18

19 Trophoblastic zone of W/2, showing strands of branching chorionic mesoderm traversing the intervillous space. × 22.

20 Hyena G81/3. The subchorial lake (scs) is prominent. Large chorioallantoic strands attach by cytotrophoblast that caps their tips ( ) The architecture is more villous than that in figure 18. × 16.

21 Trophoblastic zone of G100/4 showing increasingly greater delicacy of fetal elements and architecture approaching that of the term placenta. Compare with figure 22. × 30.

22 Term placenta of L/5. The lacy appearance in this section results from an almost complete transformation to the villous condition. Mallory × 13

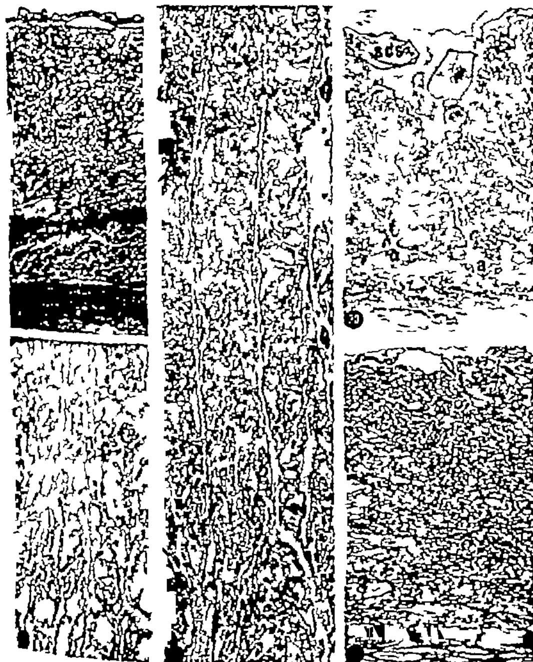


PLATE 7

EXPLANATION OF FIGURES

23 Villi of S/1 showing relatively thick and less well vascularized mesodermal cores than those in figures 24 and 25 × 132.

24 Villi of G100/4 showing decrease in proportion of connective tissue and greater vascularity × 132.

25 Villi of L/5 at term. The mesodermal cores are reduced to a minimum resulting in intimate approximation of fetal capillaries and maternal blood. Masson × 82.

26 High power view of villi of S/1 (fig. 23) The cores are relatively dense and there is a suggestion of double layered trophoblast. Arrow points to cell of the Langhans type in the inner cytotrophoblast. Masson. × 573.

27 Villus of G100/4 (fig. 24) An increase in vascularity and decrease in connective tissue are apparent, as compared with figure 26. Mallory × 502.

28 Villi of L/5 at term (fig. 25) There is minimal connective tissue with fetal capillaries closely approximated to the syncytiotrophoblast. Mallory × 502.

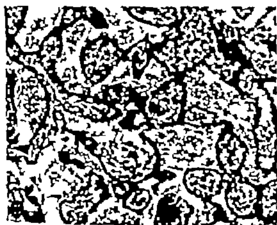












PLATE 8

EXPLANATION OF FIGURES

29 Villi at term (L/5) Arrow points to fetal capillary indenting the trophoblastic lining to assume an "intraepithelial" position. The placental barrier is here reduced to an attenuated syncytial epithelium and the fetal capillary wall. Mallory × 504.

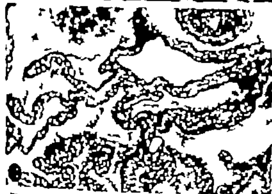
30 The trophoblastic zone of L/5 immediately beneath the allantochorion. A large allantoic vessel ( ) appears in the chorionic mesoderm, from which exceedingly well vascularized villi radiate obliquely outward toward the decidua. Mallory × 96.

31 Oil immersion photomicrograph of villus of W/2. The double layered trophoblast is readily seen at this magnification to consist of ( ) columnar cells of the Langhans type and (s) syncytium. Within the core of the villus fetal capillary (f) is seen. The maternal side of the placental barrier is represented by (m) Laminae within the syncytium are barely discernible. See figure 33. Thin section. Azure II. × 917

32 Low power electron micrograph of villus of W/2. A syncytial nucleus is represented by ( ) a fetal capillary by (f) and the intervillous space containing maternal erythrocytes by (m) The trophoblastic epithelial basement membrane is evident at the bottom of the picture Millonig lead hydroxide. Formalin fixed. × 3,136.

33 Electron micrograph of W/2 showing double layered trophoblastic epithelium. The darker nucleus ( ) is syncytial; the smaller nucleus (c) is cytotrophoblastic, of the Langhans type Microvilli ( ) corresponding to the "brush border" project from the outer surface of the syncytium. Structures resembling podocytes (p) project from the inner surface of the syncytium. Longitudinal lamellae (l) course through the syncytial cytoplasm. Millonig lead hydroxide. Formalin fixed and postosmicated. × 9,856.






c
m
f
31


m
f


11

PLATE 9

EXPLAN TION OF FIGURES

34 The interlobular groove of the term placenta (L/5). The allanto-chorionic plate, in which large vessels run, covers both lobes. Masson. × 16.

35 The chorionic epithelium in the region of the groove shown in figure 34. This tall cytotrophoblast is in contact with maternal blood and histotrophe. Masson. × 104.

36 Paraplacental chorion and endometrium of 9/1. Th chorionic epithelium is cuboidal. There is an extensive reaction in the subjacent endometrium, with pycnosis of maternal epithelial cells and degeneration of endometrial cells to form ymplasma. Separation of chorionic epithelium from its mesenchyme is an artefact. × 131.

37 Portion of trophoblastic zone adjacent to the subchorial sinus. The arrow indicates breakdown of a syncytial bridge converting the labyrinthine lamellae to villi. × 119









PLATE 10

EXPLANATION OF FIGURES

38 Placental margin of S/1. A crescent of gestational endometrial tissue is carried up from the base to the level of the subchorial sinus. Arrow indicates the transition from cyto- to syncytio-trophoblast. × 24.

39 Higher power view of area indicated by arrow in figure 38. The columnar trophoblast (c) undergoes gradual transition to syncytio-trophoblast ( ). × 75.

40 Placental margin of G81/3. The placenta is deeply undercut by double layer of allantochorion ( ) extending deep int the angle of separation from the underlying endometrium ( ). Unlike the situation in true circumvallation, the chorionic membrane is applied to both fetal and maternal surfaces. × 7

41 Chorionic epithelium of the placental margin of W/2. The cytotrophoblast is in contact with disintegrating maternal blood (b) and histotrophe (d) and resembles that lining the interlobular groove. Compare with figure 35. PAS. × 99

42 High power view of cytotrophoblast t placental margin of L/5. The epithelium is very tall with delicately vacuolated cytoplasm and prominent nuclei and nucleoli. Mallory × [illegible].











PLATE 11

EXPLANATION O FIGURES

43 Giant decidual" cells (g) in L/5 with clumps of nuclei of degenerating maternal epithelial elements (ey) × 504

44 Endometrial cells with single and multiple nuclei surrounded by maternal blood in the junctional zone of L/5. The termination of the trophoblastic zone is seen above. Mallory × 35.

45 Junctional zone of $/1 Both columnar ( ) and syncytial ( ) attachments to the basal endometrium are seen. Mallory × 35.

46 A frond of cytotrophobalst contacts maternal blood and endometrium in L/5 Mallory × 292.









PLATE 12

EXPLANATION OF FIGURES

47 Hyena G81/3. Stout columns of chorionic mesoderm extend from the chorionic plate to the decidua. From the subchorial lake the circuitous course of the maternal blood can be followed without interruption throughout the trophoblastic zone to the basal plate. × 18.

48 Base of trophoblastic zone in G81/3. The syncytial attachment to the decidua is seen. Compare with figure 49 × 104

49 In this area of G81/3 the terminal villi are capped by cellular trophoblast that attaches to the maternal tissue in the junctional zone. Compare with figure 48. × 104

50 High power view of the columnar trophoblastic attachment in the junctional zone of L/5. The cytotrophoblast here resembles that of the marginal and interlobular areas. Compare with figures 35, 41 and 42. Mallory × 292.









PLATE 13

EXPLAN TION F FIGURES

51 Placental margin of G81/1 A large maternal artery courses through a crescent of decidua to empty directly into the subchorial sinus. The arterial wall ends abruptly t its junction with the sinus. The arrows indicate area of sinus shown under higher magnification in figure 52. PAS. × 14

52 Area of subchorial sinus t placental margin indicated by arrows in figure 51. The syncytial lining of the sinus undergoes transition to the cytotrophoblast of the margin in the encircled area. PAS. × 20

53 The marginal maternal artery surrounded by decidual" tissue, in G81/3. The vessel is seen reaching the level of the subchorial sinus. Arrow indicates direction of blood flow In serial sections, wide communications of the unbranched artery with the sinus are seen. A large allantoic vessel appears at ( ) × 13

54 A smaller maternal artery of G81/3, entering through a septum of maternal tissue, communicates directly with subchorial sinus (scs). Arrow indicates direction of blood flow Compare with figures 51 and 53 × 13.

55 Venou drainage t base f placenta of G81/3. M ternal blood in the intervillou space escapes directly into three tributaries that form (see arrows) larger vein in the subplacental network. Masson. × 24

56 Venous exit at base of placenta of G81/3 The maternal blood leaving in direction of arrows is in contact with trophoblast (t) and gestational endometrium (d) × 86.



The Enzyme Histochemistry of the Osteoclasts of Normal and *ia* Rats [1]

CHESTER E. HANDELMAN, ANNA MORSE AND JAMES T. IRVING
Forsyth Dental Center and Harvard School of Dental Medicine Boston, Massachusetts

ABSTRACT Enzymes involved in oxidative metabolism as well as acid phosphatase were studied histochemically in osteoclasts from newborn normal rats and their littermates who suffered from a generalized defect in bone resorption (the *ia* rat). The osteoclasts of normal rats demonstrated intense activity for DPNH and TPNH diaphorase as well as succinic, malic and lactic dehydrogenase. Isocitric and glutamic dehydrogenase were less than one-half as active but no less definite. In the *ia* rat the reaction for the diaphorases and dehydrogenases were exactly as observed in the normal. Acid phosphatase was observed in normal osteoclasts as a general cytoplasmic reaction and also in a band of concentrated activity at the junction of the cell and bone. The osteoclasts from "*ia*" animals had greater acid phosphatase activity (more than twice as reactive) than the normal. However, the "junctional band" was only rarely observed in this anomaly. The junctional band may represent sites into which enzymes such as acid phosphatase are secreted in the resorption process and therefore only associated with active osteoclasts. It is possible that the "*ia*" rat may successfully form but not secrete the enzyme.

Bone resorption is an integral part of the morphogenesis as well as the renewal of the osseous system and commences almost as soon as bone formation occurs. The osteoclast actively participates in the resorption process (Hancox and Boothroyd, '61) by dissolution of the bone crystal and organic matrix. The *ia* (incisor absent) rat is a mutant strain characterized by severe impairment of physiological bone resorption (Bhaskar, Weinmann, Schour and Greep, '50). An excessive amount of bone accumulates in spite of the presence of a large number of osteoclasts (Morse and Greep, '60). The failure of the alveolar bone to resorb results in the ankylosis of the incisor and its absence from the oral cavity (Schour, Bhaskar, Greep and Weinmann, '49). The condition is apparently outgrown at about 30–60 days of age (Kenny, Toepel and Schour, '58 and Bhaskar, Weinmann, Schour and Greep, '50).

Walker ('61) was the first to evaluate dehydrogenase histochemistry of normal bone tissue. His results indicated a unique absence of isocitric dehydrogenase and TPNH diaphorase in the osteoclasts which were otherwise rich in citric acid cycle dehydrogenases. Walker then postulated that citrate and lactate would accumulate and actively promote decalcification of bone and calcified cartilage. A similar proposal has been advanced by Neuman and Neuman ('58). Balogh, Dudley and Cohen ('61) failed to substantiate the absence of isocitric dehydrogenase and TPNH diaphorase as reported by Walker but stated that glutamic dehydrogenase was absent.

Schajowicz and Cabrini ('58) have demonstrated acid phosphatase in normal osteoclasts and Burstone ('59a and '59b) has found this enzyme in these cells and also in bone matrix. DeDuve ('59) has associated this enzyme with several catabolic processes.

The aim of the present study was to re-evaluate the enzyme histochemistry of normal osteoclasts and investigate the same complement of enzymes of the osteoclasts of the *ia* rat. By so doing, insight into the nature of the resorption failure in the *ia* rat and more importantly the significance of various enzymes in the normal osteoclastic processes might be achieved.

---

[1] This project was supported in part by Research Grant No. D-1803 from the National Institute of Dental Research.

A post-doctoral research fellow supported by the National Institute of Dental Research at the time this work was done.

METHODS AND MATERIALS

The *ia* trait is transmitted as a simple Mendelian recessive factor (Greep 41) *Ia* rats and normal littermates from our own colony were obtained in approximately equal numbers by breeding homozygous males with heterozygous females. Rats were sacrificed by decapitation at three days of age and the maxillary alveolar bones and tibias were removed for study At this age it is still possible to cut the bones and teeth without prior decalcification. All results reported were obtained on at least four different litters.

Oxidative enzymes Tissue frozen in isopentane cooled by a dry ice-acetone mixture was cut in a cryostat at 6 μ and mounted on glass slides. For the demonstration of enzymes the following methods were used for succinic dehydrogenase that of Seligman and Rutenburg ('51) for diphosphopyridine nucleotide (DPN) linked dehydrogenases, malic, lactic and glutamic the method of Nachlas Walker and Seligman (58a) for reduced diphosphopyridine nucleotide (DPNH) diaphorase DPNH (0 5 mg/ml) was substituted as sole substrate in the aforementioned procedure for the triphosphopyridine nucleotide (TPN) linked isocitric dehydrogenase the method of Nachlas Walker and Seligman ('58b) and for reduced triphosphopyridine nucleotide (TPNH) diaphorase TPNH (0 5 mg ml) was substituted as substrate In the demonstration of all the dehydrogenases and diaphorases tetranitroblue tetrazolium was substituted for nitroblue tetrazolium to minimize artifactual staining on lipid-aqueous interfaces (Sedar Rosa and Tsou '62)

Control sections were incubated in the absence of the reduced coenzyme in the case of the diaphorases, and in the absence of the organic acid substrates in the case of the dehydrogenases. Unfixed sections were incubated in the various substrates for 30 or 60 minutes at room temperature and then post fixed in formalin and dehydrated and mounted in permount

Acid phosphatase The following adaptation of the Barka and Anderson (62) azo dye procedure for acid phosphatase gave excellent results for bone from newborn animals. The tissue was prepared after Holt ('59) using formol-calcium (neutralized to pH 7 0) for 32 hours at 4 C, followed by immersion in a solution of 0 88 M sucrose and 1% gum acacia at 4°C for two or more days. This last step restores much of the enzyme activity inhibited by fixation and aids in preservation of histological details. The gum-sucrose solution also made it possible to cut the fixed tissue in the cryostat. In some experiments tissue was decalcified in a solution of 10% versene (ethylenediaminetetraacetate) and 0 1 M tris (hydroxymethylaminomethane) which was adjusted to pH 6 95 (H M Fullmer personal communication) The decalcification followed the usual treatment with gum-sucrose and was performed at 4 C with constant agitation for three days the decalcifying solution being changed daily

Sections cut in the cryostat at 6 μ were mounted on albuminized slides and dried for several hours. Slides were incubated at either 0 C or 25 C in a medium containing hexazonium pararosanaline and naphthol AS-TR as substrate (Barka and Anderson 62) Control slides consisted of the following sections incubated without substrate (the naphthol AS-TR), sections incubated in the complete medium plus inhibitor (0 005 M sodium fluoride) and sections inactivated by heat (in distilled water at 90 C for 30 minutes) prior to incubation.

In all the experiments, livers and kidneys from adult rats were processed simultaneously for comparison.

RESULTS

Normal rat. The actively growing tibial epiphysis of the three day old normal rat contains osteoclasts predominantly in two zones: some are near the junction of the calcified cartilage and primary spongiosa (chondroclasts) and a greater number are found resorbing the distal ends of the trabeculae to accomodate the marrow cavity (fig. 1) Bone adjacent to the embryonic tooth contains osteoclasts actively remodeling the bone to provide for the expansion of the developing incisor tooth germ (fig. 4) Osteoclasts from these different anatomic locations showed similar oxidative ability in each of the various substrates

Osteoclasts of normal animals demonstrated intense activity for DPNH and TPNH diaphorase as well as malic lactic and succinic dehydrogenase. In these cases, the diformazan stain reached maximum intensity by approximately 30 minutes of incubation at room temperature (figs. 1 and 4) Isocitric dehydrogenase (figs. 3 and 5) and glutamic dehydrogenase (fig. 6) were less than one half as active but no less definite than the more reactive dehydrogenases Control sections incubated without substrate were negative. The osteoclasts were outstanding in their content of enzymes involved in oxidative metabolism when compared to that exhibited by the connective tissue cells and the other bone cells (osteoblasts being about one-half as active) The osteoclast generally equaled the liver parenchymal and the kidney tubular cells in its ability to oxidize the various substrates.

Acid phosphatase using the method of Burka and Anderson on tissue fixed in formol-calcium is visualized in the form of small cytoplasmic granules of the azo dye as well as a diffuse cytoplasmic stain. The reaction seen in the osteoclasts was rapid, maximum coloration without over staining being achieved by approximately 3 to 4 minutes at room temperature. It is interesting to note that under similar conditions liver and the tubules of the kidney did not achieve optimal staining until approximately 45 and 30 minutes respectively

Because of the rapidity of the reaction in osteoclasts, bone was incubated at 0 C to time the reaction more carefully and these results will be described in detail. In the bones of normal rats, a band of concentrated acid phosphatase activity was often observed at the junction of the osteoclast and bone matrix (figs. 12 and 14) This band became obvious after 15 minutes incubation when the general cytoplasmic activity of the osteoclast was hardly apparent. The general cytoplasmic reaction was seen by 30 minutes incubation and the junctional staining became more intense. The observation of the junctional band was independent of the plane of sectioning. This band persisted when either whole tissue or sections were decalcified in versene. Osteoclasts were also found lacking a junctional band of acid phosphatase but showing the generalized cytoplasmic reaction. Osteoclasts varied in the intensity of their reactions the normal osteoclasts of the secondary spongiosa in particular were more active than those of the primary spongiosa (fig. 7) and the osteoclasts resorbing the bone adjacent to the incisor (fig. 9) are less active than the osteoclasts found in the tibia

After one hour incubation in the cold excessive staining occurred in the osteoclast However the bone matrix was usually negative; infrequently a limited area of bone beyond the junctional band was stained (fig. 14) In contrast to this result in fixed tissue, bone matrix was almost totally stained when fresh tissue was cut in the cryostat and incubated without prior fixation. Fluoride in the substrate greatly inhibited the reaction and control sections treated with heat or incubated without substrate were negative.

The ia rat. The tibia of the *ia* rat shows little internal remodeling (Bhaskar Weinmann Schour and Greep '50) As a result, the trabeculae are thickened and the spongiosa displaces much of the marrow cavity (figs. 2 and 8) Osteoclasts are found on the surfaces of the trabeculae in great numbers throughout the extensive spongiosa and at times form a continuous layer of cells (fig 13) In the maxilla the failure in resorption results in an accumulation of unresorbed alveolar bone which in turn causes the incisor tooth to remain small and become distorted in shape (Schour et al. 49) The dental epithelium is disrupted by spicules of unresorbed bone (figs. 5 10 and 11) The osteoclasts are more numerous than in the normal animal and are found throughout the expanse of alveolar bone.

In the *ia* rat the osteoclasts demonstrated positive reactions for the diaphorases and all the dehydrogenases tested. The activities of these enzymes were exactly the same as those observed in the normal littermates (figs 2 and 5)

In contrast to the similarity in the oxidative enzymes, the acid phosphatase activity was greatly increased in *ia* osteoclasts (figs. 8 10 11 and 13) Optimal staining occurred in the cytoplasm after 15 minutes of incubation at 0 C while at

least 30 minutes were required for the normal osteoclast. The reaction product also appeared to be more granular and to occupy a greater proportion of the cytoplasm in the *ia* rat. The concentrated activity at the junction between osteoclast and bone so common in normal bone was infrequently observed in *ia* bone (fig 13) The *ia* osteoclasts unlike their normal counterparts showed little variation in activity almost all cells manifesting an intense reaction The bone matrix of *ia* rats was negative in properly fixed tissue Acid phosphatase activity was entirely absent without the presence of napthol AS-TR in the substrate and after pretreatment by heat. Fluoride added to the substrate greatly inhibited the reaction.

DISCUSSION

Biological oxidation-reduction reactions catalyzed by the dehydrogenases and diaphorases represent the major sources of energy in tissues The osteoclasts whether of normal or *ia* rats were remarkable for their intense activity in the oxidative enzymes studied. The reactions were comparable to those of the surrounding muscle tissue and undoubtedly reflected the high energy requirements of osteoclasts Baker and Klapper ('61) and Irving and Handelman ('64) found that other giant cells demonstrate high levels of oxidative enzymes.

Positive reactions were obtained for TPNH diaphorase isocitric dehydrogenase and glutamic dehydrogenase in the osteoclasts of both normal and *ia* rats. These enzymes have been reported as absent in normal osteoclasts (Walker '61 and Balogh Dudley and Cohen '61) Fullmer in a recent study ('64) has demonstrated that normal osteoclasts can exhibit maximal activity for the diaphorases and several dehydrogenases (including isocitric dehydrogenase) under appropriate conditions, and reasons that weak or negative reactions could be due to inadequate substrate concentrations These results do not negate the theory of acid decalcification attributed to osteoclasts by Walker ('61) since it is not possible to draw any conclusions as to *in vivo* metabolic dynamics from a histochemical investigation The methods are at best semi-qualitative and the conditions of enzyme demonstration need not reflect the *in vivo* situation. The role of citrate as a decalcifying agent" in bone resorption is still a matter of controversy

De Duve ('59) associated acid phosphatase and other hydrolases with a special group of lytic particles which he called lysosomes." He identified such particles in the liver and kidney and suggested their possible involvement in intracellular digestion (phagocytosis, athrocytosis and pinocytosis) as well as autolysis and necrosis Barka ('62) considered that acid phosphatase reactions stained structures associated with pinocytotic and reversed pinocytotic (secretion vacuoles) processes.

The osteoclasts proved to be unusually active with respect to acid phosphatase Maximum coloring without overstaining was achieved about ten times more rapidly in osteoclasts than in liver or kidney tissue. A consistently higher enzyme content (at least twice as active) was found in the osteoclasts of the *ia* rat. Morse and Greep ('60) found the "*ia* osteoclast to have more PAS-positive, diastase resistant granules than the normal cell, and it may be that the increased enzyme content is associated with these glycoprotein granules. Novikoff ('61 especially page 443) in his review of lysosomes and related particles states that PAS-positive material which is resistant to salivary digestion is associated with lysosomes. However lysosome-like particles have as yet not been demonstrated in ultrastructural studies of osteoclasts.

Previous techniques have demonstrated acid phosphatase in bone and dentine matrices (Burstone '59a and '59b) Gomori ('56) states that acid phosphatase is quite soluble in unfixed cryostat sections and even to some extent in formalin fixed frozen sections. Holt ('59) has suggested preparing the tissue using cold formol-calcium followed by treatment with cold hypertonic sucrose containing gum acacia, since he considers this procedure maintains the phospholipid membranes surrounding the enzyme and fixes the enzyme *in situ* Using this technic, bone matrix is found to be almost devoid of acid phosphatase activity Occasionally the matrix just beyond the junction with the normal osteo-

clast did stain. However such extracellular localization must be interpreted with caution.

The band of concentrated acid phosphatase activity observed at the junction of the normal osteoclast and bone matrix may well be functionally significant. Since this band manifests itself before the general cytoplasmic reaction becomes apparent it is unlikely to be a site of nonspecific absorption of soluble reaction products or of the final dye. Decalcification of the tissue does not interfere with the demonstration. The presence of many normal and almost all *ia* osteoclasts exhibiting the general cytoplasmic reaction but not the junctional reaction also argues against a nonspecific artifactual absorption of enzyme or reaction products in the junctional zone. Indeed, this band may represent sites into which enzymes are secreted in the resorption process and are therefore only apparent when associated with active osteoclasts. This hypothesis is supported by the observation that osteoclasts from the *ia* rat, which have a partial bone resorption failure, only rarely demonstrate the junctional band of activity An alternate explanation is that bone undergoing osteoclasis is so altered that soluble dye is preferentially absorbed.

Hancox and Boothroyd ('61) have examined sites of osteoclasis with the electron microscope They described a narrow zone of altered bone an extracellular "junctional zone and a ruffled border of innumerable cytoplasmic processes The precise localization of the acid phosphatase of the junctional band awaits ultrastructural examination. However localization of enzyme on bone matrix beyond the surface of altered bone is unlikely because of the limited diffusion in bone (Neuman, Mulryan and Martin, '60)

Burstone ('59) has described an acid phosphatase reaction in the bone matrix adjacent to osteoclasts. The junctional band described in this paper need not be comparable to Burstone's observations since the band is narrower and does not appear to be on the bone matrix. This zone also is more reactive than the general cytoplasm of the osteoclast.

Greulich ('61) has reported a rind" of increased radio-density between active osteoclasts and bone in microradiograms of decalcified bone He tentatively concludes that this rind represents a focal accumulation of proteinaceous material possibly in part enzymes concerned with bone destruction He notes that there has been no demonstration of concentrated enzyme activity in this junctional zone The observation of acid phosphatase in a band of similar size and location to Greulich's radio-dense rind lends credence to the idea that lytic enzymes accumulate at the junction between active osteoclasts and bone

A number of investigations have been carried out in an attempt to determine the cause of the failure of bone resorption in the *ia* animals. This does not appear to lie in the bone matrix, since bone from an *ia* rat transplanted into a normal animal is remodeled in a normal way (Gillette Mardfin and Schour '56) and such bone will resorb in tissue culture (Goldhaber personal communication) The extracellular environment of the cell appears in many ways normal Kenney Topel and Schour ('58) have found that the calcium and phosphorus metabolism of *ia* animals suggested normal endogenous parathyroid function

Since large doses of parathyroid extract given at an early age improve the dental anomaly and bone formation (Bhaskar Schour Greep and Weinmann, '52) it has been suggested that the osteoclasts are unresponsive to parathyroid hormone at normal levels (Gillette, Mardfin and Schour '56) Another finding which suggests that the defect lies in bone cells has been reported by Vaes and Nichols ('63) They found in an *in vitro* study with bone slices that the *ia* abnormality was associated with a partial block in the oxidation of citrate to keto-glutamic acid, and that the *ia* bone maintained unusually high steady-state calcium concentrations. It is impossible with such a technic to identify the cells responsible for these findings Bone from an *ia* animal is anatomically different from normal bone and this also makes biochemical studies difficult to interpret.

One significant difference in the present findings in the *ia* osteoclasts compared with those from normal animals is a higher content of acid phosphatase which can be

correlated with the histochemical findings of Morse and Greep ('60) already referred to. Also the osteoclasts of *ia* rats contained a consistently high concentration of this enzyme while the normal was variable in activity Another significant difference in the *ia* rat is the infrequence of the band of concentrated acid phosphatase at the junctional zone It is conceivable that *ia* osteoclasts can form but not secrete this enzyme which seems to be closely associated with catabolism Agents such as parathyroid hormone which normally activate osteoclasis may be needed in higher amounts for the activation of this mechanism. The microenvironment of the *ia* bone can successfully initiate differentiation of osteoclasts from what Young ('63) calls the osteoprogenitor pool. However some factor is missing which carries these cells into full function.

ACKNOWLEDGMENT

The authors wish to acknowledge the assistance of Mr John Heeley in preparing the photomicrographs used herein

LITERATURE CITED

Baker B L and Z. F Klapper 1961 Oxidative enzymes the foreign body giant cell. J Histochem. Cytochem., 9 713–714

Balogh, K., H. R Dudley and R. S Cohen 1961 Oxidative enzyme activity in skeletal cartilage) and bone. Lab Investig., 10 839–845.

Barka T 1962 Cellular localization of acid phosphatase activity J Histochem. Cytochem., 10 231–232

Barka, T and P J Anderson 1962 Histochemical methods for acid phosphatase using hexazonium pararosanilin coupler J Histochem. Cytochem., 10 741–753

Bhaskar S. N I. Schour R O Greep and J P Weinmann 1952 The corrective effect of parathyroid hormone on genetic anomalies in the dentition and the tibia of the *ia* rat. J Dent. Res 31 257 270.

Bhaskar S. N J P Weinmann, I. Schour and R. O Greep 1950 The growth pattern of the tibia in normal and *ia* rat Am. J Anat., 86 439–477

Burstone M. S. 1959a Histochemical demonstration of acid phosph tase activity in osteoclasts. J Histochem Cytochem 7 39–41

——— 1959b Acid phosphatase activity of calcifying bone and dentine matrices J Histochem. Cytochem., 7 147 148

DeDuve C. 1959 Lysosomes new group of cytoplasmic particles I Subcellul P rticles. [Ed. J Hayashi] Ronald Press New York pp 128–159

Fullmer H. M. 1964 Dehydrogenase in developing bone of the rat. J Histochem. Cytochem 12: 210–214

Gillette R., D. F Mardfin and I Schour 1958 Osteogenesis in subcutaneous rib transplants between normal a d *ia* rats. Am. J. Anat., 99 447–471.

Gomori, G. 1956 Histochemical methods for acid phosphatase. J Histochem Cytochem., 41 453–461

Greep R. O. 1941 An hereditary absence of the incisor teeth. J Hered., 32 397–398

Greulich R. C. 1961 Organic mass distribution in bone matrix undergoing osteoclastic resorption. Arch. oral. Biol., 3 137 142.

Hancox, N M 1956 The Osteoclast. In: The Biochemistry and Physiology of Bone. [Ed. G H Bourne] Academic Press, New York. Chapter 8 pp. 220–224

Hancox N M and B. Boothroyd 1961 Motion picture and electron microscopic studies on the embryonic avian osteoclast. J Biophys. and Biochem. Cytol 11 651–661

Holt, S J 1959 Factors governing the validity of staining methods for enzymes and their bearing upon the Gomori acid phosphatase technique. Exp Cell. Res. Suppl., 7 1 27

Irving, J T and C. S. Handelman 1964 Bone destruction by multinucleated giant cells. In: Mechanisms of Hard Tissue Destruction [Ed. R. F Sognnaes] American Association for the Advancement of Science Washington, D. C.

Kenney A D W Toepel and I. Schour 1958 Calcium and phosphorus metabolism in the ia rat. J Dent. Res., 37 432–443.

Morse A., nd R. O Greep 1960 Histochemical observations on the ribonucleic acid and glycoprotein content of the osteoclasts of the normal and *ia* rat. Arch. oral Biol., 2 38–43

Nachlas, M. M D G Walker and A. M. Seligman 1958a A histochemical method for the demonstration of diphosphopyridine nucleotide diaphorase. J Biophys Biochem. Cytol., 4: 29–38.

——— 1958b The histochemical localization of triphosphopyridine nucleotide diaphorase J Biophys. Biochem. Cytol., 4 467–472.

Neuman W F and M. W Neuman 1958 The Chemical Dynamics of Bone Mineral. Univ of Chicago Press, Chi go, Ill. Chapter 6 157–166.

Neuman, W F B. J Mulryan and G R Martin 1960 A hemical iew of osteoclasis based on studies with yttrium. Clinical Orthopaedics No. 17 Lippincott Philadelphia; pp. 124–134

Novikoff A. B. 1961 Lysosomes and Related P rticles. In The Cell, vol. II. [Eds J Brachet nd A. E Mirsky] Academic Press New York. Chapte VI 424–488

Schajowicz, F and R L. Cabrini 1958 Histochemical localization of acid phosphatase in bone tissue. Science 127 1447 1448.

Schour I., S N Bhaskar R. O Greep and J P W Inmann 1949 Odontome-like formations in mutant train of rats. Am J. Anat 85 73–112.

Sedar A. W C. G. Rosa and K-C Tsou 1962 Tetranitro-blue t trazolium and the electron histochemistry of succinic dehydrogenase J Histochem. Cytochem., 10 506–508.

Seligman, A. M., and A. M. Rutenberg 1951 The histochemical demonstration of succinic dehydrogenase. Science, *113* 317–320.

Van, C. M., and G. Nichols, Jr. 1963 Bone metabolism in mutant strain of rats which lack bone resorption. Am. J Physiol., 205 461–466.

Walker D G 1961 Citric acid cycle in osteoblasts and osteoclasts histochemical study of normal and parathormone-treated rats. Bull. Johns Hopkins Hosp *106* 80–99

Young, R. W 1962 Cell proliferation and specialization during endochondral osteogenesis in young rats. J Cell Biol., *14* 357–370.

PLATE 1

EXPLAN TION OF FIGURES

Figures 1 through 6. Oxidative enzymes in newborn normal and "ia" rat bones. All reactions performed at room temperature using the tetrazolium salt TNBT No counterstain was used.

1 Normal tibia incubated 30 minutes for DPNH diaphorase. The epiphyseal cartilage (C) is t the top and the marrow cavity (M) at the bottom. Osteoclasts are exceedingly reactive and can be seen in the region of the calcified cartilage (top arrows) and about the distal ends of the trabeculae (bottom arrows) × 100

2 "Ia rat tibia incubated 30 minutes for DPNH diaphorase. A comparable section to figure 1 with the epiphyseal cartilage (C) at the top. The osteoclasts (arrows) are increased in number but they are equally reactive. The trabeculae show little remodeling and obliterate the marrow cavity × 100

3 Normal tibia incubated 60 minutes for isocitric dehydrogenase. The typical enzyme reaction is seen in the multinucleated osteoclasts (arrows) clustered bout the distal ends of the trabeculae. × 250.

4 Normal maxilla incubated 30 minutes for TPNH diaphorase. The incisor tooth is t the top (A = ameloblasts; S.I. = stratum intermedium) Three osteoclasts (arrows) at edge of the labial alveolar bone (B) show the typical enzyme reaction. × 250.

5 "Ia rat maxilla reacted 60 minutes for isocitric dehydrogenase The dental epithelium is interrupted and distorted (top arrow) by spicules of bone Osteoclasts are seen (bottom arrows) surrounding these spicules. Osteoclasts are also seen t the edge of the l bial alveolar bone (B) which in this section has been torn way The activity in these ia" osteoclasts is comparable t the normal (fig 3) × 250.

6 Normal osteoclasts from the maxillary alveolar bone adjacent to the expanding first molar This section was incubated 60 minutes for glutamic dehydrogenase. × 400.

PLATE 1

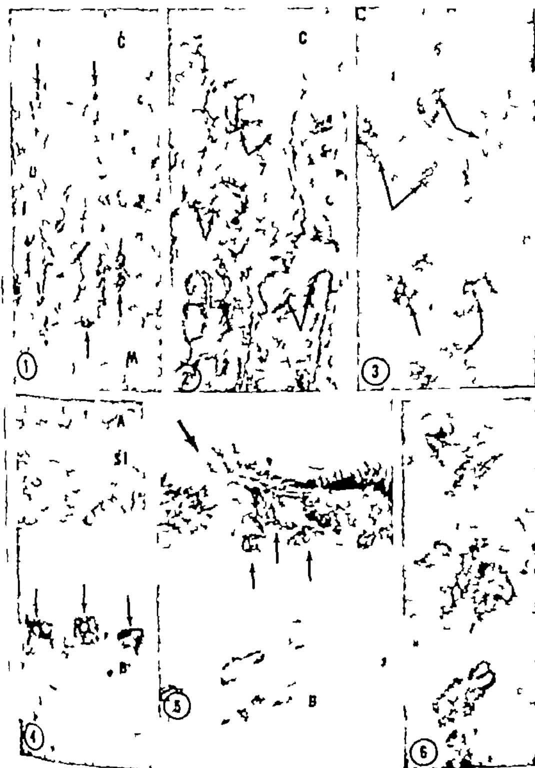


PLATE 2

EXPLAN TI N OF FIGURES

Note Figures 7 through 11 demonstrate acid phosphatase in newborn normal and *ia* rat bones. Tissue was fixed in cold formol-calcium followed by cold gum-sucrose solution. Sections were incubated in medium containing n phthol AS-TR and hexazonium pararosanaline at 0 C

7 Normal tibia incubated 60 minutes for acid phosphatase. The epiphyseal cartilage (C) is at the top and the marrow cavity (M) is at the bottom. A moderate reaction is seen in osteoclasts near the calcified cartilage (top arrows) and more intense reaction is noted in osteoclasts at the distal ends of the trabeculae (bottom arrows) Note th zone of concentrated activity t the junction between the bone matrix and the cell. The matrix is negative. No counterstain × 100

8 *Ia* rat tibia incubated 60 min tes for acid phosphatase. A comparable section to figure 7 with the epiphyseal cartilage (C) at the top The osteoclasts are more intensely reactive than the normal. The bone matrix is negative The trabeculae are unresorbed and obliterate the marrow cavity despite the presence of great number of osteoclasts. N counterstain. × 100.

9 Normal maxilla incubated 60 minutes for acid phosphatase. A weak reaction is noted in th osteoclasts (arrows) along the edge of the labial alveolar bone (B) Note the orderly arrangement of the dental organ (A, ameloblasts and O odontoblasts) Cou terstain hematoxylin. × 110

10 *Ia* maxilla incubated 30 minutes for acid phosph tase. An intense ctivity is noted in the osteoclasts (arrows) Compare with the less reactive osteoclasts seen in the normal (fig 9) The alveolar bone (B) impinges upon the base f the developi g incisor This results in folding and disruption of the dental epithelium (DE) in several places. Counterstain hematoxylin. × 110.

11 *I* maxilla incubated 30 min tes for acid phosphatase. Note the intense enzymatic reaction in the osteoclasts (arrows) which surround spicule of bone (B) that interrupts the continuity of the dental epithelium (DE) Counterstain hematoxylin. × 250


C
C
M
7
8
A
O
B
B
DE
B
DE
B
9
10
11

PLATE 3

EXPLANATION OF FIGURES

Note Figures 12 through 14 demonstrate cid phosphatase in newborn normal and *ia* rat bones. *Tissue was fixed in cold formol-calcium fol*lowed by a cold gum-sucrose solution. Sections were incubated in a medium containing naphthol AS-TR and hexazonium pararosanaline at 0 C.

12 Normal tibia incubated 30 minutes for acid phosphatase. Osteoclasts (arrows) are found t the distal ends of the bony trabeculae (B) Note the concentration of enzyme in the "junctional band, as well as the less intense cytoplasmic reaction. The bone matrix is negative. N counterstain. × 250

13 "Ia tibia incubated 15 minutes for acid phosphatase. Despit the shorter incubation period, the osteoclasts (arrows) are more reactive than those of the normal. Much of the reaction product is granular in nature Note in these osteoclasts the absence of the "junctional band" of concentrated activity which is observed in the normal (fig. 12) The bone is negative. No counterstain × 250

14 Normal tibia incubated 45 minutes for acid phosphatase. A series of osteoclasts are seen in Howship' lacunae Note the junctional band f activity (arrows) as well as the cytoplasmic reaction. This junctional zone may parallel the striated border of the osteoclast. However some bone matrix activity is noted beyond this zone (right rrow) Counterstain hem toxylin. × 500.


B
B
12
13
14

An Electron Microscopic Study of the Cementum, Sharpey's Fibers and Periodontal Ligament in the Rat Incisor [1,2]

IRVING B. STERN

Department of Periodontics and Endodontics, School of Dentistry, University of Washington, Seattle, Washington

ABSTRACT The rat incisor is a continuously erupting, so-called rootless, tooth. It differs from human or similar "rooted" teeth in that its generative cells persist at the base of the tooth. These cells are derived from the invagination of oral epithelium which forms the dental lamina and the developing dental organ. This epithelium becomes a vase-shaped structure surrounding a condensation of connective tissue elements called the dental papilla. The cells on the labial aspect of the epithelial dental organ specialize to form enamel. The cells on the lateral and lingual aspects remain undifferentiated and are called Hertwig's epithelial sheath. The odontoblasts are derived from the dental papilla. The hard tissues of the tooth form continuously at the base, and the tooth erupts into the oral cavity where the incisal edge is worn by abrasive action during gnawing (Brunn, 1887; Addison and Appleton, '15; Schour and Massler, '42).

Hertwig's sheath extends from the base of the tooth to a short distance beyond the point where dentin formation commences. At this level the epithelial cells separate and the sheath disintegrates. As these cells separate, cementoblasts and collagen fibers appear adjacent to the newly forming dentinal surface. Apatite crystals are deposited in the matrix of collagen fibers and a thin layer of cementum results (Selvig, '63). Since Hertwig's sheath is persistent at the base of the tooth, this initial phase of cementogenesis is continuous.

In rooted teeth, on the other hand, initial cementogenesis is completed when the root becomes fully formed, and Hertwig's sheath has been expended. There may be subsequent progressing depositions of cementum to form one or several strata. This initial stratum is called "primary cementum" and the successive layers are called "secondary cementum." Primary cementum contains fine fibrils arranged radially (fiber cementum). Secondary cementum generally contains cells (osteocementum) but it may be acellular. Regardless of category, cementum contains matrix (intrinsic) fibers, and also, in most cases, Sharpey's (extrinsic) fibers (Lehner and Plenk, '36; Ech, '46; Held, '51; Schmid, '51; Sicher, '62).

During the course of eruption of the rat incisor, the periodontal fibers which are attached to the cementum move with the tooth until they somehow undergo dissolution prior to the entry of the tooth into the oral cavity. A similar picture is obtained during the more limited period of eruption of rooted teeth. The mechanisms of formation, reorganization and dissolution of the periodontal fibers are all matters of biologic importance. Moreover, investigations of these phenomena may have some bearing upon understanding those pathologic processes which involve the detachment of the gingiva from teeth and the exfoliation of teeth from their sockets.

Mammalian teeth are attached to their sockets by the periodontal ligament. This ligament contains connective tissue fibers coursing between the cementum and the alveolar bone. Such fibers also extend from the cementum to the lamina propria of the gingiva, securing the gingiva to the tooth. The embedded ends of the periodontal fibers are referred to as Sharpey's fibers.

Adaptation to changes in tooth position incident to growth, eruption, and to function is accomplished by the remodeling of alveolar bone, the reorganization of the periodontal fibers and by the apposition of cementum. Cementum is not remodeled, as is bone, by an interplay of resorptive and appositional phenomena. While cementum resorption may occur, apposition

[1] This investigation was supported by State of Washington Initiative 171 Funds for Biologic Research and by U.S. Public Health Service Training Grant no. 5T1-GM-136 from the Division of General Medical Sciences.

[2] This investigation was carried out during the tenure of a Special Research Fellowship from the National Institute of Dental Research, United States Public Health Service, with the Department of Anatomy, School of Medicine, University of Washington.

is the predominant mechanism for the alteration of cementum. The deposition of cementum therefore results in a gradual increase in its width and a concomitant increase in the length of Sharpey's fibers

In recent years electron microscopy has been employed in the examination of cementum. The earliest electron micrographs of cementum were obtained from replicated preparations of human cementum (Gerould, 44 Matsumiya and Takuma, 54 Takuma, '58 Awazawa, '61 '63) These micrographs demonstrate the irregular disposition of the fibrillar matrix of the cementum and the perpendicular arrangement of Sharpey's fibers.

Thin sections of decalcified cementum (Thilander '61 Stern, '62 Selvig, '63) and undecalcified cementum (Frank and Nalbandian '63 Selvig, '63 Albright and Flanagan '62) provide micrographs of greater clarity than the replicated preparations and are more informative. Frank and Nalbandian ('63) and Selvig ('63) have examined the early development of cementum in humans and in mouse incisors. Thilander ('61) has been concerned with periodontal disease in the rat molar Albright and Flanagan ('62) have reported on calcification of newly formed cementum in teeth from adult hamsters and humans.

The present study provides a description of the ultrastructure of rat cementum just prior to its eruption. The periodontal fibers and the cementoblasts were also studied to gain a further insight into the relationship between the cementum and the periodontal ligament in this continuously erupting tooth.

MATERIALS AND METHODS

Specimens were obtained under Nembutal anesthesia from 14 white rats older than 55 days weighing 225 to 300 gm The mucosa below the gingiva was reflected and portions of the incisors with bone and gingiva in place were obtained by cutting through the hard tissue with high speed dental apparatus under coolant. The erupted portion of the tooth was then trimmed away The specimens were fixed for two hours in ice cold 2 or 4% osmium tetroxide buffered to pH 7.4 (approx.) with s-collidine (Bennett and Luft '59) The tissue was washed in distilled water and then decalcified from 7 to 17 days in 5% formalin and 0.25 molar EDTA at pH 8.0 The tissue was washed again and then dehydrated in increasing concentrations of ethanol and embedded in Epon (Luft, '61) The specimens were mounted on aluminum specimen holders with epoxy cement and oriented so that the dentinocemental junction was perpendicular to the block face Sectioning was done with a Porter-Blum ultramicrotome and glass knives. Sections 1 to 2 μ in thickness were mounted on glass slides and stained with aqueous toluidine blue These sections were then examined with the light microscope to judge whether the specimens were properly oriented and to assure that the cementum would be included in the trimmed block face. At the same time the quality of the preparation was inspected and specimens which exhibited undue signs of damage were discarded (5 animals in all) The acceptable specimens were sectioned for electron microscopic examination Sections were picked up on grids coated with a thin carbon film and stained with uranyl acetate (Watson, '58) or lead tartrate (Millonig, '61) Microscopy was performed with RCA 2C and 4 electron microscopes equipped with a specially stabilized power supply

LIGHT MICROSCOPIC OBSERVATIONS

The rat incisor is an arc-shaped tooth which is roughly triangular in cross section (figs. 1 2) The bulk of the tooth consists of dentin which is coated on its anterior (labial) surface with enamel and on its posterior (lingual) and lateral surfaces with cementum (figs. 1 2) Unlike the rat molar or human teeth in which the cementoenamel junction rings the tooth in a horizontal plane the rat incisor has two cementoenamel junctions which course the length of the tooth as the lateral borders of a single stratum of acellular cementum (fig 1) The inner surface of this layer (the dentinocemental junction) is smooth and relatively regular (figs 3, 4) while the outer surface is more irregular because of the extending fibers (fig. 3) and small protruding tubercles may be evident (fig 4) This layer of cementum attains a thickness of 1 μ to 2 μ prior to eruption

Fiber bundles course from the surface of the cementum around the cells and of the periodontal ligament to the alveolar bone (fig. 5) or to the gingival epithelium (fig. 6) The cellular elements tend to be oriented and compressed between the fiber bundles (figs. 3 5) At times the fiber bundles course directly to the bone, and at other times, they are interrupted in the middle of the ligament by loosely organized fiber bundles which seem to run parallel to the tooth surface The cells have a variety of shapes ovoid, spindle, or occasionally stellate, and the nuclei are ovoid or elongated and contain one or more prominent nucleoli (figs. 3 4). The ligament also contains numerous capillaries and nerve fibers lying between the fiber bundles.

ELECTRON MICROSCOPIC OBSERVATIONS

Cellular structure

The cells adjacent to the cementum (figs. 7 8) are plump, ovoid or slightly elongated cells and have numerous cytoplasmic extensions. Their nuclei are generally ovoid and regular in outline and contain one or more promient nucleoli.

These cells are separated from the cementum by a zone of collagen fibrils one quarter micron to several microns in width. This zone does not appear to be cementoid (unmineralized cementum matrix) The cytoplasmic processes only occasionally come into contact with the cementum (fig. 14)

The cytoplasm of the cementoblasts contains an abundance of rough surfaced endoplasmic reticulum. The cisternae of the endoplasmic reticulum are dilated and appear to contain a flocculent, or slightly granular or filamentous material. The cisternae communicate with each other and with the nuclear envelope (fig. 10) The membranous components of the endoplasmic reticulum are not very obvious, possibly having been rendered pale by the preparatory procedure. When cut *en face* groups of ribosomes are seen to be arranged in delicate, closely juxtaposed, parallel arrays (fig. 11)

Cells farther away from the cementum have similar appearance, but the long, spindle-shaped form occurs with greater frequency The preparatory procedure which involves chelation and post-fixation for a rather prolonged time leads to the formation of several typical artifacts. Cytoplasmic membranes may become less distinct (figs. 8 10–13) The nuclear margin appears to become more prominent (figs. 7 8 10) On the other hand, the ribosomes and the collagen fibrils are unchanged in appearance. The endoplasmic reticulum is indicated by the linear array of ribosomes. The plasma membrane may be evident (figs. 12, 13) but is often indicated by a narrow pale zone separating the cytoplasm from the collagen fibrils (fig. 10)

Periodontal ligament

The periodontal fibers extend from the cemental surface and in a wavy course pass around the cells and their processes (figs. 7 8) The fibers range from approximately ¼ μ to 5 μ in width Each periodontal fiber consists of a bundle of submicroscopic fibrils. The periodicity of the fibrils ranges from 500 A to 600 A, and their diameters range from 300 A to 400 A. Very fine fibrils which are less than 100 A in diameter and which have no apparent periodicity are also noted (figs. 10 11) Each collagen fibril is distinct and separate from adjacent fibrils.

The fibrils within a bundle are rather uniformly spaced and despite their wavy course tend to be parallel. While it is possible to follow a single fibril for several microns, it ultimately passes out of the plane of section and other fibrils enter the plane. Fibrils may cross each other in different planes and produce a palisade-like arrangement (figs. 7 8)

As they insert into the cementum the periodontal fibrils are arranged perpendicular to the surface (figs. 7 8 9 15) Even when they run parallel or tangential to the cemental surface (fig. 18) they turn, before inserting and enter the cementum in an approximately perpendicular position (figs. 14 18) Other angles of insertion are infrequent. When they do occur cellular elements are found positioned in close relationship to the inserting fibrils (figs. 8, 14)

Cementum

After decalcification, the cementum has a stippled or finely reticulated appearance. It is about as dense as the adjacent dentin from which it is separated by a slightly irregular opaque line the dentinocemental junction (figs. 7–9) Collagen fibrils within the dentin may be observed running parallel to the dentinocemental junction (figs 8 9 14 20) and similarly disposed collagen fibrils may be observed within the cementum (fig 9) In some instances the junction has an irregular appearance however the dentin and cementum are clearly delineated (fig. 20) There is never any indication of a space between the two tissues and the collagen fibrils do not cross the dentinocemental junction. On occasion, however a discontinuous dense line may be seen in the cementum adjacent to the dentinocemental junction, and separated from it by a narrow less dense zone (fig. 22)

The cemental surface appears as a line as dense as the dentinocemental junction (fig 8) and is studded with projections of varying size (figs. 8 9 14 15) These projections are roughly conical in shape ranging from 0.6 μ to 2.0 μ in diameter and from 0.3 μ to 1 0 μ in height. The small conical projections (figs. 8 14 15) are associated with individual periodontal fibrils. Where a number of fibrils enter the cementum as a bundle a larger projection may be found (figs. 9 17) Densities which are evident in cross-section (figs. 8 16) and in longitudinal sections of these projections may exhibit periodicity

The fibrils which are embedded in the cementum may have characteristic collagen banding, although this banding may be difficult to perceive (figs. 15 18). They may be traced inward for a variable distance from the cemental surface. Near the surface they tend to be parallel and to continue in the orientation of their insertion (figs. 7 9 14 18) As they are traced deeper into the cementum they turn and may have a more diagonal and divergent orientation (figs. 8 17 18 20) At times the fibrils appear to end in the vicinity of a discontinuous, somewhat diffuse zone of density which may be evident near the center of the cementum (figs. 21 22)

It has already been noted that the deep-lying intrinsic fibrils course parallel to the dentinocemental junction (fig. 8) Frequently irregularly arranged thin dense lines are found in the position usually occupied by the intrinsic fibrils (fig. 19). These densities may also have a more diagonal and parallel arrangement (fig. 20). When the plane of section is fortunate, a continuity can be demonstrated between the dense lines and the periodontal fibrils (figs. 14 20)

DISCUSSION

Use of decalcified material

Fully calcified tissues are difficult to section. Moreover the apatite crystals tend to obscure the collagen and ground substance. Sectioning across hard and soft tissue junctions presents the additional problem of tearing or pulling at the interface during sectioning. This problem can be overcome by persistence, or by examining embryonic tissues in the early stages of calcification, or by the use of decalcified preparations.

Decalcification has been utilized in many electron microscopic studies and may be obtained through the action of acids (Scott, '52 Albright et al., '52 Bernick et al., '52; Shroff et al., '54 Takuma et al., '56 Frank, '57; Takuma, '60 Johansen and Parks, '62; Selvig, '63) Others have employed chelation with EDTA (Robinson and Watson, '52 '55 Takuma et al., '56 Frank, '5? Lenz, '58; Arwill, '58 '60 Yaeger '61 Thilander '61; Mjör '62 Shroff '62; Stern '62 Knese and v Harnack, '62). It is also possible to section calcified tissues and then decalcify the sections on the grids with potassium permanganate, uranyl acetate or phosphotungstic acid, all of which produce some degree of demineralization (Dudley and Spiro, '61), or with acids or EDTA (Yaeger '61).

Examination of EDTA decalcified preparations indicate that chelation leads to changes. These changes are produced to varying degree in different preparations so that inspection must be employed as a means of eliminating the more extensively altered material.

The alteration of the density of the cytoplasmic membranes as observed in this

study is of interest. When formalin fixed bone is chelated with 0.125 molar EDTA at pH 7.4 for ten days there is no significant alteration in the nitrogen content of the solution (Cook and Ezra-Cohen, '62). One might presume, therefore, that the paling of membranes observed in this study was not produced by a hydrolysis of the protein by the EDTA, although the more alkaline pH (8.0) may have played some such role. On the other hand, Klein and Ginzberg ('60) produced a loosening of plant cell walls by immersion of the tissue in 0.1 molar EDTA prior to fixation. They attribute this loosening to the withdrawal of metal cations which cross-link a protein-gel that acts as a cementing substance between these cells. Sedar and Forte ('63) have produced a depletion of the intercellular opaque material of the desmosome in gastric mucosa by *in vitro* treatment with 1 to 4 mM EDTA, which is reversible upon the addition of Ca. Disruption of various microbiota can be produced or potentiated by treatment with EDTA, which presumably acts by withdrawal of Ca from the cell membrane and/or the cell wall (Merkel and Nickerson, '53; Repaske, '58; Koller and Hartsell, '61; Humphrey and Vincent, '62; Hemmens, '63). Danielli and Davson ('34) have indicated that the adjacent lipo-protein molecules which constitute the plasma membrane are cross-linked with calcium ions which decrease the permeability (and therefore the solubility) of the plasma membrane. Accordingly one might speculate about the possible relationship between the chelation of calcium and the observed disruption of membranes.

Cellular structure and function

Electron micrographs of cementoblasts bear a general resemblance to the published electron micrographs of such collagen producing cells as fibroblasts (Karrer, '60; Kajikawa, '61; Peach, Williams and Chapman, '61; Ross and Benditt, '61, '62; Movat and Fernando, '62; Fernando and Movat, '63) and osteoblasts (Knese and Knoop, '58; Dudley and Spiro, '61; Cameron, '61), particularly with regard to the highly developed endoplasmic reticulum. The work of Palade and Siekevitz ('56), among others, indicates that the rough surfaced endoplasmic reticulum is related to protein synthesis.

The delicate paired clusters of ribosomes seen in cementoblasts are similar in appearance to arrangements of ribosomes seen in cells known to be forming collagen. Hemoglobin synthesis has been related to a cluster of ribosomes which is termed a polyribosome or polysome (Warner, Rich and Hall, '62). It is possible that the arrays of ribosomes seen in collagen producing cells may bear some special relationship to the formation of collagen precursors (Ross and Benditt, '64).

Presumably the rough surfaced endoplasmic reticulum discharges collagen precursors into the cisternae. There are no collagen fibrils within the cisternae, however. The flocculent, granular or filamentous material seen in the cisternae may represent some precursor of collagen precipitated by the fixation. The contents of the cisternae pass out of the cell and the molecules may then aggregate to form fine fibrils of less than 100 Å in diameter. These fibrils do not exhibit any periodicity. It has been inferred that such fibrils are precollagenous in nature (Porter and Pappas, '59; Godman and Porter, '60; Chapman, '61; Peach, Williams and Chapman, '61; Ross and Benditt, '61; Fernando and Movat, '63). While direct evidence is lacking, it has been presumed that additional molecules then aggregate side to side on the fine fibrils to form typical collagen fibrils.

It is highly probable that cementoblasts function in a manner similar to other collagen forming cell types and form the collagen fibrils of the cementum and the adjacent periodontal ligament. On the other hand, one cannot exclude the possibility that cells which lie a short distance from the cementum, but not immediately adjacent to it, may also contribute to these fibrils.

In addition to fibrillogenesis and cementogenesis, the cementoblasts may also be involved in the formation of lytic substances. Formational and lytic activity is apparent in osteocytes (Baud, '62). Enzymes capable of breaking down the collagen have been demonstrated in bone cells (Woods and Nichols, '63) and in other connective tissues cells (Gross, Lapiere and Tanzer, '63). It is possible, therefore,

that the cells of the periodontal ligament possess the means of maintaining the cementum and its associated fibrils by lytic as well as formational activity

Fibers of the periodontal ligament

The periodontal fibers transmit forces exerted in biting to the bone and stabilize the tooth in its socket. It has been assumed that in order to do this the fibers travel directly from the cementum to the bone (v Brunn, 1891) An earlier concept pictured the ligament as organized in two sets of fibers one attached to the cementum the other to the bone (de Terra, 11) consistent with the organization of fibers within the dental sac. This earlier concept has been revised and re-introduced by Sicher ('23 '59) who postulates that there is an intermediate plexus which represents a splicing or braiding together of both sets of fibers in the center of the ligament. An intermediate plexus ostensibly would permit a continued adaptive readjustment between the two fiber sets thus mediating eruption while still maintaining tooth attachment. Continuous durable fibers firmly attached to both bone and cementum it was argued would prevent tooth *eruption. On the other hand, fibers* inserted and interwoven in an intervening zone of irregularly arranged argyrophilic fibers could be continuously rearranged during eruption and still maintain a functional attachment (Sicher '23 '59) The possible adaptive mechanism of this plexus as suggested by Wassermann '51 consists of a splitting or fraying of fibers into fibrils and protofibrils which reassociate with similar fine units of adjacent fibers permitting the escalation of the tooth

A subsequent suggestion by Wassermann, '56 that fibrolysis may provide a store of molecular components which are *immediately reconstituted into fibrils*, implies that fibrils can be disconnected and reconnected. Further radioautographic and electron microscopic findings indicate that the cells of the ligament are actively synthesizing protein. Within one hour after administration of H^3 Proline cells in the periodontal ligament of the rat molar are labeled; in 4 to 12 hours the label is found over collagen fibers (Crumley '62; Stallard, '63) The cells of the periodontal ligament of the rat incisor shown in *figures* 10 and 11 contain an extensive endoplasmic reticulum and fine extracellular fibrils are found adjacent to these cells Such findings are similar to those observed in other collagen forming systems.

Since there is no indication that collagen fibrils splice or join at an ultrastructural level, and since a chemical bonding between adjacent fibrils is highly unlikely because they are separated by distances much larger than 5 Å, other explanations must be sought. There is the possibility that the ground substance may play a stabilizing role between adjacent fibrils (Jackson '53) On the other hand, the protein synthesis within the ligament may be related to the maintenance or replacement of pre-existing fibrils to facilitate both eruption and attachment.

Cementum — fibers

The embedded ends of the periodontal fibers are by convention, called Sharpey's fibers. (Sharpey 1856 had described fibers which had perforated into lamellar bone from the surrounding periosteum). Since the deep ends of these fibrils are embedded during the early phases of cementum for*mation one* should examine their path from the dentinocemental junction to the surface for an evaluation of the relationship of these fibrils to cementum formation. The following structures, listed in order may be evident when the cementum is examined in such manner There sometimes is a structure adjacent to the dentinocemental junction (b.m., fig. 22) which may represent a remnant of the basement membrane of Hertwig's sheath, (Paynter and Pudy '58 Selvig, '63) There may also be many thin irregularly disposed, dense lines (d.l., figs. 14 19 20) that appear in some sections (figs. 14 20) to be continuous with *Sharpey's fibrils*. These, therefore, may represent fibrils which were incorporated in the cementum early in cementogenesis. Selvig, ('63) reports such fibrils are first laid down parallel or at an angle to the epithelial sheath and gradually form an irregular meshwork in the cementum. The Sharpey's fibrils turn and then course toward, and exit, from the cemental surface in a perpendicular direction (figs. 7 9 14 18 20) The zones of increased

lensity which may occasionally be evident in the center and other areas of the cementum (figs. 8, 9 17 18 21 22) may be produced by sectioning across the fibrils.

The course of the fibrils forms a curve that appears to represent the resultant of the interaction of eruptive movement and functional pull. The depth of the fibril may be considered as a factor of time since increasing portions of the periodontal fibrils are incorporated by the apposition of cementum. Thus in examining the cementum just prior to eruption, one may well be provided with a record of the deposition of fibrils extending not only back to their initial formation, but also reflecting their role in continuous eruption (fig 23).

If, as v Brunn (1891) has proposed, there is a detachment of old fibers from the cementum followed by an attachment of new ones, then the old ends should remain embedded in the cementum. Isolated ends, other than those produced by sectioning, are not evident in the electron micrographs. If all alterations were limited to the zone of the intermediate plexus, then the fibers that enter the cementum perpendicularly should become embedded rectilinearly The observed paths of Sharpey's fibrils are curved. Therefore such a path cannot be explained by the continued incorporation of perpendicular fibrils. It is unlikely that the fibrils bend during their incorporation — Gustafson and Persson ('57). It is more probable that they are less static than has been assumed and are capable of being altered and reconstructed. Such an alteration may occur as part of a generalized aggregation of collagen precursors to maintain or to re-establish fibrils throughout the periodontal ligament.

Exceptions to the described path of Sharpey's fibrils occur in the form of oblique insertions found in the proximity of cells or cellular processes (figs. 8 14) where the periodontal fibrils course obliquely around the cell. The embedded portion of these fibrils maintains the same oblique direction. From the depth of the oblique insertion it may be inferred that the adjacent cell was present in the same relative position earlier in the course of eruption. Messier and Leblond '60 on the basis of radioautographic labeling find that there is an intense local proliferation of cells at the base of the rodent incisor and that labeled cells migrate along the lengthening root of the tooth It would appear that these cells are carried along with the erupting tooth and are concerned with the maintenance of the adjacent fibrils.

Cementum — calcification

Gustafson and Persson ('57) suggest that the perpendicular extension of the periodontal fibers from the cementum (in human teeth) protects the fibers, and that when tooth position is altered additional cementum is deposited in order to re-establish the perpendicularity

Our observations indicate that the cemental surface is formed into conical projections oriented about single fibrils or bundles of fibrils in the direction of their course. The course of a fibril tends to be roughly perpendicular to the surface but, regardless, the conical projection follows the fibril, and therefore may be formed in response to fibril pull. Cemental spurs that form in the direction of prevailing stress may be observed on human teeth (Kronfeld, '28 Gottlieb and Orban, '31) Smaller tubercles also attributed to fiber pull are visible in the light microscope (Heuser '62) These spurs tubercles and the ultramicroscopic projections might be compared with the tuberosities that form on bones in response to the pull of ligaments and tendons (Weidenreich '23; Dolgo-Saburoff '29 Petersen, '30 Amprino and Cattaneo '37 Vis '58) Where tendons and ligaments attach directly to bone without an intervening periosteum the formation of the tuberosity appears to represent a special instance of bone formation (Weidenreich, '23, '30; Knese, '57; Vis, '58; Knese and Biermann, '58) in which there is a direct transformation of the fibers into bone, or *tendonous osteogenesis* (Weidenreich '23 Knese, '56) The progressive extension of calcification along the periodontal fibril may represent another example of this phenomenon. Functional pull may be only one facet of this process. Selvig ('63) indicates that the mineral crystals are deposited in close association with the fibrils. One could specu-

late that physical and chemical changes at this site permit the extension of calcification along the fibrils.

Cementum — ground substance and fibrillar matrix

The cementum of rat incisors does not appear to be as extensively fibrillar as that of rat molars (Thilander '61) or of human teeth (Tonge and Boult, '58; Awazawa, '63 Frank and Nalbandian '63) After decalcification, therefore the interfibrillar structure becomes quite prominent. It appears to be a sponge-like network composed of circumscribed areas of less density enclosed by areas of greater density The less dense zones are irregular and range from 150 Å to 450 Å in diameter Structure of similar appearance has been demonstrated between fibrils in decalcified bone by Yaeger ('61) in osteoid by Dunning ('58) and in rat tail tendon by Bondareff ('57) These workers have interpreted these less dense and more dense zones as ground substance In tracing the path of a collagen fibril in the cementum it becomes apparent that the fibril is outlined by a dense component. The dense lines with which Sharpey's fibrils are continuous are similarly outlined and are apparent due to the condensation of this dense component.

SUMMARY

The cementum of rat incisors has the following organization in the region adjacent to the gingival attachment. Remnants of the basement membrane of Hertwig's sheath are sometimes found adjacent to the dentinocemental junction. Next to this zone irregular dense lines are present and run more or less parallel to the dentinocemental junction. They appear to be remnants of the irregular meshwork of fibrils formed in the initial stages of cementogenesis They are continuous with the deeper portions of Sharpey's fibrils The Sharpey's fibrils converge, turn, and pass outward approximately perpendicular to the surface of the cementum. The depth of the fibrils can be considered in terms of time, and their path reflects the role of fibrils in tooth eruption.

The fibrils exit from the surface of the cementum and are associated with projections of the cemental surface. These projections may be likened to the tuberosities which form at the insertion of tendons and ligaments to bone. They may be formed in response to fibril pull and/or the fibrils may provide a path for the advancing front of calcification.

Sharpey's fibrils with oblique insertions occur in conjunction with fibrils that course obliquely around adjacent cells. This observation and those of others indicate that the cementoblast has a long-term association with the root of the tooth and is carried along during eruption.

The cementoblasts contain an extensive endoplasmic reticulum with dilated cisternae Fine fibrils of less than 100 Å diameter are found in close proximity to these cells. Synthesizing activity occurs in the vicinity of mature cementum and may be related to the maintenance or replacement of periodontal fibrils. The embedded fibril exhibits a continuity with its periodontal extension from the time of its initial formation to the time of eruption into the oral cavity The embedded portion of the fibril forms a curved path and this path together with the continuation of synthesizing activity lend support to the hypothesis that tooth attachment during eruption is mediated by generalized aggregation of collagen precursors to maintain or to re-establish fibril continuity

ACKNOWLEDGMENTS

The author is indebted to Drs. H. Stanley Bennett and Maurice J Hickey for the opportunity to do this study to Drs. John H Luft and Richard L. Wood for their patient guidance during the training period and subsequent work and to Dr Russell Ross for critical suggestions in the preparation of the manuscript.

LITERATURE CITED

Addison, W H. F and J L. Appleton 1915 The structure and growth of the incisor teeth of the albino rat. J Morph., 26: 43–96.

Albright, J T and J B. Flanagan 1962 Electron microscopy of cementum. Abstracts 40th general meeting, Internat. Assoc Dent. Res St. Louis, pp. 77

Albright, J T D. B. Scott, V M. Mosley and R W G. Wyckoff 1952 Fixation, dehydration and dehydration of dental tissues for electron microscopy J Dent. Res 31 4[illegible]–484.

Bogdan, R., and R. Cattaneo 1937 Il substrato istologico delle varie modalità di inserzioni tendinee alle ossa nell'uomo. Zschr. f. Anat. u. Entw 107 680–705.

Bradl, T 1959 Innervation of the teeth. Trans. Roy Schools of Dent., Stockholm and Umea., 3 pp. 7–83.

—— 1960 Studies on the ultrastructure of dental tissues 1. Some microstructural details of dentine. Acta Morph. Neerlando-Scand., 3 147–158.

Busares, Y 1961 Electron microscopy of carious cementum — with special reference to early caries — J Nihon U School of Dent., 4: 93–106.

—— 1963 Electron microscopy of human cementum. J. Nihon U School of Dent., 5: 117–137

Bard, C. A. 1962 Morphologie et structure infrastructurale des osthocytes. Acta Anat., 51: 208–225.

Bennett, H. S., and J H. Luft 1959 s-Collidine as basis for buffering fixatives. J Biophysic. and Biochem. Cytol., 6 113–114.

Berwick, L., R. F Baker, R. L. Rutherford and O. Warren 1952 Electron microscopy of enamel and dentin. Oral Surg., Oral Med. & Oral Path 5 669–694.

Bondareff, W 1957 Submicroscopic morphology of connective tissue ground substance with particular regard to fibrillogenesis. Geront., 1 222–233.

v. Brunn, A. 1887 Ueber die Ausdehnung des Schmelzorganes und seine Bedeutung für die Zahnbildung. Arch. Mikros. Anat., 29 367–383.

—— 1891 Beiträge zur Kenntniss der Zahnentwicklung. Arch. Mikros. Anat., 38 142–156.

Cameron, D. A. 1961 The fine structure of osteoblasts in the metaphysis of the tibia of the young rat. J Biophysic. and Biochem. Cytol., 9: 583–595.

Chapman, J. A. 1961 Morphological and chemical studies of collagen formation I. The fine structure of guinea pig granulomata. J Biophysic. and Biochem. Cytol., 9 639–651

Cook, S F and H. E. Ezra-Cohen 1962 A comparison of methods for decalcifying bone. J Histochem. and Cytochem., 10: 560–563.

Crumley P J. 1962 Collagen formation in the periodontium of the rat — histological and radioautographic study Thesis, University of Washington, Seattle, 1–78.

Danielli, J F and H. Davson 1934 A contribution to the theory of permeability of thin films. J. Cell. and Comp. Physiol., 5 495–508.

de Terra, P 1911 Vergleichende Anatomie des Menschlichen Gebisses und der Zähne der Vertebraten. Gustav Fischer Jena, pp. 105–107 110–112, 123–124.

Dolgo-Saburoff, B. 1929 Über Ursprung und Insertion der Skelettmuskeln. Anat. Anz., 68 80–87.

Dudley H. R., and D Spiro 1961 The fine structure of bone cells. J Biophysic. and Biochem. Cytol., 11 627–649.

Dunning, W C. 1958 Submicroscopic structure of frozen-dried epiphyseal plate and adjacent spongiosa of the rat. J Ultra. Res., 2. 245–260.

Egli, A. R. 1946 Über die Struktur des Faserzementes. Schweiz. Monatschr. Zahnheilk., 56 23–38.

Fernando N V P and H. Z. Movat 1963 Fibrillogenesis in regenerating tendon. Lab. Invest., 12: 214–229

Frank, R. M. 1957 Contributions à l'étude au microscope électronique des tissus calcifiés normaux et pathologiques. Thèse Faculté de Médecine de Strasbourg, pp 1–96.

Frank, R. M., and J Nalbandian 1963 Comparative aspects of development of dental hard structures. J Dent. Res., 42: 422–437

Gerould, C. H. 1944 Ultramicrostructures of the human tooth as revealed by the electron microscope. J Dent Res., 23: 239–245.

Godman, G. C., and K. R. Porter 1960 Chondrogenesis, studied with the electron microscope. J Biophysic. and Biochem. Cytol., 8 719–760.

Gottlieb, B., and B. Orban 1931 Die Veränderungen der Gewebe bei übermässiger Beanspruchung der Zähne, Leipzig, Georg Thieme, pp. 7–225.

Gross, J C. M. Lapiere and M. L. Tanzer 1963 Organization and disorganization of extracellular substances The Collagen System in Cytodifferentiation and Molecular Synthesis, edited by M. Locke, New York, Academic Press, pp. 175–202.

Gustafson, A.-G., and P.-A. Persson 1957 The relationship between the direction of Sharpey's fibres and the deposition of cementum. Odont. Tidsk., 65 457–463.

Held, A.-J 1951 Cementogenesis and the normal and pathologic structure of cementum. Oral Surg., Oral Med., Oral Path., 4: 53–67

Hemmens, W F 1963 Effect of ethylenediamine tetraacetic acid on the cell fragility of brewers yeast. Nature, 200: 383–384

Hesser H. 1962 Wird die Zementoberfläche des menschlichen Zahnes durch die Funktion gestaltet? Deut. Zahnaerzt. Zschr., 17 661–667

Humphrey B and J M. Vincent 1962 Calcium in cell walls of Rhizobium trifolii. J gen. Microbiol., 29 557–561

Jackson, D. S. 1953 Chondroitin sulphuric acid as a factor in the stability of tendon. Biochem. J 54. 638–641

Johansen, E., and H. F Parks 1962 Electron-microscopic observations on sound human dentine. Arch. oral Biol., 7 185–193.

Kajikawa, K. 1961 The fine structure of fibroblasts of mouse embryo skin. J of Electron-microscopy 10: 131–144

Karrer H E. 1960 Electron microscope study of developing chick embryo aorta. J Ultrastruct. Res., 4: 420–454.

Klein, S., and B. Ginzberg 1960 An electron microscopic investigation into the effect of EDTA on plant cell wall. J Biophysic. and Biochem. Cytol., 7 335–338.

Knese, K.-H. 1956 Die periostale Osteogenese und Bildung der Knochenstruktur bis zum Säuglingsalter. Zschr. f. Zellforsch., *44* 585–643.

Knese, K.-H., and H. Biermann 1958 Die Knochenbildung an Sehnen- und Bandansätzen in bereich ursprünglich Chondraler Apophysen. Zschr. f Zellforsch., *49* 142–187

Knese, K.-H., and M. v Harnack 1962 Über die Faserstruktur des Knochengewebes. Zschr. f. Zellforsch., *57* 520–558.

Knese K.-H., and A. M. Knoop 1958 Elektronenoptische Untersuchungen über die periostale Osteogenese. Zschr. f Zellforsch., *48* 455–478

Kronfeld, R. 1928 Zement und Sharpeysche Fasern. Zschr f. Stomatol., *26* 714–734

Lehner J and H. Plenk 1936 Die Zähne, In Handbuch der Mikroskopischen Anatomie des Menschen, edited by Möllendorff, W., Vol. V-3. Berlin, Julius Springer pp. 619–628.

Lenz, H. 1958 Elektronenmikroskopische Untersuchungen der organischen Matrix des Schmelzes und des Dentins. Mikroskopie., *13* 75–82.

Luft, J H. 1961 Improvements in epoxy resin embedding methods. J Biophysic. and Biochem. Cytol., *9* 409–414.

Matsumiya, S., and S. Takuma 1954 Atlas of electron micrographs of the human dental tissues. Tokyo, Tokyo Dental College Press, p. 119–120.

Merkel, J R., and W J Nickerson 1953 Release of mitochondria from yeast cells by the action of metal- chelating agents. Proc. N t. Acad. Sci., *39* 1008–1013.

Messier B., and C. P Leblond 1960 Cell proliferation and migration as revealed by radioautography after injection of thymidine-H^3 into male rats and mice. Am. J Anat., *106* 247–285.

Millonig, G. 1961 A modified procedure for lead staining of thin sections. J Biophysic. and Biochem Cytol., *11* 736–739

Mjor I. A. 1962 The bone matrix adjacent to lacunae and canaliculi. Anat. Rec., *144* 327–339

Movat, H. Z., and N V P Fernando 1962 The fine strutcure of connective tissue. 1 The fibroblast. Exp. and Molec. Path., *1* 509–534

Noller E. C and S. E. Hartsell 1961 Bacteriolysis f Enterobacteriaceae I. Lysis by four lytic systems utilizing lysozyme. J Bacteriol., *81* 482–491.

Palade G. E., and P Siekevitz 1956 Liver microsomes. An integrated morphological and biochemical study J Biophysic. and Biochem. Cytol., *2* 171–213.

Paynter K. J and G. Pudy 1958 A study of the structure, chemical nature and development of cementum in the rat. Anat. Rec., *131* 233–251.

Peach, R., G. Williams and J A. Chapman 1961 A light and electron optical study of regenerating tendon. Am. J Path., *38* 495–513.

Petersen, H. 1930 Die Organe des Skeletsystems. VIII Die Verbindung des Knochengewebes mit anderem Geweben im knochenen Skeletstück. In Handbuch der mikroskopischen Anatomie des Menschen, edited by W Mollendorff Vol. II-2. Berlin, Julius Springer, pp. 587–619

Porter K. R., and G. D Pappas 1959 Collagen formation by fibroblasts of chick embryo dermis. J Biophysic. and Biochem. Cytol., *5* 153–166.

Repaske R. 1958 Lysis of gram-negative organisms and the role of Versene. Biochem et Biophys. Acta., *30* 225–232.

Robinson, R. A., and M. L. Watson 1952 Collagen-crystal relationships in bone as seen in the electron microscope. Anat. Rec., *114* 383–409

——— 1955 Crystal-collagen relationships in bone as observed in the electron microscope. III. Crystal and collagen morphology as function of age. Annals New York Acad. Sci., *60* 596–628.

Ross, R., and E. P Benditt 1961 Wound healing and collagen formation I. Sequential changes in components of guinea pig skin wounds observed in the electron microscope. J Biophysic. and Biochem. Cytol., *11* 677–700.

——— 1962 Wound healing and collagen formation. II. Fine structure in experimental scurvy J Cell Biol., *12* 533–551.

——— 1964 Wound Healing and Collagen Formation IV Distortion of ribosomal patterns of fibroblasts in scurvy J Cell Biol., *22* 365–390

Schmid, P 1951 Polarisationsmikroskopische Untersuchungen über den Faserverlauf des Zahnzementes des Menschen. Zschr. f. Zellforsch., *36* 319–332.

Schour, I., and M. Massler 1942 The Teeth. In The Rat in Laboratory Investigation, edited by J Q Griffith and E. J Farris, Philadelphia J B Lippincott, pp. 102–163.

Scott, D. B. 1953 Microscopic studies of dental tissues. I. Electron microscopy of tooth structure. Oral Surg Oral Med. and Oral Path. *5* 527–535.

Seder A. W and J G Forte 1963 The influence of calcium on the junctional complex between oxyntic cells in the gastric mucosa. J Cell Biol., *19* 64A.

Selvig, K. A. 1963 Electron microscopy of Hertwig' epithelial sheath and of early dentin and cementum formation in the mouse incisor Acta Odont. Scand., *21* 175–186.

Sharpey W 1856 J Quain Elements of Anatomy 6th ed., edited by W Sharpey and G. V. Ellis, London Walton and Maberly p. cxx.

Shroff, F R. 1962 Bacterial progression in carious dentine the effect of the calcified peritubular wall. Austral. Dent. J., *7* 433–438

Shroff F R., K. I. Williamson and W S. Bertaud 1954 Electron microscopic studies of dentin. The true nature of dentinal canals. Oral Surg., Oral Med., and Oral Path., *7* 662–670.

Sicher H. 1923 Bau and Funktion des Fixationsapparates der Meerschweinchenmolaren. Zschr. f. Stomatol., *21* 580–594.

—— 1959 Changing concepts of the supporting dental structures. Oral Surg., Oral Med., and Oral Path., 12: 31–35.

—— 1962 Orban's Oral Histology and Embryology St. Louis, C. V Mosby pp 45–48, 163–184.

Stallard, R. E. 1963 The utilization of H³-proline by the connective tissue elements of the periodontium. J Am. Soc. Periodont., 1 185–188

Stern, I. B. 1962 An electron microscopic study of the gingival attachment to rat incisor; the cementum and mode of connective tissue fiber attachment. Anat. Rec., 142: 282–283.

Takuma, S. 1956 Electron microscopy of dental tissues by use of the replica method. Dent. Abst., 1957 2: 399–400.

—— 1960 Electron microscopy of the developing cartilagenous epiphysis. Arch. Oral Biol., 2: 111–119.

Takuma, S., Y. Kurahashi, N Yoshioka and A. Yamaguchi 1956 Some considerations of the microstructure of dental tissues revealed by the electron microscope. Oral Surg., Oral Med., and Oral Path., 9 328–343.

Thilander, H. 1961 Periodontal disease in the white rat. Trans. of the Royal Schools of Dent., Stockholm and Umeå, no. 6 pp. 9–99

Tonge, C. H and E. H. Boult 1958 Observations on the optical and electron microscopy of human cementum. J Dent. Res., 37 760.

—— 1958 Collagen in human cementum shown by electron microscopy Nature 182 459–460.

Vis, J H. 1957 Histologic investigations into the attachment of tendons and ligaments to the mammalian skeleton. Proc Kon. Ned. Akad. Wet., Ser C, 60 147–157

Warner J R., A. Rich and C. E. Hall 1962 Electron microscope studies of ribosomal clusters synthesizing hemoglobin. Science 138 1399–1403.

Wassermann F 1951 Electron microscopic study of the submicroscopic network of fibrils as component of connective tissue. Anat. Rec 111 145–173.

—— 1956 V The intercellular components of connective tissue origin, structure and interrelationship of fibers and ground substance. Ergebn. Anat. Entwickl., 35 240–333.

Watson, M. L. 1958 Staining of tissue sections for electron microscopy with heavy metals J Biophysic. and Biochem. Cytol., 4 475–485.

Weidenreich F 1923 Knochenstudien. I. Teil. Über Aufbau und Entwicklung des Knochens und den Character des Knochengewebes. Zschr. f Anat. u. Entwickl., 69 382–466.

Woods, J F and G. Nichols 1963 Collagenolytic activity in mammalian bone. Science, 142. 386–387

Yaeger J A. 1961 The vacuolar nature of bone ground substance. Arch. Oral Biol., 5. 168–172.

All electron micrograph are of tissues fixed in buffered osmium tetroxide and decalcified with EDTA. The tissues shown in the light micrographs are similarly treated unless the notation is otherwise.

Abbreviations

C, cementum
D dentin
DCJ dentinocemental junction
PDL, periodontal ligament
AB alveolar bone
GE, gingival epithelium
pr projection of cemental surface
pf periodontal fibril
Sf Sharpey' fibril
ff fine fibril
dl, dense line
dz, dense zone
ofi oblique fibril insertion
cb cementoblast
cp, cell process
n, nucleus
ne nuclear envelope
er endoplasmic reticulum
ci, cisterna
m, mitochondrion
pm, plasma membrane

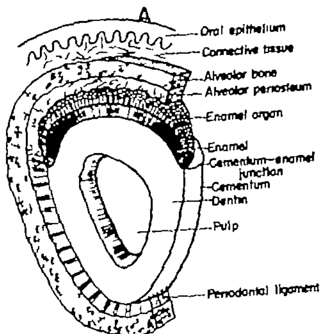
PLATE 1

EXPLAN TION OF FIGURES

1 Diagram of cross-section of rat incisor and adjacent tissues. The anterior surface of the tooth (A) faces the upper border of the diagram.

2 Diagram of longitudinal section of rat incisor and adjacent tissues. The anterior surface (A) of the tooth faces the left margin of the diagram

ULTRASTRUCTURE OF CEMENTUM AND SHARPEY'S FIBERS



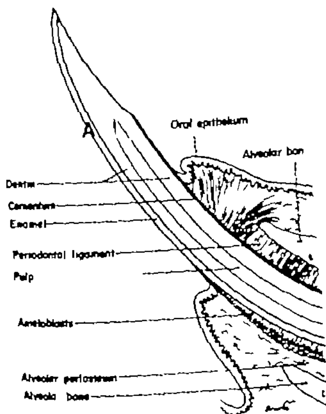


PLATE 2

EXPLANATION OF FIGURES

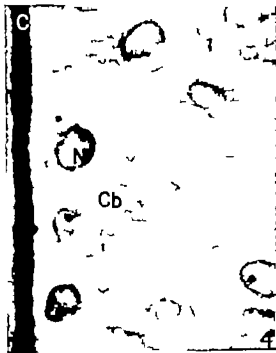
3 Light micrograph of cementum and periodontal ligament showing insertion of periodontal fibers. Formalin fixed, EDTA decalcified, embedded in paraffin. × 600.

4 Light micrograph showing structure of the cells adjacent to the cementum. × 1,300.

5 Light micrograph of the periodontal ligament. Cells indicate course of fibers from cementum to alveolar bone. × 115.

6 Light micrograph showing relationship of the gingiva to the cementum. × 260.


3


C
N
Cb
4


C
PDL
AB
5


D
C
GE
6

PLATE 3

EXPLAN TION O FIGURE

7 A lower magnification electron micrograph showing cementum, dentin and adjacent periodontal ligament. Portions of several cementoblasts are evident. Periodontal fibers and their constituent fibrils are shown. The periodontal fibrils course to the cemental surface in a perpendicular direction and insert into the cementum as Sharpey fibrils. × 9,500


DCJ
D
C
Sf
Cb
c
pf
n
5.0
pf

PLATE 3

EXPLANATION OF FIGURE

7 A lower magnification electron micrograph showing cementum, dentin and adjacent periodontal ligament. Portions of several cementoblasts are evident. Periodontal fibers and their constituent fibrils are shown. The periodontal fibrils course to the cemental surface in a perpendicular direction and insert into the cementum as Sharpey's fibrils. × 8,500


D
pr
cb

PLATE 5

EXPLANATION OF FIGURE

9 A higher magnification electron micrograph of the cementum showing its reticular ppearance and the contained Sharpey fibrils associated with the cemental projections. Magnification × 35,000 (From Orban's Periodontics by D Grant, L B. Stern and F M. Everett — C. V Mosby St. Louis, '63)


pf
Sf
C
D
DCJ
pf
9

PLATE 6

EXPLANATION OF FIGURES

10 Electron micrograph of a portion of cementoblast showing the extensive rough surfaced endoplasmic reticulum. Periodontal fibrils and also fine fibrils are adjacent to the cell. A cisterna is shown communicating with the nuclear envelope. × 17,000.

11 Electron micrograph of cementoblast showing the extensive endoplasmic reticulum. Delicate paired arrays of ribosomes may be noted at the arrows. Periodontal fibrils and also fine fibrils less than 100 Å in width are indicated. Magnification × 19,000.

PLATE 7

EXPLANATION OF FIGURES

12 Electron micrograph f a mitochondrion is shown to indicate state of preservation of membranes. Magnification × 12,000.

13 Electron micrograph of section of plasma membrane is shown to demonstrate state of preservation. Magnification × 20,000.

14 Electron micrograph showing a cell process of cementoblast in contact with the cementum. Periodontal fibrils are shown entering the cemental surface at the cemental projections. The fibrils can be traced to the dense lines lying close to the dentinocemental junction. Magnification × 35,000.


pf
pm
m
pf
pm
er

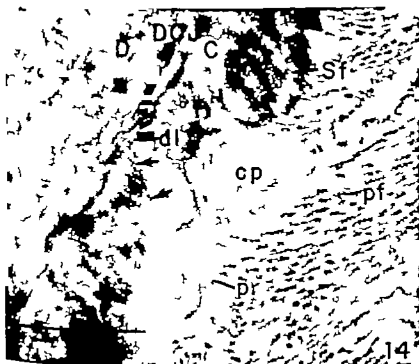

D
DCJ
C
Sf
dl
cp
pf
pr
14

PLATE 8

EXPLANATION FIGURE

15 High magnification electron micrograph of cementum showing continuity of periodontal and Sharpey' fibrils. Arrows indicate periodicity of collagen. Several interperiod bands are evident. Magnification × 67,000.

pr
Sf
pf
cp
c
pcj
pr
15

PLATE 9

EXPLANATION OF FIGURES

16 Electron micrograph of projections of the cemental urface There is a density in the cross-section. In the longitudinal section the fibrillar structure of the density is evident. Magnification × 24 000.

17 Electron micrograph of a projection of the ceme tal surface containing a central density Compare its conical shape with the two bundles of fibril inserting int the cementum in the lower portion of the picture. Magnification × 31,500.

18 Electron micrograph of periodontal fibrils turning to enter the cementum in perpendicular direction. Note the reticulated appear ance of the interfibrillar material (arrow) in the cementum. × 41,000.


C
pr
Sf
pf
pf
Sf
16


Sf
pr
C
C
pf
Sf
pf
pf
17


D
DCJ
C
dz
Sf
0.5
pf
18

PLATE 10

EXPLANATION OF FIGURES

19 Electron micrograph of dense lines near the dentinocemental junction. They appear to be arranged more or less parallel with the dentinocemental junction. × 29,000.

20 Electron micrograph of dense lines arranged in several diagonal layers. The arrows indicate the continuity of one of these with periodontal fibril. Magnification × 26,000.

21 Electron micrograph showing a broad, dense zone which is seen in the center of the cementum. Such dense zones may be produced by sectioning through fibrils. Magnification × 31,000.

22 Electron micrograph showing a clear zone and dense zone adjacent to the dentinocemental junction. This structure may represent remnant of the basement membrane of Hertwig's sheath. Magnification × 6,600.


f
f
19


spf
Dc
D
dl
Sf
dl
20


dz
pf


bm
D
cp
pf
bm

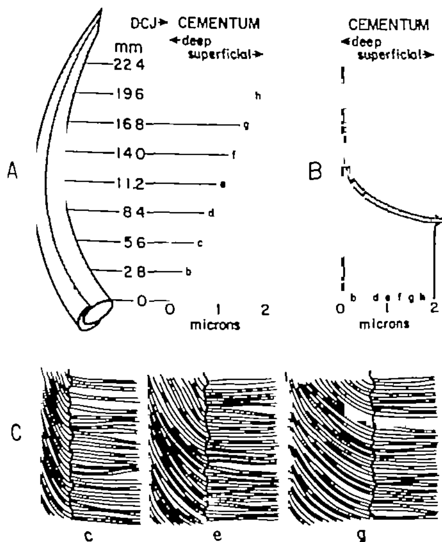
PLATE 11

EXPLANATION OF FIGURES

23A Points in the cementum may be interpreted in terms of time by observing the level of eruption and the width f the cementum. In this diagram an eruptive rate of 2.8 mm per week and an even rate of increase in width have been assumed. Points through "h" can be analyzed according to the ordinates and abscissae of the graph.

23B A single fibril taken from segment in the vicinity of "h" of previous diagram (23A) illustrates the curved path f the fibril.

23C The cementum taken t points "c and g" of figure 23B shows the width of the cementum at each stage. The formation of the curved Sharpey' fibrils from the perpendicular periodontal fibrils can be explained a bending of fibrils or by presuming series of dissol tions and reformations of the periodontal fibrils during their progressive incorporation into the cementum.


A
DCJ ► CEMENTUM
◄ deep
superficial ►
mm
22 4
19 6
16 8
14 0
11 2
8 4
5 6
2 8
0
b
c
d
e
f
g
h
0 1 2
microns
B
CEMENTUM
◄ deep
superficial ►
b d e f g h
0 1 2
microns
C
c
e
g

Histochemical Studies on Seromucous- and Mucous-secreting Cells of Human Salivary Glands [1]

BRYCE L. MUNGER
Department of Anatomy Washington University School of Medicine St. Louis, Missouri, and the Armed Forces Institute of Pathology Washington, D C

ABSTRACT Human salivary and lacrimal glands have been studied with variety of methods to demonstrate polysaccharides in tissue section. On the basis of these studies, an attempt has been made to clarify the classification of exocrine cells. Serous cells secrete proteinaceous material without significant polysaccharide in the secretory granules such as the pancreatic acinar cell and gastric chief cell. Seromucous cells secrete watery product, but the secretory granules contain variable amounts of mucopolysaccharide in the secretory granule. Typical seromucous cells are found in the parotid gland, lacrimal gland, submaxillary gland and eccrine sweat glands. Mucous cells liberate a viscous product rich in mucopolysaccharide. The typical mucous cell is the intestinal goblet cell. Other examples are the mucous portion of the submaxillary gland, the entire sublingual gland, bronchial gland, and Brunner' gland. Human pancreatic acinar and gastric chief cells are unique as compared to other species since the secretory granules of these cells, usually considered to be serous, contain small amount of neutral mucopolysaccharide.

Classification of exocrine glands into types based on the nature of the secretion product date from the work of R. Heidenhain (1868) who recognized a distinction between mucous and albuminous (now termed serous) glands, the former secreting viscous mucoid material, the latter secreting proteinaceous material of more watery consistency Since that time numerous studies have characterized the structure and histochemical properties of secretory cells. This information is summarized in exhaustive reviews of Stormont ('32) Zimmerman ('27) and more recently Schätzle ('62) Leblond ('50) proposed a major revision in the classification of glandular cell types based on the intense PAS positivity (diastase-resistant) of secretory granules in the rat parotid gland. This reaction indicated the presence of a distinct carbohydrate moiety within the secretory granules of a cell classically regarded as serous. Thus, Leblond ('50) proposed that the parotid gland be termed "seromucoid" as distinct from the pancreatic acinar cell and gastric chief cell of purely serous nature. Recently Shackleford and Klapper ('62) have reinvestigated the carbohydrate histochemistry of the salivary glands of various species, and based on their findings they propose to use the term seromucous for those glands containing an acidic mucopolysaccharide in the secretion product. The parotid gland in their opinion is serous in nature.

The importance of these considerations is manifold. First, to understand the cellular mechanisms involved in glandular secretion, cells of similar function must be recognized as such. Secondly the variations in secretory products of a group of cells must be understood at the cytologic level to provide meaningful interpretations of the biochemical data relating to the secretory product of the gland *in vivo*. Finally these considerations are related to concepts as to the pathogenesis of cystic fibrosis of the pancreas which has been variously considered as a generalized disease of exocrine glands, a disease of mucous glands, and by the present author and co-workers (Munger Brusilow and Cooke, '61) as a disease of mucous and seromucous glands. The present study is an attempt to elucidate the relationships of the serous, mucous, and seromucous cells of the human exocrine glands.

[1] This study was supported in part by research grant E-201 from the American Cancer Society, and United States Public Health Service grants GM-07784 and GM 10102 from the Institute of General Medical Sciences.

Formerly Captain, USAF MC (Res.).

MATERIALS AND METHODS

Well preserved human tissues were obtained from the material presented to the department of surgical pathology and were fixed in 10% formalin or 10% neutral buffered formalin. The tissues studied included 3 parotid 4 submandibular 2 sublingual, 2 lacrimal glands, 2 portions of pancreas and 2 sections of fundic mucosa of the stomach. The tissue was embedded in paraffin and sectioned at 5–6 µ. Sections were stained with the PAS technic (Lillie, '54) always with diastase digested controls, toluidine blue at pH 5 6 for metachromasia (Lillie, 54) alcian blue (Mowry '56) colloidal iron (Mowry '58) aldehyde fuchsin (Spicer and Meyer '60) the combined alcian blue-PAS technic (AB-PAS) (Mowry '56) and the combined aldehyde fuchsin-alcian blue technic (AF AB) (Spicer and Meyer '60)

OBSERVATIONS

Based on arguments presented in the discussion the following definitions will be used throughout the present report:

Serous cell. A cell secreting a "watery product, containing no demonstrable polysaccharides in the secretory granules.

Seromucous cell. A secretory cell, usually considered to be serous but containing demonstrable polysaccharide in its secretory granules (Leblond, '50)

Mucous cell. Cells resembling goblet cells of the intestine in histologic and histochemical characteristics secreting a viscous product rich in polysaccharide.

The secretory granules of the acinar cells of the *human parotid gland* are intensely eosinophilic and intensely PAS positive (figs. 1 2, 3) The intensity of the PAS reaction does not diminish with diastase treatment. The PAS positivity is exactly limited to the individual secretory granules and delineates them from the surrounding cytoplasm In sections stained with colloidal iron (fig. 4) and alcian blue, only a faint diffuse background staining is present throughout the cells. This type of cell is termed a seromucous cell based on arguments presented in the discussion.

Small PAS positive granules are likewise present in the apical cytoplasm of the secretory duct (fig. 3) Other staining reactions of these granules could not be exactly determined, but they were most certainly not strongly positive with alcian blue or colloidal iron. Aldehyde fuchsin and mucicarmine stains are negative and no metachromasia is present in human parotid glands. The combined technics (AB-PAS AF AB) are not informative.

In rare instances a mucous acini with or without a seromucous demilune (serous demilune) are present in the human parotid gland, similar to those of the submandibular gland. No goblet cells were observed in the ductal system. No significant variation was observed among different specimens studied.

The *lacrimal glands of man* are identical in all respects to the parotid in staining characteristics.

Human submandibular glands are predominantly seromucous (serous) and contain scattered mucous acini which in some instances are capped by seromucous demilunes (fig 5) The mucous elements are positive with virtually all of the stains employed in the present study (figs. 6–12), except they are not eosinophilic. Mucous cells are PAS positive (diastase resistant), alcian blue positive, colloidal iron positive aldehyde fuchsin positive, metachromatic with toluidine blue, and mucicarmine positive. The intensity of a given staining reaction in these mucous acini varies from cell to cell. Whereas PAS stains uniformly all mucous cells, aldehyde fuchsin (fig. 8) toluidine blue (figs. 9 10) alcian blue (fig. 11) colloidal iron (fig 12) stain irregularly The metachromasia with toluidine blue and the reaction to aldehyde fuchsin (figs. 8, 9 10) are the most variable some mucous cells reacting weakly others intensely This variability of reactivity cannot be correlated with the quality of cytologic preservation or proximity to the edge of the block of tissue. The intensity of reaction of alcian blue (fig. 11) is more uniform. Colloidal iron produces an appearance in the mucous cells of very dark blue staining material clumped in masses with the intervening cytoplasm clear The result is a reticulated appearance to the cytoplasm of a single mucous cell. The combined alcian blue-PAS stain results in a confusing picture. Some cells and occasion-

ally entire mucous acini will stain obviously blue, others red and still others a reddish purple. Thus gradations are present between alcian blue positive and PAS positive mucous acini in the same gland. A similar admixture of colors results from the combined aldehyde fuchsin-alcian blue stain. All types of reactivity can be seen within a single mucous acini or between different acini. Unfortunately these preparations are impossible to illustrate successfully in black and white reproduction since all cells will appear dark grey

The zymogen granules of the seromucous portion (usually considered to be serous) of the submandibular gland stain in a manner similar to that of the parotid gland. They are eosinophilic and PAS positive, and negative with mucicarmine alcian blue, colloidal iron, and aldehyde fuchsin. Ducts containing distinct secretory granules could not be identified in the submandibular glands.

Some acini within the submandibular gland have a predominantly serous appearance but the amount of PAS reactive material in the apex of the cell is much greater than in surrounding seromucous acini (figs. 6 7) Such cells resemble the cells of mucous acini containing fewer secretory vacuoles than usual, but the cells do not appear to be classical mucous-filled cells. In careful examination of the other stains mucous acini are present in which the cells have only sparse secretory granules which react with colloidal iron, alcian blue, and aldehyde fuchsin. These cells are considered to be small mucous cells based on arguments presented in the discussion.

Each specimen examined presented identical histochemical characteristics, if well preserved. However in large blocks of tissue secretory granules of acinar cells could not be stained in the central portion of the block. If secretory granules could not be resolved and hence the stainability of same clearly delineated from that of the background cytoplasm, the results in these areas were disregarded.

The *sublingual gland* in H and E stained preparations appears to have a mixed complement of cells (figs. 13 14) Individual acini of the sublingual gland vary in the types of cells they contain. While some acini contain large mucous-filled cells other acini are composed of cells with few secretory granules. All gradations can be found between these two extremes. It is impossible on the basis of appearance to decide if many acini are mucous or seromucous.

However on the basis of the other stains employed, no clearly defined seromucous cells could be identified in the human sublingual gland. A variability in staining reactions is present, best illustrated by toluidine blue metachromasia (fig 15) and the PAS technic (fig 16) The PAS reaction (fig. 16) is uniformly intensely positive throughout the gland, varying only in the number of PAS positive secretory granules in the apices of the cells. Toluidine blue metachromasia (fig. 15) mucicarmine (fig. 17) colloidal iron (fig. 18) alcian blue (figs. 19 20) and aldehyde fuchsin (fig 21) all evidence a variable reaction throughout the gland. Yet even those cells containing scant secretory vacuoles are positive for acidic components, unlike seromucous cells of the parotid or submandibular glands. In cells having scant secretory granules, the granules are intensely positive with both alcian blue and colloidal iron. Aldehyde fuchsin, on the other hand, is less reactive in the sparsely granulated cells and of variable strong intensity in the mucous-filled cells In the AB-PAS procedure some cells (as described by Quintarelli, '61) are predominantly colored by one or the other and some cells take both colors becoming deep lavender or purple The lightly granulated cells are always colored with alcian blue, the mucous-filled cells by PAS alcian blue or both stains. In the combined AF-AB technic a similar variability is present, sparsely granulated cells are alcian blue positive, mucous-filled cells are aldehyde fuchsin positive or mixed in color

Human pancreatic acinar cells exhibit a weak to moderate PAS positivity in the apical region of the cell which appears to be roughly confined to the area of individual zymogen granules (fig 22) This observation confirms that of Lillie ('50) By way of contrast, goblet cells in the pancreatic duct in the same specimen will stain intensely PAS positive similar

to the parotid gland but the zymogen granules of the pancreas are only weakly positive The zymogen granules are alcian blue aldehyde fuchsin colloidal iron and mucicarmine negative

The human gastric chief cells are similar in staining characteristic to human acinar pancreas. The individual zymogen granules are not PAS positive, but the apical region of the chief cells is diffusely stained Mucous cells in the surface are also PAS positive. It is not possible to ascertain the quality of preservation of this specimen since gastric mucosa obtained at surgery is difficult to preserve

By way of contrast, we also studied cat *salivary* and *lacrimal glands* and our findings *confirm those of Shackelford and* Klapper ('62) The cat parotid secretory granules are eosinophilic intensely PAS colloidal iron and alcian blue positive (figs 23 24) but not metachromatic nor are they mucicarmine positive. The secretory ducts also contain PAS positive secretory *granules. The submandibular gland* is mixed Seromucous and mucous elements have similar staining properties i.e PAS alcian blue and colloidal iron positive (figs. 25 26 27) Mucous elements *however stain irregularly with* colloidal iron and alcian blue similar to those of the human Secretory ducts also contain PAS positive secretory granules

The cat lacrimal glands contain weakly PAS alcian blue and colloidal iron positive secretory granules

DISCUSSION

Based on the information available to date the exocrine gland cells of mammals can be characterized as being purely *serous* (pancreas and chief cells of the gastric fundic glands in most species and most likely human as well) purely *mucous* (sublingual mucous portions of the submandibular Brunner's glands, bronchial mucous glands etc) and *seromucous* (parotid seromucous (serous) portion of submandibular lacrimal Paneth cells and mucoid cells (Munger '61) of the eccrine sweat glands) The basis for this classification rests on the histochemical nature of the secretory product of the cells. As Stormont ('32) points out the pancreatic acinar cell is the prototype of the serous cells, and the zymogen granules of the pancreas of most species are unreactive with PAS (Lillie, '50) or with any of the other known methods for demonstrating carbohydrates. A similar cell is the chief cell of the fundic glands. These two cells are known to secrete digestive enzymes but substances present with zymogen granules other than the specific digestive enzymes are not known. While the term sero-zymogenic as proposed by Stormont ('32) for such cells is appropriate the term serous or zymogenic is adequate and concise characterizing their *functional capabilities and their secretory* process.

The term seromucoid has been used previously in the literature with *rather* implications and definitions. Schafer ('08) used *the* term *with respect to a* gland that had a mixed cellular composition i.e. the submandibular gland was a seromucosen Drüsen Stormont ('32) called the cells of the parotid "seromucous in the introduction to *his paper* but later in the same article proposed the term special serous" for these cells Leblond ('50) noting the carbohydrate moiety present in the mouse parotid gland termed these cells seromucous, denoting a cell classically considered to be serous but secreting as one of its products a carbohydrate. More recently Shackelford and Klapper ('62) defined seromucous as those cells of the salivary glands containing acidic carbohydrates in the secretory granules. As pointed out in the present study and by Lillie ('50) the acinar pancreas and gastric chief cell do not contain appreciable amounts of mucopolysaccharide in most species. If we consider such cells as the prototype of serous cells then the parotid and lacrimal glands are distinctly different. These latter glands *do* secrete a mucopolysaccharide and fit Leblond's ('50) criteria for being seromucous cells. The present report gives added substance to Leblond's ('50) concept and emphasizes the differences of glandular histochemistry which undoubtedly parallel differences in glandular function Shackelford and Klapper ('62) have emphasized the *acid* moiety of the secreted carbohydrate and as a result of this reasoning the mucous portions of submandib-

-lar and sublingual glands are also considered as being seromucous. Yet by structure (Ferner and Gansler '61; Leeson and Jacoby '59) as well as histochemical -r (Lillie, 49 Schlitzle, '62) these -s, usually referred to as mucous, are similar to goblet cells of the intes- (Palay '58) and cells of Brunner's the bronchial mucous glands (Spicer -). Similarities in the chemical nature and viscosity (Gottschalk and Thomas -) of the cellular secretions of these -ds are not presently known. However to consider submandibular mucous -s as seromucous would mean that cells Brunner's glands or bronchial mucous might also be considered as sero- since they too react with methods demonstrate acidic carbohydrate. This -er possibility leads, then, to denying existence of a mucous cell.

In an attempt to clarify these problems -s proposed to classify glandular secre- -n as follows: Cells possessing cytologic -d histochemical evidence of mucous -retion (the goblet cell being the proto- -e) should be termed *mucous*. Cells -reting a "watery" secretion usually -taining enzymes and lacking polysac- in the secretion product (acinar -creas of most species being the proto- -) should be termed *serous*. Cells cyto- -ically similar to serous cells but con- -ning polysaccharide in the secretory -nule should be termed *seromucous* as -gested by Leblond ('50) (the parotid -nd being the prototype) regardless of -e nature of the carbohydrate moiety.

The biochemical properties of the secre- -n of a seromucous cell, exemplified by -e secretory cells of parotid gland, are -rently poorly understood. As contrasted -h the submandibular gland, the parotid -nd has received little attention from -chemists (Nisizawa and Pigman, '59 -izawa and Pigman '60 Quintarelli, -al., '61). The sialomucins are known -be largely responsible for the acidic -bohydrate moiety of submandibular -cin, but the nature of carbohydrates of -rotid origin is not known. Understand- -g the biochemical nature of parotid se- -retion is hindered by the histochemically -served species variation (Lillie 49; -ackelford and Klapper '62). Yet, despite this biological diversity one point is constant, i.e., the parotid gland cells of all species studied to date contain a histochemically demonstrable carbohydrate moiety in the secretory granules.

The pancreatic acinar cell and gastric chief cells are usually regarded as being unreactive with histochemical methods to demonstrate carbohydrate. But, as pointed out by Lillie ('50) human tissue is somewhat of a biological curiosity. Whereas most species are unreactive a distinct but weak reactivity is present in the region of the zymogen granules of human pancreatic acinar cells and gastric chief cells. It is difficult to assess the importance of the weak PAS-positivity of these zymogen granules. The carbohydrate component of the zymogen granules of pancreas and gastric chief cell is relatively insignificant when compared to the carbohydrate component of other seromucous cells. In addition, the proteins or lipids in the zymogen granules of the pancreas could be responsible for this PAS-positivity. No histochemical proof exists that this PAS-positivity indeed indicates a carbohydrate. Until the biochemical properties of seromucous secretion (parotid) have been compared to that of the pancreas, the seromucous component of pancreatic acinar secretion must remain undefined. On the basis of present knowledge we regard the pancreatic acinar cell as most likely being purely serous.

The submandibular gland of most species is a mixed gland containing seromucous acini, similar in properties to acini of the parotid gland, combined with varying numbers of mucous acini. Sialic acid is a very prominent component of this glandular mucoprotein (32% in bovine submandibular gland mucin (Nisizawa and Pigman, '59) and variable but prominent in dog submandibular saliva (Dische et al., '62)). Since acid hydrolysis and treatment with influenza virus neuraminidase abolish the acidic properties of the mucous acini (Quintarelli et al. '61) the mucous acini most likely secrete a sialomucin. But, the PAS reactivity of the mucous acini is only slightly decreased by such treatment and the PAS reactivity of the seromucous demilunes is not affected. While the evidence is good that the mu-

PLATE 1

EXPLANATION OF FIGURES

1 Human parotid gland, H and E. The acinar cells are filled with eosinophilic secretory vacuoles (black in photomicrograph) × 385.

2 Human parotid gland, H and E. A higher magnification of the preparation seen in figure 1 × 1,200.

3 Human parotid gland, PAS. The secretory vacuoles of the acinar cells are intensely positive. Very small PAS positive secretory granules can be seen in the apex of the duct cells. × 1,200.

4 Human parotid gland, colloidal iron. No distinct reactivity is present; only diffuse background staining. × 395.


1




3

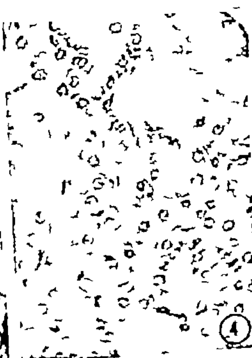

4

PLATE 1

EXPLANATION OF FIGURES

1 Human parotid gland, H and E. The acinar cells are filled with eosinophilic secretory vacuoles (black in photomicrograph) × 385.

2 Human parotid gland, H and E. A higher magnification of the preparation seen in figure 1. × 1,200.

3 Human parotid gland, PAS. The secretory vacuoles of the acinar cells are intensely positive. Very small PAS positive secretory granules can be seen in the apex of the duct cells. × 1,200.

4 Human parotid gland, colloidal iron. No distinct reactivity is present; only a diffuse background staining. × 395.


5


6


7


8

PLATE 3

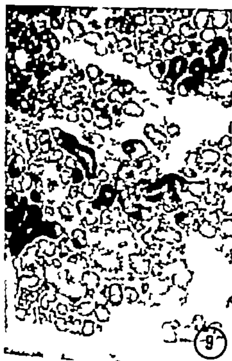
EXPLANATION OF FIGURES

9 Human submandibular gland, toluidine blue. The mucous acini are variably but definitely metachromatic (dark grey) × 100.

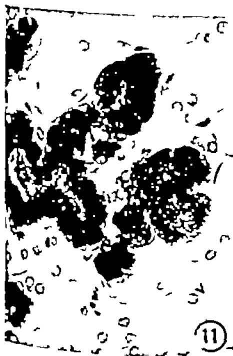
10 Human submandibular gland, toluidine blue. The sharp line of demarcation between the metachromatic (grey) and orthochromatic (colorless) staining of mucous and seromucous acini can be seen. × 395.

11 Human submandibular gland, alcian blue. The mucous acini alone are intensely reactive (dark grey) × 395.

12 Human submandibular gland, colloidal iron. The mucous acini react in an irregular but intense manner; the intense blue color is mainly limited to the cell margins. × 395.


9


10


11


12

PLATE 4

EXPLANATION O FIGUR

13 Human sublingual gland, H and E. The gla d appears homogeneous and consists of one type of acinus. × 100.

14 Human sublingual gland, H and E. The acinar cell contain varying amount of mucinou material in the apical cytoplasm. × 395.

15 Human sublingual gland toluidine blue. Varyi g degrees of metachromasia are present (the cytoplasm having varying shades of grey in the micrograph) × 100

16 Hum n sublingual gland, PAS All acinar cell co tain PAS positi material in the pical cytoplasm. In some cell this can be resolved as discrete granules; in others as confluent ma ses or in intermediat conditions. × 395




14





PLATE 5

EXPLANATION OF FIGURES

17 Human sublingual gland, mucicarmine. The dy is taken up irregularly from cell t cell. × 395

18 Human sublingual gland, colloidal iron. The entire gland stains irregularly as do mucou cells of the ubmandibula gland. × 100.

19 Human sublingual gland alcian blue. The ariability of staining is evident as different shades of grey in the micrograph. 500

20 Human sublingual gland, alcian blue Distinct secretory granules can be seen in some cells and confluent masses in others. × 500.

21 Human sublingual gland, aldehyde fuchsin Marked differences are present in the reactivity from cell to cell. × 500


17


18




20



PLATE 6

EXPLANATION OF FIGURES

22 Human acinar pancre s, PAS. The apical portion of the acinar cells is PAS positive × 500

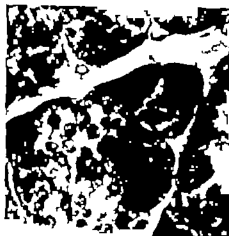
23 Cat parotid gland, H and E. The secretory vacuoles are weakly eosinophilic. × 110.

24 Cat parotid gland, colloidal iron. The secretory acuoles are intensely positive × 110.

25 Cat submandibular gland H and E. The gla d is predominantly mucoid but some serous (?) demilunes can be seen. × 110.

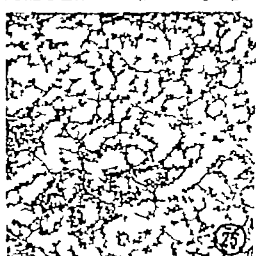
26 Cat submandibular gland, colloidal iron. A mottled but litt e re ctivity is present throughout the gland. × 110

27 Cat submandibular gland alcian blue A homogeneous nd intense reaction is present in all secretory cells. × 110.




23


24


25


26


27

Spermatogenesis in Animals as Revealed by Electron Microscopy

I. THE FINE STRUCTURE AND FUNCTION OF ENDOPLASMIC RETICULUM AND OF PECULIAR BODIES APPEARING IN ATYPICAL MATURING SPERMATIDS AND NUTRITIVE CELLS OF CIPANGOPALUDINA MALLEATA REEVE [1,2,3]

GONPACHIRO YASUZUMI

The Electron Microscope Research Laboratory Department of Anatomy Nara Medical University Kashihara, Nara, Japa

ABSTRACT In an early stage of metamorphosis of typical spermatids of pond snail, *Cipangopaludina malleata* Reeve, numerous vesicles of a circular form appear in the juxtanuclear region. These vesicles represent the rough surfaced endoplasmic reticulum of the typical spermatids. As amorphous contents within the vesicles increase in density an amount, Palade granules 130 to 150 A in diameter attached to the external surface of the vesicles, disappear gradually and at the same time an apparently single layered limiting membrane is transformed to double layered structure.

It has been revealed that a Feulgen-positive material appearing in the vesicles transforms into PAS-positive material in the atypical maturing spermatids, and such material is transported as D bodies through intercellular spaces into the nutritive cell. In the nutritive cell, G bodies make their appearance as transitional form of mitochondria. Structural changes from homogeneous appearance to concentric and parallel lamellar structures have been traced in both bodies. It is noticeable fact that lamellar structure is often found surrounding an electron-lucent space of both bodies. An occurrence of the electron-lucent space within both bodies suggests that the contents of the bodies may be transported via the tubular system of the endoplasmic reticulum in the mantle to the typical maturing spermatids.

Turnbull blue tests have shown that the dense particles, 50 to 70 A in diameter appearing in the D and G bodies are organic iron compounds. It is interesting that lipid is found in helical appearance along the typical maturing spermatid head part, suggesting that lipid is located in the cytoplasm surrounding the nucleus.

As the development of typical spermatids of a pond snail, *Cipangopaludina malleata* Reeve proceeds, numerous elongate pseudopodia develop from the surface of the nutritive cell and extend towards the lumen of the seminiferous tubule. These greatly elongated pseudopodia approach the maturing spermatids and adhere to the surfaces of their heads and middle pieces. The nutritive cell pseudopodia coalesce forming a sheet which takes the shape of a thin-walled mantle. As the development of the pseudopodia proceeds dense mitochondria and large inclusion bodies of varying density gradually increase in number in the nutritive cell. When the typical spermatids have reached a certain degree of maturity they are set free leaving the mantle empty. At this stage the inclusion bodies and the mitochondria decrease remarkably in number. Thus it has been suggested that these cytoplasmic components function as nutritive substances which pass from the cytoplasm of the nutritive cell into the spermatids through tubular elements of the endoplasmic reticulum in the mantle (Yasuzumi, Tanaka and Tezuka, '60).

While numerous light microscopic studies have dealt with the characterization of the chemical nature of granular ele-

[1] The paper invited to the VIIth International Congress of Anatomy Symposium on Fine Structure.
[2] The publication of the extra plates were supported by grants from the Joseph Henry Fund of the National Academy of Science and the Rockefeller Foundation.
The publication of the extra plates of the papers VII and III of this series were supported by grants from the Joseph Henry Fund of the National Academy of Science.
[3] This study was supported by Grant RG-6387 from the United States Public Health Service.

ments appearing in the Sertoli cells of vertebrates relatively little attention has been paid to the origin or fine structure of these granules (Leblond, 50 Arzac 50; Montagna and Hamilton, '51 '52 Mancini, Nolarco and De La Balze 52; Cavazos and Melampy '54 and Daoust and Clermont, 55) The present study is oriented towards elucidating the origin the chemical constitution and the fine structure of bodies appearing in the nutritive cell.

It has already been revealed at a high magnification that the smooth-surfaced vesicular elements of endoplasmic reticulum which contain dense granules are limited by a double layered unit membrane in atypical maturing spermatids of the pond snail (Yasuzumi, Tanaka, Tezuka and Nakano 59) But the relation between the fine structure of the limiting membrane of these vesicles and their contents has remained unknown. The description of this structural pattern and a discussion of its functional significance form the topics of this paper

MATERIAL AND METHODS

Fixation and embedding destined for electron microscope study The testes of *Cipangopaludina malleata* Reeve were fixed in 1% osmium tetroxide adjusted with Veronal acetate buffer to pH 7 3 without NaCl Fixation was continued for one hour at 10 C After fixation the tissue was dehydrated without washing in distilled water using a graded series of ethyl alcohol solutions The tissue was impregnated with a solution containing absolute alcohol and mixture (a a) of 20% methyl methacrylate and 80% *n*-butyl methacrylate for one hour at 18 C The blocks were finally embedded in the same resin, with polymerization effected by 2 6-dichlorobenzoyl peroxide at 46 C

Microtome and electron microscope For comparative examination of cytoplasmic components appearing in the nutritive cell and the spermatids with the electron and light microscopes alternate thin (about 10–20 mμ) and thick (about 1 μ) sections were cut with glass knives on either a Porter Blum microtome or a Shimadzu microtome Thin sections were examined in a Siemens electron microscope Elmiskop I or an Akashi electron microscope model TRS-50 or an electron microscope of the Japan Electron Optics Company model JEM T5 Micrographs were taken at magnifications ranging from 2,000 to 40,000

Ordinary light microscopy and cytochemical tests The thick sections were affixed to glass slides and the embedding material was removed with amyl acetate. After 15 minutes of hydrolysis they were stained with the Feulgen technique. The periodic acid-Schiff reaction for 1–2 glycol linkages (McManus 48 Hotchkiss, '48) was performed on other similar sections which were previously treated with or without saliva. Some specimens were then counterstained with 0 1% methylene blue Methyl green-pyronin stain was applied to paraffin sections fixed in absolute alcohol Control sections were treated with ribonuclease before they were stained with the methyl green-pyronin

Procedure for organic iron compounds (Macallum, 08).

1 Testes were fixed in 95% alcohol for 24 hours

2 Washed in iron-free distilled water for a few minutes.

3 Placed in 5% gelatine solution for two hours at 40 C.

4 Placed in 5% formalin for 30 minutes.

5 Frozen sections were placed in the organic conversion solution (4% sulfuric acid in 95% alcohol) for 4 days at 35 C

6 Sections were washed in 90% alcohol followed by iron free distilled water

7 Placed in Turnbull's blue reagent for 20 minutes

8 Washed in water containing eosin

9 Dehydrated and mounted in benzol balsam

Procedure for inorganic iron compounds The material mentioned above was stained with the Turnbull's blue reagent without treatment with the organic iron conversion solution.

RESULTS

Endoplasmic reticulum containing amorphous substances or dense granules in the atypical spermatids At an early stage of the metamorphosis of the atypical spermatid the interspace between the two layers of the nuclear envelope is clearly visible A considerable number of vesicles in a circular form appear in the juxtanuclear re-

gon. The vesicles contain only a fine flocculent precipitate similar to that present in the perinuclear space. The limiting membrane of the vesicles appears apparently to be a single layer. These vesicles represent the rough-surfaced endoplasmic reticulum of the atypical spermatid. Small dense Palade granules 130 to 150 A in diameter are found attached to the surfaces of the vesicles and isolated in the cytoplasmic matrix. The nucleus contains a large number of small granules which, in general, appear to be disposed at random, although in some places they seem to be arranged in short, coiled strands (fig. 1).

As the metamorphosis of the atypical spermatid proceeds, the amorphous substance in the vesicles come to be aggregated gradually into denser masses. At the same time, the apparently single layered limiting membrane of the vesicles tends to be transformed into a compound structure consisting of two dense lines with a separating less dense zone (fig. 2). This limiting membrane corresponds to Robertson's unit membrane (Robertson '57 '59). The amorphous substance of low density within the vesicles is aggregated into denser masses, leaving a clear area around them. The Palade granules disappear gradually from the surface of the vesicles and at the same time their limiting membranes become thicker assuming a double layered or unit structure (figs. 3 4 and 5). Some of the vesicles containing a dense mass lie in close association with the plasma membrane and appear to open through a pore into the intercellular space (figs. 3 and 4). In more advanced stages, the large dense granules can be seen isolated in the intercellular space (figs. 4 9 10 11 and 12).

At a late stage of metamorphosis of the atypical spermatids most of the vesicles become filled with dense granules of varying size and number. On the other hand it is very difficult to find manifestations of the rough-surfaced endoplasmic reticulum in any area of the cytoplasm (fig. 6). A voluminous Golgi complex is usually situated in the juxtanuclear region. As the metamorphosis of the atypical spermatid proceeds, the nucleus moves towards the anterior pole of the cell body while the Golgi complex appears to be displaced in the opposite direction and is usually found in the posterior part of the cell, which contains lamellae granules and vesicles of different sizes. In the Golgi zone vesicles containing dense granules are scarcely visible (fig 6).

At later stages in which the atypical spermatids show a considerable elongation, the vesicles containing dense granules come to be concentrated at the periphery of the cell and occasionally contain relatively large dense granules which presumably arise from the fusion of smaller intravesicular granules. One can see clearly that some of the dense granules are discharged into the intercellular space, while most of the vesicles containing large dense granules become concerned with the formation of the sheath of the middle piece of the atypical spermatid (fig. 7). As Yasuzumi and Tanaka ('58) and Yasuzumi, Tanaka and Tezuka ('60) have already reported, the nucleus is reduced to a thin arched profile which envelops a bundle of tail filaments. The nucleus comes to be lodged in a deep indentation of the nutritive cell, where the substance of the atypical spermatid is separated from the cytoplasm of the nutritive cell by their respective cell membranes (fig. 7).

Cytochemical observations of the atypical spermatid. In early stages the cytoplasm of the atypical spermatid is uniformly basophilic, revealing a positive RNA-reaction. In the middle stage of its development the cytoplasm is filled with numerous vesicles containing fine granules which give a positive Feulgen-reaction but the sheath of the middle piece, which is composed of a series of vesicles containing dense granules, fails to stain with basic dyes and shows a strong positive PAS-reaction (fig 19).

Dense bodies appearing in the nutritive cell. At the early stage of spermatogenesis, dense mitochondria and elements of endoplasmic reticulum composed of variable sub-units can be seen in the nutritive cell. The endoplasmic reticulum appears in the form of small round or oblong profiles of vesicles. They are often arranged in rows where some of them may presumably represent sections through tubules (fig. 8). As spermatogenesis proceeds, numerous dense bodies of different

forms appear in the nutritive cell (figs. 7 9 10 11 and 12) Figure 9 shows cells in which the atypical spermatid cytoplasm and the adjacent cell surface of the nutritive cell are in a state of vigorous activity with similar dense granules seen within the vesicles of the atypical spermatid within the intercellular space and in invaginations of the nutritive cell membrane The dense material in the invaginations of the nutritive cell increases in amount and accumulates to form a dense body having an irregularly festooned outline and an inhomogeneous appearance. Such bodies will hereafter be referred to as "D bodies. It is noticeable that the plasma membrane shows a wide or narrow area of defect or discontinuity in regions immediately adjacent to the D body Denser particles 50 to 70 A in diameter are visible at the periphery of the body (fig. 10)

An interesting complex structure is found in an oval-shaped D body 1 7–2.4 μ in diameter which displays numerous laminated structures of varying size shape and density Here many ill-defined electron-lucent spaces occur in the body Dense layers approximately 25 A wide are arranged alternately with less dense layers 30 A wide and dense lines and granules seem to have a tendency to become arranged in parallel or concentric array Isolated or clustered denser particles 50 to 70 A in diameter appear in the D body (fig 11)

The D body 1 3–1 7 μ in diameter appearing in figure 12 is more round and more complex in structure than the one shown in figure 11 This body is limited by a double layered unit membrane and contains laminae as well as dense masses of different sizes Apparently each layer of the laminae is not a single dense layer but a double layered structure like a unit membrane Fine dense particles 50 to 70 A in diameter are distributed in the masses Numerous electron lucent spaces tend to occur at the periphery of the body

Periodic acid Schiff reaction of the nutritive cell An ordinary light micrograph of seminiferous tubules stained by the PAS reaction shows numerous large granules giving a positive PAS reaction in the nutritive cell where the sheath of the middle piece of atypical spermatids can be seen (fig. 20) PAS-positive granu are found also in the Golgi zone germ cells. It has already been reveal that the Golgi zone contains a PAS po tive material in other animals (Gres and Zlotnik 48 Gersh 49; Leblond a Clermont, '52 and Cavazos and Melamp '54) A positive reaction with the P stain is usually attributed to 1 2 glyc linkages and is commonly interpreted evidence for the presence of carbohydra

Mitochondria and globoid bodies in th nutritive cell. Numerous mitochondr and globoid bodies, which are less den than the D bodies appear also in th nutritive cell to which typical maturin spermatids are attached. However the are scarely visible in the nutritive cell which are in close relation to atypical de veloping spermatids (fig 7) The mit chondria are smaller and more variable i shape than those described in the typica spermatids (Yasuzumi and Tanaka, '5 and Yasuzumi Tanaka, Tezuka and Na kano 59) Characteristically the mit chondria contain a small number of tubu lar or vesicular cristae and a matrix o medium density (figs 8 10 12 14 an 16) The globoid bodies of medium o low density seem to be a transition for of mitochondria because a few mit chondria 0.2–0 3 μ in width are seen gated in which their limiting membrane and internal organization are not alway clearly visible. If membranes are cut ver obliquely and are parallel to the plane of sections they do not show sharply (fig 13) The globoid bodies are larger tha mitochondria in size and will be hereafter designed as "G bodies One type of G body 0 8 to 1 4 μ in diameter which ma represent the first transition stage is filled with an amorphous substance of medium density in which dense particles are sca tered (fig 14 A) In the second transi tion stage the G body 0 8–1.2 μ in diam eter is bounded by a double layered limit ing membrane and contains dense particles either in random distribution or in a clus ter within the matrix of low density (fi 14 B) In the third transition stage the G bodies 0 7–1 1 μ in diameter appear being limited by a double layered mem brane to contain two smaller bodies in its heterogeneous matrix: one of which

is enveloped by a double layered membrane, the other being composed of a homogeneously dense mass which is encircled by denser particles 50 to 70 A in diameter (fig. 14 C)

Other types of G bodies in the third stage of transition can be seen at high magnification in figures 15 and 16 The one shown in figure 15 is cut so as to reveal the well defined double dense contour in its enveloping membrane. In it is an amorphous matrix concentrated in at least 5 places. Dense particles 40 to 100 A in diameter are found in random distribution and in clusters in the matrix. The other example shows an amorphous material and contains lamellar structures which are arranged either concentrically or in parallel at the periphery of the body Two smaller dense inclusions of different sizes are found in the less dense matrix. Very dense particles 50 to 70 A in diameter, surround the homogenously dense inclusion and are scattered in the matrix. The peripheral lamellar structure is closely associated with a series of vesicles which are enveloped by a double layered limiting unit membrane (fig. 16)

In the next or 4th stage of transition of the G body electron lucent spaces occur in the body In the example shown in figure 17 an oval-shaped body incompletely limited by a double layered membrane shows two concentric lamellar structures of different sizes, each containing electron-lucent areas. The lamellar structures consist of dense layers about 30 A wide arranged alternately with intervening less dense layers about 30 A in width. The matrix is composed of homogeneously dispersed fine granules of medium density dense inclusions, and very dense particles 50 to 70 A in diameter which are found isolated or in clusters (fig. 17) The G body develops finally into an electron-lucent body in which remain a few particles of low and high density and a lamellar element at the periphery of the body (fig. 18).

Turnbull's blue test for organic iron compounds. The dense particles, 50 to 70 A in diameter appearing in the D bodies and G bodies are similar to organic iron particles in density and size as described by Farrant ('54) and Bessis and Breton-Gorius ('57 '59a, '59b) The Turnbull's blue test for organic iron compounds shows a number of dark blue granules in nutritive cells in which numerous maturing spermatids appear attached to its surface. Such granules are rare in very early stages of spermatogenesis They are different in number and size in different cells. They are characteristically found in the nutritive cell, and have never been observed in germ cells (fig. 21) The inorganic iron test was negative in both nutritive and germ cells.

Staining by Sudan III In the preparation stained by Sudan III dark reddish granules appear at the periphery of the seminiferous tubules as Montagna and Hamilton ('51) have observed in the human testis but only a few granules are present in the nutritive cell. This suggests that D bodies and G bodies are not lipoidal. However a helical structure is found along the major axis of the maturing spermatid nucleus. This appearance suggests that there are lipides either in the cytoplasm surrounding the nucleus in a helical configuration or in the mantle which is provided with the endoplasmic reticulum in a canalicular form (fig 22) (Yasuzumi, Tanaka and Tezuka, '60)

DISCUSSION

This report is a follow-up of earlier studies (Yasuzumi and Tanaka, '58) Yasuzumi, Tanaka, Tezuka and Nakano '59; and Yasuzumi, Tanaka and Tezuka, '60) The fine structure of the endoplasmic reticulum in the atypical spermatid and of peculiar bodies appearing in the nutritive cell have been analyzed in detail Possible origins of these bodies will now be discussed.

In an early stage of metamorphosis of atypical spermatids, one does encounter circular profiles that can be definitely identified as elements of the rough-surfaced endoplasmic reticulum. These elements display dense granules 130 to 150 A in diameter adhering to the external surface of their membranes. In this stage it has been noted that the cytoplasm is remarkably basophilic and contains RNA on the basis of cytochemical tests, as described previously on several cells of other animals (Schachman Pardee and Stanier '5

Palade and Siekevitz, '52 Chao and Schachman '56 Tso Bonner and Vinograd '56 Palade and Siekevitz, '56 Cota Robles Marr and Nilson, '58 Tissières and Watson '58 and Blondel and Turian '60) As the metamorphosis of the atypical spermatid proceeds the Palade granules disappear gradually from the surface of the vesicles and at the same time the contents of vesicles increase in density and amount. The cytoplasm loses its basophilic character and no longer shows evidence of RNA. The contents of the vesicles appear finally as dense granules of varying size and number It has already been reported that there is a close relationship between the increase of the dense granules in the vesicles and the progressive reduction of the nucleus which at least completely loses its DNA components (Yasuzumi and Tanaka '58)

The limiting membrane of the vesicles representing the rough-surfaced endoplasmic reticulum which contain an amorphous substance appears as a single dense layer about 50 A thick, as noted previously by Karrer ('60) As the contents of the vesicles increase in density and amount, the limiting membrane is transformed into a double layered structure i.e Robertson's unit membrane ('57 '59) and becomes continuous with the plasma membrane which shows always the unit membrane characteristics. It is assumed that the vesicles which apparently represent a vesicular form of the smooth-surfaced endoplasmic reticulum, are connected with one another to make a continuous channel from the perinuclear space to the intercellular space. Through such a pathway the nuclear material seems to be transported from the nucleus into the intercellular space In the present study it has been noted that the rough-surfaced endoplasmic reticulum connected with RNA-synthesis is transformed into the smooth-surfaced endoplasmic reticulum which plays an important role in transport of the nuclear material It has already been suggested by Bennett ('56) and Porter ('56) that the endoplasmic reticulum may function as an intracellular conductor directing and facilitating intracellular movements.

Cytochemical tests have shown that th dense granules in the vesicles of the atyp cal spermatids are composed of a Feulgen positive material but the dense granule aggregated to form the middle piec sheath lose their basophilic character an are transformed into PAS-positive mate rial. Such a cytochemical change is ver interesting, but it is difficult to explain i the present study how the Feulgen-posi tive material is transformed into the PA! positive material

It is apparent that the D bodies appea ing in the nutritive cell represent th coalescence of granular material derive from the atypical spermatid vesicles. Thi material had previously been discharge into the intercellular space through th channels mentioned above. It then wa incorporated into the nutritive cell in th following manner: The dense granule derived from the atypical spermatids fir become attached to the plasma membrane of the nutritive cell Then minute invagi nations of the membrane form, enfoldin the adherent granules. These cause the coalescence of the dense material. A nar row area of defect or discontinuity of the nutritive cell membrane adjacent to the D body may possibly be evidence of adap tation serving the transfer of the materia (fig 10) Finally the invaginated mem brane is pinched off forming the D body (figs. 11 and 12) This activity of the nu tritive cells reminds one of the pinocytotic activity described in the amoeba by Chap man-Adresen and Holter ('35) in the lung tissue by Karrer ('58) and in the young rat glomerular epithelium by Farquhar and Palade ('60) Cytochemical tests have shown that the D body is compose of PAS-positive material. This D body cor responds to the chromatoid body describec in the previous papers (Yasuzumi and Tanaka, '58 and Yasuzumi, Tanaka and Tezuka, '60)

One of the striking features in the nu tritive cells is a series of G bodies from mitochondria. A few mitochondria, meas uring 0.2 to 0 3 μ in diameter are aggre gated to G bodies 0.8 to 1.2 μ in diamete which are filled with an amorphous sub stance of medium density As the matura tion proceeds the changes occurring in the internal structure of the G bodies lea

a limitation or condensation of its elements which finally are converted to an electron-lucent body leaving a lamellar structure at its periphery The complex change in the structure of mitochondria has already been reported in several cells of other animals (Payne '52 Hess '55; Dempsey '56 Lever '56 Harford, Hamilton, Parker and Revensway '56 De Robertis and Sabatini, '58 Yasuzumi and Ishihara, '58 Zelander '59 Yasuzumi, Ishihara, Nakano, Kise and Takeuchi, '60; and Duncan and Hild, '60) In the present study it was fortunately possible to trace the changes of the mitochondria of the nutritive cell through the successive steps of spermatogenesis. It is very easy to differentiate the G body which originates from mitochondria, from the D body because the former is less dense than the latter.

Both D and G bodies arise from different origins, but have something in common. Both bodies often appear to contain small internal structures seen as densely stripped whorled lamellae with light centers of different sizes and shapes. The diameter of these lamellae is much smaller than those of the Golgi complex. Extremely dense particles 50 to 70 A in diameter are found scattered or in clusters within the bodies Both bodies are encountered in intimate association with the endoplasmic reticulum. These morphological features suggest that nutritive elements in the bodies could conceivably move into the mantle where they could participate in the developing activities of the typical spermatids.

The Golgi complex in the nutritive cell was not studied in detail since there seemed to be no relationship between D and G bodies and the Golgi complex which appeared only as a vesicular structure in a narrow space (fig 7)

The very dense particles 50 to 70 A in diameter found in the G and D bodies are similar in density and size to organic iron particles as described by Farrant ('54), Palade ('56) Bessis and Breton Gorius ('57 '59a, '59b) and Farquhar and Palade ('60) In the present study granules which are positive in the Turnbull's test for organic iron compounds were seen only in the nutritive cell where maturing spermatids appear attached to its surface A test for inorganic iron was negative.

It was noted that the D and G bodies were not lipid since they did not stain with Sudan III. Yet it is interesting that typical maturing spermatid heads show a positive lipid reaction in a helical pattern about the head It is not sure whether the lipid exists within the mantle or in the cytoplasm. However the lipid seems to be located in the cytoplasm forming a helix around the maturing nucleus since the lipid is rarely found in the nutritive cell from which the mantle develops. It has been revealed that the cytoplasm spiraling around the nucleus is sloughed off when the typical spermatid has reached a certain degree of maturity (Yasuzumi, Tanaka and Tezuka, '60). The present study suggests that the mechanism by which the cytoplasm sloughs off the nucleus may be related to lipid degeneration of the cytoplasm.

ACKNOWLEDGMENT

The author wishes to explain his grateful appreciation to Professor H. Stanley Bennett for his assistance in revising the manuscript.

LITERATURE CITED

Arrac, J P 1950 Glycogen in human testicular biopsy material. J Clin. Endocrinol., 10 1465–1470.

Bennett, H. S. 1958 The sarcoplasmic reticulum of striped muscle. J Biophys. Biochem. Cytol., 2: suppl., 171–174.

Bessis, M. C., and J Breton-Gorius 1957 Iron particles in normal erythroblasts and normal and pathological erythrocytes. Ibid., 3 503–504

——— 1959a Différents aspects du fer dans l organisme. I. Ferritine et micelles ferrugineuses. Ibid., 6 231–236.

——— 1959b Différents aspects du fer dans l'organisme. II. Différentes formes de l'hémosidérine. Ibid. 6 237–240.

Blondel, B and G. Turian 1960 Relation between basophilia and fine structure of cytoplasm in the fungus *Allomyces macrogynus* Em. Ibid 7 127–134

Ca azos, L F and R. M. Melampy 1954 A comparative study of periodic acid reactive carbohydrates in vertebrates. Am. J Anat., 95 467–490.

Chapman-Andresen C., and H. Holter 1955 Studies on the ingestion of ^{14}C glucose by pinocytosis in the amoeba Chaos chaos. Exp. Cell Res. suppl 3 52–63.

Chao, Fu-Chuan, and H. K. Schachman 1956 The isolation and characterization of a macromolecular ribonucleoprotein from yeast. Arch. Biochem. Biophys., 61 220–230.

Cota-Robles, E. H., A. G. Marr and E. H. Nilson 1958 Submicroscopic particles in extracts of *Azotobacter agilis*. J Bact., 75 243–252.

Daoust, R., and Y Clermont 1955 Distribution of nucleic acids in germ cells during the cycle of the seminiferous epithelium in the rat. Am. J Anat., 96 255–283.

Dempsey E. W 1956 Variations in the structure of mitochondria. J Biophys. Biochem. Cytol., 2 suppl., 305–312.

De Robertis, E., and D Sabatini 1958 Mitochondrial changes in the adrenocortex of normal hamsters. Ibid., 4 667–670.

Duncan D and W Hild 1960 Mitochondrial alterations in cultures of the central nervous system as observed with the electron microscope. Z. Zellforsch., 51 123–135.

Farquhar M. G., and G. E. Palade 1960 Segregation of ferritin in glomerular protein absorption droplets. J Biophys. Biochem. Cytol., 7 297 304

Farrant, J L. 1954 An electron microscopic study of ferritin. Biochem. Biophys. Acta, 13 569–576.

Gersh, I. 1949 A protein component of the Golgi apparatus. Arch. Path., 47 99–109

Gresson, R. A. R., and I. Zlotnik 1948 A study of the cytoplasmic components during the gametogenesis of *Bos taurus*. Quart. J Micr Sci., 89 219–228.

Harford C G., A. Hamlin E. Parker and T van Ravensway 1956 Globoid structures in the cytoplasm of rapidly growing *H La* cells. J Biophys Biochem. Cytol 2 suppl 347–350.

Hess, A 1955 The fine tructure of young and old spinal gangli Anat. Rec 123 399–423.

Hotchkiss R D 1948 A microchemical reaction resulting in the staining of polysaccharide tructures in fixed ti sue preparations. Arch. Biochem 16 131–141

Karrer H E 1958 The trastructure of mouse lung The alveolar macrophage J Biophys. Biochem Cytol 4 693–700

——— 1960 Electron microscopic study of the phagocytosis proces in lung Ibid 7 357–366.

Leblond, C P 1950 Distribution of periodic acid-reactive carbohydrates in the adult rat. Am. J Anat 86 1–49

Leblond, C P and Y Clermont 1952 Spermatogenesis of rat, mouse hamster and guinea pig as revealed by the "periodic acid-fuchsi sulfurous acid" technique Ibid., 90 167–215.

Lever J D 19.6 Physiologically induced changes in adrenocortical mitochondria. J Biophys. Biochem. Cytol. 2 uppl., 313–318.

Macallum, A. B. 1908 Die Methoden und Ergebnisse der Mikrochemie in der biologischen Forschung. Ergeb. Physiol 7 552–652.

Mancini, R. E., J Nolazco and F A De La Balze 1952 Histochemical tudy of normal dult human testes. Anat Rec 114 127 14

McManus, J F A. 1948 Histological and histochemical uses of periodic acid. Stain Tech., 23 99–108.

Montagna, W and J. B Hamilton 1951 Histological studies of human testes. I. The distribution of lipids. Anat. Rec., 109 635–66

——— 1952 Histological studies of human testes. II. The distribution of glycogen and other HIO_4-Schiff reactive substances Ibid 112 237 250.

Payne F 1952 Cytological changes in the cell of the pituitary thyroids, adrenals and sex glands of ageing fowl. In Cowdry' Problems of Ageing, 3rd ed., A. I. Lansing, ed. Williams and Wilkins Co., Baltimore, pp. 381–402

Palade, G. E. 1956 The endoplasmic reticulum. J Biophys. Biochem. Cytol., 2 suppl 85–98.

Palade G. E., and P Siekevitz 1956 Liver microsomes. An integrated morphological and biochemical study Ibid., 2 171 200.

——— 1956 Pancreatic microsomes An integrated morphological and biochemical study Ibid., 2 671–690.

Porter K. R. 1956 The sarcoplasmic reticulum in muscle cells of amblystoma larvae. Ibid 2 suppl., 163–170.

Robertson, J D 1957 The cell membrane concept. J Physiol 140 58P 59P

——— 1959 The ultrastructure of cell membranes and their derivatives. Biochem. Soc Symp 16 3–43

Schachman, H. K. A. B. Pardee and R. Y Stanier 1952 Studies on the macromolecular organization of microbial cells. Arch Biochem Biophys 38 245–260.

Tissières, A., and J D Watson 1958 Ribonucleoprotein particles from *Escherichia coli*. Nature, 182 778–780

T'o, P O P J Bonner and J Vinograd 19 Microsomal nucleoprotein particles from pea seedlings J Biophys Biochem. Cytol 2 451 466.

Yasuzumi, G. and R Sugihara 19.8 A comparative electron microscopic study on the Yoshida sarcoma cells of ascites tumor cells Yoshida sarcoma cells of human cancerous peritonitis ascites cells Cancer Res 18 116 1170

Yasuzumi G R Sugihara S Nakano, T Ito and H T Ikeuchi 1960 Submicroscopic structure of cell necrobiosis of Yoshida sarcoma revealed by lectron microscopy Ibid 3 339–343

Yasuzumi G., and H. Tanaka 1958 Spermatogenesis in animal revealed by lectron microscopy VI. Researches on the spermatozoon-dimorphism in pond snail, *Cipangopaludina malleata*. J Biophys. Biochem Cytol 4 621–632.

Yasuzumi G., H Tanaka and O Tezuka 19 Spermatogenesis in animals revealed by lectron microscopy VIII. Relation between the nutritive cells and the developing spermatid in a pond snail, *Cipangopaludina malleata Reeve* Ibid., 7 499–504

[illegible], G. H. Tanaka, O. Tezuka and [illegible] [illegible] The ultrastructure of organelles appearing in spermatids and nutritive cells of *Cipangopaludina malleata*. Z. Zellforsch., [illegible]: [illegible]–643.

Zelander T 1959 Ultrastructure of the mouse adrenal cortex. An electron microscopical study in intact and hydrocortisone-tre ted male adults. J Ultrastructure Res., suppl., 2: 5–111

PLATE 1

EXPLANATION OF FIGURE

1 Section through an early atypical spermatid of *Cipangopaludina malleata* Reeve showing part of nucleus (N) perinuclear space (PS) and vesicles (V) which represent the rough-surfaced endoplasmic reticulum of the atypical spermatid. The karyoplasm is composed of fine granules dispersed without clear regularity of patterns, though the granules seem to be arranged in coiled strands t the points marked by the arrows. The vesicles (V) limited by single layered membrane contain amorphous substance AMS) of low density Dense granules 130 to 150 A in diameter appear attached to the xternal surfaces of the vesicles (V) and free in the cytopl smic matrix. × 130,000

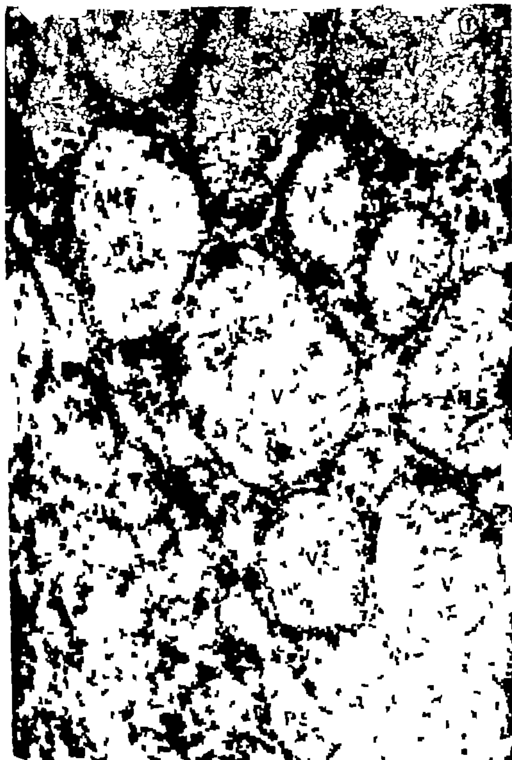

1
V
V
V
PS
V
V
V
PS

PLATE 3

EXPLANATION OF FIGURES

4 Two dense large granules (DG) can be seen in the intercellular space Note that the rough-surfaced endoplasmic reticulum contains amorphou substances (AMS) and that the smooth-surfaced endoplasmic reticulum invests dense large granules (DG). The limiting membrane of one of the vesicles containing dense granules leads to the plasm membrane t the point marked by the arrow × 48,000.

5 As the metamorphosis of the atypical spermatid proceed many of the vesicles come to contain the dense large granules. It is clearly visible that the vesicles are limited by double layered (unit) membrane (arrows) at high magnification. The plasma membrane (PM) shows also a double layered structure The perinuclear space (PS) is visible × 138,000.

DG
DG
AMG
M

PLATE 5

EXPLANATION OF FIGURE

7 A longitudinal section of an atypical maturing spermatid lodged in deep indentation in the surf ce of nutritive cell (NC) showing an irregular outline. The atypical spermatid nucleus (N) is reduced to a thin arched profil which envelops bundle of tail filaments (TF) The middle piece is surrounded by an env lope composed of series of vesicles filled with a dense material. The nucleus (NN) of the nutritive cell (NC) shows a flat profile. Peculiar dense bodies (DB) and globoid bodies (GB) and vesicles (V) of different sizes can be seen in the nutritive cell (NC) The Golgi zone (GZ) is composed of small vesicles and group of small vesicles surrounded by single membrane (arrow) × 15,200.



PLATE 7

EXPLANATION OF FIGURE

10 A dense granule (DG) and amorphous substances (AMS) are found in the intercellular space between two atypical spermatids (ASP) and the nutritive cell (NC). At the periphery of the nutritive cell, an irregularly shaped D body (DB) with inhomogeneous appearance appears attached to the mitochondrion (M) and endoplasmic reticulum (ER). The plasma membrane of the nutritive cell (NC) is discontinuous at the parts marked by the white arrows. Very dense particles 50 to 70 A in diameter are found at the periphery of the D body. The vesicles representing the smooth surfaced endoplasmic reticulum and the plasma membrane show double layered structure at the points marked by the black arrows. × 77,000.

M

A

ER

ER

DB

ER

ASP

NC

AMS

DG

ASP


15
V
GB
V

PLATE 9

EXPLANATION OF FIGURE

12 A "D" body (DB) limited by a double layered membrane (white arrows) contains laminae and dense masses of different sizes. Numerous electron lucent spaces occur in the body. Apparently each layer of the laminae is not a single unit but a double layered structure (black arrows). Fine dense particles, 50 to 70 A in diameter, are distributed in the mass. Mitochondria (M) provided with tubules or cristae are filled with a matrix of intermediate density. The endoplasmic reticulum (ER) appears often attached to the limiting membrane of the D body (DB) and the mitochondria (M). A dense granule (DG) can be seen in the intercellular space between the nurse cell (NC) and the atypical spermatid (ASP). × 81 000.


13
V
M
LM
V
N
V
V
V

PLATE 12

EXPLAN TION OF FIGURE

15 G body (GB) ppearing in the nutritive cell in high magnification depicts a ell defined double layered unit limiting membrane (white rrows) A amorphous matrix is concentrated in at least 5 places (black arrows) Dense particles re found in random distribution and in clusters in the m trix. Vesicles (V) appear losely attached to the G body × 157,000.


15
V

PLATE 13

EXPLANATION OF FIGURE

16 G body (GB) appearing in the nutritive cell (NC) at high magnification. It is enveloped by double layered unit membrane (white arrow) The body consists of an amorphous material and contains lamellar structures which are arranged either concentrically (CC) or in parallel (PL) at the periphery of the body Two smaller dense inclusions (DI) of different sizes can be seen in the less dense matrix Denser particles 60 to 70 Å in diameter either surround the homogeneously dense incl sion or are scattered in the matrix. The peripheral lamellar structure (black arrow) seems to be associated with one of series of vesicles which are enveloped by a double layered limiting unit membrane. A mitochondrion (M) of small size i visible showing little internal organization. × 154,000


16
BL
NC
B
CC
V
V
PL
V
V
V
M

PLATE 15

EXPLANATION OF FIGURES

19 This picture displays an ordinary light micrograph of the PAS-reaction in the sheath *of the middle piece of atypical spermatids which were fixed with 1% osmium tetroxide* adjusted with Veronal-acetate buffer to pH 7.3. The sheath gives a positive PAS-reaction × 4000

20 This picture shows an ordinary light micrograph of seminiferous tubules which were fixed in 1% osmium tetroxide adjusted with Veronal acetate buffer to pH 7.3 and stained by the PAS-reaction. Numerous granules giving positive PAS-reaction appear in the nutritive cell and in the Golgi zone (arrows) of germ cell. At the right, lower side of the figure the sheath of the middle piece of typical spermatids can be seen, being stained by the PAS-reaction. The basement membrane (BM) of the seminiferous tubule shows a positive PAS-reaction. × 4000

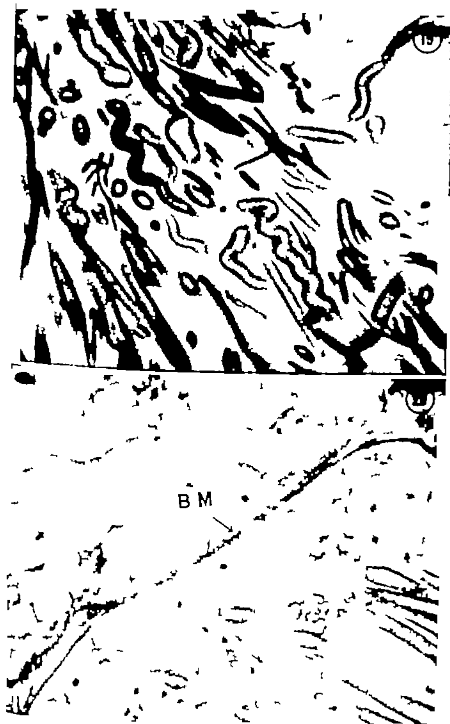

B M

PLATE 16

EXPLANATION OF FIGURES

21 An ordinary light micrograph of seminiferous tubules with maturing sperm shows granules giving positive Turbull's blue reaction for organic iron compounds in the nutritive cell. Background counterstained by eosin. × 2000.

22 An ordinary light micrograph of seminiferous tubules fixed in 1% osmium tetroxide adjusted with Veronal-acetate buffer to pH 7.3 and stained with Sudan III and methylene blue It shows dark reddish granules at the periphery f the seminiferous tubules, and only few granules (black arrow) in the nutritive cell. A helical structure stained with Sudan III can be seen at the head part of the typical maturing perm tids (white arrows) The nuclei of germ cells and the sheaths of middle pieces of typical spermatids are stained by methylene blue. × 4000


21


22

(Blattner and Williamson, '51 Williamson et al. '56 Robertson et al. '60) resulted in abnormalities of several embryonic organs including the lens. The high titers of influenza A and Newcastle disease viruses necessary for initiation of lens defects resulted in severe retardation or complete necrosis of the lens followed shortly by death of the embryo. However in embryos infected at the 48-hour stage by mumps virus, there was survival for 3–15 days after inoculation and the occurrence of virus-induced cataracts in many of these embryos (Williamson et al. '57)

The present report is concerned with the incidence origin, and development of characteristic mumps-induced lens cataracts in embryos infected at various stages during the early formative phases

MATERIALS AND METHODS

Chick embryos were inoculated at each of the following five incubation ages: 36 48 60 72 and 96 hours. The number of experimental and control embryos injected in each age group is shown in table 1

The Enders strain of mumps virus was used and was obtained from American Type Culture Collection. This virus was inoculated in 10 dilution into the allantoic cavities of eight-day chick embryos. The infectious allantoic fluids were harvested after incubation at 35 C for seven days. The fluid was harvested from each egg separately and tested for hemagglutinating activity Fluids showing titers of 1–500 or more were pooled and dispensed in ampoules for storage at −70 C For inoculation into embryos the suspensions were diluted in buffered saline (pH 7.2 to the required infectivity

Infectivity titers were determined by inoculating 10-fold dilutions of the virus suspensions into the allantoic cavities of groups of eight-day-old embryos. These were tested after seven days for virus growth as indicated by hemagglutinability of the allantoic fluids. The ID_{50} was calculated by the method of Kärber ('31)

The eggs were from flocks of New Hampshire reds, and were incubated in a forced-draft incubator at 37 C. The embryos were prepared for inoculation by cutting a square window in the shell over the embryo The shell membrane was then ruptured and the inoculum injected through the vitelline membrane and over the embryo In the 96-hour group, in which the amniotic membrane covered the embryo the inoculum was injected into the amniotic cavity The amount of inoculum was 0 05 ml in all cases. Optimum titers of the virus to yield a high percentage of viable defective embryos after inoculation at 48 hours of incubation had been previously determined (Williamson et al '57). Comparable titers were employed in the present study with an ID_{50} of 10^{4} to 10^{5} per 0 05 ml of inoculum. Control embryos were inoculated with normal allantoic fluids in dilutions equal to those of the experimental groups. All embryos were staged according to the criteria of Hamburger and Hamilton ('51) at the time of inoculation

TABLE 1

Incidence of lens cataracts observed grossly in chick embryos three or more days after inoculation in five age groups

Group	Hours of incubation at inoculation	Total eggs virus-inoculated	Range of developmental stages inoculation	Experimental embryos observed at three or more days postinoculation: Number of embryos	Number with cataracts	Percentage incidence of cataracts
I	36	263(209)	8–13	72	63	83
II	48	364(262)	9–15	173	115	67
III	60	209(164)	13–18	93	20	22
IV	72	193(186)	15–20	105	9	9
V	96	152(136)	20–23	83	0	0

Incubation temperature 37°C.
In parentheses are the numbers of control eggs which were injected with non-infectious allantoic fluid [illegible] seen in experimental embryos
None of the control embryos developed typical cataracts
Hamburger-Hamilton stages.
Cataracts were not observed grossly prior to three days postinoculation

After inoculation, the shell opening was covered with a glass cover slip and the edges sealed with paraffin. Surviving embryos were examined daily up to 14 days postinoculation, by observation through the shell opening under 24 × magnification. Hamburger-Hamilton staging was done whenever possible, although development of the membranes obscured the view of the older embryos.

At 24-hour intervals after inoculation groups of surviving embryos were harvested and fixed in Bouin's fluid. Embryos were harvested up to seven days postinoculation in the 36-hour group up to eight days in the 48-hour and 60-hour groups up to 14 days in the 72-hour group, and up to ten days in the 96-hour group. At the time of fixation all embryos were examined under the dissecting microscope for gross appearance of cataracts as well as other abnormalities. Also, the developmental stage (Hamburger-Hamilton) was determined. In addition, in most of the harvested groups, five experimental and two control embryos were serially sectioned and stained for microscopic examination. Altogether, 180 experimental and 80 control embryos were sectioned. The stains used were Delafield's hematoxylin and eosin, and eosin and methylene blue.

OBSERVATIONS

Incidence of lens cataracts

The five age groups studied are listed in table 1 along with the number of virus-inoculated and control embryos as well as the range of developmental stages at inoculation in each group. The characteristic type of lens cataract induced by virus inoculation was not observed grossly in any of the control embryos nor in any of the experimental embryos prior to three days postinoculation. As described previously (Williamson et al., '57) the cataract appears at three days after inoculation as a small and dense white opacity centrally or slightly eccentrically located. As development proceeds, both the opacity and the lens become larger with the cataract maintaining its central position.

Table 1 also indicates the numbers of embryos examined grossly 3–14 days after inoculation. These numbers do not represent true survival figures since some embryos, which might have survived the virus infection, were harvested for histological study during the first two postinoculation days.

The incidence of lens cataracts detected by gross examination in embryos living three or more days after inoculation is also indicated in table 1 The incidence ranges from 88% in the youngest age group to none following inoculation in the oldest age group. It is evident from these figures that susceptibility of the lens to damage by the virus was high in the youngest embryos inoculated and that this susceptibility declined with advancing developmental age.

In table 2 the incidence of cataracts is related to the developmental stage and the status of lens morphology at the time of inoculation. There was a high incidence (ranging from 87 to 43%) in embryos inoculated prior to the time the lens vesicle closes off a low incidence when inoculated at the time of closure and no incidence when inoculated after separation of the lens vesicle from the surface ectoderm. It can be stated then that the mumps-induced defect is produced only after direct contact with lens tissue at a time when this tissue is susceptible, and that this critical period is during early formative phases, i.e. during placode pit and early vesicle stages Following this critical period, it is apparent that the developing lens either is protected by overlying tissue which is not susceptible and therefore cannot transmit the virus or the lens tissue itself is capable of resisting viral invasion.

Cataracts occurred bilaterally in a majority of affected embryos, but in many cases were more extensive in the right lens. In subsequent histological examinations the pathological changes were often found to be more advanced in the right lens. In a few cases cataracts occurred unilaterally either in the right lens or in the left lens. These observations are in contrast to those of Langman ('60) who found that cytotoxic effects of lens antiserum were located unilaterally on the left side in 70% of the embryos tested

In addition to the specific lens-cataract type of defect in the older embryos there was exhibited a consistent inhibition

TABLE 2

Incidence of lens cataracts observed grossly in chick embryos three or more days postinoculation — correlated with developmental stages and lens morphology at inoculation

Stages at inoculation	Lens morphology at inoculation	Number of embryos observed 2–14 days post-inoculation	Number of observed embryos with cataracts	Percentage incidence of cataracts
8–10	Surface ectoderm and optic vesicle in contact (stage 10)	52	45	87
11–13	Lens placode	133	99	74
14–16	Lens pit and early vesicle with lens pore	138	59	43
17–18	Lens pore closing and lens vesicle separating from surf ce ectoderm	101	9	9
19–25	Lens vesicle separated from surface ectoderm	113	0	0

Hamburger-Hamilton stages.

the growth of the amniotic membrane and also a moderate inhibition of embryonic growth in general. In other words, the embryos surviving three days or longer with cataracts were observed to be somewhat smaller than the control embryos, but not otherwise abnormal except for spraddling in some cases. It should be noted that in previous studies a few embryos inoculated at the 48-hour period and surviving for 12 to 15 days did show defects of feathering pigmentation of the optic cup and of lid and skin development around the eye (Williamson et al. '57)

Histogenesis of lens cataracts

Before proceeding with a description of the histogenesis of the mumps-induced cataract it should be noted that a low inci dence of tissue damage in other surface ectodermal structures such as neural tissue auditory placodes and visceral arch ectoderm was observed in histological preparations This tissue damage was degenerative in character and was seen in embryos harvested the first and second postinoculation days Embryos surviving three or more days rarely exhibited any specific developmental defects, other than lens cataracts in organs arising during this early period of development. It is possible that the damage observed in organs other than the lens prior to the third day represents defects which are lethal to the em bryo or it may be that some embryos n toxic effects from the large doses of v inoculated. Nevertheless the fact that mumps-induced cataracts are compat with survival of the embryos up to at l the fifteenth postinoculation day is marked contrast to the short survival ti of embryos inoculated with two o myxoviruses at titers which produce cific organ defects (Williamson et al., '56 Robertson et al. '55 '60)

Histological examinations confirm t cataracts occurred only in embryos ino lated prior to stage 18 (i.e prior to sep tion of the lens vesicle from the surf ectoderm) as indicated earlier by g observations (table 2) However a cha teristic microscopic lesion was found to present in lenses at least 24 hours prio the gross appearance of the lens opaci This first indication of lens abnorma was rarely observed earlier than two d following inoculation and consisted of terations in the cytoplasm of differe ating lens fiber cells. Figure 1 show lens vesicle from an embryo which l been inoculated at 48 hours incubat and allowed to develop for two days bef fixation and subsequent preparation microscopic study This lens is somew retarded in growth but otherwise the c defect detectable in this type of prep

tion is the presence of numerous eosinophilic inclusions in the cytoplasm of the differentiating lens fibers. It is noteworthy that these characteristic inclusions are also present in the anterior epithelium and are sometimes present in the cytoplasm of the equatorial cells, their incidence in this region is much lower than in the differentiating lens-fiber cytoplasm. Variations in the size and shape of the inclusions are shown more clearly at higher magnification in figure 2.

By the end of the third day after inoculation there is a marked cytoplasmic vacuolization, nuclear pyknosis, and necrosis of the centrally located lens fibers (fig. 3). Eosinophilic inclusions are present in the differentiating lens fibers peripheral to the central degenerating area. The inclusions are throughout the cytoplasm but are more numerous at the anterior ends of the lens fibers. Also, they are present in the area of necrosis and in the lumen along with basophilic bodies of various sizes and irregular shapes as well as other debris resulting from cellular degeneration (fig. 4). It should be noted that the eosinophilic inclusions are rarely present in the anterior epithelium and are not numerous in the equatorial cells.

The characteristic histopathology is more extensive five days after virus inoculation (figs. 5–6). The most centrally located lens fibers are completely destroyed and the ones beginning differentiation along the periphery contain the characteristic eosinophilic inclusions. It is evident that growth and differentiation of the lens proceed while central lens fibers become progressively more extensively damaged, with the cataract becoming larger as the lens becomes larger but remaining in a central position and involving only differentiating lens fibers.

By seven days after virus inoculation the lens fibers are almost completely destroyed (figs. 7–8). The equatorial epithelium now has abnormal masses of cells extending from it internally. This same abnormal type of cell proliferation also involves the anterior epithelium. It is noteworthy that the lens capsule remains intact, even in lenses where the cataract is extensively developed (see figs. 3–8).

DISCUSSION

During active phases of lens organogenesis it is evident from our experiments that differentiating lens-fiber cells are strikingly more susceptible to damage by mumps virus than are the anterior or equatorial cells. Such specific tissue manifestations of viral activity during organogenesis have been noted previously. For example, in young embryos infected with Newcastle virus (Robertson et al. '55) or influenza A virus (Robertson et al., '60) an alar-basal difference in susceptibility was noted during the process of neurulation. Subsequently in a study of proliferative patterns during neural organogenesis no correlation was found between differences in mitotic densities and viral susceptibility (Corliss and Robertson '63). It therefore seems that differences in susceptibility to viruses during organogenesis can be due to morphogenetic mechanisms other than cell proliferation. Related to this is the observation by Noyes and Mellors ('57) employing the fluorescent antibody technique that most of the papilloma virus could be found in the nuclei of the differentiated keratinizing cells in superficial regions of the papillomas in the cottontail rabbit. Subsequently Noyes ('59) demonstrated by means of microcautery technique that the papilloma virus could be extracted from the keratinized layers of cells, and not from the actively proliferating cells at the base of the papillomas. Electron microscopic observations by Stone et al. ('59) indicated that the spherical virus particles, presumably representing the fully infective virus, could be found only in the differentiating and fully keratinized cells of the upper part of rabbit papillomas while finely granular viral material was found limited to the nucleoli in the cells of the deeper germinative layers. Gross ('61) has suggested that the virus of rabbit papilloma exists in two forms: an immature non-infective virus in the proliferating cell layers and the mature infective virus present in the upper keratinized part of the papilloma. A different conclusion was reached by Saxén et al. ('62) who applied polyoma virus to in vitro cultures of mouse kidney rudiment and found that the metanephrogenic

mesenchyme is highly susceptible whereas tubules differentiating from both the ureteric bud and metanephrogenic tissue are resistant to the cytolytic effects of the virus. This was confirmed in a later study using the fluorescent antiserum technique to locate the sites of viral replication (Vainio et al. '63a) However when the effects of vesicular stomatitis virus (VSV) were compared with those of polyoma virus an important difference was noted (Saxén et al. '63 Vainio et al., '63b) It was found that the mesenchymal condensations which represent the first detectable step in tubulogenesis resist polyoma virus but are highly susceptible to VSV and support its replication. These varying observations indicate that, as might be expected, the basis and patterns of viral susceptibility of tissues during developmental phases vary with different viruses. There are undoubtedly also variations due to the techniques used the tissues employed, and the state of development of the tissues.

Susceptibility of developing lens tissue to the pathogenic effects of mumps virus is related to the developmental stage at the time of inoculation. The lens is not affected when inoculation occurs after closure of the lens vesicle and its separation from overlying ectoderm Similar results were obtained in experiments with other viruses (Robertson et al. '55 '60) with respect to placode organs which roll up into a vesicle or tube and detach from surface ectoderm in the course of their development. The important differences between mumps and the other viruses studied (NDV and influenza) are the survival of mumps-infected embryos for much longer periods of time and the fact that the lens cataract is the only defect observed, among organs differentiating at the time of virus inoculation which is compatible with survival for three or more days after inoculation. Whether the specific pathological changes observed in the lens are due to a particularly rich source of materials necessary for viral replication or to a high degree of susceptibility of the lens fibers to the damaging effects of the virus is not known. Although the virus is known to increase in titer in tissues of the developing embryos the virus has not acually been demonstrated in the lens or in of the early embryos. Since there abundant extraembryonic tissues such as chorion and amnion which are readily available for viral replication, it is certain whether the specific damage is due to replication of the virus or to some other secondary effect associated with the ence of the virus. However viral antigen has been demonstrated in the epithelial cells of the skin, in the oropharynx, naso-pharynx, trachea and bronchi of chick embryos inoculated at eight days incubation by Watson ('52) and it seems likely that tissues of the early embryonic stages may also be susceptible to infection by the mumps virus. Further studies are planned to see if the viral antigen can be located in specific tissues of the early embryos. The specificity of the damage for the lens fibers presents an interesting point for speculation. It was observed that the lens capsule remained intact regardless of the severity of the damage to the lens. It may be that the lens tissue, infected at the time that the lens vesicle lies open, later becomes an incubation chamber after closure of the lens vesicle and separation from the overlying ectoderm, with the lens capsule serving as a barrier to the escape of liberated virus. In this way the virus in the lens might build up to a very high titer, more rapidly than is possible in other tissues of the embryo. In considering the longer survival of mumps-infected embryos and the slower development of abnormalities when compared to the effects of influenza and Newcastle disease it is probably relevant that the mumps virus appears to have a much longer latent period and a slower growth cycle than the other viruses (Treagan and Fong, '62)

The earliest manifestation of mumps-induced changes in lens tissue is the occurrence of prominent eosinophilic inclusions in the cytoplasm of the differentiating lens fibers. These inclusions are of various sizes and shapes, and are often surrounded by a clear zone. Similar inclusions were described by Brandt ('58) in cells of tissue cultures of the chorioallantoic membrane and the amniotic membrane of chick embryos infected with New-

cella and mumps viruses. In the case of mumps virus, Brandt used two strains and found the characteristic inclusions in tissues infected with the Enders strain, the strain used in our experiments but did not find the inclusions in tissues infected with the Lawn strain. In subsequent work, Brandt ('61) as well as Lebbo et al. ('63) found similar inclusions in mammalian cell types infected with mumps. In Brandt's fluorescent antibody studies, the viral antigens were found to be more widely and evenly distributed in the cytoplasm of infected cells than were the inclusions in similar preparations. Therefore these inclusions probably do not represent concentrated virus. Brandt suggested the possibility that a major component of the inclusions is a cellular protein which is altered as a result of viral action in such a way as to permit its aggregation and shrinkage when fixed with an acid fixative.

The period of greatest susceptibility of differentiating lens fibers to the pathogenic effects of mumps coincides with the time of initial formation of lens proteins. According to Maisel and Langman ('61) the lens-fiber protein, beta crystalline, appears at the onset of lens-fiber differentiation. At approximately the same time a continuous increase in the concentration of RNA begins in the lens-fiber cytoplasm (McKeehan, '58) It is possible that these qualitative and quantitative changes may be involved in the specific pathological changes induced in the lens by mumps virus.

SUMMARY

1. Critical inocula of the Enders strain of mumps virus were injected over the blastoderm at 36 48 60 72 and 96 hours of incubation (Hamburger Hamilton stages 8–25) Surviving embryos were harvested at daily intervals up to 14 days postinoculation.

2. Observations on gross and serially sectioned specimens revealed that, of the organs differentiating at the time of inoculation with mumps virus, the lens was the only one consistently exhibiting abnormal development. By comparison, maldevelopment in other organs or tissues was occasionally observed up to the third day postinoculation but rarely observed in embryos surviving three or more days.

3. A high incidence of characteristic lens cataracts was observed but only in embryos which had been inoculated prior to Hamburger Hamilton stage 18 i e., prior to separation of the lens vesicle from surface ectoderm. Cataracts did not develop in embryos inoculated after this stage of development. This indicates that the susceptible stages of lens development, under the conditions of our experiment are the placode, pit and early vesicle stages.

4 An analysis of the histopathogenesis of lens cataracts in embryos inoculated at stages 8–17 indicates that development of this abnormality occurred exclusively in differentiating lens fibers until seven days postinoculation at which time the equatorial and anterior regions also showed marked pathological changes.

5 The earliest histopathological manifestation of virus infection occurred in lens vesicles two days after inoculation and was indicated by the presence of numerous prominent eosinophilic inclusions in the cytoplasm of differentiating lens fibers and sometimes also a few such inclusions in the equatorial cells. Following this, centrally located fibers exhibited progressive cytoplasmic vacuolization nuclear pyknosis, and necrosis. Growth and differentiation of the lens proceeded peripherally while central degeneration progressed towards the periphery The cataract thus became larger as the lens enlarged but remained in a central position.

6 It can be concluded from our observations on mumps-infected chick embryos that (1) the initiation of characteristic *lens cataracts occurs in high incidence if* mumps virus is inoculated over the blastoderm immediately prior to or during the early formative phases of lens development, (2) lens cataract is the only specific organ defect, among organs differentiating at the time of inoculation (3) the histopathological manifestation of viral activity is first evident in the early lens fibers and (4) the central location and progressive enlargement of the cataracts result from degenerative changes continuously occurring in the cells differentiating into lens fibers.

LITERATURE CITED

Blattner, R. J and A. P Williamson 1951 Developmental abnormalities in the chick embryo following infection with Newcastle disease virus. Proc. Soc. Exp Biol. and Med., 77 819–821

Brandt, C. D 1958 Inclusion body formation with Newcastle disease and mumps viruses in cultures of chick embryo cells. Virology 5 177–191

——— 1961 Cytopathic action of myxoviruses on cultivated mammalian cells. Virology 14 1–10.

Cordes, F C. 1949 Cataract formation in the human embryo after Rubella. Arch. Ophth., 42 596–605.

Cordes, F C., and A. Barber 1946 Changes in lens of embryo after Rubella. Arch. Ophth., 36 135–140.

Corliss, C E., and G. G. Robertson 1963 The pattern of mitotic density in the early chick neural epithelium. J Exp Zool., 153 125–140.

Dekaban, A., J O'Rourke and T Cornman 1958 Abnormalities in offspring related to maternal rubella during pregnancy Neurology 8 387–392.

Erickson C. A. 1944 Rubella early in pregnancy causing congenital malformations of eyes and heart. J Pediat., 25 281–283.

Gregg, N. McA. 1941 Congenital cataract following German measles in mother Trans. Ophth Soc. Australia, 3 35–46

Gross, L. 1961 Oncogenic Viruses. Pergamon Press, New York. Chapter 2, 27–34

Hamburger V and H. L. Hamilton 1951 A series of normal stages in the development of the chick embryo. J Morph., 88 49–92

Helweg Larsen, H. F and E. L. Nielsen 1948 Forandringer i fosterlinse efter rubeolae? Ugesk. f laeger 110 1394–1396.

Kärber G. 1931 Beitrag zur kollektiven Behandlung pharmakologischer Reihenversuche Arch. exp Path. Pharm., 162 480–483.

Langman, J 1960 The effect of lens antiserum on chick embryos. Anat. Rec., 137 135–140.

Leilo J J Szántó and P Albrecht 1963 Mumps virus infection of Hela cells studied by the fluorescent antibody method. Acta Virol., 7 3 –41

Maisel H and J Langman 1961 An immunoembryological study on the hick lens. J Embryol. Exp Morph., 9 191 201

McKeehan, M. S. 1956 The relativ ribonucleic acid content of len and retina during lens induction in the chick. Am. J Anat 99 131 156.

Noyes, W F 1959 Studies on the Shope rabbit papilloma virus. II. The location of infective virus in papillomas of the cottontail rabbit. J Exp. Med., 109 423–428.

Noyes, W F and R. C. M llory 1957 Fluorescent ntibody detection of the antigen of the Shope papilloma virus in papilloma of the wild and domestic rabbit. J Exp. Med 106 555–562.

O'Rahilly R., and D B Meyer 1959 The early development of the eye in the chick. Acta Anat., 36 20–58.

Reese, A. B. 1944 Congenital cataract an other anomalies following German measles i the mother Am. J Ophth., 27 483–487

Rhodes, A. J 1961 Virus infections and co genital malformations. In First Internation Conference on Congenital Malformations, p 106–116 J B Lippincott Co., Philadelphia.

Robertson, G. G., A. P Williamson and R. J Blattner 1955 A study of abnormalities i arly chick embryos inoculated with Newcast disease virus. J Exp. Zool., 129 5-43.

——— 1960 Origin of myeloschisis in chic embryos infected with influenza-A virus. Yal J Biol. and Med., 32 449–463.

Saxén, L., T Vainio and S. Toivonen 19 Effect of polyoma virus on mouse kidney rud ment in vitro J Nat. Cancer Inst., 29 597–63

——— 1963 Viral susceptibility and embry onic differentiation. 1 The histopatholog mouse kidney rudiments infected with polyom and vesicular stomatitis viruses in vitro Act path. Microbiol. Scand., 58 191 204.

Stone R. S., R. E. Shope and D. H. Moor 1959 Electron microscopic study of the devel opment of the papilloma virus in the skin o the rabbit. J Exp. Med., 110 543–546.

Swan, C. 1944 A study of three infants dyin from congenital defects following maternal rubella in the early stages of pregnancy J Path. and Bact., 56 289–295.

Swan, C., and A. L. Tostevin 1946 Congenital bnormalities in infants following infectious diseases during pregnancy with special reference to Rubella A third series of cases. Med. J Australia, 1 645–659

Swan, C., A. L. Tostevin, B. Moore H. Mayo and G. H. B Black 1943 Congenital defects in infants following infectious diseases during pregnancy Med. J Australia, 2. 201 210

Traegan, L., and J Fong 1962 Mumps viru replication. J Immunol. 89 730–735.

Vainio, T L. Saxén and S. Toivonen 1963a Acquisition of cellular resistance to polyoma virus during embryonic differentiation. Virol ogy 20: 380–385.

——— 1963b Viral susceptibility and embry onic differentiation. 2. Immunofluorescence studies of viral infection in the developin mouse kidney in vitro Acta path. Microbi Scand., 58 205–211

Watson, B. K. 1952 Di tribution of mumps virus in tissue cultures as determined by fluorescein-labeled antiserum. Proc. Soc Exp. Biol and Med., 79 222–224

Williamson, A. P R. J Blattner and G. G. Robertson 1953 F ctors influencing the pro duction of developmental defects in the chick embryo following infection with Newcastle disease virus. J Immunol 71 207 213

Williamson, A. P R. J Blattner and L. Simonsen 1957 Cataracts following mumps virus in arly chick embryos. Proc Soc. Exp Biol and Med., 96 224–228.

Williamson, A. P L. Simonsen and R. J Blattner 1956 Specific organ defects in arly chick embryos following inoculation with influenza A virus. Proc Soc. Exp. Biol. and Med 92 334–337

PLATES

PLATE 1

EXPLANATION OF FIGURES

1 Section through the right lens of an embryo harvested two days after inoculation with mumps virus at 48 hours incubation. × 100.

2 Section through the same lens as in figure 1 but at higher magnification. The prominent cytoplasmic inclusions in the lens-fiber cytoplasm are eosinophilic, and represent the first indication of mumps-induced pathological changes. × 500.

3 Section through the right lens of an embryo harvested three days after inoculation with mumps virus at 48 hours incubation. Note the extensive destruction of lens fibers. × 100.

4 Section through the same lens as in figure 3, but at higher magnification. Note the normal anterior and equatorial cells, and the more extensive lens-fiber degeneration in the central region. × 400.





2



3



4

Experimental Production of Perfect Cyclopia by Removal of the Telencephalon and Reversal of Bilateralization in Somite-stage Chicks

K. T. ROGERS
Biological Laboratories Harvard University Cambridge Massachusetts and Department of Anatomy University of Michigan, Ann Arbor Michigan

ABSTRACT The telencephalon was removed with iridectomy scissors in stages from 1 to 20 somites, with the vast majority of operated chicks being t 5 to 10 somites. The most chance of successfully producing yclopia ppears to be at 6 to 7 somites. Twelve cyclopean embryos, with operated stages ranging from 5 to 10 somites, were produced mong the first 271 operations. Subsequently 398 operations, concentrated on 9- to 10-somite embryos, proved that cyclopia is very much less apt to follow this sort of operation t these stages than at the ery slightly younger stages.

Serial sections of the cyclopean embryos were stained with modification of the Bodian protargol stain. An oral hypophysis is usually present in these embryos, making them in this respect similar to the majority of cyclopean embryos for which this point is reported in the literature, but making them different from experimentally produced cyclopean amphibian embryos reported in the literature. The sequence of fusion of extrinsic ocular muscle components and the patterns of their nerves, as the cyclopean defect becomes more severe, indicates that the reversal of bilateralization is ventralization.

Coupled with biochemical work on the chick and the more recent of the biochemical work of others on amphibia, the results allow one to suggest that experimental stimuli resulting in the cyclopean mode of development may act either on prechordal substrate or on neural tissue of telencephalon and diencephalon, or on both substrate and neural tissue, and that they may be effective over a considerable period of time, up to and including the period of actual bilateralization of the optic primordia.

Early attempts to explain cyclopia mainly hinged on interpretation of the origin of the eyes. Speer (1819) and Tiedemann (1828) believed that cyclopia arises through more or less perfect fusion of the originally separate eyes and concomitant fusions of various other paired head structures. Huschke (1832) opposed this view; he believed that the eyes normally arise as a single median vesicle and that in cyclopia a developmental arrest causes the eye and forebrain to remain single. As a result of his constriction experiments on Triton eggs in cleavage stages Spemann ('04) supported the view that the cyclopean eye arises by fusion of the parts of two eyes. From his observations on cyclopean embryos produced by $MgCl_2$ treatment, Stockard ('07) agreed with the fusion theory but reversed his stand ('08 and later papers) and argued repeatedly that the cyclopean eye forms as a result of failure of division of the optic anlage

The view that the prechordal substrate is all-important in directing the bilateralization of the anterior part of the head by inductive action came from the operative experiments on amphibian prechordal substrate (Adelmann, '30 '37 Alderman, '35 '38 Lehman '38) in which the precise time of application of the initial stimulus was known and from experiments in which amphibian embryos were kept in lithium solutions (Lehmann, '33 '36 '37 '38; Adelmann '34 Hall, 42) in which the effective time of action of the experimental stimulus is not known with such precision. Although a considerable body of evidence has accumulated showing that the neural tissue may be very important in its own right in the events of head bilateralization, some workers have overlooked this evidence and continue to hold

Author's address, Proctor Foundation and Department of Anatomy, University of California Medical Center San Francisco, California.

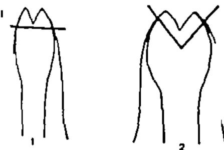
that the prechordal substrate is solely responsible (Kawakami, '55; Giroud, Delmas and Martinet, '63).

Since the telencephalon is usually strongly reduced in cyclopia it was felt in the present work that removal of the telencephalon at the time the optic vesicles are bilateralizing might result in reversal of bilateralization or fusion of optic vesicles to form a single median eye. St. Warynski and Fol (1883) first reported an experiment designed to test the possibility of reversal of bilateralization of optic primordia to form the cyclopean eye. They destroyed the anterior tip of the medullary plate of 24-hour chicks with a hot needle, but were not able to produce cyclopia. Levy ('05) in a series of experiments on regulation in *Triton taeniatus* obtained one synophthalmic individual after removal of part of the forming optic vesicles and diencephalon, along with all of the telencephalon. Pasquini ('27) obtained one synophthalmic individual by fusion and regulation after implanting most of an extra optic vesicle in *Pleurodeles waltli*. Wolff ('34) produced cyclopia perfecta by point x-raying the region of the head process in 18- to 22-hour chicks, but he was unable to obtain cyclopia perfecta either by x-ray or by electrocautery treatment after the eye primordia had formed. Huber ('48) again failed to produce cyclopia perfecta by electrocautery but reported "la pseudocyclopie" (displacement of the two eyes). It seemed significant that in the work on the chick the methods employed produce changes in adjacent tissues that are probably unfavorable for regeneration and fusion of like tissues, and that eye fusions of other sorts have been accomplished by utilizing a cutting tool that leaves a clean wound surface (Born, 189?; Pasquini, '27; Detwiler, '29 and others). In the present work, therefore, iridectomy scissors were employed for tissue removal.

The primary results of the present study were reported in abstract some years ago (Rogers, '51). At that time the viewpoint that the neural tissue is important in determining head organization was not accepted. Additional operations were subsequently done to add data on the question of the developmental time during which cyclopia can most easily be caused by this sort of operation. Further biochemical studies on the chick over the last six years have demonstrated that LiCl can produce perfect cyclopia in this animal (Rogers, '63). Furthermore they have shown that LiCl inhibits protein synthesis and probably RNA synthesis more in neural tissue, particularly the forming optic vesicles of early somite stages, than in prechordal substrate (Rogers, '64). These results collectively support the viewpoint that the neural tissue is indeed important in the modification of head organization that follows LiCl treatment. Evidence in the same direction had also been accumulated from several different kinds of experiments with amphibian material (Lallier, '52, '53; Lombard, '52; Masui, '56, '59, '60, '61 and Ogi, '61; see summarization in Rogers, '64). It seems appropriate to report now in detail the operative results on the chick that indicate that modification of the neural tissue can be just as important as modification of the prechordal substrate in the disturbance of normal head bilateralization in the course of development.

MATERIALS AND METHODS

About 270 Barred Rock, 225 White Rock, 175 White Leghorn, and smaller numbers of Barred Rock ♀ X Rhode Island Red, New Hampshire and Indian River ♂ and White Rock ♀ X Cornish ♂ eggs were used. Eggs were incubated at 38.5 C for 28 to 51 hours before operation. A shell window about 9 mm square was cut with a hack saw blade on which the teeth had been ground to a narrow edge. The vitelline membrane was torn and lifted away from the head of the embryo with no. 5 watchmakers forceps. The operation was then performed with sharpened iridectomy scissors. Various means to position the head were tried, such as the use of forceps, glass needles and hair loops, but the best results were obtained with the scissors alone. A single cut, straight across, removed the telencephalic area, or two cuts meeting in a V removed the telencephalic area and some of the medial di-



Figures 1 and 2

cephalic area, as illustrated in figures 1 and 2. The straight cut was employed for most of the embryos of 1 to 7 somites, and the two cuts, for most of those of 8 to 20 somites.

The first 271 operations were done on embryos of 1 to 20 somites with the great majority being at 5- to 10-somite stages. An attempt was made over the next 116 operations to select as many 10-somite embryos as possible by incubation time alone. As might be expected this method was only partially successful. For the last 112 operations, therefore, shell windows were opened but sealed after observation of the embryo if it has not yet reached 10 somites, to be reopened for operation at the indicated time With this method all the embryos were operated upon at stages from 9 to 13 somites with the great majority at 10 somites.

After the operation, shell windows were sealed with paraffin and eggs incubated further. Daily candling was employed to detect when embryos died, and in some cases eggs were then reopened soon enough that the embryos were useful for histological preparations. Eggs were incubated for a total of 4 to 9 days, the majority for 7 days Of the 204 embryos that were alive at the end of the incubation period, most had been incubated for seven days.

Selected embryos were fixed in Allen's PFA3 modification of Bouin's fluid, sectioned at 10 μ, and stained with the modification of the Bodian stain previously described (Rogers '32) From the first 271 operations, 33 embryos were sectioned and mounted. Other embryos were fixed and saved for assessment of their morphological state but were not sectioned when it was found that they were not cyclopean.

RESULTS

Among the first 271 operations 12 embryos were produced that would be classed as cyclopean if they occurred in the human (table 1) Of these the first six listed in the table are perfect cyclopean. In addition to the embryos listed in the table a series of morphological stages intermediate between the normal embryo and the perfect cyclopean condition were also obtained and sectioned. Four of these, illustrating typical stages in reduction of bilaterality will be presented along with a well-developed cyclopean embryo and an additional cyclopean embryo illustrating still further reduction in bilaterality Descriptive notes as complete as those to be presented for the first embryo below were recorded from slide study for a normal 7 day embryo and for 18 experimental embryos. A complete description of the best-developed cyclopean embryo will be reported followed by descriptions that note only the significant differences from case to case for a series of five additional embryos that demonstrate the steps involved in increasing union of primordia in cyclopia and in increasing ventralization of head organization.

Because of the frequent complete absence of the telencephalon and because of the normal recurved position of the diencephalon in relation to the rhombencephalon, it would lead to confusion to attempt to describe nearby structures in a spatial framework related to the flexed brain axis. Therefore a descriptive axis has been used that is related solely to that of the hind brain in the region of the eye muscles and their nerves. To illustrate, anterior and dorsal have been indicated in figure 9 To avoid conflict, the tip roof and floor of the diencephalon are referred to rather than its anterior dorsal, and ventral aspects

Embryo no 261 (figs 8–11 15–17 21). Operated upon at 6 somites 35 hours of incubation. A transverse cut was made across the anterior edges of the forming optic vesicles. When the egg was reopened seven and one-fourth days after the start of incubation, the embryo was alive and moving normally was covered by a normal amnion and was supplied by normal extra-embryonic vessels. The eye was

that the prechordal substrate is solely responsible (Kawakami '55 Giroud, Delmas and Martinet, '63)

Since the telencephalon is usually strongly reduced in cyclopia it was felt in the present work that removal of the telencephalon at the time the optic vesicles are bilateralizing might result in reversal of bilateralization or fusion of optic vesicles to form a single median eye. St. Warynski and Fol (1883) first reported an experiment designed to test the possibility of reversal of bilateralization of optic primordia to form the cyclopean eye They destroyed the anterior tip of the medullary plate of 24-hour chicks with a hot needle but were not able to produce cyclopia. Levy ('05) in a series of experiments on regulation in *Triton taeniatus* obtained one synophthalmic individual after removal of part of the forming optic vesicles and diencephalon along with all of the telencephalon. Pasquini ('27) obtained one synophthalmic individual by fusion and regulation after implanting most of an extra optic vesicle in *Pleurodeles waltli*. Wolff ('34) produced cyclopia perfecta by point x raying the region of the head process in 18- to 22-hour chicks but he was unable to obtain cyclopia perfecta either by x-ray or by electrocautery treatment after the eye primordia had formed. Huber ('48) again failed to produce cyclopia perfecta by electrocautery but reported "la pseudocyclopie (displacement of the two eyes) It seemed significant that in the work on the chick the methods employed produce changes in adjacent tissues that are probably unfavorable for regeneration and fusion of like tissues and that eye fusions of other sorts have been accomplished by utilizing a cutting tool that leaves a clean wound surface (Born 1897 Pasquini, '27 Detwiler '29 and others) In the present work, therefore iridectomy scissors were employed for tissue removal.

The primary results of the present study were reported in abstract some years ago (Rogers '51) At that time the viewpoint that the neural tissue is important in determining head organization was not accepted. Additional operations were subsequently done to add data on the question of the developmental time during whi[ch] cyclopia can most easily be caused by t[his] sort of operation. Further biochemi[cal] studies on the chick over the last [...] years have demonstrated that LiCl c[an] produce perfect cyclopia in this anim[al] (Rogers '63) Furthermore they h[ave] shown that LiCl inhibits protein synthes[is] and probably RNA synthesis, more [in] neural tissue particularly the forming [op]tic vesicles of early somite stages, th[an] in prechordal substrate (Rogers '6[4]) These results collectively support the vi[ew]point that the neural tissue is ind[eed] important in the modification of head [or]ganization that follows LiCl treatm[ent]. Evidence in the same direction had a[lso] been accumulated from several differ[ent] kinds of experiments with amphib[ian] material (Lallier '52, '53 Lombard '[...] Masui, '58 '59 '60 '61 and Ogi, '61; [...] summarization in Rogers '64) It see[ms] appropriate to report now in detail [the] operative results on the chick that indic[ate] that modification of the neural tissue c[an] be just as important as modification of t[he] prechordal substrate in the disturbance [of] normal head bilateralization in the cou[rse] of development.

MATERIALS AND METHODS

About 270 Barred Rock, 225 Wh[ite] Rock, 175 White Leghorn and smal[l] numbers of Barred Rock ♀ X Rhode Isla[nd] Red New Hampshire and Indian River and White Rock ♀ X Cornish ♂ eggs w[ere] used. Eggs were incubated at 38.5°C [for] 28 to 51 hours before operation A sh[ell] window about 9 mm square was cut w[ith] a hack saw blade on which the teeth h[ad] been ground to a narrow edge. The vi[tel]line membrane was torn and lifted aw[ay] from the head of the embryo with no[. 5] watchmakers forceps. The operation w[as] then performed with sharpened iridecto[my] scissors. Various means to position t[he] head were tried such as the use of f[or]ceps glass needles and hair loops but t[he] best results were obtained with the sci[s]sors alone A single cut, straight acro[ss] removed the telencephalic area or t[wo] cuts meeting in a V removed the tele[n]cephalic area and some of the medial



Figures 1 and 2

operative area, as illustrated in figures 1 and 2. The straight cut was employed for most of the embryos of 1 to 7 somites and the two cuts, for most of those of 8 to 20 somites.

The first 271 operations were done on embryos of 1 to 20 somites with the great majority being at 5- to 10-somite stages. An attempt was made over the next 116 operations to select as many 10-somite embryos as possible by incubation time alone. As might be expected, this method was only partially successful. For the last 32 operations, therefore, shell windows were opened but sealed after observation if the embryo if it has not yet reached 10 somites, to be reopened for operation at the selected time. With this method all the embryos were operated upon at stages from 9 to 13 somites, with the great major ity at 10 somites.

After the operation, shell windows were sealed with paraffin and eggs incubated further. Daily candling was employed to determine when embryos died, and in some cases eggs were then reopened soon enough that the embryos were useful for histolog ical preparations. Eggs were incubated for a total of 4 to 9 days, the majority for 7 days. Of the 204 embryos that were alive at the end of the incubation period, most had been incubated for seven days.

Selected embryos were fixed in Allen's Py modification of Bouin's fluid, sec tioned at 10 µ, and stained with the modi fication of the Bodian stain previously de scribed (Rogers, '52). From the first 271 operations, 33 embryos were sectioned and studied. Other embryos were fixed and saved for assessment of their morpholog ical state, but were not sectioned when it appeared that they were not cyclopean.

RESULTS

Among the first 271 operations 12 em bryos were produced that would be classed as cyclopean if they occurred in the human (table 1) Of these the first six listed in the table are perfect cyclopean. In addition to the embryos listed in the table a series of morphological stages in termediate between the normal embryo and the perfect cyclopean condition were also obtained and sectioned. Four of these illustrating typical stages in reduction of bilaterality will be presented along with a well-developed cyclopean embryo and an additional cyclopean embryo illustrating still further reduction in bilaterality De scriptive notes as complete as those to be presented for the first embryo below were recorded from slide study for a normal 7 day embryo and for 18 experimental em bryos A complete description of the best-developed cyclopean embryo will be re ported, followed by descriptions that note only the significant differences from case to case for a series of five additional em bryos that demonstrate the steps involved in increasing union of primordia in cyclo pia and in increasing ventralization of head organization

Because of the frequent complete ab sence of the telencephalon and because of the normal recurved position of the dien cephalon in relation to the rhombenceph alon it would lead to confusion to attempt to describe nearby structures in a spatial framework related to the flexed brain axis. Therefore a descriptive axis has been used that is related solely to that of the hind brain in the region of the eye muscles and their nerves. To illustrate anterior and dorsal have been indicated in figure 9 To avoid conflict, the tip roof and floor of the diencephalon are referred to rather than its anterior dorsal, and ventral aspects

Embryo no 261 (figs. 8–11 15–17 21). Operated upon at 6 somites 35 hours of incubation. A transverse cut was made across the anterior edges of the forming optic vesicles. When the egg was reopened seven and one-fourth days after the start of incubation, the embryo was alive and moving normally was covered by a nor mal amnion, and was supplied by normal extra-embryonic vessels. The eye was re

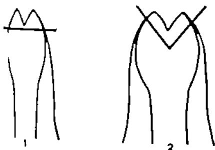
that the prechordal substrate is solely responsible (Kawakami, '55 Giroud Delmas and Martinet, '63)

Since the telencephalon is usually strongly reduced in cyclopia it was felt in the present work that removal of the telencephalon at the time the optic vesicles are bilateralizing might result in reversal of bilateralization or fusion of optic vesicles to form a single median eye. St. Warynski and Fol (1883) first reported an experiment designed to test the possibility of reversal of bilateralization of optic primordia to form the cyclopean eye They destroyed the anterior tip of the medullary plate of 24-hour chicks with a hot needle but were not able to produce cyclopia. Levy ('05) in a series of experiments on regulation in *Triton taeniatus* obtained one synophthalmic individual after removal of part of the forming optic vesicles and diencephalon, along with all of the telencephalon Pasquini ('27) obtained one synophthalmic individual by fusion and regulation after implanting most of an extra optic vesicle in *Pleurodeles waltli.* Wolff ('34) produced cyclopia perfecta by point x raying the region of the head process in 18- to 22 hour chicks, but he was unable to obtain cyclopia perfecta either by x ray or by electrocautery treatment after the eye primordia had formed Huber (48) again failed to produce cyclopia perfecta by electrocautery but reported "la pseudo-cyclopie (displacement of the two eyes) It seemed significant that in the work on the chick the methods employed produce changes in adjacent tissues that are probably unfavorable for regeneration and fusion of like tissues and that eye fusions of other sorts have been accomplished by utilizing a cutting tool that leaves a clean wound surface (Born 1897 Pasquini '27 Detwiler '29 and others) In the present work, therefore iridectomy scissors were employed for tissue removal

The primary results of the present study were reported in abstract some years ago (Rogers '51) At that time the viewpoint that the neural tissue is important in determining head organization was not accepted Additional operations were subsequently done to add data on the question of the developmental time during whi[illegible] cyclopia can most easily be caused by th[illegible] sort of operation. Further biochemic[illegible] studies on the chick over the last [illegible] years have demonstrated that LiCl c[illegible] produce perfect cyclopia in this anim[illegible] (Rogers '63) Furthermore they ha[illegible] shown that LiCl inhibits protein synthes[illegible] and probably RNA synthesis, more [illegible] neural tissue particularly the forming [illegible] tic vesicles of early somite stages, th[illegible] in prechordal substrate (Rogers, '6[illegible] These results collectively support the vie[illegible] point that the neural tissue is inde[illegible] important in the modification of head [illegible] ganization that follows LiCl treatme[illegible] Evidence in the same direction had al[illegible] been accumulated from several differe[illegible] kinds of experiments with amphibi[illegible] material (Lallier '52, '53 Lombard [illegible] Masui, 56 '59 '60 '61; and Ogi, 61: [illegible] summarization in Rogers, '64) It see[illegible] appropriate to report now in detail t[illegible] operative results on the chick that indica[illegible] that modification of the neural tissue c[illegible] be just as important as modification of t[illegible] prechordal substrate in the disturbance [illegible] normal head bilateralization in the cour[illegible] of development.

MATERIALS AND METHODS

About 270 Barred Rock, 225 Wh[illegible] Rock, 175 White Leghorn, and smal[illegible] numbers of Barred Rock ♀ X Rhode Isla[illegible] Red, New Hampshire and Indian Riv[illegible] and White Rock ♀ X Cornish ♂ eggs w[illegible] used. Eggs were incubated at 38.5°C [illegible] 28 to 51 hours before operation. A s[illegible] window about 9 mm square was cut [illegible] a hack saw blade on which the teeth [illegible] been ground to a narrow edge The v[illegible] line membrane was torn and lifted a[illegible] from the head of the embryo with [illegible] watchmakers forceps. The operation [illegible] then performed with sharpened iridect[illegible] scissors. Various means to position [illegible] head were tried such as the use of [illegible] ceps glass needles and hair loops but [illegible] best results were obtained with the [illegible] sors alone A single cut, straight acr[illegible] removed the telencephalic area or [illegible] cuts meeting in a V removed the te[illegible] cephalic area and some of the medial [illegible]



Figures 1 and 2

ephalic area, as illustrated in figures 1 and 2. The straight cut was employed for most of the embryos of 1 to 7 somites, and the two cuts, for most of those of 8 to 20 somites.

The first 271 operations were done on embryos of 1 to 20 somites, with the great majority being at 5- to 10-somite stages. An attempt was made over the next 116 operations to select as many 10-somite embryos as possible by incubation time alone. As might be expected, this method was only partially successful. For the last 12 operations, therefore, shell windows were opened but sealed after observation if the embryo if it has not yet reached 10 somites, to be reopened for operation at the indicated time. With this method all the embryos were operated upon at stages from 9 to 13 somites, with the great major ity at 10 somites.

After the operation, shell windows were sealed with paraffin and eggs incubated further. Daily candling was employed to detect when embryos died, and in some cases eggs were then reopened soon enough that the embryos were useful for histolog ical preparations. Eggs were incubated for a total of 4 to 8 days, the majority for 7 days. Of the 204 embryos that were alive at the end of the incubation period, most had been incubated for seven days.

ected embryos were fixed in Allen s PFA modification of Bouin s fluid, sectioned at 10 µ, and stained with the modification of the Bodian stain previously described (Rogers '52) From the first 271 operations 33 embryos were sectioned and studied. Other embryos were fixed and saved for assessment of their morphology, but were not sectioned when it appeared that they were not cyclopean.

RESULTS

Among the first 271 operations, 12 embryos were produced that would be classed as cyclopean if they occurred in the human (table 1) Of these the first six listed in the table are perfect cyclopean. In addition to the embryos listed in the table a series of morphological stages intermediate between the normal embryo and the perfect cyclopean condition were also obtained and sectioned. Four of these illustrating typical stages in reduction of bilaterality will be presented along with a well-developed cyclopean embryo and an additional cyclopean embryo illustrating still further reduction in bilaterality De scriptive notes as complete as those to be presented for the first embryo below were recorded from slide study for a normal 7 day embryo and for 18 experimental embryos. A complete description of the best-developed cyclopean embryo will be reported, followed by descriptions that note only the significant differences from case to case for a series of five additional embryos that demonstrate the steps involved in increasing union of primordia in cyclopia and in increasing ventralization of head organization.

Because of the frequent complete absence of the telencephalon and because of the normal, recurved position of the dien cephalon in relation to the rhombenceph alon it would lead to confusion to attempt to describe nearby structures in a spatial framework related to the flexed brain axis. Therefore, a descriptive axis has been used that is related solely to that of the hindbrain in the region of the eye muscles and their nerves To illustrate anterior and dorsal have been indicated in figure 9 To avoid conflict, the tip roof and floor of the diencephalon are referred to rather than its anterior dorsal, and ventral aspects.

Embryo no 261 (figs 8–11 15–17 21). Operated upon at 6 somites 35 hours of incubation. A transverse cut was made across the anterior edges of the forming optic vesicles. When the egg was reopened seven and one-fourth days after the start of incubation the embryo was alive and moving normally was covered by a nor mal amnion and was supplied by normal extra-embryonic vessels. The eye was mo-

TABLE 1

Cyclopean embryos from the first 271 operations

Embryo number	Somite stage operated	Type of cut	Total incub.	State of embryo	Oral hypophysis	Eye
			days			
43	7	transverse	5	dead a short time	present	single pigmented vesicle
83	9 or 10	V-wedge	5½	alive	—	single retinal cup and lens
261	6	transverse	7¼	alive	present	large median eye and lens
266	5	transverse	7¼	dead	present	single pigmented vesicle
268	6 or 7	transverse	7¼	dead	absent	single pigmented vesicle
269	6 or 7	transverse	7¼	alive	present	single pigmented vesicle
25	4 or 5	transverse	5	alive	—	single retinal cup, single lens with two centers
47	*8 or 9*	*transverse*	*5¼*	*alive*	—	*double retinal cup, each part with a lens*
171	5 or 6	transverse	7	alive	present	single orbit, pigment on right
183	8	shallow V-wedge	7	dead a short time	present	single orbit, pigment on each side of midline
191	7	V-wedge	7	alive	absent	single orbit, pigment on right
246	6	V-wedge	7¼	alive	present	single orbit, pigmented vesicle on each side of midline

dian, of about normal size and showed a clear median choroid fissure in the fresh state The telencephalon was greatly reduced. See figures 8–11

Sections show that the eye is bilaterally organized, with a median, frontal lens slightly larger and more spherical than the normal lens and of normal histological form The choroid fissure extends from the medio-posterior edge of the pupil back around the curvature of the eye dorso-anteriorly through 31% of the sections of the eye (figs. 15 and 16) Tapetum, sensory retina (with a fair number of mitoses in the stratum germinativum) the abundance distribution, and form of the nerve fibers just under the internal limiting membrane and the forming scleral condensations and corneal regions are all normal for the age. Ciliary folds are developing in a normal course (fig. 15) but have passed slightly beyond the stage seen in the control. The form of the eye is unusual only in the presence of lateral infoldings of [illegible] wall on each side, ventro-posteriorly [illegible] the region of the lens. The two major fol[illegible] are symmetrically placed; one of these [illegible] shown on the embryo's right in figure 1[illegible] while its counterpart on the left appear[illegible] three sections farther down in the serie[illegible] The eye is attached to the diencephal[illegible] at the dorso-anterior end of the choroid fi[illegible]sure A normal optic nerve papilla is lack[illegible]ing, and it is difficult to be sure whethe[illegible] this tissue should be interpreted as opti[illegible] stalk or as diencephalon proper Relation[illegible] make it seem however that the stalk ha[illegible] not formed and that the diencephalon i[illegible] interposed between the two sides of th[illegible] tapetum at this level as it is in higher sec[illegible]tions.

Thick bundles of optic fibers from th[illegible] two sides of the retina run into this dien[illegible]cephalic tissue and many of them certainl[illegible] decussate there (fig. 17) The abundance of these fibers the small size of the tissu[illegible]

sea into which they run, and the fact that most of them do not continue farther makes it impossible to follow decussating fibers clearly to the opposite side of the diencephalon in higher sections. Upward in the series of sections the diencephalon widens out into easily recognizable form, with the infundibulum appearing in normal relation behind the optic chiasma. A saccus infundibuli of almost precisely normal size is present, with its cavity confluent with that of infundibulum, and by way of the latter with the cavity of the diencephalon. Surrounding the saccus infundibuli is the tip of the hypophysis which shows completely normal form and cellular constitution, and which is attached to the roof of the oral cavity by a slender tube (for terminology see Hamilton, '52, pp. 310–311) Still higher in the sections, the diencephalic cavity is enclosed between the diencephalic tissue and the sensory retina. It can be seen in figure 11 that the diencephalic cavity is still continuous with the much reduced primary optic cavity and that the tapetum of the eye is a direct continuation from the diencephalic tissue on each side. Above and behind the eye the diencephalon is more normal, as in the control, and a normal epiphysis is attached to its roof (fig 8) In front of the epiphysis is a median telencephalon, greatly reduced in size with walls of 4 or 5 cells thickness in most places. Distally from its attachment to the diencephalon the telencephalic vesicle is displaced slightly to the left by the eye which bulges up anteriorly somewhat farther on the right than on the left (figs. 8 and 9). The mesencephalon is normal, as is the remainder of the body posterior to it.

There remain to be described the relations of the extrinsic eye muscles and their associated cranial nerves. (For detailed description of the development of the eye muscles of the chick see Adelmann, '27 and for their nerves, Carpenter '06.) In the normal 7-day chick the eye muscles, except for the extreme insertion ends of few of them, lie in the area between the eyes, the greatest diameter of the eyes considered. In the cyclopean condition the muscles have to be formed laterally to the eye, or behind the eye or be discarded. With this in mind, the relations of the muscles to the eye in this series of embryos can be described by comparing their positions with those of the control embryo.

In the sections of no. 261 the superior oblique muscles are encountered first, lying lateral to the eye one on each side, with the greatest bulk of the muscle about one-third of the way back from the ventral surface of the eye. The superior oblique is supplied by N IV in normal fashion except that the muscle and its nerve are lateral to the eye. The superior rectus in a comparably sectioned control is seen in cross-section, beginning at its insertion, dorso-medial to the eye. In this embryo it sweeps ventrally and laterally around the eye, nearly in the plane of section, to meet the insertion of the superior oblique just dorsal to the greatest diameter of the eye. In other words, its long axis has been shifted greatly toward that expected for the lateral rectus. The quadratus is between the origin f the superior rectus and the eye on each side just as it is in the control, but in the cyclopean this means that the quadratus is medial to the superior rectus rather than lateral to it as in the normal chick.

The ophthalmic branch of N. V passes peripherally from the trigeminal ganglion between the superior rectus and the quadratus, as in the control, but here, because of the reversed relations of these two muscles, the nerve passes medially to the superior rectus in the most lateral portion of the substance of the quadratus instead of laterally to the rectus in the most medial part of the quadratus. A communicating ramus to the ventral tip of the ciliary ganglion to join N III is sent through the substance of the quadratus, as in the control. Just ventral (peripheral) to this, unlike the control, the ophthalmicus of each side has small ovoid mass of ganglion cells on it (see Rogers, '57a, for description of ganglion cells on the eye muscle nerves of the normal chick) and then the nerve passes around the eye laterally in a course otherwise similar to the medial path of the control nerve. It follows the direction of N. IV but is lower down in the sections until it reaches well out toward the ventral part of the eye, when it ascends in the sections to end near the superior oblique muscle, as does the normal opthalmicus at this stage.

The lateral rectus of each side is in the expected position below and slightly lateral to the superior rectus, but it sweeps forward around the eye only about half as far as does the superior rectus. As in the control, N VI supplies the quadratus and pyramidalis muscles near their junction and just lateral to the ciliary ganglion, and then sends large trunk to enter the lateral rectus on its ocular surface. At this forking of N. VI, unlike the control, there is small communicating ramus between the fork and the dorso-lateral corner of the ciliary ganglion on each side. At the same section level the ciliary ganglion, on the left only branches into two masses downward in the sections. One is located at the level of the dorsal part of the ciliary ganglion of the right side, but the other is more ventral, or just lateral to the optic-diencephalic junction. It is from the ventral fork that the major ciliary nerve to the orbit arises on the left side. In sections just bove the dorso-anterior end of the choroid fissure the ciliary ganglia are (bnormally) connected with each other across the midline by few fibers dorsal to the eye. At this level the origin of the paired inferior

recti — medial recti masses are first seen just medial to the ciliary ganglia, one on each side of the midline. Also at this level it is apparent that after passing through few sections of thinned-out muscle, indicating the beginning in development of the separation of quadratus and pyramidalis, the denser tissue of the pyramidalis has been reached. The latter with its main mass just lateral to the ciliary ganglion, passes an attenuated arm of muscle medially under the fork of the ciliary ganglion on the left, and in the corresponding angle of the ganglion and its ciliary orbital branch on the right, thence toward the midline just below the area of ttachment of th eye to the diencephalon, but not meeting in the midline The relation of the pyramidalis to the ciliary ganglion and this orbital branch and to the optic stalk is exactly the same as the control, even through the changed relations in this cyclopean head cause the projection of the muscle to be in medial direction instead of ventral as in the control

At the posterior ends of the ciliary ganglia (dorsal fork on the left) the nerve trunks leaving the ganglia t once supply the origin of the inferior recti on their faces away from the eye (as is the case at the ventral ends of the ganglia in the control) The medial recti are apparently not separated off or t best are represented on the left only by a small slip of muscle lying ventral and slightly medial to the main mass of that side. The nerve trunks, after supplying the inferior recti (mainly with motor fibers passing through the ganglia) instead of branching as they normally do to medial rectus and inferior oblique of each side pass to the midline where the right and left trunks unite just dorsal to the inferior recti — medial recti masses, and then as unified group of nerve fibers follow the muscle masses downward These muscles fuse with each other in the midline toward their insertions fter flanking the horoid fissure and following down through the sections (the inferior rectus of the control follows down along the horoid fi sure from the region of the papilla) A the fused insertion of the inferior recti — medial recti ma ses thin out in going down through the sections the completely f sed inferior obliques ppear nearly in their place but very slightl farther way from the eye (insertion of inferior recti nd inferior obliques meet in the control) The fused trunk of N III which came down through the sections just dorsal t the inferior recti — medial recti ma s, ends by branching into the fused inferior oblique mass on its ocular surface

Embryo no 228 (fig 6). Operated upon at 11 or 12 somites 36 hours of incubation A deep wedge of tissue was removed with two cuts The embryo was alive and enclosed in an amnion after six and one-half days of total incubation The eyes appear nearly adjacent but otherwise normal in size and form with a choroid fissure in each The cerebral hemispheres are much reduced. Infundibulum and h pophysis are normal, but there is no epip ysis. The right eye has a normal papi where nerve fibers leave the eye and pa through a short, broad stalk into the encephalic wall On the left a flatten papilla is present, around which fibe leave the vitreal surface of the gangli cell layer and proceed to the outside of t eye but there is no stalk at this point, a fibers do not leave the eye At some d tance from this, a tiny cord of stalk ce touches the pigment epithelium from t outside and sensory retina fuses to t pigment epithelium from the inside in small area. Tapetum and sensory reti are separate between this point and t formed papilla region. The stalk thicke and joins the diencephalon but it conta no nerve fibers.

The eye muscles and their innervation are usual in only a few respects. The medial rect of the left especially is shortened, and it does project out between the eyes as is from its ori s the normal. The inferior obliques are fused their origin in the midline but they separ toward their insertions. The branches of N I on each side enter the muscles independently each other lateral to the fusion of the muscl in the midline.

Embryo no 216 Operated upon at somites thirty-four and one-half hours incubation A deep wedge was remove The embryo was alive and contained in well-formed amnion at six and one-h days of total incubation The eyes we nearly adjacent and each had a choro fissure as in the previous case Maxilla processes had grown down posteriorly the eyes and were not directed so as push against them from their lateral fac Sections show that the telencephalon nearly or completely lacking. The infund ulum and hypophysis are normal but t epiphysis is absent Retinas and lenses normal as is the papilla region of the l eye with nerve fibers passing out of t eye through a very short stalk and cross in the floor of the diencephalon The ri eye has no stalk, but over a very sm area its pigment epithelium is continued a reflection of the diencephalic wall, w its sensory retina projecting into the di cephalic cavity (see fig. 19 a section embryo no 107 for an exactly similar lationship but one of greater extent

[illegible] the surfaces of the diencephalon [illegible] eye). In place of the normal stalk, the sensory retina becomes continuous with the diencephalic tissue at another [illegible] (similar to fig. 14, embryo no. 197) and nerve fibers cross from the retina into diencephalic tissue.

An advance over the previous case in the [illegible] of moving the eye muscles out from between the eyes is seen. The inferior rectus on the right only (side of closest association of eye and diencephalon) is displaced very slightly [illegible] around the eye. The medial rectus of the left side is near the inferior rectus and does not extend between the eyes farther than the optic stalk. The medial rectus of the right side seems to be present, but it is reduced and lies adjacent to the inferior rectus [illegible] that side. The inferior obliques are fused at their origins in the midline; the branches of N III of the two sides enter them separately. In this case, unlike the preceding, superior muscles are involved. The right superior rectus is more lateral than normal, as are both superior obliques. The right superior oblique is displaced farther than the left, but neither extends back into the narrow strip of tissue between the eyes. The right N IV passes directly over the eye rather than between it and the diencephalon, and the right ophthalmicus has been diverted [illegible] corresponding distance upward.

Embryo no. 197 (figs. 14 and 19) Operated upon at 11 somites thirty-six and one-half hours of incubation. A wedge of tissue was removed. At seven days the embryo was alive and enclosed in an amnion. The eyes are of normal size and very nearly touch each other The left maxillary process had grown down around the posterior curvature of the eye and then forward again to the midline. On the right side, however, the process had grown only a short distance along the posterolateral curvature of the eye and it falls far short of the midline leaving a gap between the right eye and the oral cavity The choroid fissure of this eye extends down to the edge of this gap Sections show that the telencephalic vesicle is single, median, thick-walled, and of moderate size. Infundibulum and hypophysis are normal, but the epiphysis is lacking. In both eyes the lens and retina are normal. Optic fibers from the left eye enter the diencephalic floor by way of a well formed optic stalk in normal fashion but [illegible] extend along the outer edge of the [illegible]lateral diencephalic wall instead of [illegible]ing. They can be traced most of the way to the mesencephalon. The right eye has no stalk, but instead is related to the diencephalon in the manner described in the preceding case but over a much greater area (fig 19) The unpigmented medial area of this eye, which could be seen in the living embryo is the area within the circumferential reflection of the tapetum from the edges of the diencephalic defect Where sensory retina is continuous with diencephalic tissue (fig. 14) in effect a flattened papilla has formed Here the optic fibers leave the ganglion layer in large numbers and many of them simply run out into the adjacent mesenchyme in ten or more large bundles and very shortly end there

With the positional relationships of the left eye fairly normal, its eye muscles and associated cranial nerves are in normal relations. On the right they are so similar to those on the right in the preceding case that they do not require separate description. The m jor difference is that, since the muscles of the left are in normal relations, the inferior oblique of the right does not meet its opposite in the midline.

Embryo no 198 (fig 20). Operated upon at 9 or 10 somites, 37 hours of incubation The embryo appeared to be alive when candled after five and one-half days of incubation but was dead when fixed at six days There was no amnion The eyes were of normal size, and adjacent to each other The right eye appeared normal The left eye however lacked a choroid fissure and there was a transparent (unpigmented) vesicular bulge of its coats ventrally Through this window one could look in through the eye into the third ventricle of the brain. A large blood vessel passed around the exterior of the eye to ring the pupil.

In section (fig 20) the sensory retina of each eye is seen to project into the diencephalic cavity The pigment epithelium is reflected from the diencephalon on each side but it has broken away as a result of tensions of growth or fixation, over a dorsal area on the left and a very small dorsal area on the right. Nerve fibers from the right eye pass into the diencephalon along the medial edge of the choroid fissure where the sensory retina is continuous with the diencephalon. Nerve fibers in the left eye which possesses no such connection with the diencephalon, do

not leave the vitreal surface of the retina. The telencephalon is apparently represented only by a small, irregular pocket from the diencephalon. The mesencephalic wall is thin and abnormally convoluted over the caudal five-eighths of the left side The hindbrain is abnormally thick walled and thick roofed in places. Infundibulum and hypophpysis are present, but there is no epiphysis.

It is apparent that the eye muscles must have moved out from between the eyes to a great degree. In development, the medial recti seem not to have separated from the inferior recti, as was true in the perfect cyclopean embryo no. 261. Inferior obliques are represented by loose interlacing strands of muscle few in number and crossing the midline in a few instances. The superior rectus of the left side has deviated from its normal course, and come to lie on plane nearly parallel to the lateral rectus instead of lying at nearly a right angle to it (compare no. 261) The superior obliques are so poorly developed that it is difficult to outline the muscle masses, although N IV proceeds out to the expected area between the eyes ventro-anteriorly

The preceding four embryos illustrate morphological stages between the normal control embryo and the well-developed cyclopean embryo The following embryo illustrates reduction of the cyclopean eye and further reduction in bilateralization of the head over that described for cyclopean embryo no 261

Embryo no 269 (fig 18). Operated upon at 6 or 7 somites 36 hours of incubation with a transverse cut. After seven and one-fourth days of total incubation the embryo was alive and enclosed in an *amnion. Sections show a single orbit with* a pigmented vesicle in its center but the ventral part of the head is bent slightly to the left so that reference to the hindbrain axis would appear to put the eye a little to the left of the midline Study of the shape of the head and orbit, and of the cranial nerves and eye muscles however shows that the eye is truly an example of perfect cyclopia. The telencephalon is absent and the diencephalon has unusually thick walls. An epiphysis infundibulum and hypophysis are present. The optic vesicle is composed of pigmented cells, and there *is no lens. The stalk of the vesicle at*taches to the dorsal wall of the vesicle to the right of its center and dorso-anteriorly to the tip of the diencephalon just to the left of its midline.

The more ventral oculomotor muscles are fu[illegible] and massed near the midline to degree [illegible] seen in any of the cases so far described. [illegible] heavy mass of muscle ventro-medial to the cil[iary] ganglia represents the unseparated inferior r[ecti] — *medial recti complex and the inferior obliq[ues]* of the two sides are fused in the midline. [illegible] ciliary ganglia, located dorsal to the eye, [illegible] heavily cross-connected by fibers supply th[e] masses. The right and left ciliary nerves pas[s] the right and left dorsal aspects of the pigmen[ted] optic vesicle (fig. 18) and there branch arc[illegible] the eye to form common, encircling set [of] nerves. The superior obliques are fused in [the] midline. Superior and lateral recti are bilater[ally] separated from their counterparts, but the [lat]eral rectus, quadratus, and pyramidalis of e[ach] side form an undivided mass of muscle that [is] laterally closely adjacent to the fused comp[lex] of inferior and medial recti noted above.

Supporting cases of cyclopia

In a general way the group of embry[os] comprising nos 43 (fig. 4 total view) 26[illegible] and 268 resemble no. 269 which has ju[st] been described All have a single, media[n] pigmented optic vesicle. The eye is pe[r]fect cyclopean but not well developed. [In] each case the lens is lacking

Embryo no 28 (fig 3 total view a[nd] fig 12, section) is representative of [a] group *including also nos. 47 (fig. 13, se*ction) and 83. The general developme[nt] of body form is poor eyes have not d[e]veloped a pigment epithelium but the opt[ic] vesicle has invaginated in each case, a[nd] a lens or lenses are present. *Embryo n[o]* 28 was operated upon at 4 or 5 somit[es] 33 hours of incubation, with a transver[se] cut. After five days of total incubation t[he] embryo was alive but spread out vent[ral] side down on the yolk. The ectamnion h[ad] just begun to rise around the embryo. T[he] heart although pulsating, had failed [to] unite into a single tube in the medline [In] sections the eye *is seen to* be attached [to] the anterior tip of the neural tube A sing[le] retinal cup of irregular shape surround[s a] lens with two distinct lens centers. T[he] outer wall of the eye is continuous w[ith] that of the brain no optic stalk ha[ving] formed This eye is not considered to [be] an example of cylopia perfecta because [of] the partly double lens. No. 47 has a par[tly] double optic cup with two lenses where[as] no. 83 has a single optic cup and a sin[gle] lens.

Embryos no 191 (fig. 5 total view) a[nd] no. 171 are similar in that both have

single, median orbit, but a pigmented stalk and small vesicle in the right side of the orbit only. No. 191 was operated upon at about 7 somites, 35 hours of incubation. A deep anterior wedge of tissue was removed. The embryo was living after seven days of incubation, and the amnion was well formed. Maxillary processes had fused posterior to a single, wide, low-triangular orbit centered in the midline. The pigmented, vesicular eye in the right side of the orbit is connected to the brain by a long pigmented stalk, clearly seen in figure 5. Sections show that the telencephalon is lacking, the diencehpalon is abnormal in form, and the mesencephalon has developed only a hint of the normal bilaterality of optic lobes. The eye is a very irregular indented, pigmented vesicle. Pituitary and epiphysis are lacking. The more ventral oculomotor muscles of each side are fused and massed near the midline. The ciliary ganglia supply these muscles and only the ganglion on the right sends a large nerve trunk out to encircle the optic vesicle. Superior obliques are fused in the midline but the superior and lateral recti are both bilaterally paired.

Embryos no. 246 (fig. 7 total view) and no. 183 both have a single median orbit with two small pigmented vesicles and stalks. No. 246 was operated upon at 8 somites, 36 hours of incubation, with an anterior wedge removed. The embryo was living after seven and one-half days of total incubation. Sections show that the telencephalon is nearly or completely lacking, the epiphysis absent, but the infundibulum and hypophysis well developed. The eyes are pigmented vesicles, heavily infolded in numerous places, but especially on the side toward the ventral surface of the head. The optic stalks extend back to the diencephalon. A small lens is present in front of the eye on the left only. The ciliary ganglia, located dorso-medial to the eye on each side, send their orbital branches to the accessory ganglion located immediately ventral to each eye. The eye muscles are very similar to those of no. 191 just described, except that the inferior recti — medial recti complexes of the two sides are fused in the midline ventro-medial to the ciliary ganglia.

The eight embryos from the first 271 operations included in table 1 that were still alive at the end of the incubation period comprise just over one-tenth of all the embryos that were alive at the time the eggs were opened.

Results of further operations

Since no new types of embryos appeared among the operations after the first 271 histological sections were not made of any of these later embryos. Although in the next group of 116 operations an attempt was made to operate on embryos of 10 somites this attempt, as stated in the methods section, was only partially successful. One embryo no. 289 operated upon at 5 somites died just after six days of total incubation. It had a single, laterally elongated orbit, symmetrically enclosing a laterally elongated, pigmented vesicle lying across the midline and centered upon it. It constitutes an additional case of cyclopia perfecta.

In the last group of 282 operations most of the embryos were operated upon at the 10-somite stage. Among these were 13 embryos of especial interest, two of which developed for a total time of six days, ten of which developed for seven days, and one for nine days. One was operated upon at 9 somites, four at 9 to 10 somites, and eight at 10 somites. One of these had eyes similar to no 228 (fig 6 total view and described above) but the eyes were not quite as close together as those of no. 228 Four embryos had eyes similar in position to those of no 228 and seven had eyes still closer together thus resembling more closely nos. 216 197 (figs. 14 and 19 sections) and 198 (fig. 20 section) all of which were described above. Several of the group of seven were dissected in the fresh state with iridectomy scissors, demonstrating that the pigment layer and in some cases even the sensory retina were absent from one or both eyes in the common, medial area of junction. The thirteenth embryo had a large single orbit with a reduced, pigmented vesicle on each side of the midline thus resembling no. 246 (fig. 7 and described above)

DISCUSSION

These experiments demonstrate that it is possible to produce cyclopia in early somite stages by a disturbance initially limited almost entirely to neural tissue more specificially that at stages of 5 to 7 somites cyclopia perfecta can be produced by removal of only the telencephalon and its lateral, covering surface ectoderm No prechordal substrate is removed in an operation employing a transverse cut just anterior to the forming optic vesicles at these stages as can be seen from serial sections of normal embryos. At stages of 8 to 10 somites it becomes increasingly difficult to produce cyclopia and more success is attained by removal of a wedge of tissue with two cuts, directed so as to include the telencephalon and the medial portion of the diencephalon between the forming optic vesicles in which the anterior portion of the medial prechordal substrate is also removed Clarke ('34) has shown that in the chick the eye forming field is still strongest medially up to the stage of 8 somites but after that time there is a medial area that will not form eye if isolated in chorioallantoic grafts At 5 to 7 somites the optic vesicles are beginning to bilateralize as can be seen in both the intact embryo and in sections The production of cyclopia at this time can be interpreted as a reversal of the normal course of events in the bilateralization of the head Since the transverse cut is most successful at this time the reversal can be ascribed to neural deficiency

The cyclopean eye still behaves at least in part as a product of bilateralized development retaining certain properties of the derivatives of the normal right and left optic fields In particular it tends still to send its otpic fibers to the opposite side of the brain It was not possible to trace these fibers past the chiasma region in embryo no 261 of the present series but amphibian embryos determined to cyclopia by centrifugation (Pasquini 42) and teleost fish embryos determined to cyclopia by chemical means (Rogers '52, '57b) usually have optic fibers from the right side of the cyclopean eye crossing to the left side of the diencephalon and from the left side of the eye to the right side of the brain The present results make it appear that the previous interpretation (Rogers '52) : this indicates fusion of forming primo should be revised and modified With a tional evidence it seems probable that stimulus acting in the early somite st likely operates in the period just before during the initiation of bilateralizatior the optic primordia In this connectio should be pointed out that in the ra autographic work cited in the introduct (Rogers, '64) it was found that LiCl hibited synthesis of protein in the la portions of the optic vesicles just at time that they are rapidly expanding erally more than it did in any other sue examined

There is now a good deal of evide that the prechordal substrate is not ne sarily the primarily modified tissue in experimental genesis of cyclopia Ther no question that substrate removal in open medullary plate stage in amphi can be the primary cause of experiment produced cyclopia but equally with question removal of the telencephalon the chick at the time the optic vesicles beginning to bilateralize can cause cy pia In the lithium experiments from to 42, cited in the introduction it was that the prechordal substrate or its de opmental precursor is primarily affec by the lithium treatment. The more re evidence of the five workers cited in introduction employing more pre methods on both amphibian and ch consistently argues against this inter tation

The total evidence to the present t allows one to suggest that experimen stimuli resulting in the cyclopean mode development may act on either prechor substrate or on the neural tissue of te cephalon and diencephalon or on both s strate and neural tissue and that they m be effective over a considerable period time up to and including the period actual bilateralization of the optic p mordia It may be added that in fort ously occurring cases of cyclopia the tial cause simply is not known except the few cases of known genetic ori (Wright and Wagner '34 Landauer '5 Production of cyclopia by experimental bridization (Moenkhaus, '10 Loeb Newman 17 Moulton 49 Rogers '5

almost certainly also has a genetic basis. But even here the causal developmental mechanisms are unknown.

The median eyes obtained in the present work are directly comparable morphologically to the cyclopean eyes obtained in chemical experiments and to those in fortuitously occurring cases. In many cases in the chemical experiments and in some cases in the operative experiments the optic stalk is shortened or eliminated so that the eye comes to be closely related to the diencephalon, with the tapetum continued as a reflection of the diencephalic walls. This is made clear by comparing figures 19 to 21 of this paper with figures 1 to 11 13 15 and 18 showing cyclopia produced by chemical means in *Fundulus* (Rogers, '52). In cyclopia produced by chemical means (Adelmann '34) or by operation (Levy '05) in amphibia, in the present bird examples and in Mall's ('17) human example, the primary optic cavity is in broad communication with the third ventricle (narrowest in Mall's example) and the tapetum is reflected from the margins of the diencephalic defect. Only the fish examples (Rogers '52) deviate at all from this fundamental pattern, and these do so with respect to the lack of open communication between the eye and brain cavities. This might be expected because of the secondary mode of origin of these cavities in the teleost. Thus it is apparent that the cyclopean eyes resulting from the present operative procedures in the bird are similar to those experimentally produced or fortuitously occurring in the other three most commonly studied vertebrate classes.

Stockard ('13) and Werber ('15) considered that the mass of two fused eyes to form the cyclopean eye would have to equal that of two separate eyes. The regulation that occurred in the work of Pasquini ('27) and Dewitter ('29) on lateral, fused eyes proves in theory that this is not necessarily true. Pasquini ('42) found that cyclopean eyes of axolotl were only slightly greater than normal size. The eye of embryo no. 261 shows that regulation causes even the well developed cyclopean eye formed by the total eye-forming field, to be of approximately normal size.

Most of the cyclopean embryos in the present series have a saccus infundibuli and oral hypophysis although the experiments were mostly performed at 10 somites or earlier in ample time to affect the primordia of the pituitary body. Rathke's pocket does not appear until about 22 somites in the chick (study of normal control series; see also Hamilton '52, p. 80). Kingsbury and Adelmann ('24) felt that in cyclopia the failure of the prechordal mesoderm to be removed from the midline not only results in a common oculomotor muscle mass but also in the absence of an oral hypophysis because of the lack of a normal mesoderm-free area for its formation. This viewpoint has recently been reiterated by Giroud Delmas and Martinet ('63) in relation to cyclopean mouse embryos produced by hypervitaminosis A of the pregnant mother. But in experimental as well as fortuitously occurring cyclopia the oral hypophysis actually is more often present than not, as was found in an exhaustive search of the literature (Rogers '57c). The present experiments did, however, result in medial massing of the eye muscles to a greater or lesser extent, related directly to the degree of reduction in bilateralization of the eye-forming tissue.

The evidence indicates that the experimental prevention of normal eye and head bilateralization is a process of ventralization, as Bäckström ('54, '62) has independently proposed for *Xenopus*. In the present cases the median eye is attached to the ventral tip of the diencephalon, the telencephalon being absent, at least ventrally. The modification of eye muscles and their nerves strongly supports this view. In the cases transitional between the normal and the cyclopean (nos. 228, 216, 197 and 198) the inferior oblique is the only muscle to fuse with its opposite and only in the most extreme case (no. 198) is the medial rectus not present as a separate muscle. The perfect cyclopean with well-developed eye (no. 261) adds the fusion of the inferior recti insertions, the fusion of the right and left oculomotor branches on their way to the fused inferior obliques, and a cross-connection of the ciliary ganglia. The superior obliques here are

lateral to the eye. The perfect cyclopean condition with reduced eye (no. 269) in addition closely masses the oculomotor muscles medially and fuses the superior oblique with its opposite. Within this framework of the significant changes in going from the less to the more severe defect, the changes of all the muscles and their nerves in all the cases studied can be seen to fit. Fortuitously occurring cyclopean embryos fit into this series with equal precision as for example Mall's ('17) 6.5 mm synophthalmic human Gemmill's ('06) perfect cyclopean trout, and Lyssenkow and Filatow's ('26) perfect cyclopean horse. In the present chick material no. 191 has a median orbit, but one pigmented vesicular stalked eye whose relations make it appear to be derived from the right optic vesicle and only the right ciliary ganglion sends a nerve to encircle the eye. Embryo no 269 has a larger pigmented, vesicular stalked eye whose relations make it appear to be the product of the optic field material of both sides of the embryo, and here both ciliary ganglia send nerves to form a common encircling net around the eye

Results of the experiments are in agreement with the feeling of Gruenwald ('45) that the choroid fissure is probably necessary for the presence of an optic nerve in cyclopia. The dispensability of an optic stalk in the formation of the nerve (Pasquini 42 on amphibian embryos) is less clear in the chick material than in the fish material already reported (Rogers '52) In the left eye of no 228 although there is a choroid fissure and optic fibers penetrate the retina to the outside of its coats the stalk is small and dislocated in relation to the papilla No nerve fibers from the eye reach the brain This may possibly be explained by the more distant relation of the eye to the diencephalon and consequent greater attenuation of the optic stalk in the chick with partially lateral eye as compared with the cyclopean fish material and Pasquini's cyclopean amphibian material. If the stalk is shortened or fails to form to the extent of relating the eye directly to the diencephalon however nerve fibers are seen to enter the diencephalon from the retina (no 228 right eye with shortened stalk, and nos. 216 and 198 right eyes with stalk not formed) In the right eye of no. 197 where the same close relationship of retina and diencephalon is seen the optic fibers do not remain in the diencephalic tissue but run out into the adjacent mesenchyme and end. This embryo is also unusual in that the fibers from the left eye do not decussate but ascend in the homolateral diencephalic wall. A case of non-decussation of the fibers from one eye has been reported in *Fundulus* by Oppenheimer ('50) T[he] close relation of the eye to the diencephalon seen in nos. 216 197 and 198 is illustrated in the right eye of no. 197 figure 14. It should be noted that the same sort of relation, also at the end of the choroid fissure occurs in the cyclopean eye of n[o.] 261 figure 17

The present results (see descriptions [of] maxillary processes) lend no support t[o] and in fact argue against, the interpret[a]tion of Mann ('37) that the maxillary pro[c]esses force the eye primordia together i[n] cyclopia when midline structures a[re] arrested. Substrate disturbances howeve[r] probably explain deficiencies in the or[al] region such as the under-development o[f] the right maxillary process of no. 197 a[l]though in this case the rest of the or[al] cavity and mandibular region is norma[l] Other undescribed cases in the series o[f] operated chicks had deficiencies in th[e] maxillary region while other embryos ap[]peared normal throughout the oral region Krafka ('45) has criticized the substrat[e] inhibition or deficiency concept with th[e] statement that substrate lack would pre[]vent normal development of the oral re[]gion. This view neglects the fact th[at] often oral region disturbances are de[]scribed even in fortuitously occurring cy[]clopean embryos. It also neglects the grea[t] regulative powers of the early embryo

SUMMARY

Various degrees of cyclopia includin[g] cyclopia perfecta, were produced at th[e] time of beginning bilateralization of th[e] optic vesicles in the chick, by removal o[f] the telencephalon with iridectomy scissors Operations were performed largely on 5 to 10-somite stages with the most chanc[e]

of success apparently at 6 or 7 somites. Twelve cyclopean embryos including six that were perfect cyclopean, were produced among the first 271 operations. The cyclopean eyes obtained are morphologically similar in form, and in the details of their relation to the diencephalon, to cyclopean eyes in several vertebrate classes, produced experimentally in a variety of ways, or *fortuitously* occurring

In these cyclopean embryos the saccus infundibuli and oral hypophysis are usually present, despite medial massing of the extrinsic ocular musculature. In this respect they are similar to the majority of experimentally produced, and especially fortuitously occurring, cyclopean embryos reported in the literature summarized in a previous publication. They are different in this regard from experimentally produced cyclopean amphibian embryos reported in the literature.

Morphological evidence, including the sequence of fusion of the extrinsic ocular muscle components as the cyclopean defect becomes more and more severe, indicates that the experimental reversal of bilateralization resulting in cyclopia is a ventralization.

Biochemical work on the chick, as well as the recent biochemical work of others on amphibian embryos, supports the major interpretation derived from the present operative work. The total evidence to the present time allows one to suggest that experimental stimuli resulting in the cyclopean mode of development may act on either prechordal substrate or on neural tissue of telencephalon and diencephalon, or on both substrate and neural tissue and that they may be effective over a considerable period of time, up to and including the period of actual bilateralization of the optic primordia.

ACKNOWLEDGMENTS

I wish respectfully to dedicate this work to Professor Leigh Hoadley under whose guidance I began work on the nervous system and eye, including the present experiments. His generosity to others, in his roles of teacher administrator and undergraduate house master has been an outstanding characteristic during his many university years.

LITERATURE CITED

Adelmann, H. B. 1927 The development of the eye muscles of the chick. J Morph., 44 29–67

——— 1930 Experimental studies on the development of the eye III. The effect of the substrate ('Unterlagerung') on the heterotopic development of median and lateral strips of the anterior end of the neural plate of *Amblystoma*. J Exp Zool., 57 223–281.

——— 1934 A study of cyclopia in *Amblystoma punctatum* with special reference to the mesoderm. J Exp. Zool., 67 217–281.

——— 1937 Experimental studies on the development of the eye. IV The effect of the partial and complete excision of the prechordal substrate on the development of the eyes of *Amblystoma punctatum*. J Exp. Zool., 75 199–237

Alderman, A. L. 1935 The determination of the eye in the anuran, *Hyla regilla*. J Exp. Zool., 70 205–232.

——— 1938 A factor influencing the bilaterality of the eye rudiment in *Hyla regilla*. Anat. Rec., 72: 297–302.

Bäckström, S. 1954 Morphogenetic effects of lithium on the embryonic development of *Xenopus* Ark. Zool., 6 527–535.

——— 1962 A link between neural induction and vegetalization. The effect of magnesium on *Xenopus* embryos. Acta Embryol. Morphol. Exp., 5 295–303.

Born, G. 1897 Über Verwachsungsversuche mit Amphibienlarven. Arch. Entwicklungsmech. Organ., 4 349–465, 517–623.

Carpenter F W 1906 The development of the oculomotor nerve, the ciliary ganglion and the abducent nerve in the chick. Bull. Mus. Comp. Zool., Harvard, 48 141–229.

Clarke L. F 1934 Regional differences in eye forming capacities of early chick blastoderms as studied in chorio-allantoic grafts. Physiol. Zool., 9 102–128.

Detwiler S. R. 1929 Some observations upon grafted eyes of frog larvae. Arch. Entwicklungsmech Organ., 161 656–668.

Gemmill, J F 1906 On cyclopia in osseous fishes. Proc. Zool. Soc., London, 1906, I 443–449

Giroud, A., A. Delmas, et M. Martinet 1963 Cyclocéphalie Morphogénèse et mécanisme de sa production. Arch. Anat. Hist. Embr 47 293–311

Groenwald, P 1945 Absence of the optic nerve in cyclopia. Anat. Rec., 91 13–20

Hall, T S. 1942 The mode of action of lithium salts in amphibian development. J Exp. Zool., 89 1–32.

Hamilton, H. L. 1952 Lillie' Development of the Chick. Henry Holt, New York.

Huber W 1946 Sur les conditions qui déterminent la synophthalmie chez les cyclocéphales à deux yeux et sur une malformation nouvelle la pseudocyclopie. C. R. Soc. Biol., 142 1063–1064

Huschke, E. 1832 Über die erste Entwicklung des Auges und die damit zusammenhängende Cyklopie. Meckel' Arch. Anat. Physiol., 1–47

Kawakami, I. 1955 Teratogenic effects of chemicals on early amphibian development, with special reference t the lithium effects. Acta Path. J p 5 suppl. 475–484
Kingsbury B F., and H. B Adelmann 1924 The morphological plan of the head. Q J Micr Sci., 68 239–286.
Krafka J 1945 Cyclopia and arhinia. Arch. of Ophthalmol., 33 128–136.
Lallier R. 1952 Chlorure de lithium et développement embryonnaire (aspects cytochimiques et morphologiques) C. R. Acad. Sci., 235 260–262.
——— 1953 Recherches sur le problème de la détermination embryonnaire chez les Amphibiens et les Echinodermes. Thèses. Paris. Imprimerie H Vaillant-Carmanne, S. A., Liège Belgique 1955.
Landauer W 1956 Cyclopia and related defect as lethal mutation f fowl. J Genetics, 54 219–235.
Lehmann, F E. 1933 Die Augen- und Linsenbildung von Amphibienembryonen unter dem Einfluss chemischer Mittel. Rev Suisse Zool., 40 251–264
——— 1936 Stehen die Erscheinungen der Otocephalie und der Zyklopie bei Triton mit Axialgradienten oder mit Störungen bestimmter Organisatorregionen im Zusammenhang? Rev Suisse Zool., 43; 535–541.
——— 1937 Mesodermisierung des präsumptiven Chordamaterials durch Einwirkung von Lithiumchlorid uf die Gastrula von Triton alpestris Arch. Entwicklungsmech. Organ., 136 112–146
——— 1938 Regionale Verschiedenheiten des Organisators von Triton insbesondere in der vorderen und hinteren Kopfregion, nachgewiesen durch phasenspezifische Erzeugung von lithium bedingten und operativ bewirkten Regionaldef kten Arch Entwicklungsmech. Organ., 138 106–169
Levy O 1905 Entwicklungsmechanische Studien am Embryo von Triton taeniatus Arch. Entwicklungsmech. Organ., 20 335–379
Loeb J 1912 Heredity in heterogeneous hybrids. J Morph., 23 1 15.
Lombard, G. L. 1952 An experimental investig tion on the action of lithium on amphibian development Thesis. Utrecht. Druk Excelsiors Foto-Offset 'Gravenh ge Netherlands
Lyssenkow N K., und W P Filatow 1926 Ein Fall von Zyklopie beim Pferd. Arch. A genh., 97 314–340
Mall F P 1917 Cyclopia in the human embryo. Contr to Embr no 15 Carnegie In t. Publ. no 226 5–33
Mann, I. 1937 Developmental Abnormalities of the Eye Cambridge University Pres Cambridge
Masui, Y 1956 Effect of LiCl upon the organizer nd the presumptive ectoderm. Annot. Zool. Jap 29 75–78
——— 1959 Induction of neural tructures under the influence of lithium chloride Annot. Zool. Jap 32; 23–30
——— 1960 Effect of lithium hloride upo differentiation of the neural-plate ectoderm o head area. Mem. Kônan Univ Sci. Ser no. 4 103–114
——— 1961 Mesodermal and endodermal di ferentiation of the presumptive ectoderm Triturus gastrula through influence of lithiu ion. Experientia, 17 458–459.
Meckel J F 1826 Ueber Verschmelzungsbil ungen. Meckel's Arch. Anat. Physiol., 1 238 310
Moenkhaus, W J 1910 Cross fertilizatio among fishes. Proc. Indiana Acad. Sci 1910 353–393.
Moulton J M. 1949 The development of Men dia-f ndulus hybrids. Biol. Bull., 97 314 (al tract)
Newman, H. H. 1917 On the production c monsters by hybridization. Biol. Bull., 32. 306 321.
Ogi, K. I. 1961 Vegetalization of the presum tive ectoderm of the Triturus-gastrula by exp sure to lithium chloride solution. Embryologi 5 384–396.
Oppenheimer J M 1950 Anomalous optic ch asma in Fund lus embryos. Anat. Rec., 10 477–484.
Pasquini, P 1927 Ricerche di embriologia spe imentale sui trapianti della vescicola ottic pr maria in Pleurodeles waltli. (I processi regolazione di differenziamento della fusio degli abbozzi oculari e l'origine della lente Boll. Ist. Zool. R. Univ Roma, 5 1–83.
——— 1942 Sulla fine struttura dell'encef nei diversi case di anomalie oculari e dell gano olf ttorio in larvette di Axolotl, ottenu da uova centrifugate. Arch Ital. Anat. Emb 47 310–341
Rogers K. T 1951 Experimental producti of cyclopia in the hick after the arisal of tw distinct optic primordia. Anat. Rec 111 4 (abstract)
——— 1952 Optic nerve pattern evidence f fusion of eye primordia in cyclopia in Fundul heteroclitus. J Exp. Zool., 120 287–309
——— 1957 Ocular muscle proprioceptl neurons in the developi g hick. J Com Neur 107 427–437
——— 1957b Optokinetic testing of cyclope and synophthalmic fish hatchlings. Biol. Bu 112 241 248
——— 1957 Presence of the pituitary in p fect cyclopia. Anat. Rec 128 213–221
——— 1963 Experimental production of p fect cyclopia in the hick by means of Li with urvey of the literature on cycl produced experimentally by rious mea Dev Biol., 8 129–150.
——— 1964 Radioautographic nalysis of t incorporation of protein and nuclei acid prec sors into arious tissues of arly hick bryos cultured in tol on medium containi LiCl. Dev Biol 9 176–190
Speer 1819 De cyclopia aive unione partiu capitis in tatu normali disjunctarum Di Halae (Cited from Meckel 1826)

Spemann, H. 1904 Ueber experimentell erzeugte Doppelbildungen mit cyclopischem Defect. Zool. Jahrb., suppl 7 429–470

Stockard, C. R. 1907 The artificial production of a single median cyclopean eye in the fish embryo by means of sea water solutions of magnesium chloride. Arch. Entwicklungsmech. Organ., 23 249–258.

—— 1908 The question of cyclopia, one-eyed monsters. Science, 28 455–456.

—— 1913 An experimental study of the position of the optic anlage in *Amblystoma punctatum*. Am. J Anat., 15 253–289

Warynski, St., et H. Fol 1883 Recherches expérimentales sur la cause de quelques monstruosités simples et de divers processus embryogéniques. Recuil Zool. Suisse 1883 1–23.

Werber E. I. 1915 Experimental studies aiming at the control of defective and monstrous development. A survey of recorded monstrosities with special attention to the ophthalmic defects. Anat. Rec., 9 529–562.

Wolff E. 1934 Recherches expérimentales sur la cyclopie. Arch. Anat. Hist. Embr 18 145–167

Wright, S., and K. Wagner 1934 Types of subnormal development f the head from inbred strains of guinea pigs and their bearing on the classification and interpretation of vertebrate monsters. Am. J Anat., 54 383–447

PLATE 1

EXPLANATION OF FIGURES

Figures 3 to 9 are photographs made with transmitted light and red filter of embryos stained with eosin and cleared in cedarwood oil. Figures 10 and 11 are photographs taken with reflected light and green filter at the end of dehydration of the embryo, after staining with eosin.

3 Embryo no. 28, dorsal view × 8. Heart primordia in this embryo failed to unite in the midline. c, lens of cyclopean eye; h, chamber of heart; w wing bud.

4 No. 43 ventral view × 5.5. The mesencephalon is above and the saccular amnion, which failed to grow over the embryo, is in front of the eye. The eye is single, median, pigmented vesicle.

5 No. 191 ventral view of head, × 6. The mesencephalon is above the single orbit, which contains a small, stalked, pigmented vesicle on the right only

6 No. 228, ventral view of head, × 6. The telencephalon is much reduced, and lies between the eyes and the optic lobes of the mesencephalon (above) See text for further description.

7 N 246, ventral view of head, × 5. The reduced telencephalon is in front of the optic lobes, and above the broad, single orbit, which contains two stalked, pigmented vesicles.

8 No. 261 ventral view of head, × 5. The notch indicating the choroid fissure can just be made out, in the midline below the pupil. The reduced telencephalon is immediately above the eye and the epiphysis ppears as a dark spot above the telencephalon. See text for further description.

9 No. 261 left side of head, × 5. Descriptive anterior ( ) and dorsal (d) are indicated. Dotted lines indicate the microtechnique plane of sectioning.

10 No. 261 uncleared, left side, × 5.

11 No. 261 uncleared, ventral view of head, × 5.

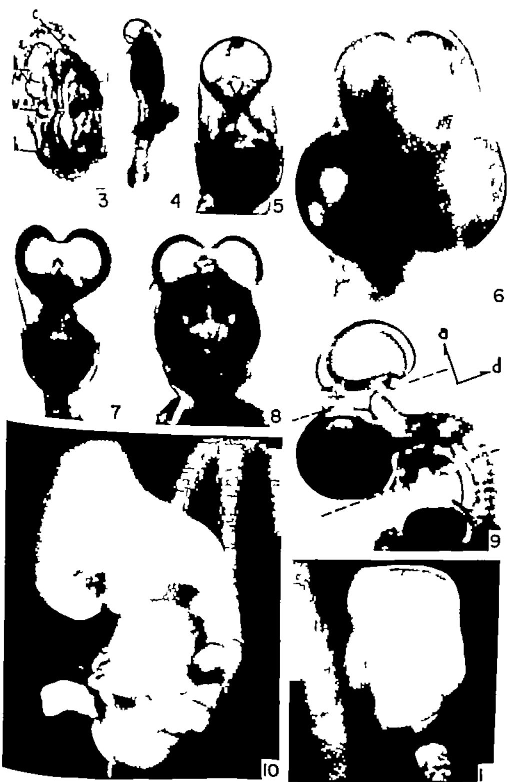

c
3
4
5
6
7
8
a
d
9
10
11

PLATE 3

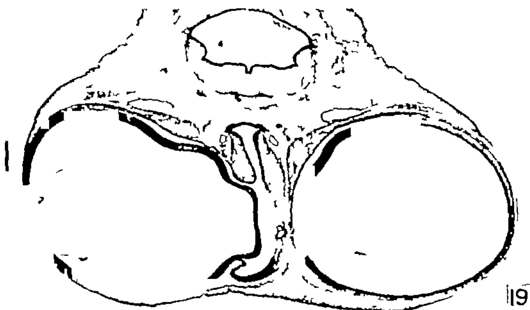
EXPLANATION OF FIGURES

Photomicrographs of 10 μ transverse sections, modified Bodian preparation.

19 Section through the eyes and diencephalon of no. 197 144 sections higher in the series than figure 14 × 14 The sensory retina on the right projects into the third ventricle through the diencephalic defect, from the edges of which the tapetum of the ey is continued direct reflection. Hindbrain is above

20 *Section through the eyes and diencephalon of no. 193 × 14* The embryo had died day earlier younger ge and greater hrinkage in preparation account for the great disparity in size as compared w th the adjacent figures The sensory retinal portion of the yes re in effect, in the third entricle, with the tapetum of each side continued from the edges of the diencephalic defect. On the embryo left t this level, the tapetum ha broken away from the diencephalon. Hind brain abov See text for further description.

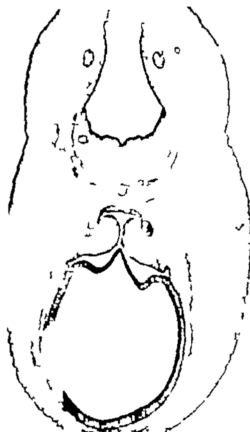
21 Section through the perfect cyclopean ey and diencephalon f no 261 106 sections higher in the series than figure 17 × 14 The pe tum ontinuou with the edges of the diencephalic defect and the primary optic vity is confluen with the third entricle Hind rain bov



19



20



21

togenesis were designated according to Leblond and Clermont ('52)

EXPERIMENTAL RESULTS

Effect of heat on distribution frequency of stages of the cycle of seminiferous epithelium. Testicular sections from animals sacrificed 2, 8 and 26 days after exposure were analyzed. In some tubules this could not be done due to complete degeneration of germinal epithelium. Such tubules were recorded as "undetermined." Results of the analysis are summarized in table 1. In the two-day group frequency of stages was similar to normal controls although there was a slight increase in stages IX to XI and decrease in stages XII and XIII. At eight days there was a drop in frequency of stages I, II and VI, while the frequency of other stages was comparable with control values. The 26-day sample showed a slight decrease in stages II, XII and XIII. The percentage of tubules in stage XIV was unchanged at all time intervals, however in the two-day group dividing primary spermatocytes were missing, and identification of this stage was based on the numbers of type A spermatogonia, spermatids at step 14 and zygotene spermatocytes.

HISTOLOGIC OBSERVATIONS

Two days after exposure

Spermatogonia. No abnormalities in the microscopic appearance were observ[ed].

Spermatocytes. A small number [of] pachytene spermatocytes in stage I show[ed] increased affinity of cytoplasm for P[AS] stain, pyknosis, karyolysis and kar[yor]rhexis (figs. 5, 9, 13). From stages II [to] IV an increasing number of cells w[ere] affected and tubules were full of cellul[ar] debris (figs. 9, 13, 17). "Ghost cells" wi[th] faint PAS-positive cytoplasm and no n[u]clear material were abundant. At stage [V] cellular debris disappeared but most sp[er]matocytes showed degenerative chang[es] (fig. 21). In stage VI the pachytene sp[er]matocytes were markedly decreased [in] numbers, but showed normal morpholog[y]. In stage VII all spermatocytes were mo[r]phologically intact (figs. 25, 29). Fro[m] stages VIII to XI morphology of pachyten[e] spermatocytes was mostly normal, [al]though counts were below control value[s] (figs. 37, 41, 45); the few remainin[g] spermatocytes at stage XII showed norma[l] morphology. By stage XIV few sho[wed] cells and little cellular debris could b[e] found, but dividing spermatocytes wer[e] [ab]sent (fig. 57).

TABLE 1

Percentage of tubules in different stages of the cycle at various time intervals after exposure to 43 C for 15 min

Stages	Controls	2 days	8 days	26 days
I	_3	_6	1	9.1
II	5.3	6_	4.9	4.4
III	_3	_6	3.8	4.3
IV	4.5	6.6	6.5	3.4
V	5.1	5.0	6.5	5.5
VI	[illegible]	[illegible]	4.4	[illegible]
VII	[illegible]	[illegible]	[illegible]	1.8
VIII	[illegible]	—	11.9	14.9
IX	[illegible]	4.4	4.6	3.5
X	[illegible]	4_	_9	3.4
XI		3.8	6_	3.5
XII	[illegible]	8.0	11.1	.5
XIII	[illegible]	3.1	4	3
XIV	[illegible]	[illegible]	3.4	4.4
Undetermined		[illegible]	_1	3.9
[illegible]	[illegible]	[illegible]	685	1173

spermatids. In stages I and II, spermatids were absent. At stages III and IV despite relatively high or normal counts large numbers of young spermatids showed morphologic changes. Giant cells containing 3 to 5 spermatid nuclei, and spermatids showing ring formation in the nucleus were abundant (fig. 17) From stage V on, spermatids appeared normal (figs. 21 25, 33, 53, 57) At stages VI and VIII, arrangement of mature groups of spermatids in some tubules was abnormal; they were retained in the deep layers of the germinal epithelium (figs. 25 29) Some mature spermatids particularly at stages VII and VIII, showed pyknosis of the head (fig. 33) In stages IX to XI, many spermatozoa were found retained in the basal layers of the germinal epithelium. Most of them showed pyknotic heads (figs. 37, 41, 45)

Four days after exposure

Spermatogonia. No abnormalities in microscopic appearance were observed

Spermatocytes. No abnormality could be detected in resting, leptotene or zygotene spermatocytes. Pachytene spermatocytes appeared normal in stage I whereas there was a progressive decrease in their numbers from stages II to V Tubules in these stages contained cellular debris and spermatocytes showed abnormalities similar to those found in the two-day group. A few spermatocytes showed giant cell formation. Pachytene spermatocytes were absent in stage VI. In stages VII and VIII, the number of pachytene spermatocytes varied widely from none to normal. The number of spermatocytes in tubules at stages IX to XI showed only a slight decrease No abnormality was detected in either number or morphology of pachytene spermatocytes in stages XII and XIII In stage XIV all cellular components were present, but most of the dividing cells showed gross abnormalities such as bizarre meiotic figures pyknotic nuclei, cytolysis and chromatolysis.

Spermatids. Spermatids in stages II to V were absent, and at stage VI only a few mostly degenerating spermatids could be seen. From stage VII on spermatids appeared normal, but large numbers of spermatozoa were retained in the basal layers of the germinal epithelium at stages VIII to XI. Most of the spermatozoa showed degenerative changes.

Six days after exposure

Spermatogonia. Spermatogonia appeared perfectly normal at all stages of spermatogenesis.

Spermatocytes No abnormality could be detected in resting, leptotene or zygotene spermatocytes or in early pachytene spermatocytes up to stage III. By stage IV there was a decrease in numbers associated with morphological abnormalities and in stages V through VIII, the primary spermatocytes were absent. Abnormal spermatocytes could be found only rarely in stages IX to XI and at stages XII and XIII, all spermatocytes were normal. In stage XIV however many bizarre meiotic figures were observed secondary spermatocytes showed marked degenerative changes.

Spermatids Only a few young spermatids were present in stages I to III, and many tubules at stage III contained none. From stage VIII on, spermatids appeared normal, although numbers of mature spermatozoa were retained in the layers of the seminiferous epithelium at stages VIII to XI.

Eight days after exposure

Spermatogonia. No abnormalities were observed.

Spermatocytes Early spermatocytes up to the zygotene stage appeared microscopically normal, as did pachytene spermatocytes in stages I and II (figs 6 10) Cells in stages III to VI showed giant cell formation or chromatolytic changes (figs. 14 18) Ghost cells and occasional degenerating spermatocytes could be found at stages VII and VIII. From stages IX to XII, only very occasionally could a pachytene spermatocyte be found. These cells exhibited normal structure (figs. 38 42, 46 50) Diakinetic spermatocytes at stage XIII were normal morphologically (fig. 54), but at stage XIV a large proportion of meiotic figures was abnormal. The secondary spermatocytes, however appeared normal (fig. 58)

Spermatids Morphological changes in young spermatids at stages I to III consisted mainly of cytolysis and chroma

tolysis (fig. 10) From stages IV to VIII, no normal spermatids were seen; those present were found in the form of giant cells containing 5 to 16 spermatid nuclei (figs. 18 22, 26) Spermatids, from stages IX, appeared normal. Retention of sperma tozoa in the basal layers of the germinal epithelium at stages IX to XI was also observed (fig. 46)

Twenty-six days after exposure

Testicular sections from this group of animals revealed a picture of regeneration.

Spermatogonia. No abnormalities were observed.

Spermatocytes Most spermatocytes showed normal structure. A few tubules *at stage XIV contained bizarre dividing* cells and pyknotic nuclei, but normal sec ondary spermatocytes (fig. 59)

Spermatids. The only changes observed were retention of spermatozoa in the germinal cell layers of tubules in stages IX and XI, as well as pyknosis of the sperm heads.

It is of interest to note that some tubules failed entirely to regenerate containing only Sertoli cells and a few spermatocytes at 26 days after the experiment. Sertoli and Leydig cells did not show any signifi cant change in morphology in any of the experimental groups.

QUANTITATIVE ANALYSIS OF THE SEMINIFEROUS EPITHELIUM

Two days after exposure

Spermatogonia. The mean number of spermatogonia per cross-section of a semi niferous tubule did not differ significantly from control values (table 2)

Spermatocytes Results of counts are summarized in table 3 There was no change in numbers of resting leptotene and zygotene spermatocytes. Counts of pachytene spermatocytes were normal in stages I and IV At stage VI, the average count was reduced from a normal of 50 to 21 cells per tubular cross-section. At stage VII, the count was normal at stage VIII *the occurrence of pachytene spermatocytes* was irregular some tubules containing normal numbers while others only a few (fig. 33) There was a slight fall in count of pachytene spermatocytes in stages IX and XI, whereas at stage XII, very few were present. No diakinetic or dividing sperm tocytes could be found in stages XIII an XIV; secondary spermatocytes and youn spermatids were absent (figs. 53 57)

Spermatids The counts are presente in table 4 The young group of spermatid at stages I and II were absent, and at stag III their number was considerably *below* normal. From stage IV on counts wer normal.

Eight days after exposure

Spermatogonia. The counts are sum marized in table 2. No deviation from con trol values was observed.

Spermatocytes. Counts of primary sper matocytes are summarized in table 3. Rest ing, leptotene and zygotene spermatocyte showed no significant variation from nor mal early pachytene spermatocytes up to stage VI were within the normal range

TABLE 2

Number of spermatogonia per cross-section of tubule at various time intervals after exposure to 43 C for 15 minutes

Spermatogonia	Stage of the cycle	Control	Days after exposure 2	8	26
A	VII	1.8 ± 0.7	1.0 ± 0.9	1.0 ± 0.8	1.2 ± 0.8
	IX	2.9 ± 1.0	2.2 ± 1.6	2.7 ± 1.2	2.2 ± 0.7
	XII	3.0 ± 1.0	2.0 ± 1.2	3.4 ± 1.5	3.4 ± 1.4
	XIV	3.8 ± 1.8	4.1 ± 1.5	5.2 ± 1.3	4.0 ± 1.1
A and Intermediate	I	6.8 ± 2.2	7.5 ± 2.4	8.8 ± 2.2	7.5 ± 2.3
	III	8.6 ± 2.9	11.8 ± 3.4	11.4 ± 1.7	10.7 ± 2.0
A, Intermediate and B	IV	14.7 ± 3.1	14.9 ± 4.2	15.3 ± 3.0	13.0 ± 2.3
B	V	23.3 ± 4.0	22.9 ± 4.1	22.5 ± 3.5	21.8 ± 2.5

Mean ± standard deviation of the mean.

TABLE 3

Number of primary spermatocytes per cross-section of a tubule at various time intervals after exposure to 43°C for 15 minutes

Spermatocytes	Stage of the cycle	Control	Days after exposure 2	8	26
Resting	VII	44.0 ±5.3	42.7± 4.3	40.9± 3.0	48.7± 4.0
Leptotene	IX		46.4±14.6	39.5±13.2	47.2± 4.6
	XI	46.2 ±4.1	53.1± 8.0	42.4±10.5	46.1± 6.6
	XII		60.7± 4.7	47.0± 7.8	59.3± 6.5
Zygotene	XIV	49.0 ±5.1	56.0± 9.3	49.9± 8.8	52.6± 8.3
	I	50.09±8.6	59.8± 7.7	51.3± 5.2	52.4±10.4
	IV		40.2±13.8	46.6± 8.1	51.5± 7.0
	VI		21.0±15.1	47.3±10.5	51.8± 7.8
Pachytene	VII	69.0 ±6.7	63.8± 7.2	1.5± 4.3	64.6± 6.4
	IX		35.2±12.8	nil	56.2± 7.6
	XI		43.6±14.3	nil	60.3± 9.0
	XII		0.7± 1.3	nil	60.0± 7.9

Mean ± standard deviation of the mean.

TABLE 4

Number of spermatids per cross-section of a tubule at various time intervals after exposure to 43 C for 15 minutes

Steps of spermiogenesis	Stage of the cycle	Control	Days after exposure 2	8	26
1	I	132.3±15.0	0.0	40.6±40.0	normal
2	II	132.3±15.0	0.0	25.1±28.0	normal
3	III	132.3±15.0	93.0±41.2	0.0	normal
4	IV	132.3±15.0	normal	0.0	normal
5	V	132.3±15.0	normal	0.0	normal
6	VI	132.3±15.0	normal	0.0	normal
7	VII	132.3±15.0	normal	0.0	normal
8	VIII	132.3±15.0	normal	0.0	normal
13	I	132.3±15.0	normal	normal	0.0
14	VI	132.3±15.0	normal	normal	29.1±37.6
15	VII	132.3±15.0	normal	normal	22.1±35.0
16	VIII	132.3±15.0	normal	normal	0.0

Mean ± standard deviation of the mean.
Normal the mean count was within 132.3 ±15.0.

but were reduced or absent in stages VII to XII. At stages XIII and XIV the number of diakinetic and dividing spermatocytes was normal.

Spermatids. The counts are presented in table 4. A significant reduction in numbers of young spermatids was noted in stage I. This was more pronounced in stage II and spermatids were absent in stages III to VIII. However in stage IX, the number of step 9 spermatids was normal. The number of spermatids continued to be normal throughout the later stages of spermatogenesis.

Twenty-six days after exposure

Spermatogonia. Counts are summarized in table 2. No significant departure from the normal range was detected.

Spermatocytes The counts of resting leptotene, zygotene and pachytene spermatocytes were within normal limits (table 3)

Spermatids. The counts are presented in table 4 The number of young spermatids in stages I through XIII was normal. Step 14 spermatids were absent in some tubules at stage XIV and step 15–19 spermatids were absent from stages I through V (figs. 7 11 15 19) In stages

VI and VII they were absent from about 50% of tubules; in stage VIII mature spermatids were also lacking from most tubules. Retention of spermatozoa was again evident in stages IX and XI (figs. 39 43)

DISCUSSION

Earlier studies concerned with the effect of heat on testes were based mainly on histologic evaluation of testicular tissue with no attempt to quantitate the changes in the germinal epithelium. The investigators employed different amounts of heat and various species of animals therefore the controversy concerning differential sensitivity of germinal epithelium cells to heat was difficult to resolve.

In experiments described here testes of adult rats were exposed to a well defined quantity of heat (43 C for 15 minutes) and sacrificed at time intervals after a single exposure. Testicular tissue was examined for cytomorphologic abnormalities, and a quantitative study was made of changes in numbers of the germinal epithelium elements. Schematic diagram of spermatogenesis and its timing based on data of Clermont et al. ('59) was constructed to help in the analysis of the

TWO DAYS AFTER EXPOSURE TO HEAT

STAGES OF CYCLE	I	II	III	IV	V	VI	VII	VIII	IX	X	XI	XII	XIII	XIV
DURATION (hours)	34 9	25 3	6 0	13 0	14 7	26 5	62 8	21 5	20 6			32 3	17 6	14 1

A (observed)	I	II	III	IV	V	VI	VII	VIII	IX	X	XI	XII	XIII	XIV
	15	16	16	17	17	18	19	19						
	1	2	3	4	5	6	7	8	9	10	11	12	13	14
	P	P	P	P	P	P	P	P	P			P	D1	D1
	In	In	In	In	B	B	R	R	L			Z	Z	Z
	A	A	A	A	A	A	A	A	A			A	A	A

B (calculated)	I	II	III	IV	V	VI	VII	VIII	IX	X	XI	XII	XIII	XIV
	15	16	16	17	17	18	19	19						
	1	2	3	4	5	6	7	8	9	10	11	12	13	14
	P	P	P	P	P	P	P	P	P			P	D1	D
	In	In	In	In	B	B	R	R	L			Z	Z	Z
	A	A	A	A	A	A	A	A	A			A	A	A

FIGURE 1

Figs. 1–3 Each figure is composed of two complete and identical diagrams of spermatogenesis (constructed on the basis of data published by Clermont et al., '52). Diagram A shows cell found damaged (shaded) or absent (heavily shaded) at the indicated time intervals after exposure to heat. Diagram B show position of these cells (found by back calculation) in the germinal epithelium at the time of exposure to heat.

The following symbols are used

A, Type A spermatogoni
B Type B spermatogonia
In, Intermediate spermatogoni
R, Resting primary spermatocytes
L, Leptotene primary spermatocytes
Z, Zygotene primary spermatocytes
Di, Diplotene primary spermatocytes
D\ Primary sperm tocytes in division.

EIGHT DAYS AFTER EXPOSURE TO HEAT

STAGES OF CYCLE I II III VI V VI VII VIII IX X XI XII XIII XIV

DURATION (hours) 34 9 23 3 60 13 0 14 7 26 5 62 8 21 3 20 6 32 3 17 6 14 1

A (observed)



B (calculated)

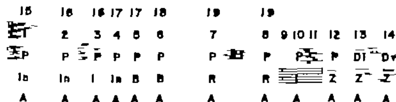


FIGURE 2

TWENTY SIX DAYS AFTER EXPOSURE TO HEAT

STAGES OF CYCLE I II III IV V VI VII VIII IX X XI XII XIII XIV

DURATION (hours) 34 9 25 5 6 0 13 0 14 7 26 6 62 8 21 3 20 6 32 3 17 6 14 1

A (observed)



B (calculated)

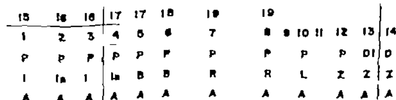


FIGURE 3

quantitative data reported here (figs. 1–3). Cells, absent or damaged at a given time interval after heat exposure were marked in the "A" part of the diagram; their position in the cycle at the time of exposure found by back-calculation was depicted in the "B" part. For example in testes obtained two days after exposure (fig. 1) spermatids were absent in steps 1 and 2, and markedly decreased in steps 3 and 4. Since step 1 requires about 35 hours and step 2 about 23 hours, spermatids exposed to heat early in step 1 should become late step 2 spermatids after 48 hours. Since step 2 spermatids were absent from testes obtained 48 hours after exposure it could be concluded that step 1 spermatids were affected by exposure to heat. Similarly early step 2 spermatids should develop into late step 4 spermatids after 48 hours but the step 4 spermatids were either absent or showed abnormal morphology. Late step 2 spermatids also require about 48 hours to reach step 6 and these were present in day 2 samples. It appears, therefore, that spermatids in steps 1 and early step 2 are susceptible to heat, while those in advanced step 2 are resistant. Since step 5 and older spermatids were normal in two-day samples it appears that all spermatids beyond early step 2 are resistant to heat, or at least the effect is not manifested two days after exposure. Forty-eight hours are required for primary spermatocytes in stage XII to become early spermatids in step 1. Since spermatids in the entire step 1 interval were absent two days after exposure to heat pachytene and diakinetic spermatocytes at stages XII and XIII and dividing spermatocytes in stage XIV must be susceptible. Calculating back for the absent pachytene and dividing spermatocytes at stages XII to XIV we came upon spermatocytes from late stages VII to first half of stage XII. Consequently all pachytene spermatocytes between late stage VII and early stage XII, must be affected by heat. Further analysis of the data indicates that zygotene spermatocytes at stage XIV and pachytene spermatocytes at stages I and II are also affected by heat. Thus results obtained from analysis of the two-day samples suggest that all primary spermatocytes from pachytenes at late stage VII to dividing spermatocytes at stage XIV and young spermatids at st[age] I are susceptible to heat, and disapp[ear] within 48 hours after exposure. Zygote[ne] spermatocytes at stage XIV, pachyte[ne] spermatocytes at stages I, II and part [of] VII, appeared to be only partially affect[ed]. Pachytene spermatocytes at stages III [to] VI and spermatids from step 2 on app[ear] to be heat-resistant. Analysis of the da[ta] obtained four days after exposure reve[aled] that the same groups of cells are heat-sen[si]tive. Reduction of pachytene spermatocyt[es] in stages VII to XI indicates that these ce[lls] are partially susceptible when exposed [to] heat in stages II and IV. Since pachyte[ne] spermatocytes were absent in stage VI, [it] may be concluded that pachytene sperm[a]tocytes in stage I are severely injured b[y] heat, gradually degenerate and disappe[ar] within four days. Furthermore, reductio[n] in numbers of pachytene spermatocytes i[n] stages II to V in the four-day sample ind[i]cates that zygotene spermatocytes in stage XII and XIII are also partially damage[d] by heat. The absence of pachytene sper[ma]tocytes in stages V to VII in the six-da[y] group indicates that spermatocytes ex[posed] to heat at stages XII and XIII ca[n] develop into zytogene and pachytene sper[ma]tocytes but they gradually disappea[r] within six days after exposure. Analysis o[f] the eight-day sample (fig. 2) confirm[s] above calculations and conclusions. It als[o] indicates that leptotene spermatocytes a[t] stage XI are damaged by heat. Pachytene spermatocytes in stage VII showed partial damage in earlier experimental groups. In this sample, absence of young spermatids from stages III to VI suggests that these spermatocytes have variable susceptibility; some degenerate during the pre-meiotic phase, others during meiosis while still others continue to form spermatids and enter early phases of spermiogenesis. Nevertheless ultimately they degenerate completely while pachytene spermatocytes at stage V and VI continue to show resistance. Results of a similar analysis of 26-day samples presented in figure 3 not only confirm conclusions derived from earlier time interval groups but provide additional evidence that pachytene spermatocytes at stages V and VI are not affected by heat since these cells develop into adult spermatozoa, as shown by the presence of steps

8 and 16 spermatids in a large number of tubules at stages VI and VII, respectively.

In summary the above discussed data show that primary spermatocytes from step XI (leptotene) to dividing spermatocytes at stage XIV are injured by heat, excepting for pachytene spermatocytes in stages V and VI. In addition, spermatids in step 1 and early step 2 of spermiogenesis are heat-susceptible. Those beyond step 2 continue with the maturation process, and form adult spermatozoa. Resting spermatocytes, spermatogonia and Sertoli cells are not affected by the amount of heat employed in this experiment.

Morphological abnormalities in degenerating cells appear to follow a definite sequence, different for spermatids and spermatocytes. Cytolytic and chromatolytic changes were very common in young spermatids in steps 1 and 2, and their rate of degeneration was comparatively rapid. Nuclei of steps 3 and 4 spermatids formed caps by peripheral accumulation of chromatin materials before actual chromatolysis. These cells were often detached from the cellular layer and enclosed in a common mass of cytoplasm forming giant cells. Giant cell formation was common for spermatids from step 4 to 8 of spermiogenesis, containing *up to 16* spermatid nuclei. The acrosomic material of spermatids enclosed by giant cells remained intact, disintegrating subsequently without further differentiation, as evidenced by the presence of giant cells containing step 4 or 5 spermatids in tubules in stages VI or VII. The earliest changes in degenerating spermatocytes occurred in the cytoplasm, which stained positively with PAS. This was followed by pyknosis chromatolysis and gradual cytolysis. Giant cell formation by spermatocytes was less common than with spermatids and occurred only in severely damaged tubules. Dividing spermatocytes deteriorated more rapidly showing nuclear fragmentation and bizarre meiotic figures.

It is apparent that the dose of heat employed in these experiments may affect cells in two different ways. First, it must interfere drastically with one or more vital functions of some cells, as evidenced by their rapid death shortly after exposure. Secondly it may produce a latent effect, since certain types of cells are able to continue their development before degenerating at a later stage of maturation. It is of interest that cells in early stages of meiosis (leptotene zygotene) are more resistant to heat than those in later stages. Earliest morphologic signs of damage in cells in pre-meiotic stages of division, were detectable in the cytoplasm, while cells in interphase, like spermatids showed earliest signs of damage in the nuclei. No explanation can be offered at this time for the surprising finding of resistance to heat of pachytene spermatocytes in stages V and VI of spermatogenesis. Spermatogonia, the youngest germinal epithelium cells, showed no morphologic changes following exposure to heat, but continued normal development with ultimate formation of spermatozoa.

Steinberger and Dixon ('59) on the basis of qualitative histologic study of testicular tissue concluded that exposure to temperatures of 43 C for 15 minutes produces a specific type of damage to germinal epithelium limited to one type of cells, primary spermatocytes. Quantitative data reported in this paper provide support for their concept of response-specificity of germinal epithelium to heat. However their conclusions concerning limitation of damage to primary spermatocytes must be modified. First, not all stages of development of primary spermatocytes are sensitive to this amount of heat, and second, in addition to primary spermatocytes the first two steps of spermatid development are also heat-susceptible.

In conclusion, this work supports the hypothesis that germinal epithelium reacts to noxious stimuli, in this case heat, in a precise and specific fashion.

LITERATURE CITED

Asdell, S. A., and G. W. Salisbury 1941 The rate at which spermatogenesis occurs in the rabbit. Anat. Rec., 80: 145–154.

Clermont, Y et al. 1959 Durée du cycle de l'epithelium seminal du rat. Arch. Anat. Micro. Morph. Exp., 48 37–56.

Clermont, Y and H. Morgentaler 1955 Quantitative study of spermatogenesis in the hypophysectomized rat. Endocrinology 57 369–382.

Leblond, C. P and Y Clermont 1952 Spermiogenesis of rat, mouse, hamster and guinea pig

quantitative data reported here (figs. 1–3) Cells absent or damaged at a given time interval after heat exposure, were marked in the A part of the diagram, their position in the cycle at the time of exposure found by back-calculation was depicted in the B part. For example in testes obtained two days after exposure (fig 1) spermatids were absent in steps 1 and 2 and markedly decreased in steps 3 and 4 Since step 1 requires about 35 hours and step 2 about 23 hours spermatids exposed to heat early in step 1 should become late step 2 spermatids after 48 hours Since step 2 spermatids were absent from testes obtained 48 hours after exposure it could be concluded that step 1 spermatids were affected by exposure to heat. Similarly early step 2 spermatids should develop into late step 4 spermatids after 48 hours but the step 4 spermatids were either absent or showed abnormal morphology Late step 2 spermatids also require about 48 hours to reach step 6 and these were present in day 2 samples. It appears, therefore that spermatids in steps 1 and early step 2 are susceptible to heat, while those in advanced step 2 are resistant. Since step 5 and older spermatids were normal in two-day samples it appears that all spermatids beyond early step 2 are resistant to heat, or at least the effect is not manifested two days after exposure Forty-eight hours are required for primary spermatocytes in stage XII to become early spermatids in step 1 Since spermatids in the entire step 1 interval were absent two days after exposure to heat pachytene and diakinetic spermatocytes at stages XII and XIII and dividing spermatocytes in stage XIV must be susceptible Calculating back for the absent pachytene and dividing spermatocytes at stages XII to XIV we came upon spermatocytes from late stages VII to first half of stage XII Consequently all pachytene spermatocytes between late stage VII and early stage XII must be affected by heat Further analysis of the data indicates that zygotene spermatocytes at stage XIV and pachytene spermatocytes at stages I and II are also affected by heat. Thus results obtained from analysis of the two-day samples suggest that all primary spermatocytes from pachytenes at late stage VII to dividing spermatocytes at stage XIV and young spermatids at st[age] I are susceptible to heat and disapp[ear] within 48 hours after exposure Zygot[ene] spermatocytes at stage XIV pach[ytene] spermatocytes at stages I II and part VII appeared to be only partially affect[ed] Pachytene spermatocytes at stages III VI and spermatids from step 2 on, app[ear] to be heat-resistant. Analysis of the d[ata] obtained four days after exposure reve[aled] that the same groups of cells are heat sen[si]tive Reduction of pachytene spermatocy[tes] in stages VII to XI indicates that these c[ells] are partially susceptible when exposed [to] heat in stages II and IV Since pachyt[ene] spermatocytes were absent in stage VI [it] may be concluded that pachytene sperm[a]tocytes in stage I are severely injured [by] heat, gradually degenerate and disapp[ear] within four days. Furthermore, reducti[on] in numbers of pachytene spermatocytes [in] stages II to V in the four-day sample, in[di]cates that zygotene spermatocytes in sta[ges] XII and XIII are also partially damag[ed] by heat. The absence of pachytene sp[er]matocytes in stages V to VII in the six-d[ay] group indicates that spermatocytes [ex]posed to heat at stages XII and XIII c[an] develop into zytogene and pachytene sp[er]matocytes but they gradually disapp[ear] within six days after exposure Analysi[s of] the eight-day sample (fig. 2) confir[ms] above calculations and conclusions. It al[so] indicates that leptotene spermatocytes [in] stage XI are damaged by heat. Pachyte[ne] spermatocytes in stage VII showed part[ial] damage in earlier experimental groups. [In] this sample absence of young spermat[ids] from stages III to VI suggests that th[ese] spermatocytes have variable susceptibili[ty:] some degenerate during the premeio[tic] phase others during meiosis while s[ome] others continue to form spermatids and [af]ter early phases of spermiogenesis. Nev[er]theless ultimately they degenerate co[m]pletely while pachytene spermatocytes [in] stage V and VI continue to show resistan[ce]. Results of a similar analysis of 20-day sa[m]ples, presented in figure 3 not only co[n]firm conclusions derived from earlier ti[me] interval groups but provide additional e[vi]dence that pachytene spermatocytes [in] stages V and VI are not affected by he[at] since these cells develop into adult sp[er]matozoa as shown by the presence of ste[p]

18 and 19 spermatids in a large number of tubules at stages VI and VII, respectively

In summary the above discussed data show that primary spermatocytes from stage XI (leptotene) to dividing spermatocytes at stage XIV are injured by heat, excepting for pachytene spermatocytes in stages V and VI. In addition, spermatids in step 1 and early step 2 of spermiogenesis are heat-susceptible. Those beyond step 2 continue with the maturation process, and form adult spermatozoa. Resting spermatocytes, spermatogonia and Sertoli cells are not affected by the amount of heat employed in this experiment.

Morphological abnormalities in degenerating cells appear to follow a definite sequence, different for spermatids and spermatocytes. Cytolytic and chromatolytic changes were very common in young spermatids in steps 1 and 2 and their rate of degeneration was comparatively rapid. Nuclei of steps 3 and 4 spermatids formed rings by peripheral accumulation of chromatin materials before actual chromatolysis. These cells were often detached from the cellular layer and enclosed in a common mass of cytoplasm, forming giant cells. "Giant cell" formation was common for spermatids from step 4 to 8 of spermiogenesis containing up to 16 spermatid nuclei. The acrosomic material of spermatids enclosed by giant cells remained intact, disintegrating subsequently without further differentiation, as evidenced by the presence of giant cells containing step 4 or 5 spermatids in tubules in stages VI or VII. The earliest changes in degenerating spermatocytes occurred in the cytoplasm, which stained positively with PAS. This was followed by pyknosis, chromatolysis and gradual cytolysis. Giant cell formation by spermatocytes was less common than with spermatids and occurred only in severely damaged tubules. Dividing spermatocytes deteriorated more rapidly showing nuclear fragmentation and bizarre meiotic figures.

It is apparent that the dose of heat employed in these experiments may affect cells in two different ways. First, it must interfere drastically with one or more vital functions of some cells, as evidenced by their rapid death shortly after exposure. Secondly it may produce a latent effect, since certain types of cells are able to continue their development before degenerating at a later stage of maturation. It is of interest that cells in early stages of meiosis (leptotene, zygotene) are more resistant to heat than those in later stages. Earliest morphologic signs of damage in cells in pre-meiotic stages of division, were detectable in the cytoplasm, while cells in interphase, like spermatids, showed earliest signs of damage in the nuclei. No explanation can be offered at this time for the surprising finding of resistance to heat of pachytene spermatocytes in stages V and VI of spermatogenesis. Spermatogonia, the youngest germinal epithelium cells showed no morphologic changes following exposure to heat, but continued normal development with ultimate formation of spermatozoa.

Steinberger and Dixon ('59) on the basis of qualitative histologic study of testicular tissue, concluded that exposure to temperatures of 43 C for 15 minutes, produces a specific type of damage to germinal epithelium, limited to one type of cells, primary spermatocytes. Quantitative data reported in this paper provide support for their concept of response-specificity of germinal epithelium to heat. However their conclusions concerning limitation of damage to primary spermatocytes must be modified. First, not all stages of development of primary spermatocytes are sensitive to this amount of heat, and second, in addition to primary spermatocytes, the first two steps of spermatid development are also heat-susceptible

In conclusion, this work supports the hypothesis that germinal epithelium reacts to noxious stimuli, in this case heat, in a precise and specific fashion.

LITERATURE CITED

Asdell, S. A., and G. W Salisbury 1941 The rate at which spermatogenesis occurs in the rabbit. Anat. Rec., 80 145–154

Clermont, Y et al. 1959 Durée du cycle de l'epithelium seminal du rat. Arch. Anat. Micro. Morph. Exp., 48 37–56.

Clermont, Y and H. Morgentaler 1955 Quantitative study of spermatogenesis in the hypophysectomized rat. Endocrinology 57 369–382.

Leblond, C. P., and Y Clermont 1952 Spermiogenesis of rat, mouse, hamster and guinea pig

as revealed by the periodic acid-fuchsin sulfurous acid technique. Amer J Anat., 90 167–215.
Mori, Akira 1952 Studies on the abnormal spermatozoa. I. Appearance of abnormal spermatozoa in the experimental cryptorchidism of the albino rat. Tohoku J Agricultural Research, 3: 15–29
Steinberger E. 1962 Quantitative study of the effect of an alkylating agent (Triethylenemelamine) on the seminiferous epithelium of rats. J Reproduction and Fertility 3: 250-259.
Steinberger E., and W. J. Dixon 1959 Some observations on the effect of heat on the testicular germinal epithelium. Fertil. and Steril., 10: 578.
Young, W. C. 1927 The influence of high temperature on guinea pig testis. J Exp. Zool., 49: 459–499

PLATE 1

EXPLANATION OF FIGURES

Testicular sections from control and experimental animals stained with PAS-Weigert hematoxylin (× 400)

Column A: Intact controls
Column B Two days after exposure
Column C Eight days after exposure
Column D Twenty-six days after exposure

Roman numerals indicate the stages of spermatogenesis.

4 Normal cellular association of germinal epithelium at stage I of spermatogenesis.

5 Note complete absence of step 1 spermatids; pachytene spermatocytes show degenerative changes with formation of ghost cells" (arrow)

6 The young group of spermatids appears morphologically normal although their count was much below normal.

7 The young spermatids are present; those at tep 15 of spermiogenesis are absent.

8 Normal cellular association of germinal epithelium at stage II of permatogenesis.

9 Step 2 spermatids are completely absent and the tubule is full of cellular debris.

10 The step 2 spermatid show chromatolytic hanges.

11 Note complete absence of step 16 spermatids.

12 Normal cellular association of germinal epithelium t stage III of sperm togenesis.

13 Some sperm tids at step 3 show degeneration. The spermatocytes show typical pyknotic changes (arrow)

14 The step 3 spermatids are bsent; pachytene spermatocytes show hrom tolytic changes.

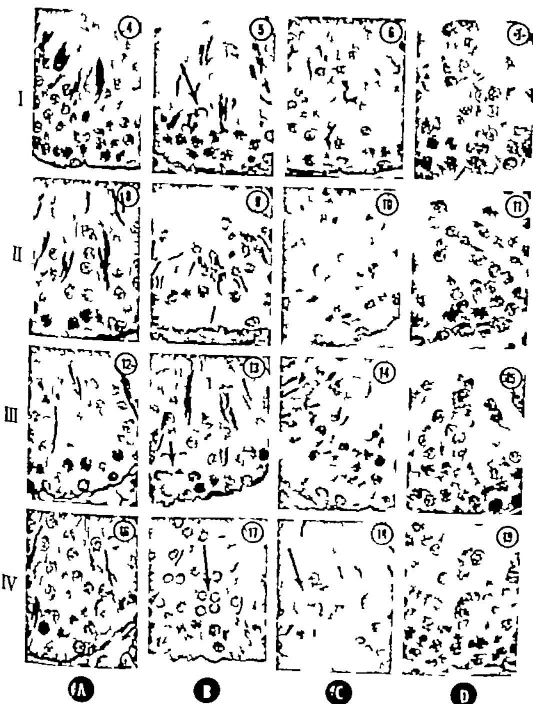
15 The tep 16 spermatid are bsent.

16 Normal cellular association of germinal epithelium t stage IV of spermatogenesis.

17 Typical ring formation in the step 4 spermatid (arrow)

18 The step 4 spermatids are bsent. The spermatocytes show degenerative changes and giant cell formation (arrow)

19 Step 17 spermatids are absent.


I
II
III
IV
4
5
6
10
11
12
13
14
17
19
A
B
C
D

('57) claimed to produce brain malformations in the offspring of pregnant mice by immunizing the mice with brain tissue Barber Willis and Afeman ('61) utilizing a similar immunizing procedure did not obtain brain malformations but reported a high incidence of eye lesions in the offspring of mothers immunized with brain antigen Both these provocative studies should be extended to determine the reason for the differences in results since other similar experiments have not yielded positive results. Steblay ('63) failed to produce nephritis in fetal lambs in spite of the presence of a fulminating autoimmune nephritis in the mothers Chandler Kyle Hung and Blizzard ('62) attempted to produce cretinism in the offspring of pregnant animals with experimentally induced autoimmune thyroiditis They were unsuccessful even though they demonstrated circulating antibodies to thyroid tissue in the fetal and newborn animals It appears that most experimental autoimmune disease depends on the accessibility of sensitized lymphocytes to the involved tissue Since in most instances the sensitized lymphocyte does not cross the placenta one would not expect autoimmune disease in the mother to be consistently reflected in the fetus

The first investigation in mammals dealing with antisera as general teratogenic agents without specificity was in '61 (Brent Averich and Drapiewski 61) Kidney antiserum was reported to be a potent teratogenic agent which produced malformations involving multiple organs and systems when injected into rats eight days pregnant David Mercier Parot and Tuchmann Duplessi ('63) repeated this work and obtained similar results The following presentation deal with the further description and characterization of this antiserum as a potent teratogenic agent when administered on four separate days of rat gestation

MATERIALS AND METHODS

Wistar rats utilized in this study were obtained from our own colony which has been randomly inbred for the past seven years. New Zealand rabbit were obtained from commercial sources for antibody production. Female rats were mated with caged males for 12 hours during the night. Those females that had been inseminated were considered to be zero hours and zero days pregnant at 9 A.M the next morning After seven eight nine or ten days of pregnancy the pregnant rats were anesthetized (sodium nembutal 30 mg kg) and laparotomized The number and condition of the embryonic sites were recorded and the abdominal incision was closed. Antiserum was injected at this time at various dosage levels: 0.125 ml 0.25 ml 0.50 ml 0.75 ml 1.0 ml and 1.25 ml per 100 grams of pregnant rat. Control (non-immunized) rabbit serum was administered to rats that were seven eight, nine or ten days pregnant at dose levels of 1.0 ml or 2.0 ml per 100 grams of pregnant rat. The intravenous subcutaneous and intraperitoneal routes were utilized although the material being presented in this paper deals mainly with the results of intraperitoneal administration Following the administration of antiserum after seven eight, nine or ten days of pregnancy the mothers were weighed daily After 21 days of pregnancy the mothers were sacrificed and the fetuses were delivered by cesarian section Maternal urine and blood were obtained for protein determinations The fetuses and placentae were examined grossly weighed and fixed in 10% formalin or Bouin's fixative for dissection or histological section

Antisera were obtained in the following manner Male and female adult rats were perfused with buffered isotonic saline via the abdominal aorta The tissues were homogenized in a Virtis tissue homogenizer and lyophilized The dry tissue powder was stored at −20 C The rabbits were immunized with 200 mg of resuspended tissue mixed with an equal amount of Freund's adjuvant and intramuscular injections of these materials were given at weekly intervals for three weeks followed by monthly injection Bleeding was performed at bi-weekly interval The blood was allowed to clot and the serum was stored at −40 C until enough was obtained to form a large pool Whole serum was used throughout the studies in this paper although fractions of this serum have also been utilized

Antisera were prepared against (1) adult rat kidney (2) rat serum, (3) rat red blood cells, (4) adult rat liver (5) maternal and fetal term placenta, (6) adult rat muscle (7) fetal skin, (8) isolated adult rat glomeruli and (9) fetal liver. These antisera were studied electrophoretically immunoelectrophoretically and by immunodiffusion analysis. The data reported in this manuscript deals mainly with the effect of rabbit anti-adult rat kidney serum. The ineffectiveness of normal rabbit serum, rabbit anti-rat serum antiserum and rabbit anti-rat red blood cell antiserum in producing malformations was previously reported (Brent, Averich and Draplewski, '61)

RESULTS

Since the teratogenicity of heterologous rat kidney antiserum has been adequately demonstrated in eight-day-old rat embryos (Brent, Averich and Draplewski, '61) the main purpose of this report is to describe in detail the quantitative and qualitative effects of this antiserum when administered to pregnant rats on various days of gestation. Other experimental teratogenic agents (uterine vascular clamping, chemotherapeutic agents irradiation, trypan blue etc.) demonstrate a triad of effects upon the embryo which includes lethality growth retardation and congenital malformations Rat kidney antiserum produces this same triad of effects at various dosage levels.

Lethal effect of kidney antiserum on seven- eight nine and ten-day-old embryos: (table 1)

The resorption rate of control embryos whose mothers are laparotomized during the period of differentiation is 8.2% (table 1) The administration of normal rabbit serum in large doses (2.0 ml per 100 grams of pregnant rat) to pregnant

TABLE 1

The growth retarding and lethal effect of rabbit anti-rat-kidney anti-serum and normal rabbit serum on rat embryos 7 8, 9 and 10 days of age

Gestational age	Dose in milliliters per 100 g pregnant rat: Normal rabbit serum	Rabbit anti-rat kidney antiserum	Number of embryos (pre-injection)	Per cent mortality	Term fetuses: Number	Weight ± S.D.	Overall per cent fetuses malformed (see tables 2 and 3)
days 7 and 8 Operative controls	0	0	97	8.2	89	4.80 ± 0.31	1.7
7	2.0	0	49	6.1	46	4.89 ± 0.64	2.2
8	2.0	0	54	3.7	52	4.74 ± 0.42	0.0
9	2.0	0	57	7.5	53	4.62 ± 0.71	1.9
10	2.0	0	41	9.7	37	4.51 ± 0.44	0.0
7	0	0.25	73	13.7	63	4.39 ± 0.3[illegible]	25.4
		0.50	66	45.4	36	3.89 ± 0.60	38.9
		0.75	71	77.5	16	3.83 ± 0.63	81.4
		1.00	52	98.1	1	2.81	100.0
8	0	0.25	68	19.0	55	4.0[illegible] ± 0.17	85.5
		0.50	87	49.4	44	4.04 ± 0.31	72.7
		0.75	68	97.1	2	1.55	100.0
		1.00	71	100.0	0	—	—
9	0	0.25	102	11.8	90	4.36 ± 0.60	34.4
		0.50	87	38.0	54	4.11 ± 0.7[illegible]	55.6
		0.75	97	100.0	0	—	—
10	0	0.25	53	7.5	49	4.45 ± 0.80	14.0
		0.50	80	13.6	69	3.80 ± 0.6[illegible]	42.0
		0.75	72	91.7	6	3.32 ± 0.33	100.0

rats on the seventh eighth ninth and tenth days of gestation resulted in an incidence of resorptions comparable to the control laparotomized animals being respectively 6 1 3 7 7.5 and 9 7% (table 1). Thus neither the administration of rabbit serum or the operative procedure contributed to the increased resorptions produced by the administration of kidney antiserum. Rabbit antiserum made against rat muscle liver plasma and skin administered to pregnant rats after eight days of pregnancy resulted in 6.2 9 1 9.2 and 4.0% resorptions respectively These resorption rates are within the range of the two previously mentioned control groups.

On the other hand, the administration of kidney antiserum to embryos aged seven to ten days resulted in an increased resorption rate which was directly related with the dose administered (table 1) In fact an increased resorption rate was present at all the stages and in all the dosage groups studied except in the ten-day-old embryos given the lowest dose (0.25 ml/100 g pregnant rat) Furthermore the mortality reached 100% in the four embryonic stages studied following the administration of 1 0 ml/100 g of pregnant rat. The dose response curve varied on different days of gestation with the eight day-old rat embryo being the most sensitive to the lethal effects of low doses of the antiserum.

Growth retarding effects of kidney antiserum when administered to seven- eight nine- and ten-day old embryos (table 1)

The growth retarding effect of kidney antiserum demonstrated the same dose response relationship as the lethal effect of this antiserum. The laparotomized control fetuses weighed 4 80 g at term and the mean fetal weights of all the experimental groups exposed to antiserum weighed significantly less (table 1) Furthermore as the dose of antiserum increased from 0.25 ml to 1 0 ml/100 g of pregnant rat, the amount of fetal stunting also increased. Thus there was an inverse relationship between fetal growth and the dose of antiserum administered As with the lethal effect of this antiserum the eight-day-old embryos were most sensitive to the growth retarding effect at low doses of the antiserum (0.25 ml/100 g rat) At higher doses all four stages that were studied had obvious growth retardation.

The normal rabbit serum, when injected into rats seven, eight nine and ten days pregnant at the dose level of 2.0 ml/100 g of pregnant rat, resulted in term fetuses of normal weight (table 1) Statistical analysis using the t test revealed no significant difference between the term fetal weights of the operative controls and any of the term fetal groups receiving control rabbit serum (table 1)

The teratogenic effect of kidney antiserum when administered to seven eight nine- and ten-day-old embryos (tables 2, 3) (figs 3–19)

The incidence of malformations in fetuses whose mothers were laparotomized during the period of differentiation, but who did not receive kidney antiserum, was 1 7% Of the 1 012 operative control fetuses, 18 were malformed. Fifteen had one malformation Nine of these had borderline hydrocephalus which was graded one plus or two plus on a one-to-four scale. The incidence of hydrocephalus in our control stock is very low Two have been observed in adults during the past five years. But the etiology of the hydrocephalus observed postnatally may not be the same as the low grade lesions observed at term It is not known at this time what percentage of hydrocephalus observed at term is truly normal. Two fetuses had unilateral microphthalmia. One fetus each had unilateral anopthalmia, a right-sided aortic arch and a cleft palate

Three other control fetuses had more than one malformation. Two fetuses had a hydrocephalic lesion associated with an eye lesion. One stunted fetus implanted at the ovarian position had multiple malformations, including an encephalocele anophthalmia club feet and evisceration.

There were 188 surviving fetuses in the control groups that were exposed to 2 0 ml /100 g of pregnant rat of normal rabbit serum when seven, eight, nine and ten days pregnant (table 1) There were no

TABLE 2

The incidence of malformations following the intraperitoneal injection of rabbit anti-rat-kidney whole antiserum in pregnant rats 7, 8, 9 and 10 days pregnant

	Dose of antiserum in milliliters/100 g of pregnant rat													
	0	0.25				0.50				0.75				1.0
Gestational age time of injection	—	7	8	9	10	7	8	9	10	7	8	9	10	7
	Malformations per term live fetus													
One malformation	15	11	4	20	6	0	13	6	8	2	0	—	—	—
Two malformations	2	4	27	7	5	0	10	9	2	5	0	—	—	—
Three or more malformations	1	0	16	4	1	14	12	15	19	6	2	—	6	1
Total malformed fetuses	18	15	47	31	12	14	35	30	29	13	2	—	6	1
Total live fetuses	1012	63	55	90	86	36	44	54	69	16	2	—	6	1
Per cent malformations	1.7	25.4	85.6	34.4	14.0	38.9	79.6	55.6	42.0	81.4	100	—	100	100

malformed fetuses in the eight- and ten-day-old groups, although one fetus in the eight-day group exhibited a shorter than usual innominate artery (table 1). There was one malformed fetus in the seven-day group (right-sided aortic arch) and nine-day group (mild hydrocephalus).

The incidence of malformations following the administration of kidney antiserum was directly related to the dose of antiserum administered (tables 1 and 2). The incidence of malformations following 0.25 ml of antiserum/100 g of pregnant rat was increased at all stages studied. At this low dose, the eight-day-old rat embryo was the most sensitive of the four stages studied, in that 85.6% of the surviving embryos were malformed. Higher doses not only increased the incidence of malformations, but also the severity of malformations (table 2). As examples of this observation, it will be noted that 15 of 63 fetuses whose mothers were seven days pregnant when given 0.25 ml of antiserum/100 g of rat were malformed, an incidence of 25.4% (table 2). None of these fetuses had three or more malformations. At the next higher dose of antiserum (0.50 ml/100 g of rat), the over-all incidence of malformations rose to 38.9% and all the 14 malformed fetuses had three or more malformations. This same phenomenon occurred in the eight-, nine- and ten-day old embryonic groups (table 2).

The dose of antiserum which produced a high incidence of malformations in the term fetuses (70–100%) also resulted in a high over-all mortality in the embryos exposed to this dose of antiserum (greater than 40%). The converse was not always true in that increased mortality did not have to be associated with an increase in malformations. As an example, rats pregnant for ten days that received 0.25 ml of antiserum/100 g had no increase in embryonic mortality (7.5%, table 1) but the incidence of malformations was seven times normal (14.0%).

The spectrum of malformations produced by kidney antiserum differed over the four gestational periods encompassed in this study. Although certain malformations were produced when antiserum was injected into seven-, eight-, nine- or ten-day-old embryos, other malformations were peculiar to one or two particular embryonic stages (table 3). Of the 522 experimental fetuses in this study, 234 were

TABLE 3

The spectrum and incidence of malformations produced by the intraperitoneal injection of rabbit anti-rat-kidney antiserum into rats 7 8 9 and 10 days pregnant

Gestational age in days	7	8	9	10
Total live term fetuses from all dosage groups on each day	116	101	144	161
Total live term fetuses with one or more malformations	43	84	61	47
Per cent live term fetuses malformed	37.1	83.2	42.4	29.2
	Per cent of malformed fetuses with particular malformation			
Gestational age in days	7	8	9	10
Situs inversus totalis	—	2.4	—	—
Ophalocele and evisceration	—	8.3	—	—
Anencephaly	—	2.4	3.3	—
Meningocele	—	1.2	—	—
Encephalocele	3.9	15.5	3.3	—
Hydrocephaly	49.0	75.0	47.5	78.7
Unilateral microphthalmia	11.7	—	9.8	8.5
Bilateral microphthalmia	17.6	—	14.8	4.2
Microphthalmia and anophthalmia	7.8	—	1.6	10.6
Unilateral anophthalmia	11.7	4.8	3.3	—
Bilateral anophthalmia	45.0	91.7	63.9	21.4
All eye malformations	93.8	96.5	93.4	46.7
Cleft palate	—	4.7	6.6	—
Facial clefts	—	2.4	6.6	—
Jaw and tongue malformations	28.0	8.3	14.8	—
Micrognathia	17.6	1.2	1.6	—
Total aortic arch anomalies	9.8	25.0	21.3	36.2
Right sided A.A.	—	2.4	3.3	—
Infantile coarctation	3.9	—	3.3	—
Situs inversus A.A. + infantile coarctation	5.8	2.4	—	—
Situs inversus A.A.	—	7.1	14.8	12.8
Other A.A. malformations	—	13.1	—	23.4
Heart anomalies	—	2.4	—	—
Diaphragmatic anomalies	3.9	2.4	—	[illegible]
Right renal agenesis	3.9	—	—	—
Left renal agenesis	1.9	15.5	21.9	—
Bilateral renal agenesis	11.7	10.7	19.1	—
Left ovarian agenesis	—	1.2	2.1	—
Left uterine agenesis	—	2.3	1.6	—
Bilateral testicular agenesis	—	—	3.3	—
Right-sided cryptorchidism	—	—	3.3	—
Left-sided cryptorchidism	7.8	2.4	6.6	—
Bilateral cryptorchidism	5.8	12.1	—	—
Bilaterally absent ears	—	2.4	—	—
Absent spleen	3.9	2.4	—	—
Syndactyly	—	—	—	20.7
Abnormal tail	—	—	—	8.5
Limb hypoplasia	—	—	—	4.2
Rectovesical fistula	—	1.2	—	—

malformed. Therefore the percentages listed in table 3 are based on 234 abnormal fetuses. Only the significantly large differences in incidence and types of malformations can be relied upon because of the small size of the group of malformed embryos. In spite of this some interesting observations can be made

Eye abnormalities as a group were the commonest malformations, occurring in 94 97 93 and 47% of the seven- eight nine- and ten-day-old malformed embryos (figs. 11 12) Severe hydrocephalus was the next most common malformation occurring in all four stages studied [illegible] 6) On the other hand micrognath

predominantly in the seven-day group (fig. 11). Evisceration, encephalocele, meningocele, situs inversus totalis and bilateral cryptorchidism were associated with the administration of antiserum to eight-day-old embryos (figs. 3, 5, 7-9, 19). Left renal agenesis and bilateral renal agenesis were associated with the nine-day-old group (figs. 15, 16) and syndactyly, tail abnormalities and limb hypoplasia were only present in fetuses from the ten-day-old group (fig. 18). Thus some malformations or group of malformations occurred in embryos from all four stages that were studied. Other malformations were associated with two or three particular stages having a peak incidence at one stage, while some malformations occurred only at one stage. This is the typical result one observes following the administration of a teratogenic agent at various dosages and periods of gestation.

The effects of other tissue antisera upon rat embryos

In the previous report (Brent, Averich and Drapiewski, '61) it was stated that rabbit antisera to rat red blood cells, muscle, brain, serum, fetal skin and liver were ineffective in producing malformations or growth retardation in rat embryos. The antisera against rat red blood cells and rat serum were very strong as measured by serial dilutions in an immunodiffusion system and therefore it appears that no teratogenic effect results from the administration of these antisera. On the other hand, it is possible that the failure to produce effects on the embryo with the other antisera is due to a low titer of the teratogenic factors rather than their complete absence. Before other tissue antisera are considered to be ineffective in producing malformations more, extensive investigations must be carried out with each specific tissue antiserum.

At the time of the first report of the teratogenic effect of kidney antiserum (Brent, Averich and Drapiewski, '61) it was also stated that rabbit anti-rat-placental serum did not produce malformations, although a significant increase in resorptions was produced by injecting this antiserum into rats 8, 9, 10 and 15 days pregnant. By increasing the dose of the placental antiserum to 1.25 ml/100 g of rat eight days pregnant, malformations have been produced. The incidence and severity of malformations resembles the effects of kidney antiserum given at the same stage of gestation. There is no question that properly prepared placental antiserum is a potent teratogenic agent in the rat, but the spectrum of malformations and the incidence of malformations on various gestational days has not been determined.

Characterization of the rabbit anti-rat-kidney antiserum

The total protein of the kidney antiserum utilized in this study was 6.8 grams per cent. The electrophoretic analysis on cellulose acetate paper revealed the following fractions and their quantities: albumin 3.54 g % (52%), alpha 1, 0.69 g % (10.2%), alpha 2, 0.58 g % (8.5%); beta 0.62 g % (9.1%), gamma 1.31 g % (19.3%). The normal rabbit serum used in this study had a total protein of 7.0 grams per cent and the following fractions: albumin 4.73 g % (67.5%), alpha 1, 0.26 g% (3.8%), alpha 2, 0.19 g% (2.8%), beta 0.76 g% (10.8%), gamma 1.04 g % (14.9%).

The immunodiffusion pattern in agar when kidney antiserum is reacted against resuspended lyophilized kidney consists of nine separate precipitin bands (fig. 1). Seven of these bands are the result of reactions between antiserum and blood serum constituents in the kidney. The remaining two bands are produced by antibodies reacting with tissue antigens in the resuspended kidney tissue. At the present time it is not known whether both these antibodies are responsible for the teratogenic effect of kidney antiserum or whether this pathologic effect resides with only one or neither of these two antibodies against kidney antigens.

Maternal effects of rabbit anti-rat kidney antiserum

Proteinuria appeared within 24 hours in the maternal rats receiving the kidney antiserum. The proteinuria at term ranged

between 3 to 10 mg of protein/ml of urine. Frequently marked changes were observed in the shape of the maternal liver at term. The liver was decreased in size and the edges were blunted as if there had been an acute decrease in size. Clinically the animals were mildly edematous and this was substantiated by their increased weight gain On rare occasions in the higher dosage groups (1 0 ml/100 g of rat) a mother would die several days after receiving the kidney antiserum. Eleven mothers out of 240 were lost in this manner The blood pressure was not measured in these animals but other investigators have reported that this antiserum produces a syndrome of hypertensive nephrosis-nephritis It is also well known that alterations in cholesterol metabolism and amino acid excretion occur in this type of experimental nephrosis. Thus, the maternal environment offered to the experimental fetuses is considerably different from that of a normal pregnancy

DISCUSSION

The experimental results leave no doubt as to the teratogenicity of kidney antiserum in the rat and, furthermore, the preliminary results with placental antiserum indicate that it is also a potent teratogenic agent Since both these antisera have had wide use in the past and have been used in pregnant animals it is interesting that a teratogenic effect had not been reported previously In 40 Seegal Loeb and co-workers began an interesting series of experiments utilizing rabbit anti rat placental serum in the pregnant rat (Seegal and Loeb 46 Loeb and Seegal 43) In later years they switched species and utilized dog placenta (Bevans Seegal and Kaplan '55 Seegal Hansson Gaynor and Rothenberg '55 McCaughney '55) Their findings indicated that both anti kidney and anti-placental serum could induce an identical form of chronic nephritis. When this antiserum was injected into pregnant rats hypertension nephritis albuminuria and edema were produced mimicking the clinical syndrome of "toxemia of pregnancy Fetal loss was increased, as evidenced by resorptions or stillbirths depending on the time during gestation that the antiserum was injected. No malformations were reported in these experiments, in spite of the fact that antiserum was administered as early as the ninth day of rat gestation. Pressman and Korngold ('57) evaluated the immunologic relationship between rabbit anti-rat-kidney antibody and Seegal's antiplacental serum. They concluded that although many of the localizing antibodies of kidney and placental antisera are common, different antibodies are concerned with the interruption of pregnancy and the production of nephrotoxicity In '61 we demonstrated that kidney antiserum, labeled with radioactive iodine localized in the kidney and placenta (Brent, Averich and Drapiewski, '61) Using fluorescent antibody techniques Steblay ('61 '62 and '63) demonstrated that anti-placental serum localizes in the glomerular basement membrane, tubules, capillaries and the media and adventitia of the arteries of the kidney He also produced an autoimmune nephritis in pregnant sheep with placental antigen yet the kidneys of the fetus were not affected during the pregnancy or during the nursing period. This autoimmune nephritis was severe enough to be fatal to the mothers in from 45 to 54 days from onset (Steblay '63)

Thus there is ample evidence to support the thesis that placental and kidney antisera have antibodies in common and that their pathological effects are similar in many respects. In spite of the relationship demonstrated between kidney and placental antisera the mechanism of teratogenesis is still elusive There are a number of possibilities that must be considered in evaluating the teratogenic effect of kidney antiserum.

1 *Biochemical or physiological alterations in the maternal organism* It is of interest that malformations were produced when kidney antiserum was injected into rats seven and eight days pregnant. This is a period quite insensitive to the teratogenic effects of irradiation. If one postulates that the seven-day-old rat embryo is not subject to environmentally induced teratogenesis then one must conclude that the alterations produced by this antiserum persisted until the embryo was subject to teratogenic stimuli. This in fact could be mediated via a persistent metabolic lesion

in the mother or a persistent alteration at the implantation site

2. *Direct action of the antiserum upon the embryo.* It is impossible to rule out a direct effect upon the embryo at the present time even though tracer studies demonstrate that little of this antiserum crosses the mature placenta near term. But during the period when malformations are readily produced there is no placenta or one just being formed. Thus the embryo might be exposed to small but significant quantities of antiserum during the four stages of gestation studied. The fact that different types of malformations were produced on the various days does not rule out the possibility that the antiserum acted directly on the embryo. Some might argue that if the embryo is directly exposed to antiserum there should be primarily kidney malformations rather than a changing spectrum of malformations on various days of gestation. But again it should be pointed out that the embryo has not even differentiated into germ layers at the very early stages studied and it has not been determined whether cells which will eventually form kidney tissue are immunologically different from other cells in the inner cell mass stage.

3. *The kidney antiserum may be interfering with trophoblast formation and function.* Because of the immunologic relationship between placenta and kidney this line of investigation may yield fruitful results. If the antiserum can produce long lasting alterations in the trophoblastic tissue, then an explanation may exist for the ability of this antiserum to result in malformations even when injected into pregnant animals only seven and eight days pregnant. This same line of reasoning applies to the maternal decidual reaction, since interference with its formation and/or function could lead to the same phenomenon that may result from trophoblast pathology. If decidual or trophoblast dysfunction can be induced by this antiserum then the teratogenic factors in the serum would be acting in a unique fashion which would warrant careful evaluation of the mechanisms involved.

Besides not knowing the site of action of the teratogenic serum, that is the *maternal organism* the *embryo* or the *deciduo-trophoblast*, we are unaware of the biochemical or physiological event triggered by the injection of the anti serum. Is the teratogenesis the result of an immune reaction between proteins and cells in the host and the humoral antibodies injected? Is histamine release host cell death, host cell dysfunction or some other pathologic event important in initiating the chain of reactions that eventually results in teratogenesis? Although it seems most likely that the immune bodies present in the kidney antiserum are the offending molecules the data to date are not incontrovertible. It is possible that the teratogenic factor is produced by rabbits responding to kidney antigen but is unrelated to kidney antibodies? Thus even if we knew the site of action of the teratogenic factors we still do not know what is taking place at that site or sites and whether an immune reaction is involved.

ACKNOWLEDGMENT

This work was supported by a research grant from the National Institute of Child Health and Human Development (HD 630)

The author was ably assisted by Mrs. C. Coyle Misses J Garaguso R. Matsumoto and J Myers and Messrs. E. George and J Hefton. Appreciation is extended to Mrs. E. Ward for typing the manuscript.

LITERATURE CITED

Barber A. N J Willis and C. Afeman 1961 Changes in the lens induced by maternal hypersensitivity in mice. Amer J Ophthal., *51* 949–953.

Bevans, M., B. C. Seegal and R. Kaplan 1955 Glomerulonephritis produced in dogs by specific antisera. II Pathologic sequences following the injection of rabbits, antidog-placenta serum or rabbit antidog-kidney serum. J Exp. Med., *102*, 807

Brent, R. L., E. Averich and V A. Drapiewski 1961 Production of congenital malformations using tissue antibodies. I. Kidney antisera. Proc. Soc. Exp. Biol. Med., *106* 523–526

Chandler R. W M. A. Kyle, W Hung and R. M. Blizzard 1962 Experimentally induced autoimmunization disease of the thyroid. I The failure of transplacental transfer of anti-thyroid antibodies to produce cretinism. Pediatrics, 961–967

Clarke, W M., and L Fowler 1960 The inhibition of lens-inducing capacity of the optic vesicle with adult lens antisera. Develop Biol., 2: 155–172.

David, G., L. Mercier-Parot and H. Tuchmann-Duplessis 1963 Action teratogene d'hetero-anticorps tissulaires. I. Production de malformations chez le rat par action d'un serum anti-rein. Comptes rendus des seances de la Societe de Biologie, 157 939, 1963.

Davis, F A. 1928 Hereditary eye defects in rabbits experimentally induced. Trans. Ophthal. Soc., 45 555–603.

Davis F A., and H. M. Smith 1930 The role of lens antigen and uveal pigment in the production of hereditary anomalies of the eye. Arch. Ophthal., 4 672–690.

Finlay G. F 1924 The effect of different species lens antisera on pregnant mice and rats and their progeny Brit. J Exp. Biol., 1 201–214

Fowler L, and W M. Clarke 1960 Development of anterior structures in the chick after direct application of adult lens antisera. Anat. Rec., 136: 194–195.

Glueckaohn-Waelsch, S. 1957 The effect of maternal immunization against organ tissues on embryonic differentiation in the mouse. J Embryol. Exp. Morph., 5 Part 1 83–92.

Guyer N F and E. A. Smith 1918 Studies on cytolysins. I. Some prenatal effects of lens antibodies. J Exp. Zool., 26 65–82.

——— 1920 Studies on cytolysins. II. Transmission of induced eye defects. J Exp. Zool., 31 171 222.

Huxley J S and A. M. Carr Saunders 1924 The absence of prenatal effects of lens-antisera in rabbits. Brit. J Exp Biol., 1 215–248.

Langman, J 1960 The effect of lens antiserum on chick embryos. Anat. Rec., 137 135–140.

——— 1963 The effects of antibodies on embryonic cells. Canad. Cancer Conf., 5 249–262.

Loeb, E. N and B C. Seegal 1943 The production of chronic nephritis in the rat following the initial injection of anti-placenta serum. II. Pathological findings. Fed. Proc., 2 99.

McCaughey W T E. 1955 The nephrotoxic action of antiplacenta serum in rats. J Obstet. Gynaec. Brit. Emp., 62: 863.

Miller W J 1958 Anti-lens sera a mutagen in rabbits. J Exp Zool., 137 463–477

Poynter C. W M., and E. V Allen 1925 Lens antigen as a factor in congenital and hereditary eye abnormalities. Amer J Ophthal., 8 184–192.

Pressman, D and L. Korngold 1957 Localizing properties of anti-placenta serum. J Immun., 78 75–78

Seegal, B. C., M. W Hanson, E. C. Gaynor and M. C. Rothenberg 1955 Glomerulonephritis produced in dogs by specific antisera. I. The course of the disease resulting from injection of rabbit antidog-placenta serum or rabbit anti-dog-kidney serum. J Exp Med., 102 789

Seegal, B C., and E. N Loeb 1940 Effect of anti-placenta serum on development of the fetus in the pregnant rat. Proc. Soc. Exp Biol. Med., 45 248–253.

——— 1946 Production of chronic glomerulonephritis in rats by injection of rabbit anti-rat-placenta serum. J Exp. Med., 84 211

Steblay R. W 1961 Closely related antigens in human placenta and kidney N ture (London), 192 1259–1261

——— 1962 Localization in human kidney of antibodies formed in sheep against human placenta. J Immun., 88 434–442.

——— 1963 Effect of injecting heterologous glomerular basement membrane preparations in pregnant sheep. Proc. Soc. Exp Biol. Med., 112: 15–18.

PLATES

PLATE 2

EXPLANATION OF FIGURES

7 Severe encephalocele in term fetus that received kidney antiserum when eight days old.

8 A small encephalocele (arrow) and absence of the external ar in term fetu exposed to kidney antiserum when eight days ld (see control fig. 10)

9 Severe encephalocele, facial cleft and failure of fusion and development of the maxillary processes in term fetus exposed to kidney antiserum when eight days old.

10 Normal term fet s with the skin di sected aw y from the e) normal external ear and normal lower jaw

11 Anophthalmia and bsence of the lower j w in a term fetus exposed to kidney antiserum when seven d ys old (see control fig. 10)

12 Anophthalmia and bsence of the external ear in term fet ex posed to placental antiserum when eight days old


7


8


9


10


11


12

Aldehyde-fuchsin Positive Material in Brain of Squirrel Monkey (*Saimiri sciureus*)

GEORGE F CRESWELL, DONALD J REIS AND PAUL D. MacLEAN
Section on Limbic Integration and B havior Laboratory of Neurophysiology National Institute of Mental Health, National Institutes of Health, Bethesda, Maryland

ABSTRACT In the squirrel monkey nerve cells in certain areas of the brain are characterized by abundant granules which stain intensely with aldehyde-fuchsin but not with chromium hematoxylin.

These cells fall into three main types Type A, with a polar clumping of the granules, characterize the region surrounding the stria terminalis in the amygdala and the supratrochlear nucleus of the mid-brain. Type B, which have heavy diffuse granulation, are found in the lateral and caudal hypothalamus and in nucleus raphes ventralis. Less heavily granulated cells classified as Type C distinguish the entire nucleus subthalamicus, and are prominent in nucleus septalis triangularis, rostral midline thalamus, and area CA2 of the rostral hippocampus. Cells of these corresponding types and distribution are not seen in the brains of cat, rat and mouse.

The cerebellum and pineal body contain extracellular material which stains with aldehyde-fuchsin but not chromium hematoxylin.

The granules of the nerve cells stain with PAS Sudan black B, and oil red O suggesting that they have carbohydrate and lipid components.

As in other species, the neurosecretory substance of the paraventricular and supraoptic nuclei is stained both by aldehyde-fuchsin and chromium hematoxylin. Material showing positive reaction to both these stains is also found in the glia of the nucleus septalis triangularis, subfornical organ, lateral hypothalamus, and locus caeruleus. All these regions, except the lateral hypothalamus, show similarly staining material in the extracellular spaces.

Of anatomical interest is the close association of the aldehyde-fuchsin positive neurons with phylogenetically ancient cellular structures and fiber systems of the brain. In the squirrel monkey they would seem to provide basis for further characterization of certain nuclei and new division of the amygdala.

This study was originally undertaken in the squirrel monkey (*Saimiri sciureus*) to explore the possibility of finding neurosecretory material (Scharrer and Scharrer '37; Bargmann, 49) in the amygdaloid region. The outcome was negative in so far as no cells were found which stained both with chromium hematoxylin and aldehyde-fuchsin. In a circumscribed part of the amygdala, however, distinctive cells were found with densely packed granules that stained intensely with aldehyde-fuchsin but were chromium hematoxylin negative. This made it of interest to explore the entire brain to learn if similar staining cells were present elsewhere This report will describe the distribution of intra and extracellular aldehyde-fuchsin positive (AFP) granular material that was found, as well as the preliminary attempt to identify its chemical nature Findings will also be given of a preliminary comparative study

MATERIALS AND METHODS

The squirrel monkey is a small, New World monkey with an average weight of about 700 g Its brain is comparable in size to that of the cat. The stereotaxic brain atlas prepared by Gergen and MacLean ('62) served as an anatomical reference for this study Material was obtained from four males and one female of adult *size but undetermined age. Four animals* were perfused with Bouin s fluid, after which the brains were dehydrated, imbedded in paraffin, and sectioned at 8 µ. Throughout the greater part of three of these brains sections were stained at every 0.5 mm and sometimes every 0.25 mm. The remaining animal was perfused with a 10% *formalin-1% agar solution*, and frozen sections were cut at 20 µ. Complete

Present address Department of Neurology, Cornell New York Hospital, 525 E. 68th Street, New York 21, New York.

Aldehyde-fuchsin Positive Material in Brain of Squirrel Monkey (*Saimiri sciureus*)

GEORGE F CRESWELL, DONALD J REIS AND PAUL D. MacLEAN
Section on Limbic Integration and Behavior Laboratory of Neurophysiology National Institute of Mental Health, National Institutes of Health, Bethesda, Maryland

ABSTRACT In the squirrel monkey nerve cells in certain areas of the brain are characterized by abundant granules which stain intensely with aldehyde-fuchsin but not with chromium hematoxylin.

These cells fall into three main types Type A, with polar clumping of the granules, characterize the region surrounding the stria terminalis in the amygdala and the supratrochlear nucleus of the mid-brain. Type B which have heavy diffuse granulation, are found in the lateral and caudal hypothalamus and in nucleus raphes ventralis. Less heavily granulated cells classified as Type C distinguish the entire nucleus subthalamicus, and are prominent in nucleus septalis triangularis, rostral midline thalamus, and area CA2 of the rostral hippocampus. Cells of these corresponding types and distribution are not seen in the brains of cat, rat and mouse.

The cerebellum and pineal body contain extracellular material which stains with aldehyde-fuchsin but not chromium hematoxylin.

The granules of the nerve cells stain with PAS, Sudan black B and oil red O suggesting that they have carbohydrate and lipid components.

As in other species, the neurosecretory substance of the paraventricular and supraoptic nuclei is stained both by aldehyde-fuchsin and chromium hematoxylin. Material showing positive reaction to both these stains is also found in the glia of the nucleus septalis triangularis, subfornical organ, lateral hypothalamus, and locus coeruleus. All these regions, except the lateral hypothalamus, show similarly staining material in the extracellular spaces.

Of anatomical interest is the close association of the aldehyde-fuchsin positive neurons with phylogenetically ancient cellular structures and fiber systems of the brain. In the squirrel monkey they would seem to provide basis for further characterization of certain nuclei and new division of the amygdala.

This study was originally undertaken in the squirrel monkey (Saimiri sciureus) to explore the possibility of finding neurosecretory material (Scharrer and Scharrer '47 Bargmann, 49) in the amygdaloid region. The outcome was negative in so far as no cells were found which stained both with chromium hematoxylin and aldehyde-fuchsin. In a circumscribed part of the amygdala, however distinctive cells were found with densely packed granules that stained intensely with aldehyde-fuchsin but were chromium hematoxylin negative. This made it of interest to explore the entire brain to learn if similar staining cells were present elsewhere. This report will describe the distribution of intra- and extracellular aldehyde-fuchsin positive (AFP) granular material that was found, as well as the preliminary attempt to identify its chemical nature Findings will also be given of a preliminary comparative study

MATERIALS AND METHODS

The squirrel monkey is a small, New World monkey with an average weight of about 700 g Its brain is comparable in size to that of the cat. The stereotaxic brain atlas prepared by Gergen and MacLean ('62) served as an anatomical reference for this study Material was obtained from four males and one female of adult size but undetermined age. Four animals were perfused with Bouin s fluid, after which the brains were dehydrated, imbedded in paraffin, and sectioned at 8 µ. Throughout the greater part of three of these brains sections were stained at every 0 5 mm and sometimes every 0.25 mm. The remaining animal was perfused with a 10% formalin-1% agar solution and frozen sections were cut at 20 µ. Complete

Present address Department of Neurology, Cornell-New York Hospital, 525 E. 68th Street, New York 21, New York.

ᶠuchsin Positive Material in Brain of
ˡMonkey (*Saimiri sciureus*)

GEORGE F CRESWELL, DONALD J REIS AND PAUL D. MacLEAN
Section on Limbic Integration and Behavior Laboratory of Neurophysiology National Institute of Mental Health, National Institutes of Health, Bethesda, Maryland

ABSTRACT In the squirrel monkey nerve cells in certain areas of the brain are characterized by abundant granules which stain intensely with aldehyde-fuchsin but not with chromium hematoxylin.

These cells fall into three main types Type A, with a polar clumping of the granules, characterize the region surrounding the stria terminalis in the amygdala and the supratrochlear nucleus of the mid-brain. Type B which have heavy diffuse granulation, are found in the lateral and caudal hypothalamus and in nucleus raphes [illegible]. Less heavily granulated cells classified as Type C distinguish the entire nucleus subthalamicus, and are prominent in nucleus septalis triangularis, rostral midline thalamus, and area CA2 of the rostral hippocampus. Cells of these corresponding types and distribution are not seen in the brains of cat, rat and mouse.

The cerebellum and pineal body contain extracellular material which stains with aldehyde-fuchsin but not chromium hematoxylin.

The granules of the nerve cells stain with PAS, Sudan black B and oil red O, suggesting that they have carbohydrate and lipid components.

As in other species, the neurosecretory substance of the paraventricular and supraoptic nuclei is stained both by aldehyde-fuchsin and chromium hematoxylin. Material showing positive reaction to both these stains is also found in the [illegible] of the [illegible], nucleus septalis triangularis, subfornical organ, lateral hypothalamus, and [illegible] [illegible]. All these regions, except the lateral hypothalamus, show similarly staining material in the extracellular spaces.

Of anatomical interest is the close association of the aldehyde-fuchsin positive neurons with phylogenetically ancient cellular structures and fiber systems of the brain. In the squirrel monkey they would seem to provide basis for further classification of certain nuclei and new division of the amygdala.

[illegible] study was originally undertaken in [the squirrel] monkey (Saimiri sciureus) to [explore] the possibility of finding neurosecretory material (Scharrer and Scharrer [and] Bargmann, 49) in the amygdaloid region. The outcome was negative in so far [as no] cells were found which stained both [with] chromium hematoxylin and aldehyde-fuchsin. In a circumscribed part of the amygdala, however distinctive cells were [found] with densely packed granules that [stained] intensely with aldehyde-fuchsin [and] were chromium hematoxylin negative. [This] made it of interest to explore the entire brain to learn if similar staining cells [were] present elsewhere. This report will [describe] the distribution of intra- and extracellular aldehyde-fuchsin positive (AFP) [granular] material that was found, as well [as] a preliminary attempt to identify its chemical nature. Findings will also be [given] of a preliminary comparative study

MATERIALS AND METHODS

The squirrel monkey is a small, New World monkey with an average weight of about 700 g. Its brain is comparable in size to that of the cat. The stereotaxic brain atlas prepared by Gergen and MacLean ('62) served as an anatomical reference for this study. Material was obtained from four males and one female of adult size but undetermined age. Four animals were perfused with [illegible] fluid, after which the brains were dehydrated, imbedded in paraffin, and sectioned at 8 µ. Throughout the [illegible] part of three of these brains, sections were stained at every 0.5 mm and [illegible] every 0.25 mm. The remaining animal was perfused with a 10% formalin [illegible] solution, and frozen sections were cut at 30 µ. Comp[illegible]

Present address: [illegible] New York Hospital, [illegible] New York, New York.

J. Comp. Neur., 115: 543-[illegible].

Abbreviations

a, Artefact
B Basal Nucleus (amygdala)
Co Cortical Nucleus (amygdala)
IC, Internal Capsule
MAB, Accessory Basal Nucleus, Medial Portion (amygdala)
N4 Nucleus of Trochlear Nerve
ST Stria Terminalis

PLATE 1

EXPLANATION OF FIGURES

All sections are stained with aldehyde-fuchsin unless otherwise indicated.

1 Section from the amygdala in region of stria terminalis (ST) showing portions of the medial accessory basal nucleus (MAB) and cortical nucleus (Co) It is in this area surrounding the stria terminalis that granulation is heaviest. a-artefact 100 ×.

2 A Type A cell from amygdala showing a single compact mass of granules. 1 100 ×

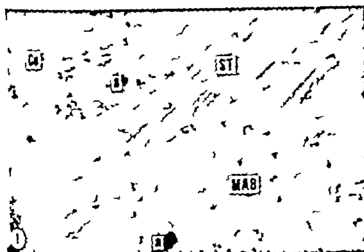
3 A Type C cell from the amygdala showing dispersed arrangement of granules. 1,100 ×

4 Opposed photographs from a section through amygdala showing striking contrast between the positively staining medial accessory basal nucleus (MAB) and the negative basal nucleus (B) 100 ×.

5 Medial accessory basal nucleus of the amygdala stained with Sudan black B 1,100 ×

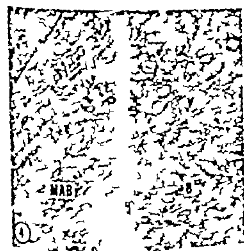
6 Nucleu septalis triangularis. In addition to neurons, granules are found in glia cells and in interstitial tissue. 400 ×

7 Subfornical organ. In this case there was heavy accumulation of AFP material in the interstitial spaces. 400 ×.

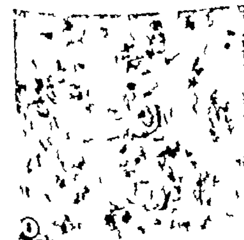

Ca
B
ST
MAB
B
1


2


3


MAB
B
4


5


6


7

Abbreviations

a, Artefact
B Basal Nucleus (amygdala)
Co, Cortical Nucleus (amygdala)
IC, Internal Capsule

MAB, Accessory Basal Nucleus, Medial Portion (amygdala)
N4 Nucleus of Trochlear Nerve
ST Stria Terminalis

PLATE I

EXPLANATION OF FIGURES

All sections are stained with aldehyde-fuchsin unless otherwise indicated.

1 Section from the amygdala in region of stria terminalis (ST) showing portions of the medial accessory basal nucleus (MAB) and cortical nucleus (Co) It is in this area surrounding the stria terminalis that granulation is heaviest. a-artefact 160 ×

2 A Type A cell from amygdala showing a single compact mass of granules. 1,100 ×

3 A Type C cell from the amygdala showing dispersed arrangement of granules. 1,100 ×

4 Opposed photographs from a section through amygdala showing striking contrast between the positively staining medial accessory basal nucleus (MAB) and the negative basal nucleus (B) 160 ×.

5 Medial accessory basal nucleus of the amygdala stained with Sudan black B. 1,100 ×

6 Nucleus septalis triangularis. In ddition to neurons, granules are found in glia cells and in interstitial tissue. 400 ×

7 Subfornical organ. In this case there was heavy accumulation of AFP material in the interstitial spaces. 400 ×

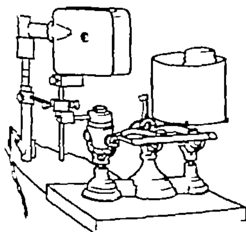


Fig. 8 Focusing apparatus concluded. Microscope with camera and beam-splitter above it, is supported on vertical steel rod that permits sliding movements of the two instruments for the preliminary focusing. This rod in turn is attached to the arm of a balance by joint that allows vertical movement on a horizontal ball-bearing axis to take place in the combination of instruments in response to the rise and fall of the ribs in breathing. The load upon the thorax well made by the rib-stays, microscope, beam-splitter and camera, had to be removed in order to avoid interference with respiration, and the following counterbalance was devised. A common type of commercial balance, without the pan, was modified for the purpose by substituting ball-bearings in place of the knife-edge of its beam, and in place of the pan, metal jar containing number 8 shot. Thus a perfect balance was provided between the weigh of the instruments connected with, and bearing upon the chest-wall, and the weight of the jar of shot. In this means an accurate focus on the lung of the breathing cat was maintained.

Special apparatus used in a few experiments has been described in the protocols.

OBSERVATIONS

Mammalia

White rat (Rattus norvegicus Berkenhout) In 38 experiments made during April '21 and June '23 on the living rat, a peculiar movement of the pipette which had been thrust into the lung was noted. If the lung were tapped near the heart, there were two oscillations of the pipette one synchronous with the heart-beat, the other caused by a momentary pause at the beginning of inspiration.

Columns of clear or sanguinous fluid, interrupted by empty spaces, appeared in pipettes that had been thrust into the lobules of the lung

Cat (Felis domestica, Briss) In 39 experiments capillary pipettes were inserted into the lungs of anesthetized cats. By measuring the thickness of the pleura and subserous coat in sections of the cat's lung, and by making casts of the bronchial system, data were obtained for designing pipettes that would project beyond their handles to enter but not to pass through a superficial lobule. Experiments in which a dye was injected into the lung from the trachea showed that such pipettes reached the interior of the lung lobule. The experimental procedure consisted in exposing approximately 1 sq cm of parietal pleura in the V and VII intercostal space while constantly observing the blood pressure as indicated by a mercury manometer connected with the left common carotid artery and the respiratory movements as recorded on a drum by a tambour. Pipettes were inserted into the lung, either through the intact pleura or after opening the pleural cavity A total of 268 pipettes were thus inserted, and of this number 184 or 69% contained clear fluid upon withdrawal.

Twenty two experiments were performed to determine the relative humidity of the air in the trachea during expiration and inspiration. The apparatus depicted in figure 2 was inserted between the cut ends of the severed trachea to collect and measure the water vapor present in the inspired and expired air No measurable differences were observed.

In five experiments motion pictures of the lung lobule were made during the process of respiration by use of the thoracic window described under materials and methods. The experiment required approximately two hours to perform and autopsy revealed little evidence of damage to the lung at the site of the window No signs of expansion or contraction of the lung lobule were seen in the motion pictures.

During the period 29 9 53 — 6:2:57 many experiments were made by Remy's reduced methylene blue method in search of evidence of fluid in the terminal bronchioles of the cat. Of these trials in which only the smallest caliber pipettes could be used, 21 retrieved a very short column of clear fluid.

There were 127 experiments on Mammalia recorded

Reptilia

Turtles Cumberland terrapin (*Pseudoemys elegans* Wied) painted turtle (*Chrysemys marginata* Agassiz) The anatomy of the turtle s lung and its relations to other viscera made intubation impossible and other methods were devised Two approaches were selected (a) removal of the plastron and (b) trephining the carapace.

In the first tests ('30–'33) the plastron was removed under anesthesia and the lungs exposed An opening was made by electro-cautery in the sinus-wall and its internal surface away from the opening was inspected. It was found to be wet and clear fluid could be collected by touch ing it with capillary pipettes. Search for parasites (routine in these experiments) yielded none Approach to the lungs by removal of the plastron is recorded for 25 experiments

Frequently employed was the method of exposing the lungs through openings made in the carapace Two square openings 2 by 2 cm were made in the cephalic part of the carapace located 1 5 to 2 cm right and left of the midline a little dissection of peripulmonary tissues revealed the lungs Through a circular aperture made in the lung by electro-cautery smooth-end capillary pipettes were introduced to make contact with the walls of the vestibule and with the septa between the sinuses at a distance from the aperture of en trance There are 20 records of this method and results A protocol of an experiment by each of the two methods follows.

11 2 33 Chrysemys marginata Spinal cord pithed at atlanto-occipital joint Plastron removed Sharp pipettes primed with paraffine oil were inserted into the caudal end of the left lung Clear fluid with drawn Through a small hole made electro-cautery in wall of cephalic end right lung six smooth-end pipettes prim with paraffine oil were inserted, a swept gently over surfaces away fro the opening On withdrawal they we found to contain clear fluid. This expe ment is cited for evidence of lung fluid a turtle that was pithed — no anesthet

4 4 51 Chrysemys marginata. Femal Urethane 3 66 cm into right thigh 9: A.M A piece 2 × 4 cm sawed out of mi dle of right half of carapace 10 50 ope ing in lung made by electro-cautery lu tapped with eight smooth-end pipette Experiment ended 11:45 turtle w breathing and active The results wer recorded as follows:

Pip. no. 1 clear fluid	0.4 mm; bubb
Pip. no. 2, sanguin. fluid	0.1 mm; bubb
Pip. no. 3, clear fluid	1.0 mm; bubb
Pip no. 4 clear fluid	0.7 mm; bubb
Pip. no. 5 sanguin. fluid	1.6 mm; bubb
Pip. no. 6, sanguin. fluid	0.1 mm; bubb
Pip. no. 7 nothing	
Pip. no 8 clear fluid	1.0 mm; bubb

Alligator (*Alligator mississippiensi* Daudin) The outer wall of the alligator lung is very thick composed as it is o much connective tissue and smooth mu cle conditions that made tapping wit pipettes difficult and necessitated the us of special techniques.

26 3 51 Alligator mississippiensi Weight 160 g. Nembutal 0 1 cm intra abd., 10:12 A.M 10 20 reptile on animal board body cavity opened by dorsal lon gitudinal incision right side and lun exposed small hole made in lung b electro-cautery 10:30 touched mucosa a spots away from this hole with eigh smooth-end pipettes Each pipette was i lung 30 seconds on removal end wa stopped with vaseline Experiment ende at 11 00 A.M heart was beating through out breathing slight Contents of pipette were recorded as follows

Pip. no. 1 lea fluid	4 5 mm; bubb
Pip. no. 2, lear fluid	2 0 mm; bubb
Pip. no. 3 lear fluid	5 0 mm; bubb
Pip no. 4 clear fluid	1.5 mm; bubb
Pip no. 5 le r fluid	0 8 mm; bubb
Pip. no. 6 lear fluid	6 0 mm bubb
Pip. no. 7 nothi g	
Pip no 8 nothing	

There were seven experiments on Alligator

Horned toad (*Phrynosoma cornutum*, Harlan) Only three living specimens of this desert inhabiting reptile were obtained.

1 12.38. *Phrynosoma cornutum*. Weight 11 g. Urethane intra abd. Respirations 28 per minute. Opened body cavity ventrally to observe entrance of cannulae into lung. Chose trachea for intubation and introduced cannulae, containing fine pipettes, into left and right bronchi and pushed them into cavities of lungs. With drew from right lung columns of clear fluid, sanguinous fluid, blood from the left lung withdrew 1.5 mm clear fluid. Heart beating at close of experiment, 11 40 A.M.

There were 55 recorded experiments on reptiles.

Amphibia

Frog (*Rana catesbiana* Shaw bullfrog; *R. clamitans* Latreille green frog *R. pipiens*, Schreber leopard frog) In preparation for several kinds of experiments frogs were pithed or decerebrated in other cases anesthesia was produced by intra-abdominal injection of urethane. Some experiments caused no pain and anesthesia was unnecessary Rhythm of heart beat and respiratory actions of mouth and body walls were noted The lung was exposed in many experiments by an opening made either dorsally or ventrally through the body-wall, and tapped with capillary pipettes. Such experiments gave some evidence of the presence in the sinuses of a clear fluid, but failure to control bleeding led to the abandonment of this method of tapping in the lung after a total of 20 experiments.

Intubation was first tried in the summer of '33 and used again in the spring of '38 with improvements of the apparatus employed. Anesthesia (urethane) was used in most cases, but in some this simple intubation operation was done without it A metal cannula 1 cm long having an outside diameter a little less than that of the rima glottidis provided with a handle was slipped through the rima into the lung A glass tube 8 cm long with an inside diameter somewhat less than that of the bore of the cannula, was used as a sheath-tube to protect the pipette when entering the lung. The distal entering-end of this sheath-tube was smoothed and its lumen closed by a very thin celloidin diaphragm.

In performing the experiment on a living frog the sheath-tube with a pipette inside and its smooth end arrested by the celloidin diaphragm was pushed through the cannula and into the central cavity of the lung. The pipette was then thrust through the diaphragm and beyond about 1 cm when contact of its tip with the free margins of septa was sought by moving the sheath-tube gently in all directions. This operation was continued for not more than half a minute The smooth point of the pipette came into contact with nothing but the celloidin diaphragm until it was free in the central cavity of the lung. The intubation method was carried out successfully in 16 experiments on bullfrogs during March '30 and results were consistently positive that is clear fluid was obtained.

1:8 51 *Rana catesbiana* This frog was moribund when the intubation experiment was made. Results: Contents of pipettes nos. (1) 0; (2) 0 (3) 1 mm column clear fluid (4) 0 (5) bubble

29 4 53. *Rana catesbiana* Anesthetic urethane 6.5 cm³ into thigh 0 00 A M Prone on animal-board 9:50 Respirations none. Glottis cocainized 10:05 Inserted cannula in rima glottidis at 10 15 and through it four pipettes with smooth tips and calibers 0.4-0.5 mm were inserted into right lung, each pipette was left for two minutes. Right lung was exposed at 10 40 and tip of cannula located ... thirds of its length within the lung which was empty of gas and relaxed The pipettes had drawn nothing. Breathing ... heart beating had ceased. Examination ... left lung was a repetition in all ... of the method used for exploring ... lung, and the results were similar ... four pipettes were empty on with... This frog was lethargic when taken ... the cold tank was injected with ... dose of urethane ... a trace ... was drawn into the right pipette ... exploring the two lungs. This ... tion of similar experiences in ... results of which had been ... accident or to faulty technique

On March 6 9 16 45 three experiments were undertaken to learn something more of the movement of the lungs and their sinuses. In preparation, a bullfrog was placed upon a meshed-wire frame and 1 cm of lipoidol was injected *via* the rima glottidis into the lungs. Observing that the heart action and rhythm of breathing were regular and rate unaffected it was clearly shown (a) that the lungs expanded cephalad in inspiration and (b) that the sinuses expanded approximately one-quarter of their diameters both dimensions retracting on expiration.

Parasites within the cavity of the frog's lung were encountered in many experiments These all trematode flukes were found in both lungs in the central cavity and in the sinuses The largest number observed in one frog was three. These parasites were active and moved about in a conspicuous surrounding of fluid filled with bubbles. Lungs were apparently healthy no thickening of sinus-walls or presence of congested blood-vessels were observed. Dr Alfred Lucas identified the flukes as *Hematotelechus medioplenus*

In the period May '51 to February '52 a series of experiments (started in St. Louis) was made with bullfrog tadpoles to learn whether water was present in their lungs when they came to the surface

11 5 51 Living tadpoles 7–8 cm long were put in a bowl containing 1 400 cm of tap-water They swam about, rose to the surface at intervals of 3 to 4 minutes One was transferred to a second bowl for a control. Lamp black, 2.5 g was mixed with the water in the first bowl. From this tadpoles were removed on May 12th 14th 15th 16th and sacrificed fixed in 10% formalin cut in serial transverse sections 10 μ through lungs in situ and stained with hematoxylin and eosin The control animal was prepared by the same technique. Study of these sections was begun in the Department of Anatomy Harvard Medical School (31 7 51) on the invitation of Professor George Wislocki. On his suggestion another series of sections was cut from the same specimen and stained with Mayer's paracarmine Under the microscope there were many particles visible in the tissues and cavities of the lung, some large some small, with rough irregular edges. Also present were black granules in the open spaces of the lung With high magnification these granules appeared separate from any cells in their vicinity

27 8 51 Trypan blue indicator Sacrificed two tadpoles rima glottidis and right gill-cover closed, that had lived 75 minutes in a 1% solution of trypan blue dissected them to expose ventral aspect of lungs. Removed cart. basihyal., made transverse opening in larynx, and introduced capillary pipette primed with mineral oil, into right "bronchus and cavity of lung withdrew blue-colored fluid. Tapped left lung, drawing 4 mm of blue-colored fluid

Prussian blue indicator Tadpoles were immersed in a 1% solution of potassium ferrocyanide for varying periods. Sought fluid in lung by capillary pipettes introduced *via* larynx. Fluid found present and ferric chloride was then drawn into the pipette Zone of contact of lung fluid and reagent the criterion: appearance of Prussian blue

Tadpole no 2 Immersed in potassium ferrocyanide solution two hours 90 minutes. Living Lungs tapped: from one drew a 7 mm column of fluid that formed a blue zone on contact with ferric chloride

Tadpole no 4 Urethane anesthesia. Each lung tapped by one capillary pipette Fluid withdrawn in both gave positive reaction with Prussian blue test.

There were 15 experiments on bullfrog tadpoles using the Prussian blue and trypan blue indicators in all of which clear fluid was withdrawn from the air spaces of the lung

Mudpuppy (Necturus maculosus Rafinesque) Eleven specimens of this perennibranch were obtained four were moribund and discarded. The method used in exploring the lungs was the same in the seven specimens examined. Under urethane anesthesia, the body-cavity was opened ventrally and the paired, sac-like lungs were tapped with capillary pipettes. The first experiment, May 8 '33 specimen a female revealed both lungs distended. Tapping the right lung resulted in filling the pipette with a column of clear fluid with a little blood 4 cm high; the lung was

filled with fluid. From the left lung were drawn a few short columns of clear fluid, and bubbles. In the other six active specimens the lungs were found expanded and short columns of clear fluid separated by bubbles were withdrawn.

There were 149 experiments on Amphibians made in the present study exclusive of the many tapping experiments that were performed.

REVIEW OF THE LITERATURE

In the literature on respiration in animals an association of this function with water appears to have been recognized by many investigators. Moist respiratory surfaces were described by Leclard (1815) Bernard (cited by Duval, 1875) Sehrwald (1886) Bohr ('00) Köppen ('21) Luciani ('11) Winternitz and Smith ('19) Voerhoff ('21) Colosi ('27 '28a, b '30) Wigglesworth ('29 '30 '31 '50) Powers et al. ('32) Clara ('36) Leiner ('38) Krogh ('41) Macklin ('36) Lee ('50) Movements of dust-cells and macrophages within or out of the alveolus are described by a number of investigators Metchnikoff ('05) Haythorn ('13–'14) Permar ('20–'21) Fried ('27) Maximow and Bloom ('30) Ross ('39) Low ('53) Phagocytic activities of free cells in the alveolus are recorded by Mavrogordato ('18) Sewell ('18–'19) Cappell ('23 '29) Mitosis of cells within the alveolus is cited by Seeman ('31) and by many others. Liljestrand and Sahlstedt ('24) found nearly complete saturation of the air in man's trachea both in inspiration and expiration (also reported by Perwitzschky '27) The presence of amniotic fluid in the lung has been found by Wialocki ('21) Bremer ('35) Snyder and Rosenfeld ('37) and Snyder ('41 '49) MacDougall and Hegner ('43) found water in the cloacal respiration of hibernating turtles. Boyd and Johnston ('40) discovered that the difference between the weight of the fresh and dried human lung was large and seasonly consistent. Concerning the musculature of the lung Ogawa ('20) found circularly arranged fibers around collecting ducts in many mammals. Baltisberger ('21) described smooth muscle surrounding respiratory bronchioles. Macklin ('22) described movements and form changes in the bronchial tree in human respiration. Hayek ('50) stressed the wide-spread distribution of smooth muscle in the human lung. He discussed the origin of secretion in the terminal branches in the absence of goblet cells and gave the evidence of Clara ('36) and Macklin ('54) that it is a secretory process of ciliated epithelium and liquidating cells. Scholander ('60) found the rate of oxygen transport enhanced by diffusion through water and by mediation of hemoglobin molecules which may carry over more than eight times as much oxygen as in straight diffusion.

SUMMARY AND CONCLUSIONS

The experiments on the white rat revealed the momentary pause in inspiration in normal breathing.

Motion pictures made on cats during successive phases of inspiration and expiration revealed no evidence of expansion and contraction of alveoli. The expansion and contraction of the lung as a whole appears to function in the filling and emptying of air in the bronchi up to the level of the pulmonary lobule.

The cat's lung is pervaded throughout with smooth muscle. It is suggested that this musculature functions in preventing the pressure of the inspired air from suddenly falling off as it passes from the narrow lumen of the trachea into the wide spaces of the lung and that this is accomplished by the constriction of the bronchi and the atrial openings in expiration, thereby establishing a partial pressure of oxygen in the alveoli that facilitates its solution.

The pneumograph curve registering the respiratory movements of the thoracic wall showed a pause in inspiration lasting but the fraction of a second before continuing its course This phenomenon was first *observed in my experiments on the white* rat and has since been noted in several instances when the cat was the subject (fig. 3) It is conceived that at the moment of the pause the rima glottidis closes; that in this fraction of a second, under intrathoracic pressure a phenomenon, suggestive of the dew-point, occurs

in the alveolus, and that molecules of oxygen in watery solution enter the blood of the pulmonary capillaries.

In the experiments on the turtle it was found that strata of clear fluid, bubbles and empty spaces occupied the pipettes that had made contact with the walls of both vestibule and sinus of the lung. All experiments save one, were made on an esthetized turtles the exception, C mar ginata pithed yielded clear fluid in six pipettes.

In tapping the lungs of the alligator many pipettes withdrew short columns of clear fluid interspersed with or followed by bubbles.

The lungs of the desert-inhabiting liz ard *Phrynosoma cornutum* yielded col umns of clear and flocculent fluid.

On the respiratory surfaces of the lungs of the adult frog a thin stratum of clear fluid was demonstrated by several methods. Intubation overcame the chance of contamination by blood and gave convinc ing evidence of wet respiratory surfaces. In breathing, the frog s lung moves ceph ad on expanding in inspiration the al ôses expand about one quarter of their diameters both dimensions retracting in expiration During the experiments on moribund and dead frogs very little fluid or none at all appeared in the pipettes on their withdrawal from the lung negative evidence supporting the claim of a normal physiological condition.

The experiments on tadpoles yielded evidence that with the closing of the gill clefts the lungs became filled with water drawn into them from the medium in which the tadpoles were immersed. From this source oxygen may enter the blood in the pulmonary circulation. A later state in the respiratory evolution is indicated by the tadpole repeated risings to the surface the head entering the atmosphere

Whereas fluid was found in the sac-like lungs of Necturus the extreme differences in the amounts call for explanation that the limited material examined thus far cannot supply

The respiration of fishes and the myriad aquatic invertebrates is dependent upon the oxygen dissolved in the seas lakes and rivers. Inter-tidal invertebrates and land invading fishes maintain a wet environment of their respiratory membranes. Terrestrial isopods and insects have wet respiratory organs. Advance toward air breathing is manifest in the fish *Ceratodus* by its possession of primitive lungs. In amphibians the skin functions in respiration both in the air and in the water vital to these animals during hibernation. The habitat of *Siren* is the mud of marshes of *Necturus* the depths of lakes and streams. Oxygen is in aqueous solutions in the lungs of reptiles and in the cloacal sac of certain hibernating turtles. It has been shown that the air-spaces of the lungs of chick-embryos are receptive to amniotic fluid. Watery fluid in the air passages of the lungs of mammalian embryos including man is recorded. The lungs of living adult mammals tolerate large quantities of water injected into them and dispose of it through the blood-circulation a fact that may be found of significance in the treatment of a drowning man.

ACKNOWLEDGMENTS

Following my retirement from teaching I continued the present research in St. Louis for the advantages of which I am much indebted to Professor Edward W Dempsey For assistance in the prepara tion of this paper for publication I am most grateful to Professor Mildred Trotter My best thanks go to Miss Elaine Harvey for help in the Library For technical help I am indebted to the skill of Mr Paul Bauer For assistance throughout I am indebted to Miss Carol Keller

LITERATURE CITED

Baltisberger W 1921 Über die glatte Muskulatur der menschlichen Lunge Zeitschr Anat. Entwicklungs., 61 219–282.

Bohr Christian 1900 Über die Haut und Lungenathmung der Frösche Skand Arch. f Phys 10 74–90.

Boyd, E. M., and G M. Johnston 1940 Seasonal Variation in the Water Content of the Respiratory Tract. Am. J Med. Sci 199 21–235.

Bremer John L. 1935 Postnatal development of Alveoli in the mammalia lung in relation to the problem of the Alveolar Phagocyte Carnegie In t. (Washi gton D C.) Publication No. 459 83–111 4 plates.

Cappell D. F 1923 Observ tions on the origin of the mononuclear phagocytes of the lung. J P th. and Bact ?8 430–432.

——— 1929 Intr vi al and supr vi tne. J P th. and Bact. (P rt II) 32

Clara, Max 1936 Vergleichende Histobiologie des Nierenglomerulus und der Lungenalveole. Ztschr. f. Mikros.-anatom. Forsch., 40: 147–280.

Colosi, Giuseppe 1927 Il popolamento delle terre emerse i fattori delli Grandi transmigrazioni. Universo (Firenze) 8(4): 359–373.

——— 1929a Ueber die Konstanz des respiratorischen mediums. (Lage des Problems und neue Beweise) Zool. Anz., 77 106–112.

——— 1929b Brevi considerazioni sulla pressione dell' ossigeno respiratorio. Soc. Ital. Sci. Natur. Atti., 67 340–344.

——— 1930 Il medium respiratorio. Riv di Patol. Sperim., 5 73–80.

Duval, Mathias 1873 Cours de médecine du Collège de France. Leçons sur les anesthésiques et sur l'asphyxie. Paris, J B. Baillière, In-8o VIII-636 p.

Fried, B. M. 1927 The origin of histiocytes (macrophages) in the lung. Arch. Path. and Lab. Med., 3 (5): 751–767

Hayek, H. v 1950 Die muskulatur im lungenparenchym des menschen. Zeitschr f Anat. u. Entwickl. Bd., 115 68–94.

Haythorn, Samuel R. 1913-14 Some histological evidences of the disease importance of pulmonary anthracosis. J Med. Research, 29 259–279

Keppen, A. 1921 Die feineren verästelungen der tracheen nach untersuchungen an Dytiscus Marginalis L. Zool. Anz., 52 132–139

Krogh, A gust 1941 Comparative Physiology of Respiratory Mechanisms (Swarthmore College, William J Cooper Foundation. Lectures, '39) VII, 172 p Univ of Penn. Press.

Leclard 1815 U tersuchungen, welche zu beweisen f heinen, das der Fotus das Schafwasser athmet. Deutsch. Arch. für Physiol. Bd., 1 164–165.

Lee Douglas H K. 1950 Physiology of tissues and organs; an introduction to the study of systematic physiology (Queensland Univ Mic. Pub. no. 11) VIII, 159 p., Charles C Thomas

Leiner Michael 1938 Die physiologie der fischatmung mit 117 Abbildungen. Leipzig. Akademische verlagsgesellschaft m.b.h., 134 p

Liljestrand, G and A. V Sahlstedt 1924 Temperatur und Feuchtigkeit der ungeatmeten Luft. Skand. Arch f. Physiol., 46 94–120.

Low Frank N 1953 The pulmonary alveolar epithelium of laboratory mammal and man. Anat. Rec., 117 241–263.

Luciani, Luigi 1911 Human Physiology trans. by Frances A Welby; with preface by J N. Langley London, Macmillan and Co Ltd. 5

MacDougall, Mary Stuart, and R. W Hegner 1943 Biology the Science of Life. 963 p. McGraw-Hill Co New York.

Macklin, Charles C. 1925 X-ray studies on bronchial movements. Am. J Anat., 35 303–320.

——— 1936 Alveolar pores and their significance in the human lung. Archives of Path., 21 202 216.

——— 1954 The Pulmonary Alveolar Mucoid Film and the Pneumonocytes. Lancet, I 1099–1104

Mavrogordato A. 1918 Experiments on the effect of dust inhalations. J Hygiene 17 439–459.

Maximow Alexander A. 1930 A Text-book of Histology completed and edited by William Bloom, Philadelphia and London, W B. Saunders Co., XIII, 833 p.

Metchnikoff, Elie 1905 Immunity in infective diseases. Trans. from the French by Francis G. Binnie. XVI, 591 p. Cambridge.

Ogawa, Chikanosuke 1920 Contributions to the histology of the respiratory spaces of the vertebrate lungs. Am. J An t., 27 333–393.

Permar H. H. 1920-21 An experimental study of the mononuclear phagocytes of the lung. J Med. Research, 42: 9–32.

Perwitzschky R. 1927 Die Temperatur und Feuchtigkeitsverhältnisse der Atemluft in den Luftwegen. Arch. Ohren, Nasen u. Kehlkopf., *117(1)*: 1–36.

Powers, Edwin B., et al. 1932 The relation of respiration of fishes to environment. Ecological Monographs, 2: 385–473.

Ross, I. S. 1939 Pulmonary epithelium and proliferative reactions in the lungs. Arch. Path., 27 478–496.

Scholander P F 1960 Oxygen transport through hemoglobin solutions. Science 131 585–590.

Seeman, G. 1931 Histobiologie der Lungenalveole. Jena, Fischer 68 p.

Sehrwald, Ernst 1886 Aus der med. Klinik des Herrn Prof. Rossbach in Jena. Ueber die percutane Injection von Flüssigkeiten in die Trachea, deren Verbreitung in der Lunge und Wirkung auf Lunge und Gesammtorganismus. Dtsch. Arch. f. Klin. Med., 39 162–200.

Sewell, W T 1918-19 The phagocytic proper ties of the alveolar cells of the lung. J Path. and Bact., 22 40–55.

Snyder F F 1941 The rate of entrance of amniotic fluid into the pulmonary alveoli dur ing fetal respiration. Am. J Ob. and Gyn., 41 224–230.

——— 1949 Obstetric analgesia and anesthesia; their effects upon labor and the child. VIII, 401 p Saunders.

Snyder F F and M. Rosenfeld 1937 Direct observation of intrauterine respiratory movements of the fetus and the role of carbon dioxide and oxygen in their regulation Am. J Phys 119 153–166.

Terry Robert J 1920 On the presence of fluid in the pulmonary alveoli. J Mo State Med. Assoc., 17 40–41

——— 1939 A thoracic window for observation of the lung in living animal. Science n.s. 90 43–44

Voerhoff K. W 1921 Über die Atmung der Landasseln, zugleich ein beitrag zur Kenntnis der Entstehung der Landtiere. Zeitschr f. Wissen. Zool., 118 365–446.

Wigglesworth, V B. 1929 Chemical bioemesis and the development of secretion cells are 124 966–987

——— 1930 A theory of trac in insects. Proc. Roy Soc.

——— 1931-32 The extent of air in the tracheoles of some terrestrial insects. Proc. Roy Soc. B, *109* 354–359

——— 1950 Insect Physiology Fourth ed. x, 134 p. Methuen.

Winternitz, M. C., and G. H. Smith 1919 Intratracheal pulmonary irrigation. p. 1255–1268, vol. 2, Contributions to Medical and Biological Research, Dedicated to Sir William Osler *New York, Hoeber*

Wislocki, G. B 1921 Note on the behavior of trypan blue injected into the developing egg of the hen. Anat. Rec., 22 267 274.

Pathways of Intestinal Lymph Drainage in Normal Sheep and in Sheep Following Thoracic Duct Occlusion [1]

TREVOR HEATH
Department of Anatomy San Francisco Medical Center
University of California, San Francisco, California

ABSTRACT The pathways by which intestinal lymph enters the blood were studied with radiologic and radioactive tracer techniques in normal sheep and in sheep after thoracic duct occlusion. It was concluded that direct connections between the intestinal lymphatics and blood vessels in the abdomen and caudal thorax in normal sheep are very uncommon if they occur at all.

During the first few days after the thoracic duct of sheep was occluded in the thorax, transfer of protein from intestinal lymph to blood was slow At this time, the abdominal lymphatics were grossly dilated and lymphatic valves incompetent. After about 1–3 weeks, the abdominal lymphatics were of more normal size and drainage of lymph protein to the blood occurred more rapidly At least some of this protein *entered the blood within lymph nodes. After 4–7 weeks, direct vascular connections* between the thoracic duct and hemiazygos vein had developed.

It is generally assumed that all the lymph from the abdominal viscera and caudal portion of the body drains into the thoracic duct which conveys it to the great veins in the neck. However in some species direct connections between the lymph and blood vascular systems have been discovered in the abdominal region which suggests that some lymph from this region may drain into abdominal veins. Silvester (12) found connections between lymphatics and the inferior vena cava at the level of the renal veins in monkeys, and Job (18) found similar connections in rats. In studies of fat absorption in sheep Heath and Morris ('62) were able to recover in thoracic duct lymph only about one-half the fat absorbed from the intestine. Failure to recover all the fat might be explained by the presence of lymphatic venous connections distal to the point of lymph collection. This paper describes the results of a series of experiments performed to determine whether such connections do in fact exist in sheep.

Two general approaches were used to provide an answer to this question. First, the amount of ^{131}I-labeled albumin that could be recovered in thoracic duct lymph following its injection into a mesenteric lymphatic was determined. Second the rate and route of passage into the bloodstream of tracer substances injected into a mesenteric lymphatic was studied at various time intervals after occlusion of the thoracic duct. It was anticipated that the results of these experiments would disclose (a) whether lymphatic venous connections exist in the abdomen and caudal thorax in normal sheep and (b) the location and nature of connections which develop during an extended interval after occlusion of the thoracic duct. It has been shown previously in dogs that, after the thoracic duct is occluded the flow of lymph into the bloodstream is temporarily impeded (Gryaznova, '63) but that collateral lymphatics or lymphatic venous connections develop within a few weeks (Blalock, Robinson Cunningham and Gray '37; Freeman, 42 Gryaznova, '63)

MATERIALS AND METHODS

The merino and crossbred ewes 1–6 years of age used in these experiments were restrained indoors in metabolism cages and had free access to water and alfalfa hay or chaff.

EXPERIMENTAL METHODS

Recovery of intestinal lymph in the thoracic duct. Cannulae were placed in the

[1] Presented in part at the Seventy-seventh Meeting of the American Association of Anatomists in Denver, 31 March – 3 April, 1964 (Heath, '64).
Present address: Veterinary School, University of Melbourne, Melbourne, Australia.

thoracic duct and a mesenteric lymphatic of 15 sheep. Five-tenth milliliter of a solution of ^{131}I labeled albumin (The Radiochemical Centre Amersham, England) was washed into the mesenteric cannula with 0.5 ml of a solution of Evans Blue. The radioactivity in thoracic duct lymph collected during the next hour was measured and then compared with the total amount initially injected. The sheep were maintained under anesthesia during this procedure. All radioactivity measurements were made by GM counting.

Drainage of intestinal lymph after thoracic duct occlusion Nine of the sheep subjected to the procedure described above were used in these experiments. In all these sheep the labeled albumin injected into a mesenteric lymphatic was completely recovered in the thoracic duct lymph indicating that functioning lymphatic venous connections were not present along the route of the intestinal lymph. The thoracic duct cannulae were then tied off At the same time the mesenteric cannula was removed and the lymphatic ligated except in one sheep (sheep A) in which the mesenteric cannula was left in place

After 9–13 days three of these sheep were anesthetized and 0 5 ml ^{131}I labeled albumin was injected into a cannulated mesenteric lymphatic At intervals up to 10 min thereafter blood samples were collected from either the caudal vena cava or the jugular vein and from veins draining lymph nodes in the abdomen These experiments were performed to see whether following thoracic duct occlusion evidence could be obtained that proteins from intestinal lymph could pass to the blood within lymph nodes

In sheep A 0 5 ml ^{131}I-labeled albumin was injected into the indwelling mesenteric lymphatic cannula on each of five successive days after the thoracic duct was occluded The levels of radioactivity in samples of jugular vein blood were measured at serial intervals up to an hour after each injection Before each injection of labeled albumin, adequate functioning of the indwelling canula was checked radiologically with an image intensifier (see below) by observing that contrast medium injected into the canula flowed freely into the efferent lymphatic. The sheep was not anesthetized during these experiments.

At intervals up to seven weeks after the thoracic duct was occluded each of the nine sheep was anesthetized, and 10–15 ml of water-soluble contrast medium (Diaginol or Arteriodione May and Baker) was injected into a mesenteric lymphatic over a period of 10–15 min. The injection pressure was not measured Mercury was substituted for the aqueous medium in two sheep examined four and seven weeks respectively after thoracic duct occlusion. The fate of the injected medium was observed directly with a Siemens Image Intensifier X ray Unit. The course of the medium through the lymphatics was periodically recorded on non-screen film (Kodirex Kodak) without the use of a grid.

In order to observe the changes in lymph node structure following thoracic duct occlusion the ducts of three sheep were ligated and seven days later mesenteric renal and hepatic lymph nodes were removed. The nodes were fixed in 10% aqueous acrolein (Luft '59) and embedded in polyethylene glycol disterate (Sidman Mottla and Feder '61) Sections were stained with hematoxylin and eosin.

In one sheep in which the thoracic duct had been occluded six weeks previously a solution of latex was injected into a mesenteric lymphatic and the distribution of latex in lymph and blood vessels observed at autopsy In the two sheep in which mercury had been used as a contrast medium, the distribution of mercury was observed at autopsy

Surgical techniques

The technique of Lascelles and Morris ('61) was used either to ligate or to cannulate the thoracic duct at the level of the ninth thoracic vertebra To inject solutions into a mesenteric lymphatic a mesenteric lymph node was exteriorized through an incision 15 cm long in the right mid flank region. In contrast to their position in many other species these nodes in sheep are situated in the mesentery about 5 cm from the intestine (fig. 1) As a result efferent lymph from these nodes passes through a relatively long segment of lymphatic before reaching the thoracic duct As the efferent lymphatics pass dorsally

Fig. 1. Schematic diagram showing the lymphatic drainage from the small intestine of a sheep. A cannula used for making injections is placed in an efferent duct from mesenteric lymph node and another for collecting lymph is placed in the thoracic duct.

they converge to form one or two collecting ducts which join lymphatics from the cecum and colon near the root of the mesentery. One of the efferent lymphatics was dissected free from surrounding tissue for about 1 cm of its length and cannulated with 1.0 mm O.D. polyethylene tubing (fig. 1). Proper placement of the cannula was checked by injecting into it a small amount of a solution of Evans Blue and observing its passage into the lymphatic.

RESULTS

Recovery of intestinal lymph in the thoracic duct. After ^{131}I-labeled albumin was injected into a mesenteric lymphatic radioactivity appeared rapidly in the thoracic duct lymph. In 13 sheep, all the injected radioactivity was recovered in the lymph usually within the first 10–15 min. In two sheep, 88 and 85% was recovered. This indicates that, in anesthetized sheep at least, all or very nearly all the intestinal lymph drains into the thoracic duct and can be collected when the thoracic duct is cannulated in the thorax.

Drainage of intestinal lymph after thoracic duct occlusion. Sheep in which flow through the thoracic duct was occluded recovered rapidly from the operation and appeared clinically normal during the experimental period.

When ^{131}I-labeled albumin was injected into a mesenteric lymphatic of sheep A immediately after its thoracic duct was occluded radioactivity appeared in the blood very slowly (fig. 2). When the experiment was repeated on this sheep on each of the next two days, the results were similar. Since the level of radioactivity in the blood increased slowly it appeared that functioning lymphatic-venous connections were not present. When the experiment on sheep A was repeated on the fifth day after thoracic duct occlusion, the level of radioactivity in the blood increased much more rapidly indicating that a more direct pathway for the drainage of lymph into the bloodstream had probably developed in the interim.

In an attempt to demonstrate the pathways by which intestinal lymph drained to the bloodstream during this period the drainage of contrast medium from a mesenteric lymphatic was studied radiologically in three sheep at intervals during the first week after the thoracic duct was occluded. During the first few days the lymphatics distal to the occlusion appeared grossly dilated (fig. 4). Contrast medium flowed in a retrograde direction along the lumbar trunk and filled efferent lymphatics from various abdominal lymph nodes. This could have occurred only if the valves in the dilated vessels had become incompetent. About 10–20 min after the contrast medium was injected, the walls of the lymphatics became indistinct and a small amount of radio-opacity appeared in the immediately surrounding area. Apparently some contrast medium was extravasating through the walls of the dilated lymphatics. The lymphatic walls also became indistinct following an intralymphatic injection of contrast medium in normal sheep but at a much less rapid rate.

By 5–7 days after thoracic duct occlusion, although some retrograde flow of contrast medium still occurred along efferent lymphatics draining abdominal lymph nodes, the abdominal lymphatics were less dilated and presumably lymph was draining more readily into the bloodstream. In each of two sheep examined radiologically eight days after th duct occlusion a radiotranslucent

sheep autopsied eight days after thoracic duct occlusion, a small amount of clotted lymph enclosed by a fibrous tissue capsule was found surrounding the thoracic duct caudal to the obstruction. This corresponded in position to the radiotranslucent area observed radiologically It seemed likely that, during the first few days after the thoracic duct was occluded, lymph escaped through the walls of the dilated duct and became encapsulated. At autopsy however there was no sign of continuing extravasation.

In two sheep in which radiological evidence suggested the passage of mercury from the thoracic duct to the hemiazygos vein four and seven weeks after thoracic duct occlusion mercury was present in the hemiazygos vein at autopsy In the first sheep mercury was also found in a small vessel joining the thoracic duct to the hemiazygos vein about 10 cm cranial to the diaphragm. In this sheep mercury was also found in a small vessel which extended from the thoracic duct to the caudal mediastinal lymph node In the second sheep mercury was found in a small vessel which emerged from the thoracic duct just caudal to the site of occlusion and passed under the fibrous capsule of a lymph node adjacent to the hemiazygos vein Because of difficulties in dissection however it was not possible to be sure whether the mercury which had entered the vein had passed along this vessel Another sheep was anesthetized six weeks after thoracic duct occlusion and latex was injected through a mesenteric lymph cannula The sheep was killed and the area of the thoracic duct dissected after fixation in formol-saline Latex was found filling both the thoracic duct and a small vessel joining the thoracic duct to the hemiazygos vein just cranial to the diaphragm (fig 3) A small amount of latex wa also found in the vein

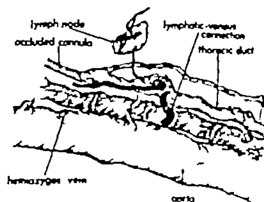


Fig. 3 Sketch of a lymphatic-venous connection in sheep, six weeks after thoracic duct occlusion. This connection between the thoracic duct and the hemiazygos vein was demonstrated after the thoracic duct was filled with latex.

DISCUSSION

In almost all cases in which labeled protein was injected into a mesenteric lymphatic in normal anesthetized sheep the protein was recovered quantitatively in the thoracic duct lymph indicating that protein was not leaving the intestinal lymphatics to enter the bloodstream in the abdomen or caudal thorax. If connections between intestinal lymphatics and veins were present in these animals they were closed and nonfunctional during the period of anesthesia. Threefoot, Kent and Hatchett ('63) suggested that lymphatic venous connections may be under autonomic control and may open when the intralymphatic pressure exceeds a critical level If this process occurs in sheep it is likely that any existing connections would have opened when the intralymphatic pressure increased following ligation of the thoracic duct However when the thoracic duct was occluded, the abdominal lymphatics remained dilated for several days indicating that drainage of lymph to the bloodstream was severely impaired. In addition immediately after the thoracic duct was occluded transfer of labeled protein from the intestinal lymph to the bloodstream was slow It is probable that the transfer which took place at this time represented protein which extravasated through the walls of the dilated lymphatics and was returned to the circulation by the right lymph duct (Yoffey and Courtice '56) Although under normal conditions the main lymphatic vessels are impermeable to large proteins (Mayerson Patterson McKee LeBrie and Mayerson '62) Courtice and Steinbeck ('51) have demonstrated that protein can extravasate from occluded lymphatics.

In normal lymph nodes of dogs the passage of proteins and of cells from lymph to blood is negligible (Mayerson, et al., '62 Sabiston Archer and Blalock, '63) Pressman, Simon, Hand and Miller ('62) have demonstrated the passage of plasma proteins into the efferent blood of dog cervical lymph nodes following intra nodal injection. In interpreting their results, it is important to consider the traumatic changes in lymph node structure which must follow the injection of relatively large volumes (2 ml) of material directly into lymph nodes. Following thoracic duct occlusion, abdominal lymph nodes become large and edematous and contain a decreased amount of lymphoid tissue (Lee '22 Blalock, Robinson, Cunningham and Gray '37) In the experiments described in the present paper extensive dilatation of medullary sinuses occurred in abdominal lymph nodes of sheep a week after thoracic duct occlusion. At this time the retrograde flow of intestinal lymph along efferent lymphatics draining intestinal, renal and lumbar nodes was demonstrated by radiological methods and the examination of efferent nodal blood indicated transfer of intestinal lymph protein to the bloodstream within these nodes With the methods used, however it was not possible to identify a route within the lymph nodes by which lymph could reach the blood.

These pathways of lymph drainage were replaced later by direct connections between the thoracic duct and hemiazygos vein just caudal to the site at which the thoracic duct had been occluded. Connections of this type have been shown to function in cats dogs and rats within the first two months after thoracic duct occlusion (Lee '22 Blalock et al '37 Threefoot, Kent and Hatchett, '63) Yoffey and Courtice ('56) suggested that these anastomotic connections may be enlargements of pathways normally present. Pathways of this type however could not be demonstrated in normal sheep.

In the experiments of Heath and Morris ('62) on the absorption of fat in sheep only about one-half of the fat absorbed from the gut could be recovered from chronic thoracic duct fistulae It has been suggested that some of the fat which was absorbed into the lymph may have entered the blood through alternate pathways and escaped collection. The evidence presented in this paper however indicates that all, or very nearly all, of the lymph from the intestines of sheep is collected from a freely flowing cannula in the thoracic duct. It is possible that if this cannula is temporarily occluded (e g by fibrin clots) alternate means of drainage such as those observed in these experiments, may develop If this did occur quantitative collection of lymph would not be possible when free flow through the cannula was again established. However in the experiments of Heath and Morris ('62) the thoracic duct cannulae were rarely occluded and never for more than a few hours. The evidence presented here indicates that total obstruction to lymph flow for at least several days is necessary before alternate pathways develop for the rapid drainage of intestinal lymph. For these reasons it is thought unlikely that lymphatic-venous connections of any type played a part in their experiments. In sheep therefore the portal vein must be considered as a possible route for the transport of a portion of the fat which is absorbed from the gut

SUMMARY

The results of tracer experiments performed on normal sheep and on sheep after thoracic duct occlusion indicate that direct connections between the intestinal lymphatics and the bloodstream in the abdomen and caudal thorax of sheep are very uncommon if they occur at all.

When the thoracic duct of sheep was occluded, during the first few days the lymphatics distal to the obstruction were widely dilated and the valves incompetent Transfer of proteins from intestinal lymph to blood was slow After about 1–2 weeks, the abdominal lymphatics were of more normal size and drainage of protein from lymph to blood more rapid. At least some of this protein entered the bloodstream within lymph nodes. After 4–7 weeks, direct vascular connections between the thoracic duct and hemiazygos vein had developed.

sheep autopsied eight days after thoracic duct occlusion, a small amount of clotted lymph enclosed by a fibrous tissue capsule was found surrounding the thoracic duct caudal to the obstruction. This corresponded in position to the radiotranslucent area observed radiologically It seemed likely that, during the first few days after the thoracic duct was occluded lymph escaped through the walls of the dilated duct and became encapsulated. At autopsy however there was no sign of continuing extravasation.

In two sheep in which radiological evidence suggested the passage of mercury from the thoracic duct to the hemiazygos vein four and seven weeks after thoracic duct occlusion mercury was present in the hemiazygos vein at autopsy In the first sheep mercury was also found in a small vessel joining the thoracic duct to the hemiazygos vein about 10 cm cranial to the diaphragm In this sheep mercury was also found in a small vessel which extended from the thoracic duct to the caudal mediastinal lymph node In the second sheep mercury was found in a small vessel which emerged from the thoracic duct just caudal to the site of occlusion and passed under the fibrous capsule of a lymph node adjacent to the hemiazygos vein Because of difficulties in dissection however it was not possible to be sure whether the mercury which had entered the vein had passed along this vessel Another sheep was anesthetized six weeks after thoracic duct occlusion and latex was injected through a mesenteric lymph cannula The sheep was killed and the area of the thoracic duct dissected after fixation in formol-saline Latex was found filling both the thoracic duct and a small vessel joining the thoracic duct to the hemiazygos vein just cranial to the diaphragm (fig 3) A small amount of latex was also found in the vein.

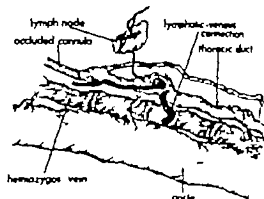


Fig. 3 Sketch of lymphatic-venous connection in a sheep, six weeks after thoracic duct occlusion. This connection between the thoracic duct and the hemiazygos vein wa demonstrated after the thoracic duct was filled with latex.

DISCUSSION

In almost all cases in which labeled protein was injected into a mesenteric lymphatic in normal anesthetized sheep the protein was recovered quantitatively in the thoracic duct lymph indicating that protein was not leaving the intestinal lymphatics to enter the bloodstream in the abdomen or caudal thorax. If connections between intestinal lymphatics and veins were present in these animals they were closed and nonfunctional during the period of anesthesia. Threefoot Kent and Hatchett ('63) suggested that lymphatic venous connections may be under autonomic control and may open when the intralymphatic pressure exceeds a critical level If this process occurs in sheep, it is likely that any existing connections would have opened when the intralymphatic pressure increased following ligation of the thoracic duct However when the thoracic duct was occluded the abdominal lymphatics remained dilated for several days indicating that drainage of lymph to the bloodstream was severely impaired. In addition immediately after the thoracic duct was occluded transfer of labeled protein from the intestinal lymph to the bloodstream was slow It is probable that the transfer which took place at this time represented protein which extravasated through the walls of the dilated lymphatics and was returned to the circulation by the right lymph duct (Yoffey and Courtice '56) Although under normal conditions the main lymphatic vessels are impermeable to large proteins (Mayerson Patterson McKee LeBrie and Mayerson '62) Courtice and Steinbeck ('51) have demonstrated that protein can extravasate from occluded lymphatics.

T

V

W

X

Y